

Springer Earth System Sciences

Jorge Rabassa *Editor*

Advances in Geomorphology and Quaternary Studies in Argentina

Proceedings of the Sixth Argentine
Geomorphology and Quaternary
Studies Congress

 Springer

Springer Earth System Sciences

Series editors

Philippe Blondel, Bath, UK

Eric Guilyardi, Paris, France

Jorge Rabassa, Ushuaia, Argentina

Clive Horwood, Chichester, UK

More information about this series at <http://www.springer.com/series/10178>

Jorge Rabassa
Editor

Advances in Geomorphology and Quaternary Studies in Argentina

Proceedings of the Sixth Argentine
Geomorphology and Quaternary Studies
Congress

 Springer

Editor
Jorge Rabassa
Laboratorio de Geomorfología y Cuaternario
CADIC-CONICET
Ushuaia
Argentina

ISSN 2197-9596 ISSN 2197-960X (electronic)
Springer Earth System Sciences
ISBN 978-3-319-54370-3 ISBN 978-3-319-54371-0 (eBook)
DOI 10.1007/978-3-319-54371-0

Library of Congress Control Number: 2017932021

© Springer International Publishing AG 2017

This work is subject to copyright. All rights are reserved by the Publisher, whether the whole or part of the material is concerned, specifically the rights of translation, reprinting, reuse of illustrations, recitation, broadcasting, reproduction on microfilms or in any other physical way, and transmission or information storage and retrieval, electronic adaptation, computer software, or by similar or dissimilar methodology now known or hereafter developed.

The use of general descriptive names, registered names, trademarks, service marks, etc. in this publication does not imply, even in the absence of a specific statement, that such names are exempt from the relevant protective laws and regulations and therefore free for general use.

The publisher, the authors and the editors are safe to assume that the advice and information in this book are believed to be true and accurate at the date of publication. Neither the publisher nor the authors or the editors give a warranty, express or implied, with respect to the material contained herein or for any errors or omissions that may have been made. The publisher remains neutral with regard to jurisdictional claims in published maps and institutional affiliations.

Printed on acid-free paper

This Springer imprint is published by Springer Nature
The registered company is Springer International Publishing AG
The registered company address is: Gewerbestrasse 11, 6330 Cham, Switzerland

Preface

The Argentine Association of Geomorphology and Quaternary studies was founded and established during the decade of the 1990s. Then, it was the optimistic effort of a small group of Argentine geologists, geographers, paleontologists, and archeologists who were expecting to generate their own space in the Earth Sciences of Argentina, where the dialogue about landscapes, landforms, as well as recent paleoclimates and paleoenvironments would be open among scientists of various concurrent disciplines. As expected, the beginnings were very difficult, until a reduced group of geomorphologists and Quaternary specialists found out that symposia, field trips, and finally, multidisciplinary congresses were the most appropriate means to improve the frequency of academic encounter of researchers in these sciences. Many countries in the world have autonomous societies for Geomorphology and Quaternary Sciences, which are then linked to the International Association of Geomorphologists (IAG) and the International Union for Quaternary Studies (INQUA), respectively. In Argentina, due to the limited number of specialists, most of them working simultaneously in both these fields of knowledge, the congruent decision was to support just only one organization, incorporating in it specialists of both areas, so as to better concentrate the valuable efforts of its members.

The Argentine Congresses in Geomorphology and Quaternary studies are held every three years. The first congresses took place in the cities of Mar del Plata, Tucumán, Córdoba, La Plata, and Río Cuarto where, in all cases, prestigious universities hosted the meetings. Finally, the 6th Argentine Congress of Geomorphology and Quaternary Studies was held in Ushuaia, Tierra del Fuego, in April 2015. Ushuaia is the southernmost city in the world, over 3000 km south of Buenos Aires, the national capital city.

This was certainly a historical fact in academic terms. This was the first time a national congress in any discipline of the Earth Sciences was held in Tierra del Fuego, and the southernmost place on Earth where a congress as such, organized by a national association, had taken place. The immense distances that separate Ushuaia from the rest of Argentina and thus, the higher costs of air fare, were some of the difficulties faced by the organizers. The Association had accepted the

proposal to organize the 6th Congress, during the previous congress in the city of Río Cuarto, Córdoba, in October 2011. That was certainly an expression of confidence by the congress members toward the Ushuaia organizing committee, who voiced later their gratitude to all participant colleagues. The Congress received the support of the Centro Austral de Investigaciones Científicas (CADIC), the Ushuaia branch of CONICET, the National Research Council of Argentina, the National Agency for Science and Technology (ANPCYT), the Argentine Minister of Science and Technology, and the academic backing of the Asociación Geológica Argentina, the Asociación Paleontológica Argentina and the Asociación Argentina de Sedimentología.

The main aim of this congress was to contribute to the progress of Geomorphology and Quaternary Studies, in all disciplines, integrated to the other Earth Sciences but closely related to the Natural and Social Sciences. Besides, the Congress provided the right environment to discuss aspects of the relationship with production, prospection, and use of natural resources, the rational treatment of waste, the protection and management of the environment, climatic change, and the availability of appropriate techniques for these purposes.

The Congress developed thematic sessions, with oral and poster presentations, most of them in plenary sessions to favor the multidisciplinary analysis of core subjects. Almost 200 participants from many different Argentine provinces and neighboring countries such as Uruguay, Chile, Brazil, and Paraguay registered, and more than 200 abstracts were reviewed by a Scientific Committee and later published in a dedicated volume which was made available to the participants upon registration.

Four distinguished foreign colleagues accepted our invitation to offer high impact lectures during the Congress. They were Dr. John Clague (Simon Fraser University, Vancouver, Canada; former INQUA President), Dr. Rene Barendregt (Lethbridge University, Alberta, Canada), Dr. Michael Smith (Kingston, London, United Kingdom, founder-editor of the "Journal of Maps"), and Dr. Piotr Migón (Wrocław University, Poland, founder-editor of the series "Geomorphological Landscapes of the World", by Springer Verlag Publishers), who did it as the official representative of the International Association of Geomorphologists (IAG). In all cases, our guest lecturers cover their own travel expenses, a fact that deeply compromises our permanent gratitude.

Since most of the participants have never been in Tierra del Fuego before, intra-Congress and post-Congress field trips were organized to expose the geological features, landscapes, and environments of the island to the Congress attendants. The Beagle Channel, the Fuegian Andes, Lake Fagnano and the Magellan Transcurrent Fault, the passage from the Scotia Plate to the South American Plate, the Austral Basin, and the dry steppes of northern Tierra del Fuego were visited and their features discussed in the field.

As President of the Organizing Committee, I would like to deeply thank all the colleagues at CADIC that worked indefatigably to make this event possible: Andrea Coronato, Juan Federico Ponce, Marilén Fernández, Romina Onorato, Mónica Salemme, Fernando Santiago, Soledad Schwarz, Jimena Oría, María Laura

Villarreal, María Soledad Candel, Lucas Turnes, Ramiro López, Diego Quiroga, Mauricio González Guillot, María Laura Borla, Leonardo Ramírez Viturro, and Pau Montero Estaña. To all of them, my eternal gratefulness.

The great Charles Darwin, the first naturalist, geologist, paleontologist, glaciologist, and anthropologist who visited Tierra del Fuego in 1833–1834, was in this island during his famous voyage on board of the HMS Beagle, under the command of Captain Robert Fitz Roy. Hopefully, Darwin's spiritual legacy has steered our visitors to appreciate the immensity, complexity, and exceptionality of the Fuegian landscapes, its past and present ecosystems, and the fascinating history of human occupation of these extreme lands which started 11,000 years ago.

This volume presents 11 papers which were carefully selected by the Scientific Committee, for their scientific quality and topical and methodological variety. In summary, these papers belong to several different disciplines, representing the ample diversity of the science community that participated in this Congress.

The first chapter of this book, by Emilia Aguilera and colleagues, is devoted to the different landscapes developed on ignimbrites in Argentina, mostly in Patagonia where these pyroclastic rocks are common. The nature of these landscapes on ignimbrites is directly related to the degree of welding of the ash-flow tuffs, and the scale of analysis, from single micro-landforms to huge, extensive, complex landscapes. The landscape characteristics are also strongly related to the age of the pyroclastic units and the exposure time of their outcrops.

Soledad Schwarz and Piotr Migoń analyzed the relationship of landscape and tourism, science and leisure, the nature of geotourism, and the educational relevance of regionally changing landscapes. Using field notes and data, different Fuegian landscapes were studied and their features identified. It is worth mentioning that sections of this paper were prepared and elaborated actually during the post-Congress field trip and original field sketches, with notes in Polish, were underwritten by Professor Migoń by means of ad-hoc files.

Soil and Geomorphology relationships were carefully studied by Pablo Bouza and colleagues, as a by-product of a technical survey done in a uranium mining district in Central Patagonia. Many dissimilar landscape units have been recognized; most of them of Quaternary age but some others as old as the Late Mesozoic. The soils developed on these landscapes were wisely and sensibly described and their pedological and geochemical characteristics scientifically considered.

The hydrology of coastal environments in Buenos Aires province was investigated by Silvina Carretero and Eduardo Kruse. The availability of water resources is highly valuable in these coastal environments, since most of the coastline is used for touristic purposes, not only as summer beaches, but also for week-end recreation all year around. The human intervention on the coastal dune systems, the best source for fresh water, has endangered the water supply to the ample beaches and growing towns. Two neighboring localities were tested for water availability and degradation of the coastal dune systems.

Diego Sebastián Fernández and María Elena Puchulu presented a detailed study about available, quantitative technologies to predict landsliding hazards in north-western Argentina. Abrupt slopes, lack of vegetation, and frequent seismic activity

favor recurrent landsliding. Different landslide susceptibility models are presented and their performance was evaluated using statistical techniques. Comprehensive and profound sensitivity analysis of the models was performed in order to evaluate how the errors associated with input factors affect model results.

The landscapes of southernmost Patagonia, north of the Magellan Straits, have been studied by Elizabeth Mazzoni to investigate their characteristics from a scenic point of view and their possibilities as touristic resources. The immensity and emptiness of the Santa Cruz province tablelands is in strong contrast with the coastal and mountain landscapes. Individual landforms and extended landscapes are discussed in terms of slope, vegetation cover, resident and migrant fauna, acting geomorphological processes, and age and cultural resources.

Karina Echevarría and colleagues have investigated the flash flood hazard in the Sierras Pampeanas of the province of Córdoba, studying piedmont basins which lack appropriate water and sediment discharge data. The importance of this study is linked to the nature of these mountain ranges, some of them being the most populated mountain environments in Argentina. These ranges are characterized by impervious bedrock, steep slopes, poor soils, sparsely vegetated basins, and strong, seasonally concentrated rainfall, which are visited by millions of tourists all year around, but mostly during summer holidays.

The nature and dynamics of deflation hollows or pans and saline, shallow lakes in northern Tierra del Fuego are discussed by María Laura Villarreal and Andrea Coronato, who have analyzed the geomorphological and morphometric characteristics of these landscapes under temperate/cold and very dry climate. The shape, size, perimeter, and density of the studied pans are examined, as well as the landforms developed in their periphery. The dry steppes of northern Tierra del Fuego are the home of the “roaring fifties”, very fast and strong winds which are the dominant geomorphological agents in the region; this paper evaluates their powerful influence on landform development.

The study of epibiosis on brachiopods along a large extent of the Patagonian coasts has been conducted by Gisela Morán and colleagues. Epibiosis is the association between two or more living organisms belonging to the same or different species as a result of surface limitation. This property is of high interest in paleoecological studies of both recent and fossil organisms. Though Quaternary brachiopods are rare, they provide an ideal biogenic substrate for studying paleoecological questions relating to encrusting biotas. The absence of encrusting biotas on the Holocene shells of this study is attributed to the fact that many of these individuals are younger age and of smaller size.

The Quaternary of the Laguna de los Pozuelos basin, located in the Puna, the region including the high Andean plains of northern Argentina, was investigated by María Camacho and Julio J. Kulemeyer. This district is located at very high elevation close to the Argentina–Bolivia border. Puna is a unique environment of the Central Andes, with complex and varied sedimentary and stratigraphic features. This is a large “altiplano”, a high altitude tableland characteristic of the Central Andes. The depression occupies a morphostructurally low area, bearing extensive shallow salt lake systems. Climatic and tectonic adjustment at the end of the Last

Glaciation Maximum reduced them to ephemeral lakes that survived during the entire Quaternary.

Margarita Osterrieth and colleagues have investigated calcium biomineralizations associated with bioclastic deposits in coastal pedostratigraphic sequences of the southeastern Pampean plains. The biomineralization process is genetically controlled, and it is the result of the metabolic activity of different organisms, either microorganisms, plants, and animals. The Quaternary pedosedimentary sequences of the southeastern coast of Buenos Aires province evolved from bioclastic and loess sediments. These biomineralizations play an important role in the development of soils, and they are very good indicators of paleoclimatic and paleoenvironmental characteristics.

The future of Geomorphology and Quaternary studies in Argentina and South America is quite promising. Every year, more and more papers dealing with these disciplines are published, both in regional and in international journals. We do hope that the present book will be a benchmark in the progress of Geomorphology and Quaternary studies in this region and the appreciation of their advancement and evolution at the international scenario. From Puna to Tierra del Fuego, from the Andes piedmont to the Buenos Aires coastal environments, from flash floods to ephemeral lakes, this book was intended to show the assortment and complexity of Argentina climates and environments, and the state of our knowledge at the beginning of the twenty-first century.

Ushuaia, Tierra del Fuego, Argentina
July 2016

Jorge Rabassa

Contents

Landscapes Developed on Ignimbrites	1
Emilia Y. Aguilera, Irene Hernando and Jorge Rabassa	
When Science and Leisure Meet: A Geotourist Itinerary in Southern Tierra Del Fuego, Argentina	49
Soledad Schwarz and Piotr Migoń	
Soil–Geomorphology Relationships in the Pichiñán Uraniferous District, Central Region of Chubut Province, Argentina	77
Pablo J. Bouza, Claudia Saín, Lina Videla, Patricia Dell’Arciprete, Estela Cortés and Julio Rua	
Hydrological Variations Associated with Geomorphological Changes in a Sand Dune Barrier of the Partido de La Costa, Province of Buenos Aires	101
Silvina Carretero and Eduardo Kruse	
Uncertainty and Sensitivity Analysis of GIS-Based Landslide Susceptibility Models in Northwestern Argentina. Implications for Future Hazard Assessment at the Basin Scale	119
Diego Sebastián Fernández and María Elena Puchulu	
Landscapes of Southern Patagonia, Argentina, Their Scenic Characteristics and Their Importance for Geotourism	141
Elizabeth Mazzoni	
Flash Flood Hazard Assessment in an Ungauged Piedmont Basin in the Sierras Pampeanas Western Region, Province of Córdoba, Argentina	181
Karina V. Echevarria, Susana B. Degiovanni, Mónica T. Blarasin and M. Jimena Andreazzini	

Characteristics and Nature of Pans in the Semi-arid Temperate/Cold Steppe of Tierra del Fuego 203
María Laura Villarreal and Andrea Coronato

Epibiosis on Brachiopods from Patagonia, Argentina (40°–55°S): Composition, Spatial Variation, and Preservation 225
Gisela A. Morán, Sandra Gordillo and M. Sol Bayer

The Quaternary of the Laguna de los Pozuelos Basin, Northern Puna, Argentina 237
María Camacho and Julio J. Kulemeyer

Calcium Biomineralizations Associated with Bioclastic Deposits in Coastal Pedostratigraphic Sequences of the Southeastern Pampean Plain, Argentina 261
Margarita Osterrieth, Natalia Borrelli, Celia Frayssinet, Lucrecia Frayssinet and Juan Cresta

Index 287

Landscapes Developed on Ignimbrites

Emilia Y. Aguilera, Irene Hernando and Jorge Rabassa

Abstract This paper analyses the landforms and landscapes developed on ignimbrites outcropping in different regions of Argentina: Portezuelo (province of Mendoza), Lihuel Calel (province of La Pampa), Pilcaniyeu (province of Río Negro), Barda Colorada (province of Chubut) and Chon Aike (province of Santa Cruz). Some of these localities show clear resemblance to landforms which are typical of sedimentary rock landscapes, whereas others expose landforms typical of granitic rock landscapes. Systems of macro- and micro-landforms have been observed, such as inselbergs, bornhardts, nubbins, castle koppies, tors, crests and pinnacles, low cliffs, whale backs, and many other, associated minor features. Landforms of micro-modelling are shown at the base of vertical slopes, as cavities of the alveolar hollows and tafoni types, with subsequent evolution to caves, caverns and rock shelters. Besides, sometimes peculiar landforms such as yardangs, mushrooms and hoodoos are observed. The dominant agents that are responsible for these features are chemical and physical weathering and aeolian erosion. The micro-modelling affecting the different ignimbrite units is a direct consequence of their particular textural and structural conditions, on which a varied set of processes and erosion mechanisms have acted and defined their shape. In other cases, the orientation of the prevailing winds and the exposure of the ignimbrite flows have a decisive contribution to their genesis and ensuing development. It is herein concluded that the heterogeneity of these rocks, mostly due to changes in the welding degree, generates diverse types of macro- and micro-landforms.

E.Y. Aguilera (✉)

Facultad de Ciencias Naturales y Museo, Universidad Nacional
de La Plata, calle 60 y 122, 1900 La Plata, Argentina
e-mail: eaguilera@fcnym.unlp.edu.ar

I. Hernando

Centro de Investigaciones Geológicas, Universidad Nacional
de La Plata, CONICET, La Plata, Argentina

J. Rabassa

Laboratorio de Geomorfología y Cuaternario, CADIC-CONICET,
9410 Ushuaia, Argentina

© Springer International Publishing AG 2017

J. Rabassa (ed.), *Advances in Geomorphology and Quaternary Studies
in Argentina*, Springer Earth System Sciences,
DOI 10.1007/978-3-319-54371-0_1

Keywords Ignimbrites · Pyroclastic flows · Granitic landscape · Late Mesozoic · Neogene · Patagonia · Argentina

1 Introduction

The landforms and landscapes developed on ignimbrites have been described and studied in five different areas of Argentina, in the provinces of Mendoza (western Argentina) and La Pampa (central Argentina) and the provinces of Río Negro, Neuquén, Chubut and Santa Cruz, in Patagonia. The geomorphological criteria applied to the five study areas have taken into consideration the morphological types, geological structure, lithology and petrology in terms of fabric and texture, palaeoclimate and tectonic stability. The combined application of these concepts allows establishing the classification of the different environments in which they were formed and the dominant processes, as well as the landform types which have been generated.

From the lithological and petrologic point of view, the ignimbrite rocks are the product of explosive volcanic eruptions and their deposits are formed from pyroclastic flows. At a large scale, they may be considered as homogeneous bodies, but at more detailed scales, they exhibit significant heterogeneity which is a consequence of the depositional regimes within the pyroclastic flow. These rocks are composed of a matrix of glassy shards, crystalline clasts, lithoclasts and vitroclasts. Their emplacement at high temperatures is reflected in the degree of welding, designating as high-degree ignimbrites those which are densely welded and as low-grade ignimbrites those which are not so welded. Differential erosion is a characteristic of the different types of ignimbrites (Ollier 1988).

Concerning tectonic stability, planation surfaces are common in the landscapes developed in cratonic areas. Several erosion processes have acted upon them. The extensive and prolonged crustal stability of these cratonic massifs, in which the planation surfaces generated by deep chemical weathering are found, is the cause of the formation of very thick weathering mantles (or their remains), partially exposing the remnants of the weathering front.

It is very important to consider also palaeoclimates, because the climate changes that have taken place since the Mesozoic have produced important modifications in the landscapes that permit to recognize formation environments and acting processes.

Contrasting landscapes are distinguished in the studied outcrops, with landforms very similar to those described in the typical “granitic landscapes” (Aguilera et al. 2014), even those developed in sandstones (Bruthans et al. 2014).

Many of the micro-modelling landforms are developed in igneous and sedimentary rocks, commonly in sandstones, but rarely in conglomerates, gneisses and porphyritic rocks (Gutiérrez Elorza 2001). Of the five studied areas, three of them include very ancient, relict and partially exhumed landforms. Among the younger units, such as the Pilcaniyeu Ignimbrite (Middle to Late Miocene: Rabassa 1974,

1975, 1978a, b) and the “Tobas del Portezuelo” (Quaternary; Llambías 1966), similar landforms have also been described. In all cases, caves, taffoni and even yardangs have been carved over these ignimbrites.

The development of rocky arcs and natural bridges is conditioned by the combination of erosion processes, by “piping” or “tunnelling”. In the genesis of yardangs, the aeolian erosion acts by means of high velocity winds blowing in a constant, permanent direction.

Although many landforms have been explained starting from sub-superficial etching processes, once these landforms have been exhumed, the differential weathering and erosion rates would have continued acting along existing fractures and specific places of less resistance in the bedrock.

2 Materials and Methods

The methodology applied consisted of field work at both regional and detailed scales, with the support of satellite imagery and aerial photographs, and the petrographic studies of thin sections in the different outcrops.

Appropriate zones were selected for grain size, clastic components, distribution, lithology, welding degree and small-scale structures. Systematic identification of flow units was completed, including different welding facies and areal distribution of the ignimbrite components.

Likewise, landforms were recognized related to the fabric and jointing of the ignimbrites.

3 Location and Description of the Study Areas

The various studied areas are five, distributed in ample regions of western and southern Argentina (Fig. 1):

- (a) The Payunia volcanic district, between 36° – 37° S and $68^{\circ}30'$ – 70° W. The Portezuelo de los Payunes is located near the town of Malargüe, province of Mendoza, Argentina, where the yardang landscape developed over the Portezuelo Ignimbrite has been described.
- (b) The Sierra de Lihuel Calel, $38^{\circ}00'$ S, $65^{\circ}36'$ W, province of La Pampa, Argentina, occupies approximately 40 km² and stands as a giant inselberg above the surrounding planation surfaces, with a maximum elevation of 590 m a.s.l.
- (c) The volcanic–pyroclastic complex of the middle Río Chubut valley is located in the province of Chubut, Argentina, between the localities of Paso del Sapo and Piedra Parada ($69^{\circ}47'$ – $70^{\circ}32'$ W and $42^{\circ}13'$ – $43^{\circ}00'$ S).
- (d) The Deseado Massif, north-eastern Santa Cruz Province, Argentina, is a morphostructural unit where the pyroclastic–volcanic complex of the Bahía Laura Group is located. This group is composed of the Chon Aike and La Matilde

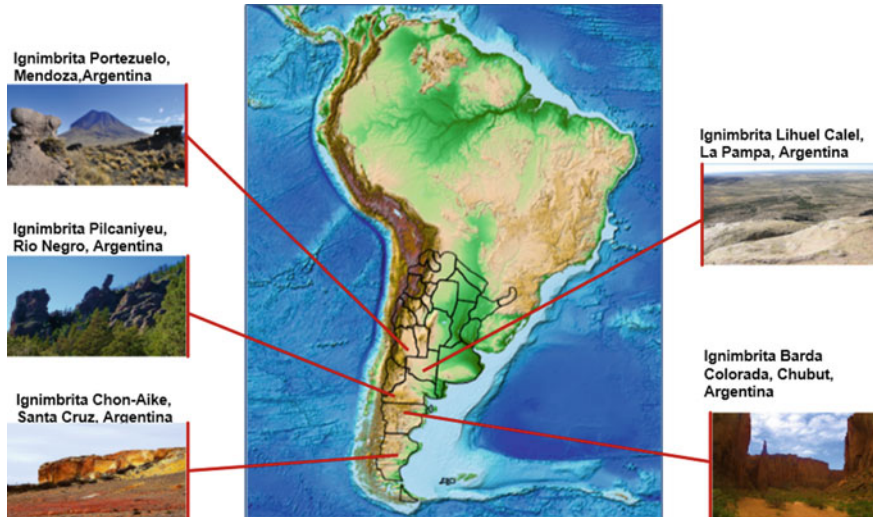


Fig. 1 Location map

formations, both merging laterally. These units are widely distributed in the Massif, and most of the observations were made in its central and eastern portions.

- (e) In western Río Negro Province, Argentina, the region between the Río Pichileufu and the town of Comallo, at the western edge of the Northern Patagonian Massif, where the Pilcaniyeu Ignimbrite has been studied.

3.1 *The Portezuelo Ignimbrite*

The Payunia volcanic district is a volcanic region covering more than 25,000 km², located in the province of Mendoza, Argentina, at the foot of the Andean ranges. The building up of the Payún Matrú volcanic complex was initiated in the Early Pleistocene. The evolution of these volcanic vents extends up to the Pleistocene–Holocene boundary, with pyroclastic flow deposits and trachyte layers interbedded with basaltic lava flows. Since the Pleistocene until Holocene, pre-historic times, the region has been a subject of extensional events, generating enormous volumes of volcanic products which are located in a retro-arc position with respect to the presently active arc (Bermúdez and Delpino 1989).

The landscape is characterized by volcanic landforms of huge dimensions, such as the El Nevado, Payún Matrú, Payún Liso and Chachahuen volcanoes, which are composed of alternating explosive and lava flow eruptions. Small and numerous volcanic cones, lava flows with a great diversity of landforms, cinder flows, volcanic bomb fields and pumice rocks are identified. In the Payunia volcanic district,

the El Nevado, Payún Matrú and Payún Liso volcanoes have generated explosive eruptions with a scale of super-eruptions (Llambías 2009). The Payún Matrú volcano is a composed shield volcano with an 8-km-diameter caldera at its summit. The ignimbrites related with the caldera formation cover a surface of approximately 4000 km², whose mantles have variable thicknesses related to the topography that has been buried, and they may be followed up to 30 km away from the eruptive vent. These ignimbrites have been given different names such as “Tobas de explosión” (Groeber 1937), “Tobas del Portezuelo” (Llambías 1966), El Portezuelo Formation (González Díaz 1972) and Portezuelo Ignimbrite (Hernando 2012). The name corresponds to the extensive outcrops found at Portezuelo de los Payunes, that is, the area between the Payún Matrú and the Payún Liso volcanoes. These pyroclastic deposits are related with the formation of the Payún Matrú caldera (Groeber 1937; Llambías 1966). Hernando (2012) obtained radiometric dates on pre- and post-caldera lavas, pointing out that the explosive eruption took place in the Late Pleistocene, between 148 and 82 ka. He also noted the impossibility of dating the Portezuelo Ignimbrite.

The ignimbrite mantles are deposits formed from pyroclastic flows, which at a large scale are considered as homogeneous bodies. However, at detailed scale, these rocks present a certain heterogeneity, as a consequence of different depositional regimes within the same pyroclastic flow.

The Portezuelo Ignimbrite is in general described as poorly welded, although it presents local variations in the welding degree, which depict a behaviour ranging from coherent rocks to mostly friable sediments, in different sectors. Hernando (2012), due to the frequent lateral and vertical changes detected, performed a differentiation of a facies series in this ignimbrite formation. In the study area, only two of these facies have been recognized.

3.1.1 Lithological Description of the Studied Section at the Portezuelo

At the lower portion of the section, a massive ignimbrite is found, with pinkish and reddish colours, pumice fragments without a substantial compaction, with crystals of feldspars, biotite, clinopyroxene and olivine and angular lithic fragments of a variety of volcanic rocks, though those of trachytic–trachyandesitic types are dominant. These trachytic facies are the most common, occupy a larger surface and integrate most of the section. In the upper portion of the profile, a massive, pinkish-reddish ignimbrite is found, highly rich in matrix, with scarce pumice fragments of up to 2 mm long. It also includes crystals of feldspars, biotite, clinopyroxene and olivine, and rare volcanic lithoclasts of 1–2 mm in diameter.

3.1.2 Yardangs

Yardangs are elongated, keel-like mounds, showing grooves and unstable sides. Their shape resembles an inverted boat, although some yardangs have instead a flat

top. These features may occur in a wide variety of lithological types (Goudie 1989, 2004). The outcrops of the Portezuelo Ignimbrite are eroded by the wind, forming yardangs of a depth of 3–6 m. In these sections, these two facies may be observed, in a neat, straight contact. These landforms were described by Llambías (1966) and Inbar and Risso (2001).

At a regional level, morphology of sand-covered crests and corridors or depressions is distinguished. In some areas, the amount of accumulated sand is so large that it gradually buried the yardangs. As it may be observed in the satellite imagery, they are thin, elongated landforms, of great areal extension which integrate large yardang fields, where the landforms occur aligned due to the dominant wind abrasion (Fig. 2a–c).

At the Portezuelo de los Payunes, the area comprised between the Payún Matrú and the Payún Liso volcanoes, the appropriate topographic conditions are met to produce the channelization of the strong, dominant winds, with a prevailing WNW-ESE direction. The intensive wind action, loaded with sand particles, impacts upon the ignimbrite sheets, deeply modelling them (Fig. 3). Their size varies between 30 and 120 m in length, and they are up to 2–6 m tall.

Yardangs are carved as elongated grooves, separated by vertical walls. In the upper part, the roof is slightly expanded as rock shelters. In addition to the observation of the neat contact between the two recognized facies of the Portezuelo Ignimbrite, the abrasion power of the wind is noted in the lower facies up to an elevation of 1.80–4.0 m, where the exposed surface has frequent rills, channels, tafoni and micro-yardangs. Contrarily, the upper portion occurs as a massive and polished surface (Fig. 4). This unit is dissected by vertical joints, which are related to the cooling conditions of the individual pyroclastic flows.

Some yardangs expose a flat top, and the groovy channel previously described is modified by strangling and thinning in certain levels of the profile, thus acquiring a more rounded morphology with tendency to mushroom shapes (Fig. 5).

The differential response of the two facies of the Portezuelo Ignimbrite to aeolian erosion may be due to the relative abundance of pumice fragments and sub-angular lithoclasts in the lower section, which is more profoundly affected by erosion. These fragments do not show intense compaction. These components are easily degraded out of the friable and scarce matrix, leaving hollows which are expanded by abrasion and deflation, thus favouring the mobilization of the eroded clasts and their subsequent removal. The upper portion of the unit is more resistant to wind erosion. This part is differentiated from the lower section because it has a greater proportion of matrix and a lower content of pumice fragments and lithoclasts, which are smaller and rarer, characteristics that confer it a much higher toughness. As most of the particles are deflated up to a certain elevation above the soil surface, the more intense erosion action takes place at the basal portion of the flow, thus originating thinner landforms at the base and more exposed ones in the upper zone.

Aeolian erosion is favoured by the scarce vegetation cover and the general aridity of the zone. Although precipitation is not frequent, they may be very intense in time and of a torrential nature, providing great erosion capacity to running

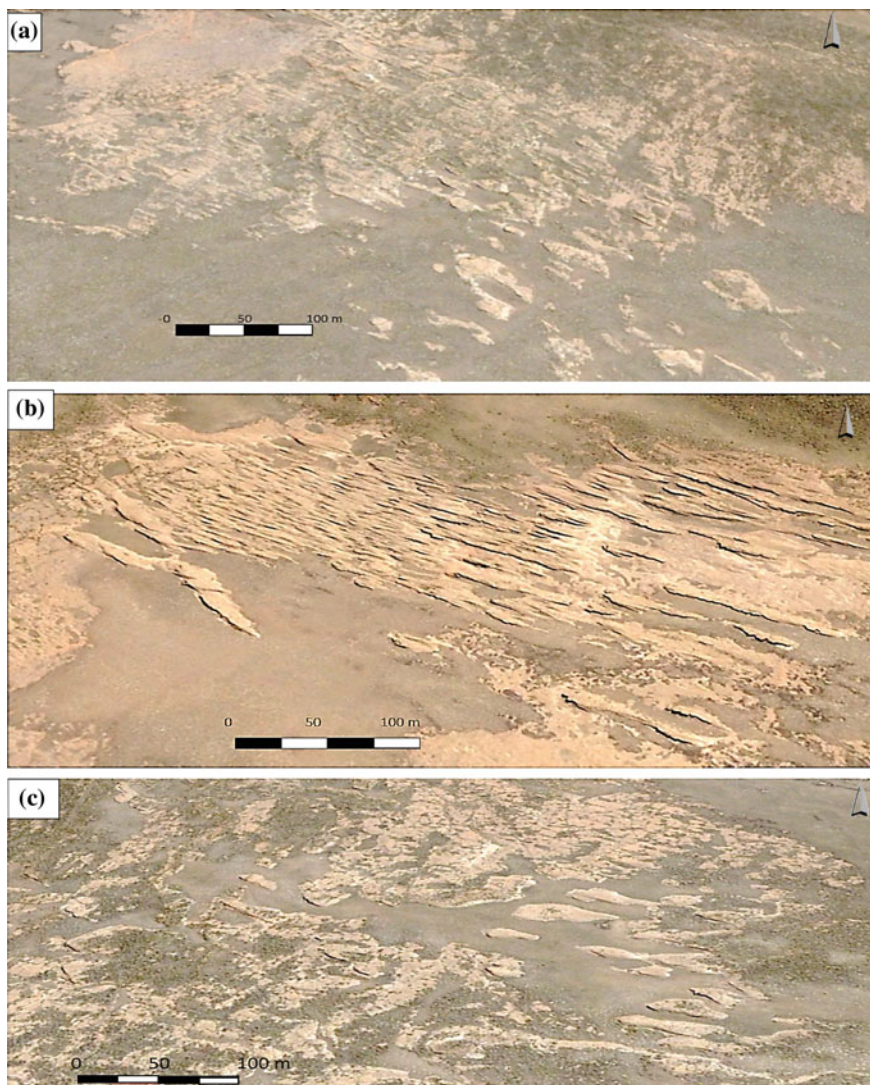


Fig. 2 Views at a regional scale of the yardang field at Portezuelo de los Payunes, province of Mendoza. Google Earth image. **a** Sand-covered crest and corridor morphology is observed. **b** Note the prevailing orientation of the landforms as WNW-ESE. The projected shadows suggest a positive relief. **c** Sand deposits gradually cover the yardang field

waters. The joints cutting the yardangs produce water migration with the development of rills and small channels in those surfaces which lack vegetation.

Another intervening process, though of lesser proportions and totally subordinated to aeolian action, is the physical weathering, which may be exposed as a

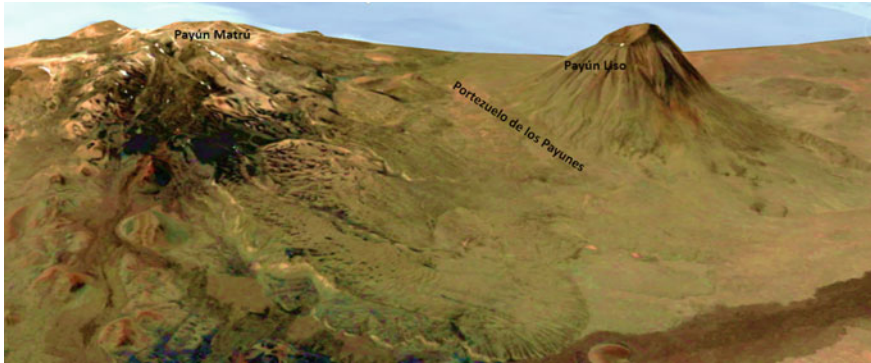


Fig. 3 3D view of the Portezuelo de los Payunes. The yardang field extends at the pass in between both volcanoes



Fig. 4 Yardangs carved as elongated channels, bounded by vertical walls. Micro-yardangs have developed along the lateral wall. At the background, one person for scale. At the foreground, a fracture with snow and ice

cryoclastic product and may be observed as wedges in which freezing water exerts powerful pressure.

It is possible that the natural wind tunnel generated at Portezuelo de los Payunes facilitates and magnifies the debris-loaded, wind erosion activity. Wind produces corrosion or abrasion on the ignimbrite surfaces, as they are permanently hammered by the coarser particles (normally, middle to coarse sands) which the wind transports, grabbing the angular clasts and excavating the surface, generating bowls, furrows and grooves, which are progressively enlarged by the constant, endless erosion of wind action (Fig. 6).

Generally, the coarser particles move by saltation between 0.45 and 1.00 m above the soil surface. However, favoured by the local topography at Portezuelo de los Payunes, the maximum elevation of the trajectory of the particles would have



Fig. 5 Flat topped yardangs near the Volcán Payén Liso. A strangled level that reflects a faster erosion rate



Fig. 6 Portezuelo de los Payunes: at the foreground, aligned yardangs are observed, following the prevailing wind direction

necessarily been of at least 2 m and even more. That is, the aeolian flux would have been greater than usual, as suggested by the yardang dimensions (Figs. 7, 8, 9 and 10). Additionally, as the wind velocity increased and generated ascending turbulence, exfoliation and particle releasing from the base of the landforms upwards, these landforms show evidence of progressive dismantling. Towards the roof of the landforms, a flux of finer materials (silt and clays) would have acted, thus producing polished surfaces, although in this portion the ignimbrite is more agglutinated and coherent, lacking large sized pumice fragments and lithoclasts which could be extracted by abrasion. It is undisputable that velocity and turbulence of the aeolian agent was more intense at the base than in the roof, but heavier particles would have acted at lower elevations because the wind was unable to rise them further up, and they were transported close to the ground by rolling. In this way, additional



Fig. 7 Fault topped yardangs with rock shelters limited by fractures



Fig. 8 Yardangs of large dimensions and varying height; a person for scale

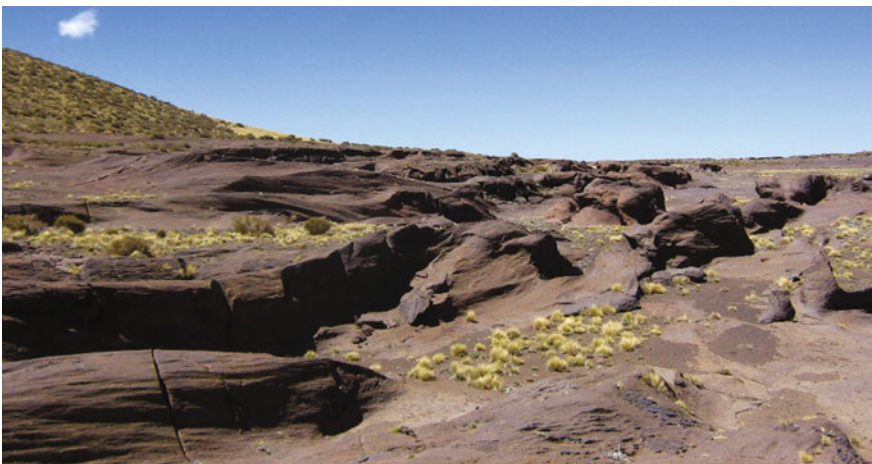


Fig. 9 Keel roofed yardangs, transversally cut by fractures



Fig. 10 Panoramic view of the yardang field at the base of the Volcán Payén Liso

erosional effects were generated due to impacts between clasts and the interaction of wind-blown particles driven by saltation.

Based upon the radiometric dating of the Payún Matrú eruptions, it is assumed that this landscape has a post-Late Pleistocene age. Concerning the concept of landscape genesis and evolution, the resulting landforms reveal that the dominant modelling process has been aeolian erosion, indicating that these are simple landscapes. From a morphoclimatic point of view, no relevant climate oscillations have taken place since their formation. Due to the fact that these landforms have been modelled by a unique morphogenetic system, this is a monogenetic landscape.

3.2 The Barda Colorada Ignimbrite

The volcanic–pyroclastic complex of the middle valley of the Río Chubut (province of Chubut; Aragón and Mazzoni 1997) developed over igneous and metamorphic rocks ranging in age from the Proterozoic to the Late Palaeozoic and volcanic and sedimentary rocks emplaced between the Jurassic and the Early Tertiary (Maastrichtian–Danian). Their more important deposits correspond to ignimbrite and lava flows, domes and smaller sub-volcanic intrusive bodies, ash falls and reworked pyroclastic rocks, which are related to igneous activity of a great caldera of about 25 km in diameter and two stratovolcanoes of lesser size, located on the northern and southern flanks of the caldera. The magmatic activity, essentially of acidic composition, was developed between the Palaeocene and the Middle Eocene (Aragón and Mazzoni 1997).

The deposits of pyroclastic flows erupted from the outburst of the Piedra Parada Caldera, in the middle valley of the Río Chubut, are distributed in an area of

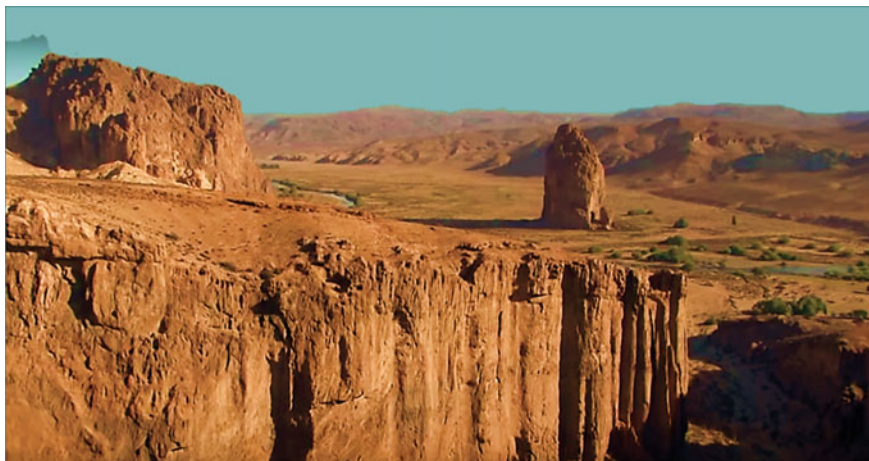


Fig. 11 Volcanic landscape in the Piedra Parada region, province of Chubut. At the foreground, the ignimbrite plateau; at the background, the Río Chubut and the Piedra Parada inselberg within the valley of such name

200 km³ and comprise an extensive plateau of rhyolitic ignimbrites recognized as the Barda Colorada Ignimbrite Formation—BCIF—(Aragón and Mazzoni 1997; Fig. 11). Mazzoni et al. (1989) recognized in the BCIF two varieties which were informally named as Lower Member and Upper Member. The Lower Member of the BCIF is of light yellowish, tuffaceous nature, with abundant lithoclasts and rounded pumice pebbles, whose size reach up to 10 cm in diameter. This unit is slightly welded, and both pumice fragments and lithoclasts are easily separated from the tuff mass. In some areas, the unit exceeds 80 m in thickness. The Upper Member of the BCIF has yellowish to brownish colour, dark “fiammes” and blackish vitrophyric colour. The more important feature of this unit is the abundance of lithoclasts and the high degree of welding.

In most cases, the exposures of the Lower Member of the BCIF are discontinuous and incomplete, due to their highly friable character, whereas the Upper Member of the formation forms structural terraces, among other features, due to its higher resistance to erosion. These deposits are characterized by different degrees of welding, from welded to highly welded, with abundance of pumice fragments and lithoclasts.

Due to the marked differences pointed out for both members, it should be noted that each member presents particular heterogeneity concerning fabric and structures. This anisotropy plays an important role concerning the erosion processes involved and the relief modelling. The fabric of the ignimbrites, with more welded zones in contact with other lesser welded ones, levels with abundant pumice fragments and lithoclasts, contacts between different cooling units, interbedded conglomerate layers, etc., and the structural characteristics, such as joints, fractures

and pseudo-stratification planar surfaces, set conditions for their massive behaviour against the morphogenetic agent action.

3.2.1 Landforms

At the regional level, the ignimbrite flows buried the previous landscape, levelled the topography, and the pre-existing fluvial valleys were fully drowned by the pyroclastic deposits (Figs. 12 and 13). Once the ignimbrite plateau was formed, new drainage networks developed, with channels which were partially different compared to the pre-existing ones. One of the more relevant effects of the coalescent pyroclastic flows forming the plateau was the change in the hydrological conditions of this region.

In general, the BCIF is situated at high elevations, around 1000 m a.s.l. Field observations performed in several localities of the plateau show that the Upper Member of the Barda Colorada Formation has columnar jointing. In these vertical cliffs, the processes of physical weathering are quite active. Weakness surfaces are developed in preferential directions, marked by the jointing. When the fractures are widened, the cliffs are affected by breaking up processes that produce collapsing and dislodging of hexagonal columns (Fig. 14) leaving new fronts with walls very close to vertical positions. Through this process, an important reduction in the relief starts, due to erosion and gravitational slumping. These erosion processes have developed an irregular landscape, dissected by deep, narrow and elongated gullies, with predominant straight channels, such as the La Buitrera, El Loro and La Horqueta canyons.

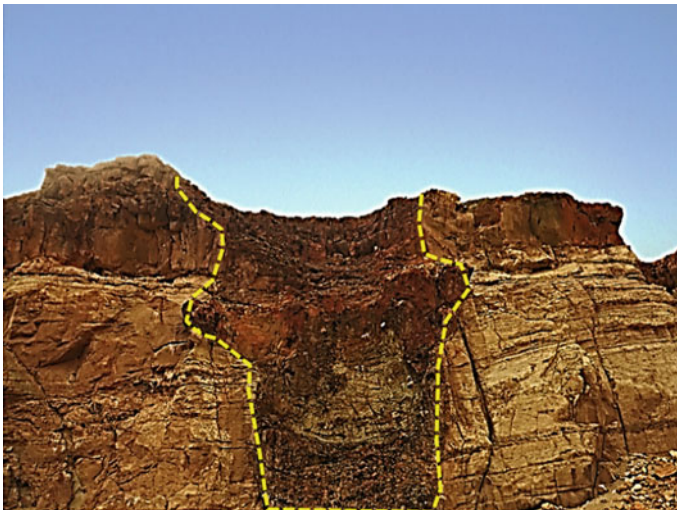


Fig. 12 Ignimbrite in-filling a fluvial valley, depicted in *yellow*



Fig. 13 Ignimbrite deposit burying a Cretaceous landscape

3.2.2 Arches, Rock Bridges, Tunnels and Corridors

Thick layers of welded ignimbrites are overlying lesser welded beds, being the latter eroded faster. This anisotropy contributes to make unstable the structure and the hard rock layers preserve their continuity, whereas the more friable strata are more easily eroded and mobilized by running water generated by high energy, intermittent rain storms.

In the rock wall fronts, at more vulnerable points, depressions generate which become deeper, forming hollows, bowls, caves, caverns and tunnels, sided by columnar structures, from which other galleries depart (Fig. 14). Due to the fracture network and in the interception of surface planes of different cooling units and cracks, water penetrates to sub-superficial levels, eroding and excavating the ground, generating tunnels and corridors, producing slumping and developing rock cliffs. The channelization of sporadic water currents at the base of the tunnels and corridors contributes to their deepening, weathering the rocks and transporting the altered and loosened materials (Fig. 15).

Concerning its morphogenesis, this landform could be explained by the process of “tunnelling” or “piping”, due to the development of a selective, sub-superficial drainage in friable materials such as these volcanoclastic rocks, whose components are mobilized in suspension with the hydrological flow.

Although the ignimbrites of the Upper Member are highly welded and tenacious, they are cut by plentiful cracks and fractures. These fractures represent weakness zones which are occupied by rainwater or even snow and ice. This structural feature affects its behaviour related to the action of the same morphogenetic process, where the nature and position of these materials play an important role in their modelling.

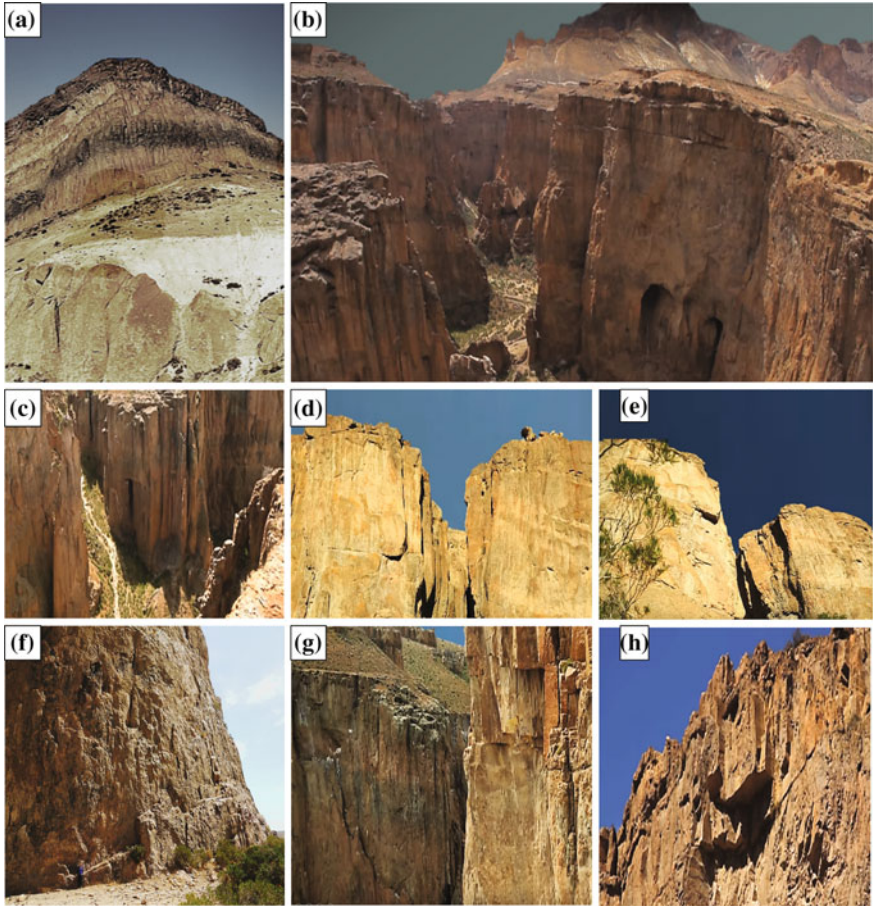


Fig. 14 Different views of columnar and pseudo-columnar structures in the Upper Member of the Barda Colorada Ignimbrite, with erosional features in vertical walls. **a** Hexagonal jointing in the upper part and the tuff-like, friable, Lower Member at the base. **b** Columnar fracturing, slumping and sliding that started at the roof. **c** Talus whose angles are close to a vertical position. **d** and **e** Massive aspect zone, with horizontal fractures that bound blocks. **f** Massive aspect zone with horizontal and oblique jointing; a person for scale. **g** and **h** Orthogonal fractures that favour the weathering processes

Another primary features in the structure of the ignimbrites are the pipes or degasification tubes which are the product of escaping gas during cooling. They represent a discontinuity in the outcrop whose dimensions make progress due to differential erosion, favouring tunnelling and piping processes.

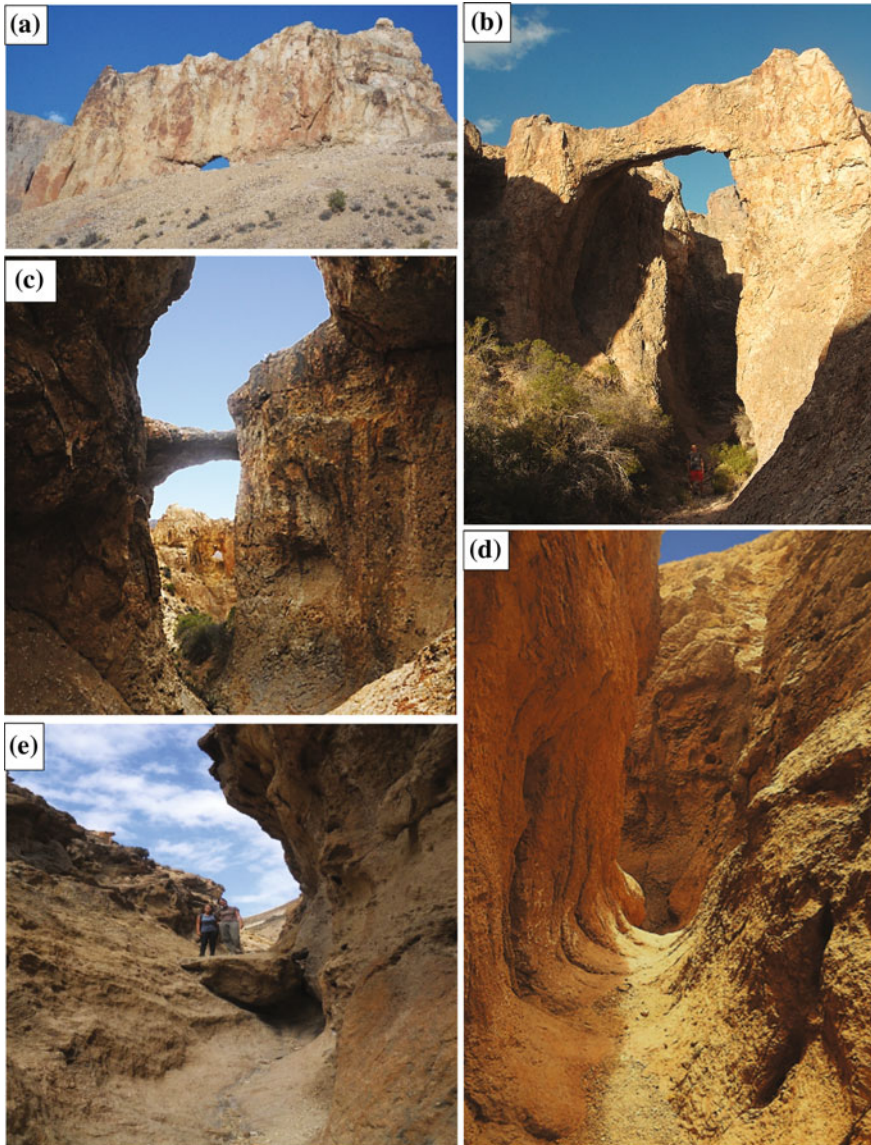


Fig. 15 Arches, rock bridges, tunnels and corridors. **a** Rocky front with generation of caves. **b** Rock arch flanked by columnar structures known as “pillars”. **c** Evolution of a rocky front into hollows, chambers and galleries flanked by columnar structures, from which subsequent galleries start. **d** Corridors generated by erosion and bedrock carving. **e** Tunnel with channelization of ephemeral streams in down-cutting processes, abraded and altered materials

3.2.3 Demoiselles and Badlands

In certain sectors, erosion landforms of slightly conical shape known as “demoiselles” are found, in which the tallness is clearly dominant with respect to the width (Fig. 16). These are elongated landforms with vertical flanks and, seldom, a more resistant level at the top befalls, perhaps due to stronger welding that resembles a hat (“demoiselles coiffées”; Godefroy 1940) (Fig. 17). These landforms are usually not isolated but forming groups instead. An orthogonal jointing is typically developed. These joint sets facilitate the erosional incision due to the channelling of the rainwater with the development of very steep slopes. These landforms may be observed at Cañadón de la Buitrera, in levels of the Upper Member of the BCIF. An important factor in the erosion process is that even though the environment has semiarid characteristics, the scarce rain events may reach prodigious intensity.

At the Lower Member of the BCIF, slopes with dissection modelling at the metric scale may be observed, in the shape of gorges, gullies and rills. By means of sub-superficial erosion, ravine-concentrated rainwater excavates the surface and drags materials developing a “badland” landscape, with tunnelling and piping as dominant processes. A very friable ignimbrite, with abundant clayey materials due to weathering of the primary minerals (basically feldspars and volcanic glass



Fig. 16 “Demoiselles”: erosion landforms of a roughly defined cone shape morphology, where the height is significantly prevailing with respect to the width. The contact between cooling units is depicted by tafoni and caves



Fig. 17 At the foreground, slender forms with vertical flanks. At the top, a more resistant level, resembling a hat, is observed (“demoiselles coiffées”)

shards), correlates with this landscape. These features may be observed at the sites of Cañadón del Loro and the Barda de los Perros.

3.2.4 Smaller Scale Features

These smaller size features are the product of a set of erosion processes that lead to the granular disintegration of the rocks. Such micro-modelling landforms are exposed in vertical walls, forming holes and hollows such as alveolar cavities and tafoni, later evolving to caves, caverns and rock shelters.

3.2.5 Alveolar Cavities, Tafoni, Caves, Caverns and Rock Shelters

These minor landforms are localized in vertical and sub-vertical joints associated with oblique orthogonal, joint networks. Coincidentally, in the areas with alveolar hollows, the rocks present a blackish to dark reddish colour, compatible with the presence of desert varnish generated by Fe and Mn precipitation.

Layers marked by pseudo-stratification seen in vertical walls exist, where sub-circular cavities with sizes between centimetres to metres in diameter dominate. It may be observed that these landforms are started in an isolated distribution, but they coalesce during growth and form larger size cavities. These cavities are located at the base of the vertical walls and along the pseudo-stratification layers, where textural and structural changes are found (Fig. 18). They may be due to

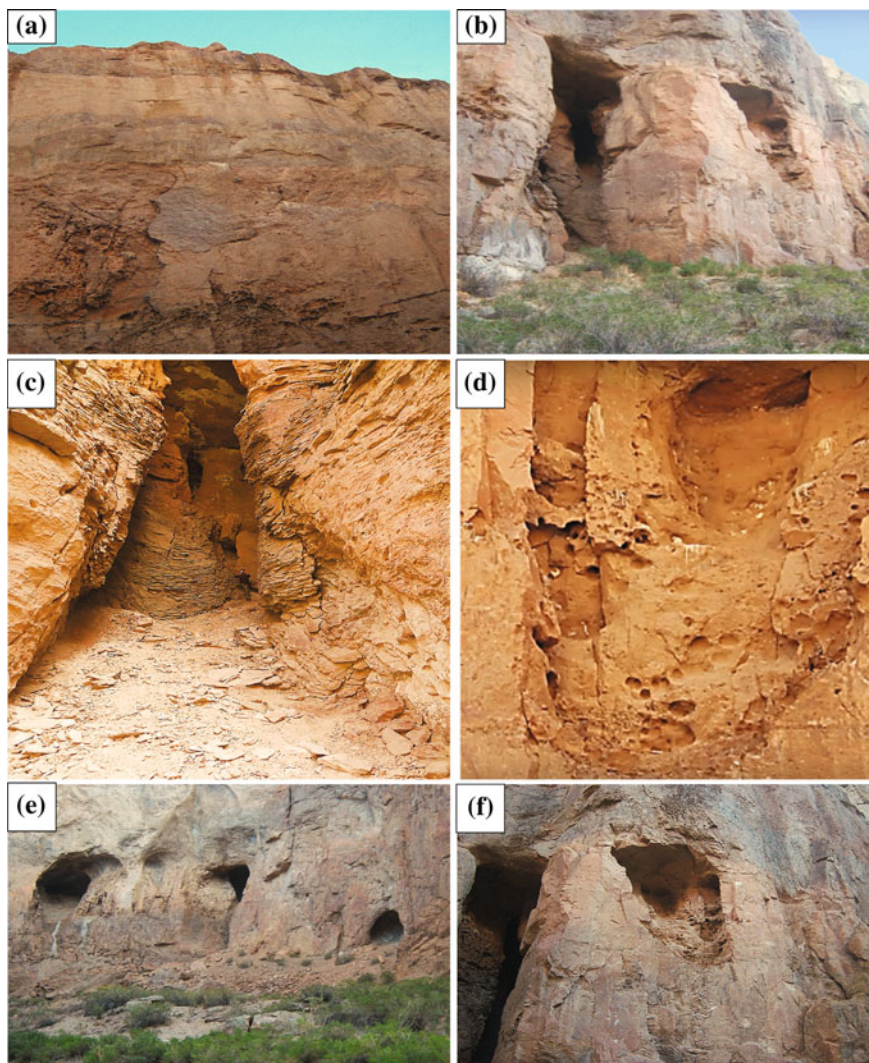


Fig. 18 Alveolar hollows, tafoni, caves, caverns and rock shelters. **a** Alveolar hollows and tafoni in vertical walls, associated with joints and descaling processes. **b** and **c** A cave developed from degassing tubes which make progress in size due to differential erosion. **d** Vertical rock wall with development of tafoni and tunnels. **e** and **f** Lenses of poorer welding degree, bearing tafoni and caves, are depicted

heterogeneous welding, levels of abundant pumice fragments and lithoclasts, convergence of joint planes or, simply, joint surfaces. These cavities evolve into caves at the Cañadón de la Buitrera, where cavern levels may be followed along discontinuity zones representing the contact between two pyroclastic flows.

3.2.6 Remarks

The igneous activity of this volcanic complex ended in the Middle Eocene, covering a Cretaceous planation surface. Since then, these units remained exposed and the modelling of these deposits started (Aguilera et al. 2010).

This morphogenetic processes, in which chemical weathering has had a dominant role compared to other external morphogenetic agents, would represent the first cycle of this landscape formation, favoured by contrasting climatic scenarios from temperate/warm, sub-humid seasonal climate. Starting in the Late Eocene, these scenarios were related to a warm/humid event towards the end of the Palaeocene and the beginning of the Eocene. Towards the end of the Eocene, the climatic conditions became temperate and dry, as a consequence of the global cooling that took place at the Eocene–Oligocene boundary. This cooler event culminated in the Late Oligocene with a warm/temperate, sub-humid seasonal climate (the Late Oligocene warming event), with permanent, meandering streams. Although during the Miocene a warm/humid event also occurs, related to the Middle Miocene climatic optimum, likewise indicating a global warming period.

The preponderance of warmer and wetter conditions favoured deep chemical weathering, with the development of weathering mantles that were later denuded and mobilized. Finally, the weathering front became exposed. Later on, during the Quaternary, another cycle under drier climate evolved, with episodic, fast run-off and aeolian action. The weathering front remained exposed to other morphogenetic agents, with the capacity of obtaining and transporting materials, thus contributing, directly or indirectly, to the creation and evolution of new landforms. Deflation became the dominant process, caused by the powerful, permanent winds, responsible for the detaching, flaking, uplifting and subsequent elimination of the finer sediments.

From the morphoclimatic point of view, this could be considered a polygenetic landscape, depicting features of different morphogenetic systems, each with its characteristics landforms.

3.3 *Sierra de Lihuel Calel*

The Sierra de Lihuel Calel, located at around 38°00'S and 65°36'W, covers approximately 40 km², and it rises as a giant inselberg from a surrounding planation surface, with maximum elevation at 590 m a.s.l. It is composed of a sequence of rhyolitic ignimbrites (Llambías 1975; Sruoga and Llambías 1992) which are part of an extensive rhyolitic plateau of Permian–Early Triassic age (Llambías and Leveratto 1975). The bedrock basement on which the ignimbrites are lying on is composed of igneous/metamorphic units of Late Proterozoic to Early Palaeozoic age (Linares et al. 1980; Tickyj et al. 1999; Sato et al. 2000).

The thickness of the Sierra de Lihuel Calel ignimbrites exceeds over 950 m, with no base or top identified. Beds are inclined towards the WNW, as part of a



Fig. 19 N-S view of the Sierra de Lihuel Calel, where beds with homocline dipping towards the WNW are shown

homocline structure, with values close to 25° in the basal levels and values closer to 15° in the coarse stratification noticed in the upper layers (Fig. 19). The sequence is composed of two cooling units, both of them of rhyolitic composition: the lowermost unit, 440 m thick, and the upper one, more than 450 m thick (Sruoga and Llambías 1992). The lower unit is composed of highly welded rhyolitic ignimbrites, partly vitrophyric or with spherulitic crystallization, with participation of volcanic breccias. The upper cooling unit is separated from the lowest one by a relatively thin cooling unit of 50 m in thickness, composed of a highly welded dacitic ignimbrite. Certain levels of the ignimbrites at Lihuel Calel were affected by marked recrystallization, being transformed in rocks of apparent porphyritic texture with micro-grained groundmass, due to the high proportion of gas components and to the slowness of the cooling during the welding of the glass shards (Llambías 1973). The age of the Lihuel Calel ignimbrites has been established by means of Rb-Sr isochrones in 238 ± 5 Ma (Linares et al. 1980) and 240 ± 2 (Rapela et al. 1996). After the intense volcanism of the Permian and Triassic periods, no more magmatic activity took place in the region and the accumulated ignimbrites were never buried again.

3.3.1 The Lihuel Calel Ignimbrite

The modelling of the more massive rocks of this unit exposes fractures by sheet development or by intersection of orthogonal joints. Both types of fractures are recognized in the Sierra de Lihuel Calel where the layering modelled the landscape basically in dome landforms. The best example is the Sierra de Lihuel Calel itself that rises from the surrounding plain as an enormous inselberg, that is, a large dimension dome. This “mega-inselberg” would be the product of the denudation of the weathering profiles, developed since the Triassic in humid, tropical climate

conditions, followed by the denudation of the weathered products in these profiles and the subsequent exhumation of an ancient etchplain.

The mega-inselberg of the Sierra de Lihuel Calel is recognized for several topographic steps, defined by the differential resistance to erosion of the ignimbrite flows. In the analysed levels, step-like slopes with landforms assigned to granitic landscapes are noted (Aguilera et al. 2014), as well as slopes resulting from the pseudo-stratification depicted by several ignimbrite layers. The Sierra de Lihuel Calel has a N-S orientation, and its outcrops show a WNW-ESE orientation, with gorges and rocky valleys similarly oriented.

A large plain develops surrounding the rock elevations, whose pediments are differentiated by a reduced areal extent compared to the regional plain. They are generally covered by regolith, thus receiving the name of “regolith pediments”. Towards the east, the regolith got to lower elevations, following the regional slope, and the landscape became monotonous. This is a planation surface or erosion surface, in the sense of Ollier (1991).

The types of inselbergs recognized here are denuded domes (bornhardts) and by evolution of some of them other residual landforms occur, such as “nubbins”, “castle koppies”, “boulders” and “tors” (Figs. 20, 21 and 22). These landforms and other smaller ones have a sub-superficial origin and are usually developed at the weathering front (Mabbutt 1961).



Fig. 20 Very degraded domes with orthogonal fractures and varied dissection degree, with stepped and convex slopes



Fig. 21 Dome landforms of the “whale back” type, with curved jointing and partially degraded to nubbins and a diversity of smaller forms

In the stratigraphic profile of the Sierra de Lihuel Calel, several units are recognized, such as rhyolitic flows, glassy layers and ignimbrite flows with varied degree of welding, which become zones more or less favourable for erosion. In addition to the lithological differences, it should be noted the important role that the joint systems play, acting as weakness planes. Following them, corridors of higher moisture content are excavated, where the weathering processes generate convex landforms, with down-wasting of sides and corners.

In the middle and upper sections of the lower cooling unit, these rocks have a similar behaviour to granitic rocks. These are massive rocks which do not preserve



Fig. 22 Curved jointing in dome shapes, associated with a vertical system with progressive development of nubbins of different scales and convex slopes

primary textures and, not without difficulties, the contacts between the different flow units may be identified. Structural and textural changes have modified the properties of the rocks, increasing their resistance to erosion, thus developing a sort of “granitic landscape”, as it can be seen in the Cerro de la Sociedad Científica. The same landscape develops in the upper cooling unit, in the Valle de las Pinturas, where rock art in caves and rock shelters are plentiful, with alveolar hollows and tafoni as secondary components.

Panoramic views of the mountain ranges show their convex slopes, highlighted by the dipping layers of the ignimbrite. Run-off takes place under surficial flow conditions, with the formation of rills and creeks following smaller topographic irregularities. The morphology of the slopes is conditioned by the spacing of the joint systems. In some sectors with large spacing, the landscape resolves in stepped

profiles (Fig. 20). Contrarily, when the jointing is closer, the morphology of the slopes is much more gentle.

Different sectors of the weathering front have been recognized in relation to the landforms present. The zone with a larger depth of the weathering front, the Valle de las Pinturas (Arroyo de las Sierras), is revealed with landforms that preserve the orthogonal jointing sets, with blocks in which it is still possible to identify corners, edges and sides. The orthogonal jointing bounds landforms of the castle koppies type (castle-like forms) (Fig. 22).

The uppermost levels, recognized in other sectors of the range, show landforms such as boulders, tors and nubbins, in the area of the Cerro de la Sociedad Científica. Landforms such as the whaleback type predominate, limited by horizontal fracturing of ample curvature radius, which is also depicted by the convexity of slopes and hills (Fig. 22). In this succession of layers of different resistance to erosion along the main slopes, a series of steps is seen, a product of differential erosion.

The landforms of the granitic landscape have been classified according to the criteria exposed by Twidale (1982), Vidal Romaní and Twidale (1998) and Migoñ (2006).

It is clear that the weathering and dismantling of the regolith has been incomplete. The landscape is characterized by flat sections interrupted by block accumulations, outcrops, nubbins and castle koppies. The regolith is preserved in the lowest areas, where residual nuclei outcrop (Fig. 23). In those sectors where the sierras preserve pseudo-stratification, due to the disposition in thick strata of

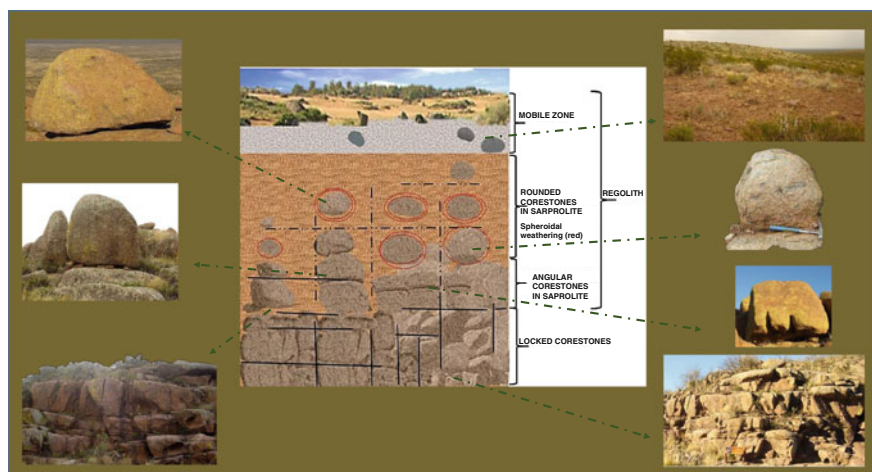


Fig. 23 Analogy between the granite landforms identified in the Lihuel Calel Ignimbrite with the typical weathering profile in granites, where the joint systems and the weathering processes generate this characteristic landscape (based upon ideas and a diagram by Ollier 1991).

the ignimbrite, and the spacing of the jointing is closer, the slopes are very gentle. Likewise, the homocline inclination of the flows generates such landforms as “mesas” or “cuestas”.

At a larger, detailed scale, the horizontal jointing is dominant with respect to the vertical one. The basal undercutting process is active where the running water erodes the slope and it weathers the bedrock, developing shelters, alveolar hollows, tafoni and gnammas. The alveolar hollows are rounded or ellipsoidal holes of centimetre size. They have developed in surfaces of medium to strong inclination (Fig. 24). Tafoni are hollows of larger size than the alveolar depressions, and they may get up to cave size. They may occur grouped with circular or elliptical geometry, and some of them with the bottom covered by debris. In some occasions, they occur oriented according to weakness planes of the ignimbrite mantles (usually, boundaries between flow units), and generally in vertical slopes (Fig. 25). The blocks or rounded boulders occur in tors, where the horizontal jointing is dominant. Blocks may preserve equilibrium position on a pedestal. On the slopes of Cerro de la Sociedad Científica, many boulders and blocks are found.

Gnammas are weathering closed depressions, which are developed on horizontal or semi-horizontal surfaces. Their size is in the order of metres. Their shapes are



Fig. 24 Alveolar hollows, reaching 50 cm in diameter. They have been developed in sheltered surfaces

Fig. 25 Tafoni somewhat larger than the alveolar hollows, oriented according to weakness planes in vertical walls of the ignimbrite sheets



circular and elliptical, and in some of them, a spillway channel may be observed or they may occur as forming sequences or chains of depressions (Fig. 26). In the landscape of the Sierra de Lihuel Calel, all types of gnammas have been recognized following the ordering provided by Twidale and Corbin (1963), who classified them according to their transversal section: gnammas in rock bottoms or pits, basin gnammas, and armchair-shaped gnammas. Descaling and scraping is generalized elsewhere, as granular disintegration and lichen colonization take place.

The study of Cerro Cortado shows that, in its slopes, the upper portion is slightly convex to flat, where highly welded ignimbrite beds form as bench that is receding due to different erosion processes. The materials that are removed from the crest are removed by hydrological erosion towards the debris slope, until they reach the pediment, which merges with the plain. The slopes depict a concave profile (Fig. 27). In these sectors, the rocks do not achieve the development of a “granitic landscape”.



Fig. 26 Gnammas: closed depressions in horizontal surfaces or gently inclined



Fig. 27 Cerro Cortado: primary structures of the ignimbrite flows, with the development of crests, cuetas and debris slopes, are shown. Concave slope merging the pediment with the plains

3.3.2 Remarks

Most of the landforms in this landscape suggest that they have been formed sub-superficially and they are recognized in the weathering front where they were generated. Thus, they correspond to corrosion and etching processes, in the sense of Wayland (1934) and Willis (1936). Due to deep weathering processes that started perhaps even during the Late Triassic, these landforms evolved in two periods, starting with the sub-superficially modelling of the weathering front and later dismantling of the regolith, thus exposing the fresh bedrock front. Mineral and textural transformations due to devitrification and/or assisted crystallization by vapour phase provide to the rock an even stronger cohesion, typical of a coherent igneous rock. This feature allows the explanation of the development process of the herein described landforms, otherwise typical of granite environments.

3.4 *The Chon Aike Ignimbrites*

3.4.1 **Geology of the Deseado Massif, Province of Santa Cruz, Argentina**

The oldest rocks in the Deseado Massif are of Neoproterozoic to Palaeozoic age. They are metamorphic rocks and are covered by Permian and Triassic sedimentary rocks. These ancient rocks occur only in very small and sparse outcrops. A significant volcanic episode took place in the Middle Jurassic, related to deep fractures in the crust, coeval with the efforts that preceded the fracturing and separation of Gondwana. These rocks are andesites, basalts and pyroclastic rocks, a product of fissure volcanic eruptions, included in Bajo Pobre Formation. Later on, during the Middle to Late Jurassic, another volcanic event occurred in the Massif, with the extrusion of volcanic and volcanoclastic rocks of the Bahía Laura Group, covering most of the Massif surface and building up an enormous, extensive plateau. This magmatic episode is related with the dismembering of the Gondwana continent, which produced the separation of South America and Africa and the opening of the South Atlantic Ocean. This volcanic event was mostly explosive, generating important volumes of pyroclastic flows, whose coalescence generated the large ignimbrite plateau. These ignimbrites and lava flows comprised by the Chon Aike Formation are associated with intense ash fall, with the subsequent tuff genesis (La Matilde Formation). During the Cretaceous and the Neogene, the Deseado Massif was a positive element of the regional landscape, and, along its margins, sedimentary rocks of continental environments were deposited, with the limited transgression of marine deposits of Atlantic provenance that accumulated from the Palaeocene to the Miocene.

3.4.2 Landforms and Landscapes

Bluffs, crests, needles, cliffs, nubbins, castle koppies and badlands

The ignimbrite sedimentary packages are the more irregular and discontinuous landscape of the Deseado Massif. Thick beds appear in the local relief, forming an extensive plateau with sub-vertical bluffs that exceed 20 m in height. They show abrupt crests and pinnacles marked with intensive vertical jointing that form prismatic columns (Fig. 28a).



Fig. 28 a Sub-vertical walls with vertical jointing that bounds prismatic columns. b Nubbins, dome landform later fractured and degraded. c and d Low and rounded hills. e Abrupt crests and needles, bound by jointing. f castle-like landforms: “castle koppie”

The dominant landforms in terms of their abundance are outcrops of small cliffs with heights between 4 and 8 m high. Low hills and rounded outcrops occur as well with different steps of outcrops, generally covered by their own regolith. Landforms of the nubbin (dome-like landforms) and castle koppies (castle wall like landforms) occur as well (Fig. 28b–d, f).

Weathering mantles

In depressed topographies, weathering mantles have been preserved, a by-product of the chemical disintegration of ignimbrites. These weathering mantles have thicknesses in the order of metres to tens of metres, where “corestones” may be observed, immersed in the regolith. The regolith is composed of multi-coloured clayey materials, with clayey packages of reddish, brownish and whitish colours. These levels are distributed in several sectors of the Massif. They basically differ in the preserved thicknesses, and they include outcrops in depressed areas, with badland morphology (Fig. 29). They occur generally in the same topographic level where more resistant, overlying layers protect them from erosion. They are overlain by Tertiary sedimentary rocks or glaciofluvial deposits.

The ignimbrite expositions have reddish colours, due to the oxidation of the iron-bearing minerals present in the original rocks, and also whitish, yellowish, light brownish and pinkish grey sediments. The ignimbrites exposed in the area have a variable degree of compaction and welding, from poorly welded to and very altered due to their high porosity, to those highly welded and massive.

Caves, caverns, tafoni and alveolar hollows

At a regional scale, the ignimbrite mantles integrate bluffs, abrupt crests and cliffs. These major structures present lesser features as caves, caverns and needles (Fig. 30). They are usually localized in levels with lesser degree of welding and compaction, or levels of a larger concentration of pumice fragments and/or lithoclasts which have been displaced from the pyroclastic matrix of the ignimbrite, due to erosion processes. In some cases, the alveolar hollows are very common and they occur so close to each other that they confer to the rock the aspect of a sponge (Fig. 31a). Textural and structural control is evident in terms of their development, genesis and later evolution, which becomes favoured by the existence of orthogonal joint networks. Another factor that contributes in this sense is that during the deposition and cooling of the pyroclastic flows, the escaping gases generate tubes and chambers (known as degasification tubes) that are afterwards enhanced by differential erosion.

Corridors, galleries and tunnels

Thick layers of welded ignimbrites overlie other lesser welded ignimbrites which become eroded by processes such as “tunnelling” and/or “piping” faster than the welded sections and the hard rock strata which contribute to the formation of corridors, galleries and tunnels (Fig. 31b, c).

The drainage network is of angular–rectangular pattern as a consequence of the structural control that the frequent joint and fracture systems exert. Water channels have an ephemeral character, and they are incised in vertical wall gorges. In interbedded locations with the Chon Aike ignimbrites, tuffs and water-lain tuffs of the La Matilde Formation are present, and when the water channels cross these



Fig. 29 Weathering mantles in badland landscape; the regolith is the product of “in situ” weathering of the ignimbrites and it shows *reddish, brownish, whitish* and *yellowish* colours

formations, alluvial plains traverse these formations developing alluvial plains and acquiring braided patterns.

Mushroom rocks/Hoodoos

In the direction of the valleys, slopes or depressed areas such as endorheic basins, different levels of degradation of the ignimbrite sheets may be observed. Relict landforms are identified due to their conspicuous morphological expression. Vertical jointing is noted, as it gradually dissected sections of irregular columns, in which corners and crests are present. These landforms are localized in the proximity of the ground, within the valley or depression. They continue to reduce their

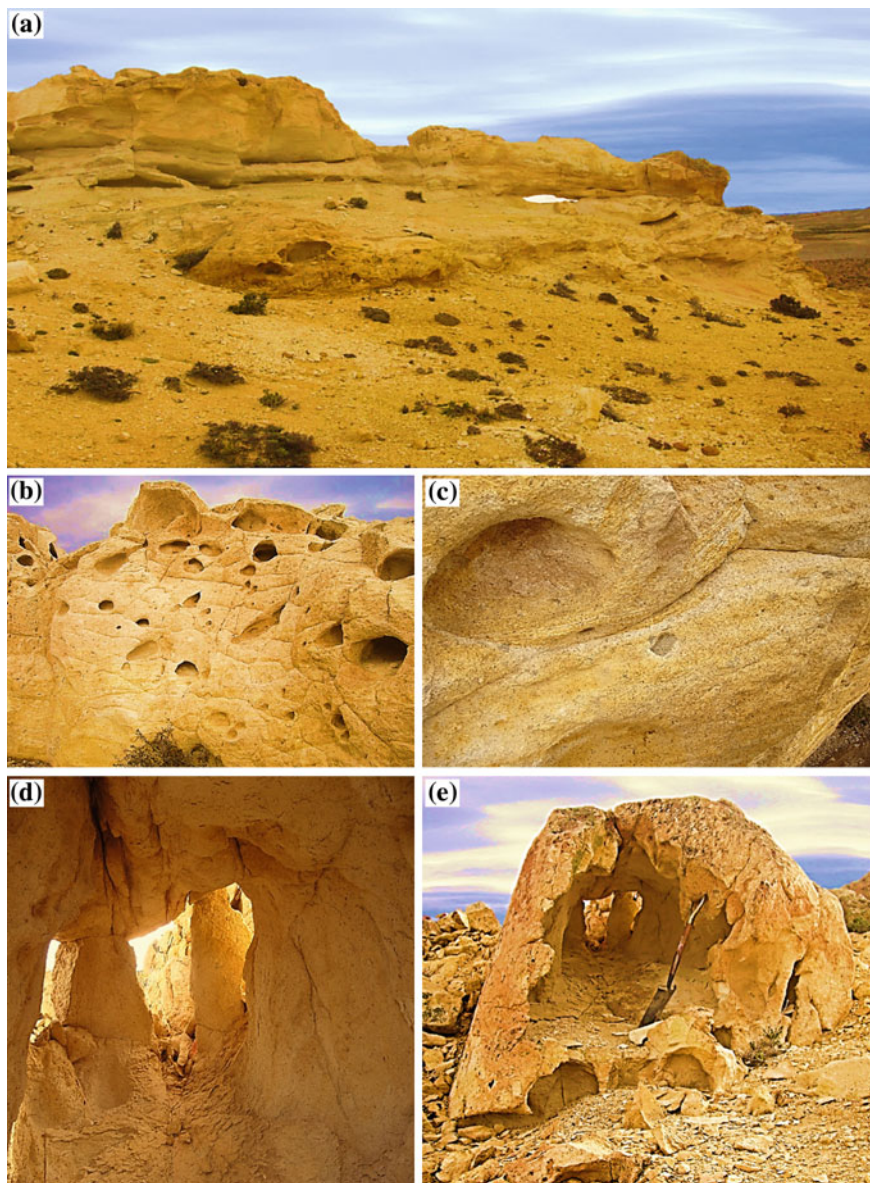


Fig. 30 Different degrees of tafoni formation. **a** Incipient arch, in formation. **b** Tafone with shelter at the *top*. **c** Detail of tafoni with Liesegang rings. **d** Grooves, pillars, cavities, arches and rock bridges. **e** Tafone with evolution towards cave or tunnel



Fig. 31 a Alveolar hollows of the honeybee type. b and c Corridors, galleries and tunnels favoured by the joint systems and the degassing tubes

volume and, due to differential erosion, they achieve the shape of a pedestal or a mushroom with bases smaller than the diameter of the upper portion above it.

In geomorphological literature, there are other terms that are used as equivalent to those cited here, such as mushroom rocks, pedestal rocks, chimney rocks, earth pillars, yardangs, demoiselles, and hoodoos, among others. In general, these names are applied according to specific geographical regions; for instance, in Utah (USA), the term “hoodoo” (Goudie 2004) is used to describe landforms of the chimney type, which in France they are known as “demoiselles”. These terms point out mostly anthropomorphic shapes than their true genesis. It is shown in several examples that the lower portion of the landform is smaller in diameter than the upper one, and it describes a concave profile. This aspect is related with slopes of the “flared slope” type. Some of these landforms may show more than one level of flared slopes. Another characteristic is that the concave slopes may present the genesis of tafoni. They rise over a platform of up to 4–5 m high and laterally

surrounded by flared slopes. The upper portion is varied in shape, since some of them have indurated porous surfaces, as a duricrust, exposing tafoni and other alveolar hollows resembling bee hives. In some occasions, the upper portion develops shelters or spiral forms (Figs. 32 and 33).

The surface of the ignimbrite is rugged and presents grains of quartz in micro-relief, with spots of clayey materials which are the product of weathering of

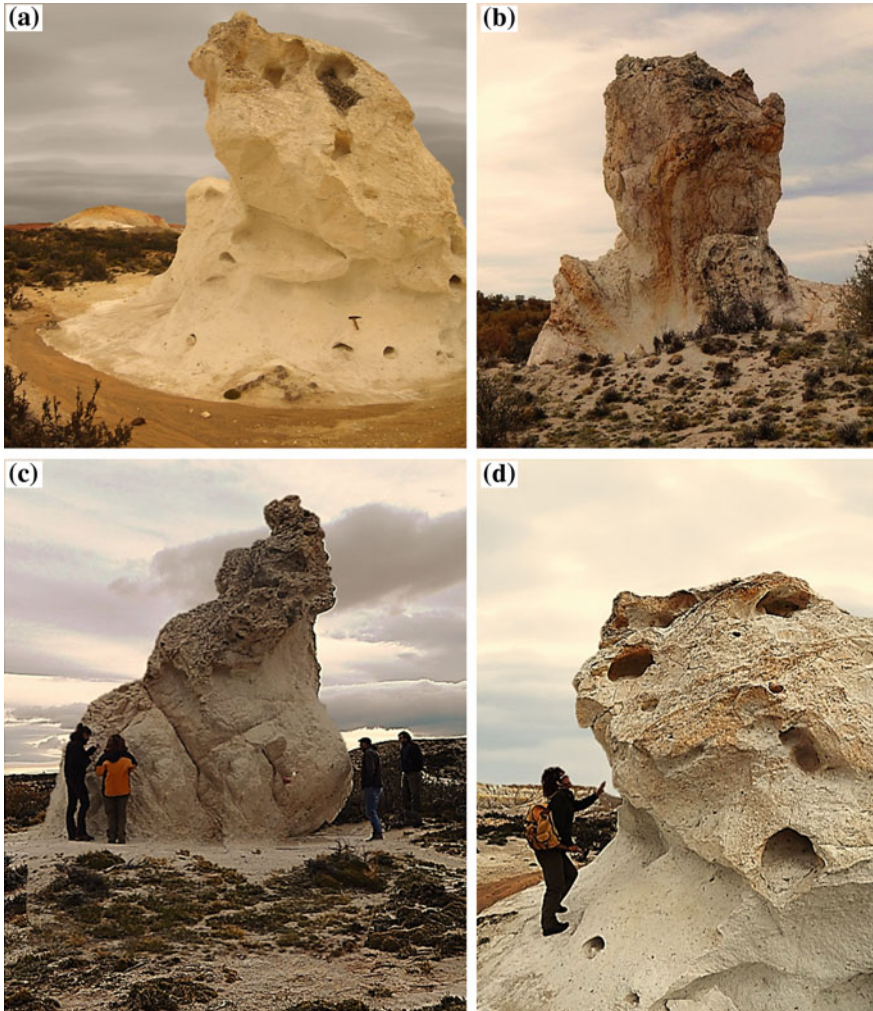


Fig. 32 Landforms in poorly welded ignimbrites. **a** Flared slopes in the periphery and tafoni formation from the base to the roof. A bird nest at the shelter. **b** Evolution to mushroom rocks with two levels of flared slopes. **c** Rounded landforms bound by fractures in the upper zone with alveolar hollows of the honeybee type. **d** Tafoni and carving in the middle zone, with a wide flared slope

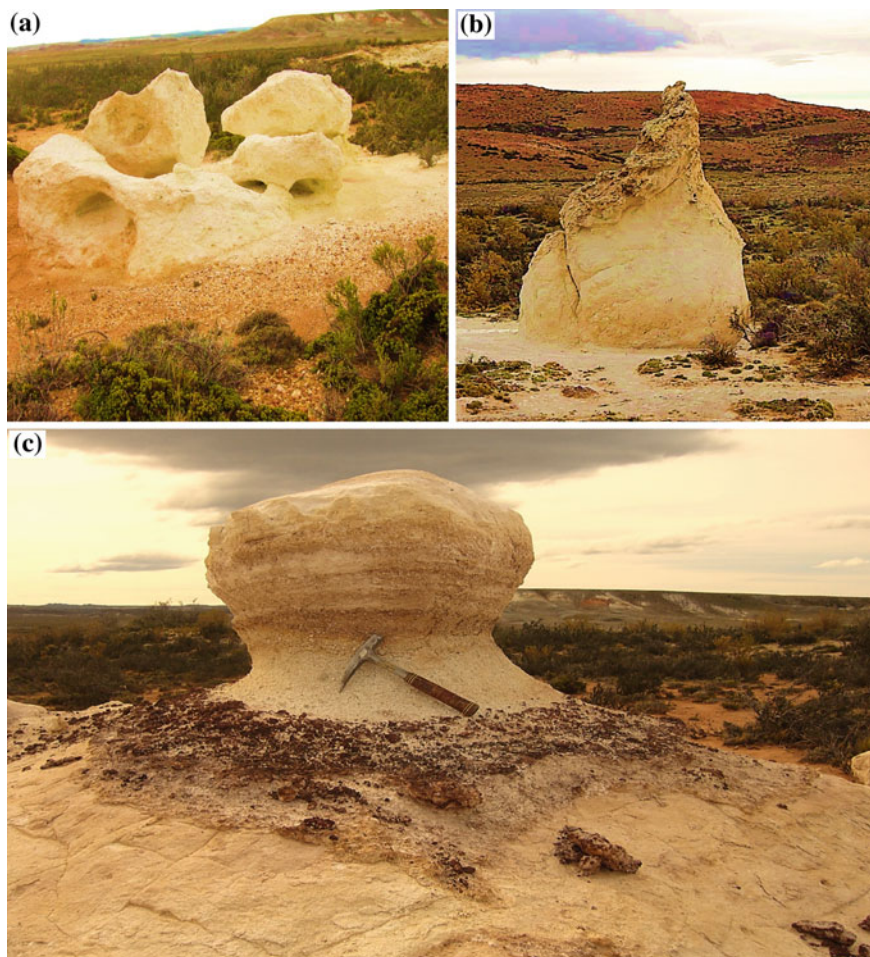


Fig. 33 Landforms developed on platforms or pedestals. **a** High erosion and relicts of a tunnel. **b** Bulb-like landform with endurated surficial duricrust, with alveolar hollows of the honeybee type. **c** Differential erosion of the soft sediments of the intermediate zone. Flared slopes merge with the platform

feldspar crystals and pumice fragments, which is an expression of differential erosion and expansion of the hollows as the result of lithoclasts.

“Pseudo-pillow” landforms

In the badland landscape, outcrops with morphology of sub-rounded hills as piled-up pillows, somewhat deformed, are observed. These landforms are pressed one against the other, with size reaching 1 m in diameter. These structures remind “pillow lavas” to the observer. They have a reddish-violet colour (Fig. 34). Thin sections analysed with a petrographic microscope permitted to recognize breccias of the peperite type, a product of the interaction between water-saturated sediments



Fig. 34 An outcrop whose morphology is noted for its piling up of cushions, somewhat deformed, which get compressed against each other, reaching sizes of 1 m in diameter. The larger structures look like valley walls

(White et al. 2000) with pyroclastic flow deposits. Peperites are of the globular type because the clasts present similar forms to those of the pillow-lava flows, surrounded by sedimentary materials (Busby-Spera and White 1987). This outcrop is interpreted as the interaction of a pyroclastic flow with a water body, most likely a lake.

3.4.3 Remarks

Due to its field relationships, fabric continuity and in situ, mineralogical composition/transformation, the alteration mantles are interpreted as fundamental components of the Late Jurassic weathering surfaces, in this case palaeoweathering surfaces and corrosion/etching plains. Over the Jurassic rocks of the Bahía Laura Group, a palaeosurface developed (Rabassa 2010; Bétard et al. 2014), a product of deep chemical weathering, under very hot and humid conditions. This landscape evolved in two phases: the first one included sub-superficial modelling of the weathering front and comprises the gradual transformation of the fresh rock into a regolith, which is the final product. The second phase involves the regolith denudation and the exhumation of the weathering front.

These landforms have been explained as due to sub-superficial etching and once they have been exhumed, differential rates of weathering and erosion would have continued acting along the existing fractures and the spots where rocks were less resistant.

Concerning the pedestal rocks and mushroom/hoodoos, it is interpreted that these landforms are the result of differential erosion rates, which have operated along the existing blocks as defined by fracture systems in the rock. The landforms that occur in the slopes were probably initiated under an ancient regolith mantle, which was later eroded and mobilized, leaving these landforms exposed perhaps to other dominant erosion processes in present climate conditions. Thus, it is very important to consider the climatic changes which have functioned since the Late Mesozoic to present times, which have imprinted important modifications to the landscape.

3.5 *Pilcaniyeu Ignimbrite, Collón Curá Formation (Middle to Late Miocene)*

3.5.1 Geology, Petrography and Stratigraphy

The stratigraphy of the Pilcaniyeu-Comallo region in western Río Negro Province, northern Patagonia, is related to the westernmost section of the Northern Patagonian Massif. It is composed of the following: (1) a lithological-structural complex known as the “Crystalline Basement”, gneisses, schists, migmatites and granitic rocks, probably of Early Palaeozoic age, metamorphosed in the Middle to Late Palaeozoic times; (2) Permian granites; (3) volcanic and sedimentary rocks probably of Late Triassic to Jurassic age; (4) Late Cretaceous sedimentary rocks; (5) the Ventana Formation, volcanic, pyroclastic and sedimentary rocks of Late Palaeocene and Eocene age; (6) the Collón Curá Formation, ashfall tuffs, ignimbrites, and conglomerates and sandstones of Middle to Late Miocene age; (7) Late Miocene and Early Pliocene basalts; (8) Pliocene piedmont deposits; (9) Quaternary glacial

sediments; and (10) Quaternary alluvial, aeolian and colluvial deposits (Rabassa 1974, 1975, 1978a). The landscapes and landforms described in this section correspond to those related to the Pilcaniyeu Ignimbrite, Middle to Late Miocene (Rolleri et al. 1975; Rabassa 1978b; Mazzoni 1993; Mazzoni and Benvenuto 1990; Mazzoni and Stura 1990). The palaeoclimatic and palaeoenvironmental conditions of this region during these times were investigated by Bondesio et al. (1978) and Vucetich et al. (1993) among many others.

The Collón Curá Formation is a set of ashfall tuffs, ignimbrites, sandstones, conglomerates and water-lain tuffs, of about 200 m in thickness, which extends for most of the western part of northern Patagonia. The outcrops of the type section are located in the Collón Curá River Valley and are laterally connected to those units described here. The petrographic description of this formation recognizes four basic lithologic types: (a) well-stratified, brownish, lithic tuffs, which are bearing insect nests and other concretions, usually with interbedded intra-formational breccias; these rocks are interpreted as regional palaeosols; (b) dacitic and rhyodacitic ignimbrites, in various welding degrees; (c) greyish, cinder ashfall tuffs, partly of a sandy nature, of very coarse stratification and usually bearing abundant land mammal fossil remains (see Bondesio et al. 1978, among many others); and (d) conglomerates, sandstones and sandy tuffs, usually well stratified and cemented by calcium carbonate. The three first types represent a continuous and clearly organized sequence and were named as Caruhé Tuff Member, Pilcaniyeu Ignimbrite Member and Las Bayas Tuff Member, respectively. The (d) type comprises a thick epiclastic sequence which has been named as the Rio Chico Conglomerate Member, interpreted as a direct signal of the uplift of the adjacent Andean Cordillera to the west. The ignimbrite member rocks have developed peculiar landscapes and landforms and will be described in greater detail.

The Pilcaniyeu Ignimbrite Member (Fig. 35) is exclusively composed of dacitic to rhyodacitic ignimbrites. The term “ignimbrite” is used here in the sense of Sparks et al. (1974, p. 115). This ignimbrite occurs in sheets of up to 40–60 m thickness, generally exhibiting various degrees in their welding. In most cases, three zones may be described: a lower one, poorly welded, which appears as a whitish cineritic tuff (Fig. 36); a middle one, of incipient welding which shows well-defined columnar jointing; and an upper one, deeply welded, which fractures in small, equidimensional blocks, usually characterized by tafoni, the result of aeolian abrasion (Fig. 37). It has not been possible to identify remnants of other uppermost zones, of lesser welding which originally were found above the deeply welded portion. These uppermost zones have been probably removed by denudation. From a petrographic point of view, there seems to be no major differences between these units. In all cases, these are dacitic to rhyodacitic ignimbrites, of vitroclastic, porphyritic texture, with quartz, intermediate plagioclase, potash feldspar (sanidine, anorthoclase) and biotite in a cinder matrix of very angular, acidic glass shards. The eruptive vents that generated these rocks have not been identified in the study area. These vents have perhaps been eroded or they were fissures, which were later sealed by the eruption products. The great extension of the outcrops of this unit and the presence of these rocks in many different, intermontane drainage basins,



Fig. 35 Pilcaniyeu Ignimbrite Member, welded zone with columnar jointing. Pichileufu River Valley, Río Negro Province

physiographically not connected, favour the hypothesis of multiple eruption vents. In most of the studied area, this ignimbrite is integrated by only one cooling unit. In only one site two superposed, welded ignimbrites are present, with an unwelded layer in between (Rolleri et al. 1975; Rabassa 1978a). It is important to note that the dispersal area of this unit is at least of 15,000 km², thus involving a huge mass of volcanic ejecta. Many fossil mammal bones and teeth and plant remains have been found in layers of this formation, usually forming part of calcareous concretions (see Bondesio et al. 1978). The identified fossils correspond to the “Santacruense-Friasense” stage, widely represented in Patagonia, which has been assigned to the Middle to Late Miocene. A concentrate of biotite crystals obtained from the ignimbrite member was dated in 15 Ma, confirming the Middle to Late Miocene age of the unit (Rabassa 1974, 1975, 1978a).

3.5.2 Landscape Evolution

This region has been emerged and exposed in a continental environment since, at least, the Triassic, as it is shown by exposures of sedimentary and volcanic rocks of Triassic and Jurassic age (Rolleri et al. 1975). Probably since the Late Jurassic and perhaps up to the Middle Cretaceous, planation surfaces developed due to deep chemical weathering, forming etchplains (Fig. 38). The regional planation surface is covered by Late Cretaceous continental sediments. Since then, the region

Fig. 36 Pilcaniyeu Ignimbrite Member, poorly welded zone with original deformation of tephra layers during the ash-flow movement. Pichileufu River Valley, Río Negro Province



has undergone successive periods of fluvial erosion, with the development of a complex fluvial network which was partially buried by Early Miocene basalts and deeply incised later during the Middle Miocene (Rolleri et al. 1975; Rabassa 1978b). The ignimbrite flows closely followed this stream network, totally burying the network and, partly, also the divides. The orogenic movements towards the end of the Oligocene started to uplift the Andean Cordillera, gradually leading to the inversion of the regional slope from the Pacific towards the Atlantic Ocean. Erosion, essentially of a fluvial nature, carved in the latest Oligocene and earliest Miocene a very well integrated, deep landscape, which had achieved a maturity stage (in a Davisian sense) when the sedimentation of the Collón Curá Formation concealed it in the Middle Miocene. Palaeosols which follow bedrock landforms are perfect witnesses of the existence of such landscape. This formation rapidly submerged the pre-existing landscape, including the outcrops of its own Lower Tuffaceous Member, when the ignimbrite flows occupied the existing drainage network and the ashfall tuffs in-filled all depressions and covered most of the



Fig. 37 Pilcaniyeu Ignimbrite Member, tafoni and block disintegration in heavily eroded zone. Pilcaniyeu, Río Negro Province

ancient divides. Only a few summits of the pre-Miocene, hilly, bedrock outcrops emerged from the ash mantles.

The in-filling of the basins and the rising of the first ranges of the Andean Cordillera built up a new positive area in the westernmost portion of northern



Fig. 38 Late Mesozoic planation surface developed on Crystalline Basement rocks, Comallo creek valley, Río Negro Province. This surface is unconformably covered by Late Cretaceous sedimentary rocks and the Collón Curá Formation (Middle to Late Miocene tuffs)

Patagonia, including the inversion of the drainage networks, from a Pacific to an Atlantic slope. Groeber (1929, p. 66, 1941) assigned this regional elevation to orogenic movements which he called the “First Phase of the Andean Movements”. The landscape developed as a consequence of these processes was rapidly in-filled by the pyroclastic sediments of the Collón Curá Formation. This accumulation was very fast and accompanied by substantial climatic changes, stopping the erosion process of the stream networks, allowing the in-filling of the landscape depressions and the preservation of the palaeolandforms. The identification and study of these landforms are strongly favoured by the deep lithologic contrast between the Collón Curá Formation and the pre-existing lithostratigraphic units.

On the central, palaeopositive block of the Northern Patagonian Massif, the pre-Collón Curá Formation landscape is characterized by the carving of integrated drainage systems in state of “maturity”. The fluvial systems where the present drainage network is located existed already in pre-Collón Curá times, as main valleys of the consequent type and smaller valleys of subsequent nature existed, adjusted to main fractures and joint systems. Ample, merging valleys generated depressions which were rapidly filled up by the Miocene tuffs. The sources of the valleys were usually found on the ancient surface of the Crystalline Basement massif. Towards the west, the palaeovalleys developed over the Palaeogene volcanic rocks. The sides of the valleys may have been as steep as 25°, as shown by the original dip of the basal lithic tuffs. In some cases, the former palaeosols cover rounded hills with peripheral dip around the buried palaeohills (Rabassa 1978b).



Fig. 39 Well-stratified ashfall tuffs of the Collón Curá Formation, in steep outcrops covered by Pliocene basalts. Río Pichileufu valley, Río Negro Province

Some of the valleys were up to 2 km wide. The valleys within the Northern Patagonian Massif were deep and elongated depressions, which augmented sharply their gradient when reaching the large tectonic basins located one to the north, the Collón Curá Graben, and another to the south, the Ñirihuau marine basin. Perhaps a rapid deepening of the network took place just before the eruption of the ignimbrites, as the Andean Cordillera was being elevated towards the west and the graben was being enlarged. In the western basins and grabens, very few sites exposed the base of the Collón Curá Formation and, therefore, little information is available about the pre-existing landscape. However, the sedimentary deposits suggest large, powerful streams with ample flooding plains of braided drainage pattern, consequently developed over the tectonically down-warped blocks.

The Collón Curá ashfall tuffs generated large mesetas and highplains, favoured by their friability and large inner friction of their clasts, mostly very angular glass shards. These landforms present abrupt walls, rock towers, and steep and sharp crests (Fig. 39). Micro-relief landforms of the “volcano-karst” type (Fairbridge 1968, p. 1205) are very frequent along the sides of these landforms. In these deposits, the slopes recede in a parallel manner, partly due to slumping of blocks, whereas at the foot of the slope, the removal of the materials generated as a result of the slumping process, and particularly the calcareous concretions, developed rounded landforms of gentle slopes. If the outcrops of the Pilcaniyeu Ignimbrite are involved, the erosion landforms are very similar, but in this case, the differential degree of welding controls the genesis of these features. Therefore, very gentle slopes are formed at the base of the outcrops (the poorly welded zone), whereas the

upper portions (deeply welded zone) show usually almost vertical rock walls, rock monuments and cliffs, displaying columnar jointing, needles, tafoni and steep cliffs.

4 Discussion and Final Remarks

In the studied ignimbrite outcrops, contrasting landscapes are frequently observed, from features related to “granite landscapes” and easily taken for such rocks, and other landforms that resemble landscapes developed in sandstones. Several further questions arise from our observations.

- (1) Why is it possible that rocks with so different lithology and texture may generate comparable landscapes?
- (2) Is it relevant to consider the age of the ignimbrite plateaus when dealing with the geomorphological analysis or is it sufficient to indicate their fabric characteristics?
- (3) Have the morphogenetic agents responsible for the generation and evolution of the landforms acted independently or are these features the result of multiple actions or even converging activities?
- (4) What is the relationship between the similarities on landform development of some ignimbrite flows and the modelling of sandstones?
- (5) Are there also similarities between ignimbrite modelling and granite rock landforms?
- (6) From a morphoclimatic point of view, are they monogenetic or polygenetic landscapes?

To answer these questions, emerging from our own field work observations, it is necessary to support the research activities with elements provided by other geological studies. The observed characteristics require the explanation of the landscape starting from structural analysis, determination of lithology and stratigraphic position of the deposits, considering the information related to the age of the outcrops and their fabric characteristics. In this sense, it should be highlighted the role of the chronology and, subsequently, the climatic changes that have taken place since the eruption of the ignimbrite flows until present times.

Since the morphogenetic agents are directly related to the climatic conditions, in the case of the Portezuelo ignimbrite only one agent would have acted in an isolated form, whereas other landscapes would have been the result of multiple processes and even several morphogenetic agents could have operated simultaneously with one of them prevailing over the others.

Concerning the fabric, it demands detailed analyses, because within even one individual flow, many fabric variations may coexist, both laterally and vertically. Moreover, these outcrops may be composed of several pyroclastic flows, superposed within one single cooling unit, each of them with their peculiar characteristics. This information allowed the definition and interpretation of landforms

according to the observation of structures and morphogenetic systems. In this manner, the generational stages of the various landforms were reconstructed, their consequence being the organization of the present landscape.

Concerning the geomorphological analysis, the landforms were defined and explained, searching for the differential resistance to erosion in specific points of the various outcrops, adding to this the identification of the successive climatic cycles that occurred since their eruption, thus becoming responsible for the present configuration of the vast majority of the ignimbrite landscapes.

The landscape of the Portezuelo de los Payunes would have started to develop sometime after the Late Pleistocene. The yardangs found in the landscape reveal that the dominant geomorphic process today is aeolian erosion and that the landscape is a simple one. From a morphoclimatic point of view, these landforms were modelled by a unique morphogenetic system, thus forming a monogenetic landscape.

The Barda Colorada and Chon Aike ignimbrites present similarities with sedimentary rocks concerning the existing set of landforms, such as rock arches, rock bridges, galleries, tunnels, corridors, demoiselles and badlands, mushroom rocks, hoodoos and minor features such as alveolar hollows, tafoni, caves, caverns and rock shelters. The integration of these landscapes results from multiple processes, sometimes acting simultaneously.

Both areas were affected by severe climatic changes since the Jurassic (the Chon Aike Formation) and the Middle Eocene (the Barda Colorada Formation), where the presence of erosion landforms was conditioned by different morphogenetic agents. The action of these agents in the creation and evolution of the landforms was eased by orthogonal jointing. These landscapes include slopes with dissection modelling, sub-superficial water erosion with “tunnelling” or “piping” processes, affecting ignimbrites with levels marked by pseudo-stratification and/or very friable deposits with abundant clayey materials as in friable sedimentary rocks.

Other sections of these ignimbrites show deeper, thorough welding, which enables the development of a specific set of landforms such as rock walls, crests, needles, pyramids, cliffs, nubbins, rowars and castle koppies, where the first ones are typical of welded ignimbrites and are positive elements of the landscape, whereas nubbins, rowars and castle koppies compare much better with granite landscapes, since these are rocks of higher cohesion.

To explain the modelling of the Lihuel Calel Ignimbrite with the development of granite landscape, it should be taken into consideration that this is a primary process, that is, mineral and textural transformations due to devitrification and/or vapour-phase, assisted crystallization, during the cooling of the unit. These transformations provided an even higher cohesion to the ignimbrite, which is typical of coherent igneous rocks. This feature permitted the explanation of the development of the landforms herein described, which are typical of granite environments.

Due to deep weathering processes which may have started as early as the Late Triassic, these landforms evolved in two stages, beginning with the sub-superficial modelling of the weathering front and posterior dismantling and denudation of the regolith and the surface exposure of the ancient weathering front.

Concerning the Pilcaniyeu Ignimbrite, the differences between the deeply welded and the poorly welded zones are so relevant that these welding facies occur as if they were totally different rocks. Welding defines large-scale features, as well as minor landforms, sometimes with strong gradation between the two end types. Future studies may allow the identification of micro-landforms which occur only in each of these welding types.

The landscapes developed on the ignimbrites cited in this work, concerning a morphoclimatic approach, correspond to a polygenetic relief bearing features of different morphogenetic systems which are defined by diagnostic landforms.

Ignimbrites are very common in volcanic landscapes of a varied scope of geological ages, thus deserving carefully dedicated geomorphological studies.

References

- Aguilera EY, Aragón E, Carretero S (2010) The palaeosurface on the Paso del Sapo Volcanic rocks, Chubut, Argentina. *São Paulo, UNESP, Geociências* 29(4):479–486
- Aguilera EY, Sato AM, Llambias E, Tickjy H (2014) The erosional surfaces and granitic landscape in ignimbrites of Sierra de Lihuel Calel, Province of La Pampa, Argentina. In: Rabassa J, Ollier C (eds) *Gondwana landscapes in southern South America, Argentina, Uruguay and southern Brazil*. Springer Earth Systems Sciences, Monograph series, pp 393–422
- Aragón E, Mazzoni MM (1997) Geología y estratigrafía del complejo volcánico-piroclástico del Río Chubut medio (Eoceno). *Revista de la Asociación Geológica Argentina* 52(3):243–256 (Buenos Aires)
- Bermúdez A, Delpino D (1989) La provincia basáltica Andino Cuyana (35–37°L.S.). *Revista de la Asociación Geológica Argentina* 44(1–4):35–55 (Buenos Aires)
- Bétard F, Peulvast JP, Rabassa J, Aguilera EY (2014) Meso-Cenozoic Palaeotopographies and Palaeolandscapes in the Deseado Massif, Santa Cruz Province, Argentina. In: Rabassa J, Ollier C (eds) *Gondwana Landscapes in southern South America, Argentina, Uruguay and southern Brazil*. Springer Earth Systems Sciences, Monograph series, pp 477–502
- Bondesio P, Rabassa J, Pascual R, Vucetich MG, Scillato Yané G (1978) La Formación Collón Curá de Pilcaniyeu Viejo y sus alrededores (Río Negro, Argentina). In: Su antigüedad y las condiciones ambientales según su litogénesis y sus vertebrados. II Congreso Argentino de Palaeontología y Bioestratigrafía and I Congreso Latinoamericano de Palaeontología, Actas, 85–99, Buenos Aires
- Bruthans J, Soukup J, Vaculikova J, Filippi M, Schweigstillova J, Mayo AL, Masin D, Kletetschka G, Rihosek J (2014) Sandstone landforms shaped by negative feedback between stress and erosion. *Nat Geosci* 7:597–601
- Busby-Spera CJ, White J (1987) Variation in peperite textures associated with differing host-sediment properties. *Bull Volcanol* 49:765–775
- Fairbridge RW (1968) *Encyclopaedia of geomorphology*. Ronald, New York
- Godefroy R (1940) *La nature alpine: exposé de géographie physique*. R. Arthaud editeur a Grenoble. 439 pages
- González Díaz EF (1972) Descripción geológica de la Hoja 30d Payún Matrú. Informe Técnico Boletín 130, Dirección Nacional de Geología y Minería. Buenos Aires
- Goudie AS (1989) Weathering processes. In: David S.G. Thomas (ed) *Arid zone geomorphology*. Wiley, London, pp 11–24
- Goudie AS (2004) *Encyclopedia of geomorphology*. Routledge, London
- Goudie AS (2007) Mega-yardangs: a global analysis: geography. *Compass* 1:65–81

- Groeber P (1929) Líneas fundamentales de la geología del Neuquén. Dirección General de Minas, Geología e Hidrología, Publicación 58, 110 pp. Buenos Aires
- Groeber P (1937) Descripción geológica de la Hoja 30c, Puntilla de Huincán, provincia de Mendoza. Informe técnico, Dirección Nacional de Geología y Minería, Buenos Aires
- Groeber P (1941) Desarrollo de la red de drenaje en América del Sur. *Holmbergia* 3(6):3–18 (Buenos Aires)
- Gutiérrez Elorza M (2001) Geomorfología climática. Ediciones Omega, Barcelona. 642 pp
- Hernando IR (2012) Evolución volcánica y petrológica del volcán Payún Matrú, retroarco andino del sudeste de Mendoza. Unpublished Doctoral Thesis, Facultad de Ciencias Naturales y Museo, Universidad Nacional de La Plata, La Plata, Argentina
- Inbar M, Rizzo C (2001) Holocene yardangs in volcanic terrains in the southern Andes. *Earth Surf Proc Land* 26:657–666
- Linares E, Llambías EJ, Latorre C (1980) Geología de la provincia de La Pampa, República Argentina y geocronología de sus rocas metamórficas y eruptivas. *Revista Asociación Geológica Argentina* 34(1):87–146 (Buenos Aires)
- Llambías EJ (1966) Geología y petrografía del Volcán Payún Matrú. *Acta Geologica Lilloana*, 8:265–315 (San Miguel de Tucumán)
- Llambías EJ (1973) Las ignimbritas de la sierra de Lihuel Calel, provincia de La Pampa. *Actas 5º Congreso Geológico Argentino* 4:55–67 (Buenos Aires)
- Llambías EJ (1975) Geología de la provincia de La Pampa y su aspecto minero. Dirección de Minas de la provincia de la Pampa, Unpublished technical report, Santa Rosa, 38 pp
- Llambías EJ (2009) Volcanes, nacimiento, estructura, dinámica, 1st edn. Vázquez Mazzini Editores, Buenos Aires, 144 pp
- Llambías EJ, Leveratto MA (1975) El plateau riolítico de la provincia de La Pampa, República Argentina. *Actas II Congreso Iberoamericano de Geología Económica* 1:99–114
- Mabbutt JA (1961) Basal surface or weathering front. *Proc Geol Assoc Lond* 72:357–358
- Mazzoni MM (1993) Sedimentación Colloncurensis en las provincias de Río Negro y Neuquén. *Ameghiniana* 30:351 (Buenos Aires)
- Mazzoni MM, Benvenuto A (1990) Radiometric ages of Tertiary ignimbrites and the Collón Curá Formation, northwestern Patagonia. In: *Congreso Geológico Argentino*, 11, 1990. *Actas*, San Juan, pp 87–90
- Mazzoni MM, Stura S (1990) El Miembro Ignimbrítico Pilcaniyeu, Formación Collón-Curá (Mioceno), provincias de Río Negro y Neuquén. *Reunión Argentina de Sedimentología*, 3, 1990. *Actas*, San Juan, pp 187–192
- Mazzoni MM, Aragón E, Merodio JC (1989) La ignimbrita Barda Colorada del Complejo Volcánico Piroclástico del Río Chubut Medio. *Revista de la Asociación Geológica Argentina* 44(1–4):246–258 (Buenos Aires)
- Migoñ P (2006) *Granite landscapes of the world*. Oxford University Press, Oxford 384 pp
- Ollier CD (1988) *Volcanoes*. Basil Blackwell, Oxford, p 228
- Ollier CD (1991) *Ancient landforms*. Belhaven, London, p 233
- Rabassa J (1974) Geología superficial en la región Pilcaniyeu-Comallo, Provincia de Río Negro. Unpublished Doctoral Thesis, Facultad de Ciencias Naturales y Museo, Universidad Nacional de La Plata, 119 pp. La Plata
- Rabassa J (1975) Geología de la región de Pilcaniyeu-Comallo, Provincia de Río Negro. *Boletín Fundación Bariloche* 17:1–125 (San Carlos de Bariloche)
- Rabassa J (1978a) Estratigrafía de la región de Pilcaniyeu-Comallo, Provincia de Río Negro. *Actas 7º Congreso Geológico Argentino*, Neuquén 1:731–746
- Rabassa J (1978b) Palaeorrelieves Cenozoicos en la región de Pilcaniyeu-Comallo, provincia de Río Negro. *Actas 7º Congreso Geológico Argentino*, Neuquén 2:77–87
- Rabassa J (2010) Gondwana Palaeolandscape: long-term landscape evolution, genesis, distribution and age. *Geociências* 29(4):541–570 (Universidade Estadual de São Paulo (UNESP), São Paulo)

- Rabassa J, Carignano C, Cioccale M (2014) A general overview of Gondwana landscapes in Argentina. In: Rabassa J, Ollier C (eds) *Gondwana landscapes in southern South America*. Springer Earth System Sciences, Monograph series, pp 201–245
- Rapela CW, Pankhurst RJ, Llambías EJ, Labudía C, Artabe A (1996) “Gondwana” magmatism of Patagonia: inner Cordilleran calc-alkaline batholiths and bimodal volcanic provinces. Third international symposium on Andean geodynamics. Saint-Malo, France, pp 791–794
- Rolleri EO, Guichón M, Rabassa J, Scanavino RA (1975) Estudio geológico del valle del Río Limay entre Piedra del Aguila y Paso Limay (provincias del Neuquén y Río Negro). In: *Actas VI Congreso Geológico Argentino*, vol 1. Buenos Aires, pp 257–266
- Sato AM, Tickyj H, Llambías EJ, Sato K (2000) The Las Matras tonalitic-trondhjemitic pluton, central Argentina: Grenvillian-age constraints, geochemical characteristics, and regional implications. *J S Am Earth Sci* 13:587–610
- Skilling IP, White JDL, McPhie J (2002) Peperite: a review of magma-sediment mingling. *J Volcanol Geotherm Res* 114:1–17
- Sparks RSJ, Self S, Walker GPL (1974) Products of ignimbrite eruptions. *Geology* 1(3):115–122
- Sruoga P, Llambías EJ (1992) Permo-Triassic leucorhyolitic ignimbrites at Sierra de Lihuel Calel, La Pampa province, Argentina. *J S Am Earth Sci* 5(2):141–152
- Tickyj H, Basei MAS, Sato AM, Llambías EJ (1999) U-Pb and K-Ar ages of Pichi Mahuida Group, crystalline basement of south-eastern La Pampa province, Argentina. *Actas II South American symposium on isotope geology*. Villa Carlos Paz, Córdoba, Argentina, pp 139–144
- Twidale CR (1982) *Granite landforms*. Elsevier, Amsterdam, p 372
- Twidale CR, Corbin EM (1963) Gnammas. *Revue de Geomorphologie Dynamique* 14:1–20
- Vidal Romani JR, Twidale CR (1998) *Formas y paisajes graníticos*. Universidade da Coruña, A Coruña, Spain, p 411
- Vucetich G, Mazzoni M, Pardiñas U (1993) Los roedores de la Formación Collón Curá (Mioceno Medio) y la Ignimbrita Pilcaniyeu, Cañadón del Tordillo, Neuquén. *Ameghiniana* 30(4): 361–381 (Buenos Aires)
- Wayland EJ (1934) Peneplains and some erosional platforms. *Geological Survey of Uganda, Annual Report and Bulletin*. Protectorate of Uganda Geological Survey, Department of Mines, Kampala, pp 77–79
- Willis B (1936) *East African plateaus and rift valleys: studies in comparative seismology*, vol 470. Carnegie Institution of Washington Publication, 358 pp
- White JDL, McPhie J, Skilling IP (2000) Peperite: a useful genetic term. *Bull Volcanol* 62:65–66

When Science and Leisure Meet: A Geotourist Itinerary in Southern Tierra Del Fuego, Argentina

Soledad Schwarz and Piotr Migon

Abstract Tierra del Fuego (Patagonia, Argentina) is a re-known place due to its location and beauty. These attributes have drawn attention to adventurers during centuries as well as to visitors from all over the world and also to local and foreign researchers during decades. Witness of this situation was the Sixth Argentine Congress of Quaternary and Geomorphology which took place on April, 2015. A field trip was organized within the frame of the Congress in order to expose the scientific knowledge of the region and to reveal several aspects of the uniqueness of Tierra del Fuego. This chapter proposes a geotourist itinerary in Southern Tierra del Fuego, taking into account the experience of the first part of day 1 of the corresponding field trip, that is, along the Ushuaia-Harberton transect. Geotourism is a modern way of tourism that focuses on experiencing the Earth geological and geomorphological features. In order to achieve this, special services and facilities can be organized, for instance guided visits, interpretative materials (such as booklets, signs, posters), viewpoints, thematic trails, among others. It is believed that this geotourist itinerary must start with the identification of georesources that may allow in the future the design of a product to enhance this transect singularities. In this sense this chapter aims to: (a) present geotourism as a modern way of tourism, (b) outline the geological and geomorphological setting of Southern Tierra del Fuego, (c) select and describe different georesources in the Ushuaia-Harberton

S. Schwarz (✉)

Universidad Nacional de Tierra del Fuego, Antártida e Islas del Atlántico Sur,
Onas 450, Ushuaia, Tierra Del Fuego, Argentina
e-mail: sschwarz@untdf.edu.ar

S. Schwarz

Centro Austral de Investigaciones Científicas, CADIC—CONICET,
Bernardo Houssay 200, Ushuaia, Tierra del Fuego, Argentina

P. Migon

Department of Geography and Regional Development, University of Wrocław,
(pl. Uniwersytecki 1 50-137), Wrocław, Poland
e-mail: piotr.migon@uni.wroc.pl

© Springer International Publishing AG 2017

J. Rabassa (ed.), *Advances in Geomorphology and Quaternary Studies
in Argentina*, Springer Earth System Sciences,
DOI 10.1007/978-3-319-54371-0_2

transect using a data-sheet designed ad hoc, and (d) discuss about geotourism as a bridge between science and leisure and how the former can be used to upraise the latter.

Keywords Georesources · Geotourism · Argentina · Patagonia · Southern Tierra del Fuego

1 Introduction

The Isla Grande de Tierra del Fuego (Fig. 1) is located at the southern end of South America, between lat. $52^{\circ} 27' 14''$ – $55^{\circ} 04' 36''$ S and long. $65^{\circ} 05' 31''$ – $71^{\circ} 46' 05''$ W. It is divided into two administrations: the Republic of Chile west of the 68° meridian and the Republic of Argentina to the east of it. This island is the largest of those of the Fuegian Archipelago.

The unique geographical position of Tierra del Fuego attractive in itself (the southernmost part of a continental landmass in the world) is enhanced by extremely diverse geoheritage, including striking sceneries of different origin.

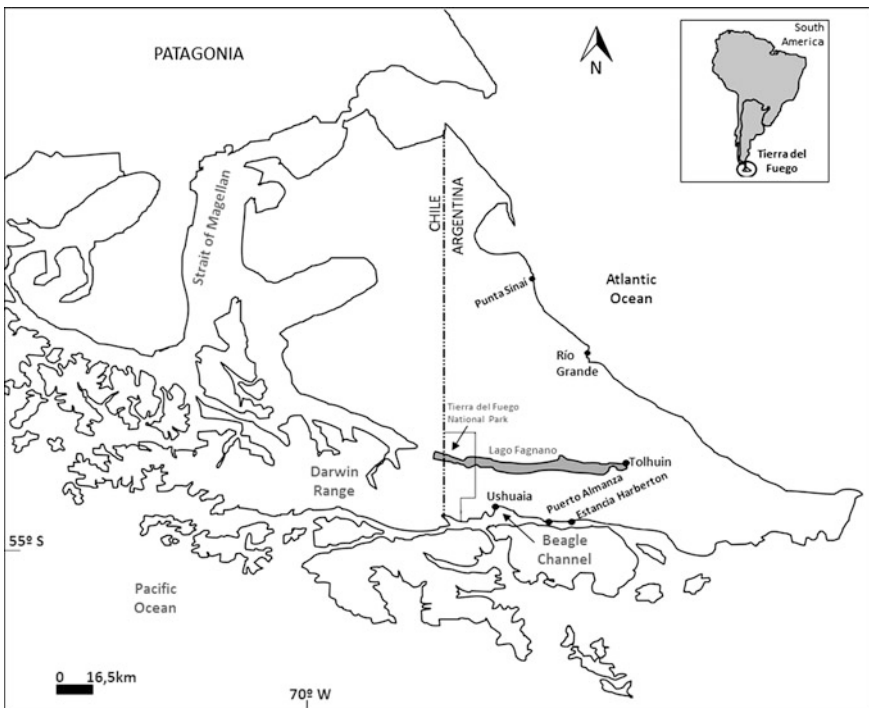


Fig. 1 General outline of Isla Grande de Tierra del Fuego

In Argentina, the province of Tierra del Fuego includes three urban locations: Ushuaia (the capital city), Tolhuin and Río Grande. The former was the venue of the Sixth Argentine Congress of Quaternary and Geomorphology which took place last April, 2015.

After three days of varied enriching lectures and even international conferences (some of which gave rise to this volume), a field trip was organized in the spirit of revealing the uniqueness of Tierra del Fuego: a geographical area which is geologically divided into two different tectonic plates: the South American plate to the North of the Magellan/Fagnano Fault and the Scotia plate to the South of it (e.g. Olivero and Martinioni 2001; González Guillot 2012) and was covered with big masses of ice during the Last Glacial Maximum which took place 24 ka B.P.—thousands of years before Present—(e.g. Rabassa 2008; Rabassa et al. 2005; Rabassa and Coronato 2007). These features bestow singularity to Tierra del Fuego and this will be exposed later.

The field trip organized within the cited Congress included an itinerary of three days around Tierra del Fuego in order to visit and to learn about special localities of geomorphological interest (Fig. 2), such as the Beagle Channel, the drumlin field of Harberton and Isla Gable, Lago Fagnano (day 1), the erratic boulder field of Punta Sinaí in northern Tierra del Fuego (day 2), Pleistocene and Holocene paleosoils (day 3) and many more features.



Fig. 2 Three-day field trip during the Sixth Argentine Congress of Quaternary and Geomorphology (Google Earth image)

Thanks to the local scientists and specialists that led the field trip, the participants were part of a geotourist practice, but without being aware of it. What is geotourism then? It is a modern way of tourism that focuses on experiencing the Earth geological features: the “geo” part of the term means geology and geomorphology and the “tourism” part of it means visiting geosites, learning, appreciating and engaging with nature and landscape (Dowling and Newsome 2010).

Martínez Fernández (2013) stated that there is a need to emphasize the appreciation and use of geological tourist attractions and in fact geotourism appreciates the abiotic environment in a natural landscape, without losing sight of its interrelations with biota and culture, but understanding that the latter have been historically more considered and integrated into tourist products and interpretative media. Under this perspective, geotourism offers a great opportunity to create new products in sparsely populated and faraway areas with incipient tourism and also to enrich the diversity of mountainous and coastal environments that currently concentrate more demand.

In this context, the itinerary proposed in this chapter starts in Ushuaia and continues through the National Road number 3 northwards and then takes place along provincial road “j” which leads to Puerto Almanza and then to Estancia Harberton (an “estancia” in Patagonia is an extensive private area or a large rural complex, similar to a ranch).

Along National Road 3, there are many winter sport centres which are also the starting point of several treks in the Fuegian Andes during the rest of the year. There are presently different viewpoints along the itinerary but only one site offers an interpretative board (in Valle Carbajal). The road “j” leads first to Puerto Almanza, a small fishery location, where there is incipient tourist infrastructure in the form of family restaurants, but for the time being these restaurants are mainly visited by local people rather than by tourists. Then, the route leads to Estancia Harberton. This is the oldest estancia in the Argentine sector of Tierra del Fuego. Its founder, Thomas Bridges, was an Anglican missionary who received a donation of land from the Argentine National Congress in acknowledgement for his work with the natives. Harberton is now managed by Thomas Goodall, a great-grandson of the founder. The estancia was declared an Argentine National Historical Monument in 1999 since it maintains its original simple buildings of wood covered with corrugated iron, its gardens, stone piers and terraces (January, 2016. Retrieved from <http://www.estanciaharberton.com/historiaenglish.html>). Originally, it operated with sheep (for wool) and cattle (for meat) but today, this well-known farm offers organized visits around the place: farm buildings, a vegetable garden, a graveyard, a museum of bones and a tea house. There is also a dock there from where small boats leave to visit an island nearby which is home of a Magellan penguin rockery, sometimes with occasional visitors of other sub-Antarctic species.

Apart from the tourist use of these roads, the transect draws attention to local and international scientists. Field and postgraduate courses organized in Ushuaia usually include this transect and different research projects were carried out in the area during the last three decades.

However, visitors just pass these roads, using them as a link between Ushuaia and Puerto Almanza or Estancia Harberton. Landscape performs as a great

backdrop but most visitors enjoy it without merely noticing its components and dynamics. Despite this, through interpretative facilities, visitors may also acquire knowledge and understanding of the geology and geomorphology, and this is in fact the key goal in geotourism (Hose 1995). In addition, from a touristic point of view, Borla (1995) made a report classifying and analysing natural and cultural resources with ecotouristic potential. In her study the biotic information was particularly detailed, as it is usually understood that flora and fauna are the main source of interest for ecotourists.

In this sense, this chapter aims to: (a) present geotourism as a modern way of tourism, (b) outline the geological and geomorphological setting of Southern Tierra del Fuego, (c) select and describe different geosites in the Ushuaia-Estancia Harberton transect as well as their educational potential, (d) discuss geotourism as a bridge between science and leisure and how the former can be used to upraise the latter.

2 Geotourism as a Modern Way of Tourism

“The beauty of many geomorphological landscapes has long been recognized, starting from travelogues of ancient travellers and scientists. Today, many such landscapes, if easily accessible, are top tourist destinations, accommodating millions of visitors annually. They come to see the scenery, which in their eyes have outstanding universal value” (Migoñ 2010, p. 11). However, geotourism is much more than just looking at landscapes.

Though modern geotourism has been practised for some time before, the term was actually undefined until the mid-1990s when Hose first definition appeared: geotourism is a form of tourism based on the provision of facilities and interpretation services that allows tourists to incorporate knowledge for understanding the geology and geomorphology of a site (including its contribution to the development of Earth Sciences) beyond the mere aesthetic appreciation (Hose 1995; in Hose 2012).

Conceptualizations of geotourism as a form of tourism have been reviewed by several authors. Since a universally accepted definition of the term does not exist, there are major disputes and confusions about its meaning (Hose 2012; Ollier 2012). As a result, it can be said that “when defining geotourism, two opposing conceptions emerge. Some scholars consider geotourism to be synonymous with geographical tourism, that is a form of tourism aimed at the integrative discovery of an area, with all its natural and human components [...] The second view considers geotourism as a form of tourism aimed specifically at the discovery of the heritage of a region [...]” (Reynard 2008, p. 225).

In this study, the latter view is adopted and although the aim of this paper is not to present the different approaches, some definitions will be given.

In Iran, Sadry (2009) suggested that geotourism is a type of tourism based on knowledge, preservation and interpretation of abiotic nature attributes. This idea

was shared in Spain by Carcavilla et al. (2011) who added that geotourism must disclose the particular characteristics of the Earth to the visitors. Dowling and Newsome (2010, p. 232) stated that geotourism is a niche within nature tourism “that specifically focuses on geology and landscape. It promotes tourism to geosites and the conservation of geodiversity and an understanding of Earth Sciences through appreciation and learning. This is achieved through independent visits to geological features, use of geotrails and viewpoints, guided tours, geo-activities and patronage of geosite visitor centres”. These authors fell within the sustainability paradigm emphasizing the importance of this type of development which is locally and economically beneficial, while geological heritage is protected. Moreover, Newsome and Dowling (2006) explained that geotourism can be seen as a system made of three subsystems: forms (landscapes, landforms, sediments, rocks and fossils), processes (tectonic activity, volcanic processes, weathering, erosion and deposition) and tourism (attractions, accommodation, tours, activities, interpretation, planning and management). In Brazil, Ruchkys (2007) understood that geotourism is the segment of tourism that has the geological heritage as the main attraction and at the same time seeks protection through conservation of resources and tourist awareness. He added that interpretation makes this heritage accessible to the lay public and promotes the development of Earth Sciences.

These various definitions converge at the following keywords: geological heritage, conservation, interpretation and learning. In this sense, Hose (2012) referred to the 3 G’s of geotourism: (1) Geoconservation: an emergent geoscience that promotes the recognition of the importance of geosites for sustainable development education; (2) Geohistory: a systematic narrative of geological and geomorphological discoveries, events, personalities and institutions, and (3) Geointerpretation: the art or science of determining and communicating the meaning of geosites, events or locations.

As to the third G, geotourism uses, in order to achieve appreciation and learning, independent visits, thematic itineraries, viewpoints, guided tours, visitor centres and interpretation materials, such as posters. At this point, and following the different approaches, it can be said that the major difference between geotourism and other forms of tourism is precisely its educational function: to teach, to instruct and to explain clearly the repertoire of georesources in different sites (Millán Escriche 2011).

Finally, “geotourism as a type of nature tourism comes to fill an empty field on the use of geological resources of the landscape in Argentina” (Martínez Fernández 2013, p. 61). In Patagonia, for instance, there are incipient geotourism initiatives in arid and sparsely populated areas, particularly in northern Patagonia. Martínez Fernández (2013) stated that Patagonia has a great geotourist potential considering the strength of this destination in the national and international offer as well as its ever-increasing number of tourists. In the past two decades, progress has been made in “ecotourism” through the creation of new products and infrastructure of the term in the tourist supply; likewise, a geotourism discussion must be encouraged. If geotourism enhances the abiotic components of a natural landscape, then this

perspective opens great possibilities to other Patagonian destinations as well as it promotes diversification of attractions in mountainous, tableland and coastal landscapes (Martínez Fernández 2013), presently still unused for these purposes.

3 Geographical Setting

The geological history of Tierra del Fuego began 150 Ma (millions of years) ago, when the area was covered by oceans from where volcanic islands emerged (González Guillot 2012). Between these islands and a continent to the north, there was an interior ocean with submarine volcanic activity that created new seabed (Stern and de Wit 2003). Some 50 Ma later, this interior ocean begun to narrow due to a change in the dynamics of the tectonic plates. The collision of these plates deformed the rocks causing faulting, folding and foliation and triggered mountain uplift (e.g. Fildani and Hessler 2005; Klepeis et al. 2010). This was the beginning of the formation of the Fuegian Andes which continued until the Miocene (Klepeis and Austin 1997; Ghiglione and Ramos 2005; Torres Carbonell et al. 2011). Successive stages of compression made the range grow in altitude and width. At the same time, major faults were formed, nowadays followed by the main valleys of the region, such as the Lago Fagnano, the Beagle Channel and the Carbajal-Tierra Mayor-Lashifasaj valleys. As these processes took place the interior ocean disappeared and the Tierra del Fuego archipelago completely emerged 2 Ma ago (e.g. Olivero and Malumián 2007).

Today, the boundary between the South American and Scotia plates (Fig. 3) is of the transform type (Diraison et al. 2000). The Magellan-Fagnano Fault extends from the Pacific Ocean through the Chilean side of Tierra del Fuego, and it continues into the Atlantic Ocean domain; the depression that occupies the Lago Fagnano follows this huge fault (e.g. Lodolo et al. 2003). The plates move along this fault with an average relative speed of 4–6 mm per year (Smalley et al. 2003, 2007; Mendoza et al. 2011). Movements along this fault, according to some authors (Cunningham et al. 1991; Kraemer 2003; Rapalini et al. 2015), have caused the curvature of the Andes in Patagonia which explains why the Fuegian Andes present a W–E trend, when the rest of the Southern Andes have a dominant N–S orientation.

According to Bujalesky (2007), the basement of the southern part of Tierra del Fuego is composed of pre-Jurassic highly deformed metamorphic rocks, covered by Late Jurassic to Early Cretaceous volcanic pyroclastic rocks and by Early Cretaceous, mildly metamorphosed, sedimentary rocks of marine origin. The northern part is composed of non-deformed Late Jurassic-Early Cretaceous rocks; the oldest exposed sediments are continental or marine Tertiary rocks, overlain by Pliocene-Pleistocene glacial deposits.

During the Quaternary, glaciations affected Tierra del Fuego (Fig. 4): five main lobes developed from an ice sheet in Darwin Range, Chile (55° S–69° W; 2000 m a. s.l.—meters above sea level—), spreading in all directions and following

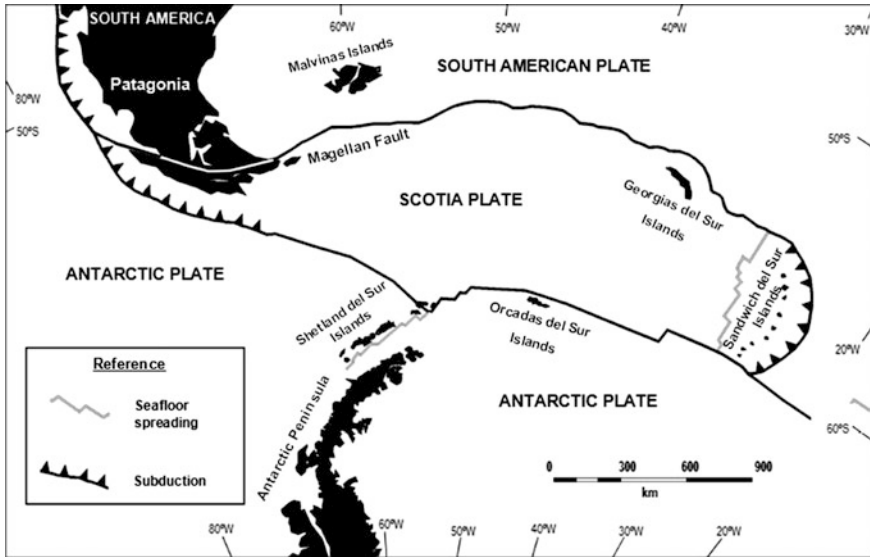


Fig. 3 Tectonic plates that affect Tierra del Fuego (modified from Bird 2003)

alignments and pre-existing fluvial valleys; small tributary glaciers occupied inner valleys (Rabassa et al. 2011; Rabassa and Coronato 2007). According to Rabassa et al. (2011), “five main glaciations have been mapped in the northern area, but only the last two have been recognized so far in the mountainous southern area”. In the former, submerged till, glaciofluvial deposits and erratic boulders have been recognized, whilst in the latter conspicuous moraines, outwash plains with kettles, drumlin fields, cirques, troughs and many other erosional and depositional landforms can be identified. The Last Glacial Maximum was attained around 24 ka B. P., and the ice recession started before 14.7 ka B.P. (Rabassa and Clapperton 1990).

These geographical characteristics impose low-hill topography, plateaus and closed depressions in the North of the Fuegian archipelago and a mountainous terrain in the South, separated by a transitional intermediate zone formed by hills, wide valleys and lake basins (Coronato 2014).

The topography, together with the latitudinal position of Tierra del Fuego and its closeness to Antarctica, which influence the climate, gives rise to three major biomes: steppe in the North, sub-Antarctic mixed forest and Andean desert in the South, and the Fuegian ecotone in the centre. All these factors determine five landscape units (Coronato 2007): steppe plains, mixed hills and valleys, forested mountains, peaty plains and coasts. Since the transect Ushuaia-Estancia Harberton is located in the “forested mountains” and “coasts” areas, only these two landscape units will be described.

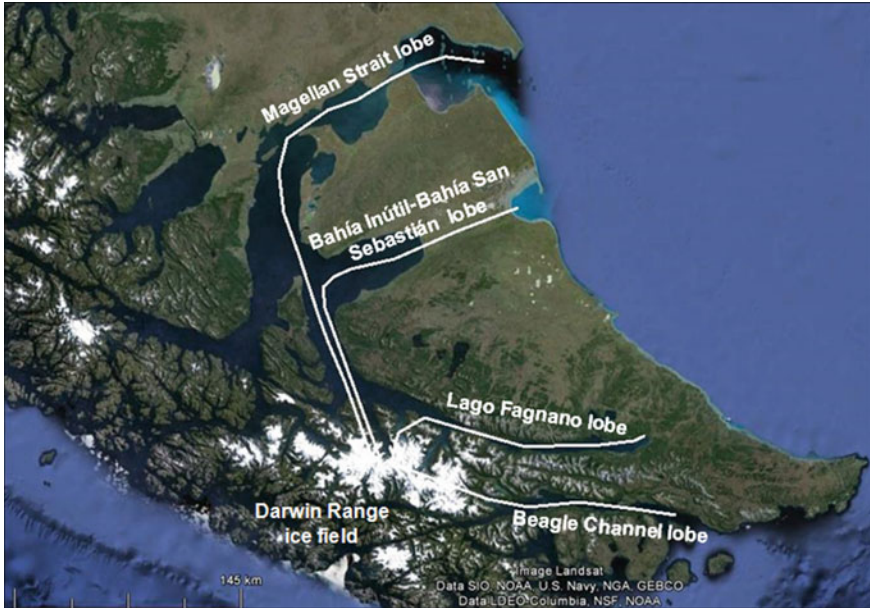


Fig. 4 Major ice lobes during the Quaternary glaciations, based on Coronato et al. (2004) (Google Earth image)

According to Coronato (2007, 2014), a mountainous topography dominates the south-western part of Tierra del Fuego. The Fuegian Andes, with W-E direction, form relatively low mountain ranges, reaching about 1000 m a.s.l. Slope steepness is considerable, and therefore, despite rather low altitude, there is a high mountain scenery with jagged peaks, rock slopes, deeply incised valleys and widespread talus. Metamorphic rocks of Palaeozoic and Mesozoic age and marine origin are stratified, folded and foliated. There are also some igneous rocks, both volcanic and plutonic. Mountain systems have been subject to minor faulting. All the landscape shows evidence of past ice modelling. Cirques, horns, truncated spurs and sharp edges are characteristic. Some glacial troughs are now occupied by lakes, whereas most of the valleys host peatbogs and *Nothofagus sp.* forest in the slopes, up to 600 m a.s.l., in the lower parts.

On the other hand, 525 km of two different coastlines describe Tierra del Fuego in the East and in the South. The former corresponds to the Atlantic Ocean coast and is situated in a stable geological area. The latter, where the transect takes place, corresponds to the Beagle Channel, situated in a seismic, tectonically active area, affected by several glaciations. High coasts in hard rocks with gravel beaches as well as low and terraced areas can be identified.

4 Ushuaia-Estancia Harberton Transect as a Geotourist Itinerary

Any geotourist itinerary must start with the identification of georesources that may allow in the future the design of a product to enhance the singularities of a transect.

Though the Ushuaia-Estancia Harberton transect offers more georesources, in this case the attention will be focused on the six most important ones (Fig. 5). The sites selected for this itinerary were all stopovers during the field trip of the Congress and are the result of an assessment and ranking process carried out during the senior thesis of the first author (Schwarz 2009), which included the design of three instruments for data collection: a fact sheet, a direct assessment sheet and a parametric assessment sheet. Some of these results were presented in other meetings (Schwarz et al. 2011; Schwarz 2013).

To describe each of the six georesources, a data-sheet was designed (Table 1), following recommendations when building a catalogue of sites of geological interest (Carcavilla et al. 2007). The sheet includes information about location (coordinates and access of the viewpoint and management), physiographic features (dimensions and altitude), lithology, type of use (economic, scientific, recreation, observation) and geodescription (formation, processes, age, among others). It also details what type of georesource is described, according to its structure (sedimentary, tectonic, hydrological or geomorphological) and materials (minerals, rocks, fossils or soils), what educational functions it has so as to learn about different geoprocesses and geosystems, which specific Earth Sciences could be promoted if geo-interpretation is offered, as well as any other information related to various aspects of nature and culture.

All the photographs included in the sheets (Tables 2, 3, 4, 5, 6 and 7) were taken by the first author during different field trips whereas all the sketches except one for



Fig. 5 Ushuaia-Estancia Harberton transect. Georesources: 1 Beagle Channel, 2 Valle Carbajal, 3 Gable island, 4 Drumlin field, 5 Bahía Cambaceres and 6 Harberton peatbog (Google Earth image)

Table 1 Data-sheet to describe georesources

Georesource					
1. Location			5. Sketch		
1.1. Coordinates					
1.2. Access					
1.3. Management					
2. Physiographic features					
2.1. Dimensions					
2.2. Altitude					
3. Type of use					
4. Lithology					
6. Photograph					
7. Geodescription					
8. Type of georesource					
8.1. Structure	8.1.1. Sedimentary		8.2. Materials	8.2.1. Minerals	
	8.1.2. Tectonic			8.2.2. Rocks	
	8.1.3. Hydrological			8.2.3. Fossils	
	8.1.4. Geomorphological			8.2.4. Soils	
9. Educational functions					
10. Geosciences promoted					
11. Other information					
12. References					

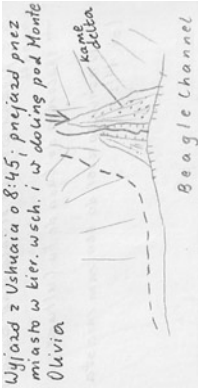

Schwarz (2016), doctoral thesis in preparation

georesource 3 were hand-drawn by the second author during the Congress field trip. Sketches include notes in Polish but these are translated into English below each respective sketch.

5 Linking Science and Leisure

The six georesources presented above are just a sample from a more extensive list of potential sites of interest. The transect Ushuaia-Estancia Harberton offers many more, such as Monte Olivia, Río Lasifashaj, Cerro Cornú, Bahía Brown and Bahía Harberton, among many others. All these natural attractions are already being used by the tourism industry, but as Manosso (2012) stated, the scientific contents offered to tourists should be more extensively explored so that these localities are not only appreciated for their aesthetic value. One way to achieve this is through thematic panels. Miranda et al. (2011) explained that these have a great effectiveness and give the chance to bring people to issues related to Earth Sciences. Panels give observers information about what they are looking at in a direct way. They are a great resource for geo-interpretation and geotourism, particularly in isolated localities.

Table 2 Georesource 1: Beagle Channel data sheet



Georesource 1: "Beagle Channel" (in Ushuaia)	
1. Location	54° 48' 18"S-68° 17' 40"W
1.1. Coordinates	Direct access from the city of Ushuaia
1.2. Access	Argentine Navy and National Coast Guard
1.3. Management	
2. Physiographic features	
2.1. Dimensions	190 km long and 5 km average wide
2.2. Altitude	0 m a.s.l.
3. Type of use	Economic. Recreation. Scientific. Observation
4. Lithology	Departure from Ushuaia at 8:45, across the town towards the east and into a valley below Mt Olivia Along the north coast the "Deformed Complex of the Fuegian Andes" develops, which consists in its lower part of a metamorphic basement on which volcanic and sedimentary rocks of Jurassic age lie, which in turn are covered by layers of marine origin from Late Jurassic-Early Cretaceous. This set is folded and metamorphosed, as the result of intense seismic activity in the area.
5. Sketch	
6. Photograph	

(continued)

Table 2 (continued)

Georesource 1: "Beagle Channel" (in Ushuaia)			
7. Geodescription	<p>A marine channel that connects the Pacific and the Atlantic oceans with a maximum depth of 280 m in the western area. Clear water with a temperature between 3 and 7 °C. Estuarine dynamic, with semidiurnal microtidal regime and a less-than-2-m range tide.</p> <p>The Channel occupies a tectonic valley that was modelled by outlet glaciers, several times during the Pleistocene. The paleo-glacier Beagle flowed from W to E during the LGM, along 200 km and with an average width of 10 km and 1200 m of thickness in its central part. The retreat of the glaciers started 14.7 ka B.P.; the progressive inflow of sea water started about 8.2 ka B.P.</p> <p>The islands and islets in the channel show signatures of subglacial erosion; the channel coasts present different landforms of glacial origin, including a drumlin field and frontal moraines that show the maximum position of the ice front during the LGM.</p> <p>In 2008, the Argentine Mining and Geological Survey declared the Beagle Channel as a Site of Geological Interest considering it a significant example of the expression of endogenous and exogenous processes.</p>		
8. Type of georesource			
8.1. Structure	8.1.1. Sedimentary		8.2. Materials
	8.1.2. Tectonic	x	8.2.1. Minerals
	8.1.3. Hydrological	x	8.2.2. Rocks
	8.1.4. Geomorphological	x	8.2.3. Fossils
9. Educational functions	Geo-interpretation may allow visitors to learn:		
	<ul style="list-style-type: none"> - about tectonic plates; - about changes in global climate and the dynamics of glacial times; and - about major changes in the sea level. 		
10. Geosciences promoted	Geomorphology Geology		
11. Other information	<p>The channel name derives from the British navy vessel used in Fitz Roy's hydrographic expeditions to South America which included a famous trip with the young Charles Darwin on board.</p> <p>Sea-mammals and birdlife including penguins live in the islands and islets of the Channel.</p> <p>Underwater kelp forests, <i>Nothofagus sp.</i> forest develops from the shore up to 600 m a.s.l.</p> <p>Archaeological sites 8000 years old, on the shore and higher old beaches.</p> <p>Different parts of the coastline are protected by the national and local governments.</p>		
12. References	<p>Borla and Vereda (2001), Borla (1995), Coronato (2007), Rabassa et al. (2000), Coronato et al. (1999), Rabassa and Coronato (2007), Bujalesky et al. (2008)</p>		

Table 3 Georesource 2: Valle Carbajal data sheet


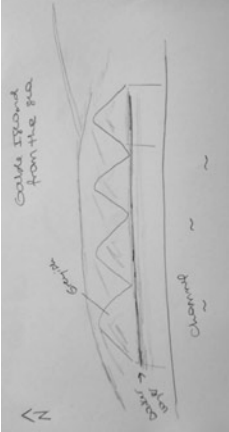

Georesource 2: "Valle Carbajal"	
1. Location	
1.1. Coordinates	54° 44' 03"S/68° 10' 52"W
1.2. Access	17 km from Ushuaia, along route "3"
1.3. Management	Public. Part of a natural reserve.
2. Physiographic features	
2.1. Dimensions	23 km long, 2.5 km maximum width
2.2. Altitude	From 150 to 1000 m a.s.l.
3. Type of use	Economic. Recreation. Observation.
4. Lithology	Lemaire Formation: phyllites and slates highly deformed, of Late Jurassic-Early Cretaceous age.
5. Sketch	 <p>5. Sketch</p> <p>Site of transfluence of a glacial tongue [right] 1-4 Hanging glaciers—glacier ice seen beneath snow cover T—peat bogs in the valley floor</p>
6. Photograph	

(continued)

Table 3 (continued)

Georesource 2: "Valle Carbajal"																	
7. Geodescription	<p>The Carbajal valley is traversed by a 100 km long major thrust fault, which includes adjacent valleys (Tierra Mayor and Lasifashaj) with a W-SE direction.</p> <p>During the Quaternary glaciations, this valley was occupied by a main outlet glacier and many alpine glaciers that descended from the Vineiguera, Valdivieso and Alvear ranges, forming an integrated glacial system.</p> <p>During the LGM, a transfluent ice lobe flowed to the south through the Olivia valley to the Beagle Channel.</p> <p>Today, the Carbajal valley shows several erosional landforms such as sharp edges, horns, cirques, hanging valleys and truncated spurs. No depositional landforms associated with the LGM can be identified here since this was the ice accumulation zone, except for some till deposits at the bottom of the valley.</p> <p>Some slopes show geomorphical evidence of rock and debris slides.</p>																
8. Type of georesource																	
8.1. Structure	<table border="1"> <tr> <td>8.1.1. Sedimentary</td> <td></td> <td>8.2. Materials</td> <td>8.2.1. Minerals</td> </tr> <tr> <td>8.1.2. Tectonic</td> <td>x</td> <td></td> <td>8.2.2. Rocks</td> </tr> <tr> <td>8.1.3. Hydrological</td> <td></td> <td></td> <td>8.2.3. Fossils</td> </tr> <tr> <td>8.1.4. Geomorphological</td> <td>x</td> <td></td> <td>8.2.4. Soils</td> </tr> </table>	8.1.1. Sedimentary		8.2. Materials	8.2.1. Minerals	8.1.2. Tectonic	x		8.2.2. Rocks	8.1.3. Hydrological			8.2.3. Fossils	8.1.4. Geomorphological	x		8.2.4. Soils
8.1.1. Sedimentary		8.2. Materials	8.2.1. Minerals														
8.1.2. Tectonic	x		8.2.2. Rocks														
8.1.3. Hydrological			8.2.3. Fossils														
8.1.4. Geomorphological	x		8.2.4. Soils														
9. Educational functions	<p>Geo-interpretation may allow visitors to learn:</p> <ul style="list-style-type: none"> – about tectonics; – about changes in global climate and the dynamics of glacial times; – how a glacier can erode the surface and leave landforms; and – about weathering and landslides. 																
10. Geosciences promoted	<p>Geology Geomorphology Glaciology</p>																
11. Other information	<p>The Olivia river runs along the valley.</p> <p>Part of the valley is today occupied by shallow lakes and peatbogs. Trees 3.7 ka old were found in these bogs.</p> <p>Presence of birdlife and beavers that affect river flows.</p> <p>Viewpoint with interpretative sign and starting point of several trails.</p>																
12. References	<p>Sarandon (1997), Rabassa and Coronato (2005), Roig and Collado (2004)</p>																

Table 4 Georesource 3: Gable island data sheet

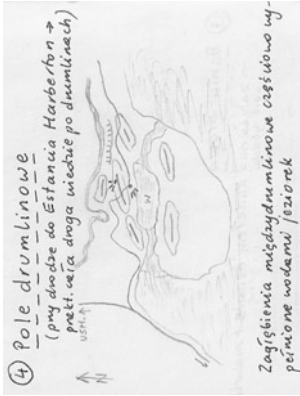

Georesource 3: "Gable island"	
1. Location	
1.1. Coordinates	54° 52' 18"S/67° 33' 43"W
1.2. Access	77 km from Ushuaia: 40 km along Route "3" (paved), 35 along Route "j" (dirt road) and 2 more km westwards along the Beagle Channel shore.
1.3. Management	Private. It is part of Estancia Harberton.
2. Physiographic features	
2.1. Dimensions	25 km ²
2.2. Altitude	0–92 m a.s.l.
3. Type of use	Observation.
4. Lithology	Bedrock is composed of metamorphosed sedimentary rocks, highly folded and deformed (Yahgán formation) and covered by Late Pleistocene glaciogenic sediments that are overlain by alluvial, aeolian and littoral sequences of Holocene age
5. Photograph	
5. Sketch	
	Gable Island from the sea Greyish (upper part), Darker layer, Channel (bottom)
6. Lithology	Bedrock is composed of metamorphosed sedimentary rocks, highly folded and deformed (Yahgán formation) and covered by Late Pleistocene glaciogenic sediments that are overlain by alluvial, aeolian and littoral sequences of Holocene age
6. Photograph	

(continued)

Table 4 (continued)

Georesource 3: "Gable island"				
7. Geodescription	This island is part of the Beagle Channel Islands affected by subglacial erosion and it corresponds to the first drumlin field described in Argentina, being composed of 70 drumlins and 5 rocky drumlins, which are up to 2.5 km long, 0.3 km wide and up to 92 m a.s.l high. The internal structure is composed of a lower basal till unit, an ice-contact stratified-drift glaciofluvial unit, a glacio-lacustrine unit and a glacially-reworked lacustro-till unit on top. The west facing drumlins suffer strong erosion by sea waves which leave a "gable" shape and gorges. The inter-drumlin depressions are occupied by mires, peatbogs and lagoons.			
8. Type of georesource				
8.1. Structure	8.1.1. Sedimentary	x	8.2. Materials	8.2.1. Minerals x
	8.1.2. Tectonic			8.2.2. Rocks x
	8.1.3. Hydrological			8.2.3. Fossils
	8.1.4. Geomorphological	x		8.2.4. Soils
9. Educational functions	Geo-interpretation may allow visitors to learn: – about changes in global climate and the dynamics of glacial times; and – about coastal landforms.			
10. Geosciences promoted	Geomorphology			
11. Other information	In the past, Estancia Harberton used to have cattle in the island.			
12. References	Rabassa et al. (1990), (2000), Coronato (2007), Coronato et al. (1999), Rabassa and Coronato (2007)			

Table 5 Georesource 4: Drumlin field data sheet



Georesource 4: "Drumlin field"	
1. Location	
1.1. Coordinates	54° 51' 17"S-67° 28' 19"W
1.2. Access	75 km from Ushuaia: 40 km along Route "3" (paved) and 35 along Route "j" (dirt road).
1.3. Management	Private.
2. Physiographic features	
2.1. Dimensions	25 km long
2.2. Altitude	From 0 to 100 m a.s.l
3. Type of use	Economic. Observation.
4. Lithology	Yaghán formation. Subglacial till deposits.
5. Sketch	
6. Photograph	
4. Drumlin field	(by the road to Estancia Harberton, the road goes across drumlins) Inter-drumlin depressions are partly filled by lakes [lower]

(continued)

Table 5 (continued)

Geosource 4: "Drumlin field"																					
7. Geodescription	Drumlins are both erosional and depositional subglacial landforms with an inverted-spoon shape that shows direction of ice flow. They typically appear in groups and were formed during the Pleistocene glaciation. The drumlins on the shore have a W-E direction while the drumlins at the mountain foot have a NW-SE direction. These different alignments indicate the existence of two ice lobes: the paleo-glacier Beagle and the paleo-glacier Lastfashaj. Several rivers traverse the field: Lasifashaj, Cambaerces, Varela, among others.																				
8. Type of geosource																					
8.1. Structure	<table border="1"> <tr> <td>8.1.1. Sedimentary</td> <td>x</td> <td>8.2. Materials</td> <td>8.2.1. Minerals</td> <td>x</td> </tr> <tr> <td>8.1.2. Tectonic</td> <td></td> <td></td> <td>8.2.2. Rocks</td> <td>x</td> </tr> <tr> <td>8.1.3. Hydrological</td> <td></td> <td></td> <td>8.2.3. Fossils</td> <td></td> </tr> <tr> <td>8.1.4. Geomorphological</td> <td>x</td> <td></td> <td>8.2.4. Soils</td> <td></td> </tr> </table>	8.1.1. Sedimentary	x	8.2. Materials	8.2.1. Minerals	x	8.1.2. Tectonic			8.2.2. Rocks	x	8.1.3. Hydrological			8.2.3. Fossils		8.1.4. Geomorphological	x		8.2.4. Soils	
8.1.1. Sedimentary	x	8.2. Materials	8.2.1. Minerals	x																	
8.1.2. Tectonic			8.2.2. Rocks	x																	
8.1.3. Hydrological			8.2.3. Fossils																		
8.1.4. Geomorphological	x		8.2.4. Soils																		
9. Educational functions	<p>Geo-interpretation may allow visitors to learn:</p> <ul style="list-style-type: none"> - about changes in global climate and the dynamics of glacial times; and - how glacial deposits look like. 																				
10. Geosciences promoted	Geomorphology																				
11. Other information	Presence of "flag" trees that show the prevailing direction of the wind (SW-NE).																				
12. References	Coronato et al. (2000), Rabassa et al. (1999), Rabassa and Coronato (2007), Arocena Bongioni (2002), Antonione (2006)																				

Table 6 Georesource 5: Bahía Cambaceres data sheet

Georesource 5: “Bahía Cambaceres”	
<p>1. Location</p> <p>1.1. Coordinates 54° 52' 17"S– 67° 17' 34"W</p> <p>1.2. Access 95 km from Ushuaia: 40 km along Route “3” (paved) and 55 along Route “j” (dirt road).</p> <p>1.3. Management Private.</p>	
<p>2. Physiographic features</p> <p>2.1. Dimensions It has a wide mouth of 830 m, whereas its penetration is around 1300 m.</p> <p>2.2. Altitude 0 m a.s.l.</p>	
<p>3. Type of use Recreation. Scientific.</p>	
<p>4. Lithology Yahgán formation: Early Cretaceous. Deep marine metamorphosed sedimentary rocks of marginal basin (black slate, tuff and sandstone).</p>	
<p>5. Sketch</p>  <p>Drumlin landscape continues (approximately 4 km to the east from Estancia Harberton), but the inter-drumlin depression is now a marine bay. Asymmetric rock knob (“roche moutonnee”) [lower left] Shoreline of a higher sea level stand, c. 3 m [lower right]</p>	
<p>6. Photograph</p> 	
<p>7. Geodescription</p> <p>Inter-drumlin depression with NW–SE direction. Separated from the Bahía Varela through a peninsula and connected by a 50-m-wide tombolo.</p> <p>Ice-moulded bedrock hills around the bay.</p> <p>Marine clear water with an average temperature of 6.5 °C and a tidal range of 1.16 m.</p> <p>Uplifted Holocene beaches.</p>	

(continued)

Table 6 (continued)

Georesource 5: “Bahía Cambaceres”					
8. Type of georesource					
8.1. Structure	8.1.1. Sedimentary		8.2. Materials	8.2.1. Minerals	
	8.1.2. Tectonic			8.2.2. Rocks	x
	8.1.3. Hydrological	x		8.2.3. Fossils	
	8.1.4. Geomorphological	x		8.2.4. Soils	
9. Educational functions	Geo-interpretation may allow visitors to learn: <ul style="list-style-type: none"> – about changes in global climate and the dynamics of glacial times; – about major changes in the sea level; – how tides affect shores; and – about coastal landforms. 				
10. Geosciences promoted	Geomorphology				
11. Other information	Presence of molluscs, algae and marine birdlife. Archaeological sites dated back to 8000 years ago, on the shore and higher old beaches. Natural shelter for sailboats.				
12. References					
Borla (1995), Coronato et al. (1999)					

Panels add valuable information to traditional itineraries, and they are an excellent complement to tour guides, who can use these posters as a practical and attractive tool to report on geological topics. At the same time, the involvement of different stakeholders enables a fundamental objective: to disseminate and promote the conservation of geological heritage (Miranda et al. 2011).

Apart from the interpretative panels that could be arranged in each of the six georesources described, we propose the following initiatives:

– Georesource 1: “Beagle Channel”

A bike and trekking path could be designed connecting different bays along the northern shore of the channel. In the path, different stopovers could include posters explaining landscape formation as well as quotations from explorers and scientists of the area, such as Charles Darwin, who described the Beagle Channel as a beautiful sheet of water surrounded by mountains, rounded and not very high, of clayey shale, covered by a dense forest (Darwin 2006).

– Georesource 4: “Drumlin field”

An interpretation centre could be built, including different rooms dedicated to the evolution of the Fuegian landscapes, such as the formation of the Andes, the Last Glaciation and the current interglacial time. Information about climate changes and glacial landforms should be given. This would be the first inter-drumlin interpretation centre in the world and could offer services like stores, bookshops and coffee-shop, among others.

Table 7 Georesource 6: Harberton peatbog data sheet

Georesource 6: "Harberton peatbog"		5. Sketch
1. Location		
1.1. Coordinates	54° 52' 54"S/67° 13' 43"W	
1.2. Access	100 km from Ushuaia: 40 km along Route "3" (paved) and 60 along Route "j" (dirt road).	
1.3. Management	Private.	
2. Physiographic features		
2.1. Dimensions	0.4 km × 0.2 km	
2.2. Altitude	25 m a.s.l.	
3. Type of use	Scientific.	
4. Lithology	Holocene peat that occupies a bedrock hollow excavated in rocks belonging to the Yaghán formation, Early Cretaceous.	

6. Photograph



7. Geodescription	Inter-drumlin depression occupied by about 11 m of <i>Sphagnum sp.</i> peatbog, without external drainage and circular shape. The base of bog was dated to 14.8 ka B.P. Paleo-climatic and environmental research resource.		
-------------------	---	--	--

8. Type of georesource

8.1. Structure	8.1.1. Sedimentary		8.2. Materials	8.2.1. Minerals	x
	8.1.2. Tectonic			8.2.2. Rocks	
	8.1.3. Hydrological	x		8.2.3. Fossils	
	8.1.4. Geomorphological	x		8.2.4. Soils	x

(continued)

Table 7 (continued)

Georesource 6: “Harberton peatbog”	
9. Educational functions	Geo-interpretation may allow visitors to learn: – about changes in global climate; and – how a glacial depression can be occupied by peatbogs.
10. Geosciences promoted	Geomorphology Geology
11. Other information	Oldest peatbog studied in Tierra del Fuego.
12. References	
Roig (2004), Rabassa et al. (2005), Roig and Roig (2007), Arocena Bongiorno (2002)	

– Georesource 6: “Harberton peatbog”

Special visits with local scientists could be arranged to this locality in order to let visitors walk on the peatbog. Together with the specialists, interpretation of the available data could promote better understanding of natural events, which could be used for scientific research. Thematic panels explaining the importance of bogs should include information on how paleoclimate history can be rebuilt after studying this georesource.

Migoñ (2010, p. 9) explained that “... natural scenery, which is essentially a combination of landforms of different sizes, shapes, origins, and ages, can be captivating”. However, and according to Manosso (2012), some natural resources are not easily seen by visitors, but with this type of scientific intermediation they can become visible and decoded. Turning a traditional visit into a geotourist one could overcome this difficulty. How? Through specific background research, at both the theoretical and application levels (Reynard 2008). Geology and Geomorphology appear to be the most suited sciences to achieve this, since “... where an untrained eye sees mainly the beauty of a physical landscape, geomorphologists go a step further, trying to answer how and why such a natural beauty has come into being” (Migoñ 2010, p. 9).

Using science for geo-interpretation must be seen as an opportunity to enrich the experience of both residents and visitors, giving them the chance to learn and understand physical natural processes, which would definitely make tourists appreciate better the Fuegian landscapes and lead to a more conservationist look. Moreover, through the implementation of the proposed initiatives, visitors would be informed and educated about local heritage, and this would probably reinforce the identity of the residents. This transect could be a proper scenery for academic practices where scientific knowledge would be spread. Approaching visitors to Earth Sciences could even awaken scientific talents.

Furthermore, since the existence of the first Fuegian geotourist itinerary could draw attention of more visitors, not only it would broaden the local tourist offer, but also alleviate other tourist saturated areas such as Tierra del Fuego National Park.

Besides, if this transect becomes a geotourist one, conservation and maintenance practices should be carried out, keeping roads in a good state, designing new paths, arranging panels and brochures. All these could derive into the generation of new local workforce.

When referring to Patagonia (and Tierra del Fuego is included) Rabassa (2008) said: “Being a land of adventure, mystery and opportunity, it is one of the least populated regions in the world and the southernmost territories with temperate continental ecosystems. It is today a chosen destination by thousands of tourists that flock from all over the world, searching for the well-promoted Patagonian enchantments”. Geotourism could definitely take advantage of these strengths.

6 Conclusions

Geographical, geological and geomorphological settings of Tierra del Fuego make it an attractive geotourist destination.

Following Reynard (2008), “by definition leisure is central for tourists. On the other hand, geotourism has among its objectives the education of Earth Sciences. The challenge is, therefore, to develop tools that combine these two aspects, leisure and education, to disseminate knowledge on geosciences towards a large public” (Reynard 2008, p. 228).

It is believed that through this geotourist itinerary in Southern Tierra del Fuego, science and leisure could be linked in a way that the forms of enhancement proposed are addressed in order to take advantage of the educational functions of each site, as well as to promote conservation, dissemination of scientific disciplines and generation of economic activities.

Taking the transect Ushuaia-Estancia Harberton and focusing on natural scenery does not necessarily mean that geotourism is practiced. However, it is assumed that this route could be turned into a geotourist itinerary if special services and facilities were organized in order to provide an enriched experience to visitors through the initiatives proposed and other innovative proposals to develop Earth Sciences and to promote sustainable economic activities involving the local population. All these would not only value each georesource as a concrete spatial unit but the whole transect between Ushuaia and Estancia Harberton, generating a sustainable development opportunity.

References

- Antonione G (2006) La genesi del drumlin tardo pleistocenicic nell’analisi geomorfologica di Estancia Harberton (Terra del Fuoco, Argentina). Unpublished Graduation Thesis in Physical Geography, Università degli Studi di Trieste, Facoltà di Scienze Matematiche, Fisiche e Naturali, Trieste, Italy, 155 pp
- Arocena Bongiorni M (2002) Atlas de la Provincia de Tierra del Fuego, Antártida e Islas del Atlántico Sur. Gobierno de Tierra del Fuego, Subsecretaría de Planeamiento. Ushuaia, Argentina, 37 pp

- Bird J (2003) An updated digital model of plate boundaries. *J G³*, 4(3):52 pp
- Borla M (1995) Relevamiento de recursos turísticos desde el punto de vista del ecoturismo a lo largo de las rutas nacionales 3 y J -Departamento Ushuaia, Tierra del Fuego. Final Report. Beca Legislatura de Tierra del Fuego. Ushuaia, Argentina, 253 pp
- Borla M, Vereda M (2001) Explorando Tierra del Fuego. Manual del viajero en el fin del mundo. Zagier & Urruty Publications, Buenos Aires, Argentina, 416 pp
- Bujalesky G (2007) Coastal geomorphology and evolution of Tierra del Fuego (Southern Argentina). *Geol Acta* 5(4):337–362
- Bujalesky G, Coronato A, Rabassa J, Acevedo R (2008) El Canal Beagle. Un ambiente esculpido por el hielo. In: SEGEMAR, 2008. “Sitios de Interés Geológico de la República Argentina. Los geólogos nos cuentan”. Ed. SCIGA, Anales 46, Buenos Aires, Argentina, pp 849–864
- Carcavilla L, López Martínez J, Durán Valsero J (2007) Patrimonio Geológico y Geodiversidad: investigación, conservación, gestión y relación con los espacios naturales protegidos. Cuadernos del Museo Geominero N°7, Instituto Geológico y Minero de España, 360 pp
- Carcavilla L, Belmonte A, Durán J, Hilario A (2011) Geoturismo: concepto y perspectivas en España. *Revista Enseñanza de las Ciencias de la Tierra de la AEPECT* (19.1), España, pp 81–94
- Coronato A (2007) El paisaje de Tierra del Fuego. In: Godoy Manríquez JC (ed) *Patagonia Total, Antártida e Islas Malvinas*. Alfa Centro Literario, BarcelBaires Ediciones, Buenos Aires, Argentina, pp 601–617
- Coronato A (2014) Territorios fueguinos: fisonomía, origen, evolución. In: Oría J and Tivoli A (eds) *Cazadores de mar y tierra. Estudios recientes en arqueología fueguina*. Editorial Cultural Tierra del Fuego, Ushuaia, Argentina, pp 43–63
- Coronato A, Salemme M, Rabassa J (1999) Paleoenvironmental conditions during the early peopling of Southernmost South America (Late glacial—early holocene, 14–18 ka B.P.). *Quatern Int* 53–54:77–92 (Elsevier)
- Cunningham W, Klepeis K, Gose W, Dalziel I (1991) The Patagonian Orocline: new paleomagnetic data from the Andean magmatic arc in Tierra del Fuego, Chile. *J Geophys Res* 96(B10):16061–16069
- Darwin C (2006) *Diario de la Patagonia. Notas y reflexiones de un naturalista sensible*. Editorial Continente, Buenos Aires, Argentina, 144 pp
- Diraison M, Cobbold P, Gapais D, Rossello E, Le Corre C (2000) Cenozoic crustal thickening, wrenching and rifting in the foothills of the southernmost Andes. *Tectonophysics* 316(1–2):91–119
- Dowling R, Newsome D (2010) *Global geotourism perspectives*. Goodfellow Publishers Ltd., Oxford, United Kingdom, 250 pp
- Fildani A, Hessler A (2005) Stratigraphic record across a retroarc basin inversion: Rocas Verdes Magallanes Basin, Patagonian Andes. *Geol Soc Am Bull* 117:1596–1614
- Ghiglione M, Ramos V (2005) Chronology of deformation in the southernmost Andes of Tierra del Fuego. *Tectonophysics* 405:25–46
- González Guillot M (2012) Breve historia de las montañas en Tierra del Fuego. *Revista La Lupa*, 2 (3):3–9. Ushuaia, Argentina
- Hose T (1995) Selling the story of Britain’s Stone. *Environmental interpretation* 10(2):16–17
- Hose T (2012) 3 g’s for geotourism. *Geoheritage* 4(1):7–24
- Klepeis K, Austin J (1997) Contrasting styles of superposed deformation in the Southernmost Andes. *Tectonics* 16(5):755–776
- Klepeis K, Betka P, Clarke G, Fanning M, Hervé F, Rojas L, Mpodozis C, Thomson S (2010) Continental underthrusting and obduction during the cretaceous closure of the Rocas Verdes rift basin, Cordillera Darwin, Patagonian Andes. *Tectonics* 29(3):24 pp
- Kraemer P (2003) Orogenic shortening and the origin of the Patagonian orocline (56°S. Lat). *J S Am Earth Sci* 15:731–748
- Lodolo E, Menichetti M, Bartole R, Ben-Avraham Z, Tassone A, Lippai H (2003) Magallanes-Fagnano continental transform fault (Tierra del Fuego, southern-most South America). *Tectonics* 22(6):1076, 28 pp

- Manosso F (2012) Potencial del geoturismo y la geodiversidad en la Serra do Cadeado, Paraná, Brasil. *Estudios y Perspectivas en Turismo* 21:332–338
- Coronato A, Martínez, O, Rabassa J (2004) Glaciations in Argentine Patagonia, southern South America. In: Ehlers J, Gibbard P (eds) *Quaternary glaciations—extent and chronology*, part IT1. Elsevier, pp 49–67
- Martínez Fernández M (2013) Invitación al Geoturismo. Reflexiones sobre geodiversidad y potencial geoturismo en la Patagonia Argentina. *Boletín Geográfico*, 34(35):61–78
- Mendoza L, Perdomo R, Hormaechea J, Del Cogliano D, Fritsche M, Richter A, Dietrich R (2011) Present-day crustal deformation along the Magallanes-Fagnano fault system in Tierra del Fuego from repeated GPS observations. *Geophys J Int* 184(3):1009–1022
- Migoñ P (ed) (2010) *Geomorphological landscapes of the world*. Springer, 374 pp
- Millán Escriche M (2011) La función didáctica del geoturismo. Propuestas para la región de Murcia. *Revista de Investigaciones Turísticas Gran Tour* 4:62–93. Universidad de Murcia, Spain
- Miranda F, Pereyra F, Lema H, Aguilar J (2011) Los paneles temáticos como herramienta del geoturismo: el caso de San Pedro, provincia de Buenos Aires, Argentina. I Simposio de Geoparques y Geoturismo en Chile. Melipeuco, Chile, (CD-ROM), pp 91–94
- Newsome D, Dowling R (2006) *Geotourism*. Elsevier, 259 pp
- Olivero E, Malumíán N (2007) Mesozoico-Cenozoico stratigraphy of the Fuegian Andes, Argentina. *Geol Acta* 6(1):5–18
- Olivero E, Martinioni D (2001) A review of the geology of the Argentinian Fuegian Andes. *J S Am Earth Sci* 14:175–188
- Ollier C (2012) Problems of geotourism and geodiversity. *Quaestiones Geographicae* 31(3): 57–61. Bogucki Wydawnictwo Naukowe, Poznań
- Rabassa J (ed) (2008) *The late cenozoic of Patagonia and Tierra del Fuego. Developments in quaternary science* 11. Elsevier, 513 pp
- Rabassa J, Clapperton C (1990) Quaternary glaciations of the Southern Andes. *Quatern Sci Rev* 9 (2/3):153–174
- Rabassa J, Coronato A (2005) Descripción del sitio (Localidad 19: Valle Carbajal). In: *Guía de campo. III Curso de campo en geomorfología y geología del Cuaternario de Tierra del Fuego*. CADIC-CONICET. Ushuaia, Argentina
- Rabassa J, Coronato A (2007) Glaciaciones del Cenozoico tardío en los Andes Patagónico-Fueguinos. In: Godoy Manríquez JC (ed) *Patagonia Total, Antártida e Islas Malvinas*. Alfa Centro Literario, BarcelBaires Ediciones. Buenos Aires, Argentina, 644–663 (1088 pp)
- Rabassa J, Serrat D, Martí C, Coronato A (1990) Internal structure of drumlins in Gable Island, Beagle Channel, Tierra del Fuego, Argentina. *LUNDQUA report*. Lund, 32, 3–5
- Rabassa J, Coronato A, Bujalesky G, Salemme M, Roig C, Meglioli A, Heusser CJ, Gordillo S, Roig F, Borrromei A, Quattocchio M (2000) Quaternary of Tierra del Fuego, southernmost South America: an updated review. *Quatern Int* 68–71, 217–240 (Elsevier)
- Rabassa J, Coronato A, Salemme M (2005) Chronology of the late cenozoic Patagonian glaciations and their correlation with biostratigraphic units of the Pampean region. *J S Am Earth Sci* 20:81–103
- Rabassa J, Coronato A, Martínez O (2011) Late Cenozoic glaciations in Patagonia and Tierra del Fuego: an updated review. *Biol J Linn Soc* 103:316–335
- Rapalini A, Peroni J, Luppo T, Tassone A, Cerredo M, Esteban F, Lippai H, Vilas F (2015) Palaeomagnetism of Mesozoic magmatic bodies of the Fuegian Cordillera: implications for the formation of the Patagonian Orocline. In: Pueyo E, Cifelli F, Sussman A, Oliva-Urcia B (eds) *Palaeomagnetism in fold and thrust belts: new perspectives*. Geological Society, London, Special Publications, 425, 16 pp
- Reynard E (2008) Scientific research and tourist promotion of geomorphological heritage. *Geografia Fisica e Dinamica Quaternaria* 31:225–230

- Roig C (2004) Antecedentes sobre turberas en Tierra del Fuego. In: Blanco D, De La Balze V (eds) Los turbales de la Patagonia. Bases para su inventario y la conservación de su biodiversidad. *Wetlands International*, 19, 33–44 (149 pp)
- Roig C, Collado L (2004) Ventana n° 6: Carbajal-Tierra Mayor. In: Blanco D, De La Balze V (eds) Los turbales de la Patagonia. Bases para su inventario y la conservación de su biodiversidad. *Wetlands International*, 19, 62–71 (149 pp)
- Roig C, Roig F (2007) Turberas de Tierra del Fuego. In: Godoy Manríquez JC (ed) *Patagonia Total, Antártida e Islas Malvinas*. Alfa Centro Literario, BarcelBaires Ediciones, Buenos Aires, Argentina, 773–781 (1088 pp)
- Ruchkys U (2007) Patrimônio Geológico e Geoconservação no Quadrilátero Ferrífero, Minas Gerais: potencial para criação de um geoparque da UNESCO. Unpublished doctoral thesis, Instituto de Geociências, Universidade Federal de Minas Gerais, Belo Horizonte, Brazil, 211 pp
- Sadry B (2009) Fundamentals of geotourism: with emphasis on Iran. Samt Organization Publishing, Tehran 220 pp
- Sarandon R (1997) Evaluación ambiental regional de la normativa de usos para los Valles Tierra Mayor y Olivia. Análisis de los aspectos de fragilidad ecológica (Provincia de Tierra del Fuego). Consejo Federal de Inversiones (CFI). Secretaría de Planeamiento y Desarrollo Provincia de Tierra del Fuego, Unpublished technical report, 109 pp
- Schwarz S (2009) Análisis de potencialidad de geositios para la conformación del Geoparque Andes Fueguinos. Unpublished Graduation Thesis in Tourism, Facultad de Humanidades y Ciencias Sociales, Universidad Nacional de la Patagonia San Juan Bosco, Sede Ushuaia. Biblioteca Universidad Nacional de Tierra del Fuego, Ushuaia, p 159
- Schwarz S (2016) Recursos paisajísticos naturales de las zonas centro y norte de Tierra del Fuego como objeto de desarrollo turístico. PhD Thesis in preparation
- Schwarz S, Coronato A, Acevedo R (2011) Geositios en los Andes Fueguinos: una metodología de análisis de potencialidad. XVIII Congreso Geológico Argentino, Actas, CD Rom, Neuquén, Argentina, pp 1252–1253
- Schwarz S, Coronato A, Acevedo R (2013) Los geoparques y las áreas naturales protegidas fueguinas: Tierra del Fuego como escenario para la geoconservación. I Simposio Argentino de Patrimonio Geológico, Geoparques y Geoturismo, and III Encuentro Latinoamericano de Geoparques, Actas, 57–58. San Martín de los Andes
- Smalley R, Kendrick E, Bevis M, Dalziel I, Taylor F, Lauría E, Piana E (2003) Geodetic determination of relative plate motion and crustal deformation across the Scotia-South America plate boundary in eastern Tierra del Fuego. *Geochem Geophys Geosyst (G³)* 4(9):19 pp
- Smalley R, Dalziel I, Bevis M, Kendrick E, Stamps D, King E, Taylor F, Lauría E, Zakrajsek A, Parra H (2007) Scotia arc kinematics from GPS geodesy. *Geophys Res Lett* 34(21):6 pp
- Stern C, De Witt M (2003) Rocas Verdes ophiolites, southernmost South America: remnants of progressive stages of development on oceanic-type crust in a continental margin back-arc basin. In: Dilek Y, Robinson P (eds) *Ophiolites in earth history*. Geological Society, London, Special Publications, 218, pp 665–683
- Torres Carbonell P, Dimieri L, Olivero E (2011) Progressive deformation of a Coulomb thrust wedge: the eastern Fuegian Andes thrust-fold belt. In: Poblet J, Lisle R (eds) *Kinematic evolution and structural styles of fold-and- thrust belts*. Geological Society, London, Special Publications, 349, pp 123–147

Soil–Geomorphology Relationships in the Pichiñán Uraniferous District, Central Region of Chubut Province, Argentina

Pablo J. Bouza, Claudia Saín, Lina Videla, Patricia Dell’Arciprete,
Estela Cortés and Julio Rua

Abstract The aim of this work was to perform a baseline study about pedologic components of the geomorphic surfaces of different origins in a sector of the *Cerro Solo* uranium ore deposit, situated in the arid central region of the province of Chubut, Argentina. This contribution was requested by the National Atomic Energy Commission of Argentina (CNEA). The geomorphological units identified in the study area were: (1) Exhumed planation surfaces, composed of rounded hills of mesosiliceous-basic volcanic rocks of Middle Jurassic age; (2) Pedisediments, consisting of four Early Pleistocene alluvial terrace levels; (3) Pediment association levels carved on the continental Cretaceous sediments; (4) Alluvial fan relicts, with three geomorphic surfaces; (5) Modern alluvial fans, composed of two coalescent alluvial fans, and (6) Alluvial plains and associated wetlands (locally known as *mallines*). The latter are located in restricted areas where the water table is discharged at the thalweg sectors of the channels. The soil parent materials are free of carbonates (e.g., alluvial

P.J. Bouza (✉) · C. Saín · L. Videla · E. Cortés

Instituto Patagónico para el Estudio de los Ecosistemas Continentales (IPEEC),
CONICET, CCT CENPAT, Boulevard Brown 2915, CP 9120 Puerto Madryn,
Chubut, Argentina

e-mail: bouza@cenpat-conicet.gob.ar

C. Saín

e-mail: saín@cenpat-conicet.gob.ar

L. Videla

e-mail: videla@cenpat-conicet.gob.ar

E. Cortés

e-mail: guadalup@cenpat-conicet.gob.ar

P. Dell’Arciprete

Centro para el Estudio de Sistemas Marinos (CESIMAR), CONICET,
CCT CENPAT, Boulevard Brown 2915, CP 9120 Puerto Madryn,
Chubut, Argentina

e-mail: dellaop@cenpat-conicet.gob.ar

J. Rua

Centro Científico Tecnológico Centro Nacional Patagónico (CCT CENPAT),
CONICET, Boulevard Brown 2915, CP 9120 Puerto Madryn, Chubut, Argentina

e-mail: bocha@cenpat-conicet.gob.ar

© Springer International Publishing AG 2017

J. Rabassa (ed.), *Advances in Geomorphology and Quaternary Studies
in Argentina*, Springer Earth System Sciences,

DOI 10.1007/978-3-319-54371-0_3

origin) and their origin could be allochthonous, mainly by aeolian influx. These soils were classified as Calcids soil suborder, and their differences are due to the different development degree of calcretization and polygenesis. The soils developed on pediments have a varied morphology and soil types depending on the age of geomorphic surface and the degree of polygenesis, this last resulting from the alternation of morphogenesis periods with pedogenic periods. The soils more developed were classified as Natrargids and Haplargids, whereas the oldest are truncated and were classified as Haplocalcids. The soils of the younger level were classified as Torriorthens. The soils formed on alluvial plains were classified as Torrifuvents.

Keywords Aridisols · Geomorphic surfaces · Exhumation planation surfaces · Pediment association · Pedisediment levels · Alluvial fans · Patagonia · Argentina

1 Introduction

The landscape of the Sierra de Pichiñán area (Fig. 1), as well as the Extra-Andean Patagonia region, is characterized by severe arid conditions. Low rainfall rate and sparse vegetation cover are typical features of arid regions and are of considerable importance for the operation and development of landforms (Thomas 1997).

Although wind is an important geomorphological agent that has deeply modified the arid region landscapes, water erosion due to short- and high-intensity rainfalls is the most intense geomorphic process in the Sierra de Pichiñán area, either as raindrop splash, surface runoff (interrill erosion) or as concentrated flow erosion, in the form of rills and badlands. Many of these landforms have large patches of bare soils (desert pavements and surface soil crusts) and thus they are exposed to wind erosion, raindrop impact, and surface runoff.

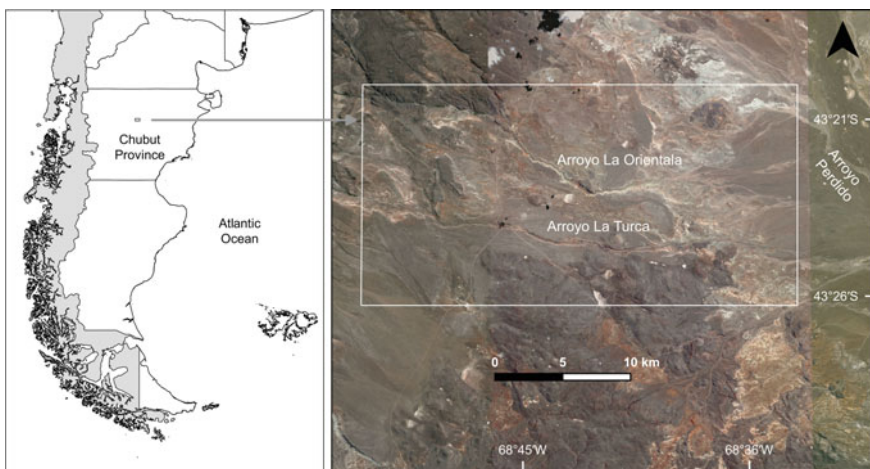


Fig. 1 Study area of Sierra de Pichiñán

Also, the scarcity of available water seems to be the limiting factor not only for plants, but also for soil formation. Chemical weathering, clays formation, translocation of particles, and ionic solutions should not occur under these conditions, and only weakly developed Entisols (Soil Survey Staff 1999) should be in the region. However, strongly differentiated soil profiles appear in these areas. These could be explained if soils processes are related to relict features of colder or wetter climates of the past (Nettleton and Peterson 1983) or if they could be attributed to the seasonally marked extreme rainfall years occurring in the present thus producing deep leaching (Buol et al. 1990). In restricted areas strongly differentiated soil profiles could be also explained in response to local dominant factors that are independent of the effect of climate and vegetation (intrazonal soils). Examples of the last are hydromorphic soils of on wetlands locally named *mallines* (Aquets).

The soil–geomorphic research emphasizes the relation between soil properties, soil development, landscape form, and geomorphic processes. Olson (1989) considers that a research in soil–geomorphology requires three investigative aspects: (1) knowledge of the surficial stratigraphy, (2) the geomorphic surface defined in time and space (Rhue 1975), and (3) correlation of soil properties to landscape feature.

In this regard, studies on soil–geomorphology relationship have used geomorphic surface concept in the context related to soil age and landscape position (Gile et al. 1981). The geomorphic surface is a unit that may be mapped and which includes a number of landforms and landscapes. This surface may be erosional or constructional and is often a combination of both (Daniels et al. 1971).

In this framework, soil–geomorphology relationship will deepen topics of interest for use as: (1) Quaternary geology (soil chronosequences and paleosols), (2) geo-ecology (vegetation distribution patterns and soil–plant relationships), and (3) soil degradation.

The aim of this work was to perform a baseline study on pedologic components of geomorphic surfaces of different origins in a sector of the *Cerro Solo* uranium ore deposit, situated in the central region of the province of Chubut. This contribution was requested by the National Atomic Energy Commission of Argentina (CNEA).

1.1 Study Area

The study region (Fig. 1) covers an area of 267 km², which is considered potentially susceptible of receiving the impacts of mining and covering the main geomorphological units of geo-ecological interest.

The oldest rocks that crop out are the Lonco Trapial Formation (Lesta and Ferello 1972) of Middle Jurassic age (Bajocian–Bathonian), composed of mesosiliceous-basic volcanic rocks, mainly lava flow facies accompanied by tuffaceous facies (Proserpio 1987). This volcanism precedes the Atlantic Ocean opening and corresponds to a wide extensional province covering a continental intraplate region (Aguilera et al. 2010). This geological unit crops out in the south-central and northeast of the study area.

Between these volcanic outcrops, an extended erosion landscape is developed. It is constituted by sedimentary rocks of fluvial and pyroclastic origin of the Chubut Group (Barremian–Santonian; Figari and García 1992). The Chubut Group is composed of the Los Adobes Formation (fluvial sediments; Early Albian) and the Cerro Barcino Formation (pyroclastic rocks; Aptian–Albian?). This latter is the geological unit with larger distribution in the area (Marveggio and Llorens 2013).

The continental Cretaceous rocks are buried by Pleistocene gravels and sandstone deposits, forming relict landforms both as plains with a plateau shape or alluvial piedmonts. This geological unit was assigned to the Renguenao Formation (Berizzo 1976) of Early Pleistocene age (Nullo 1983) and its genesis is related to pedisediments and old alluvial plains widely distributed in the area.

The climate of this area is cold and dry with an important annual oscillation. The rainfall is only 200 mm/a. January temperatures average is 19 °C, whereas on July the average is 3 °C. Absolute maximum and minimum are 38.3 and −24.2 °C, respectively (1981–1990 average, Servicio Meteorológico Nacional, SMN). The temperature and moisture regime for the relieved area are mesic and aridic, respectively (Beeskow et al. 1987).

1.2 Methodology

The geomorphic surfaces were defined by digitalization on screen from satellite images and aerial photographs analysis (1:60,000; Instituto Geográfico Nacional, www.ign.gob.ar). Cartographic adjustments were performed by means of field control.

The present work follows a hierarchical classification adapted from Peterson (1981) that uses the geographic scales, genetic relationships and shapes of the topographic forms. A geomorphological unit is the landform defined by morphogenetic criteria such as relict landforms. Relict landforms comprise remaining parts of a same geomorphic surface which has been otherwise degraded by erosion. An erosional relict must be older than the destructive erosion cycle. Recognition of relict geomorphic surfaces is the basic tool for establishing relative ages of the different surfaces. Landform elements are used to separate different geomorphic processes observed within a unit (e.g., nebkas, aeolian pans, and discontinuous patches of desert pavements). Landform elements are normally not represented in regional maps but mapped only at high-scale surveys.

Descriptions of the morphological soil profile and the sampling of the soil horizons were based on fifty-four soil pits following the criteria of Schoeneberger et al. (2002). Another seven soil pits were performed as soil control profiles (Fig. 2). The classification of the soils was according to the Soil Survey Staff (1999). Each soil sample was air-dried and screened (2 mm mesh size) to separate the gravel and estimate its percentage. In the finer earth fraction, the physical and chemical properties were determined using methods suggested by the US Salinity Laboratory Staff (1954), Page et al. (1982), and Klute (1986).

Sampling sites for vegetation types were selected through aerial photographs of scale 1:60,000. In each area of 2500 m² (50 m × 50 m), dominant communities and perennial species were registered. The abundance was estimated using the method proposed by Braun-Blanquet (1979).

2 Soil–Geomorphic Relationship: Origin and Pedogenic Features

The landscape in the study area is strongly expressed by a combination of the arid conditions, soil parent materials, and vegetation.

The fluvial process is the dominant geomorphic processes, although at present it is only manifested by the ephemeral action of the Arroyo La Turca and La Oriental (“arroyo” = creek) (Fig. 1). These two streams are tributaries of the Arroyo Perdido, located east and out of the study area.

In the surrounding area of the Cerro Solo ore deposits, the geomorphological units identified were: (1) Exhumed planation surfaces, (2) Pedisediment levels, (3) Pediment associations, (4) Alluvial fan relicts, (5) Modern alluvial fans, and (6) Alluvial plains and associated wetlands (*mallines*) (Fig. 2).

Geomorphic surfaces from pedisediment levels, pediment associations, alluvial fan relicts, and modern alluvial fans were distinguished (Fig. 2). Furthermore, small

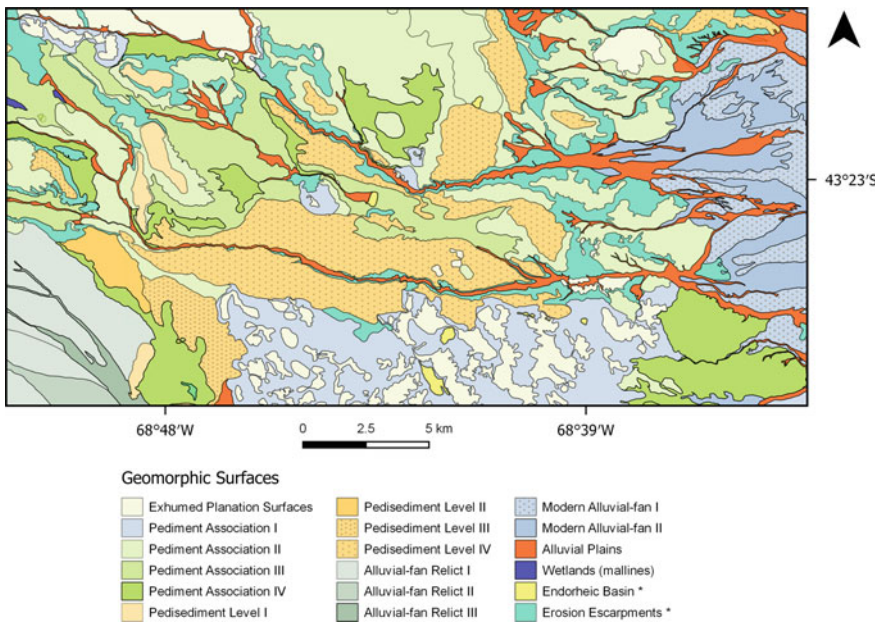


Fig. 2 Geomorphic surface of study area

endorheic basins and erosion escarpments were recognized in most geomorphological units. Geomorphic surfaces were identified by a Roman number according to the descending order of relative age on the basis of two relative age parameters: morphostratigraphic position and soil profile development.

The most important diagnostic horizons observed in Aridisols of the study area were: argillic, natric, calcic, petrocalcic, and gypsic. The physical and chemical properties of selected representative soil profiles are shown in Table 1.

Since the soil parent materials of the exhumed planation surfaces, pedisediment levels, alluvial fan relicts, and modern alluvial fans are free of carbonates and since the Ca^{2+} released during weathering is not adequate to explain the CaCO_3 content in the soils, this mineral must have an allochthonous origin, mainly by aeolian influx. These carbonates were dissolved and redistributed in the soils by leaching water at determined depth where a new carbonate (pedogenic) was precipitated by evaporation (Fig. 3).

2.1 Exhumed Planation Surfaces

These landforms correspond to Gondwana paleosurfaces and is the result of deep chemical weathering and/or pedimentation processes, occurred in very stable tectonic environments and mostly under hypertropical climates, extremely wet, extremely arid, or seasonally changing (Rabassa et al. 2010, 2014).

In the study area, the exhumed planation surfaces are recognized by their rounded hills of mesosiliceous volcanic rocks from the Lonco Trapial Formation (Fig. 4a).

The soils are shallow with large amount of coarse and sharp rocky fragments. However, soils show signs of color changes and petrocalcic crusts between rock fragments. On the southern rocky outcrop, Calcic Lithic Petrocalcids occurred, with A-Bwk-2Bkm/R-R horizon sequence (profile 29; Fig. 4a). The vegetation is a shrub steppe community composed by *Nardophyllum obtusifolium*, *Nassauvia glomerulosa*, *Prosopis denudans*, *Lycium ameghinoi*, and *Atriplex lampa*.

On the other hand, in the northeastern part of the study area, Lithic Torriorthents were developed with an A-Bw/R-R horizon sequence (Profile 41; Fig. 4b). The vegetation is composed by a shrub steppe of *Mulguraea ligustrina*, *Senecio flaginoides*, *Mullinum spinosum* and *Nassauvia glomerulosa*.

2.2 Pedisediment Levels

A pedisediment is a sedimentary layer (alluvial deposit), eroded from the shoulder and back slope of an erosional slope that lies on and is, or was, being transported across a pediment (Peterson 1981). This geomorphological unit consists of at least

Table 1 Soil properties of selected soil profiles

Horizons	Depth (cm)	Color (dry)	Structure ^a	Boundary ^a >2 mm (%)	Clay	Silt (%)	Sand (%)	EC ^b (dSm ⁻¹)	pH (1.2, 5)	CEC ^b (cmol/kg)	CaCO ₃ (%)	SOM ^b Soluble salts (%)					ESP (%)					
												Na ⁺	K ⁺	Ca ⁺	Mg ²⁺	Cl ⁻		CO ₃ ²⁻	HCO ₃ ⁻	SO ₄ ²⁻		
Exhumed planation surfaces, Calcic Lithic Petrocalcids, profile 29																						
A	0-2	10YR 5/3	sg	ai	21	8.4	49.7	41.9	0.7	8.1	32.2	4.4	2.15	1.2	17.2	12.8	3.3	0.6	0.1	2.4	8.3	0
Bwk	2-25	7.5YR 5/6	sbk, m, 2	aw	15	23.1	49.1	27.8	0.4	8.6	40.9	15.8	1.68	1.0	4.6	8.0	1.0	0.2	0.0	1.6	6.5	0
2Bkm/R	25-44	7.5YR 8/2	pl, m, 3	ai	36	12.5	48.8	38.6	0.4	9.0	13.5	88.1	nd	2.0	1.9	4.9	1.4	0.3	0.2	1.4	6.4	0
2Ck/R	44-70	7.5YR 8/2	sg	ai	45	21.1	27.1	51.8	0.4	9.0	17.4	71.4	nd	2.0	3.1	4.1	2.0	0.2	0.1	1.3	5.7	0
R	>70	Rock fragments from LT F																				
Exhumed planation surfaces, Lithic Torriochents, profile 41																						
A	0-11	10YR 5/3	gr, m, 1	aw	48	26.5	30.8	42.8	0.4	7.5	48.3	1.3	1.84	2.1	0.3	5.5	3.3	0.3	0.0	1.2	4.1	0
Bw/R	11-38	7.5YR 5/6	sbk, m, 1	ai	70	16.0	33.3	50.7	0.3	7.4	58.3	1.6	nd	2.8	0.2	5.3	4.0	0.3	0.0	1.0	3.3	0
R	>38	Rock fragments from LT F																				
Pedisestment level I, Typic Haplocalcid profile 33																						
A1	0-6	10YR 6/3	sg	as	17	22.2	15.3	62.5	0.3	7.1	25.7	1.2	1.01	0.4	16.5	4.5	4.0	0.2	0.0	1.3	4.4	0
A2	6-24	10YR 4/4	sbk, m, 2	ai	9	21.7	28.1	50.2	0.3	8.1	39.1	1.8	0.70	0.5	6.9	4.3	1.6	0.2	0.0	1.0	2.7	0
Bt	24-40	10YR 5/4	sbk, m, 2	ai	9	27.9	21.6	50.5	0.3	8.3	43.5	1.9	0.69	0.4	5.4	4.0	2.6	0.3	0.0	0.9	2.6	0
2Ck1	40-64	10YR 7/4	sbk, f, 1	aw	31	18.5	13.5	68.1	0.3	8.5	30.4	21.7	nd	0.6	3.7	4.4	2.8	0.1	0.0	1.1	4.5	0
2Ck2	64-84	10YR 8/1	sg	as	38	11.9	11.6	76.6	0.3	8.9	26.1	30.9	nd	1.0	2.3	2.7	2.1	0.3	0.0	0.9	2.3	0
3Ck	>84	10YR 8/3	sg		24	10.6	5.9	83.6	0.3	8.9	23.0	19.9	nd	1.5	2.1	2.9	2.3	0.9	0.0	1.0	2.9	0
Pedisestment level IV, Typic Haplocalcid, profile 40																						
A	0-4	10YR 7/3	pl, f, m	as	33	16.9	20.5	62.6	1.3	8.1	25.7	2.2	0.67	0.4	0.5	24.9	9.6	0.2	0.0	1.1	22.3	0
Bk	4-35	10YR 5/3	sbk, m, 2	gw	25	17.6	19.8	62.7	0.4	8.5	28.3	4.1	0.53	0.5	0.1	7.4	1.4	0.3	0.0	1.1	4.5	0
C	35-63	10YR 6/3	sg	as	24	19.7	10.6	69.7	0.5	8.8	26.1	6.8	0.80	3.1	0.1	3.6	1.1	0.2	0.0	1.6	4.6	1
2Ck	63-89	10YR 8/3	sg	aw	32	21.4	2.9	75.7	0.7	9.2	23.9	29.2	0.38	4.9	0.1	2.5	0.5	0.2	0.0	2.0	6.5	3
3Bwtkb	89-140	7.5 YR 8/2	sbk, m, 2	gw	12	11.3	22.9	65.8	1.3	9.3	26.5	51.5	0.29	11.5	0.1	1.7	0.5	5.6	0.0	1.1	16.1	10
3Ck	>140	10YR 7/4	sg		43	6.9	25.3	67.8	7.0	8.1	29.1	12.7	nd	45.2	0.4	48.1	21.8	11.6	0.0	0.9	129.8	7

(continued)

Table 1 (continued)

Horizons	Depth (cm)	Color (dry)	Structure ^a	Boundary ^a >2 mm (%)	Clay Silt (%)	Sand EC ^b (dSm ⁻¹)	pH (1.2, 5)	CEC ^b (cmol/kg)	CaCO ₃ (%)	SOM ^b Soluble salts (mmol/L)					ESP (%)							
										Na ⁺	K ⁺	Ca ²⁺	Mg ²⁺	Cl ⁻	CO ₃ ²⁻	HCO ₃ ⁻	SO ₄ ²⁻					
Pediment level I, Typic Natrargids, profile 30																						
Av	0-5	10YR 5/3	pl. f, 2	as	21.0	22.5	56.5	3.2	8.0	45.7	1.4	0.64	28.7	43.0	15.4	6.4	7.6	0.2	1.8	59.2	8	
Bm	5-23	5YR 4/6	gr. f, 2	gs	46.0	28.5	25.5	10.2	9.0	39.1	59.4	0.68	84.3	32.0	8.8	3.3	95.7	0.0	1.7	28.5	27	
Btkn	23-36	5YR 4/6	pr. m, 3	gs	61.4	17.7	20.9	9.9	9.1	39.1	21.7	0.39	82.6	26.0	8.0	4.3	84.1	0.0	1.2	33.5	27	
Ck1	36-48	5YR 4/4	m	aw	7.9	66.2	25.9	7.8	9.1	41.7	26.0	nd	73.0	22.0	6.3	2.0	57.7	0.0	1.1	29.5	28	
Ck2	>48	5YR 4/4	m		8.9	72.4	18.7	17.8	8.3	36.5	27.1	nd	144.3	28.0	51.1	14.4	87.3	0.0	0.9	114.7	21	
Pediment level II, Typic Torriorthents, profile 32																						
A	0-7	7.5YR 5/4	sg	as	14.4	47.1	38.5	0.3	7.3	41.7	1.3	0.48	0.6	16.0	4.6	1.4	0.4	0.0	0.9	3.5	0	
Bwk	7-24	7.5YR 4/4	sbk. m, 2	as	36.9	28.5	34.6	0.3	8.0	51.3	4.1	0.86	0.9	3.5	4.5	1.7	0.1	0.0	1.1	4.0	0	
2Ck	>24	Green mudstones from CH G																				
Pediment level II, Typic Haplocalcids, profile 11																						
A	0-8	7.5YR 8/5	pl. m, 1	aw	23	22	56	0.3	8.3	30.3	1.8	0.61	0.2	0.1	0.5	0.1	0.1	0.0	1.8	0.4	0	
Btk	8-21	7.5YR 6/4	sbk. c, 2	gw	5	27	30	44	0.4	8.3	40.7	0.65	0.5	0.0	0.9	0.1	1.3	0.0	2.5	0.3	0	
Bk	21-32	7.5YR 8/4	sbk. m, 2	aw	7	11	48	41	0.3	8.4	32.9	0.47	0.9	0.0	0.5	0.1	0.4	0.0	1.8	0.5	1	
Ck	>32	7.5YR 8/2	m		33	10	40	51	2.6	7.8	25.0	48.3	nd	1.3	0.0	1.9	0.2	0.4	0.0	0.5	4.0	0
Pediment level III, Typic Natrargids, profile 31																						
Av	0-4	10YR 6/3	pl. f, 2	as	24.1	21.7	54.3	1.3	8.1	15.2	1.4	0.58	10.4	12.0	3.9	4.8	3.7	0.1	2.2	14.3	5	
2Bt1	4-14	5YR 4/4	sbk. m, 3	gs	38.7	25.5	35.8	1.4	8.7	36.5	1.2	0.53	14.3	4.0	2.5	4.8	10.3	0.0	0.7	5.1	8	
2Bt2	14-27	5YR 5/6 (h)	sbk. f, 2	gs	44.6	37.4	18.0	4.8	8.8	15.2	5.7	1.00	36.5	7.0	9.8	3.3	40.1	0.0	1.1	6.9	13	
2Bkn	27-50	5YR 5/6	sbk. m, 2	as	3	10.4	63.5	26.2	7.0	9.0	62.6	0.34	61.7	10.0	12.6	7.3	52.7	0.0	1.4	39.8	18	
2Cky	>50	7.5YR 5/4	sbk. m, 1		5	10.2	70.9	18.9	12.1	8.2	53.9	6.5	93.9	8.7	60.3	29.4	59.1	0.0	1.4	182.1	13	
Pediment level III, Typic haplalgids, profile 21																						
A	0-7	10YR 5/4	sg	as	11	12	77	0.3	7.1	15.7	1.0	0.68	0.7	0.5	5.5	3.8	0.1	0.0	1.3	3.9	0	
C	7-20	10YR 5/4	sbk. m, 1	as	9	15	11	74	0.1	7.0	23.0	1.0	0.55	3.4	0.3	2.3	0.4	0.1	0.0	0.4	0.9	2

(continued)

Table 1 (continued)

Horizons	Depth (cm)	Color (dry)	Structure ^a	Boundary ^a >2 mm (%)	Clay (%)	Silt (%)	Sand (%)	EC ^b (dSm ⁻¹)	pH (1–2, 5)	CEC ^b (cmol/kg)	CaCO ₃ (%)	SOM ^b (%)	Soluble salts					ESP (%)				
													Na ⁺	K ⁺	Ca ²⁺	Mg ²⁺	Cl ⁻		CO ₃ ²⁻	HCO ₃ ⁻	SO ₄ ²⁻	
2BU	20–36	7.5YR 5/4	sbk, m, 3	gs	4	30	10	60	0.2	38.6	1.0	0.41	0.9	0.1	2.1	2.0	0.1	0.0	0.6	1.9	0	
2BU2	36–50	7.5YR 5/4	sbk, c, 2	gs	8	24	18	59	0.1	39.1	1.1	0.38	0.7	0.1	2.0	1.0	0.4	0.0	0.4	1.3	0	
2C	50–70	10YR 5/4	m	aw	5	19	9	72	0.3	31.3	1.2	nd	1.0	0.1	5.4	2.4	0.1	0.0	1.4	2.9	0	
3Ck	70–98	10YR 7/4	sg	as	23	14	0	86	0.2	17.7	2.4	nd	0.9	0.1	3.1	1.6	0.5	0.0	0.9	1.9	0	
4C	>98	2.5Y 7/4	m		0	16	10	74	0.3	17.2	6.0	nd	1.3	0.1	4.9	2.5	0.2	0.0	1.3	5.0	0	
Pediment level IV, Typic Torriorthents, profile 14																						
A1	0–13	7.5YR 6/4	gr, c, 1	aw	6	25	30	45	0.4	8.3	34.4	2.1	0.39	0.5	0.1	7.0	4.5	0.4	0.0	1.1	7.1	0
A2	13–31	7.5YR 6/4	sbk, m, 2	gw	11	23	28	49	0.4	8.3	35.0	3.3	0.47	0.7	0.1	5.6	3.4	0.2	0.1	1.2	8.3	0
2Bk	31–56	5YR 6/4	sbk, m, 3	gw	11	20	32	48	0.4	8.5	38.1	6.5	0.37	2.2	0.1	3.3	0.3	0.3	0.1	1.4	9.5	0
2Ck	>56	5YR 7/3	sg		7	23	21	56	1.4	8.8	35.0	6.3	nd	11.1	0.1	4.5	2.7	8.3	0.1	1.2	8.9	5
Pediment level IV, Lithic Torriorthents, profile 28																						
A	0–10	10YR 4/4	gr, f, 3	gs	36	16.2	16.5	67.3	0.2	7.0	15.2	1.2	0.80	0.6	25.5	2.2	1.9	0.1	0.1	0.4	3.8	0
2B/R	10–46	7.5YR 4/4	sbk, f, 3	ai	45	21.1	35.4	43.6	0.8	8.1	37.0	3.0	1.03	6.5	12.9	3.7	3.0	1.0	0.1	3.0	5.1	3
R	>46	Reddish sandstone	from Ch G																			
Alluvial fan relict I, Typic Haplocalcids, profile 22																						
A1	0–20	10YR 5/3	sbk, m, 3	gw	19	25	12	63	0.3	8.5	24.8	4.6	0.79	0.4	0.1	5.1	2.7	0.3	0.0	0.8	6.2	0
A2	20–37	10YR 5/4	sbk, m, 2	gw	21	17	20	63	0.3	8.6	23.0	7.3	0.90	0.5	0.1	6.1	1.9	0.1	0.0	0.8	6.5	0
2Bk1	37–61	10YR 7/4	m	as	34	17.6	13.2	69.2	0.4	8.7	23.0	16.5	nd	1.0	0.1	5.8	3.1	0.4	0.0	1.2	7.3	0
2Bk2	61–73	10YR 8/2	pl, m, f	as	59	15.4	7.4	77.2	0.4	8.8	22.2	28.2	nd	1.1	0.1	4.3	3.7	0.7	0.0	0.9	7.9	0
3Ck	>73	10YR 5/3	sg		20	12.7	0.0	88.9	0.3	9.1	15.2	8.9	nd	1.6	0.1	3.3	2.8	0.6	0.0	0.9	7.2	0
Alluvial fan relict II, Typic Haplocalcids, profile 25																						
A	0–22	10YR 4/4	sbk, m, 2	aw	12	28.8	23.5	47.7	0.3	8.2	21.3	1.0	0.71	0.6	0.4	3.6	2.7	0.1	0.0	0.9	5.0	0
C	22–43	10YR 4/6	sbk, m, 2	aw	46	10.8	28.5	60.7	0.3	8.6	25.2	1.0	0.50	0.7	0.4	3.5	3.0	0.2	0.0	1.2	4.1	0
2Bw	43–77	7.5YR 5/4	sbk, f, 2	aw	62	17.9	1.2	80.9	0.3	8.6	16.5	0.9	0.18	1.0	0.3	2.7	3.3	0.1	0.0	0.9	2.9	0

(continued)

Table 1 (continued)

Horizons	Depth (cm)	Color (dry)	Structure ^a	Boundary ^a >2 mm (%)	Clay Silt (%)	Sand EC ^b (dSm ⁻¹)	pH (1,2,5)	CEC ^b (cmol/kg)	CaCO ₃ (%)	Soluble salts (mmol/L)					ESP (%)					
										Na ⁺	K ⁺	Ca ²⁺	Mg ²⁺	Cl ⁻		CO ₃ ²⁻	HCO ₃ ⁻	SO ₄ ²⁻		
2C	77-96	7.5YR 5/6	sg	aw	65	10.8 3.2	86.0 0.3	8.7	8.7	1.1	1.5	0.2	2.3	2.0	0.1	0.0	1.0	3.4	0	
2Ck	96-120	7.5YR 8/2			60	14.0 0.0	86.0 0.4	9.1	11.7	15.8	3.7	0.2	3.5	3.0	0.1	0.0	1.5	7.4	1	
3C	>120	Sandy gravel deposits																		
Alluvial fan relict III, Typic Haplocalcids, profile 26																				
A1	0-5	10YR 4/4	sbk, m, 1	gs	33	16.8 25.0	58.2 0.3	7.9	22.6	1.4	0.82	0.3	0.5	6.2	1.7	0.1	0.0	1.2	5.1	0
A2	5-27	10YR 5/4	sbk, m, 2	gw	26	13.1 33.6	53.3 0.4	8.5	25.7	1.5	0.49	0.3	0.1	7.0	3.4	0.2	0.1	1.2	8.4	0
Ck	27-44	10YR 5/4	sg	ai	36	8.2 21.1	70.7 0.4	8.5	23.0	6.2	nd	0.3	0.1	9.3	3.4	0.5	0.0	1.4	12.0	0
2Bk(m)	44-135	10YR 8/2	sgs, pl, m, 3	as	36	14.0 11.7	74.3 0.3	8.7	17.4	41.1	nd	0.9	0.0	5.6	3.6	0.6	0.1	1.2	5.6	0
3C	>135	10YR 5/3	sg		12	5.1 2.4	92.5 0.6	9.8	11.3	3.2	nd	4.7	0.0	1.5	0.8	0.1	0.0	1.7	6.3	4
Modern alluvial fan I, Typic Natrargids, profile 44																				
AV	0-4	10YR 7/3	pl, f, 3	aw	13	28.9 15.7	55.5 3.5	8.8	18.3	1.2	0.54	33.5	0.6	7.5	3.4	30.2	0.7	1.6	5.6	13
2Btm	4-11	7.5YR 4/4	sbk, f, 3	aw	2	39.5 14.8	45.7 5.8	8.8	36.1	1.3	0.25	50.4	0.6	7.4	2.9	52.7	0.0	0.8	3.0	19
2Bkn1	11-21	7.5YR 5/4	sbk, m, 3	as	4	41.3 16.8	41.9 9.6	9.0	45.2	7.0	0.57	84.3	0.5	11.0	4.7	86.5	0.0	1.3	29.7	25
2Bkn2	21-43	7.5YR 5/6	sbk, m, 2	gs	28	7.0 53.1	39.9 8.4	9.2	70.4	19.0	0.77	84.3	0.5	7.9	4.0	69.7	0.0	1.5	40.6	28
2Ck	43-92	7.5YR 5/4	sg	as	22	10.0 5.5	84.5 13.2	9.0	25.2	8.1	nd	121.7	0.5	48.9	22.0	48.4	0.0	0.8	169.3	18
3Ck	>92	7.5YR 7/4	m		4	11.9 4.8	83.4 8.2	9.5	12.2	5.6	nd	80.0	0.5	8.7	4.8	49.2	0.0	1.1	76.6	25
Modern alluvial fan I, Typic Haplargids, profile 6																				
A	0-11	10YR 7/2	pl, f, 2	as	14	19 16	65 0.4	8.4	21.7	0.7	0.45	2.0	0.1	0.4	0.2	0.3	0.0	2.6	0.4	3
2Bt	11-26	7.5YR 4/4	pr, f, 3	as	7	33 28	38 0.4	8.7	41.3	1.3	0.45	2.7	0.0	0.2	0.1	0.5	0.0	2.1	0.5	6
2Btk	26-44	7.5YR 5/4	sbk, m, 3	gs	24	10 17	73 0.5	9.0	31.7	4.2	0.28	3.1	0.1	0.2	0.1	0.9	0.0	2.4	0.9	7
2Ck	44-76	7.5YR 6/2	sg	as	37	8 1	91 0.5	9.2	19.6	3.9	nd	4.1	0.0	0.2	0.0	1.2	0.0	2.9	0.6	11
3Ck	76-100	7.5YR 6/4	sbk, m, 1	as	8	5 10	84 2.0	9.5	19.6	1.3	nd	30.4	0.1	0.8	0.3	29.2	0.0	3.4	2.8	31
4Ck	>100 (150)	7.5YR 6/4	sg		10	7 5	88 3.0	9.3	17.4	4.2	nd	24.0	0.0	0.7	0.3	25.9	0.0	1.2	2.4	27

(continued)

Table 1 (continued)

Horizons	Depth (cm)	Color (dry)	Structure ^a	Boundary ^a >2 mm (%)	Clay Silt (%)	Sand EC ^b (dSm ⁻¹)	pH (1.2, 5)	CEC ^b (cmol/kg)	CaCO ₃ (%)	SOM ^b Soluble salts (mmol/L)					ESP (%)								
										Na ⁺	K ⁺	Ca ²⁺	Mg ²⁺	Cl ⁻		CO ₃ ²⁻	HCO ₃ ⁻	SO ₄ ²⁻					
Modern alluvial fan II, Typic Torriorthents, profile 7																							
A	0–19	10YR 5/3	pl. c, 1	as	16	17	14	69	0.2	7.9	23.5	0.9	0.26	0.6	0.2	0.4	0.1	0.1	0.0	1.7	0.2	0	
C	19–42	10YR 6/3	sg	ai	16	16	14	70	0.2	7.8	24.3	0.8	0.29	0.8	0.1	0.4	0.1	2.4	0.1	1.5	0.3	1	
2Ck1	42–92	10YR 6/4	sg	aw	22	8	4	89	0.3	9.4	17.8	7.6	nd	2.5	0.0	0.1	0.0	0.1	0.0	2.1	0.2	9	
2Ck2	92–142	10YR 6/4	sg	as	13	6	0	93	0.2	9.8	16.5	5.0	nd	3.7	0.0	0.1	0.0	0.5	0.0	3.0	0.6	11	
3Bkb	>142	7.5YR 7/4	sbk, m, 1		17	7	6	88	0.7	9.8	21.3	7.6	nd	7.6	0.0	0.2	0.0	3.0	0.0	2.7	1.2	19	
Modern alluvial fan II, Sodic Haplocalcids, profile 5																							
A	0–11	10YR 5/3	pl. c, 1	as	14	8	79	12	0.3	8.2	22.2	0.9	0.30	0.6	0.2	0.4	0.1	0.2	0.0	1.7	0.3	0	
C	11–45	10YR 6/4	sbk, m, 1	aw	14	10	15	75	0.4	8.4	29.6	0.6	0.25	1.3	0.0	0.4	0.1	0.9	0.0	1.9	0.4	1	
2Bk	45–125	7.5YR 6/4	sbk, c, 1	aw	6	4	3	93	5.0	8.5	27.8	30.3	0.17	41.5	0.0	5.2	1.8	4.6	0.0	1.0	28.8	19	
2Ck	125–165	7.5YR 6/4	sg	as	12	3	41	56	6.6	8.2	26.1	10.4	nd	53.9	0.0	5.3	2.1	14.0	0.0	0.8	34.5	23	
3Bkb	>165 (190)	7.5YR 6/4	sbk, m, 3		1	9	49	42	8.0	8.6	37.4	15.9	nd	62.3	0.1	5.5	2.3	34.4	0.0	0.8	31.2	26	
Alluvial plains, Typic Torriorthents, profile 37																							
A	0–4	5YR 6/4	pl. f, 3	aw	0	35.0	36.8	28.3	0.7	8.4	51.3	3.5	1.65	2.0	0.8	10.0	6.5	0.3	0.0	2.9	4.7	0	
C	4–21	7.5YR 6/4	sbk, m, 2	as	1	25.0	23.2	51.9	1.2	8.7	33.0	1.6	0.45	6.1	0.6	11.8	2.3	2.2	0.0	0.9	3.3	1	
2Ck	21–80	7.5YR 6/4	sbk, c, 1	as	4	26.1	17.7	56.3	0.5	9.3	36.5	9.2	nd	5.7	0.2	1.9	0.7	0.2	0.0	1.8	4.5	4	
R	>80	Reddish sandstone from Ch G																					
Alluvial plains, Typic Torriorthents, profile 18																							
A1	0–18	10YR 6/4	pl. m, 1	as	14	28	29	43	0.4	8.0	30.3	2.1	0.63	0.3	0.6	5.7	1.9	0.3	0.0	1.1	1.8	0	
A2	18–28	10YR 6/4	sbk, m, 2	aw	12	29	25	46	0.4	8.4	34.4	1.7	0.56	0.8	0.7	2.1	0.9	0.7	0.0	1.0	1.9	0	
Ck1	28–75	5YR 6/4	sg	aw	23	25	23	52	0.4	8.9	28.7	8.5	0.49	1.8	0.1	3.6	2.1	0.1	0.0	1.5	4.3	0	
Ck2	>75	5YR 6/4	sg		23	18	27	55	0.6	9.3	26.1	6.4	nd	4.8	0.1	1.9	0.8	0.5	0.0	1.6	6.8	3	

(continued)

Table 1 (continued)

Horizons (cm)	Color (dry)	Structure ^a	Boundary ^a >2 mm (%)	Clay Silt (%)	Sand EC ^b (dSm ⁻¹)	pH (1.2, 5)	CEC ^b (cmol/kg)	CaCO ₃ (%)	SOM ^b (%)	Soluble salts (mmol/L)					ESP (%)						
										Na ⁺	K ⁺	Ca ²⁺	Mg ²⁺	Cl ⁻		CO ₃ ²⁻	HCO ₃ ⁻	SO ₄ ²⁻			
Wetlands (mallines), Aquic Torrifluvents, profile 43																					
A	0-22	10YR 3/3 m	as	0	50.8	31.7	17.5	4.8	8.7	62.6	8.6	2.12	44.3	1.2	13.3	19.4	9.3	0.0	5.1	74.5	11
C1	22-41	7.5 YR 4/4 gr, f, 2	as	0	25.7	55.3	19.9	5.1	8.7	48.7	6.5	1.03	43.9	1.2	14.7	32.6	13.1	0.0	2.4	83.3	9
C2	41-61	10YR 3/3 m	as	0	18.0	66.7	15.3	3.3	8.8	48.7	11.9	nd	29.6	0.6	9.7	21.3	8.4	0.0	2.0	56.7	8
C3	>61 WT	Water table																			
Wetlands (mallines), Aquic Haplocalcids, profile 20																					
A	0-22	10YR 6/3 sbk, c, 3	as	1	27	36	37	4.5	9.2	40.7	14.4	1.39	49.6	0.6	7.4	9.3	36.3	0.0	2.4	71.5	17
Bwk	22-30	10YR 7/3 sbk, m, 2	aw	0	13	50	37	1.1	9.3	45.4	12.7	0.53	16.5	0.1	1.5	3.5	3.4	0.0	1.4	17.5	11
2Ab	30-40	10YR 6/2 sbk, m, 1	aw	3	13	37	50	0.8	9.1	38.6	8.6	0.39	7.1	0.1	2.0	1.9	1.8	0.1	1.4	13.4	5
2Bwkb	40-50	5 YR 6/4 sbk, m, 2	gw	7	22	44	34	0.8	9.4	41.7	10.1	0.22	7.4	0.1	2.6	3.0	0.9	0.0	1.2	4.5	4
2Bklb	50-75	10YR 7/2 sbk, m, 2	gs	0	22	24	54	0.8	9.5	28.2	21.3	0.20	6.4	0.1	1.3	2.4	1.1	0.0	0.9	11.9	5
2Bk2b	>75	10YR 7/3 sbk, m, 2		16	15	23	62	1.0	9.6	24.5	21.1	0.18	9.3	0.1	1.7	2.3	1.5	0.0	1.3	9.2	6

Roman numerals indicate chronosequence levels (geomorphic surfaces)

LTF Lonco Triapial Formation; Ch G, Chubut Group

^aAbbreviations for morphological description are from Schoeneberger et al. (2002); structure: gr granular, sg single grain, m massive, pl platy, pr prismatic, sbk subangular Blocky, size: vf very fine, f fine, m medium; grade: 1 weak, 2 moderated, 3 strong; boundary, distinctness: a abrupt, g gradual; topography: w wavy, s smooth, i irregular

^bSoil properties: EC electrical conductivity; SOC soil organic carbon; ESP exchangeable sodium percentage; CEC cation exchange capacity

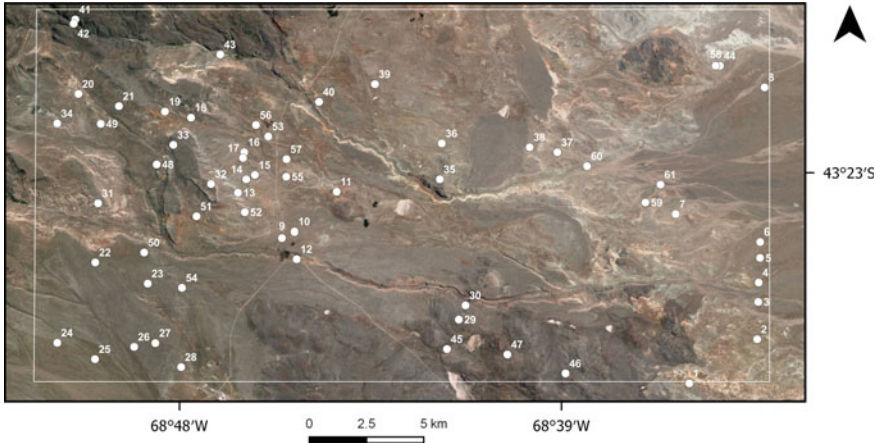


Fig. 3 Location of soil profiles

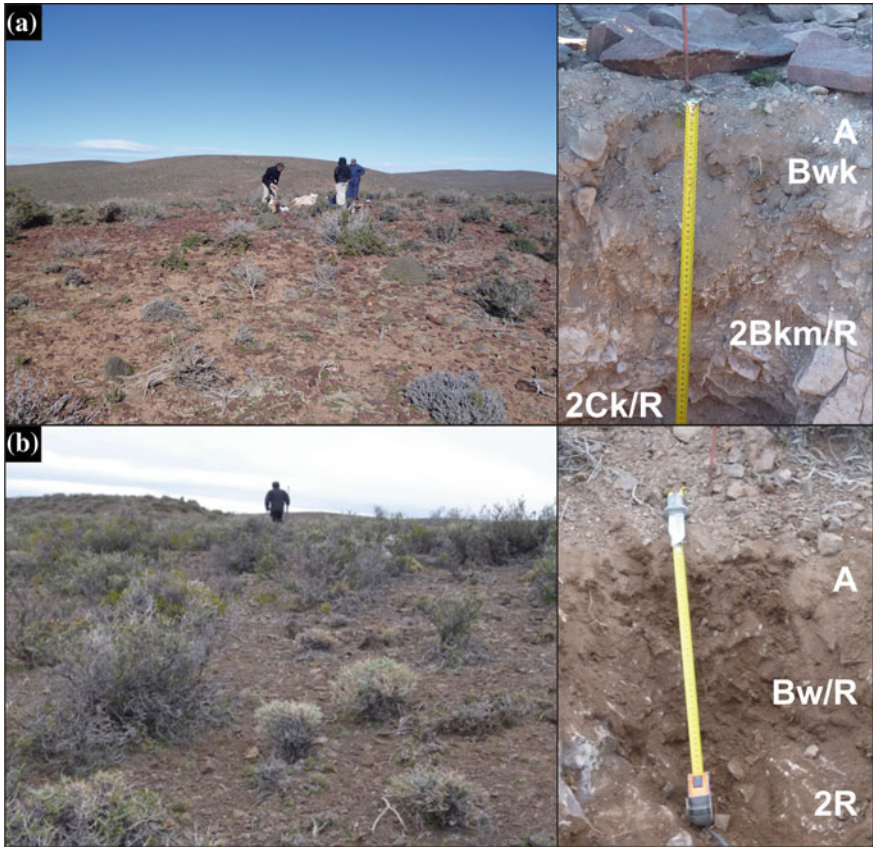


Fig. 4 Exhumation planation surface, Lonco Trapial Formation; a Calcic Lithic Petrocalcids (profile 29); b Lithic Torriorthents (profile 41)

four levels of relict pedisediment (geomorphic surfaces between 830–570 m a.s.l.; Figure 5). The slope of pedisediments is planar with a slight tilt to the east and southeast (1–1.5%). These deposits correspond to the Renguenao Formation and are composed of sandy gravel sediments (1–6 m) deposited on pediments carved on continental sedimentary rocks of the Chubut Group. Rhyolites and andesites are the main component of the gravel size fraction, and in smaller proportion basalts. In the coarse fraction (>2 mm), fragments of mudstone and calcitic concretions from the Chubut Group were also observed.

The soils of the pedisediment levels were classified as Typic Haplocalcids. The soils of pedisediment I have an A1-A2-Bt-2Ck1-2Ck3-3Ck horizon sequence (e.g., profile 33; Fig. 5a). Although clay coatings were observed in the subangular blocks, the amount of illuvial clay is not enough to define an argillic horizon.

In general, the pedisediment levels I–III are observed as isolated relicts in the northwest of the study area, between 850 and 750 m a.s.l. Vegetation communities

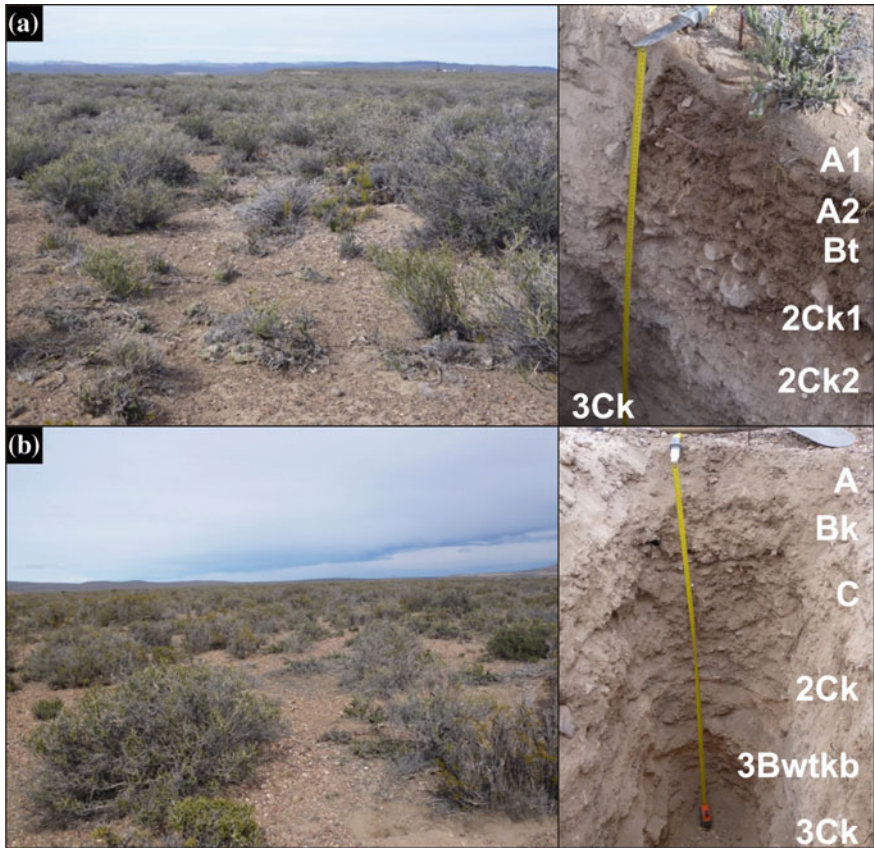


Fig. 5 Pedisediment levels, Typic Haplocalcids; **a** level I (profile 33); **b** level IV (profile 10)

(35% cover) are considered shrub steppe composed by *Mulguraea ligustrina*, *Nardophyllum obtusifolium*, and *Nassauvia glomerulosa*.

The Pedisediment level IV covers a greater area and it is distributed between 730 and 560 m a.s.l. mainly along the La Turca creek. In profile 10, pedogenic gypsum nodules occur at depth (>180 cm), indicating a *per descensum* origin of the soil solutions. In profile 40, a pinkish-buried paleosol is observed at 90 cm in depth with clay coatings between subangular blocks of 3Bwtkb horizon (Fig. 5b). Vegetation (20% cover) of this geomorphic surface is a shrub steppe composed by *Ephedra ochreatea*, *Mulguraea ligustrina*, *Chuquiraga avellanadae*, and *Nardophyllum obtusifolium*.

2.3 Pediment Associations

A pediment is defined by a gently and short slope transport surfaces of bedrock, covered by a thin alluvium, developed between an upland area where erosion dominates (i.e., the erosion scarps) and a lower plain where active aggradation dominates (i.e., *Bajadas* or Coalescent alluvial fans). Dohrenwend and Parsons (2009) defined this sequence of landforms and processes on hillslope as a pediment association.

In the study area, this geomorphological unit corresponds to an erosional landscape of the Chubut Group. This unit is highly dissected, recognizing at least four levels of pediments caused by local changes in base level (Fig. 6a, b).

The parent materials are composed of varied sedimentological facies (mudstone, sandstone) of the Cerro Barcino Formation (Chubut Group) and a thin colluvial layer of the same material re-transported.

However, whereas all geomorphic surfaces have similarities in their parent materials significant differences in their morphological, physical and chemical properties are clearly observed (Table 1). This variety of soil types is depending on the age of geomorphic surface and the degree of polygenesis, this last resulting from the alternation of morphogenesis periods with pedogenic periods.

The pediment level I is confined between the rounded hills of the exhumed planation surface (Fig. 6a). The soils have a certain pedological evolution with natric horizons formation. The general horizon sequence is Av-2Btn-2Btkn-2Ck1-2Ck2 and the soils were classified as Typic Natrargids (e.g., profile 30) with a shrub steppe vegetation community (30% cover) composed of *Atriplex lampa*, *Chuquiraga avellanadae*, and *Nassauvia ulicina*. In inter-shrubs spaces, the natric horizon (2Btn-2Btkn) is exhumed by raindrop impact and surface water runoff erosion where vesicular horizons and desert pavements are developing at the surface.

The soils of pediment level II have lithological discontinuities that indicated erosion–deposition processes with A-2Bwk-2Ck1-2Ck2 (e.g., profile 32; Fig. 6c) or A-Btk-Bk-Ck (e.g., profile 11) horizon sequences, where the soils were classified as Typic Torriorthents and Typic Haplocalcids, respectively. The vegetation of Torriorthents (20% cover) is predominantly shrub steppe and sub-shrubby steppe

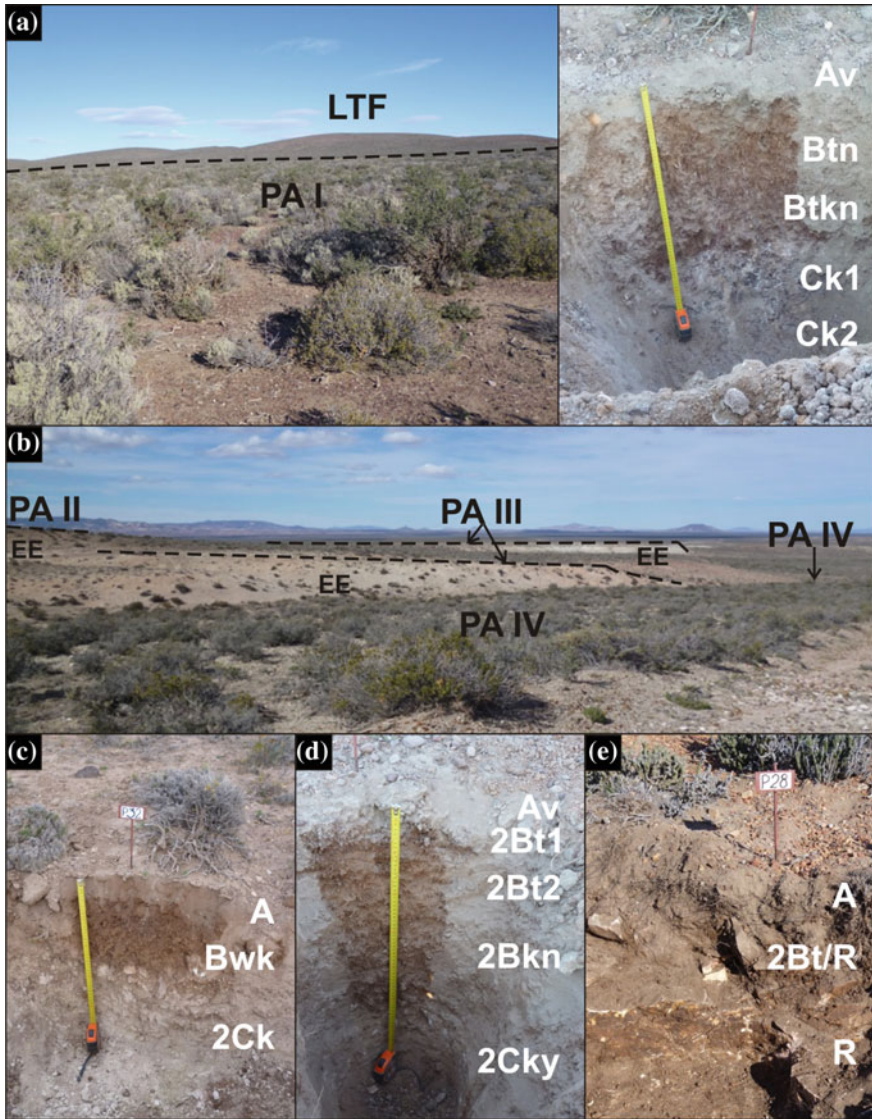


Fig. 6 Pediment associations; **a** PA I Pediment Association I, Typic Natrargids (profile 30), LTF Lonco Trapial Formation; **b** PA II–IV Pediment association levels; EE erosion scarp (Chubut Group); **c** PA II, Typic Torriorthents (profile 32); **d** PA III, Typic Natrargids (profile 31); **e** PA IV, Lithic Torriorthents (profile 28)

dominated by: *Chuquiraga avellanadae*, *Nardophyllum obtusifolium*, *Mulguraea ligustrina*, and *Prosopis denudans*, whereas in Haplocalcids, the vegetation (30% cover) is a sub-shrubby steppe with isolated shrubs dominated by *Nassauvia glomerulosa* and *Franquenina sp.*

The pediment level III occupies an area larger than pediment level II, and the soils show prominent argilic horizons (Bt1-Bt2; Bt-Btk) with greater degree of development (Table 1). The soils were classified as Typic Natrargids (e.g., profile 31; Fig. 6d) and Typic Haplargids (profile 21). The vegetation of pediment level III (25% cover) is predominantly shrub steppe dominated by: *Chuquiraga avellanadae*, *Prosopis denudans*, *Jarava speciosa*, *Lycium ameghinoi*, and *Nassauvia sp.*

The soil morphology of the profiles may differ in the degree of evolution and erosion or burial. The surface horizons may vary from thin layers vesicular (Av), A horizons or A-C horizon sequences that overlie argilic horizons.

The pediment level IV is more associated with erosion scarps of sedimentary rocks of the Chubut Group. This is observed mainly in the headwaters of the La Turca and La Oriental creeks. The soils have a weak development, where the soil parent material is exposed or covered by a thin alluvial–colluvial deposit (covered pediment). The soil profile is simple; the partially pedogenized Cretaceous sedimentary rocks are covered by alluvial–colluvial parent materials (A1-A2, A-C, or A-C1-C2-C3 horizons). According to the occurrence and depth (<50 cm) of the lithic contact, the soils were classified as Typic Torriorthents (profile 14) and Lithic Torriorthents (profile 28; Fig. 6e). The vegetation associated with these soils (25% cover) is predominantly shrub steppe and sub-shrubby steppe dominated by *Nardophyllum obtusifolium*, *Nassauvia glomerulosa*, *Prosopis denudans*, and *Lycium ameghinoi*.

2.4 Alluvial fan Relicts

This geomorphological unit is composed of three levels of relict alluvial fans (geomorphic surfaces) situated to the southwest of the study area on the eastern piedmont slope of the Sierra de Pichiñán.

Typic Haplocalcids are the soil types derived from these geomorphic surfaces. However, whereas their parent materials are gravel and sand deposits, free of carbonates, gypsum and soluble salts, important differences in their morphological, physical, and chemical properties are neatly observed (Table 1).

The soils of alluvial fan relict I (Fig. 7a) have sandy loam and loamy sand surface horizons (A1-A2 or A-C horizons) that lies on calcic (2Bk1-2Bk2 horizons; e.g., profile 22). Their vegetation is a shrub steppe composed by *Nassauvia glomerulosa*, *Nassauvia axilaris*, *Colliguaja integerrima*, and *Nardophyllum obtusifolium*.

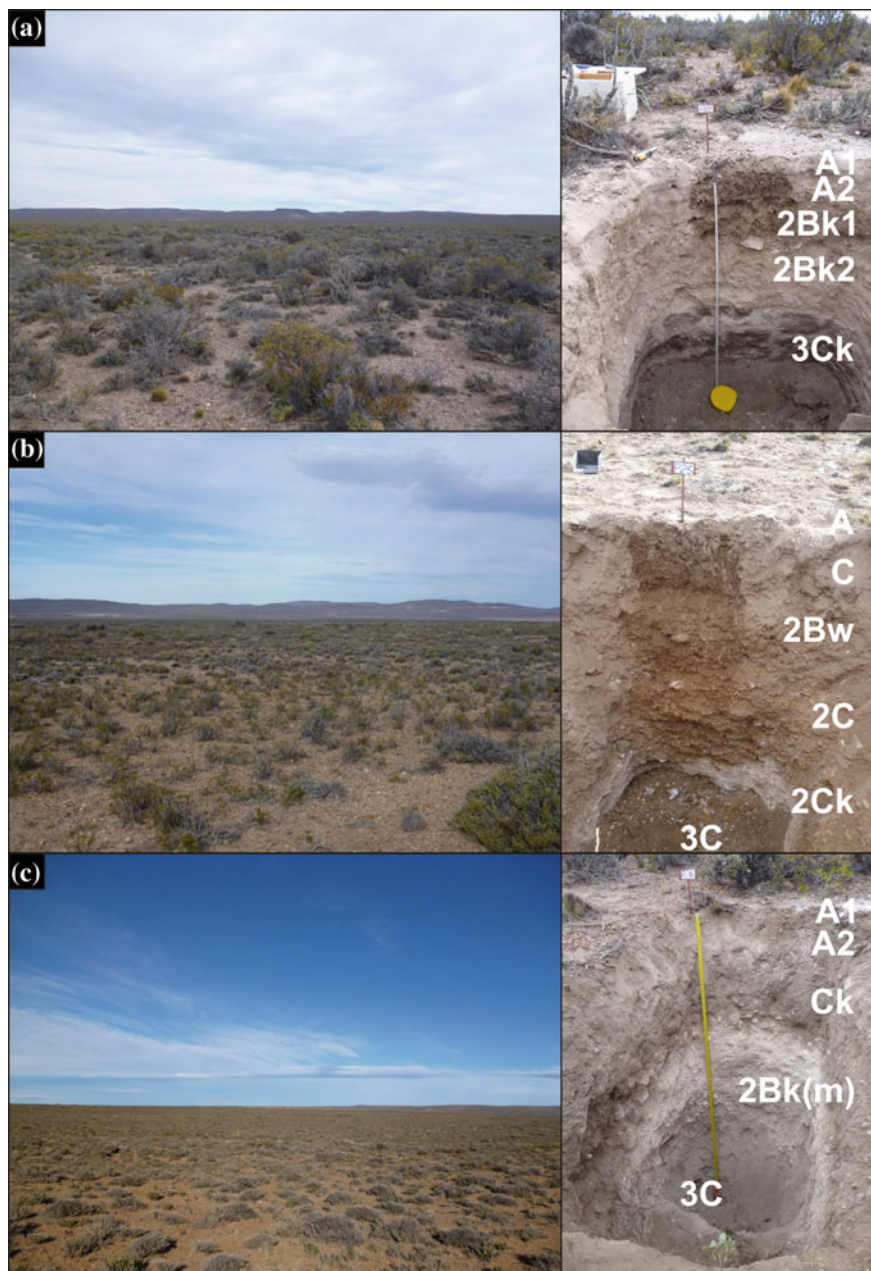


Fig. 7 Alluvial fan relicts, Typic Haplocalcids; **a** Alluvial fan relict I (profile 22); **b** Alluvial fan relict II (profile 25); **c** Alluvial fan relict III (profile 26)

The soils of alluvial fan relict II geomorphic surface (Fig. 7b, profile 25) have less pedogenic carbonate content than soils of Alluvial fan I, and present a color change at discontinuity from dark yellowish brown (10 YR 4/6; A-C horizons) to brown and strong brown (7.5YR 5/4, 5/6; 2Bw-2C-2Ck horizons). The vegetation of alluvial fan II is a sub-shrubby steppe dominated by *Grindelia chilensis*, *Maihuenia patagonica*, *Colliguaja integerrima*, and *Ephedra ochreatea*.

Alluvial fan relict III (Fig. 7c) is an erosional geomorphic surface that is superimposed at the alluvial fan I. The soil profile described on pit 26 shows this relation; the A1-A2-C horizons bury the 2Bk-3C horizons; this last sequence of horizon corresponds to the soil of alluvial fan I. In 2Bk horizon, petrocalcic crust fragments were observed, presumably incorporated from older geomorphic surfaces with petrocalcic horizons.

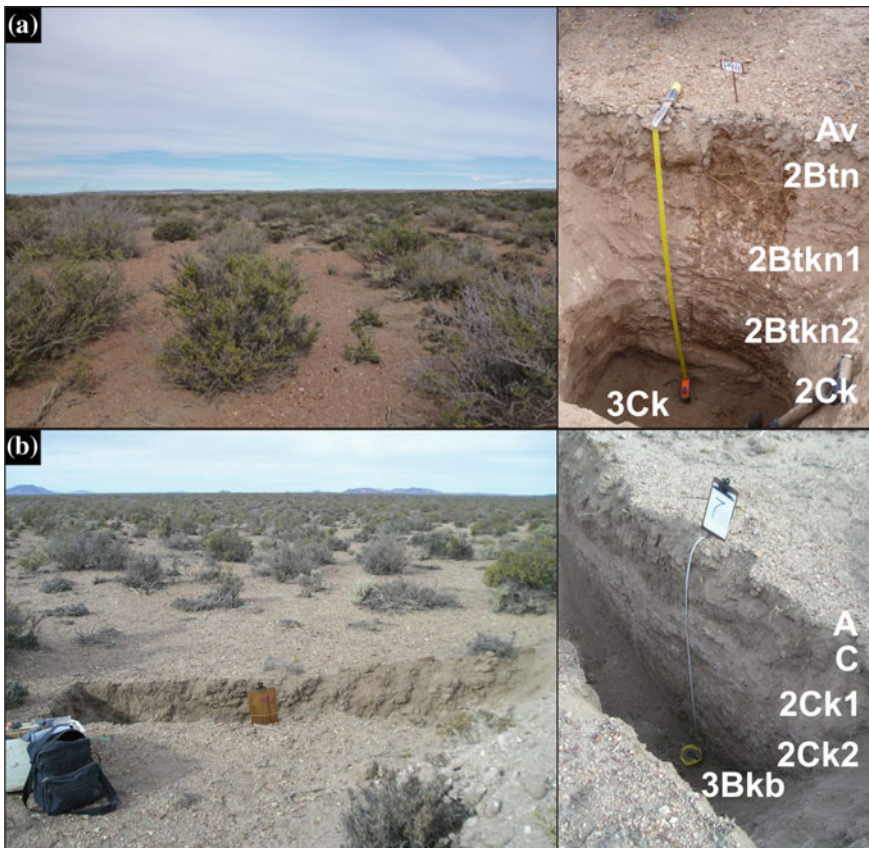


Fig. 8 Modern alluvial fans; **a** Modern alluvial fan I, Typic Natrargids (profile 44); **b** Modern alluvial fan II, Typic Torriorthents (profile 7)

2.5 Modern Alluvial fans

This geomorphological unit (Fig. 8) is located east of the study area and is formed by sedimentary accumulations from the La Turca and La Orientalita creeks.

The soil parent materials are alluvial deposits composed by the finer fraction of soil (<2 mm) and gravels from Cretaceous fragments of mudstones and sandstones of the Chubut Group.

In this unit, two modern alluvial fans were distinguished; modern alluvial fan I has soils with certain pedologic evolution as Typic Natrargids (e.g., profile 44; Fig. 8a) and Typic Haplargids (e.g., profile 6). The vegetation of this geomorphic surface is a shrubby steppe (20% cover) dominated by *Lycium ameghinoi*, *Chuquiraga avellanadae*, *Atriplex lampa*, and *Nassauvia ulicina*. Modern alluvial fan II buries the modern alluvial fan I. The soils were classified as Sodic Haplocalcids (profile 5) in the distal fan and Typic Torriorthents (profile 7; Fig. 8b) in the proximal fan. In both profiles, a 3Bkb horizon at 150 cm in depth is correlated with 2Bk horizons of soils from the modern alluvial fan I. The vegetation of Modern alluvial fan II surface is a shrubby steppe (30% cover) dominated by *Lycium ameghinoi*, *Chuquiraga avellanadae*, *Atriplex lampa* and *Nassauvia ulicina* and *Prosopis denudans*.

2.6 Alluvial Plains and Associated Wetlands (Mallines)

This geomorphological unit corresponds to the active alluvial plains of the La Turca and La Orientalita creeks, tributary streams and the *bajadas* of endorheic basins.

Soils are poorly developed, and its parent materials are composed of alluvial deposits of fine particle size (<2 mm and fine gravels) that are overlying reddish sedimentary rocks of the Chubut Group. The soils were classified as Typic Torrifluvents (e.g., profile 37; Fig. 9a) accompanied by Typic Torriorthents (e.g., profile 18). The vegetation of alluvial plains is a shrubby steppe (20% cover) composed by *Junellia tridactylis*, *Lycium ameghinoi*, *Chuquiraga avellanadae*, and *Prosopis denudans*.

Wetlands, locally named *mallines*, are located in restrained areas of the La Turca and La Orientalita creeks with underground water discharge at the thalweg sectors of the channels. The soils have water table and horizons with redox depletions (chroma ≤ 2) within 100 cm of the soil surface, and thus, the soils were classified as Aquic Torrifluvents (e.g., profile 43) and Aquic Haplocalcids (profile 20; Fig. 9b). The vegetation of wetlands is a grass steppe (50% cover) dominated by *Juncos sp.*, *Dystichlis sp.*, and *Carex banksii*.

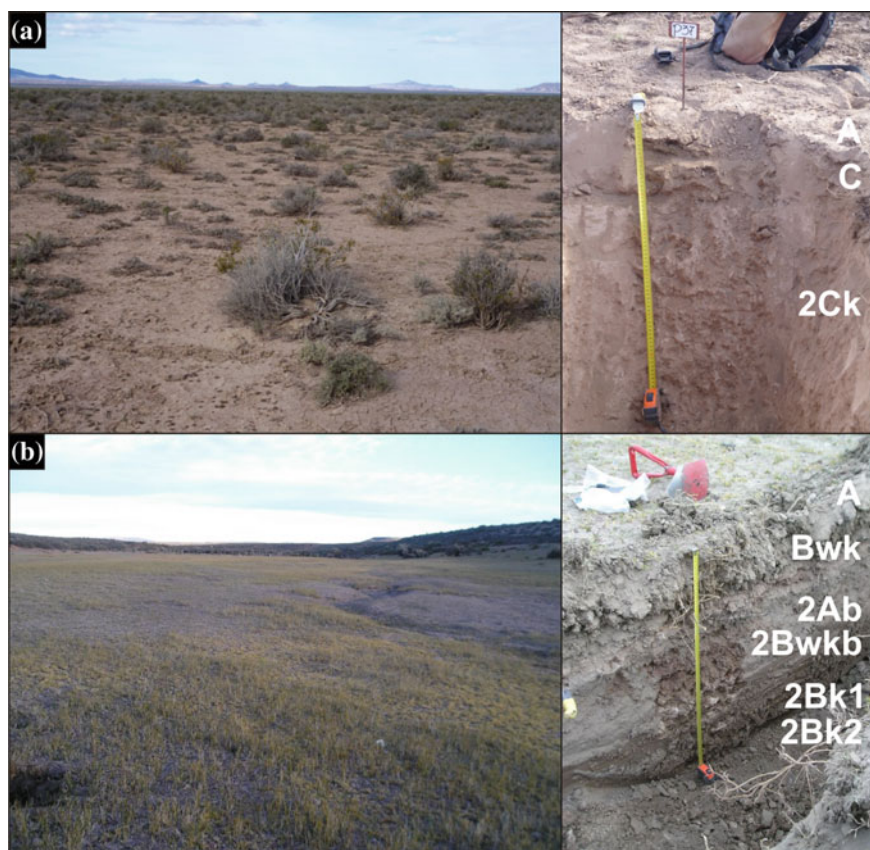


Fig. 9 a Active Alluvial plains, Typical Torrifluvents (profile 39); b wetlands (“mallines”), Aquic Haplocalcids (profile 20)

3 Perspectives and Future Work

From the preceding paragraphs, it is concluded that the study of geomorphology–soil relationship is not only a tool to correlate unconsolidated deposits, but also to characterize the pedological contents and vegetation communities associated with the geomorphological units and geomorphic surfaces. Also, this information could be used to determine the productivity indexes (or soil-quality index) at landscape scales (Schaeztl et al. 2012), for instance, the different geomorphic surfaces.

Acknowledgements This research project has been funded by the National Atomic Energy Commission of Argentina (CNEA, Comisión Nacional de Energía Atómica; Agreement CNEA-CONICET S/RP 303/11). The authors would like to thank the helpful reviews of Dr. Jorge Rabassa and Dr. Andrés Bilmes which improved the final version of this manuscript.

References

- Aguilera EY, Aragón E, Carretero S (2010) The paleosurface on the paso del sapo volcanic rocks, Chubut. Argent. Geociências, São Paulo 29(4):479–486
- Beeskow AM, del Valle HF, Rostagno CM (1987) Los sistemas fisiográficos de la región árida y semiárida de la provincia del Chubut, Argentina. SECYT Delegación Regional Patagonia. Bariloche, Río Negro, Argentina, 142 p
- Berizzo JA (1976) Estado actual del conocimiento en el área de influencia del yacimiento Los Adobes. Vertiente oriental de la Sierra de Pichiñán. Departamento Paso de Indios. Comisión Nacional de Energía Atómica, (unpublished). Córdoba, 23 p
- Braun-Blanquet J (1979) Fitosociología. Bases para el estudio de las comunidades vegetales. Blume, Barcelona
- Buol SW, Hole FD, Mcracken RJ (1990) Génesis y clasificación de suelos, 2nd edn. Trillas, México, p 417
- Daniels RB, Gamble EE, Cady JG (1971) The relation between geomorphology and soil morphology and genesis. Adv Agron 23:51–88
- Dohrenwend JC, Parsons AJ (2009) Pediments in arid environments. In: Parsons A, Abrahams A (eds) Geomorphology of desert environments. Springer, Netherlands, pp 377–411
- Fígari E, García D (1992) Análisis litofacial y arquitectónico de los depósitos continentales mesocretácicos aflorantes en el Cerro Fortín, Provincia del Chubut, Argentina. 4° Reunión Argentina de Sedimentología, Actas, La Plata, vol 1, pp 119–126
- Gile L, Hawley HJ, Grossman RB (1981) Soil and geomorphology in the basin and range area of southern New Mexico. Guidebook to the desert project, Memoir 39. New Mexico Bureau of Mines and Mineral Resources, p 222
- Klute A (1986) Method of soil analysis, physical and mineralogical methods, part 1, 2nd edn, Agronomy Monograph 9. ASA and ASSA, Madison, p 1173
- Lesta P, Ferello R (1972) Región extrandina del Chubut y norte de Santa Cruz. In: Leanza A (ed) Geología regional Argentina. Academia Nacional de Ciencias, Córdoba, pp 601–654
- Marveggio N, Llorens M (2013) Nueva edad de la base del grupo Chubut en la mena uranífera Cerro Solo, provincia del Chubut. Revista de la Asociación Geológica Argentina, Buenos Aires 70(3):318–326
- Nettleton WD, Peterson F (1983) Chapter 5, Aridisols. In: Wilding L, Smeck N, Hall G (eds) Pedogenesis and soil taxonomy II, The soil orders. Developments in soil science 11B. Elsevier, Amsterdam, pp 165–215
- Nullo F (1983) Descripción geológica de la hoja 45c, Pampa de Agnia, Provincia del Chubut. Servicio Geológico Nacional, Boletín 199, Buenos Aires, p 94
- Olson CG (1989) Soil geomorphic research and the importance of paleosol stratigraphy to quaternary investigations, midwestern USA, vol 16, Catena supplement. Catena Verlag, Cremlingen, pp 129–142
- Page AL, Miller RH, Keeney DR (1982) Methods of soil analysis, chemical and microbiological properties, Part 2, 2nd edn, Agronomy Monograph 9. ASA and SSSA, Madison, p 1159
- Peterson F (1981) Landforms of the basin and range province defined for soil survey. Max C. Fleischmann College of Agriculture, Agricultural Experiment Station. Technical Bulletin 28, p 52
- Proserpio CA (1987) Descripción geológica de la hoja 44-e, Valle General Racedo, Provincia del Chubut. Dirección Nacional de Geología y Minería, Boletín 201, Buenos Aires, p 102
- Rabassa J, Carignano C, Cioccale M (2010) Gondwana paleosurfaces in Argentina: an introduction. Geociências, São Paulo 29(4):439–466
- Rabassa J, Carignano C, Cioccale M (2014) A general overview of Gondwana Landscapes in Argentina. In: Rabassa J and Ollier C (eds.), Gondwana Landscapes in southern South America. Argentina, Uruguay and southern Brazil, 201–246. Springer Earth System Sciences, Dordrecht, p 545

- Rhue RV (1975) Geomorphology, geomorphic processes, and surficial geology. Houghton Mifflin Company, Boston, p 246
- Schaetzl RJ, Krist FJ, Miller BA (2012) A taxonomically based ordinal estimate of soil productivity for landscape-scale analyses. *Soil Science* 177(4):288–299
- Schoeneberger PJ, Wysocki DA, Benham EC, Broderson WD (2002). Field book for describing and sampling soils, version 2.0. Natural Resources Conservation Service, National Soil Survey Center, Lincoln, p 226
- SMN, Servicio Meteorológico Nacional (1981–1990) Climatic variables registered at 87814 Meteorological Station. <http://www.smn.gov.ar>
- Soil Survey Staff (1999) Soil taxonomy. A basic system of soil classification for making and interpreting soil surveys, 2nd edn. Agricultural handbook 436. Natural Resources Conservation Service, USDA, Washington, p 869
- Thomas D (1997) Arid zone geomorphology. Process, form and change in drylands, 2nd edn. Wiley, Chichester, p 713
- U.S. Salinity Laboratory Staff (1954) Diagnosis and improvement of saline and alkali soils. Agricultural handbook, vol 60. USDA, Washington, DC, p 160

Hydrological Variations Associated with Geomorphological Changes in a Sand Dune Barrier of the Partido de La Costa, Province of Buenos Aires

Silvina Carretero and Eduardo Kruse

Abstract The evolution of land use in San Clemente del Tuyú and Santa Teresita (Partido de La Costa [La Costa District], Buenos Aires, Argentina) is analysed in association with the increase in population and the presence or absence of a water supply service, in order to assess changes in the hydrological system through time. A multi-temporal analysis was undertaken on Landsat satellite images, differentiating types of land use. Water balances were estimated, and the recharge for each situation was evaluated. An increase in urbanized surface at the expense of the natural sand dune environment can be observed, which entails larger impervious surfaces that are unsuitable for the infiltration and recharge of the aquifer. In both areas, a decrease in groundwater reserves occurred; in Santa Teresita, there was even a deterioration in the chemical quality of water due to sea water intrusion. It can be concluded that the urbanization process has had a negative impact on the water system in the sand dune barrier area, affecting the infiltration and recharge processes. The presence of managed supply systems acquires relevance as a conditioning factor to avoid saltwater intrusion processes. It is essential to implement land-use planning strategies that would protect the areas unaffected by urbanization that may be of use as a reservoir for the future supply of freshwater.

Keywords Land use · Freshwater reserves · Anthropogenic modifications · Argentina

S. Carretero (✉) · E. Kruse
Facultad de Ciencias Naturales y Museo, CONICET and Universidad
Nacional de La Plata, Cátedra de Hidrología General. Calle 64 N° 3,
La Plata, Argentina
e-mail: scarretero@fcnym.unlp.edu.ar

© Springer International Publishing AG 2017
J. Rabassa (ed.), *Advances in Geomorphology and Quaternary Studies
in Argentina*, Springer Earth System Sciences,
DOI 10.1007/978-3-319-54371-0_4

1 Introduction

Coastal sand dunes can be found in a wide variety of climate regimes, and their formation depends on the availability of sand and on the winds, with vegetation development having a role in their fixation (de Seoane et al. 2007). In many cases, these environments have been degraded by anthropogenic activities—which increased significantly in the last 50 years—as it happened in New Zealand and the Netherlands, where many of the coastal systems are irreversibly altered or have disappeared (Martínez et al. 2008). Coastal dunes comprise approximately 15% of the world's coasts, with the largest barriers coinciding with tectonically stable margins, such as the east coast of the USA (3100 km) and the Gulf of Mexico coast (1600 km). There are also barrier chains along the east coast of South America (960 km), the east coast of India (680 km), the North Sea in Europe (560 km), the east of Siberia (300 km) and the north of Alaska (900 km) (FitzGerald and Buynevich 2006).

Due to their morphological characteristics and infiltration capacity, coastal dunes constitute groundwater recharge areas and freshwater reservoirs. In many cases, these reservoirs are the only source of supply to the coastal population and they act as barriers protecting from sea water intrusion (Martínez and Vázquez 2006).

There are examples of sandy coasts where aquifers have been studied, monitored and managed, for instance in the Netherlands, Belgium, the south of Italy and north-east Spain. Coastal aquifers are often of small magnitude, but they acquire relevance in the coverage of human needs, ranging from urbanization to irrigation (Custodio 2010).

Coastal aquifers have certain characteristics that make them significant from the point of view of the genesis and functioning of the natural spaces related to them. They tend to be environment with high morphological dynamism in permanent evolution. This causes morphological changes (the ones at a smaller scale are perceptible at a human timescale) that generally have an impact on the configuration of the hydrographical network and its relationship with groundwater: the quantity, location and/or extension of the aquifer recharge, discharge areas, channel route and flow volume (Manzano 2002).

Land use, particularly in urban areas and concerning its relationship with groundwater quantity and quality, has been widely addressed (Bellot et al. 2007; Houlahan and Findlay 2004; Kim 2004; Kim et al. 2003; Park et al. 2005; Weng 2001; Zuquette et al. 2004). The general influence of urbanization on the hydrological cycle includes the increase in surface run-off along roofs, pavements, streets, etc. that may drain towards the main network or main receiving body (Basile and Riccardi 2000), the modification of the natural fluctuations in groundwater levels (Batrak and Semenov 2008), the decrease in natural infiltration and the alteration of the surface run-off processes (Kruse et al. 2004).

Even though it is assumed that recharge related to precipitations decreases due to the increase in impervious surfaces in an urban area, different studies state that it may be maintained or that it may rise despite the increase in impervious areas.

Infiltrating water may come from surfaces with secondary permeability (road surfaces, pavements, car parks), infiltration ponds, irrigation, losses from the sewage system and freshwater supply system (Lerner 2002; Lerner and Barrett 1996; Hibbs and Sharp 2012; Sharp 2010; Sharp et al. 2013; Wiles and Sharp 2008). However, Seiler and Gat (2007) present other studies in which they observe a decrease of over 10% in the recharge due to drainage discharging into the sea.

In South America, aquifers in coastal dunes coincide with the deposits of the Atlantic coast (Rebouças 1999). Bocanegra et al. (2010) indicate the presence of small clastic aquifers occurring in dunes, of local interest, which are strategic water reservoirs. The most serious supply problems arise in coastal aquifers located in highly populated areas in south-east Brazil, extending towards north-east Uruguay (Almagro and Custodio 2004).

The eastern coast of the Province of Buenos Aires could be included among those places with the above-mentioned characteristics. From the mid-twenty-first century, this region has experienced a strong demographic increase, with a chaotic urbanization process and expansion of the economic activities, especially those related to the numerous seaside resorts, which led to a higher freshwater supply requirement (Kruse et al. 2012). This urban growth has contributed to the modification of the environment and, therefore, of the distribution concerning both land use and hydrological behaviour. In this region, the only source of drinking water (groundwater) shows limited development and is restricted to the water table occurring in the dune fringe (Carretero 2011). Besides the anthropogenic factor, this region is vulnerable to coastal erosion and saltwater intrusion, especially related to high-energy storm waves associated with strong south-easterly winds (“sudestadas”) (Pousa et al. 2007). The excessive exploitation of the resource due to the lack of domestic water service has brought sea water intrusion problems (Carretero et al. 2013c; Perdomo et al. 2013). Another factor to be taken into consideration is the rise in sea level related to climate change, which may affect the hydrogeology of the region in the future (Carretero et al. 2013a).

In the sandy coast of Buenos Aires, it is useful to establish the relationships between the changes in land use and groundwater quantity and quality, as the increase in stable population, together with the arrival of tourists in the summer months, is intimately linked to the consumption and management of water reserves.

In the study area, the processes of urbanization, dune destruction and soil becoming impervious affect the groundwater regime, as a consequence of the decrease in infiltration and the restriction of recharge areas (Carretero and Kruse 2010, 2014; Carretero et al. 2014). The process of urbanization to varying degrees, which brings about a decrease in possibilities for water excess infiltration restricts the natural recharge areas of the aquifer and, therefore, the available freshwater reserves.

The lack of hydrogeological data is a problem affecting the study, knowledge and understanding of coastal aquifers in South America. Bocanegra et al. (2010) point out the lack of characterization studies to support the planning and management of resources, and the lack of observation networks. In Argentina,

according to a report on water management (Planas et al. 2000), there is no database or information system on water resources, neither at a national or provincial level, which may support the management.

This situation is not unlike the one in the coast of the Province of Buenos Aires, where the lack of hydrogeological data—both historical and current—and the lack of an integral monitoring network at a regional level make it necessary to use tools and methodologies—such as the use of satellite images, which has already been applied for several decades (Byrne et al. 1980)—to recognize variations in water resources and to analyse variations in coastal regions (Huang et al. 2012; Kuleli et al. 2011; Ray et al. 2012; Shalaby and Tateishi 2007).

In this work, the evolution of land use in two localities in the Partido de La Costa [La Costa District] is analysed in association with population growth and the presence or absence of a water supply service, in order to assess changes in the hydrological system along time.

2 Study Area

The localities of San Clemente del Tuyú and Santa Teresita (Partido de La Costa, Buenos Aires) are located on a sand dune barrier (Fig. 1a). It should be noted that the inhabitants depend for the supply of water on a phreatic aquifer occurring in the above-mentioned coastal barrier, which is limited to the east and west by marine salt water and continental brackish water, respectively. The recharge to the water system only occurs by infiltration of precipitation excesses (Carretero 2011). Most of the localities in the Partido de La Costa have no drinking water service, and their inhabitants are supplied by means of individual domestic wells, with no water treatment or control of the volumes extracted. The sewage system has a wider distribution in the most important localities. It is believed that there are no significant losses from the water supply network that would feed the water table, as the network is in general in good condition and has been functioning for less than 20 years; the same applies to the sewage system.

The predominant economic activity is tourism: there are no industries, livestock farming, agriculture, or other important activities, which is why it is believed that water use is exclusive for human consumption. The population, which depends solely on the coastal aquifer for water supply, increases significantly during the summer.

The climate is humid temperate, with a dry season during the cold months (April–September) and a rainy season during the warm months (October–March). The mean annual precipitation fluctuates between 900 and 1000 mm, with 60% occurring in the months with higher evapotranspiration, which is why the highest recharge takes place during the dry season (Carretero and Kruse 2012).

The sand dune barrier extends along 70 km between Punta Rasa, to the north, and Punta Médanos, to the south, with a width ranging from 2 to 4 km. It borders to

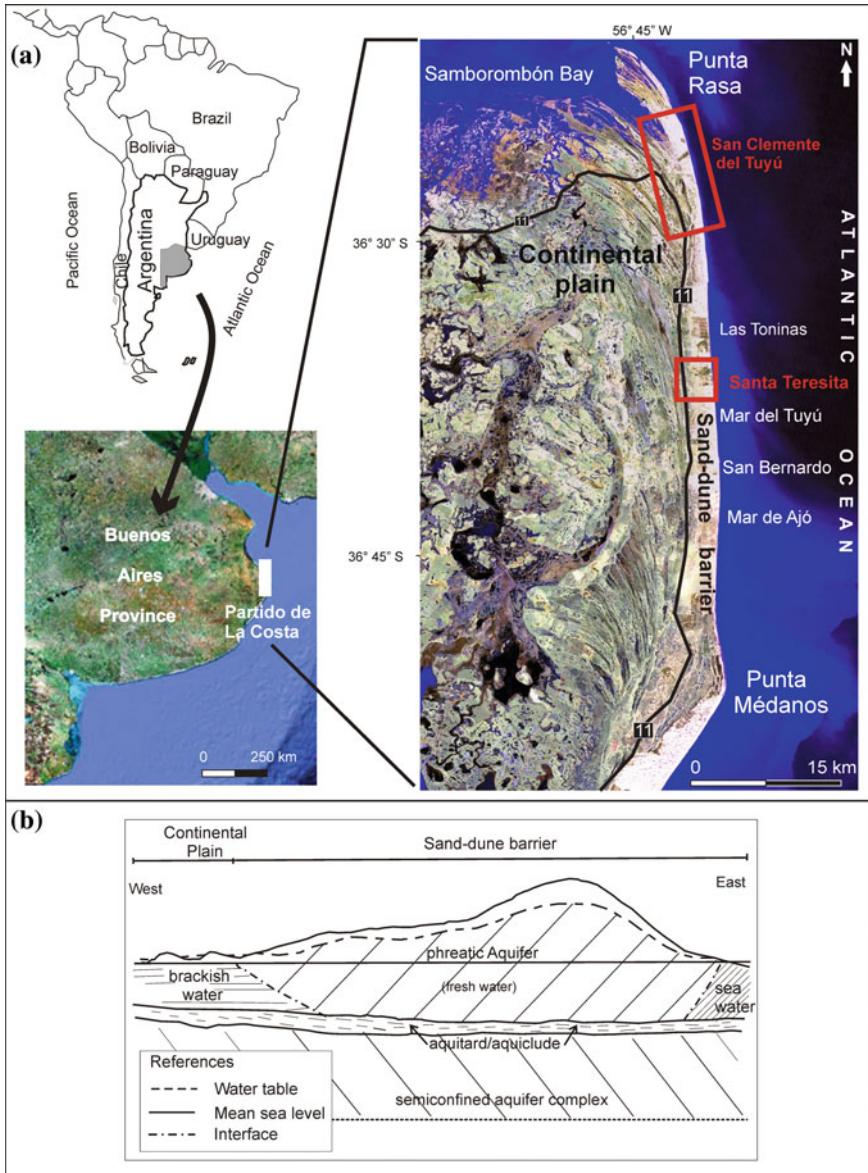


Fig. 1 a Study area. b General hydrodynamic diagram

the west with the continental plain, which is characterized by heights lower than 2 m.a.s.l. and the predominance of silty and clayey materials, with gullies oriented in a south-east–north-west direction, draining towards the Samborombón Bay.

The sand dunes in the barrier are low, with heights between 2 and 11 m.a.s.l., and fixed by sparse vegetation. In this environment, soils are sandy, with no horizon development, excessively drained and unstable.

The hydrodynamic and hydrochemical behaviour of groundwater is conditioned by the geomorphological environment. In the sand dune barrier, the water is of low salinity and mainly of the Ca–HCO₃ type, whereas in the continental plain the water shows high salinity and is of the Na–Cl type (Carretero et al. 2013b). The high Fe and Mn concentrations represent the greatest problem as regards the chemical quality in the region (Carretero and Kruse 2015).

The sand dune barrier is the main recharge area for groundwater, which then flows along a short stretch and discharges in two opposite directions: towards the sea and towards the continental plain to the west (Fig. 1b). The main freshwater aquifer is composed of dune sands (aeolian sediments) overlying barrier sands of variable thickness—between 7 and 20 m, depending on the height of the dunes—and it is bounded by two interfaces: a freshwater–brackish water interface towards the continent and a freshwater–saltwater interface towards the sea; this unit overlies aquitard/aquiclude sediments. In the Punta Médanos sector, an underlying semi-confined aquifer composed of sand and silty–clayey sand can be recognized; this unit overlies plastic clays.

3 Methodology

Fieldwork was undertaken, and the geomorphological, hydrogeological and land-use characteristics were assessed. Based on the contribution by Carretero et al. (2014), the areas of interest in the Landsat TM satellite images were selected for 1986 and 2010. This selection was based on the fact that there are historical data (CFI 1990) and current samplings (2012) that made it possible to draw isophreatic curve and electric isoconductivity maps.

A multi-temporal analysis was carried out on Landsat TM satellite images with a spatial resolution of 30 m, which were obtained from USGS/EROS (Earth Resources Observation and Science, <http://glovis.usgs.gov>). Each of the images consists in two scenes from February, in order to compare appropriately the maps and avoid introducing errors due to seasonal variation.

The images were rectified radiometrically with the gain and offset values from the metadata file, following Chander et al. (2009), and subsequently corrected geometrically before mosaicking using a WGS84 datum and UTM projection with ENVI™ software (Exelis VIS). It was not necessary to apply an atmospheric correction, as the multi-date classification procedure was carried out using spectral features obtained from each image (Song et al. 2001). In order to map land cover/land use, a decision tree classification algorithm was used. Each pixel was assigned to one of the six classes of pixels with similar spectra by means of a series of binary splits. The classes are bright sand, dark sand, dense vegetation, sparse vegetation,

bare soil and urbanized area. A statistical analysis was applied to every set, and a comparison of the mean radiance spectra was undertaken to corroborate class separation.

The study area was delimited to the localities of San Clemente del Tuyú and Santa Teresita, using Ruta Nacional 11 (National Route 11) as a limit to the west and the sea to the east. The output layers were manually reprocessed with a GIS (geographic information system) tool; and based on images and field surveys, four classes corresponding to the more significant land uses (mobile dune, semi-fixed dune, fixed dune and urbanized area) were determined. The changes that took place in the sand dunes were evaluated by calculating the areas affected by such changes and the percentage variations for each land-use type across the years studied.

The water balances were estimated by means of the methodology proposed by Thornthwaite and Mather (1955), based on precipitation data from the Servicio Meteorológico Nacional (SMN; National Weather Service of Argentina) station in Santa Teresita and a rain gauge set in San Clemente del Tuyú. Data from nearby stations, which are located outside the study area, have been added in order to have a more detailed outlook on the water balances at a regional level. Daily mean ET_0 (reference evapotranspiration) values, estimated according to Penman-Monteith (Allen et al. 1998), were used.

An infiltration value was assigned to each type of land use, and the recharge for each situation was evaluated. Besides, population growth was considered, analysing the statistics of the INDEC (1981, 2010) for the localities of the Partido de La Costa. Based on such data, the mean annual water demand for the region was estimated. Considering 200 L/d as average consumption (Planas et al. 2000), the volume necessary to supply the permanent inhabitants was calculated.

4 Land Use and Its Evolution

The analysis of satellite images resulted in a territory classification into four classes of land use: mobile dune, semi-fixed dune, fixed dune and urbanized area (Fig. 2). In the first three classes, the sandy substrate is preserved and covered by different percentages of vegetation.

The mobile dune occurs adjacent to the beach, along the coastline towards the west, and it maintains its natural transport dynamics due to the winds from the east. Although the presence of vegetation can be observed, it is very sparse and shows no signs of urbanization.

Slightly farther from the coast occurs the semi-fixed dune, showing a higher percentage of vegetation, which is capable of retaining sand. This fixation process represents the natural evolution of the mobile dune towards the semi-fixed dune. In some sectors, although the vegetation is not so abundant, the fixation phenomenon occurs due to sand compaction, as is the case in roads and streets, which constitutes a case of anthropogenic modification. The percentage of houses or urbanization features is minimal.



Fig. 2 Land-use classification **a** mobile dune, **b** semi-fixed dune, **c** fixed dune and **d** urbanized area

The area classified as fixed dune is located further into the continent and is covered by abundant vegetation. As in the semi-fixed dune, the signs of anthropogenic alteration are minimal.

Finally, the class comprising the urbanized areas, where the natural characteristics of the dune cannot be observed, was defined. This is the sector that has been modified the most with respect to the natural environment: It is composed of buildings and—in certain areas—paved streets, which represent practically impervious surfaces.

In the image analysis (Fig. 3), an increase in urbanized surfaces at the expense of the natural sand dune environment can be observed, implying larger impervious surfaces unsuitable for the infiltration and recharge of the aquifer. Although this process can be recognized in both localities, it is of a larger magnitude in Santa Teresita than in San Clemente del Tuyú (Table 1). On the other hand, the mobile dune has practically disappeared in Santa Teresita, replaced by the urban grid, whereas in San Clemente it is only partially reduced. A slight advance of the fixed dune (vegetation) over the mobile dune can be observed, interfingered with the semi-fixed dune in certain sectors, which is part of the natural process of evolution of the sand dune barrier.

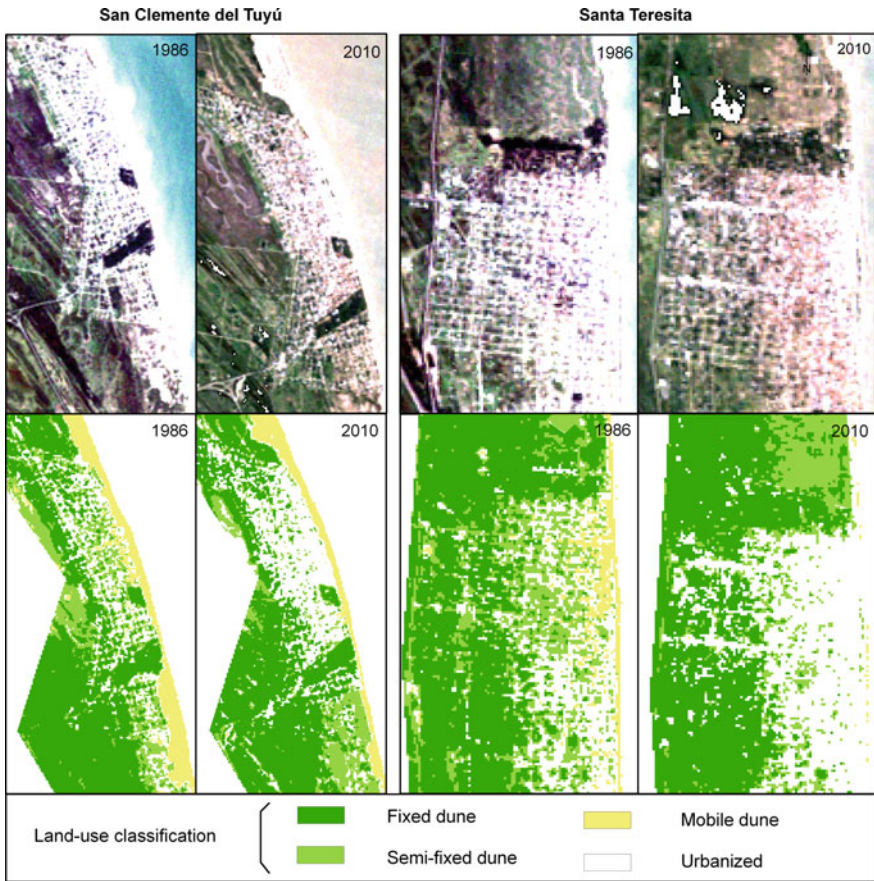


Fig. 3 Land-use changes between 1986 and 2010

Table 1 Area, estimated recharge and variation percentage corresponding to the land-use classification for the years studied

		Area (km ²)		Recharge (hm ³)		Variation (%)
		1986	2010	1986	2010	2010–1986
San Clemente	Mobile dune	2.06	1.24	0.9	0.6	-40
	Semi-fixed dune	3.41	2.95	1.2	1.0	-14
	Fixed dune	9.54	9.40	2.97	2.9	-1
	Urbanized	1.97	3.40	0.13	0.2	72
	Total	17.0	17.0	5.2	4.7	-9
Santa Teresita	Mobile dune	0.57	0.03	0.3	0.01	-95
	Semi-fixed dune	2.07	1.78	0.7	0.6	-14
	Fixed dune	4.17	3.58	1.3	1.1	-14
	Urbanized	1.22	2.64	0.1	0.2	117
	Total	8.0	8.0	2.4	1.9	-18

5 Modifications to the Hydrological System

The only water input into the aquifer comes from precipitations. The water balances (Table 2) and Carretero and Kruse (2010) show that there is no appreciable climate variability, with a mean annual precipitation of 968 mm and a water surplus of 444 mm, which—through infiltration—constitute the only recharge to the groundwater system.

The comparative analysis of the water-table contour maps (Fig. 4) shows that in San Clemente, the curves fluctuate between 0.5 and 2.5 m.a.s.l., both for 1987 and 2012. However, it can be observed that the contour of 1 m.a.s.l. is displaced towards the interior, and an areal reduction in the contours of 1.5 and 2.5 m.a.s.l. occurs in the period studied.

In Santa Teresita, water-table heights vary from 1.5 to 5 m.a.s.l. in 1987, with a decrease by 2012 to 1 and 3.5 m.a.s.l.

These changes in phreatic morphology are evident in the water-level change map (Fig. 5), where the highest generalized decrease in the levels (2.5 m) can be observed in Santa Teresita.

On the other hand, the hydrochemistry (Fig. 6) indicates that in Santa Teresita, a saltwater intrusion phenomenon has occurred in certain sectors along Avenida Costanera (Coastal Avenue), whereas in San Clemente del Tuyú the chemical quality has remained within the same parameters throughout the period analysed.

Depending on the area and the geomorphological characteristics of each of the land-use classes, a percentage of infiltration of the water excesses in the water balance was defined for each class. In the mobile dune, the infiltration of the water excesses occurs over 100% of its surface, in the semi-fixed dune in 80%, whereas in the fixed dune it is reduced to 70%.

According to different authors and in different cities (Auge 2005; Kruse et al. 2013; Vázquez Suñé and Sánchez-Vila 1997; Wiles and Sharp 2008), urbanized areas have been assigned infiltration values ranging from 6 to 36% of the precipitations. As regards this case study, it is assumed that 15% of the excess infiltrates over small surfaces and the rest constitutes surface run-off discharging into the sea.

Table 2 Average water balance. Values are expressed in mm/year. PET (potential evapotranspiration), ETr (real evapotranspiration)

Station	Period	Precipitation	PET	ETr	Water surplus
Punta Indio	1925–2008	965	747	523	441
Dolores	1959–2008	944	690	519	424
Santa Teresita	1990–2007	995	684	525	468
San Clemente	2003–2012	911	698	472	436
Average		968	707	522	444

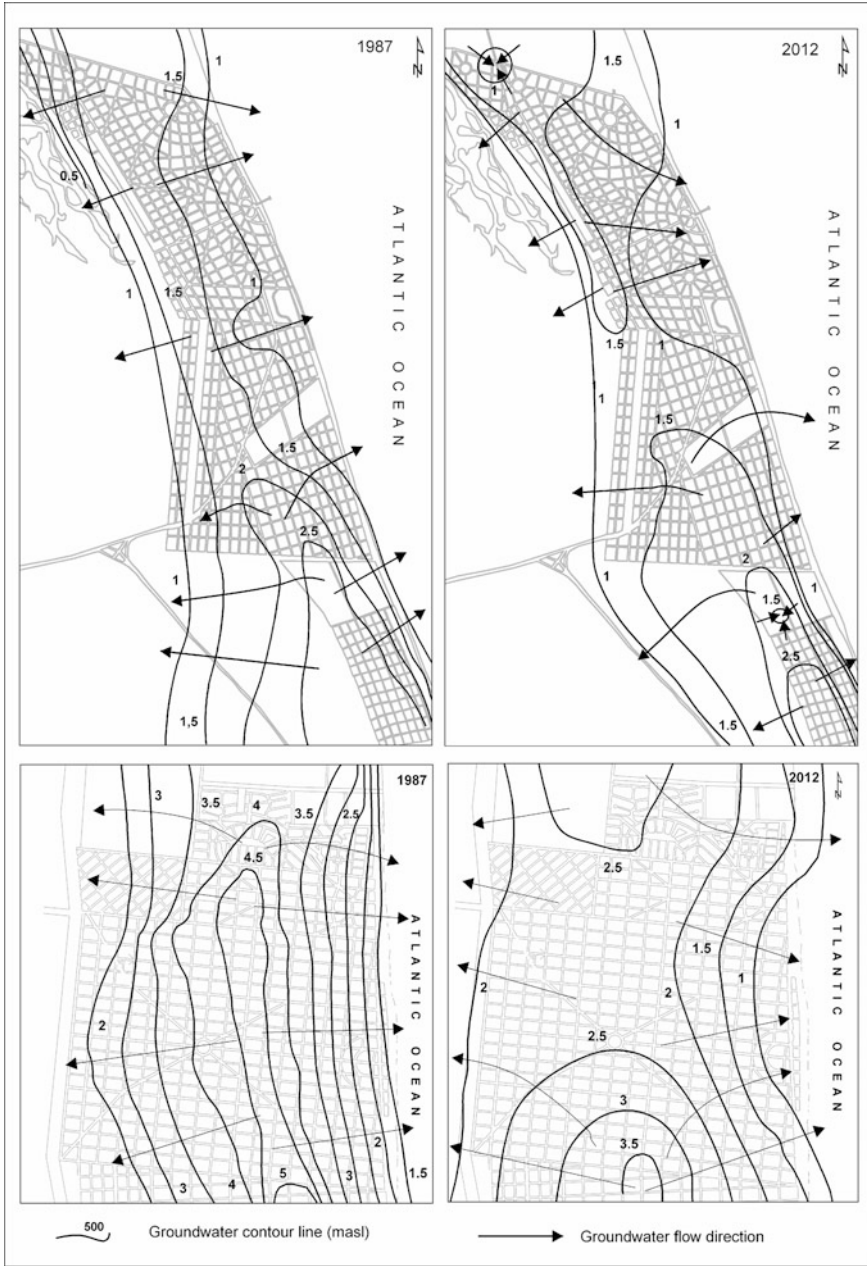


Fig. 4 Water-table contour maps: San Clemente (above) and Santa Teresita (below)

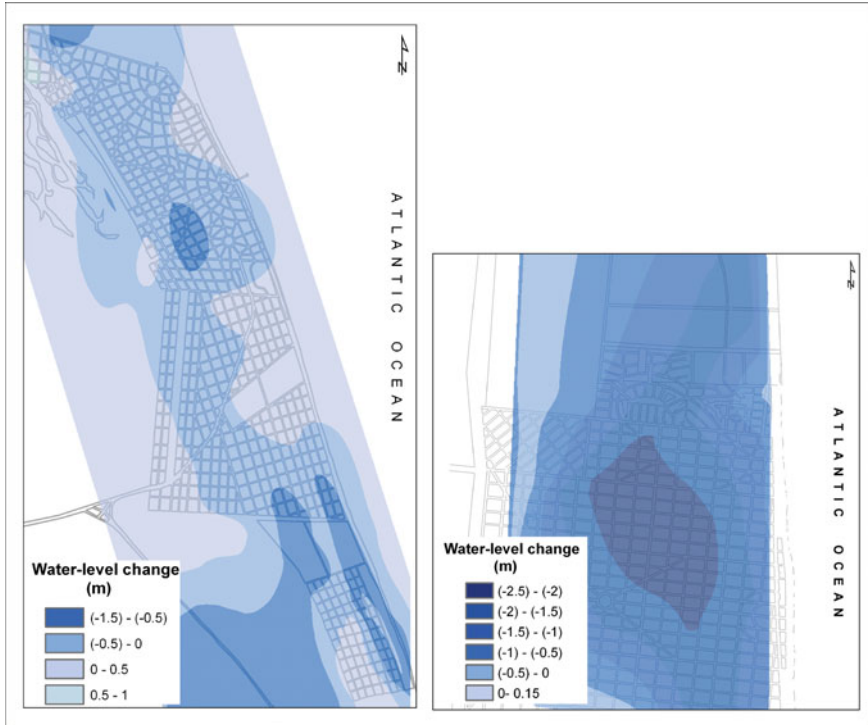


Fig. 5 Water-level change maps: San Clemente (*left*) and Santa Teresita (*right*)

Based on the areas calculated for each land use and the infiltration percentage assigned, the theoretical volume of water recharging into the aquifer and the interannual variations were estimated (Table 1).

If the variations depending on land use are considered, it can be observed that in the urbanized area, even though the numbers seem to indicate that there is an increase in recharge, this is only caused by its areal expansion. This is an apparent increase, since despite the fact that it is the sector with highest areal increase, it is also the one with the lowest infiltration capacity. At this point, the aspect to be noted is that urbanization has developed by replacing the natural sand dune environment, which has the highest infiltration capacity. This leads to a reduction in total recharge, resulting in twice as much recharge reduction in Santa Teresita compared to San Clemente.

In Santa Teresita, the groundwater reserves in the mobile dune decreased by 95%, whereas in San Clemente they did so by 40%; in the semi-fixed dune, the decrease is similar in both localities (14%).

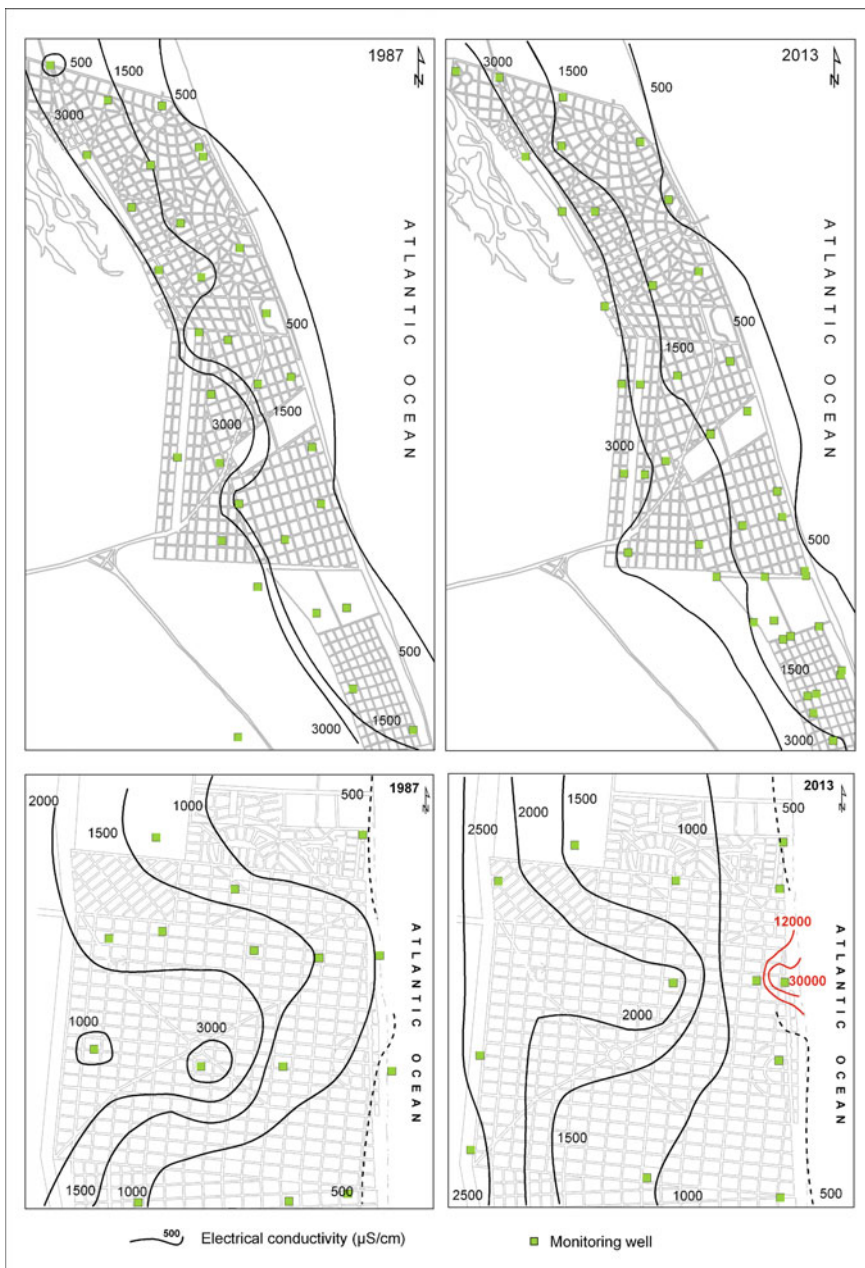


Fig. 6 Iso-electrical conductivity maps: San Clemente (*above*) and Santa Teresita (*below*)

Table 3 Population variation and water consumption

	Population		Growth rate	Water demand (hm ³ /year)	
	1986	2010		1986	2010
San Clemente	6482	13071	2.0	0.5	1.0
Santa Teresita	9052	22943	2.5	0.7	1.7

As well as a decrease in the reserves due to the increase in urbanized areas, a decrease associated with a growth in population and an increase in consumption in both areas occurred (Table 3). It should be noted that the chemical quality of the water has only deteriorated in Santa Teresita.

It is proposed that the conditioning factor in this case is the presence or absence of a water supply service in the localities. In San Clemente del Tuyú, the drinking water supply system mainly feeds the city centre, where the restaurants, hotels and largest buildings are located, on Avenida Costanera. The resource is obtained by means of a well system at a depth of 6 m, from a pumping field located to the south, out of the urbanized area, in the semi-fixed dune. Wellpoint systems and Ranney wells were used, in which the extraction volumes reach 13 and 7 m³/h, respectively (Fig. 7). The average daily extraction volumes in the summer fluctuate between 1500 and 1800 m³; out of season, the average is 500 m³. There is a water purification plant, where water is treated (mainly Fe and Mn abatement) for its subsequent distribution.

On the other hand, Santa Teresita lacks such a service, and most of the urban development is on the coastal road, where large buildings and hotels extracting water with no control whatsoever can be observed.

Both localities share the same geohydrological environment and water balance excesses. They also show certain percentages of impervious surfaces and a greater urban development on Avenida Costanera, which is logical given that, due to its proximity to the sea, it is a major tourist attraction. They differ in the deterioration of the chemical quality of the water, as an advance of the freshwater/saltwater interface occurs in Santa Teresita. The only variable that seems to make a difference is the absence of a water supply network in this locality. This lack implies that users must be supplied by domestic wells, with no control over the quantity and quality of the water resource extracted. At a domestic level, this scheme may not seem to be too detrimental, but the perspective changes radically when taking into consideration the presence of hotels and buildings in a location that is near the saltwater wedge and in which the number of people per unit area is high. The result is a process of sea water intrusion and a deterioration of the resource.

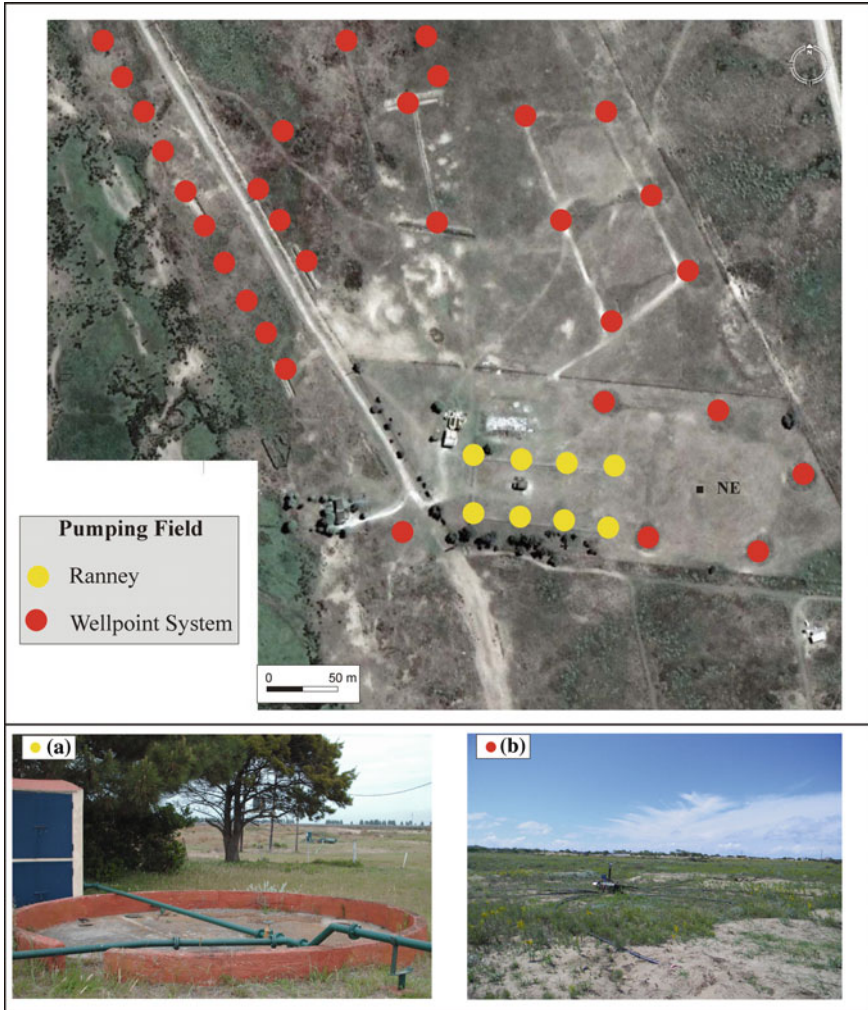


Fig. 7 Pumping field in San Clemente

6 Conclusions

The reduction in the mobile dune, which has been replaced by the establishment of cities in front of the sea, is noticeable. The fixed dune has replaced the semi-fixed dune in small sectors.

It can be observed that the urbanization process (impervious surfaces) has had a negative impact on the water system in sand dune barrier areas, affecting the processes of infiltration and recharge.

According to the methodology applied, the freshwater recharge has been reduced twice as much in Santa Teresita compared to San Clemente.

The presence of controlled drinking water supply systems acquires relevance as a conditioning factor to avoid saltwater intrusion processes in seaside localities.

The implementation of land-use planning strategies is essential to protect the areas not affected by urbanization that may act as a reservoir for future supply to the population.

References

- Allen RG, Pereira LS, Raes D, Smith M (1998) Crop evapotranspiration—guidelines for computing crop water requirements. FAO Irrigation and Drainage Papers 56. FAO, Rome
- Almagro L, Custodio E (2004) Caracterización hidrogeoquímica de las aguas subterráneas de la Formación Chuy en la franja costera del Este del Uruguay fronteriza con Brasil. *Bol Geol y Min* 115:357–378 (Montevideo)
- Auge M (2005) Hidrogeología de La Plata Provincia de Buenos Aires. In: de Barrio RE, Etcheverry RO, Caballé MF, Llambías EJ (eds) *Geología y Recursos Minerales de la Provincia de Buenos Aires Relatorio del XVI Congreso Geológico Argentino*. Asociación Geológica Argentina, La Plata, Buenos Aires, pp 293–326
- Basile PA, Riccardi GA (2000) Procesos hidrológicos urbanos. In: Orsonino HE, Zimmermann ED, Basile PA (eds) *Hidrología procesos y métodos*. Universidad Nacional de Rosario, Rosario, pp 253–280
- Batrak G, Semenov S (2008) Groundwater's dynamic regime in urban territories 33rd international geological congress abstract CD HYH-01 general contribution to hydrogeology. Oslo, Norway
- Bellot J, Bonet A, Peña J, Sánchez J (2007) Human impacts on land cover and water balances in a coastal Mediterranean county. *Environ Manage* 39(3):412–422
- Bocanegra E, Da Silva Cardoso, Jr G, Custodio E, Manzano M, Montenegro S (2010) State of knowledge of coastal aquifer management in South America. *Hydrogeol J* 118:261–267
- Byrne GF, Crapper PF, Mayo KK (1980) Monitoring land-cover change by principal component analysis of multitemporal Landsat data. *Remote Sens Environ* 10:175–184
- Carretero S (2011) Comportamiento hidrológico de las dunas costeras en el sector nororiental de la provincia de Buenos Aires. Unpublished doctoral thesis. Facultad de Ciencias Naturales y Museo, Universidad Nacional de La Plata, Argentina. http://sedici.unlp.edu.ar/bitstream/handle/10915/4918/Documento_completo.pdf?sequence=1. Accessed 20 Nov 2014
- Carretero S, Kruse E (2010) Modificaciones en las áreas de recarga del acuífero freático en los médanos costeros de San Clemente del Tuyú, provincia de Buenos Aires. *Revista Asociación Geológica Argentina* 66(4):466–474 (Buenos Aires)
- Carretero S, Kruse E (2012) Relationship between precipitation and water-table fluctuation in a coastal dune aquifer: northeastern coast of the Buenos Aires province, Argentina. *Hydrogeol J* 20:1613–1621
- Carretero S, Kruse E (2014) Impacto de la urbanización en la infiltración en un área costera, Argentina. *Tecnología y Ciencias del Agua* 5(6):5–24
- Carretero S, Kruse E (2015) Iron and manganese content in groundwater on the northeastern coast of the Buenos Aires province, Argentina. *Environ Earth Sci* 73(5):1983–1995
- Carretero S, Rapaglia J, Bokuniewicz H, Kruse E (2013a) Impact of sea level rise on saltwater intrusion length into the coastal aquifer, Partido de La Costa, Argentina. *Cont Shelf Res* 61–62:62–70

- Carretero S, Dapeña C, Kruse E (2013b) Hydrogeochemical and isotopic characterisation of groundwater in a sand-dune phreatic aquifer on the northeastern coast of the province of Buenos Aires. *Isot Environ Health Stud* 49(3):399–419
- Carretero S, Kruse E, Rojo A (2013c) Condiciones hidrogeológicas en Las Toninas y Santa Teresita, Partido de La Costa. In: González N, Kruse E, Trovatto MM, Laurencena P (eds) *Temas actuales en hidrología subterránea*. Editorial de la Universidad Nacional de La Plata (EDULP), La Plata, pp 28–35
- Carretero S, Braga F, Kruse E, Tosi L (2014) Temporal analysis of the changes in the sand-dune barrier in the Buenos Aires Province, Argentina and their relationship with the water resources. *Appl Geog* 54:169–181
- CFI (1990) Evaluación del Recurso Hídrico Subterráneo de la Región Costera Atlántica de la Provincia de Buenos Aires Región 1 Punta Rasa-Punta Médanos Informe Final Tomo 1 Hidrología Subterránea. CFI, Buenos Aires
- Custodio E (2010) Coastal aquifers of Europe: an overview. *Hydrogeol J* 18:269–280
- Chander G, Markham BL, Helder DL (2009) Summary of current radiometric calibration coefficients for Landsat MSS TM ETM+ and EO-1 ALI sensors. *Remote Sens Environ* 113:893–903
- de Seoane CLV, Gallego Fernández JB, Vidal Pascual C (2007) *Manual de restauración de dunas costeras*. Ministerio de Medio Ambiente, Dirección General de Costas, Spain
- FitzGerald DM, Buynevich IV (2006) Coastal barriers. In: Iribarne O, Isla F (eds) *Coastal zone and estuaries. Encyclopedia of life support systems (EOLSS) developed under the Auspices of the UNESCO*, Eolss Publishers Oxford, UK. <http://www.eolss.net/outlinecomponents/Coastal-Zones-Estuaries.aspx>. Accessed 21 Ago 2014
- Hibbs BJ, Sharp JM Jr (2012) Hydrogeological impacts of urbanization. *Environ Eng Geosci* 18:3–24
- Houlahan J, Findlay C (2004) Estimating the ‘critical’ distance at which adjacent land-use degrades wetland water and sediment quality. *Landscape Ecol* 19:677–690
- Huang J, Gilmore Pontius R Jr, Li Q, Zhang Y (2012) Use of intensity analysis to link patterns with processes of land change from 1986 to 2007 in a coastal watershed of southeast China. *Appl Geogr* 34:371–384
- INDEC (Instituto Nacional de Estadística y Censos de la República Argentina) (1981) Censo Nacional de Población Hogares y Viviendas, Buenos Aires. <http://www.indec.gov.ar>. Accessed 15 July 14
- INDEC (Instituto Nacional de Estadística y Censos de la República Argentina) (2010) Censo Nacional de Población Hogares y Viviendas, Buenos Aires. <http://www.indec.gov.ar>. Accessed 15 July 14
- Kim Y-Y (2004) Analysis of hydrochemical processes controlling the urban groundwater system in Seoul area, Korea. *Geosci J* 8(3):313–318
- Kim Y, Lee K, Koh D, Lee D, Lee S, Park W, Koh G, Woo N (2003) Hydrogeochemical and isotopic evidence of groundwater salinization in a coastal aquifer: a case study in Jeju volcanic island, Korea. *J Hydrogeol* 270:282–294
- Kruse E, Varela L, Laurencena P, Deluchi M, Rojo A, Carol E (2004) Modificaciones del ciclo hidrológico en un área del Noreste de la Provincia de Buenos Aires, Argentina. In: Junta Directiva AIH-GD (eds) *Serie Hidrogeología y Aguas Subterráneas 11*, Instituto Geológico Minero de España, Madrid
- Kruse E, Carretero S, Pousa J, Guaraglia D (2012) Critical problems for the fresh water supply to summer resorts on the eastern coast of the Buenos Aires province Argentina. In: Rossi AE, Miranda LS (eds) *Argentina: environmental geographical and cultural issues*. Nova Science Publishers, New York
- Kruse E, Carol E, Mancuso M, Laurencena P, Deluchi M, Rojo A (2013) Recharge assessment in an urban area: a case study of La Plata Argentina. *Hydrogeol J* 21:1091–1100
- Kuleli T, Guneruglu A, Karsli F, Dihkan M (2011) Automatic detection of shoreline change on coastal Ramsar wetlands of Turkey. *Ocean Eng* 38:1141–1149
- Lerner DN, Barrett MH (1996) Urban groundwater issues in the UK. *Hydrogeol J* 4:80–89

- Lerner DN (2002) Identifying and quantifying urban recharge: a review. *Hydrogeol J* 10:143–152
- Manzano M (2002) El papel de los acuíferos costeros en la gestión del medio natural. In: Bocanegra E, Martínez D, Massone H (eds) *Groundwater and human development*. ALSHUD, Mar del Plata, pp 2017–2024
- Martínez ML, Vázquez G (2006) Coastal sand dune and barrier island. In: Iribarne O, Isla F (eds) *Coastal zone and estuaries. Encyclopedia of life support systems (EOLSS) developed under the Auspices of the UNESCO Eolss Publishers*. Oxford, UK. <http://www.eolss.net/outlinecomponents/Coastal-Zones-Estuaries.aspx>. Accessed 21 Ago 2014
- Martínez ML, Psuty NP, Lubke RA (2008) A perspective on coastal dunes. In: Martínez ML, Psuty NP (eds) *Coastal dunes ecology and conservation ecological studies*, vol 171. Springer, Heidelberg, pp 3–10
- Park S-S, Kim S-O, Yun S-T, Chae G-T, Yu S-Y, Kim S, Young K (2005) Effects of land use on the spatial distribution of trace metals and volatile organic compounds in urban groundwater Seoul, Korea. *Environ Geol* 48:1116–1131
- Planas AC, Gaviño Novillo M, Mendiburo N, Calcagno A, Urbano Jáuregui L (2000) Informe sobre la gestión del agua en la República Argentina. JVP Consultores, Buenos Aires
- Perdomo S, Carretero S, Kruse E, Ainchil J (2013) Identificación de la intrusión salina en Santa Teresita (Buenos Aires) mediante la aplicación de métodos eléctricos. In: González N, Kruse E, Trovatto MM, Laurencena P (eds) *Temas actuales en hidrología subterránea*. Editorial de la Universidad Nacional de La Plata (EDULP), La Plata, pp 44–49
- Pousa J, Tosi L, Kruse E, Guaraglia D, Bonardi M, Rizzetto F, Schnack E (2007) Coastal processes and environmental hazards: the Buenos Aires (Argentina) and Venetian (Italy) Littorals. *Environ Geol* 51:1307–1316
- Ray DK, Pijanowski BC, Kendall AD, Hyndman DW (2012) Coupling land use and groundwater models to map land use legacies: assessment of model uncertainties relevant to land use planning. *Appl Geogr* 34:356–370
- Rebouças ADC (1999) Groundwater resources in South America. *Episodes* 22(3):232–237
- Seiler K-P, Gat JR (2007) Man's impact on the groundwater recharge. *Groundwater recharge from run-off infiltration and percolation*. Springer, Netherlands, pp 187–200
- Shalaby A, Tateishi R (2007) Remote sensing and GIS for mapping and monitoring land cover and land-use changes in the Northwestern coastal zone of Egypt. *Appl Geogr* 27:28–41
- Sharp JM Jr (2010) The impacts of urbanization on groundwater systems and recharge *AQUAmundi* 1:51–56
- Sharp JM, Krothe JN, Mather JD, Garcia-Fresca B, Stewart CA (2013) Effects of urbanization on groundwater systems. In: Heiken G, Fakundiny R, Sutter J (eds) *Earth science in the city: a reader*. American Geophysical Union, Washington DC
- Song C, Woodcock CE, Seto KC, Lenney MP, Macomber SA (2001) Classification and change detection using Landsat TM data: when and how to correct atmospheric effects? *Remote Sens Environ* 75(2):230–244
- Thornthwaite C, Mather J (1955) The water balance. *Climatology* 8:1–37
- Vázquez Suárez E, Sánchez-Vila X (1997) Cálculo de balance y recarga en la ciudad de Barcelona. In: Custodio E, Llamas MR, Samper J (eds) *La evaluación de la recarga a los acuíferos en la planificación hidrológica*. Textos del Seminario celebrado en Las Palmas de Gran Canaria, Instituto Tecnológico Geominero de España, Madrid
- Weng Q (2001) Modelling urban growth effects on surface runoff with the integration of remote sensing and GIS. *Environ Manage* 28(6):737–748
- Wiles TJ, Sharp JM Jr (2008) The secondary permeability of impervious cover. *Environ Eng Geosci* 14:251–265
- Zuquette L, Pejon O, Dos Santos Collares J (2004) Land degradation assessment based on environmental geoindicators in the Fortaleza metropolitan region state of Ceará, Brazil. *Environ Geol* 45:408–425

Uncertainty and Sensitivity Analysis of GIS-Based Landslide Susceptibility Models in Northwestern Argentina. Implications for Future Hazard Assessment at the Basin Scale

Diego Sebastián Fernández and María Elena Puchulu

Abstract Different landslide susceptibility models are applied in this contribution at the basin level, and their performance is evaluated using statistical techniques. Global sensitivity analysis of the models is performed in order to evaluate how the errors associated with input factors affect the model results. Three single models (logistic regression (LR), weight of evidence (WE) and factor of safety (FS)) were applied in a subtropical river basin located in the province of Tucumán, northwestern Argentina. Shallow landslide/debris-flow inventory maps from different basins situated at the pre-Andean mountainous region were used as training set areas. Statistical indicators show that the LR model outperforms the other in its predictive capacity taking into account both positive and negative results according to the degree of fit between the observed field data and susceptibility map obtained. Results showed that the LR model provided the best prediction accuracy of landslide susceptibility models used in the Jaya Watershed with ROC curve equal to 0.802, whereas the worst performance was obtained by the WE model with ROC curve equal to 0.713. LR model demonstrates a more robust behavior than the others, according to the balance between true-positive and true-negative indicators.

Keywords Landslide susceptibility models · Performance evaluation · Global sensitivity · Tucumán · Argentina

D.S. Fernández (✉)

Servicio Geológico Mínero Argentino (SEGEMAR), Delegación Tucumán,
Miguel Lillo 251-2P, 4000 Tucumán, Argentina
e-mail: diefer@csnat.unt.edu.ar

D.S. Fernández · M.E. Puchulu

Facultad de Ciencias Naturales and Instituto Miguel Lillo, Universidad Nacional
de Tucumán, Miguel Lillo 205, 4000 Tucumán, Argentina

© Springer International Publishing AG 2017

J. Rabassa (ed.), *Advances in Geomorphology and Quaternary Studies
in Argentina*, Springer Earth System Sciences,
DOI 10.1007/978-3-319-54371-0_5

1 Introduction

Landsliding is one of the most widespread hazards in mountainous areas, and it can be particularly devastating when it occurs adjacent to human settlement and infrastructure. Landslide susceptibility constitutes a key stage in the spatial landslide risk assessment framework. Its main goal is to predict the areas prone to suffer landslides, based on environmental factors such as slope, lithology, strength of materials, depth. The spatial probability of landsliding can be obtained either through dynamic modeling or through analyzing the relationships between the locations of past landslide events (inventory map) and the environmental factors. There are numerous methods for determining the susceptibility to landsliding, which basically can be grouped into 4 classes: probabilistic methods, statistical methods, heuristics methods and deterministic methods.

Probabilistic methods contemplate different models (i.e., Poisson model, density estimation, Gaussian mixture model) and are based on a detailed inventory of multitemporal landslide where it comes to determining the probability of occurrence of different magnitude landslides at specific terrain slopes (Lee 2015).

Statistics methods, bivariate or multivariate, have been widely developed and are based on the relationship between landslide observed locations and the geo-environmental characteristics of the area under the premise that landslides tend to occur under the same conditions as those which occurred recently (Mancini et al. 2010). The specific combination of environmental factors will vary for different landslide types, landslide depths and landslide volumes (Van Westen et al. 2006).

The heuristic approach is a direct, or indirect, mostly qualitative method that depends on how well and how much the investigator understands the geomorphological processes acting upon the terrain (Guzzetti et al. 1999). Direct approach is based on geomorphological maps, and indirect approaches involved different techniques like Boolean logic, fuzzy logic, multiclass overlay or spatial multicriteria evaluation. Instability factors are ranked and weighted on the basis of their importance assumed according the expert judgment of the earth scientist.

Deterministic models are physical-based methods that require detailed dataset about spatial variation of parametric values related to hydrological conditions (subsurface flow), soil thickness and soil cohesive strength (Iverson 2000; Claessens et al. 2007). Stability conditions are generally evaluated by means of a static model, such as the “infinite slope model”, where the local equilibrium along a potential slip surface is considered (Guzzetti et al. 1999).

In Argentina, landslide susceptibility models were applied in pre-Andean and Andean regions. Most of them are statistical and heuristics models. Relative frequency model (Moreiras 2005) and probabilistic model (Moreiras 2009) were used in central Andean region, and multivariate logistic regression was applied in northwestern pre-Andean region (Fernández and Puchulu 2015). An indirect heuristic approach, a combination of qualitative maps, was applied by Bejerman (2005). The statistical index (Wi) and logistic regression models were applied and verified for analysis of flows vulnerability in a portion of the dry frontal Andes and

western Pre-Andes of Argentina (Esper Angillieri 2012). Spatial prediction validation was contemplated during this work allowing the models comparison.

All these methods have advantages and disadvantages when analyzing the landslide susceptibility, but performance evaluation in predicting the location where these events can occur should be determinant. Several studies with focus on landslide susceptibility models performance evaluation using different techniques have been published (Carrara 1983; Van Westen et al. 1999; Crosta and Frattini 2003; Lee et al. 2003; Yesilnacar and Topal 2005; Carrara et al. 2008). Evaluation of robustness and reliability of a landslide model is a difficult task because the uncertainty is a fact of landslide susceptibility zoning and none of the methods are particularly accurate. Frattini et al. (2010) made a revision on different available techniques to evaluate the performance of landslide susceptibility models; then, they applied them for debris-flow susceptibility in Northern Italy. Among these techniques, cutoff-independent statistic methods are commonly used, such as the receiver operating characteristic (ROC) curves and success rate curves for validation purposes. Whereas these techniques are appropriate for comparing the performance of the model, they do not provide sufficient information about the error of the model or the degree of error introduced by the input factors. For this reason, uncertainty analysis (UA) and sensitivity analysis (SA) are required in model evaluation in any field where models are used. UA allows assessing the uncertainty associated with the model response as a result of uncertainties in the model input. SA studies how the variation in the model output can be apportioned to different sources of variations, and how the given model depends upon the information fed into it (Crosetto et al. 2000).

The goal of this study is to evaluate the performance of three landslide susceptibility commonly used models at the hydrological basin level with emphasis on the respective sensitivity and uncertainty analysis. The models were selected taken into account their capability of providing reliable results under a GIS environment.

2 Materials and Methods

2.1 Study Area Characteristics

The study area covers the Jaya River basin located in the eastern side of the pre-Andean mountain ranges of the province of Tucumán, approximately 100 km southwest of the provincial capital city, San Miguel de Tucumán, in the NW region of Argentina (Fig. 1). The relief of the province is characterized by the presence of the pre-Andean ranges that are located in the western part with a general north-south direction. This arrangement generates a marked altitudinal gradient from east to west, with extreme values of 300 m a.s.l. in the lower areas of the plain and more than 5000 m a.s.l. in the upper parts. Mountain fronts act as orographic barrier to the humid winds and control the distribution of the precipitations of the area.

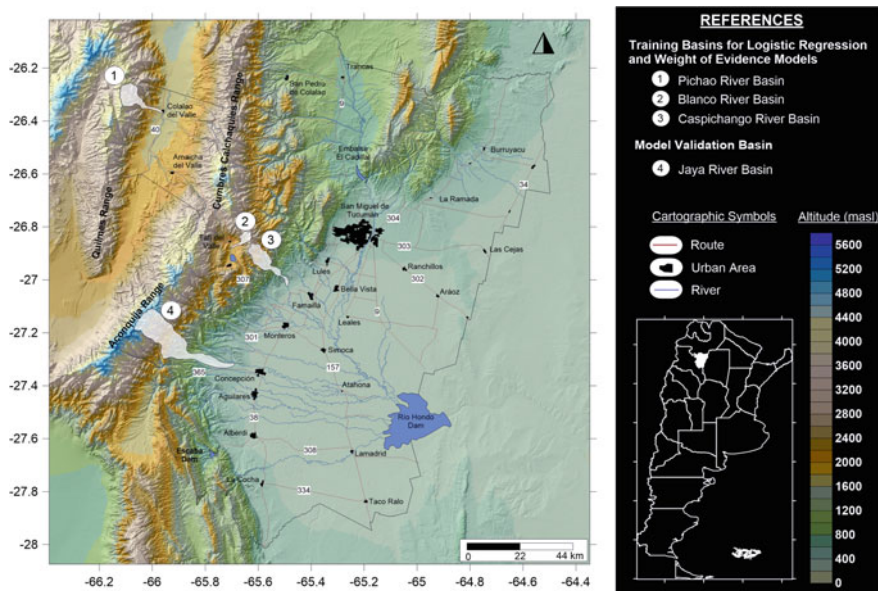


Fig. 1 Location map of the study area

Precipitations range from 500 mm per year in the eastern plain to 2000 mm per year in mountainous area. To the west, in altitudinal valleys, precipitation descends to 250 mm per year. Vegetation is strongly influenced by precipitation distribution. Mountain area is covered by rain forest, locally called “Yungas” whereas in western valleys xerophyte vegetation predominates.

The Jaya River basin covers an area of 275 km² that develops in the eastern flank of the Aconquija Range with a local relief of 4383 m (Fig. 2). Climate in the area under study is subtropical with dry winters and a monsoon storm regime in Summer. The climatic factors in subtropical regions are known to display greater variation among seasons than those observed in tropic regions. Mean annual precipitation is 1800 mm, 70% of it occurring in summer.

The geological setting of the area is characterized by a crystalline basement composed of banded schists, migmatites and igneous intrusive rocks, which occupy almost 90% of the area corresponding to its headwaters. Sedimentary rocks of Cretaceous, Paleogene and Neogene age occupy the lower slopes of the basin ranges. Cretaceous and Paleogene rocks are composed of conglomerates and sandstones with carbonate cement. A Neogene sedimentary sequence is composed of siltstones and sandstones with interbedded gypsum and limestone beds.

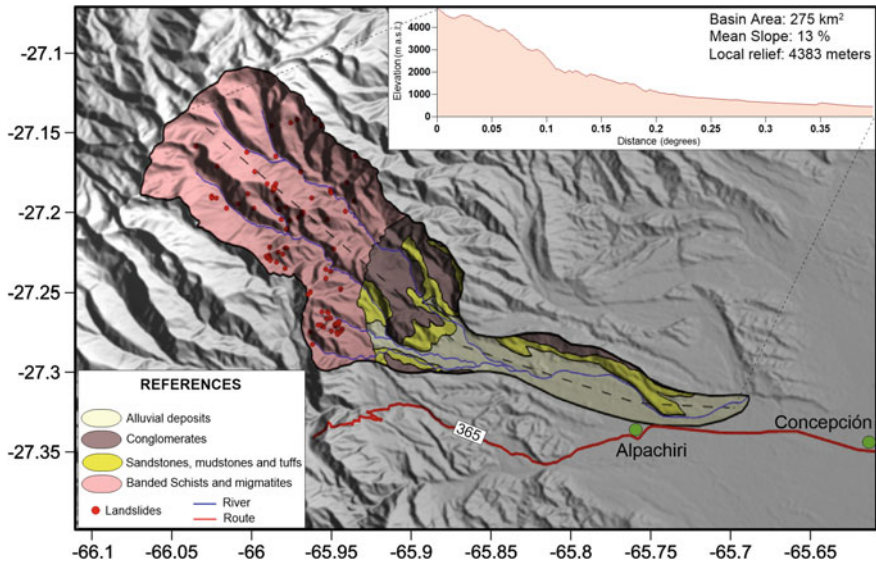


Fig. 2 Jaya River basin characteristics

2.2 Landslide Types and Distribution

More than 300 landslide events (slides, flows, rock falls) were recognized in the pre-Andean mountain front of the province of Tucumán (Fernández 2008). The types of movements described are shallow landslides, debris flows, debris avalanches, rock falls and complex movements. These movements are triggered by heavy rains with a monsoon behavior that take place during the summer months (December–March). Extreme precipitations events (>100 mm/day) were reported by Fernández and Lutz (2003) in the eastern part of the mountainous area during “El Niño” southern oscillation phenomena. The analysis of the control factors (precipitation, slope angle, aspect, lithology) was made on the basis of a landslide inventory under a GIS environment (Fernández 2009). The spatial distribution of these movements is controlled mainly by slope angle and rock weathering as principal causal factors. The majority of the landslides (>83%) were registered in slopes with angles between 10° and 30° in weathered crystalline rocks.

A detailed landslide inventory was prepared for landslide susceptibility analysis for shallow landslides and debris flows that are the most common types of movements. Data collection was performed using high-resolution multitemporal satellite images (CBERS 2B and Google Earth) and aerial photographs. The inventory was developed in two steps: First landslide events were mapped in three training basin areas, and then, it was done for the Jaya River basin. Three hydrological basins were used as training areas under different climate regimes, such as the Caspichango River basin (Subtropical climate), the Blanco River basin

(semiarid) and the Pichao River basin (arid). Locations of these basins is shown in Fig. 1. This information was used to create statistical susceptibility models that were applied in the Jaya River basin.

2.3 *Landslide Susceptibility Models*

(a) Logistic Regression Model

Among the wide range of statistical methods proposed in the assessment of landslide susceptibility, logistic regression (LR) analysis has proven to be one of the most reliable approaches (Dai and Lee 2002; Ayalew and Yamagishi 2005; Lee 2005; Guzzetti et al. 2006; Chen and Wang 2007; Mancini et al. 2010). Basically, LR analysis relates the probability of landslide occurrence as a dependent dichotomous variable (presence or absence of landslide) to predict or to evaluate its relationship with other independent control variables.

The relationship between the occurrence and its dependency on several variables can be expressed as:

$$Y = \text{Logit}(p) = \ln(p/(1-p)) = C_0 + C_1X_1 + C_2X_2 + \dots + C_nX_n \quad (1)$$

where P is the probability that the dependent variable (Y) is 1, $p/(1-p)$ is the likelihood ratio, C_0 is the intercept of the regression function, and C_1, C_2, \dots, C_n are coefficients, which measures the contribution of independent factors (X_1, X_2, \dots, X_n) to the variation in Y .

Coefficients are estimated through the maximum likelihood criteria and correspond to the estimation of the more likely unknown factors. Although the processing of the geographical data used in this study was performed in the GIS environment, the LR analysis was carried out by the SPSS statistical package.

The selection of the training basins was based on their climate characteristics. The Caspinchango River basin presents mean annual precipitation that can reach 1800 mm with mostly rain forest vegetation. The Blanco River basin presents a semiarid climate regime with mean annual precipitation of 400 mm and high grasslands vegetation. The Pichao River basin presents a severe hydrological deficit with mean annual precipitation of 250 mm and characterized by a patchwork xerophyte vegetation cover. As a consequence of the difference in climatic and land cover settings, those basins located over eastern side of the principal ranges (Aconquija and Cumbres Calchaquíes ranges) show a predominance of shallow landslides over debris flows, whereas in western dry highlands areas debris flow events predominate.

The dependent variables were derived from the landslide inventory, and for independent variables, 11 control factors with influence over landslide initiation were selected and mapped. Control factors were classified in three groups: (1) morphometric causal factors (slope, aspect, USLE LS factor, profile curvature,

plan curvature, direct insolation), (2) hydrological factors (distance to stream channels, topographical wetness index (TWI), stream power index (SPI) and Melton ruggedness number (MRN) and (3) vegetation cover factor (NDVI index). Morphometric factors were obtained from SRTM 30-m digital elevation model. Artifacts from digital elevation models (DEM) were removed using a mesh denoising algorithm of Stevenson et al. (2010), and then, sinks were filled using Planchon and Darboux (2001) algorithm for hydrological factors determination. Normalized difference vegetation index (NDVI) was used for vegetation cover-type discrimination, which was calculated using Landsat TM satellites images (Fig. 3).

For statistical analysis, 152 landslides areas and 152 areas with no evidence of landslides were randomly selected from the three training basins. Logistic regression was applied using forward stepwise technique which at each step, the independent variables (control factors) are incorporated to the model on a basis of their significance (p -values < 0.05). This technique selected 5 of 12 original variables, and the regression equation was created (Table 1).

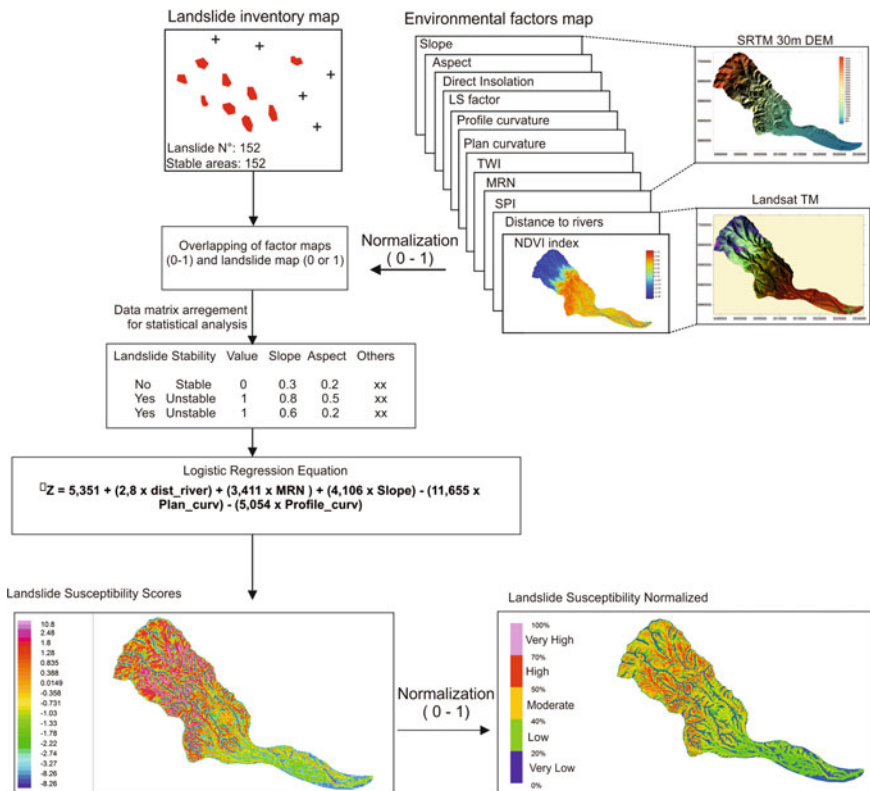


Fig. 3 Schematic representation of landslide susceptibility assessment using logistic regression model

Table 1 Variables in the equation with significance indication and logistic regression equation obtained for landslide susceptibility model

Input factors	95% confidence level					
	B	S.E.	Wald	df	Sig.	Exp(B)
Profile_Curvature	-5.054	1.698	8.856	1	0.003	0.006
Plan_Curvature	-11.655	2.371	24.175	1	0.000	0.000
Slope	4.106	1.386	8.768	1	0.003	60.680
MRN	3.411	1.636	4.347	1	0.037	30.297
Distance to river	2.800	0.678	17.042	1	0.000	16.441
Constant	5.351	1.674	10.217	1	0.001	210.890

Model equation

$$Z = 5.351 + (2.8 \times \text{dist_river}) + (3.411 \times \text{MRN}) + (4.106 \times \text{Slope}) - (11.655 \times \text{Plan_curv}) - (5.054 \times \text{Profile_curv})$$

Table 2 Overall statistics of the logistic regression model that involved 5 variables

Classification table				Model summary		Hosmer and Lemeshow test		
Observed	Predicted Stability			Cox and Snell R^2	Nagelkerke R^2	Chi-square	df	Sig.
	Stable	Unstable	% Correct					
Stability	130	22	85.5	0.497	0.663	11.097	8	0.196
Stable	22	130	85.5					
Unstable			85.5					
Overall percentage								

The overall model statistics of the logistic regression conducted in this study using SPSS is shown in Table 2. A Hosmer-Lemeshow test showed that the goodness of fit of the equation can be accepted because the significance of chi-square is larger than 0.05. The value of Cox and Snell R^2 (0.497) and Nagelkerke R^2 (0.663) showed that the independent variables can explain the dependent variables in a way. Besides, the predicted accuracy of the model is 85.5%.

(b) Weight of Evidence Model

This Weight of Evidence Model (WE) was proposed initially by Agterberg et al. (1993) and Bonham-Carter (1994) for mineral exploration mapping, and adapted by Van Westen et al. (2000) for landslides zonation. The model is based on the following assumptions (Carrara et al. 1995): (i) future landslides will be triggered under the same circumstances as in the past, (ii) all controlling factors are known and included in the model, (iii) all past and present landslides are identified in the study area.

For the application of this method into a GIS environment, the equation proposed by Van Westen et al. (1997) was applied:

$$\ln W_i = \ln \left(\frac{\text{DensClas}}{\text{DensMap}} \right) = \ln \left(\frac{\frac{\text{Area}(S_i)}{\text{Area}(N_i)}}{\frac{\sum \text{Area}(S_i)}{\sum \text{Area}(N_i)}} \right) \tag{2}$$

where W_i is the assigned weight for an specific parameter (slope class, altitude); DensClas is the landslide density for the class or parameter considered; DensMap is the landslide density for the study area; Area (S_i) is the area with landslide presence in the class or parameter considered; and Area (N_i) is the total area for the class or parameter considered.

This method is based on a cross-operation between a landslide map with a specific parameter map. As a result of cross-mapping, a cross-tabulation is obtained between landslide spatial distribution and the parameters that control their occurrence. This cross-table is used to calculate landslide density for each control parameter. A standardization of landslide density values is obtained thro the relation between partial densities for each factor and general density for the entire study area (Fig. 4). Natural logarithm assigns a negative weight when landslide density is lower than normal values and positive weight when is higher than normal values. Combining two or more weighted maps, a susceptibility map can be generated. Values of the susceptibility map are obtained by aggregating values obtained for each factor maps separately. Geo-environmental factors introduced in the model are slope, aspect, lithology, direct insolation and altitude.

$$W_i = W_{\text{slo.}} + W_{\text{asp.}} + W_{\text{lit.}} + W_{\text{dir.ins.}} + W_{\text{alt.}} \tag{3}$$

These parameters were suggested by Esper Angillieri (2012) as good predictors for debris flows. Geomorphometric parameters (elevation, slope and aspect) were obtained in the same way that in the logistic regression model. Solar direct insolation map was calculated under SAGA GIS using ASTER-GDEM filtered DEM and for 27° south latitude and 65° south longitude following criteria suggested by Boehner and Antonic (2009). Lithological map of the Jaya River basin was obtained from Dal Molin et al. (2003). Assigned weights for parameters under analysis are listed in Table 3.

(c) Infinite slope model

The stability of a slope is usually expressed in terms of factor of safety (FS), which is the balance between resisting and driving forces such that

$$FS = \frac{\text{Resistance of the soil to failure (shear strength)}}{\text{Forces promoting failure (shear stress)}} \tag{4}$$

In equilibrium analysis, an FS = 1 when both forces are exactly equal, but in natural environments, there is no absolute stability. Where FS < 1, the slope is in condition for failure; where FS > 1, the slope is likely to be stable. Most natural hillslopes upon which landsliding can occur have FS values between about 1 and

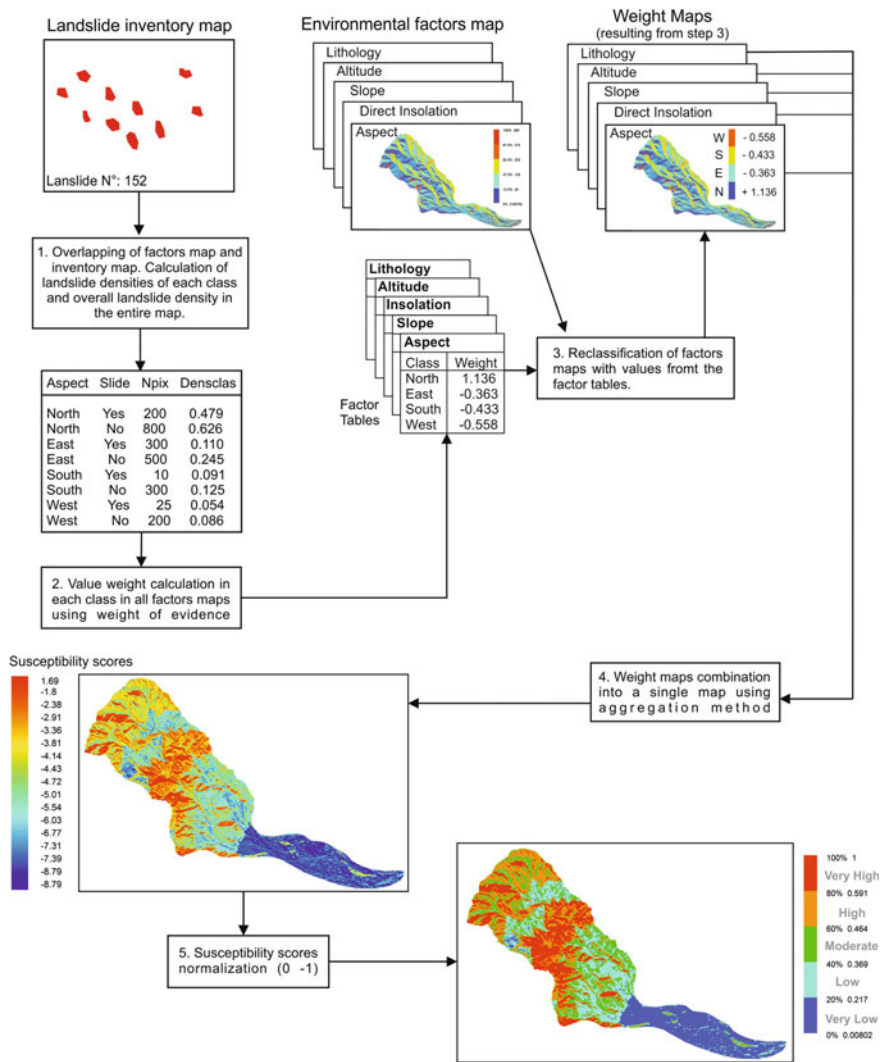


Fig. 4 Schematic representation of landslide susceptibility assessment using weight of evidence model

1.3 (Selby 1993). Generally, the infinite slope model is appropriate for shallow translational landslides because it is assumed that the mobile slice is uniform in thickness and rest on a slope of constant angle and infinite extent. The formula to calculate the Safety Factor (Brunsden and Prior 1984) reads:

Table 3 Weights obtained for the five geo-environmental factors under analysis

Geo-environmental factors	Classes	Weights
Lithology	Banded schist, migmatites	0.055
	Granites	0.449
	Sandstones, mudstones and tuffs	0
	Conglomerates	0
	Alluvial deposits	0
Altitude (masl)	<1000	-2.400
	1000-2000	-0.558
	2000-3000	1.000
	3000-4000	-2.174
	>4000	0.000
Slope (°)	<5	-1.322
	5-15	-0.832
	15-25	-0.452
	25-35	-0.034
	>35	1.158
Aspect (°)	315-45	1.136
	45-135	-0.363
	135-225	-0.433
	225-315	-0.558
Direct insolation (WH/m ²)	<2.94	-1.655
	2.94-3.78	-3.243
	3.78-4.21	-4.561
	4.21-4.85	-3.204
	>4.85	-3.005

$$FS = \frac{c' + (\gamma - m\gamma_w)z \cos^2 \beta \tan \theta'}{\gamma z \sin \beta \cos \beta} \tag{5}$$

where c' is the effective cohesion, g is the unit weight of soil, m is the vertical height of the water table above the slide plane as a fraction of the soil thickness above the plane, γ_w is the unit weight of water, z is the depth of failure surface below the surface, θ is the angle of friction, and β is the slope angle.

The analysis of FS was driven under the slope stability module of SAGA GIS. The input parameters were obtained from the ASTER GDEM filtered DEM (slope in radians), local soil characteristics from Moscatelli et al. (2005) and field observations (depth to potential shear plane). The normalized water table height usually has a range of 0-1 for non-artesian conditions (Haneberg 2004). The global frictional angle was settled in 33°. The infinite slope model was applied in the Jaya River basin and then was compared with the landslide inventory map of the basin.

2.4 Performance Evaluation of Landslide Susceptibility Models

Final landslide susceptibility maps obtained for each model can be appreciated in Fig. 5. Zoom windows of a representative area show the differences in susceptibility classification criteria registered by the three techniques.

The most relevant criterion for quality evaluation is the assessment of model accuracy, which is performed by analyzing the agreement between the model

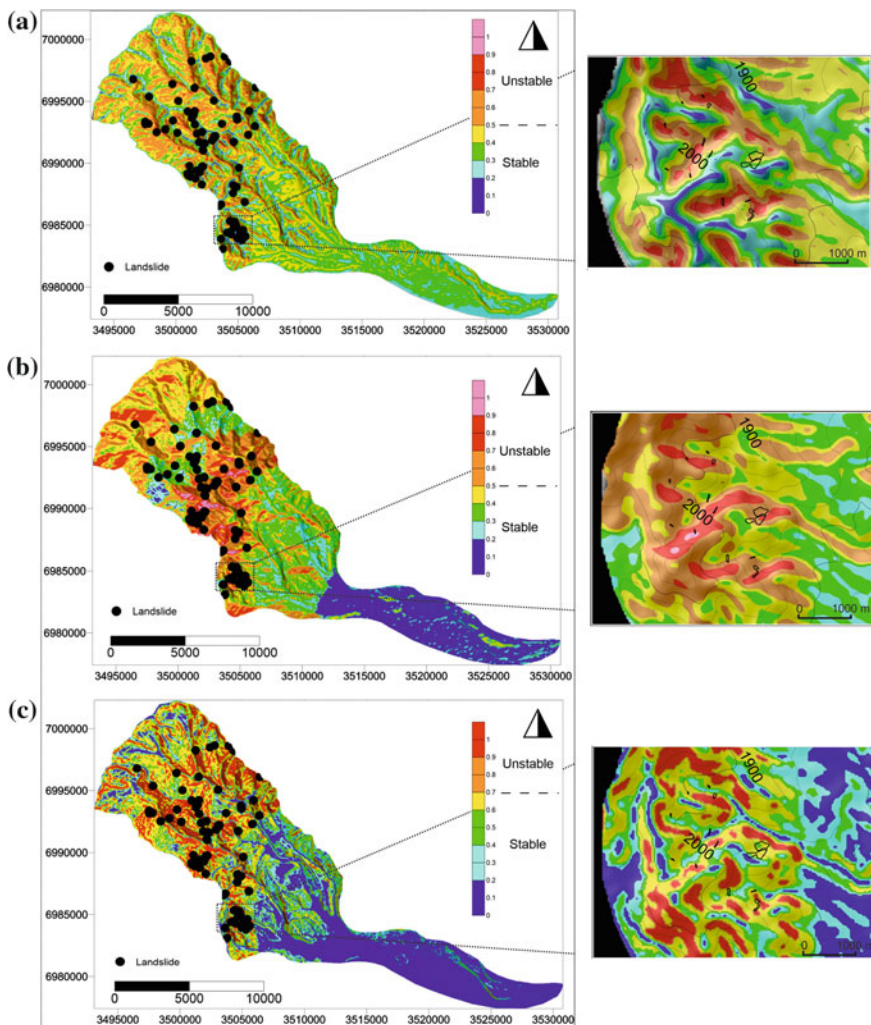


Fig. 5 Final classified modeled susceptibility maps for each model (LR, WE and FS respectively) and zoom view in a representative zone

results and the observed data. In this study, the performance of the susceptibility models was evaluated by using accuracy statistics and ROC curves. The analysis was implemented with a random selection of one hundred mapped landslides and one hundred areas with no evidence of landslides. Since the observed data comprise the presence/absence of landslides within a certain terrain unit, a simpler method to assess the accuracy is to compare these data with a binary classification of susceptibility in stable (1) and unstable units (0). This classification requires a cutoff value of susceptibility that divides stable terrains (susceptibility less than the cutoff) and unstable terrain (susceptibility greater than the cutoff). As a consequence of this analysis, a classification of the areas under analysis can be made in true-positive areas (TP), where a landslide was observed in an area mapped as unstable, false-positive areas (FP), where an area without landslides is classified as unstable, true-negative areas (TN), where an area without landslides is classified as stable, and false-negative areas (FN) where an area with landslides is classified as stable. This procedure is based on equivalent methods suggested by several authors (Guzzetti et al. 2006; Frattini et al. 2008, 2010; Van den Eeckhaut et al. 2006).

For evaluation purposes, three statistical cutoff-dependent methods were calculated. The threat score or critical success index (Gilbert 1884) measures the fraction of observed and/or classified events that were correctly predicted. The Gilbert's skill score (Gilbert 1884) measures the fraction of observed and/or classified events that were correctly predicted, adjusted for true positives associated with random chance. The Pierce's skill score (Pierce 1884) uses all elements of contingency table and does not depend on event frequency. The LR model outperforms all others with all the statistics, whereas the WE model is always the worst. Overall, the threat score and Gilbert's skill score both show smaller differences among the models, whereas the Pierce's skill score, a measure of the degree of success, throw best results for the LR model (Fig. 6a).

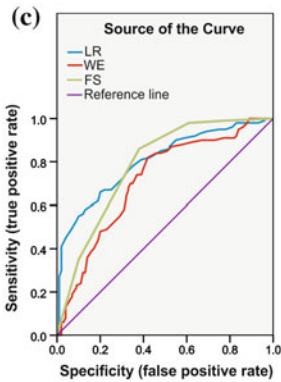
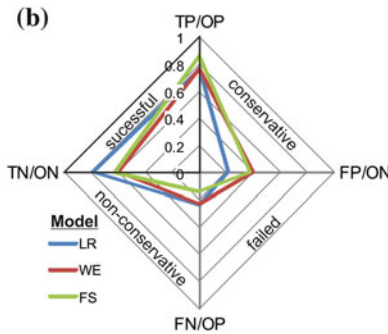
These latter indices work with two (TP, FP) or three (TP, FP and FN) indicators, and none of them work with the fourth indicator (TN) so their analysis is only partial. To deal with this situation, the four indicators were used in a radar diagram according to the classification proposed by Mergili et al. (2014). The LR model achieved better performance than the others because it has exhibited balanced results between the numbers of TP and TN (Fig. 6b). On the other hand, it also shows a less conservative behavior because they displayed a higher number of FN.

Validation of the outputs from the different models was done through ROC curve. This is the most commonly used cutoff-independent performance technique for landslide susceptibility models. The area under the ROC curve (AUC) can be used as a metric to assess the overall quality of a model (Hanley and McNeil 1982): the larger the area, the best the performance of the model over the whole range of possible cutoffs. The points on the ROC curve represent (FP, TP) pairs derived from different contingency tables created by applying different cutoffs. Points closer to the upper right corner correspond to lower cutoff values. An ROC curve is better than another if it is closer to the upper-left corner. The LR has reached the best performance with an area under the curve of 0.802 followed by FS model (0.785)

(a)

Model	Cutoff value	Model Performance				Threat score	Gilbert skill score	Pierce's skill score
		TP	TN	FP	FN			
LR	0.40	76	79	21	24	0.63	0.38	0.55
WE	0.46	77	60	40	23	0.55	0.23	0.37
FS	0.70	86	62	38	14	0.62	0.32	0.48

$$* TPrandom = \frac{(TP+FN)(TP+FP)}{T}$$



(d)

Test Result Variable(s)	Area	Std. Error ^a	Asymptotic Sig. ^b	Asymptotic 95% Confidence Interval	
				Lower Bound	Upper Bound
LR	.802	.031	.000	.742	.863
WE	.713	.037	.000	.641	.785
FS	.785	.032	.000	.721	.849

Fig. 6 Techniques for evaluating the performance of landslide susceptibility models. **a** Accuracy statistical cutoff-dependent methods applied (*TP* true positive, *TN* true negative, *FN* false negative, *FP* false positive). **b** Radar diagram for the evaluation of the degree of success in landslide prediction occurrence. **c** Receiver operator characteristics (ROC) curves obtained for the different models. **d** ROC curve test results for the three models under the study

and WE model (0.713) with a significance <0.05 and with a standard error of approximately 3% (Fig. 6c, d). The area under the ROC curve obtained for LR shows a very good ability of the model to discriminate the two terrain classes (stable and unstable) according to interpretation guidelines given by Brenning (2013).

3 Uncertainty and Sensitivity Analysis

The combination of uncertainty and sensitivity analyses is crucial to the validation and calibration of prediction models (Chen et al. 2009). Uncertainty analysis (UA) focuses on how uncertainty in input data, parameters, etc., propagates through the model and affects the model output, whereas sensitivity analysis (SA) considers uncertainty in the opposite direction (from the output back to the input) determining how much each individual source of uncertainty contributes to output uncertainty (Crosetto and Tarantola 2001). Sensitivity analysis has also been defined as a process that aims to assess the response of a model to changes in input parameters (Ligmann-Zielinska and Jankowski 2008).

Global sensitivity analysis was performed using the Monte Carlo (MC) approach method in order to determine the uncertainty of the model and the sensitivity associated with the errors in the model input factors. The basis for using the MC method in error propagation analysis is that the original data are perturbed repeatedly by the realization of the modeled error. The procedure involved a sequence of steps starting with identifying sources of uncertainty associated with the input factors of the models under evaluation.

Errors in input factors of the three models were obtained in different ways depending on the characteristics of each factor. In the case of logistic regression model, the error related to distance to rivers was calculated using root-mean-square error (RMSE) (Eastman et al. 1993). In the case of topographical factors derived from the SRTM DEM, the layer errors were calculated by creating random field maps. The random field map of the DEM was generated assuming a Gaussian distribution with a mean of zero and a standard deviation equal to the RMSE of DEM. According to Rodriguez et al. (2006), the absolute height error calculated for SRTM 30 m in South America is 7.5 m. A new DEM was created with the random

Table 4 Error input factors and associated distributions

Model	Input factor	Distribution
Logistic regression	Error distance measure to rivers	$U: [-0.003; 0.003]$
Logistic regression	Random error of MRN	$G: [\bar{x}:0.52; \sigma: 0.09]$
Logistic regression	Random error of profile curvature	$G: [\bar{x}:0.4; \sigma: 0.02]$
Logistic regression	Random error of plan curvature	$G: [\bar{x}:0.53; \sigma: 0.003]$
Logistic regression, weight of evidence and factor of safety	Random error of slope	$G: [\bar{x}:0.44; \sigma: 0.09]$
Weight of evidence	Random error of altitude	$G: [\bar{x}:0.003; \sigma: 0.13]$
Weight of evidence	Random error of aspect	$G: [\bar{x}:0.06; \sigma: 0.4]$
Weight of evidence	Random error of direct insolation	$G: [\bar{x}:0.25; \sigma: 0.95]$
Weight of evidence	Error of lithology	$G: [0; 0.02 \times \text{n.v.}]$
Factor of safety	Error of cohesion	$G: [0; 0.02 \times \text{n.v.}]$
Factor of safety	Error of height of water table	$G: [0; 0.02 \times \text{n.v.}]$

Uniform, U :[standardized range], or normal, G :[mean, std. dev.]; some of the distribution parameters are a function of the nominal input values (n.v.)

errors added, and the derived topographical factors were calculated. Error maps of topographical parameters were obtained performing grid differences between grids with random errors and the original factor grids. Finally, for every error propagation map, mean and standard deviation were calculated in order to be introduced as error input parameter in the MC analysis. In the case of errors associated with lithology (WE model), cohesion (FS model) and height of water table (FS model), variations of 20% were assumed. The list of errors in the input factors with their distribution types used in the simulated scenarios is shown in Table 4.

MC analysis was performed using Latin hypercube procedure with 1000 interactions with the software Simlab for the three models under study. Uncertainty results from the analysis are shown in Fig. 7a, c, e, where distribution histogram, and in Fig. 7b, d, f, where sensitivity analysis results are shown.

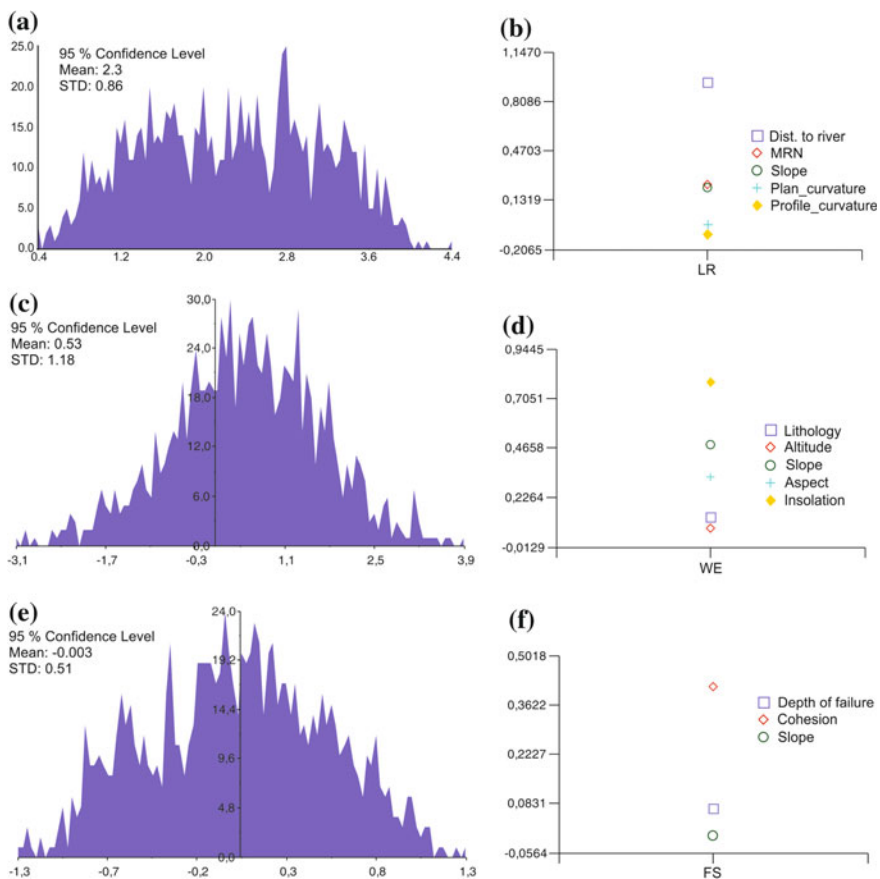


Fig. 7 Global sensitivity analysis of the models under study. To the *left* model error histograms of distribution where mean error and standard deviation were calculated for logistic regression (a), weight of evidence (c) and factor of safety (e). To the *right* sensitivity analysis results are shown where the input errors influence on total output can be appreciated for logistic regression (b), weight of evidence (d) and factor of safety (f)

mean and standard deviation for each model error were calculated. The error values correspond to the models output before the normalization. In the case LR model, the error was 2.3 ± 0.86 which implies an error of 16.6% over the output range of the model. The WE model error was 0.53 ± 1.18 which implies an error of 16.3% over the output range, and FS model a lower uncertainty with an error of -0.003 ± 0.51 that correspond to a 5.3% of the output range.

The sensitivity indices obtained for parameters model are shown in Fig. 7b, d, f. In the LR model, distance to river parameter has the greatest influence over the prediction uncertainty with an effect of 30% over the output error followed by MRN and Slope with 7.5 and 7%, respectively. In WE model, insolation has the greatest effect with a 46% followed by slope (28%) and aspect (19%). In the case of FS model, cohesion values have the greatest effect on model output error with more than 80%.

Variations over final normalized LR model map due to mean error plus standard deviation are given in Fig. 8. Final model maps with error were created using random fields operation. The final maps obtained by adding or subtracting the error calculated by the uncertainty analysis yielded results showing an increase in the percentage of the area classified as unstable within the basin (LR > 0.4). The error ranged between 3.6% (subtraction of error + STD) and 8% (addition of mean error + STD).

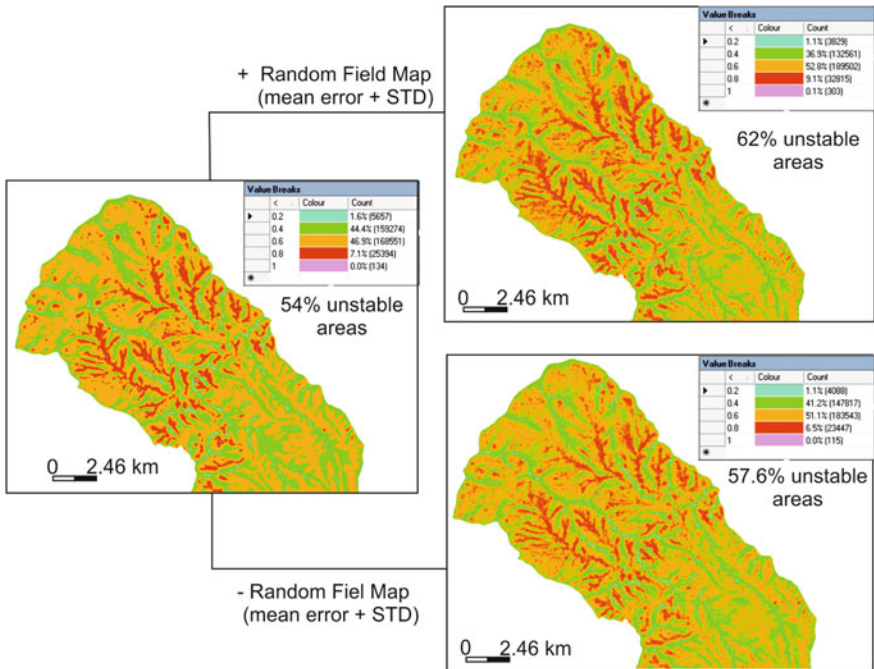


Fig. 8 Variation scenarios of logistic regression landslide susceptibility map generated from adding (a) or subtracting (b) a random field of mean error + standard deviation

4 Discussion and Conclusions

The LR model has reached a better performance than WE and FS models. Statistical indicators showed that the LR model outperforms the other in its predictive capacity taking into account both positive and negative results according to the degree of fit between the observed field and susceptibility map obtained. The FS model gave higher values for statistical TP (86/100), but its overall performance was affected due to the FP values (38/100). ROC curve approach reveal moderate differences among models. LR model obtained a ROC curve area of 0.802 followed by the FS model with a ROC curve area of 0.785. Statistically, LR model demonstrates a more robust behavior than the others because the proportion between true-positive and true-negative units is almost the same.

The deterministic model FS has shown a good performance despite the degree of simplification with which it worked, particularly in the influence of groundwater level variations, and the difficulties related to spatial variation of the geotechnical parameters that involve this model. This model achieved the best results in the degree of fit between the sectors of high susceptibility and landslides observed in the field. However, it showed overgeneralization in the allocation of unstable areas so it generated a large number of false negatives.

The WE model show the worst performance with a ROC curve value of 0.713. Low performance of the WE model would be related to the factors of control included in the analysis. In the case of the Jaya River basin, all landslide processes were observed in only one type of lithology (crystalline rocks); then, this layer would not have made a significant contribution to the prediction of landslides areas. Controls factor of the WE model were taken from Esper Angillieri (2012) where this model had a better performance than logistic regression to delimitate debris flow vulnerability areas. Nevertheless, in that work the model performance was evaluated only by TP indicators and no cutoff-independent method was applied.

Sensitivity analysis allowed to know which way the errors associated with input factors contribute to the total model error. The distance to river factor presents the highest error over the final output of the LR model. This error was calculated by measuring the error between the center channel distances that were obtained by concentric buffer and the real distances measured from an aerial photograph. The main error arises for simplification in the distance calculation obtained by the buffer method that does not take into account small local variations in the watercourse. This plus the fact that the error was incorporated with a uniform distribution for the entire area has a large influence in the final error of the model. This error could decrease if a control of the buffers layer is made with high-resolution satellite imagery or aerial photographs.

Direct solar insolation and slope errors account for almost 75% of total variance in the WE model output. These two parameters are derived from the original DEM whose error was modeled for the calculation of topographical parameters. Solar insolation error depends on the accumulated error derived from the DEM plus aspect and slope calculation errors. The only ways to reduce the uncertainty related

to this parameter would be working with solar radiation maps obtained by remote sensing or improving the quality of the DEM.

The analysis of the uncertainty introduced by the parameters error of the FS models has shown that cohesion errors have the major influence followed by depth to the failure plane and the slope. These results agree with the variations obtained by Rogers and Selby (1980) in landsliding areas due to changes in the value of the model parameter. They found that FS is very sensitive to changes in values of cohesion and groundwater levels, moderately sensitive to values of slope and failure plane depth and rather insensitive to values of angle of friction. The error introduced by the cohesion could be reduced in the event of having direct measurements of this parameter in the different types of materials present in the basin.

The methodology applied in the analysis of the performance of different landslide models at hydrological basin scale has been adequate. Statistical indicators analysis involves implications for future land-use planning. An evaluation of terrain misclassification costs must be taken into account. A terrain unit interpreted as stable is subject to a high degree of uncertainty because the evidence of instability can be invisible due to factors such as the forest cover, low resolution of satellite images or anthropogenic perturbation of the landscape. False-positive error type in landslide susceptibility mapping can be a non-error and requires further investigations to discern between real or a false error. The consequences of this type of error are only economical because a terrain that was misclassified as unstable cannot be used for residential purposes and therefore there is no danger for people. Instead, false-negative error type can conduct to classify as stable an area that actually can suffer landslide processes, and therefore, both economical and human losses can occur. From the three models under study in this paper, the LR model produced the greatest number of false-negative errors and the fewest false-positive errors. The FS model presented almost half of number of false-negative errors than the LR model. High levels of risk would show low cost ratios (false negative/false positive). The analysis of these results shows that the FS model tends to minimize the risk to society compared to the other models despite showing a lower statistical performance than LR model. A careful analysis should be done between model prediction capacity and risk consequences.

References

- Agterberg FP, Bonham-Carter GF, Cheng Q, Wright DF (1993) Weights of evidence modeling and weighted logistic regression for mineral potential mapping. In: Davis J, Herzfeld U (eds) *Computers in geology*. Oxford University Press, New York, pp 13–32
- Ayalew L, Yamagishi H (2005) The application of GIS-based logistic regression for landslide susceptibility mapping in the Kakuda-Yahiko Mountains, Central Japan. *Geomorphology* 65:15–31
- Bejerman NJ (2005) Landslide susceptibility along a sector of the state road E55 (Córdoba, Argentina). In: *Proceedings of Géoline*, Lyon, France, 2005

- Boehner J, Antonic O (2009) Land surface parameters specific to topo-climatology. In: Hengl T, Reuter HI (eds) 2008 geomorphometry: concepts, software, applications. Developments in soil science, vol 33. Elsevier, 772 pp
- Bonham-Carter GF (1994) Geographic information systems for geosciences: modelling with GIS. Pergamon Press, Oxford
- Brenning A (2013) Statistical and machine-learning classification methods. Geostat, 61 pp (University of Waterloo)
- Brunsdon D, Prior DB (1984) Slope stability. Wiley, New York, 620 pp
- Carrara A (1983) A multivariate model for landslide hazard evaluation. Math Geol 15:403–426. doi:10.1007/BF01031290
- Carrara A, Cardinali M, Guzzetti F, Reichenbach P (1995) GIS technology in mapping landslide hazard. In: Carrara A, Guzzetti F (eds) Geographical information systems in assessing natural hazards, pp 135–176
- Carrara A, Crosta G, Frattini P (2008) Comparing models of debris flow susceptibility in the alpine environment. Geomorphology 94:353–378. doi:10.1016/j.geomorph.2006.10.033
- Chen Z, Wang J (2007) Landslide hazard mapping using logistic regression model in Mackenzie Valley. Canada Nat Hazards 42(1):75–89
- Chen Y, Yu J, Shahbaz K, Xevi E (2009) A GIS based sensitivity analysis of multicriteria weights. 18th World IMACS/MODSIM Congress, Cairns, Australia. <http://mssanz.org.au/modsim09>
- Claessens L, Knapen A, Kitutu M, Poesen J, Deckers J (2007) Modelling landslide hazard, soil redistribution and sediment yield of landslides on the Ugandan footslopes of Mount Elgon. Geomorphology 90:23–35. doi:10.1016/j.geomorph.2007.01.007
- Crosetto M, Tarantola S (2001) Uncertainty and sensitivity analysis: tools for GIS-based model implementation. Int J Geogr Inf Sci 15(5):415–437
- Crosetto M, Tarantola S, Saltelli A (2000) Sensitivity and uncertainty analysis in spatial modelling based on GIS. Agric Ecosyst Environ 81:71–79
- Crosta GB, Frattini P (2003) Distributed modeling of shallow landslides triggered by intense rainfall. Nat Hazards Earth Syst Sci 3(1–2):81–93
- Dai FC, Lee CF (2002) Landslide characteristics and slope instability modeling using GIS, Lantau Island, Hong Kong. Geomorphology 42:213–228
- Dal Molin C, Fernández DS, Escosteguy L, Villegas D (2003) Hoja Geológica 2766-IV “Concepción”, provincias de Tucumán, Santiago del Estero y Catamarca. Boletín N° 342. 41 pp. Programa Nacional de Cartas Geológicas de la República Argentina. Servicio Geológico Minero Argentino, Buenos Aires. ISSN 0328-2333
- Eastman JR, Kyem P, Toledano J, Jin W (1993) GIS and decision making. Explorations in geographic information systems, vol 4. UNITAR United Nations Institute for Training and Research
- Esper Angillieri, MY (2012) Análisis de la vulnerabilidad por flujos en masa en la provincia de San Juan (oeste de Argentina). Revista de la Sociedad Geológica de España 25(3–4):145–156 (Madrid)
- Fernández DS (2008) Los movimientos en masa de la provincia de Tucumán: Tipos, características y distribución. In: Proceedings of 17th Argentine geological congress I. Buenos Aires. pp 284–285. ISBN 978-987-22403-1-8
- Fernández DS (2009) Eventos de remoción en masa en la Provincia de Tucumán: Tipos, características y distribución. Revista de la Asociación Geológica Argentina 65(4):748–759 (Buenos Aires)
- Fernández DS, Lutz MA (2003) Procesos de remoción en masa y erosión fluvial en la Quebrada del Río Los Sosa, Provincia de Tucumán. Revista de la Asociación Geológica Argentina 3 (2):155–167 (Buenos Aires)
- Fernández DS, Puchulu ME (2015) Modelación de áreas susceptibles de deslizamientos mediante análisis espacial y regresión logística multivariante. VI Congreso de Geología del Cuaternario y Geomorfología. Ushuaia, pp 293–294. ISBN: 978-987-3767-34-0

- Frattoni P, Crosta GB, Carrara A, Agliardi F (2008) Assessment of rockfall susceptibility by integrating statistical and physically-based approaches. *Geomorphology* 94(3–4):419–437
- Frattoni P, Crosta G, Carrara A (2010) Techniques for evaluating the performance of landslides susceptibility models. *Eng Geol* 111:62–72. doi:[10.1016/j.enggeo.2009.12.004](https://doi.org/10.1016/j.enggeo.2009.12.004)
- Gilbert GF (1884) Finley's tornado predictions. *Am Meteorol J* 1:166–172
- Guzzetti F, Carrara A, Cardinali M, Reichenbach P (1999) Landslide hazard evaluation: a review of current techniques and their application in a multi-scale study, Central Italy. *Geomorphology* 31:181–216. doi:[10.1016/S0169-555X\(99\)00078-1](https://doi.org/10.1016/S0169-555X(99)00078-1)
- Guzzetti F, Reichenbach P, Ardizzone F, Cardinali F, Galli M (2006) Estimating the quality of landslide susceptibility models. *Geomorphology* 81:166–184
- Haneberg WC (2004) A rational probabilistic method for spatially distributed landslide hazard assessment. *Environ Eng Geosci* 10:27–43. doi:[10.2113/10.1.27](https://doi.org/10.2113/10.1.27)
- Hanley JA, McNeil BJ (1982) The meaning and use of the area under a receiver operating characteristic (ROC) curve. *Radiology* 143(1):29–36
- Iverson RM (2000) Landslide triggering by rain infiltration. *Water Resour Res* 36(7):1897–1910. doi:[10.1029/2000WR900090](https://doi.org/10.1029/2000WR900090)
- Lee S (2005) Application of logistic regression model and its validation for landslide susceptibility mapping using GIS and remote sensing data. *Int J Remote Sens* 26(7):477–491
- Lee CT (2015) Review and perspectives on methodology for landslide hazard analysis. In: 10th Asian regional conference of IAEG
- Lee S, Ryu JH, Min K, Won JS (2003) Landslide susceptibility analysis using GIS and artificial neural network. *Earth Surf Proc Land* 28:1361–1376
- Ligmann-Zielinska A, Jankowski P (2008) A framework for sensitivity analysis in spatial multiple criteria evaluation. *Geogr Info Sci* 217–233
- Mancini F, Ceppi C, Ritrovato G (2010) GIS and statistical analysis for landslide susceptibility mapping in the Daunia area, Italy. *Nat Hazards Earth Syst Sci* 10:1851–1864. doi:[10.5194/nhess-10-1851-2010](https://doi.org/10.5194/nhess-10-1851-2010)
- Mergili M, Marchesini I, Alvioli M, Metz M, Schneider-Muntau B, Rossi M, Guzzetti F (2014) A strategy for GIS-based 3D slope stability modelling over large areas. *Geosci Model Dev* 7:2969–2982. doi:[10.5194/gmd-7-2969-2014](https://doi.org/10.5194/gmd-7-2969-2014)
- Moreiras SM (2005) Landslide susceptibility zonation in the Rio Mendoza valley, Argentina. *Geomorphology* 66(1–4):345–357
- Moreiras SM (2009) Análisis estadístico probabilístico de las variables que condicionan la inestabilidad de las laderas en los valles de los ríos Las Cuevas y Mendoza. *Revista de la Asociación Geológica Argentina* 65(4):780–790 (Buenos Aires)
- Moscattelli G, Godagnone R, Salazar L, Plaza J, Nakama V, Cuenca M (2005) Estudios de suelos para la reconversión del sector agropecuario. Departamentos de Famailá, Monteros, Simoca y Chicligasta, Provincia de Tucumán. Ediciones INTA, Buenos Aires, 134 pp
- Pierce CS (1884) The numerical measure of the success of predictions. *Science* 4:453–454
- Planchon O, Darboux F (2001) A fast, simple and versatile algorithm to fill the depressions of digital elevation models. *Catena* 46:159–176
- Rodríguez E, Morris CS, Belz JE (2006) A global assessment of the SRTM performance. *Photogram Eng Remote Sens* 72(3):249–261
- Rogers NW, Selby MJ (1980) Mechanisms of shallow translational landsliding during summer rainstorms: North Island, New Zealand. *Geografiska Annaler* 62a:11–21
- Selby MJ (1993) *Hillslope materials and processes*. Oxford University Press, New York, 451 pp
- Stevenson JA, Sun X, Mitchell NC (2010) Despeckling SRTM and other topographic data with a denoising algorithm. *Geomorphology* 114(3):238–252
- Van den Eeckhaut M, Vanwallegheem T, Poesen J, Govers G, Verstraeten G, Vandekerckhove L (2006) Prediction of landslide susceptibility using rare events logistic regression: a case-study in the Flemish Ardennes (Belgium). *Geomorphology* 76(3–4):392–410
- Van Westen CJ, Rengers N, Terlien MT, Soeters R (1997) Prediction of the occurrence of slope instability phenomena through GIS-based hazard zonation. *Geol Rundsch* 86:404–414

- Van Westen CJ, Seijmonsbergen AC, Mantovani F (1999) Comparing landslides hazard maps. *Natural Hazards* 20:137–158. doi:[10.1023/A:1008036810401](https://doi.org/10.1023/A:1008036810401)
- Van Westen CJ, Soeters R, Sijmons K (2000) Digital geomorphological landslides hazard mapping of the Alpago area, Italy. *Int J Appl Earth Obs Geoinf* 2(1):51–60
- Van Westen CJ, Van Asch TW, Soeters R (2006) Landslide hazard and risk zonation-why is still so difficult? *Bull Eng Geol Environ* 65:167–184. doi:[10.1007/s10064-005-0023-0](https://doi.org/10.1007/s10064-005-0023-0)
- Yesilnacar E, Topal T (2005) Landslide susceptibility mapping: a comparison of logistic regression and neural networks methods in a medium scale study, Hendek region (Turkey). *Eng Geol* 79(3–4):251–266

Landscapes of Southern Patagonia, Argentina, Their Scenic Characteristics and Their Importance for Geotourism

Elizabeth Mazzoni

Abstract Cartography was compiled based upon the visual interpretation of multi-spectral and 3-dimension digital models, prepared from the superposition of Landsat images with digital elevation models, plus documentary sources and field work. Landscape Units were identified and mapped in southern Santa Cruz province, Argentine southern Patagonia (51° 30'–52° 20'S). The study area covers 17,000 km² extending from the Atlantic Ocean coast to the Andean Cordillera, following a new track of the National Route 40, one of the longest of the South American continent, noted for its geographic characteristics. The integrated concept of Landscape is applied in this paper to analyze the touristic potential of the region. The landscape cartography for the southernmost portion of Argentine Patagonia is presented in this paper. This cartography has been prepared at a scale of 1:250,000, and two units of hierarchical levels have been recognized: Landscape Types and Landscape Units. Their spatial distribution and characteristics are clearly related to the natural environment conditions, particularly the geological and geomorphological processes that have acted in the region since the Middle Tertiary to present times. The peculiar features of each Landscape Type are presented and the available touristic resources are discussed, which may be useful in the development of several unconventional tourism modes, such as geotourism and ecotourism. At the analyzed scale (1: 250,000), the geomorphological aspects define the landscape variability, which includes landscapes modelled by glacial, fluvial, littoral, aeolian and volcanic processes, acting upon two large geological units, the Southern Austral Basin and the Southern Patagonian Andes, from the Middle Tertiary (around 25–30 million years ago) until present times. The impact of human activity in the area is still poorly significative in the configuration of most of these landscapes.

Keywords Landscape units and types • Southern Patagonia • Touristic resources • Ecotourism • Digital cartography • Satellite imagery • Digital elevation models • Late Cenozoic

E. Mazzoni (✉)

Universidad Nacional de la Patagonia Austral, Río Gallegos,
Santa Cruz, Argentina
e-mail: elimazzoni@yahoo.com.ar

1 Introduction

National Route 40 (NR 40) crosses the entire territory of Argentina from its northern boundary with Bolivia in the province of Jujuy (La Quiaca, 22° 07' 20"S–65° 32' 54"W; 3503 metres above sea level (m a.s.l.) to Cabo Vírgenes (52° 20' 1" S–68° 21' 15"W; 34 m a.s.l.) in the province of Santa Cruz. Due to its great extension, more than 5100 km long, the numerous towns that it links and the landscapes that occur along its pathway, Route 40 is visited by many national and foreign tourists. Transportation means are varied, but always in a sort of “adventure” mode: cars, bicycles, motorbikes, 4-wheel drive trucks or motorhomes.

The southernmost section has recently seen modifications in its track. The pavement of part of it is under construction, and other portions have not been built yet. The first 450 km, starting at the northeasternmost point of the Magellan straits, will connect the Patagonian space, from the Atlantic Ocean coast to the Andean Cordillera, mostly following the Río Gallegos watershed. Likewise, it will link the cities of Río Gallegos, the provincial capital seat, and Río Turbio, which are, respectively, located at the east and west ends of the study area (Fig. 1).

The touristic planning and use of this new section of the road needs the identification and classification of the scenic resources of the region, most of them related to the natural landscape, due to the very low density population, ample empty spaces and the extensive economic activities which, with very limited examples, have slightly modified the physical features of the territory.

In consideration to these objectives, the components of the landscape were analyzed and units of varied hierarchy were identified and described (Landscape Types, LT; Landscape Units, LU). The resulting cartography and the characteristics of each landscape are herein presented, with an indication of its potential from a touristic point of view.

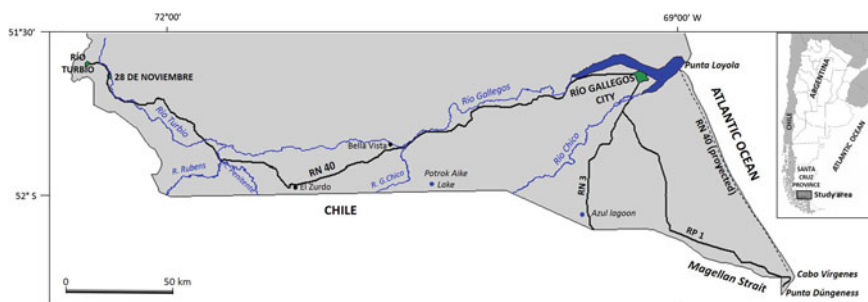


Fig. 1 Location of the study area and the towns and sites cited in the text

2 Study Area

The study area, located in the southernmost portion of the province of Santa Cruz, Argentina, has an approximate extension of 17,000 km². It goes from the Atlantic Ocean coast in its easternmost side to the international boundary with Chile at its southern and western borders, between geographical coordinates 51° 30'–52° 20'S latitude and 68° 21'–72° 26'W longitude (Fig. 1). Most of this area is located within the Río Gallegos watershed, the main river of the region, with a limited discharge of 15 m³/s. Throughout the basin, different landscapes are found, whose natural characteristics are basically a consequence of the geological and paleoenvironmental history of the region, particularly from the Middle Tertiary (around 25–30 million years ago) till present times.

Volcanic and glacial episodes have modified the original topographic features of the landscape, which are due to the distribution of two main, geological, morphostructural units (Ramos 1999): the Southern Patagonian Andes, at its western fringe and the Southern Austral Basin, characterized by predominant tablelands which are the consequence of repeated epeirogenic cycles across its geological history. In the study area, the Andean Ranges represent only a minor portion of its surface. The rest of the area is part of the tableland landscape, with a stepped topography that descends towards sea level, extending from the Andean piedmont towards the Atlantic Ocean coast. The tablelands are composed of Mesozoic and Tertiary sedimentary rocks of the Austral Basin, covered by shingle formations at different elevations. The extensive horizontal surfaces with scarce, low and homogeneous vegetation cover which always allows the observation of the horizon constitutes the typical image of Patagonia away from the Andean piedmont (Fig. 2). However, in the study area, landscapes departing from this classical model are found, in which heterogeneity is basically defined by lithological and geomorphological features.

The aforementioned environmental changes, particularly the cold events that took place during the Pleistocene, not only have given a peculiar surficial morphology to the terrain, but also have provided sub-surface features of special interest, such as cryogenic structures and landforms that expose regional permafrost past conditions (Ercolano et al. 1997). Among them, sand wedges are the most important (Bockheim et al. 2009) and occur in the different landscape explained below, easily identifiable in road cuts (Fig. 3). Whether the polygonal, patterned ground features are responsible for the pattern of present vegetation distribution which is observed in images of high spatial resolution, is presently under study (Mazzoni 2012).

The very southern geographical position of the area has strong influence in the climatic conditions, with a very low mean annual temperature of only 6 °C. The seasonal displacement of the Southern Pacific Ocean Anticyclone largely determines the distribution of winds and precipitations. Winds blow from the West with high intensity and frequency, particularly during the summer months, with gusts

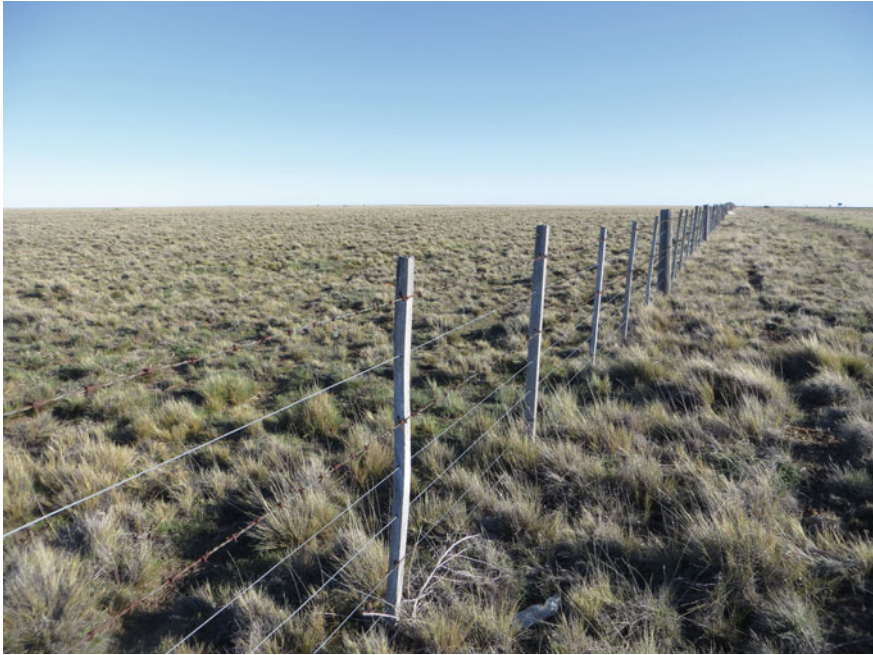


Fig. 2 Typical landscape of the Patagonian tablelands. *Photographs* E. Mazzoni

that exceed 100 km/h. The humid air masses coming from the southern Pacific Ocean generate orographic storms on the western side of the Andes. Then, the winds continue as dry gasps towards the interior of the South American continent, forcing a precipitation gradient in a W–E direction, with average annual values that range from 450 to 240 mm, decreasing in such direction. The wedge shape that the continent has at these latitudes allows also the penetration of air masses coming from the S and SE, smoothing the continental climate effect and providing also high snow cover. Heliophany is of less than 2200 h/year.

Vegetation is adjusted to the climatic conditions, mostly to the aforementioned W–E precipitation gradient. In the westernmost zone, a mesophile forest dominated by the caducifoliated species *Nothofagus pumilio* (“lenga”) and *Nothofagus antarctica* (“ñire”), alternating with grassland. The central and eastern area show a steppe of cespitouse, mat-forming grasses (“coirones”) whose bushes, 30–40 cm tall, form a homogeneous stratum, occasionally interrupted by isolated shrubs of *Berberis buxifolia* (“calafate”) or *Junielia tridens* (“mata negra”). The plant cover ranges around 60–70%, with low grasses of fodder interest that grow in between the “coirón” bushes (León et al. 1998).

To these zonal biomes, the presence of wet meadows should be added, a sort of small oases that receive the local denomination of “mallines” or “vegas” (Boelcke 1957; Cabrera 1976; Mazzoni and Vázquez 2004), whose location is related to local



Fig. 3 Cryogenic structures (sand wedges) exposed in road cuts and shoulders. *Photographs* E. Mazzoni. Upper photograph: Isabel Cruz. Lower photographs: Elizabeth Mazzoni

conditions of moisture concentration. These wetlands have a great environmental and economic importance, because they provide water and food to sheep and cattle, and also to the natural fauna, which may be clearly observed in different landscapes. Besides, they provide scenic attractions.

The use of space is mainly of an extensive nature, associated with the traditional economic activity for the region, sheep breeding. The rural space is organized in very large properties, ranches which are locally called “estancias”, most of them with surfaces larger than 20,000 ha, particularly in the lowlands, east of the Andes. Some of these “estancias” combine sheep breeding with touristic offer, providing lodgement, typical gastronomy, and other specific activities such as shearing demonstration, horse riding and trout fishing. Their main housing facilities, known as the “cascos”, constitute examples of traditional architecture. Westwards, the wetter conditions and the change from the steppe ecosystem to sub-andean grasslands, allow also cattle raising.

In the central eastern zone of the Austral Basin, oil and gas exploitation takes place, both in the continent and off shore conditions, which has grown rapidly in recent times. This activity is a priori considered as in conflict with the regional touristic development. In the western area, underground coal mining is the dominant activity since 1940.

The urban centres are distributed along the E–W axis in the Río Gallegos watershed: the city of this name is the most important urban area, with an estimated population at present of 105,000 inhabitants (INDEC 2013). In the western area, the towns of 28 de Noviembre and Río Turbio are located, whose development was historically related to coal mining. As a whole, these two towns, separated by only 12 km, have a joint population of approximately 15,000 inhabitants (INDEC 2010).

3 Landscape Units. Concepts and Methodology

The term “landscape” has several uses and its meaning has varied with time. In its more general concept, landscape refers to a synthetic visión of the territory (Troll 1966; González Bernáldez 1981) in which a physical dimension (the territory), a subjective and cultural dimension (the values that the people attribute to it upon perception) and a temporal dimension (Council of Europe 2000) are merging. Thus defined, landscape is the external and visible physiognomy of a certain geographic space, the result of the interaction of abiotic, biotic and anthropic factors with time (Bolòs 1992; Mateo Rodríguez et al. 2007), and it is also the representation that culture makes of it, the individual and social perception that it generates (Nogué and Vela 2011).

Considering landscapes as geosystems, they may be delimited and thus, cartographically represented. The landscape diversity allows to establish hierarchical structures. At a more general level, landscape differentiation is defined in most of the cases by the structural conditions (lithology and relief). Most authors are coincident in pointing that the terrain morphology is the main factor for a preliminary differentiation of the landscape at the surface of the Earth (Serrano Giné 2012). Concerning the analytical scales, the cartographic representation of the landscapes may consider three levels: the Landscape Units (LU), the Landscape

Types (LT) and the Landscape Type Associations (LTA). The first units correspond to the level of lower generalization, and it is defined as a combination of elements which generates, at a certain scale, a particular physiomy, a differentiated morphological organization, that makes a portion of the territory distinguishable from others (Mata Olmos 2011).

The landscape classification adopts different criteria according the objectives of the study. From a touristic point of view, those with unique or singular characteristics, due to natural or cultural conditions, merit special consideration. Some of the landscapes herein presented have exceptional features, mainly associated with their physical characteristics.

In relationship with the study of regional landscapes, Mazzoni (2001) recognized large morphogenetic units along the belt comprised between 69° and 72°W and from the northern boundary of the Río Gallegos watershed to the 52°S, as a basis for the analysis of the spatial distribution and geomorphological characterization of the endorheic basins of southern Santa Cruz province. Mazzoni and Vázquez (2004) mapped landscape units at a 1:1,000,000 scale for this provincial space, and López et al. (2011) identified larger units for the entire Patagonian region.

The methodology used is based on the analysis and correlation of each landscape component, considering the following: (1) structure (geology, lithology, topography, relief); (2) climate and hydrology; (3) soil and biota and (4) occupation of space and soil use. As a cartographic base, satellite images were elaborated with 1, 2, 3, 4, 5 and 7 bands of the Landsat 7 images, corresponding to the 228–229 and 230/096 path and rows, and the digital elevation model (DEM) obtained from the Shuttle Radar Topography Mission (SRTM, NASA-USGS). This made available a multispectral, three-dimensional representation of the study area (Fig. 4), thus widening the possibility of a clear visualization of the different landscape elements and textures. In relation to this, it may be pointed that the products thus obtained provide an instantaneous vision of all landscape components with superficial expression, making it an ideal tool for geographical synthesis work. The revision of diverse documentary sources, including images of high spatial resolution of the Google Earth program, the previous knowledge of the terrain and field surveying contributed also to the identification and delimitation of the units. Concerning the soil use, it may be cited that the territorial organization at the chosen scale (1:250,000) depends basically upon the physical environment characteristics, since they are exclusively related to the use of natural resources.

Processing of satellite images and DEMs was performed by means of the Erdas imagine 9.1 software and Global Mapper 11, respectively. The screen identification of the Landscape Units was completed in a GIS framework (ArcGis 9.2), where the different information layers were loaded. Cartography was elaborated at a 1:250,000 scale, in the Transverse Mercator, projection system, reference ellipsoid and datum WGS84, central meridian 69°W.

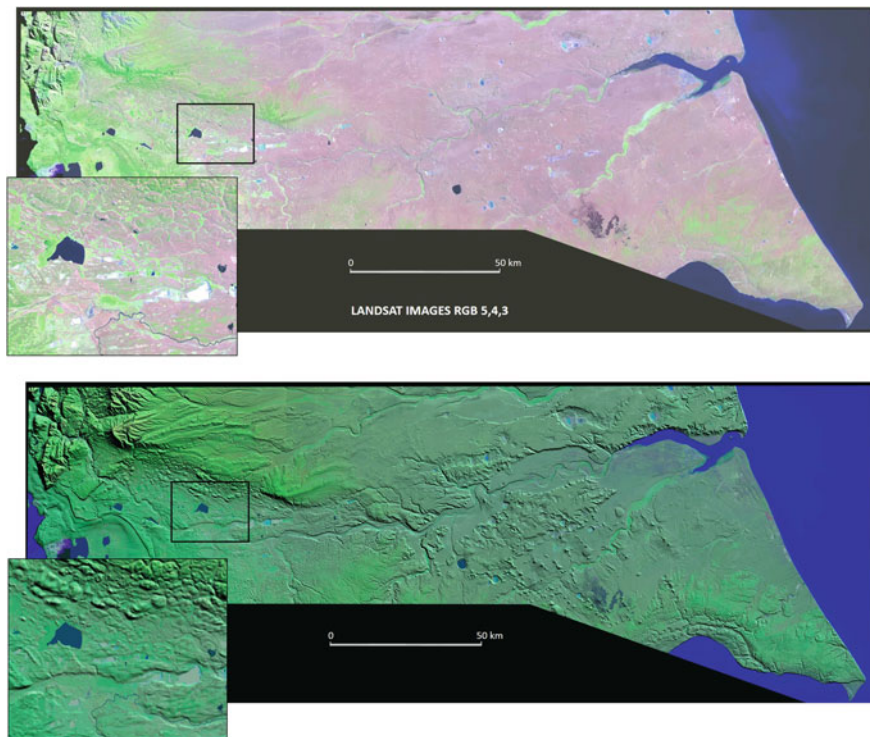


Fig. 4 Satellite mosaics of the study area elaborated with Landsat images 228, 229 and 230/096 (*above*) and with those same images plus the SRTM digital elevation model (*below*). The *boxes to the left* permit the observation with greater detail of the information provided by each remote sensing product. In the first one, the various types of cover are clearly differentiated (lithology, water bodies, plant cover, etc.), whereas the topographic dissimilarities are shown in the second one. The water body observed in the figure is “Laguna C ndor”, a water body which is cited in other places of this work

4 Landscapes of Southern Patagonia, Argentina

In the study area, eight landscape types have been recognized, most of them composed of different units (Table 1; Fig. 5). Seven of them represent the natural features of the terrain and the remaining one corresponds to the urban spaces where the territorial transformations achieve their higher expression. Due to the working scale, some of the units have not been identified in the map, though their existence is mentioned in the text.

The areal distribution of each unit, shown in Fig. 6, describes that the glacial and glaciofluvial landscapes represent almost 50% of the total area, the sedimentary rock tablelands cover an area of around 25%, whereas the fluvial landscape occupies 12.4% of the studied region. These are the three Landscape Types with the larger areal representation.

Table 1 Landscapes of southern Patagonia, Argentina

Landscape type	Landscape units	Surface		
		km ²	Sub-total	
			km ²	%
Coastal landscape	Estuary of the Gallegos and Chico rivers Beach and tide ridges and plains. Marshes	190.2	639.9	3.8
		417.0		
		32.7		
Sedimentary rock tableland landscape	Surface of the tablelands Slopes/flanking pediments Colluvial and alluvial fans. Bahadas	3552.3	3953.6	23.3
		385.3		
		16.0		
Volcanic landscape	Basaltic tablelands and plains. Slopes	1361.1	1369.7	8.1
		8.6		
Fluvial and fluvio-glacial channelled landscape	Alluvial plains and permanent drainage lines Terraces Wadi systems	805.8	2110.9	12.4
		736.3		
		568.8		
Glacial and glaciofluvial landscape	Moraines and glaciolacustrine and glaciofluvial plain systems Outwash surfaces	7455.0	8063.6	47.4
		608.6		
Mountain (andean cordilleran) landscape	Mountain relief with dominant rocky outcrops	258.3	258.3	1.5
Closed basin (endorheic) landscape	Depressions with ephemeral lakes. Lacustrine ridges and beaches. Permanent lakes	523.2	556.9	3,3
		7.6		
		26.1		
Urban landscape	City of Río Gallegos, towns of 28 de Noviembre and Río Turbio	40.9	40.9	0.2
Total area		16,993.8	16,993.8	100

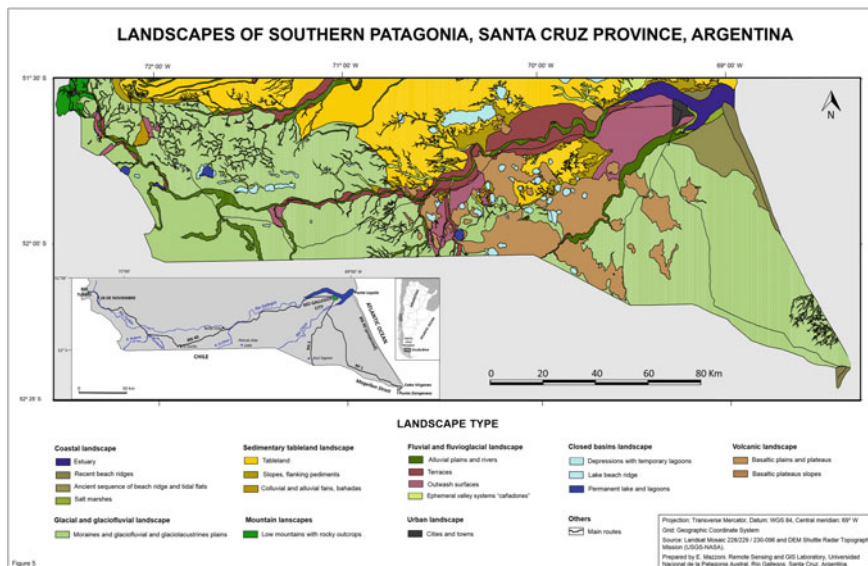


Fig. 5 Map of Landscape Types of southern Santa Cruz province

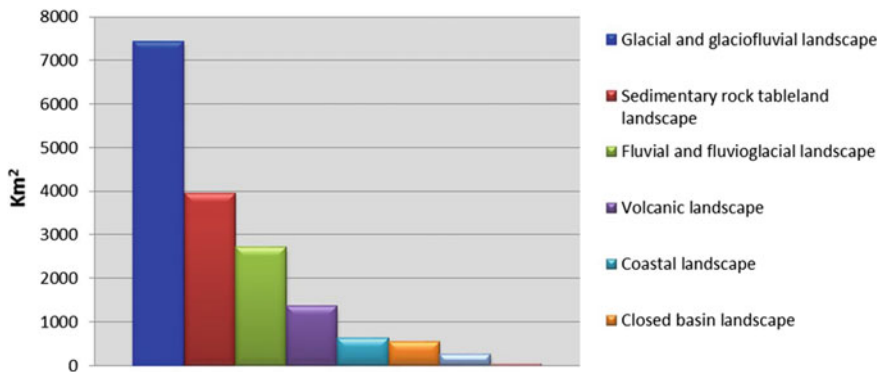


Fig. 6 Areal distribution of the Landscape Types of southern Santa Cruz province

5 Coastal Landscape

Several units may be recognized in this landscape, some of them integrating singular areas, particularly due to their geomorphological features. It includes the estuary of the Gallegos and Chico rivers and the Atlantic Ocean coast, that extends southwards towards the Magellan Straits, where two geographical features of high interest are found, the Cabo Vírgenes and Punta Dungeness.

The estuary has a length of 45 km and a width of over 5 km. From the hydrological point of view, water masses of varying density and composition, coming from the continent and from the sea, are interacting in this landform. In this case, this interaction is increased by strong currents (up to 12 knots) and the tide action, since this zone is characterized as macrotidal, with a mean tide amplitude of 5.5 m and exceptional values in between 12 and 14 m.

Morphologically, the estuary has asymmetrical margins (Fig. 7). The northern border is composed of cliffs, with a height above 130 m a.s.l., which has been deeply affected by mass-movement processes. The scars of landslides and slumps expose the rocks that form the sedimentary rock tablelands, extending north from the estuary. This margin has been also dissected by fluvial action, which has excavated complex channel systems, in whose mouths the removed and mobilized sediments have originated alluvial fans and bahadas. The southern margin is much lower, modelled by glaciofluvial processes. In both margins, coastal sedimentation has generated intertidal plains and marshes, with very complex discharge channels which, as seen from above, show a very peculiar morphology. The marshes are covered almost exclusively by *Sarcocornia* sp., a halophile species whose pigments vary seasonally from greenish during the summer to reddish and brownish in winter (Fig. 8).

The estuary as a whole has been declared as an “International Importance Site” of the “Hemispheric Reserve Network of Beach Birds”, because it is a relevant place concerning the migration scale of many thousands of Trans-American



Fig. 7 Estuary of the Río Gallegos, seen facing towards the mouth into the southern Atlantic Ocean. The differences in elevation between both margins are clearly noticed. Towards the N (*left* in the photograph), the sedimentary rock tablelands are exposed, with elevations over 100 m a.s.l. and being dissected by deep canyons. Towards the S, the landscape is composed of lower, ample plains, modelled by glaciofluvial processes. The lower level has been colonized by shrubs which are better adapted to saline environments. *Photographs* E. Mazzoni



Fig. 8 The estuary of the Gallegos and Chico rivers hosts several marshy areas. These marshes are high productivity ecosystems daily impacted by tidal fluctuations, which model complex drainage systems. The plant species that colonize these environments change seasonally in aspect and colour, with *reddish shades* in Winter and *greenish* ones during the Summer (*photographs* at *left and right*, respectively). Many birds use these wetlands as a seasonal habitat or as place for nesting. *Photographs* E. Mazzoni. Left photograph: Elizabeth Mazzoni; Right photograph: C. Albrieu

continent and Patagonian protected birds. Likewise, some marsh areas are protected sites of provincial or municipal interest (Ferrari et al. 2002, 2005).

The Atlantic Ocean coast extends from Punta Loyola, the southeastern end of the estuary, down to Punta Dungeness, with a total length of 100 km (Fig. 1). It has a linear shape, with very few features along its extension. In its northern half, the topography is low and the coast is composed of littoral ridges that have blocked ancient intertidal plains (Codignotto 1976). These landforms extend up to 15 km towards the interior of the continent, showing a continued accretional process from the Middle Pleistocene until today (Ercolano 2010). Contrarily, in the southern half, the morphology of the coast is composed of cliffs, with elevations over 60 m in the higher places. Here, littoral erosion dominates, favouring also mass-movement processes.

The Atlantic Ocean coast culminates southwards at Cabo Vírgenes, with an elevation of 34 m a.s.l. The lighthouse of that name is located here, which has been active since 1904; from the lighthouse, the eastern mouth of the Magellan Straits may be observed (Fig. 9). From a geographical point of view, it is the southernmost point of the continental Atlantic coast of South America and the eastern border of the Magellan Straits, which connects both the Pacific and Atlantic oceans.

At the contact between the Atlantic Ocean and the Straits of Magellan, a peculiar landform of marine accretionary processes takes place, which is known as Punta Dungeness. It is a triangular portion of land, around 8 km on each side, located at the foot of the paleocliff that during the Middle Holocene was the paleo-coastline of the Straits of Magellan (Codignotto 1990). It is composed of littoral ridges separated by muddy areas and marshes (Fig. 9). The ridges are composed of marine gravels, and they reach 3.5 m above the level of the adjacent marshes. Dating performed in the most recent ridge (western side) yielded a radiocarbon age of 900 years B.P. (Uribe and Zamora 1981), whereas the oldest ones would have a radiocarbon age of more than 2500 years B.P. (González Bonorino 2002). The accumulation of these materials was due to the wave action related to two different marine environments, the Atlantic Ocean to the E and the Straits of Magellan to the W. Global sea level changes have probably played a central role in the development of this landform. In its eastern beach, the second-largest penguin rockery of Argentina is located, which every year gathers thousands of Magellan penguins (*Spheniscus magallanicus*; Fig. 10). From a political point of view, the territory of Punta Dungeness is shared with the Republic of Chile.

Concerning its touristic interest, the contact between the Atlantic Ocean coast and the Straits of Magellan, represented by the already mentioned landforms of Cabo Vírgenes and Punta Dungeness, is specially relevant both for its geomorphological singularity as well as for its geographic, ecological and historical importance. This inter-oceanic pathway was discovered in 1520 by the expedition of Ferdinand of Magellan. Later on, in 1584, at the foot of the cliff that separates both landforms, the first human occupation of Patagonia was founded, the “Ciudad en Nombre de Jesús” (that is, the City on the name of Jesus), as part of the Spanish Empire (under the rule of Phillip II) plan for controlling the Magellan Straits



Fig. 9 Aerial view of the coastal landscape in the northern sector of the study area. The littoral morphology is composed of littoral ridges, in which the wreckage of the Norwegian ship “Marjorie Glen” is still grounded. This vessel caught fire and stranded near Punta Loyola in 1911. *Photographs E. Mazzoni*

pathway (De Negris and Senatore 2008). During the nineteenth century, this zone was affected by a gold fever, and a small town with shops, mining camps, workshops and police was established (Luque 1995). However, this urban project did not succeed, due to the very rigorous life conditions at this site, cold climate and lack of food resources, the same obstacles that lead to the failure of a Spanish fortress founded 300 years before.



Fig. 10 High spatial resolution image obtained from the Google Earth website, showing Cabo Virgenes, Punta Dúngeness and the paleoclimatic divide that divides them (indicated in *broken line*). The sequence of sedimentary deposits which comprises the cusped landform may be seen. The youngest beach ridges are devoid of vegetation. The location of the penguin rockery is portrayed in green. The photographs at the *right* of the figure show the terrain characteristics and a nesting Magellan penguin. *Photographs* E. Mazzoni

6 Sedimentary Rock Tableland Landscape

This is the landscape unit which better represents the lowland environments of Patagonia (Figs. 2 and 7). In the study area, it is composed of the sub-horizontal strata of the Santa Cruz Formation (Russo et al. 1980), of Middle Tertiary age (Miocene). It is a very thick, continental sedimentary sequence, composed of tuffs, tuffaceous clays, claystones, and sandstones of light greyish colours, with abundant content of vertebrate fossils, mainly mammals. The quantity and variety of these fossils make it one of the stratigraphic units of richer paleontological content in the whole of South America (Tauber 1999).

The rocks of this formation outcrop along the sides of the fluvial valleys and larger depressions, in the N margin of the Río Gallegos estuary and along the cliffs of the Atlantic Ocean coast. The surface of these outcrops is covered by layers of rounded gravels, of less than 0.50 m in thickness. These gravels most likely correspond to ancient glaciofluvial deposits, of Pliocene to Early Pleistocene age. In general, these gravel layers extend along large areas of the Patagonian plains and they are known as the “Patagonian Shingle Formation” (Darwin 1842) or “Rodados Patagónicos” (Fidalgo and Riggi 1970).

The landscape of sedimentary rock tablelands extends continuously northwards from the Río Gallegos valley, and it also occurs southwards, where it is partially covered by volcanic rocks and glacial deposits. The topography is horizontal to

sub-horizontal, with elevations that progressively increase towards the W, from around 130 m a.s.l. in the Atlantic Ocean coast up to 1050 m a.s.l. in Meseta Latorre, not far from the international boundary with Chile (see Fig. 23, right).

The friable materials that compose this landscape favour the action of erosion processes, even though the regional slope is very gentle. Along the Atlantic Ocean coast and the northern margin of the Río Gallegos estuary, it forms cliffs which are affected by mass-movement processes. The surface of the tableland is also deeply down-cut by ephemeral wadi systems, which drain towards the Río Gallegos estuary, to the Atlantic Ocean or towards the closed depressions excavated in this unit. According to their dimensions, some of these endorheic drainage systems have been identified in the maps. Towards the western sector, the tablelands are dissected by the drainage channels which, towards the NE, drain towards the Río Coyle watershed, located north from the study area. Smaller channels, tributaries of the Río Turbio (within the Río Gallegos basin) also have eroded the landscape towards the S.

Due to the intense regional winds, the homogeneity of the surface and the scarce plant cover, the aeolian action is strongly exposed. Its greatest expression occurs in the hydro-aeolian depressions, or “bajos sin salida”, that is, deflation hollows which, due to their size and frequency, have been identified as a particular landscape. However, minor features generated by aeolian activity are observed over the entire surface, particularly in the vegetation-free areas where the finer soil matrix has disappeared and the clasts have been faceted as ventifacts.

The plant cover is, in this landscape, a homogeneity factor, due to its regular distribution and composition. Visually, the aforementioned bushy grasses provide a general yellowish brown, ochre, tawny aspect to the landscape, that differentiates it from the tablelands of northern Patagonia, characterized by its larger percentage of shrubs and lesser plant cover. Likewise, the flat and extensive topography permits the observation of the horizon line without interruptions (Fig. 11).



Fig. 11 Day (*left*) and sunset (*right*) views of the sedimentary rock tableland landscapes, characterized by flat, horizontal relief and ample surfaces, where the horizon line is fully witnessed without disruptions. The *central* photograph shows the different facets of the northern Patagonian tablelands, where the shrubby vegetation dominates, but with still a high percentage of nude soils. *Photographs E. Mazzoni*

7 Volcanic Landscape

The “Pali-Aike Volcanic Field” is located S of the Río Gallegos, dispersed over a huge area of 1500 km². It is a landscape with peculiar characteristics resulting from retro-arc fissure eruptions, with mafic lavas which erupted since the Late Pliocene to the Holocene, with volcanic activity that extended until around as recently as 5000 years B.P. (Skewes and Stern 1979; Mejia et al. 2004). This volcanic activity was originally described by Altevogt (1969), Codignotto (1975) and Skewes (1978), and later studied in detail by Corbella (2002), who noted that, within the Argentine territory, these eruptions belong to a unique case of recent volcanism near urban areas, because the city of Río Gallegos is located at only 23 km from the nearest vents.

Morphologically, this volcanic field is composed of basaltic tablelands and plains, scoria and cinder cones and abundant maars. The volcanic vents are grouped or aligned along structural lines of a predominant NW–SE direction (Fig. 12a). The relative relief varies between 20 and 100 m, approximately, whereas the maximum elevations reach around 160 m a.s.l.

The younger basaltic flows, which are clearly identified in satellite images for their darker tones and more irregular, rugose surfaces, present numerous surficial features such as tubes, tunnels, caverns, inflated surfaces, crests, tumulus and “hornitos” (Corbella 2002). In those places where the flows have in-filled existing valleys, they appear restricted to channels (Fig. 12b).

Maars represent another particular geomorphic feature of this region. They are depressions of smooth topography and large dimensions, with a sedimentary ring of slightly higher relief, which surround these depressions totally or partially (Fig. 12c). Their formation is related to phenomena of high explosivity which are produced when the lavas get in contact with surficial or underground waters, ice or permafrost (Ollier 1967). In this region, their abundance may be related to the interaction of lavas with water in a periglacial environment of saturated or frozen soils (Corbella et al. 1990). Among them, the Bismarck, Potrok Aike, Carlota and Los Flamencos maars should be cited, developed over different bedrock types (Coronato et al. 2013). The Potrok Aike maar (51° 58’S–70° 23’W; Fig. 1) encloses the more important permanent water body of the eastern section of the study area, with a surface of 800 ha and a depth of 100 m (Gebhardt et al. 2011).

In addition to these noted geomorphological features, complex volcanic relief should also be cited (Fig. 12d), as volcanic cones built within the maar craters and coalescent explosion centres (Corbella 2002).

The older basaltic flows have generated tablelands, following a process of inversion of relief (Fig. 13), which are placed up to 130 m over the surrounding landscape (Mazzoni and Rabassa 2010). Dating of the lava flows covering these tablelands have yielded radiometric ages preferably within a range of ca. 3.8 Ma to ca. 0.85 Ma, with some volcanic activity as old as 8 Ma (Mercer 1976; Meglioli 1992; Corbella 1999; Mejia et al. 2004; Zolitschka et al. 2006). Knowing the age of the basalt flow and the local relief between the tableland surface and the

(a)



(b)



(c)



(d)



◀**Fig. 12** Features of the volcanic landscape. **a** Aerial and surface views of the scoria and tephra cones situated along structural arrangements. **b** Channelled recent lava flows. **c** Outlook view of the Bismark maar. At the background, several small volcanoes are perceived. **d** Complex landscapes where several landforms befall isolated or superposed, particularly volcanic cones and maar craters. *Photographs a, b and d* E. Mazzoni; *c* D. Grima



Fig. 13 View of the basaltic plateaus located in various topographic levels within the Río Gallegos watershed. At the foreground, one of the tablelands near Estancia Bella Vista may be seen, with a relative height of 35 m above the surrounding level, excavated by the fluvial action of the Gallegos Chico and Gallegos rivers, which join nearby. *Photographs* E. Mazzoni

surroundings, a regional denudation rate may be established. This rate has yielded values between 1.3 and 3.5 cm/1000 years, comparable with results obtained for similar landscapes in other regions of Patagonia (Mazzoni 2007) and the U.S.A. (California, 1–3 cm/1000 years; Marchand 1971).

The margins of these tablelands are affected by mass-movement processes, particularly rock falls and slumping, which originate a lobulated topography characterized by lobes and hummocks (Fig. 14). The process of evolution of these landscapes has been described by Mazzoni (2007) and Mazzoni and Rabassa (2007). The erosional remnants form isolated hills, locally known as “cerros mesa” (i.e., “table hills”). Some examples are, together with other volcanic necks, very well noted in the central-western portion of the study area, above the smooth glacial topography of the surroundings (i.e., the mounts Philippi, 385 m a.s.l., Domeyko, 363 m a.s.l., Cuadrado, 231 m a.s.l. and Gay, 180 m a.s.l.; Fig. 15). These basaltic outcrops have been assigned to the Late Miocene (Panza and Franchi 2002), with ages around 8 Ma (D’Orazio et al. 2001; Meglioli 1992). These are feeding volcanic chimneys, presumably of sub-aerial volcanic centres of approximately 500 m in mean diameter, which clearly expose many columns of thermal contraction joints (Corbella et al. 2014).



Fig. 14 Slopes of basaltic tablelands. The *upper left* photograph shows the characteristics of the boundaries of the volcanic tablelands, modelled by mass-movement processes such as slumping, which generate a topography of lobes and hummocks, among which multiple springs are located favour the generation of frequent wetland ecosystems, locally known as “mallines”. To the *right*, features of the upper scarp and the collapsed blocks are observed (consistent with the thickness of the lava flows). *Below* archaeological evidence of human occupation of this landscape is seen in those caves originated from lava flow channels. The caves were used as refuge and shelter by humans. The basaltic scarps expose rock art, such as engraving and rock wall painting. *Photographs* E. Mazzoni

From a hydrological point of view, the basaltic tablelands covered by rocks of high secondary permeability behave as aquifers, catching the scarce precipitation that occurs in the region. Water outcrops later on in the slopes, providing water resources and allowing the development of azonal ecosystems of wet grasslands (locally known as “mallines”), which offer water supply and food to wildlife, sheep and cattle (Mazzoni 1987, 2007; Mazzoni and Rabassa 2013). In numerous opportunities, the water of these springs supplies also the outposts and main houses of the ranches (Fig. 14).

Due to its peculiar landscape, this unit has been the scenario of varied types of use by human populations since around 10,000 years ago (Borrero et al. 2004; Borrero and Charlín 2010), because it had a very good offer of refuge and water supply. As a testimony of this occupation, many rock walls have rock painting and carving (Carballo Marina et al. 2008) (Fig. 14). In the area of Monte Philippi and other rocky hills, burials with funerary goods have been found (Ortiz Troncoso 1973).



Fig. 15 View of the Philippi (*left*) and Domeyko (*right*) hills, which are actually volcanic necks, eroded by glacial action during the glaciation events which operated within the Río Gallegos watershed. At the foreground, the topography of gently sloping hills, which form the surrounding glacial landscape, is observed. *Photographs* E. Mazzone

Presently, extensive sheep breeding takes place in the area, as in the rest of the study area. Only in isolated spots, this landscape is used with touristic purposes, in the place known as “Laguna Azul” ($52^{\circ} 04'S-69^{\circ} 35'W$), where a geological park has been created. It includes recent basaltic flows and a lake of such name, which has a longer axis of 500 m, and it is almost 60 m deep and occupies three nested craters (Fig. 16). The darker colours of the lava flow, the lack of soil development, its irregular texture, the intense bluish colour of the water body with riparian vegetation and the relative relief of up to 50 m, with very steep slopes, make these landforms very attractive. Likewise, in the hollows and caves of the rocky landscape, different bird species nest, among which the “bandurria austral” (*Theristicus melanopis*) should be mentioned (Albrieu et al. 2004). In the Chilean side of this volcanic field, a National Park has been developed.

In addition to these noted geomorphological features, complex volcanic relief should also be cited (Fig. 11d), as volcanic cones built within the maar craters and coalescent explosion centres (Corbella 2002).



Fig. 16 Oblique aerial photograph of “Laguna Azul”, which occupies three nested craters. In darker shades, the youngest lava flows erupted from this volcano are recognized along the central flow channel. At the background, several aligned volcanic vents are identified. The difference in elevation of these vents is close to 100 m. *Photographs* E. Mazzoni

8 Fluvial and Fluvioglacial Channelled Landscape

The landscape diversity of the study area includes also the valleys of the fluvial streams that integrate the Río Gallegos watershed, whose main tributaries are the Turbio, Los Penitentes, Zurdo, Gallegos Chico and Chico rivers. The streams of the western sector (especially the Río Penitentes and its tributary, the Río Rubens) flow with a meandering pattern, sometimes wandering drainage, with a glacial morphology of low relative relief. The rest of the tributaries have carved their valleys on which terraced levels may be observed (Fig. 17).

The Río Gallegos valley is composed of several terraces excavated during the deglaciation after various Pleistocene glaciations, when the discharge was notably larger than today, which merely drains $15 \text{ m}^3/\text{s}$. This river is, as in most allochthonous streams of the extra-Cordilleran environment of Patagonia, a “diminished river” with respect to the valley where it flows. In the widest sector, the valley reaches up to 14 km wide, where an extensive terrace located 30 m above the present stream channel is found. The superficial morphology of this terrace level exposes channels which are related to an ancient braided pattern. Contrarily, the present stream flows with meandering pattern and it has slightly carved its floodplain (Fig. 18).



Fig. 17 *Left* view of the Río Penitentes, to the West of the study area, which has a drifting flow within a glacial environment of low relative relief. *Right* the Río Turbio flows with a meandering pattern within a valley where it has excavated several terrace levels. *Photographs* E. Mazzoni



Fig. 18 The lower Río Gallegos valley, where meandering pattern and terraced levels are detected. Following the microtopography of the flood plain, the vegetation cover varies between a grassy steppe, a shrubby plain or wet meadows. The rural population settled in the higher places of the landscape. *Photographs* E. Mazzoni

Towards the E, the joining of meltwater coming from the Gallegos and Chico valleys, formed a very wide outwash plain along the lower sections of both rivers, which extends into the estuary. The city of Río Gallegos and the main communication systems are found in this unit.

From a visual point of view, the morphology of the terraces is similar to the tableland landscape, with comparable vegetation cover and soil use. The high permeability of the sediments forming them forces that the soil has very low water retention.

The Río Chico valley is noted for the amplitude of its alluvial plain, which in some areas is more than 3.5 km wide. Through this landform several small streams flow, with a total discharge of only 3 m³/s (Caballero 2000). The slow and scattered flow irrigates an extensive wetland surface (Mazzoni and Vázquez 2004), which gives the area a general greenish tone, and it is the habitat of many autochthonous wildlife species, including birds that use it as a place for feeding, resting and nesting (Ferrari et al. 2005). Moreover, it is the location where the human settlement takes place in two large ranches. The view of the valley, of contrasting colours compared to the steppes, volcanic cones and associated lava flows is of great scenic value (Fig. 19).

From the point of view of the touristic and sport activities, the Río Gallegos valley and its main tributaries, such as the Gallegos Chico and El Zurdo valleys, are used for sporting fishery of salmonids, mainly the brown, fontinalis and rainbow trouts, which has evolved into an activity of international importance.

This landscape is also composed of the different systems of wadis and dry valleys, mainly developed on top of the sedimentary rock tablelands. These are ephemeral streams in channels of trapezoidal transversal section, that have flat bottom and abrupt sides, usually showing dendritic drainage pattern in map view. They achieve a depth of around 10 m and a total length of 15 km, enlarged by headwater erosion. In the SE sector of the study area, these channels dissect the glacial morphology.



Fig. 19 Valley of the Río Gallegos Chico, whose extensive flood plain is irrigated by multiple channels that feed rich “mallines” ecosystems, used by wildlife, sheep and cattle. The valley is partially bounded by basaltic flows, erupted from the volcanic vents identified in the *left* photograph. To the *right* of the picture, a detailed view of the cattle ranch “Marcachaiké”. Photographs E. Mazzoni

9 Glacial and Glaciofluvial Landscape

This landscape has an ample distribution in the study area. Due to the high latitude of the region, the Patagonian mountain ice-sheets and their discharge glaciers covered almost completely in the past the southern portion of the South American continent. The area was affected at least by five main Pleistocene glacier advances (Caldenius 1932; Meglioli 1992; Rabassa 2008; Coronato and Rabassa 2011, among others) during the last 1 Ma (million years). To the N of the Río Gallegos valley, there is also evidence of glaciations that occurred even before that date (Ercolano et al. 2015).

The advance of the ice front took place both from the Patagonian Cordilleran range located to the W, as well from the Magellan Strait lobe, situated towards the S. The only portion of the study area that was directly affected by the piedmont glaciers extends as a wedge open towards the Atlantic Ocean, with a vortex located close to the Estancia (i.e., ranch) Bella Vista (51° 50'S, 70° 43'W, Fig. 1). The maximum Pleistocene ice advance is known as the “Great Patagonian Glaciation” (GPG, Mercer 1976) happened approximately between 1.01 and 1.1 Ma (Mercer 1976; Meglioli 1992; Ton-That et al. 1999; Singer et al. 2004, among others) and reached the present Atlantic Ocean coast S of the Río Gallegos valley, extending also over the adjacent portion of the present continental shelf. East of the Cordilleran front the ice expanded forming large, although relatively thin, piedmont lobes (Rabassa 2008). After the GPG, other glacial advances outspread with a farther more restricted spatial distribution, whose sedimentary deposits are located, successively, in the westernmost and lowermost portions of the landscape (Rabassa 2008).

In the study area, the dominant glacial morphology corresponds to sedimentary, accumulation landforms. Systems of terminal and basal moraines alternate with drumlinoid forms and glaciofluvial plains (Mazzoni 2001). Likewise, some features are associated with landforms modelled during the ice disintegration processes. The dominant topography shows hills of gentle slopes with abundant erratic boulders. The most relevant example is a giant erratic boulder situated just aside the RN 40 (51° 53' 10"S–70° 42' 00"W), which is a remarkable feature of the landscape due to its large size. This glacial boulder originated several hundred kilometres away at the Andean Cordillera, and it was originally described by Caldenius (1932) in his pioneer work on the Patagonian glaciations. The boulder is so big that it can be identified even in aerial photographs and high-resolution satellite imagery (Fig. 20).

The moraine systems correspond to different glacial events that took place in the region. The relative relief of these landforms is more relevant towards the W where the units corresponding to the more recent advances are located (Río Turbio Glaciation, Meglioli 1992). The main morphological expressions appear in the SW boundary of the study area, where the terminal moraines have a relative elevation of 50 m. These moraines act as the water divide between Argentina and Chile. From this position and towards the central portion of the study area, two other moraine

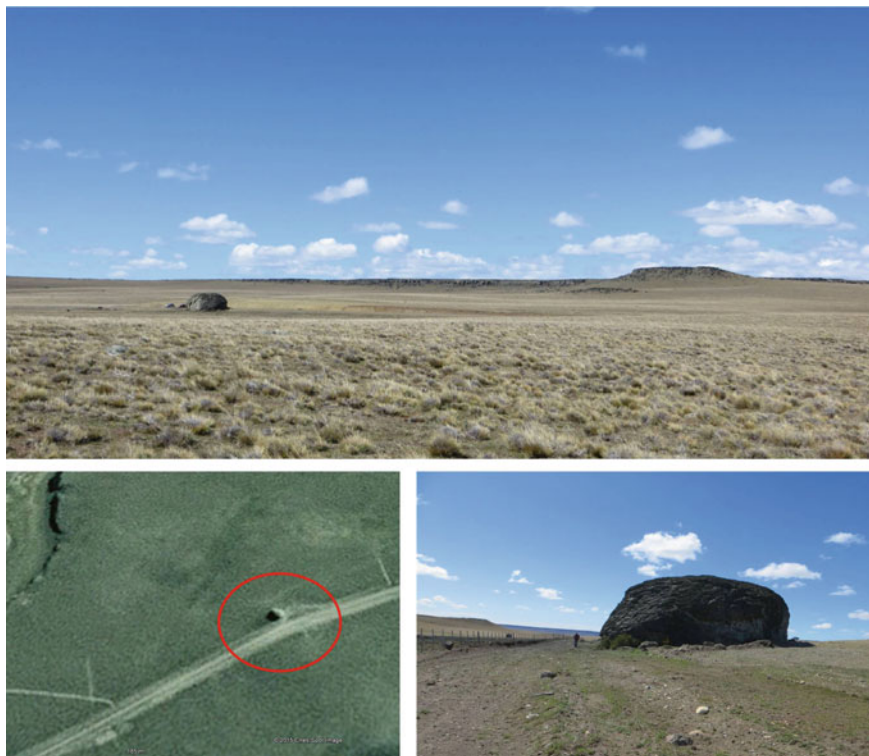


Fig. 20 Erratic boulder located in the vicinity of Estancia Bella Vista. In the *upper* photograph, its position in the landscape is depicted. Sideways, to the *left* of it, two vehicles are size references. In the *lower right* photograph, there is a person for scale. The boulder has a maximum diameter of 25 m, which allows its identification in high-resolution satellite imagery. Due to its geographical position, this boulder should be attributed to a glacier advance during the Great Patagonian Glaciation, around approximately 1.1 Ma. *Image* Google Earth program. *Photographs* E. Mazzoni

arcs occur. That one located at an easternmost position is interpreted as the outer boundary of the GPG or “Bella Vista Glaciation” (Meglioli 1992), that reaches the geographical longitude of $70^{\circ} 43'W$ in the Río Gallegos valley, being clearly identified in the watershed between the Gallegos and Coyle rivers (Fig. 18). Lateral moraine arcs are clearly observed S of Meseta Latorre (Fig. 22a). In the south-eastern margin of the study area, moraines corresponding to the GPG and the subsequent glaciation are observed. They were deposited by the ice lobes flowing towards the N–NE of the huge glacier that eroded the valley where the Magellan Straits is today. These landforms are very well preserved, with a maximum local relief of 10 m (Fig. 21).

From the site of Bella Vista towards the W, the glacial landscape shows a diversity of features which are clearly identified in aerial photographs and satellite



Fig. 21 Moraines in the Cabo Vírgenes zone. The main house of one of the largest cattle ranches of the area is located amid these landforms. *Photographs E. Mazzoni*

imagery. They are a set of subglacial landforms of very subdued relief, some of them aligned and others modelled during the different stages of ice disintegration (Fig. 22).

Among the first ones, several drumlin fields, flutes and megafutes are noted. One of them is located on the N margin of the Río Gallegos (Estancia Sofía), where elongated and sub-parallel landforms several kilometres long have a dominant orientation W–NE. These landforms have been assigned a GPG age, although current studies by Bettina Ercolano (UNPA) and Andrea Coronato (CADIC) may suggest that these landforms are a bit younger than the GPG (Fig. 22c; Bettina Ercolano, personal communication). This landscape has been carefully preserved, in spite of its great age, thanks to the extreme climatic aridness of this environment and the lack of surficial runoff during most of the Quaternary (Ercolano et al. 2004). Probably, these landforms are among the oldest, well-preserved subglacial landforms of the entire planet outside Antarctica, which gives them a special high value for scientific tourism.

Another example occurs in the proximity of Arroyo (i.e., creek) El Zurdo and the site of this name, immediately S of the boundary with Chile, well beyond the limits of the study area. Nevertheless, they are mentioned here because they are located in the surroundings and their unique morphology. Glasser and Jansson (2008) and

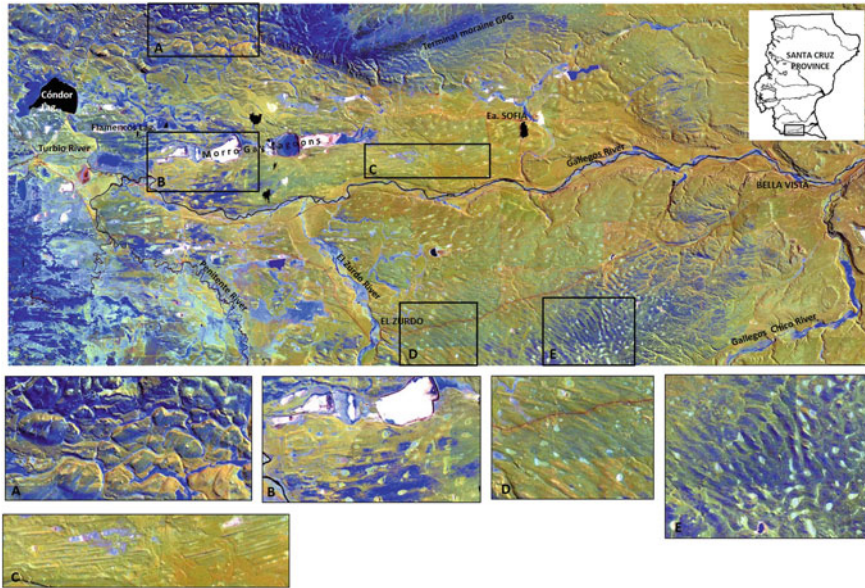


Fig. 22 Landsat satellite imagery composed within the infrared bands (7, 5, 4) that permits a neat identification of the relief landforms modelled by the glacial action in the *middle portion* of the Rio Gallegos basin. The chromatic differences indicate variations in the vegetation cover. The bluish colours correspond to grasslands, wet meadows (“mallines”) or forest areas. The detached images show details of the moraine fields, the alignment features and the kettles holes

Darvill et al. (2014) have named them as “glacial alignments”, but without providing a detailed description. A third group of elongated landforms with approximate S–N orientation are found S of the small village of 28 de Noviembre (51° 41' S–72° 13' W), which may correspond also to a drumlin field or similar forms. These landforms were interpreted by Furque and Caballé (1987) as aeolian deposits overlying glaciofluvial sediments, whereas Glasser and Jansson (2008) have mapped them as terminal moraines.

The rest of this unit shows topography where hills-hummocks and small basins-depressions alternate with various orientations and local relief. Possibly, many of these depressions were originated during the deglaciation processes, when large chunks of ice lost contact with the main ice body and remained in the landscape, totally or partially covered by glaciofluvial and glaciolacustrine sediments, and then forming hollows when the ice blocks melted away and the overlying sediments collapsed. These depressions, known as “kettles holes”, originated ponds and swamps (most of them of a seasonal nature) which are presently used as water and food sources for the wildlife and cattle. It should be mentioned the lake and ponds system located between 51° 45' S–71° 42' W and 51° 50' S–71° 12' W, composed of the Cóndor, Morro Gay and Flamenco lakes (Fig. 22b). The first of these lakes, with 960 hectares and having a permanent regime, is the largest wetland in the area.

There is evidence of recurrent human colonization in the surroundings (Gómez Otero 1991; Charlín 2012), contrarily to the rest of the central-western zone of the study area, which has been interpreted as just a transit zone due to its very poor archaeological record (Borrero and Charlín 2010).

Another group of hills may belong to moraines formed in a transversal position regarding the ice flow direction. This type of moraines has been named as “ribbed moraines”, “washboard moraines”, “De Geer moraines”, etc. (Prest 1968), and their genesis is not fully understood, being perhaps the result of superimposed subglacial processes. The morphology of these moraines transforms laterally and gradually within the study area (Fig. 22d, e). These peculiar landforms are the subject of a doctoral thesis presently under development by Mr. Pau Montero Estaña (CADIC-CONICET), under the supervision of Bettina Ercolano and Jorge Rabassa (CADIC).

In this glacial environment, the drainage has also been modified by the ice. In addition to the already mentioned abundant lakes and ponds, sinuous and shallow flow lines where water flows very slowly, allowing wetland formation, alternate between the glacial lobes and hills. In Fig. 23, this is clearly observed between the Cónдор and Morro Gay lakes. Some of the creeks, as Los Penitentes and Rubens, flow by wandering channels with meandering pattern in an alluvial plain of extremely low gradient, with frequent abandoned meanders and ox-bow lakes (Fig. 17, left).

The morphology of gentle hills is characteristic of this landscape and provides a different profile to the dominant tableland of the rest of extra-Andean Patagonia. From E to W, this landscape shows a gradual change in its vegetal cover following the precipitation gradient. Towards the western sector, the grassland steppe is replaced by the Sub-Andean grassland, the open forest and wetlands, a condition that enables cattle rising, alternating with traditional sheep farming.



Fig. 23 Wetlands in the glacial landscape. The lower areas located amongst the hills forming the glacial accumulation landscape forces the moisture concentration in the soil profile and thus, the creation of ponds. Towards the E, water bodies have a seasonal regime (*left*). In other parts of the study area, wet meadows, shallow courses and permanent lakes are found. In the *central* photographs, the aforementioned Laguna Cónдор and the Monte Philippi volcanic neck are located. At the *right*, moraine fields to the south of Meseta Latorre are seen, where wetlands are interconnected in the lowlands. This is one of the westernmost exposures of the sedimentary rock tablelands. *Photographs* E. Mazzoni

10 Andean Cordillera Landscape

This landscape occupies the western portion of the study area, with a mountain relief composed mainly by a homoclinal structure locally affected by secondary faults and folds (Pereyra et al. 2010). The geology is composed of continental and marine Cretaceous sedimentary rocks (the Cerro Cazador and Cerro Dorotea formations) and similar units of the Early Tertiary (Río Turbio Formation), carrying coal seams (Malumián and Panza 2000), whose exploitation is the main economic activity in this sector.

The topography has a lower altitude than the rest of the Southern Patagonian Andes, with elevations of less than 800 m a.s.l. The slopes are strong and abrupt, with plentiful evidence of mass movement processes. The fold system was cut by the glacial and fluvial action, exposing the different structural features that, although they have a cover of glaciofluvial sediments, soil development and vegetation, they may be clearly appreciated at the terrain or in satellite imagery (Fig. 24). The smaller tributaries are adjusted to these structures whereas the streams of higher order have crossed them transversally. The higher summits have thin debris cover associated with cryoclastic processes (Pereyra et al. 2010).

The plant cover combines the *Nothofagus* forest (the dominant southern beech) with Sub-Andean grasslands (Fig. 25). The forest formations are mainly composed of the caducifoliated *Nothofagus* species, such as “lenga” (*N. pumilio*) and “ñire” (*N. antarctica*), which gets into particularly attractive, reddish and yellowish tones during the Fall. The forest is concentrated on the slopes, although in the surroundings of the mining structures and the town of Río Turbio (see paragraph 2.8) it appears seriously degraded by timbering and forest fires. Likewise, the flood plain of the Arroyo San José is partially covered by sterile coal deposits, which have substantially modified the topography and the soil and environmental characteristics of these landforms and the surroundings (Mazzoni 2000; Pereyra et al. 2010).



Fig. 24 View of the Cordilleran landscape, where the town of Río Turbio is located, the farthest locality to the west of the study area. Dipping strata defining the main landscape features are observed in the summits and uncovered slopes. The forest ecosystem, partially degraded, is preserved in discontinuous patches. *Photographs E. Mazzoni*



Fig. 25 The rural environment permits the picturing of different countrysides in the mountain landscape. To the *left*, the glaciofluvial modelling of the San José creek (a tributary of Río Turbio) and glacial accumulation features are illustrated in the central zone. At the background, the highest summits of the glacier-covered Southern Andes may be seen in Chile. The *central* photograph shows the fluvial channel that occupies the eastern edge of this landscape (the Primavera creek), where National Route 40 is placed sidelong towards the N. To the *right*, the slopes show the effect of mass-movement processes, particularly solifluction. In all photographs the distribution of vegetation may be seen, where forest spots alternate with grassland or steppe patches, following moisture distribution. *Photographs* E. Mazzoni

Due to its geographical location, this landscape unit integrates to the Glaciares National Park, towards the N of the study area in Argentina, and to the Torres del Paine National Park towards the W in Chile, in both cases with exceptionally scenic landscape resources.

11 Landscape of Endorheic Basins

These basins are depressions located in different landscapes that are generically known as “bajos sin salida” (basins without outgoing discharge; Methol 1967), whose genesis is attribute to multiple processes among which aeolian deflation is a relevant agent (Fidalgo 1972; Martínez 2012). In the study area, they occur on top of the sedimentary rock and volcanic tablelands and in the glacial landscape, in all cases with different morphological characteristics (Mazzoni 2001) (Fig. 26). Those of larger size are found in the sedimentary rock tableland landscape, with dimensions that reach up to 13 km of longer diameter and 80 m in depth. Physical and chemical weathering, mass-movement processes and deflation intervene in their genesis and development.

The volcanic landscape shows a high frequency of depressions, whose origin is associated with phreato-magmatic explosions (Corbella 2002; Coronato et al. 2013) and craters of eruptive vents, some of them aligned or nested. Maars are those of larger size, particularly that which is occupied by Lake Potrok Aike, with an almost perfect circular shape and a diameter of 3.4 km (Fig. 27). On top of the basaltic tablelands, frequent shallow basins occur, originated by differential processes during the cooling of the lava flows (collapsed depressions; Mazzoni 2001, 2007; Mazzoni and Rabassa 2010).

The glacial landscape has the greatest density of depressions in the study area, with morphology of scarce local relief. They are located in moraine and subglacial



Fig. 26 Endorheic basins found in different Landscape Types. *Left* lowland located on a sedimentary rock tableland; at the foreground, the aeolian plume is shown, with an erosion, desert pavement over a clayey bedrock. Scattered shrubs enable the genesis of nebkas. *Centre* a small basin in a volcanic environment is partially bounded by a basaltic scarp. *Right* a system of lowland basins modelled by glacial action; being close to the National Route 40, they are easily reachable spots for bird watching. *Photographs* E. Mazzoni



Fig. 27 View of the Laguna Potrok Aike, one of the more important depressions of the region, which hosts a lake more than 100 m deep. Its origin is attributed to a phreato-magmatic explosion (Gebhardt et al. 2011; Coronato et al. 2013). *Photographs* E. Mazzoni

landform fields. The larger depression may have been excavated by the direct action of the ice during its advance or by the melting away of ice block remnants, as it is the case of the aforementioned Lake C ndor (Fig. 23, centre).

The morphology of the larger “bajos” shows frequent coastlines, which reflect environmental changes in the region, as the water level within the depression changed (Schavitz 1991, 1994; Stine and Stine 1990). These depressions are also associated with aeolian deposits which extend towards the E for many kilometres,

as aeolian “tongues” (“lenguas”; Movia 1972) or “plumes” (“plumas”; Mazzoni 2001; Mazzoni et al. 2002; Mazzoni and Vázquez 2009) oriented following the dominant westerly winds. These aeolian features are more abundant towards the E of geographical longitude 71°W, where the precipitation and plant cover are smaller. The sediments that form these “plumes” are predominantly clayey in the depressions on the sedimentary rock tablelands, excavated in the Santa Cruz Formation beds. Contrarily, the depressions situated in the volcanic fields have “plumes” predominantly composed of sand. These plumes are longer than the aforementioned ones and sometimes more than 10 km long, recording important changes with time. Wadis and canyons drain towards the larger depressions, and their ephemeral streams contribute to extend their watersheds by headwater erosion.

12 Urban Landscape

The urban landscape includes the three urban centres situated along the axis formed by the Gallegos and Turbio rivers. Each city is located in different geographical environments.

The city of Río Gallegos (51° 37'S–69° 13'W) is the seat of the government of Santa Cruz Province, with a population estimated in 105,000 inhabitants. Its origin is related to the occupation of lands for sheep rising towards the end of the nineteenth century (García 2000). The pattern of its urban design varied following according to the different epochs of city growth. Downtown, it has a checker distribution with the Town Hall, the church and the oldest school in town around the central square, according to the Spanish tradition. Many buildings (as the Cathedral) have a picturesque traditional architecture of the end of the nineteenth century, using wood and tin painted in brilliant colours (Fig. 28). In general, the buildings are of just one or two stories. The city is located on the outwash plain that connects the mouths of the Gallegos and Chico rivers, in the southern margin of the estuary, from where the maritime littoral landscape may be observed towards the N and NE and the volcanic landscape towards the SW, the eruptive vents and volcanoes being noted in the horizon. Río Gallegos has a long waterfront from where the marshy protected area may be seen with the many bird species that inhabit it.

The town of 28 de Noviembre (51° 35'S–72° 12'W) is located in the sub-humid glacial landscape with an estimated population of 8000 inhabitants. Founded in 1957 as a political-administrative centre, its urban pattern occupies the bottom of the Río Turbio valley, surrounded by small agricultural production units. Its urban structure shows a regular design and the construction corresponds mainly to social housing programs (Fig. 29).

In the W section of the study area, the city of Río Turbio (51° 32'S–72° 20'W) is located (Fig. 24). Its development is fully associated with coal mining activities that started in the 1940s. The city grew in the Cordilleran landscape, with an estimated population of 9500 inhabitants. The pattern design is irregular, being partially



Fig. 28 Partial aerial view of the city of Río Gallegos, in which its location may be analyzed, bounded by the estuary formed by the Gallegos (at the foreground) and Chico rivers at their mouth. In the image to the *left*, the Río Gallegos cathedral, a symbol of traditional architecture of the region, may be seen. *Photographs E. Mazzoni*



Fig. 29 Landscape view of the town of 28 de Noviembre, located in a fluvio-glacial environment under sub-humid climate conditions. Behind the town, the Río Turbio, with its meandering channel pattern, a wide terraced level at the intermediate plane, and the Meseta Latorre at the background may be observed. The forest ecosystem occurs mostly along the slopes of the cited tableland. In the *box* at the *right*, a detail of buildings of social housing. *Photographs E. Mazzoni*

adjusted to the local topography. The scenic attraction of its surroundings is due to relief differences, fluvial streams and the forest, but it is gravely affected by the residual materials of coal mining. Nevertheless, the original mining facilities (“Mina 1”) and the *trocha angosta* train in which the coal is transported towards the city of Río Gallegos may become a real touristic attraction. It should be considered that this is the only place in Argentina where this type of mining takes place (Fig. 22). Among the recreational offer, the city has a small winter sport centre.

13 Final Remarks

The southern fringe of Patagonia which is traversed by National Route 40 has peculiar features that differentiate it from the rest of the regional territory, both in its Cordilleran environment as in the extra-Cordilleran region. These particular characteristics are a consequence of its geographical position, the geological processes that affected it and its historical development, initiated in AD 1520 with the discovery of the Magellan Strait. Before then, the aboriginal occupation left isolated testimonies, rock-art or lithic instruments, within discontinuous modes of space use.

The spatial heterogeneity expresses in different landscape types and units that have been identified according to the natural agents and dominant processes that intervened in their genesis. A large part of the area was affected by direct glacial action or meltwater activity. Likewise, numerous cryogenic structures are found, though at the surficial level.

Among the particular features of the landscape, Cabo Vírgenes, Punta Dungeness and the estuary of the Gallegos and Chico rivers should be mentioned in the coastal region. The Pali-Aike volcanic field has a unique morphology composed of many aligned eruption centres and vents, with maars and recent lava flows. The landscape associated with the piedmont glaciations has characteristics that are exclusive of this area of Argentina. Wetlands are abundant (marshes, lakes, ponds and wetlands), appropriate to wildlife and migratory bird observation. Similarly, the sedimentary rock tableland landscape is noted for the homogeneous grass cover of *Festuca gracillima* (“coirón fueguino”), whose bushes give a ochre tone to the plains. The low density of population with ample natural space in which no obvious signs of human activity are detected comprises another important aspect of the Patagonian landscapes, combined with the scattered rural settlements, the extensive “estancias”.

The cartography of these landscapes is a helpful tool for the territorial planning and management. Particularly, in this case, cartography works very well as a base for the inventory and classification of touristic resources as alternative and sustainable activities, such as ecotourism, rural tourism, trekking and outdoors adventure and scientific tourism.

Acknowledgements To Dr. Jorge Rabassa, for the critical reading of a preliminary draft of this manuscript.

This work was developed as part of the Research Project “Corredor Austral RN40 (Santa Cruz): análisis de su potencialidad turística y propuestas para planificar su desarrollo sustentable”, based in the Río Gallegos Campus of the Universidad Nacional de la Patagonia Austral.

References

- Albrieu C, Imberti S, Ferrari S (2004) Las Aves de la Patagonia Sur, el estuario del Río Gallegos y zonas aledañas, Argentina. Editorial Universidad de la Patagonia Austral, Río Gallegos, 204 pp
- Altevogt G (1969) Der postglaciale vulkanismus südlich von Río Gallegos, Provinz Santa Cruz, Süd-Argentinien. *Geologie und Paläontologie* 12:3–15

- Bockheim J, Coronato A, Rabassa J, Ercolano B, Ponce JF (2009) Relict sand wedges in southern Patagonia and their stratigraphic and paleo-environmental significance. *Quatern Sci Rev* 28:1188–1199
- Boelcke O (1957) Comunidades herbáceas del Norte de la Patagonia y sus relaciones con la ganadería. *Revista Investigaciones Agrícolas* 11: 5–98 (Buenos Aires)
- Bolòs M (1992) *Manual de Ciencia del Paisaje. Teoría, Métodos y Aplicaciones*, Colección Geográfica. Editorial Masson, Barcelona, p 273
- Borrero L, Manzi L, L'Heureux G, Martin F, Franco N, Charlin J, Barberena R, Campán P (2004) Arqueología del campo de lava Pali Aike, Argentina. *Resúmenes XV Congreso Nacional de Arqueología Argentina*, p 368 (Río Cuarto)
- Borrero L, Charlin J (2010) *Arqueología de Pali Aike y Cabo Vírgenes* (Santa Cruz, Argentina). Buenos Aires, Editorial Dunken, 152 p
- Caballero J (2000) Hidrografía y recursos hídricos. In: García A. and Mazzoni E (dir.) *El Gran Libro de la provincia de Santa Cruz*. Millenium Ediciones and Alfa Centro Literario, Madrid, pp 116–139
- Cabrera AL (1976) Regiones fitogeográficas argentinas. *Enciclopedia Argentina de Agricultura y Jardinería*. Editorial ACME, Buenos Aires, pp 1–85
- Caldenius C (1932) *Las Glaciaciones Cuaternarias en Patagonia y Tierra del Fuego*. Ministerio de Agricultura de la Nación, vol 95. Dirección General de Minas y Geología, Buenos Aires, 148 p
- Carballo Marina F, Manzi L, Campán P, Belardi JB, Tiberi P, Manera A, Sáenz JL (2008) Distribución del registro arqueológico en la cuenca del Río Gallegos (Santa Cruz): línea de base y aporte a la preservación del patrimonio. In: Borrero L, Franco N (eds) *Arqueología del extremo sur del continente americano*. CONICET-IMHICIHU, Buenos Aires, pp 175–225
- Charlin J (2012) *Materias primas líticas y uso del espacio en las nacientes del Río Gallegos: el caso de Laguna Cóndor* (Estancia Glencross, Santa Cruz, Argentina). *Magallania* 40(1):163–184 (Punta Arenas, Chile)
- Codignotto J (1975) *Geología y rasgos geomorfológicos de la Patagonia Austral extraandina, entre el río Chico y la Bahía de San Sebastián*. Unpublished Doctoral Tesis, Universidad de Buenos Aires, 76 p
- Codignotto J (1976) Nota acerca de algunos aspectos geológicos de la costa patagónica comprendida entre Punta Loyola y el Cabo Vírgenes. *Servicio de Hidrografía Naval, Boletín* 6 (3): 257–263 (Buenos Aires)
- Codignotto J (1990) Evolución en el Cuaternario alto del sector de costa y plataforma submarina entre Río Coig, Santa Cruz y Punta María, Tierra del Fuego. *Revista de la Asociación Geológica Argentina* 45(1–2):9–16 (Buenos Aires)
- Corbella H (1999) *Dataciones radimétricas en Pali Aike, Patagonia Austral*. XIV Congreso Geológico Argentino, Salta, Actas, 2, pp 265–268
- Corbella H (2002) El campo volcano-tectónico de Pali Aike. In: Haller M (Ed.), *Geología y recursos naturales de Santa Cruz*. Relatorio del XV Congreso Geológico Argentino, El Calafate, I 18:258–301 (Buenos Aires)
- Corbella H, Ercolano B, Coronato A, Tiberi P (2014) Tectónica distensiva, magmatismo y glaciaciones en la cuenca superior y media del Río Gallegos. XIX Congreso Geológico Argentino, Actas. Córdoba, Patagonia austral
- Corbella H, Pomposiello C, Malagnino E, Trincherro E, Alonso S, Chelotti L, Díaz T, Firpo L (1990) Volcanismo lávico y freatomagmático postglacial asociado al campo de fracturación austral, Provincia de Santa Cruz, Argentina. XI Congreso Geológico Argentino, Actas 2:383–393 (Buenos Aires)
- Coronato A, Ercolano B, Corbella H, Tiberi P (2013) Glacial, fluvial and volcanic landscape evolution in the Laguna Potrok Aike maar area, Southern Patagonia, Argentina. *Quat Sci Rev* 71:13–26
- Coronato A, Rabassa J (2011) Pleistocene glaciations in Southern Patagonia and Tierra del Fuego. In: Ehlers J, Gibbard PL, Hughes PD (eds) *Quaternary glaciations, extend and chronology. Developments in quaternary science*, vol 15. Elsevier, Amsterdam, pp 715–727

- Council of Europe (2000) European landscape convention. Florencia, Available at: <https://rm.coe.int/CoERMPublicCommonSearchServices/DisplayDCTMContent?documentId=0900001680080621>. Accessed: 08 Feb 2017
- Darvill CM, Stokes CR, Bentley MJ, Lovell H (2014) A glacial geomorphological map of the southernmost ice lobes of Patagonia: the Bahía Inútil – San Sebastián, Magellan, Otway, Skyring and Río Gallegos lobes. *J Maps*
- Darwin C (1842) On the distribution of erratic boulders and on contemporaneous unstratified deposits of South America. *Trans Geol Soc Lond Ser 6(2):415–431*
- De Negris ME, Senatore MX (2008) Arqueología histórica en los confines del imperio. La ciudad del Nombre de Jesús (Estrecho de Magallanes, Siglo XVI). *Telar 6:129–144* (Instituto Interdisciplinario de Estudios Latinoamericanos, Facultad de Filosofía y Letras, Universidad Nacional de Tucumán, San Miguel de Tucumán)
- D’Orazio M, Agostini S, Innocenti F, Haller MJ, Manetti P, Mazzarini F (2001) Slab window related magmatism from southernmost South America: the Late Miocene mafic volcanic from Estancia Glencross Area (52°S, Argentina—Chile). *Lithos 57:67–89*
- Ercolano B (2010) Evolución de la costa comprendida entre el Río Gallegos y Chorrillo de los Frailes. Unpublished Doctoral Theses, Facultad de Ciencias Exactas y Naturales Universidad de Buenos Aires, Buenos Aires, 244 p
- Ercolano B, Mazzoni E, Rabassa J (1997) Fossil wedges and other periglacial structures near Río Gallegos, Argentina, Southernmost South America. In: 7th international conference on permafrost. abstracts, Yellowknife, Canada
- Ercolano B, Mazzoni E, Vázquez M, Rabassa J (2004) Drumlins y formas drumlinoides del Pleistoceno Inferior en Patagonia Austral, Provincia de Santa Cruz. *Revista de la Asociación Geológica Argentina 59(4):771–777* (Buenos Aires)
- Ercolano B, Tiberi P, Marderswald G, Coronato A, Corbella H (2015) Morfología glacial pedemontana en el interfluvio de los ríos Coyle y Gallegos, Patagonia Austral, Argentina. In: Ponce J, Candel MS, Fernández M, Oria J, Villarreal ML (eds) VI Congreso Argentino de Cuaternario y Geomorfología. Abstracts, Editorial Utopías, Ushuaia, pp 221–222
- Ferrari S, Albrieu C, Gandini P (2002) Importance of the Río Gallegos estuary, Santa Cruz, Argentina, for migratory shorebirds. *Water Study Group Bull 99:35–40*
- Ferrari S, Imberti S, Albrieu C (2005) Áreas de importancia para la conservación de las aves en Santa Cruz. In: Di Giacomo AS (ed) Áreas de importancia para la conservación de las aves en Argentina, sitios prioritarios para la conservación de la biodiversidad. Asociación Ornitológica de La Plata, Buenos Aires, pp 412–414.
- Fidalgo F (1972) Consideraciones sobre los bajos situados al norte de la provincia de Santa Cruz. V Congreso Geológico Argentino. *Actas 5:123–137* (Córdoba)
- Fidalgo F, Riggi JC (1970) Consideraciones geomorfológicas y sedimentológicas sobre los Rodados Patagónicos. *Revista Asociación Geológica Argentina 25:430–443* (Buenos Aires)
- Furque G, Caballé M (1987) Estudio geológico y geomorfológico de la cuenca superior del Río Turbio. CFI/Universidad Nacional de La Plata, unpublished technical report, Provincia de Santa Cruz, p 72
- García A (2000) El origen de las localidades de Santa Cruz y algunos aspectos de su desarrollo. In: García A and Mazzoni E (dir.), *El Gran Libro de la Provincia de Santa Cruz 1:575–646* (Editorial Millenium – Alfa Centro Literario. Madrid)
- Gebhardt AC, De Batist M, Niessen F, Anselmetti FS, Ariztegui D, Kopsch C, Ohlendorf C, Zolitschka B (2011) Origin and evolution of the Laguna Potrok Aike maar, Southern Patagonia. *J Volcanol Geoth Res 201:357–363*
- Glasser NF, Jansson KN (2008) The glacial map of southern South America. *J Maps 2008:175–196*. doi:10.4113/jom.2008.1020
- Gómez Otero J (1991) Discusión sobre el límite occidental del territorio de los Proto-Tehuelches y Tehuelches meridionales en el extremo Sud de Patagonia (cuenca del Río Gallegos). *Waxen 6(3):3–22*

- González Bonorino G (2002) Erosión y acreción litoral durante el Holoceno. In: Haller M (ed)., Geología y recursos naturales de Santa Cruz. XV Congreso Geológico Argentino, Relatorio, 1, 20: 317–324 (El Calafate and Buenos Aires)
- González Bernáldez F (1981) Ecología y Paisaje. Blume Editores, Madrid, 256 p
- INDEC (2010) Censo Nacional de Población y Vivienda. Instituto Nacional de Estadística y Censos. Buenos Aires. On line: <http://www.censo2010.indec.gov.ar/>. Accessed: 10/03/2015
- INDEC (2013) Estimaciones y proyecciones de población 2010-2040. Instituto Nacional de Estadística y Censos, Buenos Aires 36 pp
- León R, Brand D, Collantes M, Paruelo J, Soriano A (1998) Grandes Unidades de vegetación de la Patagonia extra-andina. *Ecología Austral* 8:125–144 (Buenos Aires)
- López C, Rial P, Elissalde N, Llanos E, Behr S (2011) Grandes unidades de paisaje de la Patagonia argentina. In Díaz BG and Calviño P (eds) Actas Jornadas Regionales de Información Geográfica y Ordenamiento Territorial 2:217–229. Ministerio Secretaría General de la Gobernación, *Proyecto SIT SantaCruz*. [www.sitsantacruz.com.ar/.../\[217-229\]_LibroJIGOT2_Ponencias_rial.pdf](http://www.sitsantacruz.com.ar/.../[217-229]_LibroJIGOT2_Ponencias_rial.pdf). Accessed 05 June 2015
- Luque E (1995) Reserva Provincial Cabo Vírgenes (Reseña Histórica). Dirección de Fauna Silvestre, Consejo Agrario Provincial, province of Santa Cruz. Río Gallegos
- Malumián N, Panza J (2000) Yacimiento Río Turbio. Hoja Geológica 5172-III. 1:250,000. SEGEMAR, Boletín 247, 125 p (Buenos Aires)
- Marchand D (1971) Rates and modes of denudation, White Mountains, eastern North America. *Am J Sci* 262:782–794
- Martínez OA (2012) Los bajos sin salida del centro-norte de Patagonia y su relación con los ciclos climáticos del Cenozoico superior. V Congreso Argentino del Cuaternario y Geomorfología, Río Cuarto
- Mata Olmo R (2011) Atlas de los paisajes de Castilla-La Mancha Ediciones de la Universidad de Castilla-La Mancha. 219 p. On line: <http://www.castillalalamanca.es/sites/default/files/documentos/20120511/atlas-clm.pdf>. Accessed 12 Feb 2014
- Mateo Rodríguez J, Da Silva E, Brito Cavalcanti A (2007) Geoecología das paisagens. Universidade Federal de Ceará, Fortaleza, Brasil, Fortaleza Ediciones
- Mazzoni E (1987) Aporte al conocimiento de los escoriales basálticos: acuíferos que posibilitan el asentamiento en zonas áridas. *Boletim de Geografia Teoretica*, 16–17, 31–34:339–342 (Brasil)
- Mazzoni E (2000) Problemática ambiental derivada de la actividad carbonífera en Río Turbio, provincia de Santa Cruz. In: García A, Mazzoni E (eds) *El Gran Libro de la Provincia de Santa Cruz*, 1, 1240-1244. Alfa Centro Literario and Editorial Millenium, Madrid
- Mazzoni E (2001) Distribución espacial y caracterización geomorfológica de “bajos sin salida” de la Patagonia Austral Extracordillerana. *Anales Instituto de la Patagonia* 29:5–24 (Serie Ciencias Naturales, Universidad de Magallanes, Punta Arenas, Chile)
- Mazzoni E (2007) Geomorfología y evolución geomorfológica de paisajes volcánicos y sus mallines asociados en diferentes ambientes de la Patagonia extra-andina. Unpublished Doctoral Thesis, Universidad Nacional del Sur, Bahía Blanca
- Mazzoni E (2012) Geografía física a escala de detalle: patrones geomorfológicos, edáficos y de vegetación mediante imágenes de alta resolución espacial en la estepa patagónica. IX Jornadas Nacionales de Geografía Física, Abstracts, p 16. Universidad Nacional del Sur, Bahía Blanca
- Mazzoni E, Rabassa J (2007) Volcanic landscapes of Patagonia: a geomorphological map of the Piedra del Águila volcanic plateau, province of Neuquén, Argentina. *J Maps* 311–322. http://www.journalofmaps.com/article_depository/samerica/Mazzoni_Escorial_1175626845.pdf
- Mazzoni E, Rabassa J (2010) Inventario y clasificación de escoriales basálticos de Patagonia en base a utilización de imágenes satelitales y SIG, Provincia de Santa Cruz, Argentina. *Revista de la Asociación Geológica Argentina* 66(4):608–618 (Buenos Aires)
- Mazzoni E, Rabassa J (2013) Types and internal hydro-geomorphologic variability of mallines (wet-meadows) of Patagonia: emphasis on volcanic plateaus. *J South Am Earth Sci* 46:170–182 (Elsevier)
- Mazzoni E, Vázquez M (2004) Ecosistemas de mallines y paisajes de la Patagonia Austral (Provincia de Santa Cruz). INTA – GTZ. Buenos Aires, 63 p

- Mazzoni E, Vázquez M (2009) Desertification in Patagonia. In: Latrubesse E (Edit.) *Geomorphology of natural and human-induced disasters in South America. Developments in Earth Surface Processes*, Elsevier, pp 351–357
- Mazzoni E, Vázquez M, Ruiz Posse E (2002) Dinámica geomorfológica de depósitos eólicos asociados a “bajos sin salida” de la Patagonia austral. IV Jornadas Nacionales de Geografía Física, Actas 165–176. Universidad Nacional de Mar del Plata
- Meglioli A (1992) Glacial geology of southernmost Patagonia, the Strait of Magellan and Northern Tierra del Fuego. Unpublished PhD dissertation, Lehigh University, Bethlehem, Pennsylvania
- Mejía V, Opdyke D, Vilas J, Singer B, Stoner J (2004) Plio-Pleistocene time average field in the southern Patagonia recorded lava flows. *Geochem Geophys Geosyst* 5(3):1–15
- Mercer J (1976) Glacial history of southernmost South America. *Quat Res* 6:125–166
- Methol E (1967) Consideraciones acerca de los “pequeños bajos sin salida”. *Revista de la Asociación Geológica Argentina* 22:295–311 (Buenos Aires)
- Movia C (1972) Formas de erosión eólica en la Patagonia. *Photointerprétation* 6/3:14–19 (Editorial Technip. Paris)
- Nogué J, Vela J (2011) La dimensión comunicativa del paisaje. Una propuesta teórica y aplicada. *Revista de Geografía Norte Grande* 49:25–34
- Ollier C (1967) Maars, their characteristics, varieties and definition. *Bull Volcanol* 31:45–73
- Ortiz Troncoso O (1973) Artefactos de sílex de una tumba de Morro Philippi, valle medio del Río Gallegos. *Anales del Instituto de la Patagonia* 4(2):131–139
- Panza JL, Franchi MR (2002) Magmatismo basáltico cenozoico extrandino. In: Haller M (ed) *Geología y recursos naturales de Santa Cruz*. Asociación Geológica Argentina, Buenos Aires, pp 201–236
- Pereyra F, Boujon P, Gómez A, Tello N, Tobío MI, Lapido O (2010) Estudio geocientífico aplicado a la evaluación de la aptitud para la urbanización en la cuenca carbonífera de Río Turbio, Santa Cruz. *Revista de la Asociación Geológica Argentina* 66(4):505–519 (Buenos Aires)
- Prest VK (1968) Nomenclature of moraines and ice-flow features as applied to the glacial map of Canada. Paper 67–57, Geological Survey of Canada, Ottawa
- Rabassa J (2008) Late Cenozoic Glaciations in Patagonia and Tierra del Fuego. In: Rabassa J (ed) *The Late Cenozoic of Patagonia and Tierra del Fuego, Developments in Quaternary Sciences*, vol 11. Elsevier, pp 151–204
- Ramos V (1999) Las provincias geológicas del territorio argentino. *Geología Argentina, Anales* 29 (3):41–96 (Instituto de Geología y Recursos Minerales. Buenos Aires)
- Russo A, Flores MA, Di Benedetto H (1980) Patagonia Austral Extrandina. In: Haller M (ed) *Geología Regional Argentina*, 2: 1431–1462. Academia Nacional de Ciencias, Córdoba
- Serrano Giné D (2012) El papel del relieve en la definición de unidades de paisaje. *Cuadernos de Investigación Geográfica* 32, 2, 123–145 (Universidad de La Rioja, Spain)
- Schavitz F (1991) Paleoeological studies of the “bajos sin salida” of northern Patagonia (Laguna Indio Muerto). Argentina (preliminary results). *Bamberger Geographische Schriften* 11:295–308
- Schavitz F (1994) Holocene climatic variations in northern Patagonia, Argentina. *Palaeogeogr Palaeoclimatol Palaeoecol* 108:287–294
- Skewes MA (1978) Geología, petrología, quimismo y origen de los volcanes del área de Pali-Aike, Magallanes, Chile. *Anales del Instituto de la Patagonia* 9:95–106 (Punta Arenas)
- Skewes MA, Stern CR (1979) Petrology and geochemistry of alkali basalts and ultramafic inclusions from the Palei-Aike volcanic field in southern Chile and the origin of the Patagonian plateau lavas. *J Volcanol Geotherm Res* 6:3–25
- Stine S, Stine M (1990) A record from Lake Cardiel of climatic change in southern South America. *Nature* 345:705–708
- Singer B, Ackert R, Guillou H (2004) $^{40}\text{Ar}/^{39}\text{Ar}$ and K-Ar chronology of Pleistocene glaciations in Patagonia. *Geol Soc Am Bull* 116(2):434–450
- Tauber AA (1999) Los vertebrados de la Formación Santa Cruz (Mioceno inferior – medio) en el extremo sureste de la Patagonia y su significado paleoecológico. *Revista Española de Paleontología* 14(2):173–182 (Madrid)

- Ton-That T, Singer B, Mörner N, Rabassa J (1999) Datación de lavas basálticas por $^{40}\text{Ar}/^{39}\text{Ar}$ y geología glacial de la región del Lago Buenos Aires, provincia de Santa Cruz, Argentina. *Revista Asociación Geológica Argentina* 54(4):333–352 (Buenos Aires)
- Troll C (1966) *Landscape ecology*. ITC/UNESCO Centre. The Netherlands, Special Publications, vol 4, 23 p
- Uribe P, Zamora E (1981) Origen y geomorfología de la Punta Dungeness, Patagonia. *Anales del Instituto de la Patagonia* 12:144–158 (Punta Arenas)
- Zolitschka B, Schäbitz F, Lücke A, Clifton G, Corbella H, Ercolano B, Habertzettl T, Maidana N, Mayr C, Ohlendorf C, Oliva G, Páez MM, Schleser GH, Soto J, Tiberi P, Wille M (2006) Crater lakes of the Pali Aike volcanic field as key sites of paleoclimatic and paleoecological reconstructions in southern Patagonia, Argentina. *J South America Earth Sci* 2:294–309

Flash Flood Hazard Assessment in an Ungauged Piedmont Basin in the Sierras Pampeanas Western Region, Province of Córdoba, Argentina

Karina V. Echevarria, Susana B. Degiovanni, Mónica T. Blarasin
and M. Jimena Andreazzini

Abstract In Argentina, in both mountain and piedmont basins, generally with insufficient hydrological data, flash floods are recurrent. The objective of this paper is to evaluate the flash flood hazard of a typical ungauged piedmont basin, the Arroyo (= creek) Chuchiras, province of Córdoba, Argentina, through the analysis of geomorphological, sedimentological, hydrological, and anthropogenic variables that control the behavior of these fluvial systems. The concept of hazard represents the susceptibility and natural fragility of a region exposed to a threat. The susceptibility was evaluated through the following indicators: slope, aspect, valley depth, landscape and landforms, and road networks. Five classes of flash flood susceptibility and hazard were defined. To assess the threat, analysis was made taking into account temporal distribution and intensity of precipitation, field hydrological evidence, and eyewitness reports. The Manning and the paleo-hydraulic methods were used to estimate mean velocity values during the extraordinary event flash flood which occurred on February 4, 2014. The flash flood hazard in the western piedmont of the Sierras Grandes de Córdoba is the result of the combination of variables: low permeability rocks in the upper basin; important topographical contrasts between the fault scarp and piedmont area; and streams with torrential regime and high energy (velocity, competence, and transport capacity) that make up distributary systems in the distal-middle piedmont and high intensity rainfalls. A 26% of the study area presents high/moderately high flash flood hazard, associated with the lower reaches and proximal-middle active alluvial fan of Arroyo Chuchiras; 64 and 10% of the investigated sector correspond to low/moderately low and moderate classes of flash flood hazard, respectively.

K.V. Echevarria (✉) · S.B. Degiovanni · M.T. Blarasin · M.J. Andreazzini
Departamento de Geología, Universidad Nacional de Río Cuarto,
Ruta Nacional Nº 36, Km 601, X5804BYA Río Cuarto, Córdoba, Argentina
e-mail: karyechevarria@yahoo.com.ar

K.V. Echevarria · M.J. Andreazzini
Consejo Nacional de Investigaciones Científicas y Tecnológicas
(CONICET), Buenos Aires, Argentina

Keywords Flash flood hazard · Ungauged piedmont basin · Geomorphology · Sierras Pampeanas de Córdoba · Argentina

1 Introduction

The occurrence of floods is the most frequent among all natural disasters, affecting both rural and urban settlements. Flooding is a global phenomenon which causes widespread devastation, economic damages, and loss of human lives. Particularly in the past twenty years, the number of reported flood events has been increasing significantly. Only in 2010, 178 million people were affected by floods and 8000 human beings were reported dead (Jha et al. 2012).

Specifically, flash floods represent one of the most dangerous and deadly geomorphological hazards. In general, they are characterized by intense rainfall in short time periods. These floods are enhanced by topography and affect rather small areas, but sometimes, they can affect larger areas (Gaume et al. 2009). In turn, the growing urbanization without land use planning in the piedmont areas has favored the impacts of these events. In this sense, there are several international projects that study the flash floods, in gauged and ungauged catchments. Among them, Gaume et al. (2009), Marchi et al. (2010), and Borga et al. (2014) may be cited, who made a review and characterization of these events in Europe. Gutiérrez et al. (1998), Hooke and Mant (2000), Phillips (2002), Fernández Lavado et al. (2007), and De Waele et al. (2010) studied geomorphological (and in some cases sedimentological) changes related to extreme flood events. On the other hand, Ogden et al. (2000), Gaume et al. (2004), Anquetin et al. (2010), Koutroulis and Tsanis (2010), Nikolopoulos et al. (2011), Catane et al. (2012), and Garambois et al. (2014, 2015) applied hydrological models, whereas Carpenter et al. (1999), Dawod et al. (2011), Bajabaa et al. (2014), and Elkhachy (2015) used GIS tools, for hydrological analysis and flash floods mapping, respectively. In addition, there are several works related with the estimation of paleo-floods, such as Williams (1984), Maizels (1983), Martín Vide et al. (2002), and Lang et al. (2004), among others.

In many towns and cities of Argentina, in both mountain and piedmont areas, these types of flood events are recurrent. Thus, those occurred in the provinces of San Luis (Luján, Concarán and Quines, 2015), Salta (Tartagal, 2006, 2008), and Córdoba (San Carlos Minas—1992– and Jesús María, Río Ceballos, and Unquillo—2015–) may be highlighted. However, few of these works included their analysis, characterization, and prevention; Ambrosino et al. (2004), Esper Angillieri (2007), Gil (2011), and Busnelli and Horta (2014) should be cited among them.

In Argentina, and particularly in the province of Córdoba, an important urban expansion without planning management is recorded in piedmont areas of the Sierras Pampeanas. The urban expansion is linked to growing touristic development during last decades. Thus, there are numerous villages settled along rivers and streams, a situation that generates different flash flood risk events. Therefore, it is necessary to develop maps of flood hazard and risk, which may contribute to build

up adequate territorial management and/or to mitigate the impacts caused by low and high recurrence floods.

Nowadays, the general tendency is to produce hazard flood maps using rainfall data and computer-based models. The data needed in these models include a comprehensive record of daily rainfall data, roughness coefficient of the channel, and detailed topographic maps or digital elevation models (DEMs). Nevertheless, when there is little data availability, the results of the models are not reliable (Fernández Lavado et al. 2007). Unfortunately, these methods may not be applied in many developing countries, like Argentina, because of insufficient data available.

In this sense, geological, geomorphological, and hydrological basic studies are relevant, as well as eyewitness reports that describe previous flood events and help to characterize the magnitude and spatial-temporal distribution of the flash flood.

In this framework, this paper presents a methodology based on the assessment of different indicators for estimating the flash flood hazard.

The analysis was made in a basin that presents the typical piedmont environmental problems in the province of Córdoba. On February 4, 2014, rainfall of 140 mm in only 3 h was recorded in the town of Villa de Las Rosas (Sierras Grandes). This unusually high precipitation triggered an important flash flood in the Arroyo Chuchiras basin.

The main objective of this work is to evaluate the flash flood hazard of the Arroyo Chuchiras basin through the analysis of the geomorphological, sedimentological, hydrological, and anthropogenic main variables that control the behavior of a piedmont fluvial basin.

2 Study Area Description

The Arroyo Chuchiras basin is located in the southern portion of the Traslasierra valley (San Javier Department, province of Córdoba, Argentina) (Fig. 1).

The Arroyo Chuchiras drains the western slope of the Sierras Grandes de Córdoba, discharging into the piedmont area, where a distal alluvial fan has developed. The climate is semiarid and mesothermal (Thornthwaite 1948), with an average annual rainfall of 628 mm, calculated from the data of a station located in the lowland plain area (the city of Villa Dolores, 1961–2014 series; data from the National Weather Service). There is a gentle precipitation gradient from the highest mountain elevations (800 mm isohyet) to the piedmont plains (700 mm isohyet; Capitanelli 1979). Almost 77% of the rainfall is concentrated both in spring and summer.

From the geological point of view and under the influence of the Sierras Pampeanas geological setting, the area shows the classical tectonic block arrangement defined by regional faults (Niña Paula, Los Molinos and Nono faults, among others). Toward the East, the Sierras Grandes are formed by metamorphic and granitic rocks (Precambrian–Paleozoic), which show the highest altitudes and rough slopes in the region. In the piedmont area, two levels of Cenozoic alluvial fans are recognized (Fig. 2) with a strongly undulated relief and evidence of neotectonic activity (Bonalumi et al. 1999).

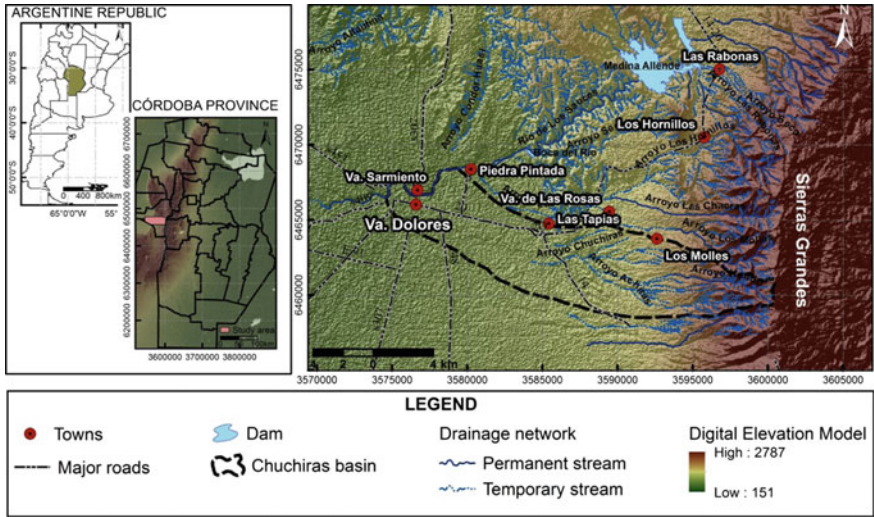


Fig. 1 Location of the study area. Digital elevation model from SRTM (Shuttle Radar Topography Mission) and hydrology features of the studied zone

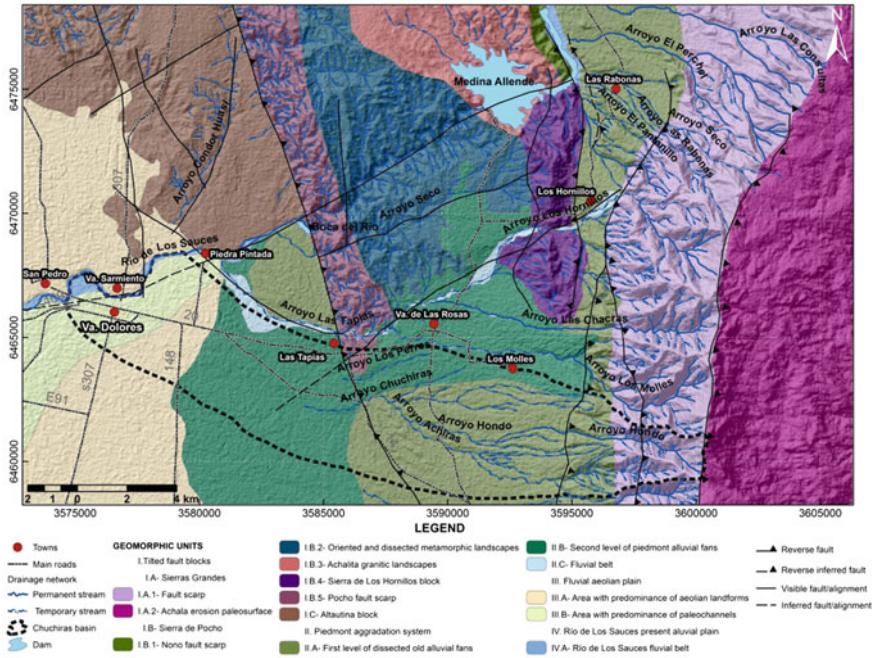


Fig. 2 Geological and geomorphological map of the study area

The Arroyo Chuchiras, like other streams in this region, has a torrential hydrological regimen associated with the almost impervious lithology and steep slopes of their upper-middle basin and with intense summer precipitation. The Arroyo Chuchiras drains an area of about 112 km². The upper mountain basin represents only 10% of the total area, and it is drained by the Hondo and Achiras streams, which have a permanent hydrological regime. In low flow conditions, instantaneous discharge values of 0.023 up to 1.40 m³/s have been measured. In the piedmont area, the Arroyo Chuchiras shows an ephemeral regime. In this environment, it receives water discharge contribution from numerous ephemeral runoff systems, which represent approximately 50% of the catchment area. In summer, the measured discharge in the trunk stream was 0.30 m³/s.

Concerning land use, the region is characterized especially by extensive cattle raising, agricultural intensive activities, soil mining for bricks, and small urbanized areas.

3 Materials and Methods

3.1 Available Data

Although studies related to water resource problems have been carried out in recent years in Argentina, the lack of instrumentation is still a limiting factor when statistically representative precipitation series are required for the flash flood analysis. Pluviometers that are already located are insufficient, and precipitation records are available for just a few years and rather discontinuous periods.

To characterize the studied storm event, data provided by residents from several piedmont towns, such as Villa de Las Rosas and Las Tapias, were used.

For the relief analysis, the following sources of information were used:

1. Digital Elevation Model—SRTM (Shuttle Radar Topography Mission) available at the Web site of the United States Geological Survey, with a spatial resolution of 30 × 30 m. Therefore, the DEM resolution is not enough to reconstruct the topography of the channel affected by the floods at a proper scale. Because of this, cross sections cannot be systematically extracted from the DEM in order to calculate discharges.
2. Topographic maps of the National Geographic Institute of Argentina have not very high detail (1:50,000 scale), and the vertical interval between contour lines is 25 m. Then, and taking into account that during floods water levels can range from centimeters to few meters, these maps are useless for flood hazard mapping. Google Earth satellite images allowed us to detect relief details which are unnoticeable in the DEM used here.
3. Finally, the obtained eyewitness reports from local residents were a very important information source. They included diverse data which gave an idea of the flash flood energy: water level during peak discharge, flood duration and

recurrence, transported sediment, preferential ways of water circulation, erosion and sedimentation sites, and damage caused by water flow, among other parameters.

3.2 Methodology

In this study, the concept of **hazard** (as stated by Cendrero 1987) represents the susceptibility and natural fragility of a region exposed to a certain **threat**. The **susceptibility** involves geological, geomorphological, lithological, hydrologic, and geotechnical aspects, among others, which together determine the behavior of an area exposed to a definite natural process (Panizza 1993). The **threat**, according to Hermelin (1991), is the probability of occurrence of a potentially destructive phenomenon, within a specific time period and for a given area.

In this work, susceptibility was evaluated through geomorphological (morphometric–morphodynamic), sedimentological, and anthropic indicators. The indicators were as follows: slope, aspect, valley depth, geomorphology (processes, features), and road networks. Each of these variables was reclassified with values between 1 and 5, the lowest values associated with a lower flash flood probability.

A set of maps related to topographic features was elaborated using DEM. A valley depth map was generated using the SAGA GIS software (Conrad 2006) and slope, and aspect maps were generated using ArcGIS 9x.

Valley depth was calculated as the vertical distance to a channel network base level. The algorithm consists of two major steps: (1) interpolation of a channel network base level elevation and (2) subtraction of this base level from the original elevation. The defined classes are not uniform because it was necessary to prepare intervals with different contour intervals to show clearly the topographic differences in both the piedmont and the plain areas.

Concerning the **slope map**, the slope tool was used, which calculates for each cell the maximum rate of change in relation to the neighbors, and it can be represented in percentage or grades. In the study area, the slopes vary between 0 and 265% (Instituto Geográfico Agustín Codazzi (IGAC) 1982). The ranges of reclassified values were assigned taking into account the water removal velocity. Then, the lowest values of flood susceptibility correspond to steeper areas, where water can flow faster, whereas the highest values were linked with lower slopes where the flooding probability is much higher.

The **aspect map** indicates the direction of each cell in relation to the north, taking each cell values between 0° (north) and 360°. This variable was analyzed according to the interference that the relief generates on the runoff direction. The west and northwest directions, which coincided with water flow pathways, represent lower values. Instead, the cells facing to the east acquire the highest values because they act as a barrier or obstacle to water flowing. The intermediate classes correspond to the remaining orientations.

For the geomorphological and anthropic variables, layers of vector format information were used, which were converted to raster format with a pixel size of 30×30 m.

The **geomorphological regional map** (scale 1:50,000) was reclassified according to the flooding probability. The higher values correspond to fluvial belts and to the active distal alluvial fans. Intermediate values were assigned to the piedmont alluvial fans, which are usually incised. The lower classes correspond to the fluvial–eolian plain without connectivity with the active fluvial systems and to the mountain sector, where the streams have deep valleys.

This analysis was complemented by another more detailed examination that provided a geomorphological scenario that restricted the active processes during the reference flash flood. Thus, the geomorphological analysis was made using Google Earth detailed images, fieldwork, and eyewitness reports. The analysis is focused on the alluvial fans and lowest channel reaches given that the highest reaches are abrupt and uninhabited. In the case of the alluvial fans, the analysis includes the observation of preferential stream channels, stagnant water, overflow in meanders, erosion, and deposition zones. Field evidence was collected looking for the following: critical points of overflow, big boulders displaced by flow energy, tree roots covered by finer sediments, vegetation influence, and sediment retention.

Moreover, the survey related to anthropic aspects focused mainly in the **road network analysis**, because it is considered the variable that generates the greater interference with the drainage network. The roads influence the runoff spatial distribution, favoring the connectivity or causing interference in the water flow. In this study, a minimal interference of the road network is considered the more favorable situation. Although the affected area can be increased, the water level and velocity would be lesser, and therefore, damage degree would be lower.

In contrast, deep roads concentrate the runoff, increasing the water level and velocity. Even though the flooded area is smaller in these cases, the impact is greater due to their magnitude. The roads that are perpendicular to water flow direction generate interference or obstruct the natural drainage.

Finally, the flash flood susceptibility **map** was obtained using map algebra tool operations contained within ArcGIS 9x. Each variable had equal weight. The susceptibility value of a cell was considered as the sum of all the values of the variables under analysis. Five susceptibility classes were defined.

To assess the **threat**, the analysis was made taking into account temporal distribution and intensities of precipitation, field hydrological evidence, and eyewitness reports. The mean velocity values and water-level heights were used to estimate the threat magnitude. In some selected sections, during low flow conditions, water discharge was measured using a flow meter. To calculate the peak discharges, the following equation was applied:

$$Q = A * v$$

where Q is the discharge, A is the area of the cross section, and v is water velocity.

Cross sections were measured, taking into account water-level marks considering vegetation, sediment distribution, erosion features, and witness reports. These methods were applied in the two major tributaries (the Achiras and Hondo streams) and in the trunk stream.

The Manning and the paleo-hydraulic (Costa 1983) methods were used to estimate mean velocity values during the flash flood occurred on February 4, 2014.

Subsequently, the Manning equation was used:

$$v = \frac{R^{\frac{2}{3}} * S^{\frac{1}{2}}}{n}$$

where R is the hydraulic radius (A/W_p), A is the cross-sectional area, W_p is the wet perimeter, S is the channel slope (calculated for a stream reach from contour lines from topographic maps), and n is the roughness coefficient. Based on channel and floodplain characteristics (dominant particle sizes, type and percentage of cover vegetation, etc.), a “weighted n ” was established (Chow 1959).

The paleo-hydraulic method is based upon obtaining the mean flow velocity by means of measuring the intermediate axis of the largest boulders moved by the flow (Costa 1983).

$$v = 0.182 * d^{0.4873}$$

where v is the water velocity, and d is the mean value of five intermediate axes of the five largest boulders displaced by flood. This method was applied in several studies (Maizels 1986; Gallardo and Colombo 1996; Beckwith 2001; Fernández Lavado 2007; Halcsik 2013).

To analyze the spatial distribution of the threat, hydro-geomorphological features and witness reports were used.

Finally, a **flash flood hazard map** was obtained based on the susceptibility classes, the threat magnitude, and spatial distribution. With this information, five classes of flash flood hazard were defined.

4 Results and Discussion

4.1 Susceptibility Analysis

4.1.1 Morphometric Indicators

The classes obtained for morphometric indicators (valley depth, slope, and aspect) and their spatial distribution are shown in Figs. 3, 4, and 5 and Table 1.

When these indicators are analyzed together, they show that the Arroyo Chuchiras upper basin has morphometric characteristics that favor a fast evacuation of channel flow. In the piedmont area, the gradients are in general between 7 and

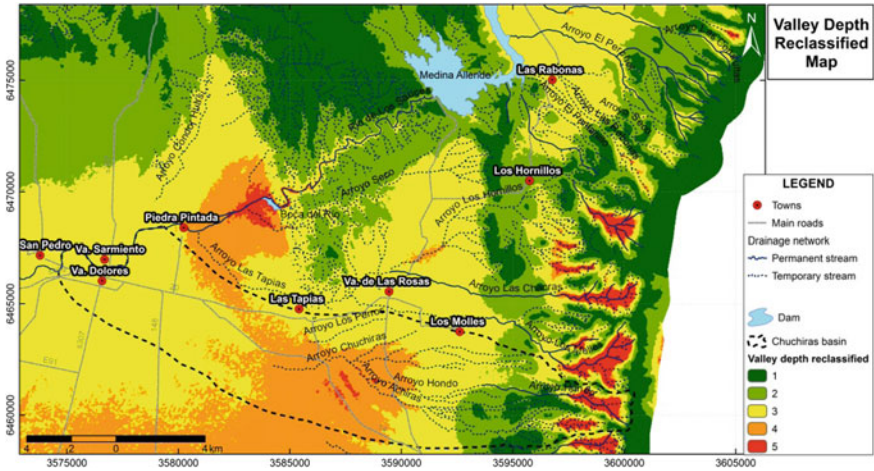


Fig. 3 Reclassified valley depth map, according to flash flood susceptibility.

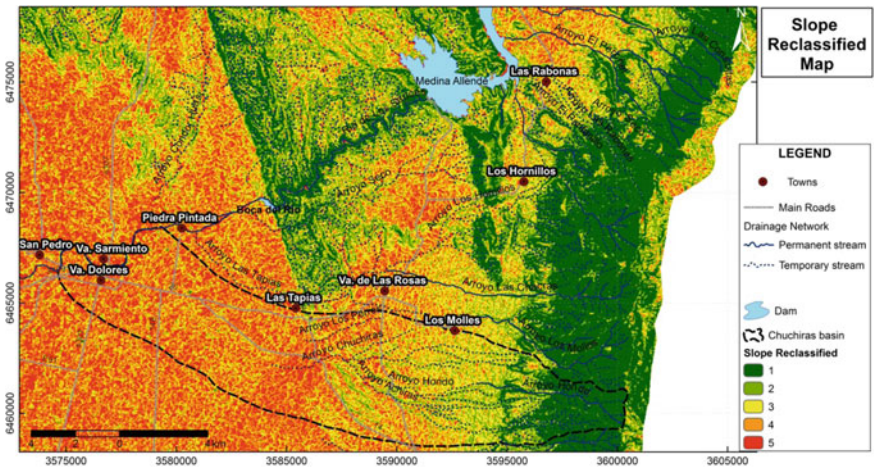


Fig. 4 Reclassified slope map, according to flash flood susceptibility.

12%, with the highest values in the uplift front of the first alluvial fan level. This environment is incised by the main stream, and it is the place where many secondary channels originate (low valley depth values). All the tributary streams converge in a sector related to the Pocho fault line. From this line to the west, the value of the slope decreases markedly and the aspect values are more variable, with a dominant northwest direction. In addition, the valley depth values increase in relation to the previous unit. From a morphometric point of view, this area shows high flash flood susceptibility.

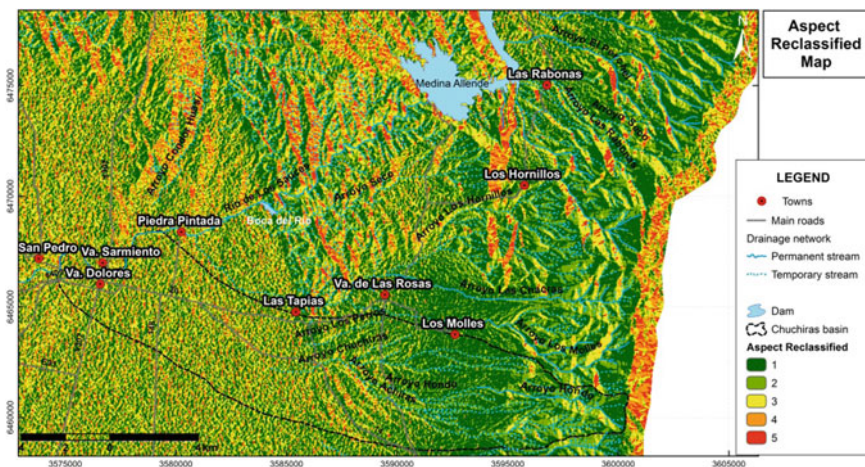


Fig. 5 Reclassified aspect map, according to flash flood susceptibility

Table 1 Susceptibility ranges for each variable

Range	Morphometry			Geomorphology	Road network
	Valley depth	Slope	Aspect		
1	0–80.56 m	>25%	225°–315°	Deep valleys, high local relief (mountain areas). Channel incision >6 m. Dominant processes: erosion, transport. Fluvial–eolian plain, without connectivity with the fluvial system	Without roads, there are not interferences
2	80.56–161.39 m	12–25%	315°–0° and 180°–225°	Defined valley, moderate/high local relief. Main channel incision between 4.5 and 6 m. Dominant processes: transport, erosion. Fluvial–eolian plain, with very low connectivity with the fluvial system	Primary and secondary roads: parallel or oblique, not deepened
3	161.39–261 m	7–12%	0°–45° and 135°–180°	Defined valley, moderate local relief. Main channel incision between 3 and 4.5 m. Dominant processes: transport, much localized avulsion and overflows. Non-channeled flow in distal alluvial fan	Primary and secondary roads: perpendicular, low deepened

(continued)

Table 1 (continued)

Range	Morphometry			Geomorphology	Road network
	Valley depth	Slope	Aspect		
4	261–290.55 m	3–7%	90°–135°	Poorly defined valleys, minimum local relief. Distributary drainage network. Main channel incision between 1.5 and 3 m. Dominant processes: avulsion, overflows, moderate–fast sedimentation. Non-channeled flow in middle alluvial fan	Primary and secondary roads: parallel or oblique, deepened
5	290.55–530.48 m	0–3%	45°–90°	Poorly defined valleys, minimum local relief. Distributary drainage network. Main channel incision <1.5 m. Dominant processes: avulsion, overflows, erosion, fast sedimentation	Primary and secondary roads: perpendicular, deepened

4.2 *Geomorphological, Sedimentological, and Morphodynamic Analysis*

The piedmont area has a flash flood susceptibility degree between moderate analysis and high (Fig. 6). The moderate class is mainly related to two different geomorphological environments: (1) the faulted and raised old fans located in the first piedmont level and (2) the distal areas of the active alluvial fan of the Arroyo Chuchiras.

In the first environment, the drainage network is formed mainly by collector channels which show different incision degree and valley development. In general, these channels have the capacity to evacuate extreme flows without generating overflow. The channels are straight to slightly sinuous with moderate to high slope, dominated by transport processes, especially of very coarse bedload. In this area, some secondary distributary channels, corresponding to historical alluvial fans of the Los Molles and San Javier streams (outside the study area), are secondarily recognized. During extraordinary floods, these channels could be reactivated and they may transfer discharge toward the Arroyo Chuchiras basin.

The second environment, by contrast, is a plain with low local relief dominated by mantle-shaped runoff or slightly channeled flow systems in larger depressions, without erosion features. The sedimentation of finer materials dominated in these distal positions.

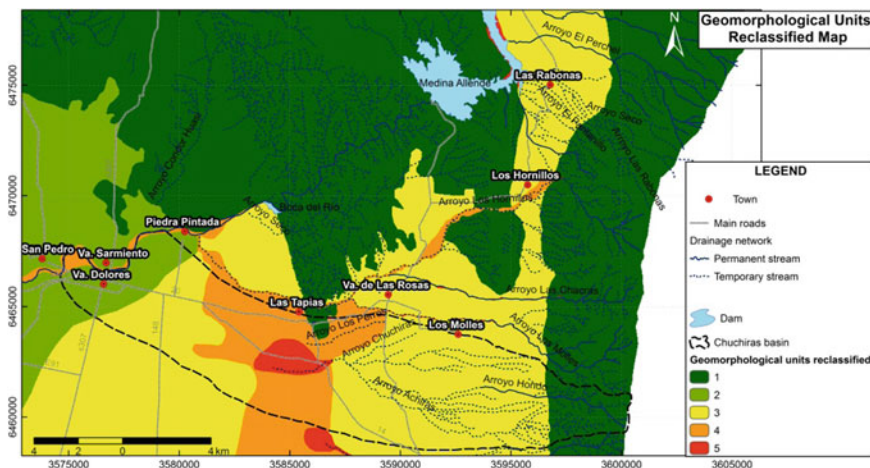


Fig. 6 Reclassified geomorphological unit map, according to flash flood susceptibility

The moderately high and high classes (approximately 15%) are associated with lower reaches and active alluvial fans of the Chuchiras and Los Perros streams, which interdigitate in the middle-distal piedmont sector. This sector shows a slightly undulating relief and local slopes that are less than 2%. The drainage network of both fans shows very few distributary courses, and it is formed by the main collector and preferential flow pathways which are generally not channeled, associated with wider and flatter topographic depressions. In the main channel, in general with lower incision, overflows during the flood events are common. It is enlarged with decreasing of the cross section by sedimentation or blockage caused by sediment and vegetation accumulation.

Lower susceptibility classes represent 60% of the area under study, and it includes the mountain basin of the Arroyo Chuchiras and also the transition zone between the distal piedmont and fluvial-olian plains. In the first case, the courses that drain the scarp have narrow and deep valleys that transport large volumes of water without possibility of overflow. The straight and steep sloped channels have high competence and transport capacity. In the second case, it includes peripheral plains of the active alluvial fan of the Arroyo Chuchiras that has minimal probability of being affected by flash flood events.

4.3 Road Network Analysis

As shown in Fig. 7, roads and routes that are located in an oblique or transversal position to the regional slope dominate the basin. Thus, there are interference situations of moderate to high degree. In general, the roads are not very deep, but in the middle-distal piedmont plains, where local relief is lower and the drainage

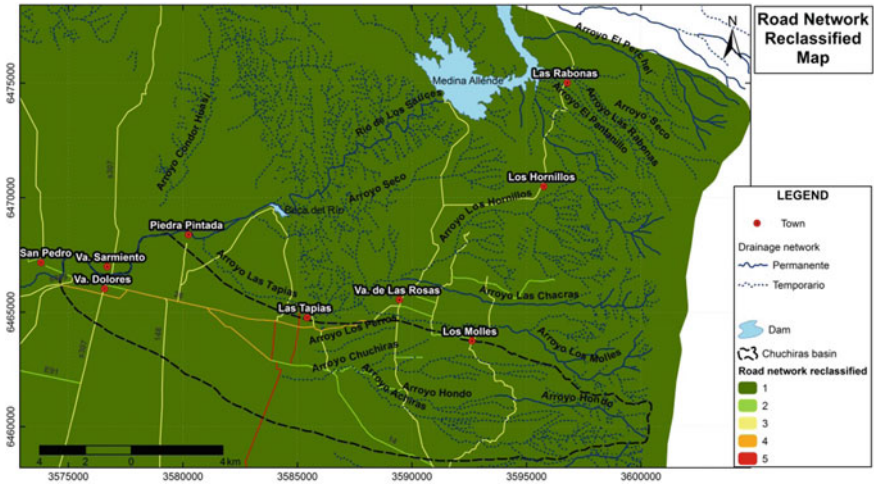


Fig. 7 Reclassified road network map, according to flash flood susceptibility

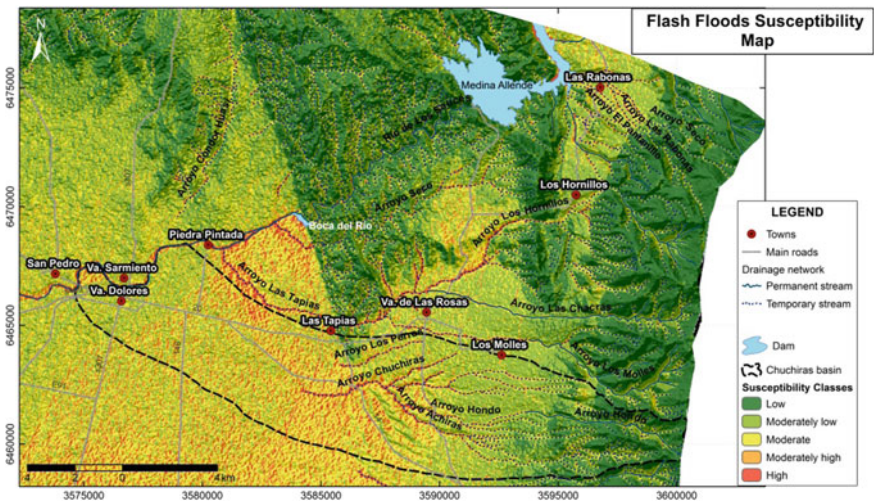


Fig. 8 Flash flood susceptibility map

network is poorly defined, there are high probabilities that the roads collect and modify water flow.

Finally, the **flash flood susceptibility map** is shown in Fig. 8. The spatial distribution of the classes is strongly conditioned by geomorphological features, slopes, and local relief. Thus, middle-distal piedmont basin (50% of the total area) presents moderate to high susceptibility, and both the proximal piedmont and the mountain sector belong to low and moderately low classes.

4.4 Threat Analysis

Concerning the magnitude of the threat, results of velocity and discharge estimates for the extraordinary event of the February 4, 2014, are shown in Table 2. High water values measured and witness reports are shown as well.

To characterize the threat, a flood discharge estimated in the order of 176–200 m³/s (recurrence of 20–30 years, according to witness reports) is considered, associated with the Arroyo Chuchiras (P1), where the velocity, water surface elevation, and clasts size values were higher than the rest of the sections considered (Figs. 9, 10 and 11). At this point in the confluence of several streams, those that have headwaters and drain a significant area in the piedmont sector become relevant. In the considered event, the estimated flow values suggest that the rainfall was higher than those recorded in the mountainous area.

When the distribution and magnitude of the threat are analyzed together, it is possible to observe that, upstream of point 1, as you indicated, the channels are incised with low chances of overflow, so the threat is concentrated in the active channel. In this sector, the estimated velocity range between 1.7 and 2.4 m/s, the size of the transported clasts is equal to or greater than 100 mm and water height is less than 1 m (P6, P7, and P8).

Downstream of P1, in the middle to lower reaches of the Arroyo Chuchiras, the threat is spatially distributed, conditioned mainly by the geomorphological characteristics and processes in the alluvial fan. At this point, water can circulate westward to national route 148 or drive along the NW–SE topographic depression toward national route 20, as it was the case in the event of flood analyzed. In this area, the depth roads constitute a pathway of water circulation, where the velocities are equal to or less than 2 m/s, with clast sizes mobilized by the stream that vary between 76 and 140 mm (P2, P3, and P4).

Flood mark observations indicate that the height reached by the water was not higher than 1.5 m, decreasing significantly in the direction of national route 20.

Table 2 Water height values measured and reported. Velocity and discharge values estimated by Manning and Paleo-hydraulic methods

	Water height (m)	Manning method		Paleo-hydraulic method		
		Velocity (m/s)	Discharge (m ³ /s)	Velocity (m/s)	Discharge (m ³ /s)	Boulders diameter (d) (mm)
P1	1.70	3.3	200	2.9	176.7	300
P2	0.40	No data	No data	1.5	No data	76
P3	1.5	No data	No data	2.0	No data	140
P4	1	No data	No data	1.7	No data	100
P6	0.6	No data	No data	1.7	No data	100
P7	0.3	1.4	3.1	2.6	5.68	230
P8	0.65	2.4	13.2	2.4	13.3	200

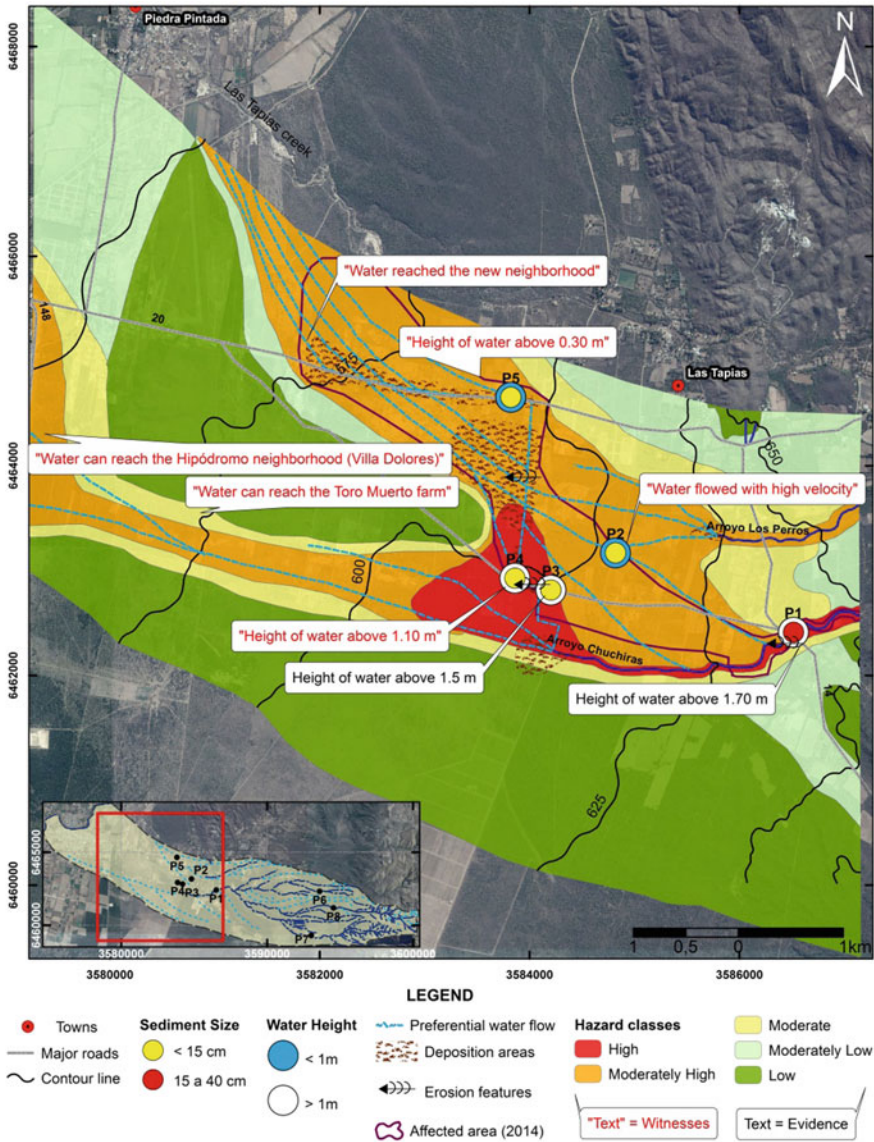


Fig. 9 Flash flood hazard map at the Arroyo Chuchiras lower basin, geomorphological and hydrological indicators and affected area during the 2014 flood



Fig. 10 Water height during the flash flood (a, b, c) and water-level marks considering the vegetation (d, e). Photograph locations in Fig. 9: a P4, b and c P5, d P1, e P3

Finally, with the available information of water height and velocity, three threat classes were defined (Table 3).

The threat behavior is as follows: (1) In P1, the threat is maximum and decreases downstream of this sections because water spreads over the alluvial fan, and consequently, the water level falls and velocity decreases and (2) during the peak discharge, water spreads over the fan, and velocity is higher in the preferential circulation channels (height threat) than in the intermediate zones (moderate–low threat).



Fig. 11 Clasts transported by the flow during flash flood event. Photograph locations in Fig. 9: **a** P4, **b** P3, **c** and **d** P1, **e** P2

Table 3 Threat classes defined for velocity and water height

Classes	Threat
High	Water height: >1 m and velocity: >2.5 m/s
Moderate	Water height: 1–0.10 m and velocity: 2.5–y 1 m/s
Low	Water height: <0.10 m and velocity: <1 m/s

Table 4 Flood flash hazard classes according to susceptibility and threat

Susceptibility	Threat		
	High	Moderate	Low
High	High	Moderately high	Moderate
Moderately high	High	Moderately high	Moderate
Moderate	Moderately high	Moderate	Moderately low
Moderately low	Moderate	Moderate	Moderately low
Low	Moderate	Moderately low	Low

4.5 *Flash Flood Hazard Map Analysis*

The classes defined by flood flash hazard and their spatial distribution are shown in Table 4 and Fig. 9, respectively.

As shown in Fig. 9, approximately 64% of the lower basin of the Arroyo Chuchiras presents low to moderately low flash flood hazard, mainly related to sectors at relatively high elevation, with a local relief generally less than 10 m. The two highest susceptibility classes (high and moderately high) account together for 26% of the total area. The high class is associated with the lower reaches and proximal-middle active alluvial fans of the Chuchiras and Los Perros streams. The moderately high class is associated with NW–SE topographic depressions, which correspond to the distal alluvial fan areas. The remaining 10% has moderate hazard and corresponds to peripheral areas of active alluvial plains (belts and fans fluvial plains).

Moreover, in Fig. 9, the flooded area during the event of February 4, 2014, is shown. In this flood, the Arroyo Chuchiras overflowed downstream when intercepting route 14 because of its reduced cross section and accumulation of vegetation, which obstructed water flow. The overflows followed natural runoff paths and partially deepened roads toward the NW–SE topographic depression, flooding route 20 and surrounding highly urbanized areas, which would be associated with moderately high and high hazard classes. In this event, flooding did not take place toward the west (the distal fan area of the Arroyo Chuchiras) due to the influence of the road network in the water flow.

As shown in Fig. 9, there is a high correspondence between the predictive map and the February 4, 2014, flood real scenario, showing also the impact of anthropogenic interventions in the natural susceptibility and the threat behavior.

5 **Conclusions**

The flash flood hazard in the western piedmont of the Sierras Grandes de Córdoba is the result of the combination of the following variables: (1) lower permeability rocks in the upper basin; (2) important topographical contrasts (local relief and slopes) between the fault scarp and the piedmont area; (3) rivers and streams with torrential regime and high energy (velocity, competence, and transport capacity) that make up distributary systems in the distal-middle piedmont; and (4) high intensity rainfalls concentrated in the summer season.

The threat magnitude is the result of the confluence of concentrated and not concentrated flows, being the latter quite relevant in the piedmont area.

The poor definition of the piedmont basin boundaries and the predominance of avulsion processes repeatedly promote the connection between neighboring basins. Thus, water transfer in between basins may occur, making difficult the threat estimation.

The road network has a moderate and more localized incidence, especially in the threat magnitude and distribution.

In basins lacking systematic information, the implementation of geomorphological methodologies shows results compatible with real scenarios. This suggests that predictive mapping could be a useful tool for land use planning and management.

Given that flooding in the area causes problems both in urban and rural areas, its mitigation requires interventions of different types. On one side, some flexible and sustainable engineering work is necessary in order to regulate the threat or to decrease the susceptibility, especially in populated areas and road infrastructure. On the other side, land use planning and management that take into account fluvial systems behavior are necessary. This will not only promote the hazard decrease but also will diminish the vulnerability, reducing this way the risk of catastrophic episodes.

Acknowledgements This chapter has been completed within the framework of research projects funded by the Secretaría de Ciencia y Técnica of the Universidad Nacional de Río Cuarto (SECyT-UNRC), the Agencia Nacional de Promoción Científica y Tecnológica of Argentina (ANPCyT), and the Ministerio de Ciencia y Tecnología of the province of Córdoba (MINCyT).

The authors would like to express their gratitude to Jorge Rabassa for his invitation to publish this chapter and for his constructive and generous review of the English text and to Mariana Chiuffo for her help with a preliminary version of the English text.

Finally, the authors thank the residents of the towns of Villa de las Rosas, Villa Dolores, and Las Tapias, for providing information of interest.

References

- Ambrosino S, Barbeito O, Bertoni JC, Daniele A, Maza JA, Ubaldo Paoli C, Serra JJ (2004) Inundaciones urbanas en Argentina. INA, Córdoba, Argentina
- Anquetin S, Braud I, Vannier O, Viallet P, Boudevillain B, Creutin JD, Manus C (2010) Sensitivity of the hydrological response to the variability of rainfall fields and soils for the Gard 2002 flash-flood event. *J Hydrol* 394:134–147. doi:[10.1016/j.jhydrol.2010.07.002](https://doi.org/10.1016/j.jhydrol.2010.07.002)
- Babajabaa S, Masoud M, Al-Amri N (2014) Flash flood hazard mapping based on quantitative hydrology, geomorphology and GIS techniques (case study of Wadi Al Lith, Saudi Arabia). *Arab J Geosci* 7:2469–2481
- Beckwith DD (2001) Sedimentologic processes and glaciogenic landforms at the Herbert Glacier Ice Front, southeast Alaska: Colorado Springs, Colorado, Colorado College, Unpublished B.S. thesis, 93 p
- Bonalumi A, Martino R, Baldo E, Zarco J, Sfragulla J, Carignano C, Kraemer P, Escayola M, Tauber A (1999). Hoja Geológica 3166-IV, Villa Dolores. Programa Nacional de Cartas Geológicas de la República Argentina, 1:250.000, 122 p., Córdoba
- Borga M, Stoffel M, Marchi L, Marra F, Jakob M (2014) Hydrogeomorphic response to extreme rainfall in headwater systems: flash floods and debris flows. *J Hydrol* 518:194–205. doi:[10.1016/j.jhydrol.2014.05.022](https://doi.org/10.1016/j.jhydrol.2014.05.022)
- Busnelli J, Horta LR (2014) Morfometría de cuencas montanas y metamorfosis fluvial, Tucumán. *Revista de la Asociación Geológica Argentina* 71(1):11–20 (Buenos Aires)

- Capitanelli RG (1979) Clima. In: Geografía física de la Provincia de Córdoba. Editorial Boldt, Córdoba, Argentina
- Carpenter TM, Sperflage JA, Georgakakos KP, Sweeney T, Fread DL (1999) National threshold runoff estimation utilizing GIS in support of operational flash flood warning systems. *J Hydrol* 224:21–44
- Catane SG, Abon CC, Saturay RM Jr, Mendoza EPP, Futralan KM (2012) Landslide-amplified flash floods—the June 2008 Panay Island flooding, Philippines. *Geomorphology* 169–170:55–63. doi:[10.1016/j.geomorph.2012.04.008](https://doi.org/10.1016/j.geomorph.2012.04.008)
- Cendrero A (1987). Riesgos geológicos, ordenación del territorio y protección del medio ambiente. 1° Curso de riesgos geológicos. Instituto Geológico Minero de España, Madrid, pp 327–333
- Chow VT (1959) Open-channel hydraulics. McGraw-Hill, New York
- Conrad O (2006) SAGA—program structure and current state of implementation. In: Böhner J, McCloy KR, Strobl J (eds) SAGA—analysis and modelling applications, vol 115. Göttinger Geographische Abhandlungen, pp 39–52
- Costa JE (1983) Paleohydraulic reconstruction of flash-flood peaks from boulders deposits in the Colorado Front Range. *Geol Soc Am Bull* 94:986–1004
- Dawod GM, Mirza MN, Al-Ghamdi KA (2011) GIS-based spatial mapping of flash flood hazard in Makkah City, Saudi Arabia. *J Geogr Inf Syst* 3:225–231. doi:[10.4236/jgis.2011.33019](https://doi.org/10.4236/jgis.2011.33019)
- De Waele J, Martina MLV, Sanna L, Cabras S, Cossu QA (2010) Flash flood hydrology in karstic terrain: Flumineddu Canyon, central-east Sardinia. *Geomorphology* 120:162–173. doi:[10.1016/j.geomorph.2010.03.021](https://doi.org/10.1016/j.geomorph.2010.03.021)
- Elkhrachy I (2015) Flash flood hazard mapping using satellite images and GIS tools: a case study of Najran City, Kingdom of Saudi Arabia (KSA). *Egypt J Remote Sens Space Sci* 18:261–278. doi:[10.1016/j.ejrs.2015.06.007](https://doi.org/10.1016/j.ejrs.2015.06.007)
- Esper Angillieri MY (2007) El aluvión del 13 de febrero de 1944 en la Quebrada del Carrizal, Departamento Iglesia, provincia de San Juan. *Revista de la Asociación Geológica Argentina* 62 (2):283–288 (Buenos Aires)
- Fernández Lavado C, Furdada G, Marqués MA (2007) Geomorphological method in the elaboration of hazard maps for flash-floods in the municipality of Jucuarán (El Salvador). *Nat Hazards Earth Syst Sci* 7:455–465
- Gallardo G, Colombo F (1996) Caracterización paleohidráulica de algunos litosomas conglomeráticos paleógenos de la cuenca del Ebro. Ejemplos en la Conca de Barberá (Tarragona). *Geogaceta* 19:109–112
- Garambois PA, Larnier K, Roux H, Labat D, Dartus D (2014) Analysis of flash flood-triggering rainfall for a process-oriented hydrological model. *Atmos Res* 137:14–24. doi:[10.1016/j.atmosres.2013.09.016](https://doi.org/10.1016/j.atmosres.2013.09.016)
- Garambois PA, Roux H, Larnier K, Labat D, Dartus D (2015) Parameter regionalization for a process-oriented distributed model dedicated to flash floods. *J Hydrol* 525:383–399. doi:[10.1016/j.jhydrol.2015.03.052](https://doi.org/10.1016/j.jhydrol.2015.03.052)
- Gaume E, Livet M, Desbordes M, Villeneuve JP (2004) Hydrological analysis of the river Aude, France, flash flood on 12 and 13 November 1999. *J Hydrol* 286:135–154. doi:[10.1016/j.jhydrol.2003.09.015](https://doi.org/10.1016/j.jhydrol.2003.09.015)
- Gaume E, Bain V, Bernardara P, Newinger O, Barbuc M, Bateman A, Blaškovicová L, Blöschl G, Borgia M, Dumitrescu A, Daliakopoulos I, Garcia J, Irimescu A, Kohnova S, Koutroulis A, Marchi L, Matreata S, Medina V, Preciso E, Sempere-Torres D, Stancalie G, Szolgay J, Tسانis I, Velascom D, Viglione A (2009) A compilation of data on European flash floods. *J Hydrol* 367:70–78. doi:[10.1016/j.jhydrol.2008.12.028](https://doi.org/10.1016/j.jhydrol.2008.12.028)
- Gil V (2011) Geomorfología fluvial de la cuenca del arroyo El Negro, Buenos Aires, Argentina. *Revista Universitaria de Geografía* 20:151–169
- Gutiérrez F, Gutiérrez M, Sancho C (1998) Geomorphological and sedimentological analysis of a catastrophic flash flood in the Arfis drainage basin (Central Pyrenees, Spain). *Geomorphology* 22:265–283

- Halscik CR (2013) Investigating late Pleistocene and Anthropocene flood deposits along North Boulder and Caribou Creek, Colorado Front Range. Unpublished graduation thesis. Beloit College, Wisconsin
- Hermelin M (1991) Introducción a la Geología Ambiental. Geología Ambiental y Geomorfología aplicada en Colombia. Asociación de Geocientíficos para el Desarrollo Internacional (AGID) Reporte 16:3–20
- Hooke JM, Mant JM (2000) Geomorphological impacts of a flood event on ephemeral channels in SE Spain. *Geomorphology* 34:163–180
- Instituto Geográfico Agustín Codazzi (IGAC) (1982) Estudio general de suelos y zonificación de tierras. Estudio general de suelos de la región nororiental del departamento del Cauca. Bogotá, Colombia
- Jha AK, Bloch R, Lamond J (2012) Cities and flooding. a guide to integrated urban flood risk management for the 21st century. International Bank for Reconstruction and Development and International Development Association, Washington, DC
- Koutroulis AG, Tsanis IK (2010) A method for estimating flash flood peak discharge in a poorly gauged basin: case study for the 13–14 January 1994 flood, Giofiros basin, Crete, Greece. *J Hydrol* 385:150–164
- Lang M, Fernández Bono JF, Recking A, Naulet R, Grau Gimeno P (2004) Methodological guide for palaeoflood and historical peak discharge estimation. In: Benito G, Thorndycraft VR (eds) Systematic, Palaeoflood and historical data for the improvement of flood risk estimation. Methodological guidelines. CSIC—Centro de Ciencias Medioambientales, Madrid
- Maizels JK (1983) Paleovelocity and palaeodischarge determination for coarse gravel deposits. In: Gregory KJ (ed) Background to palaeohydrology: a perspective. Wiley, pp 101–139
- Maizels JK (1986) Modeling of Paleohydrologic change during deglaciation *Géographie physique et Quaternaire* 40(3):263–277. doi:[10.7202/032648ar](https://doi.org/10.7202/032648ar)
- Marchi L, Borga M, Preciso E, Gaume E (2010) Characterization of selected extreme flash floods in Europe and implications for flood risk management. *J Hydrol* 394:118–133. doi:[10.1016/j.jhydrol.2010.07.017](https://doi.org/10.1016/j.jhydrol.2010.07.017)
- Martín Vide JP, Martín Moreta PJ, López Querol S, Machado MJ, Benito G (2002) Tagus river: historical floods at Talavera de la Reina. In: Thorndycraft VR, Benito G, Barriendos M, Llasat MC (eds) Palaeofloods, historical data & climatic variability. Applications in flood risk assessment, CSIC—Centro de Ciencias Medioambientales, Madrid
- Nikolopoulos EI, Anagnostou EN, Borga M, Vivoni ER, Papadopoulos A (2011) Sensitivity of a mountain basin flash flood to initial wetness condition and rainfall variability. *J Hydrol* 402:165–178
- Ogden FL, Sharif HO, Senarath SUS, Smith JA, Baeck ML, Richardson JR (2000) Hydrologic analysis of the Fort Collins, Colorado, flash flood of 1997. *J Hydrol* 228:82–100
- Panizza M (1993) Riesgo geomorfológico y vulnerabilidad ambiental. Quaderni Instituto Italo Latino Americano (IILA), Serie Scienza 6. México
- Phillips JD (2002) Geomorphic impacts of flash flooding in a forested headwater basin. *J Hydrol* 269:236–250
- Thornthwaite C (1948) An approach towards a rational classification of climate. *Geogr Rev* 38 (1):221–229
- Williams GP (1984) Paleohydrologic equations for rivers in developments and applications of geomorphology, pp 343–367

Characteristics and Nature of Pans in the Semi-arid Temperate/Cold Steppe of Tierra del Fuego

María Laura Villarreal and Andrea Coronato

Abstract This work has the aim of presenting the geomorphological and morphometric characteristics of deflation hollows or pans which occur in northern Tierra del Fuego under temperate/cold climate. The shape, size, perimeter and density of each pan are analysed, as well as the landforms developed in their periphery. The study was conducted in the San Sebastián Bay and between the Chico and Grande rivers, grouped according to the geomorphological unit in which they were generated. Digital terrain models and optical images were used to digitalize the perimeter of the depressions and shallow lakes and to discriminate geomorphological features. The studied pans are deflation landforms generated in diverse geomorphological environments of fluvial and marine origin. The higher density of pans per square kilometre is found amongst the geomorphological units of marine origin, whereas those of larger size correspond to geomorphological units of fluvial environments, which are not functional in present times. All these closed depressions have aeolian accumulation landforms placed leeward.

Keywords Pans · Morphometry · Deflation · Aeolian landforms · Tierra del Fuego

1 Introduction

Argentine Patagonia and the Isla Grande of Tierra del Fuego are the continental and insular ends of South America, which extend under climatic conditions where the wind is the main geomorphological agent. The strong and constant winds from the NW, W and SW originated in the southern half of the South Pacific Anticyclone

M.L. Villarreal (✉) · A. Coronato
ICPRNA-Universidad Nacional de Tierra del Fuego,
Avenida De los Nires 2382, 9410 Ushuaia, Argentina
e-mail: mlauravillarreal@gmail.com

A. Coronato
CADIC-CONICET, Bernardo Houssay 200, 9410 Ushuaia, Argentina

overpass the Patagonian and Fuegian Andes and blow leeward over the plains and low mountain chains. These winds take part in the relief modelling where they find soils with scarce vegetation fully devoid of them. The presence of snow, ice or water in soils and sediments prevents the aeolian action during southern winter months. Contrarily, during the remaining part of the year, and mainly in spring and autumn, when the maximum wind intensity takes place, wind generates strong deflation on soils and surficial sediments. The extensive cover of grasslands and shrublands that form the Patagonian and Fuegian steppes protects ample portions of the landscape from aeolian action, but the areas which have been affected by overgrazing and man-made action on the territory expose to erosion of the poorly developed soils or sandy/silty, unconsolidated surface sediments. These particles are removed by aeolian action and then accumulated in short distances, thus developing accumulation landforms. The finest materials are incorporated to the higher atmosphere dust (Gaiero et al. 2015; Gili et al. 2016).

The deflation hollows that are presented in this paper were defined under the term “pans” by Goudie and Wells (1995) as topographic lowlands or closed depressions which are formed in dry lands as a result of the combination of aeolian deflation and salt weathering, a product of a high rate of evapotranspiration. In the aforementioned paper, a world distribution of the dry lands is presented, including there the Argentine Pampas.

The modelling action of the wind in landscapes of temperate/cold climate in the southern hemisphere is still little known. However, a vast record of aeolian processes and landforms for the Canadian Arctic zone and the northernmost portion of Europe has been reported by Seppälä (2004). In the southernmost end of South America, the morphological types and the relationship between dune migration and vegetation cover in coastal desertic lands of NE Patagonia and Península Valdés (42°S) have been described, by means of remote sensing techniques and aeolian models (del Valle et al. 2008, 2010). The development of deflation hollows, named as “endorheic depressions” or “bajos sin salida”, was described by Mazzoni (2001) for the southern portion of the province of Santa Cruz, (51°14′–52°S) in a variety of morphogenetic units such as Patagonian Gravels tablelands, basaltic mesetas and fluvial and glaciofluvial valleys. Likewise, in the aeolian plumes derived from them, several landforms as lunettes (clay dunes) and sandy dunes of various types were identified. Deflation hollows today occupied by water bodies in the Argentine Pampas were interpreted as sources for fine-grained materials forming clay dunes during dry climatic periods during the Late Holocene (Dangavs 1979). In Tierra del Fuego, Arche and Vilas (2001) suggested the development of lunettes in the Holocene supratidal deposits of San Sebastián Bay (Fig. 1), whereas Villarreal et al. (2014) described the formation of aeolian mantles as a result of deflation in shallow lakes with exposed dry beds.

In this chapter, the morphometric characteristics of aeolian landforms and their relationship with the geomorphological emplacement of deflation hollows generated in cold/subhumid environments and in different geomorphological units are

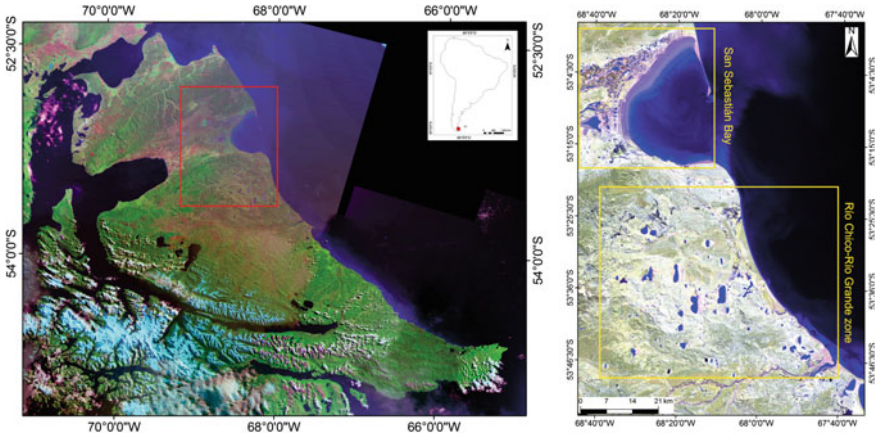


Fig. 1 *Left* Localization of the Isla Grande de Tierra del Fuego. *Right* Location of the study area, northern Tierra del Fuego. *Source* Satellite image Landsat ETM 227-97, year 2001, provided by the Comisión Nacional de Actividades Espaciales of Argentina (CONAE) and Image SID 19-50, obtained from the United States Geological Survey (USGS)

presented. Besides these, landforms are grouped into two geographical zones: the surroundings of San Sebastián Bay and the territory comprised between the Grande and Chico rivers.

2 Methods

A Geographical Information System (GIS) database was performed using ArcGis v.10 and the digital terrain model MDE-Ar as a topographic base of 30-m resolution, provided by the Instituto Geográfico Nacional of Argentina (IGN). Using the QuickBird satellite images available in Google Earth®, the pans were digitalized and the geomorphological units in which they are emplaced were mapped. A layer containing the perimeter outline of the pans was added, and a morphometric analysis was performed considering the variables proposed by Hutchinson (1957). They are: surface (A), perimeter (L), maximum length (L_m) as the distance in a rectilinear direction between the two farthest opposite points, maximum amplitude (A_m) as the corresponding maximum distance between the margins of the hollow, and the perimeter development (DL) applying the formula:

$$DL = L / (2\sqrt{A \cdot \pi})$$

Due to differences found amongst the results of the application of this methodology with the visual determination of the landforms, a classification based upon the Relationship of Axes Length (RAL) was presented. In this classification,

Table 1 Classification of pans according to their shape, based upon perimeter development (DL) and relationship of axes longitude (RAL)

Shape types			
After Hutchinson (1957)		RAL	
DL \leq 1.4	Circular	RLE = 1	Circular
DL 1.5 \geq	Elliptic	RLE 1.1 \geq	Elliptic

the so-called circular shape is that one in which the two axes have identical length, and thus, the circular shapes correspond to values of RAL smaller than 1.1, whereas the elliptical shapes respond to values of RAL higher than 1.1 (Table 1), which means that one of the axes is longer than the other.

Pans density, considered as $D = \text{number per km}^2$, was calculated for each geomorphological unit

The climatic analysis was performed with weather records available from the Servicio Meteorológico Nacional (or SMN, the National Meteorological Survey of Argentina), at Río Grande meteorological station, corresponding to the 1959–2010 period. A hydrological balance analysis was done according to the Thornthwaite and Mather (1957) method, based upon precipitation (P) as the water input to the system and evapotranspiration (ETP) as water output.

3 Study Area

The San Sebastián Bay (SSB) is part of a very wide valley, which has been suggested of tectonic origin (Diraison et al. 2000), which had been modelled by glaciers in several glaciations during the Early to Middle Pleistocene. The zones of low elevation of the present SSB were reworked by the Middle Holocene marine transgression (Rabassa et al. 2009). These processes originated diverse landforms as marsh areas, littoral ridges, cheniers, and tidal plains and channels (Bujalesky 1997).

Likewise, the Río Chico–Río Grande zone (RCH-RG) is formed by low hill ranges composed of sedimentary rocks of marine and deltaic environments (the Carmen Sylva Formation, Early to Middle Miocene) changing to continental environment (the Castillo Formation, Middle Miocene) (Codignotto and Malumián 1981; Olivero et al. 2006). Three geomorphological units have been differentiated in this region: (1) a highly dissected hill range system, eroded by transitory or ephemeral stream channels that are draining to endorheic basins (Fig. 2) integrated in palaeo-drainage systems towards the Atlantic Ocean (Coronato 2014); (2) a glaciofluvial fan, of Middle Pleistocene age (Bujalesky et al. 2001) that forms a landscape of stepped plains of gentle slope (Coronato 2014) composed of sand and gravel deposits; and (3) a much reduced extent of palaeo-bays or ancient drainage lines which have been recurrently invaded by the marine transgressions that occurred during the Middle Pleistocene (Bujalesky et al. 2001).



Fig. 2 Laguna Carmen, in the range region between the Río Chico and the Río Grande. It is a typical deflation hollow or pan that bears a shallow lake which sometimes becomes dry during the summer. This photograph was taken at the beginning of the summer, after the period of snow melting

The climate of this region is subhumid, cold/temperate, with significant influence from the South Pacific Anticyclone, which provides wind coming from the NW, W and SW. Wind is constant during the entire year, with a predominant direction from the W, WNW and SW (Fig. 3). The mean velocity is 23.7 km h^{-1} , while maximum is of up to 152 km h^{-1} . The annual calm days are of only 6.6%, which clearly indicates the persistent action of the wind throughout the whole year. The mean annual precipitation is 324.6 mm, imposing semi-arid conditions. Snow precipitation takes usually place between May and August, although snow storms may occasionally occur before and after these dates. The mean annual temperature is $5.5 \text{ }^{\circ}\text{C}$. The mean temperature of the coldest month (August) has been established in $-2 \text{ }^{\circ}\text{C}$ and that of the warmest month (February) is $10 \text{ }^{\circ}\text{C}$ (Tuhkanen 1992). The hydrological balance of the 1974–2010 period shows a clear deficit during most of the year, concentrated during November and April, which corresponds to the months with higher mean monthly temperature (Fig. 4). Deficit increases in January and, between May and August, there is a recharge because the precipitation values exceed those of evapotranspiration. This reserve will be environmentally used between September and October (Fig. 4).

The region is part of the Fuegian Steppe, formed by grasslands and shrublands. The vegetation in the steppe is dominated by *Festuca gracillima* (locally named as “coirón”) (Fig. 5). The soil characteristics between the SSB and RG-RCH zones determine the development of different species. In the first of them, such shrub species as *Lepidophyllum cupressiforme* (locally known as “Mata Verde”) and herb species of the *Sedum* genus occur. In coastal areas, where there is an important

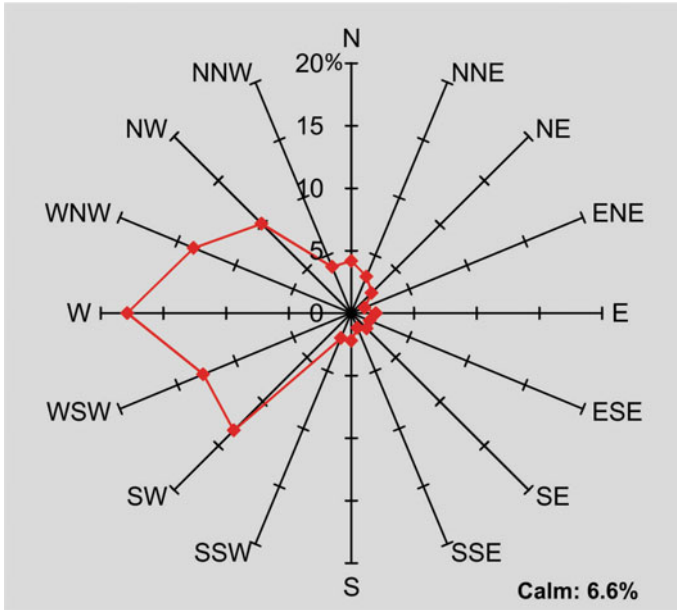


Fig. 3 Frequency of wind direction in northern Tierra del Fuego, according to climatological data from the Servicio Meteorológico Nacional of Argentina (SMN), Río Grande meteorological station, 1959–2010 period

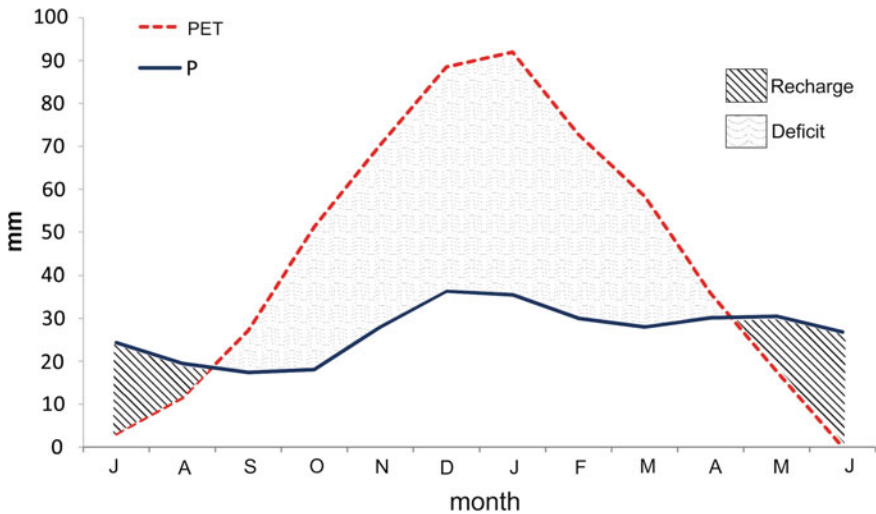


Fig. 4 Hydrological balance, 1974–2010 period, Río Grande station (SMN). *PET* potential evapotranspiration, *P* precipitation

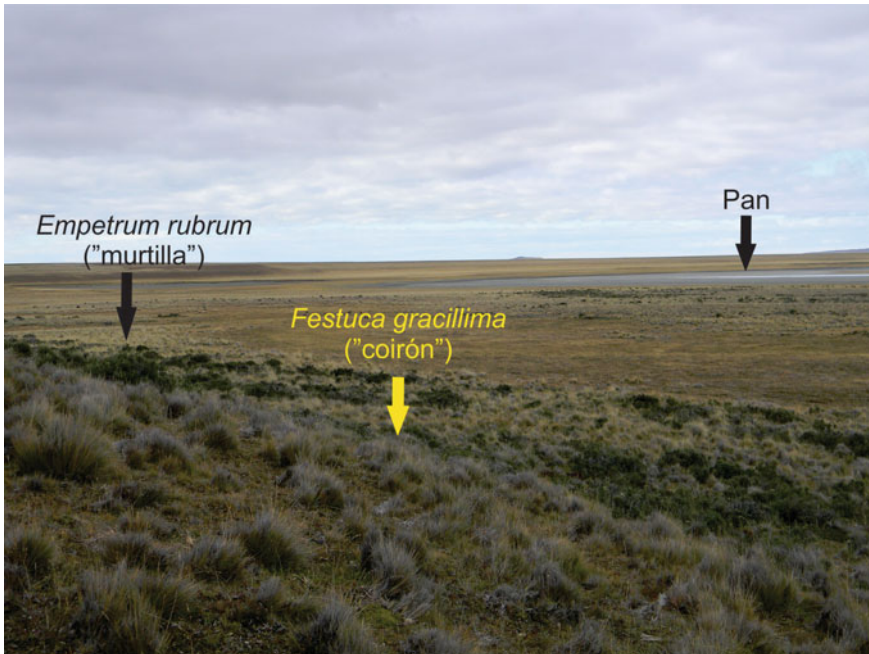


Fig. 5 Vegetation of degraded shrubby steppe due to overgrazing nearby Laguna Escondida, one of the pans that host shallow and temporary water body

saline content and large tidal influence, some characteristic species as *Salicornia ambigua* appear. Otherwise, *Empetrum rubrum* (known here as “murtilla”), *Chilotrachium diffusum* (“mata negra”), *Hordeum cosmosum* and different *Poa* species are found in the RCH-RG zone. Cespitose species such as *Bolax gummifera* and *Azorella trifurcata* (Moore 1983; Collantes et al. 1989) may be recognized in this zone as well.

4 Morphometric Characteristics and Landforms

Based upon cartographic and morphometric analysis and the direct field observation, it may be stated that most of these pans are the depositional centres of endorheic basins which receive short and ephemeral streams, a product of superficial run-off. During the periods of hydrological excess, many of them sustain a small, shallow water body, locally affected by wave action as a consequence of permanent and intense action of the constant western winds. This generates significant erosion in the eastern coastal areas of these depressions and the development of 1- to 2-m scarp local relief. Contrarily, the western coasts do not show changes in slope. During the summer, water is evaporated from the shallow lakes and their dry



Fig. 6 Deflation produced in Laguna Grande by westerlies winds with bursts of up to 120 km h^{-1} over the Laguna Grande, in the Río Grande–Río Chico zone. It is a shallow lake that acts as a pan during the drought season. Note the linear character of the deflation plume and the separated, starting point of each of them, due to differential desiccation of the exposed bottom of the lake

bottoms become exposed, thus starting deflation (Fig. 6). The wind effect on the exposed depression bottoms causes overdeepening of the pans. According to Arche and Vilas (2001), in some places this process reaches up to approximately 2.5 m deep, reaching the phreatic level which acts as the base level for wind erosion, and a dynamic equilibrium is achieved between deflation energy and the interstitial moisture that generates the sediment resistance to be blown away. The migration of the eastern margin of the pan towards the east is caused by wave erosion on the leeward direction. Meanwhile, the water remnants at the windward margin of the basin disappear (Fig. 7).

5 San Sebastián Bay (SSB)

This bay is the most significant coastal feature along the Atlantic Ocean shore of the Isla Grande de Tierra del Fuego, extending between 53° – $53^{\circ}18'S$ and $68^{\circ}11'$ – $68^{\circ}33'$ W. It develops along 65 km, between Cabo Nombre and the gravel spit Península El Páramo which closes it in the N, and the moraines of the San Sebastián Drift (Meglioli 1992) that form a coast with cliffs in the S. It is affected by a very high tide amplitude, with up to 10 m. The coastline has the looks of a semicircular coastal plain, developed in a larger depression, probably of tectonic origin (Diraison et al. 2000) which has been deeply modified by Pleistocene glaciers (Coronato et al. 2004).

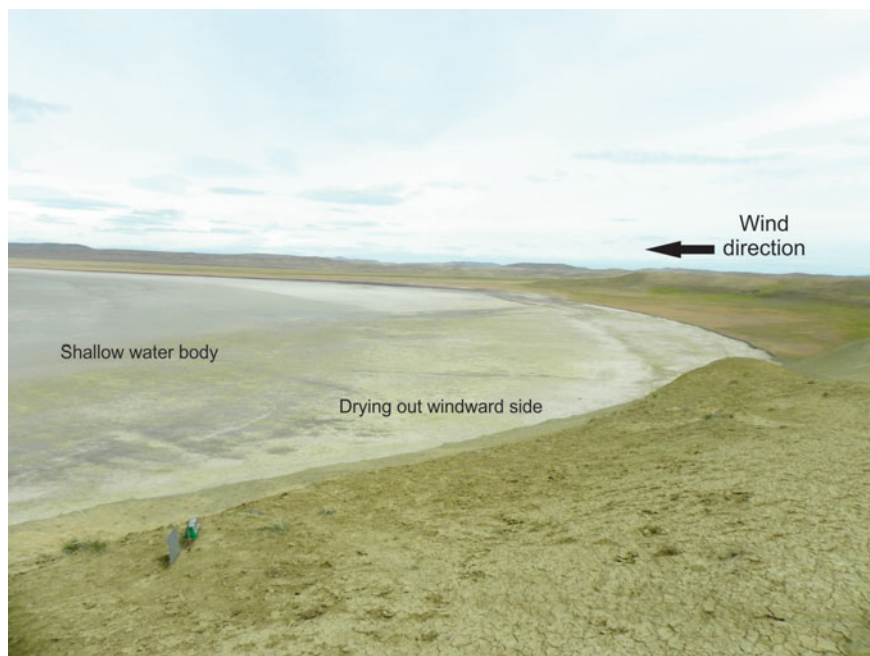


Fig. 7 Western sector of Laguna O'Connor, a pan containing a shallow water body, with progressive drying out eastwards

In the western end of this tectonic depression, Bahía Inútil is found, which opens to the Magellan Straits. In between both bays, morainic belts of Middle Pleistocene age were formed by Middle Pleistocene glaciations (Lagunas Secas Drift, Meglioli 1992). This tectonic depression of open ends affects marine and continental sedimentary rocks of Neogene age.

The pans develop in fossil marshes, formed by finer sediments of supra- and inter-tidal environments (Arche and Vilas 2001), in gravel ridges and cheniers. Besides, tidal plains and channels are also present in the littoral morphology of this area (Vilas et al. 2000). This fossil littoral environment is the result of the advance of the sea up to 7 km inland from the present coastline, between 5616 ± 282 and 509 ± 41.5 cal. yr BP (Vilas et al. 2000), that is, as a consequence of the post-glacial global sea level advance during the Middle Holocene marine transgression.

The pans developed in San Sebastián Bay are shallow depressions, generally 1 m deep, which in some cases present not very well-defined margins, either by the interconnection of several depressions or by the presence of drainage lines as fossil tide channels remnants. The dominant orientation of their longer axes is W–E or SW–NE. They have a highly variable size and type of grouping, depending upon the type of sediments and landforms on which they were formed. Three groups are distinguished: marsh pans, chenier pans and littoral ridges pans (Fig. 8).

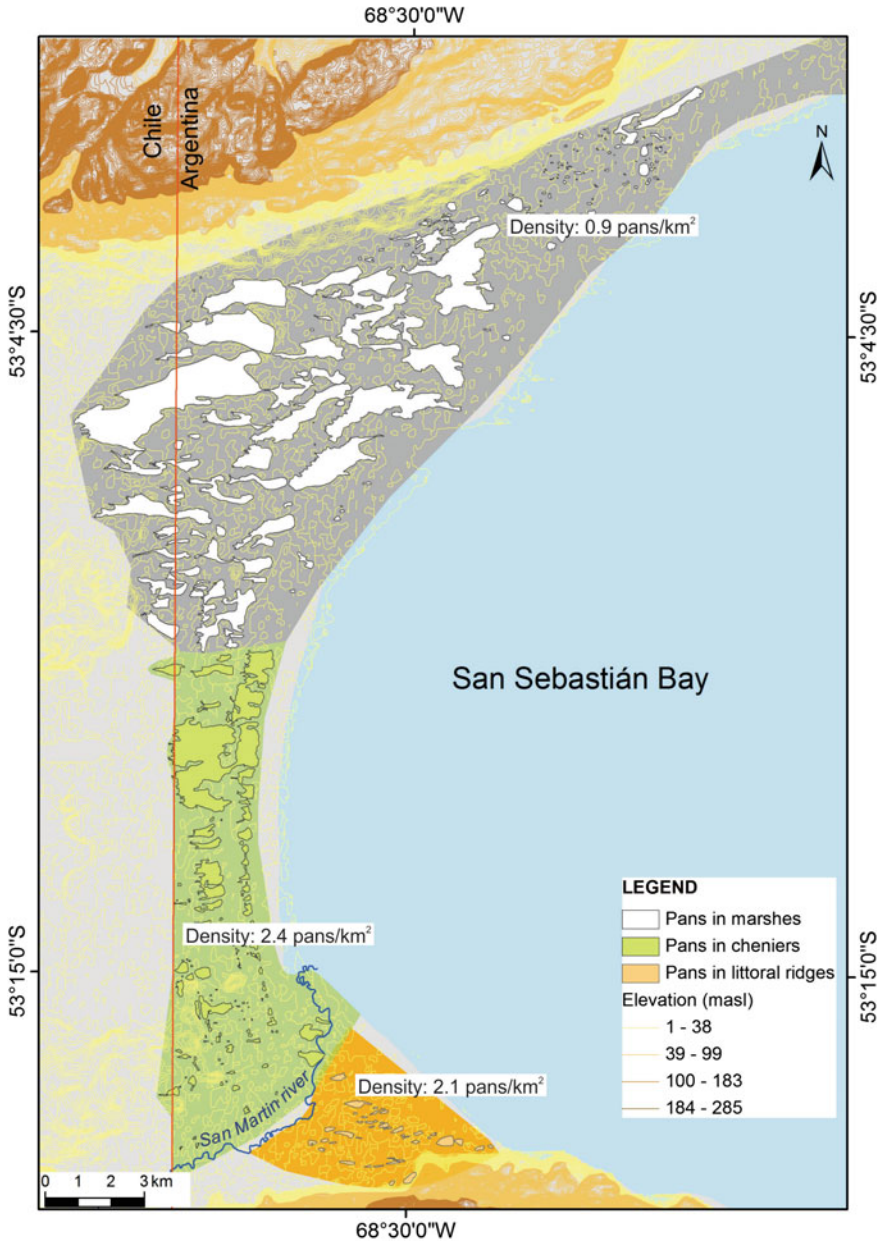


Fig. 8 Distribution and density of pans in the zone of San Sebastián Bay taking into consideration their geomorphological emplacement. The geomorphological units follow Vilas et al. (2000)

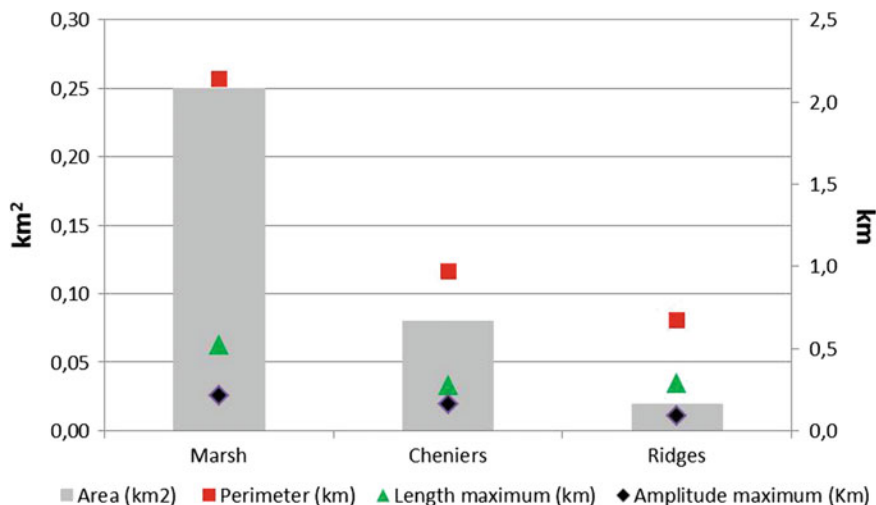


Fig. 9 Average morphometric characteristics of pans developed in San Sebastián Bay, according to the three groups of landforms

6 Marsh Pans

A large number of these hollows ($N = 151$) are developed in the northern portion of the bay, reaching a total surface of 162 km^2 , the greater extent of all groups in this zone. In this sector, a basin density of 0.9 pans per km^2 is found. Many of them are interconnected by means of temporary drainage lines of the superficial run-off system. The mean surface of these basins is 0.25 km^2 , with a range between 0.0002 and 7.3 km^2 . This group represents the larger mean size of the pans that develop at SSB. Approximately 84% of the landforms of this group have an areal surface smaller than the mean value (Fig. 9). Towards the NE, the mean area diminishes, with depressions of more regular margins. DL oscillates between 1.0 and 4.3 , being this the highest value with respect to the other groups of the bay, corresponding to several interconnected bays by means of channels and whose individual identification is difficult. In general, the margins of the basins are irregular in shape and the long axis has a SW–NE orientation. The dominant shape depends upon the method used; according to DL, the circular shapes predominate (64%); however, according to RAL, 94% of them present an elliptical shape.

7 Chenier Pans

These basins are developed in the central-south portion of SSB, and they reach a total number of 127 . They form three aligned ridges in a N–S direction, projecting a semicircle in physical accordance with the coastal plain. They cover an area of

53 km² which gives a pans density of 2.4 pans per km². The mean surface is significantly smaller than in the previous group, reaching 0.08 km², within a range of 0.0001–4.2 km². The surface area is smaller than in those basins developed in the S and E of the chenier zone. Approximately 88% of the landforms of this group have a surface development smaller than the mean value of the group. The longest axis has an E–W direction.

According to DL, whose values vary between 1.0 and 2.6, most of these landforms have circular shape (73%); following the RAL criteria, 92% of the basins are elliptical.

8 Littoral Ridges Pans

These pans reach a total of 40 along the southern sector of the bay and they are located between two groups of littoral ranges, covering a smaller areal extent with respect to the previous groups at SSB. Density is 2.1 pans per km². These basins have a mean surface of 0.02 km², within a range of 0.03 and 0.12 km², which suggest that these are the smallest hollows of three groups. The whole group presents elliptical shapes, in which the long axis is oriented, mainly, in a W–E direction. At least 70% of the pans of this group present surface values lower than the mean. The DL index records that 56% of them are basins with circular shape, whereas RAL indicates that all the basins of this group have elliptical shape, in which the longest axis is oriented in a W–E sense. Note that the marsh basins have a larger surface development, L, Lm and Am than those described in cheniers and littoral ranges (Fig. 9).

9 The Río Chico–Río Grande (RCH-RG) Zone

The sector that comprised between the Chico and Grande rivers has a hilly range relief of low altitude (150–300 m a.s.l.) with strong fluvial dissection, in some cases with sub-horizontal summits. A set of endorheic basins, some of them totally closed, contain ephemeral shallow lakes which occur amongst the hilly ranges. In the N sector of this divide, glaciofluvial fans developed with their apexes in the upper valley of the Río Chico and formed terrains of gentle slope which extend up to the present coastal zone.

The development of deflation hollows is recognized in the three geomorphological units studied (Fig. 10).

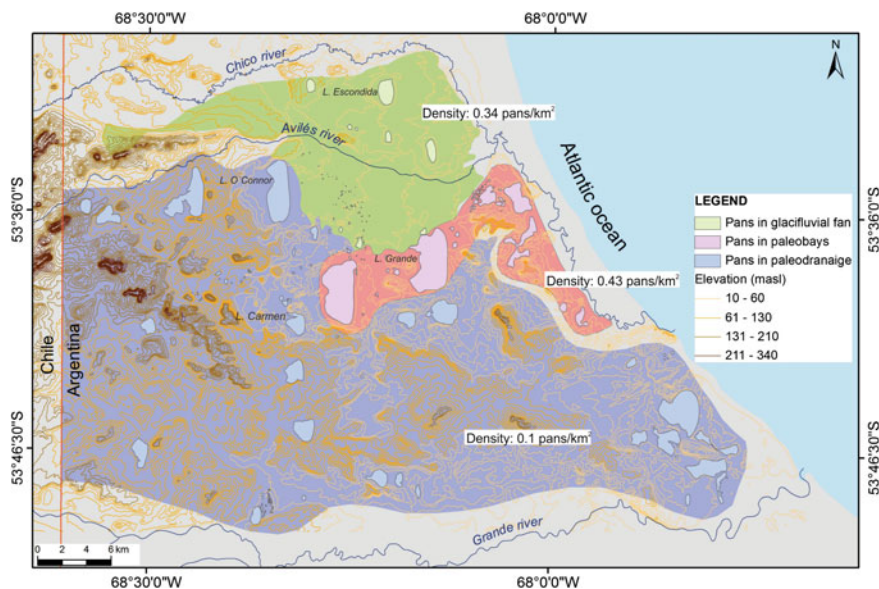


Fig. 10 Distribution and density pans in the zone comprised between the Chico and Grande rivers, according to the geomorphological units identified

10 Glaciofluvial Fan Pans

On the glaciofluvial fan, 81 pans have been carved developing 235 km² of depressed surface, limited towards the E by the Río Chico (or Carmen Sylva Creek). This group presents a pan density of 0.34 per km². The mean surface of these basins is 0.06 km², between a maximum value of 2.2 km² and a minimum one of 0.0001 km². The mean pan perimeter (*L*) of this group is 0.43 km, and the maximum length and width present values of 0.16 and 0.1 km, respectively, reaching the smaller morphometric values of the RCH-RG zone (Fig. 10). Approximately 90% of these basins have a surface smaller than the mean value. South of the Río Avilés, a greater hollow density is observed, although with smaller surface development (Fig. 10) related to channels oriented in a NW–SE direction. The values of the different measured parameters are markedly lower in this group with respect to the remaining ones which do not form the RCH-RG unit (Fig. 11). In the E and SW sectors of this group, hollows have not been developed, thus making for a very low density. According to DL, approximately 91% of the depressions are of circular shape; however, according to the RAL analysis, it is suggested that all basins in this area have an elliptical shape (RAE = 1.3–4.3). The axes of maximum length have a predominantly N–S orientation.

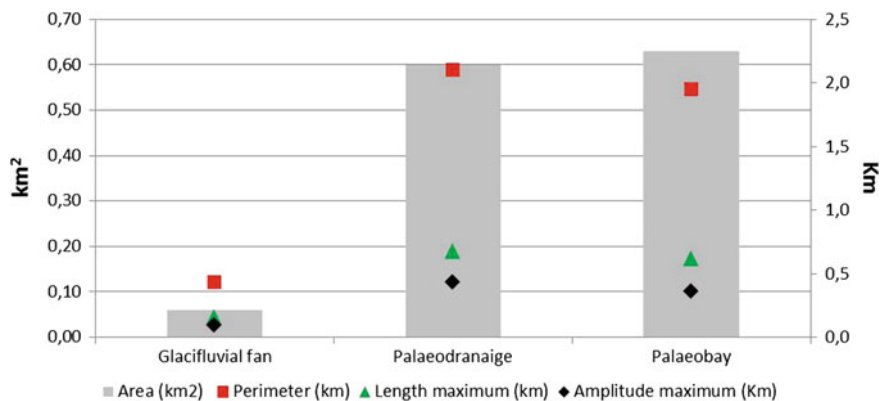


Fig. 11 Mean morphometric characteristics of pans developed between the Chico and Grande rivers, according to the geomorphological units observed

11 Palaeo-drainage Pans

The palaeo-drainage pans amount up to 90, located south of the previous group and west of the international boundary between Argentina and Chile. They occupy 1087 km², being the most extended area of the RCH-RG zone, and reach a very low density (0.1 pans per km²). They present a mean surface of 0.6 km² (ranging between 0.0004 and 7.6 km²), of which 81% is found below the mean value. The mean *P* value is 2.1 km, whereas *Lm* and *Am* reached values of 0.68 and 0.43 km, respectively (Fig. 11). The palaeo-drainage system in between the hilly ranges reflects surficial run-off conditions with greater yields than those of the creeks that flow along the present drainage basins. These water currents carved their valleys in a general direction SW–NE, and they are integrated within the Avilés and Grande rivers, or they discharge directly into the Atlantic Ocean palaeo-littoral environment. Based upon the DL analysis, the elliptical shape characterizes approximately 80% of the basins and 97% according to the RAL criteria.

12 Palaeo-bay Pans

The palaeo-bay basins include 51 depressions. They cover an area of 118.25 km², which is found in contact with the southernmost end of the glaciofluvial fan and part of the palaeo-drainage unit, limited towards the E by the Río Chico (Fig. 10). This group presents a density of 0.43 pans per km² and a mean surface of 0.63 km² in a range of values which oscillate between 0.002 and 12 km². The mean perimeter (*L*) is 1.95 km, and the variables maximum length and width have values of 0.62 and 0.36 km, respectively. Approximately 92% (47 pans) of them present a surface area lower than the mean value. Considering the DL index, the circular shapes

predominate (84%), whereas according to RAL, 94% of them have an elliptical shape.

13 Landforms Developed from Pans

In the SSB zone, megaripples developed along the eastern margin of the pans have been identified, which generate later climbing dunes (Arche and Vilas 2001), composed of silty–clayey materials (Fig. 12). However, the most frequent landforms generated from the deflated basin materials are nebkhas, also known as “coppice dunes”, as it has been mentioned by Cooke et al. (1993) and Gile (1975). These landforms are generated from the obstacles opposed by the dominant vegetation to the wind-transported particles, generally *Lepydophyllum* sp. Some dunes of the “lunette” type are also developed in this zone, and due to the shrubby vegetation effect, they develop asymmetrical shapes around branches and leaves. Pellet formation of particles 1–3 mm in diameter occur (Arche and Vilas 2001). Circular dunes are associated with other types of grassy vegetation, composed of *Sedum* sp., of smaller size than *Lepydophyllum* sp. Aeolian mantles are also developed in this zone, sometimes reaching up to 4 m in thickness.

In the RCH-RG zone, landforms generated leeward the pans are perched dunes on the cliffs, or phytogenetic dunes or nebkhas (Fig. 13) and the aeolian mantles (Fig. 14), (Coronato and Villarreal 2014; Villarreal and Coronato 2014; Villarreal et al. 2014). The perched dunes are found downwind of the depressions that occur on sedimentary rock cliffs, formed by wave erosion forced by the wind when blowing on the surface of a water body that may be transitorily occupying the pans.

The rocks exposed to the wind coming from the western quadrant receive the impact of the air on their weathered particles, and these are incorporated to ascending “twisters” that mobilize them towards the top of the cliff, thus forming a

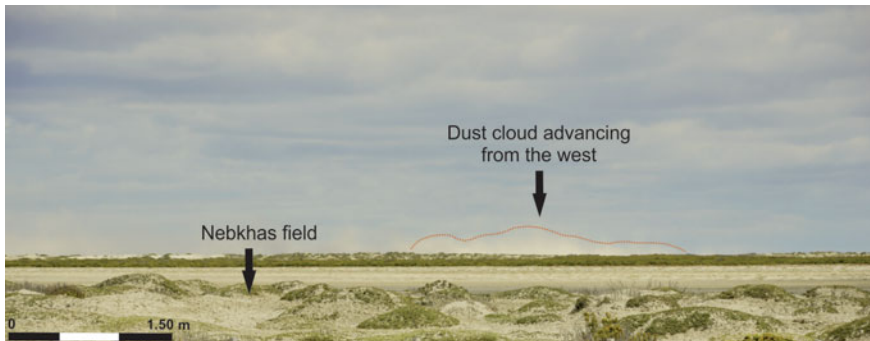


Fig. 12 Pan formed in marsh morphology of San Sebastián Bay zone with nebkhas development on halophyte vegetation in the leeward margin. At the background, a dust cloud formed by deflation advances from the west (photograph by Soledad Schwarz)

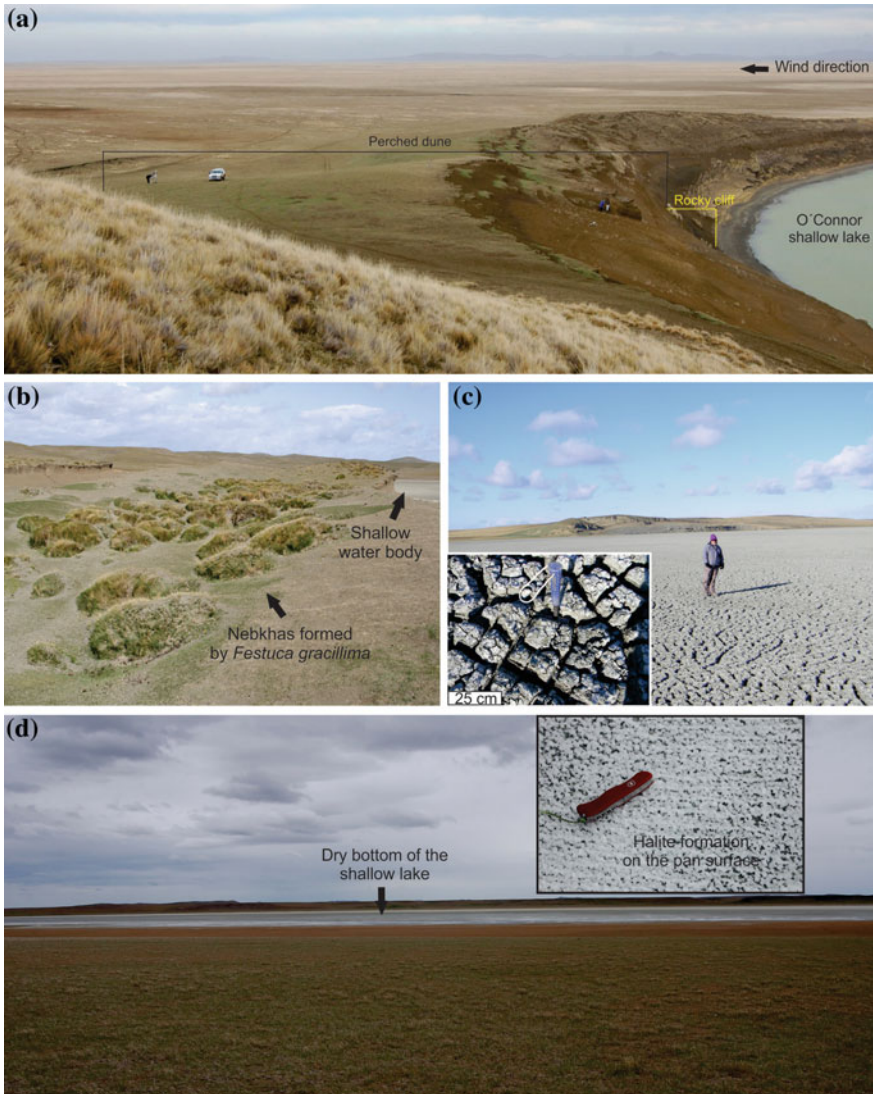


Fig. 13 Landforms originated from pans. **a** Perched dune on Lake O'Connor sedimentary rocky cliff. Note the asymmetric slopes of the dune and the erosion processes in the upward slope. **b** Nebkhas formed by sandy-silty particles and developed on *Festuca gracillima* bushes over a cliff at Laguna Amalia. **c** Lake Arturo shallow lake in dry conditions, playing the roll of a pan during the autumn. Desiccation cracks are 1–2 cm wide. **d** Escondida shallow lake in dessicating process. At the front, degraded vegetation covered by the aeolian dust mantle; in the small picture: halites formed by surface crystallization during desiccation cover the eastern side of the pan bottom

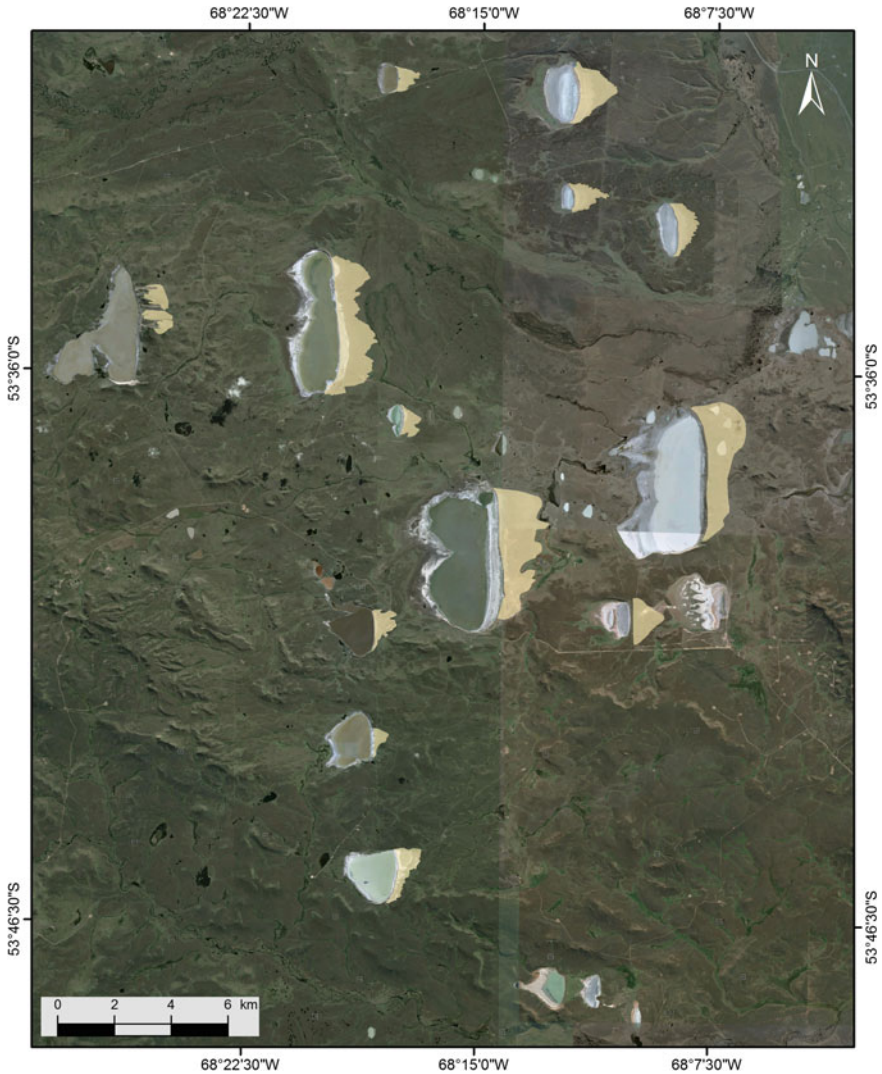


Fig. 14 Pan distribution in the RCh-RG zone, the bigger containing ephemeral, shallow water lakes. In all of the pans, aeolian mantles are developed leeward. They extend over cliffs and lacustrine terraces. Mantles are shown by polygons over the Google Earth® image

sedimentary pile. Besides, when the pans have lost the water body due to dessication or hydrological deficit, they supply sedimentary load to deflation which mobilizes leeward. Partly, these sediments are deposited at the top of the cliffs, forming part of the perched dunes. This type of dunes is found, mainly, within the palaeo-drainage group, where the pre-existing water currents would have intensified the erosion of certain cliffs, for instance, in the zone of Amalia and O'Connor

shallow lakes (Fig. 1). The dune formed on the NW slope of this shallow lake is composed of silty deposits, whereas in Laguna Arturo, they are of the silty–clayey–sandy type (Coronato et al. 2011). The aeolian mantles are concentrated in the glaciofluvial fan pans group, in which they reached a larger development in relation to the other ones. These are sheet-like deposits developed leeward depressions, composed of deflation particles from the dry bottoms of the shallow lakes, mostly during the summer season (December–February). They are composed of sandy–silty–clayey or silty–clayey sediments and, according to their provenance, they provide an important salt content (Fig. 13) to the soil in which they are deposited (Crosta et al. 2014; Villarreal et al. 2014). The modification in the properties of the soils due to the salt supply modifies the vegetation cover, in which *F. gracillima*, a dominant species in the region, is replaced by *H. cosmosum*, *Poa alopecurus*, *Deschampsia flexuosa* and cespitose species, such as *B. gummifera* and *A. trifurcata* (Villarreal et al. 2014). The aeolian mantles become adapted very well to the micro-landscape on which they are deposited, without generating new relief. Nevertheless, they are recognized by means of satellite imagery as diffuse spots extending downwind of the depressions.

14 Pans in Tierra del Fuego and Other Regions of Argentina

Pans are erosion landforms that develop under semi-arid climate conditions. In Tierra del Fuego, these landforms occur in its northern portion of the island and they are concentrated in two geographical zones of different characteristics according to the origin of their geomorphological emplacement. The density of these landforms in the different geomorphological units varies between 0.1 and 2.4 pans per km². These values are higher to those proposed by Goudie and Wells (1995) for different sectors of Argentina, where a range of density was established between 0.05 and 0.9 pans per km² for basins generated in palaeo-lacustrine, palaeo-drainage, interdune and coastal surface environments. In Tierra del Fuego, the pans are carved on coastal environments such as cheniers, marshes, littoral ridges, and palaeo-bays or in the inner portion of glaciofluvial or palaeo-drainage fans. These are different geomorphological emplacements than those previously described by Goudie and Wells (1995), which expands the set of landforms subject to the possible formation of pans. At a regional scale, in southern Extra-Andean Patagonia, deflation basins are developed in terraced tablelands, volcanic mesetas and terminal and ground moraines (Mazzoni 2001), although they present a smaller mean density than in Tierra del Fuego. In the northern portion of the Isla Grande de Tierra del Fuego, the basins of the RCH-RG zone present defined perimeter and many of them are depressions which are not interconnected. Contrarily, the basins formed in marshes and cheniers have irregular margins and they appear interconnected, which suggests aeolian erosion affecting tidal palaeo-channels in the marsh

plains and the occurrence of morphometric changes in the future. These pans should be considered as the most dynamic of the region.

According to Raedeke (1978) and Arche and Vilas (2001), one of the characteristics that identify the pans of Tierra del Fuego is their migration process towards the east, due to the effect of persistent westerlies on wave action, when these depressions hold transitory water bodies. In these periods, wind energy removes the surface of the water and generates waves that erode the leeward coast and progressively desiccate the water body, exposing the upward dry bottom. This process is produced both in the SSB pans and in those carved in the glaciofluvial fan and the palaeo-bays of the RCH-RG sector, all of them occur in geomorphological units in which the deflated material is of sedimentary origin. Contrarily, in some pans developed in the hill ranges zone, migration towards the east is impeded due to the occurrence of rocky outcrops of up to 20 m high, thus generating cliff recession erosion processes due to wave action. In those periods in which the basins are lacking water content, wind excavates the exposed bottoms, increasing depth and generating deflation and dust clouds.

The morphometric characteristics studied in each group of pans present clear differences, either between the two studied zones or even within them. The pan density is larger in the SSB zone, mainly in marsh and chenier areas. The mean surface area of pans is higher in the marsh and palaeo-bay geomorphological units. Concerning shape types and following the RAL index, most of the basins have elliptical shapes and extend their long axes perpendicularly to the dominant wind direction. In the SSB zone, the marsh and chenier basins are under intense dynamics. However, the pans found in the littoral ridge sector, where the availability of loose sediment is lower, resemble the shape of the basins of the adjacent RCH-RG zone. The aeolian mantles are present in both studied zones, although they have larger surface area in the SSB zone when compared to the RCH-RG one, which suggests that deflation is more effective here for short-distance accumulation dust, perhaps because winds speed is higher than in the hilly range area, promoting both desiccation and particle remotion. Nebkhas occur in both studied areas as well, and in SSB, they are the more abundant accumulation landforms, while they are blocked by halophilous vegetation in SSB; in the RCH-RG zone, nebkhas are formed by *F. gracillima* (“coirón”) and they appear in slope terrains or in degraded soils away from the cliffs. Perched dunes are also some of the accumulation landforms associated with pans with cliff shores, but they are found only in the palaeo-drainage unit of the range portion of the RCH-RG zone.

15 Final Remarks

Pans in northern Tierra del Fuego are distributed in different geomorphological environments, which causes that they have diverse morphometric and morphological characteristics. In all cases, these features promote the genesis of various types of landforms along their leeward margins, such as phytogenetic dunes or

nebkhas, with several species which act as obstacles to the wind, lunettes, perched dunes over cliffs and aeolian mantles. The highest density of pans occurs in the San Sebastián Bay (SSB) zone, where the marshy and chenier environments offer drier, fine-grained sediments, and where the wind has high intensity and persistency and there is a lack of topographic obstacles. Contrarily, the low hilly ranges of the RCH-RG zone generate obstacles to the air flow, generating interference to the wind influence as landscape modeller. Besides, during part of the year, these hollows retain a water body that occupies almost the entire depressions, thus diminishing the erosion potential by deflation. In the SSB zone, the higher density of pans is found here in the “palaeo-bay” unit, where sediments affected by deflation correspond to mixed deposits of marine and glaciofluvial origin, reworked by the sea during the various marine transgressions that took place in the region during the Middle Pleistocene.

Considering the morphometric parameters, the mean area of the pans in SSB is 0.12 km^2 , which is the mean value lower than those of the RCH-RG zone (0.43 km^2), which brings up the analysis of the influence of the fluvial modelling previous to the erosion effect of the wind in this region. The hollows excavated on ancient glacial deposits of the SSB region found in the marsh and chenier zones would be a direct geomorphological response to the deflation effect over fine-grained sediments, whereas those of the RCH-RG zone would be a secondary morphological result upon non-functional valley bottoms, eroded on sedimentary rocks or sandy-gravelly, thin fluvial deposits.

Concerning the shape of the pans, there are some differences regarding the analytical method applied. The application of an alternative method to the classical methodology proposed by Hutchinson (1957) allowed us to determine that, of the six geomorphological units in which pans appear, only in the palaeo-drainage hollows, where the shapes are notably elliptical, there are coincident results amongst the applied methodologies (DL and RAL). This reveals that, for the intermediate shapes, those between the circular and the elliptical shapes, which are the ones with higher frequency in the region, the RAL or the relationship of axes length describes in a similar way as with the visual interpretation as it is done from remote sensing analysis or digital terrain models. This parameter is considered as more appropriate than the DL parameter (Hutchinson 1957) to characterize the shape of pans in this region.

The deflation hollows developed in northern Tierra del Fuego are a geomorphological feature characteristic of semi-arid zones, although in this case, conditions as cold temperatures with seasonal snowfall and soil freezing are added. The persistence of the wind during the ice and snow-free season favours the progressive excavation of pans with consequent genesis of short-distance, accumulation landforms and ample provision of atmospheric dust. The pans of larger size have a role as transitory water bodies, whose progressive desiccation depends upon the westerlies persistence and velocity.

The formation of these shallow lakes adds one more component to the steppe landscape, and it offers appropriate habitats for bird wildlife, although in many cases the turbidity and salinity of the water do not allow its use for drinking water or irrigation supply.

Pans—seasonally filled of water or dry—are remarkably active landforms in the subantarctic landscape of southern South America. Their activity is triggered by the interplay of the Southern Pacific Ocean high-pressure systems and the Polar Front which determines the intensity of winds and promotes dust supply to the southern hemisphere oceans and atmosphere.

Acknowledgements The authors are deeply grateful to the owners and personnel of the Los Flamencos, María Behety, San Julio and El Salvador ranches for allowing the access to the study sites and to the members of EARG (Río Grande) for logistic facilities. Mr. Ramiro López (CADIC-CONICET) participated in field activities. They are also thankful to Jorge Rabassa, for his invitation to publish in this volume and for his suggestions and the English-style improvement on a first draft of this paper.

References

- Arche A, Vilas F (2001) Sedimentos eólicos de grano fino en la Bahía de San Sebastián, Tierra del Fuego, Argentina. *J Iberian Geol* 27:159–173
- Bujalesky GG (1997) Patrón espacial y dinámica de canales de sobrelavado de la costa atlántica septentrional. *Revista Asociación Geológica Argentina* 52(3):257–274. Buenos Aires
- Bujalesky G, Coronato A, Isla F (2001) Ambientes glaciifluviales y litorales Cuaternarios de la región del Río Chico, Tierra del Fuego, Argentina. *Revista de la Asociación Geológica Argentina* 56(1):73–90. Buenos Aires
- Codignotto J, Malumán N (1981) Geología de la región al N del paralelo 54° L.S. de la Isla Grande de Tierra del Fuego. *Revista de la Asociación Geológica Argentina* 36(1):44–88. Buenos Aires
- Collantes MB, Anchorena J, Koremblit G (1989) A soil nutrient gradient in Magellanic Empetrum heathlands. *Vegetatio* 80:183–193
- Cooke RU, Warren A, Goudie A (1993) *Desert geomorphology*. UCL Press, London, 526 pp
- Coronato A (2014) Territorios fueguinos: fisonomía, origen y evolución. In: Oría J, Tivoli A (eds) *Cazadores de mar y tierra. Estudios recientes en arqueología fueguina*. Editorial Cultural Tierra del Fuego, Ushuaia, pp 43–63
- Coronato A, Villarreal ML (2014) Modelado eólico en ambientes lagunares de la estepa fueguina, Argentina. In: XIX Congreso Geológico Argentino, Córdoba 2014. CDROM, S13–46. Asociación Geológica Argentina, Buenos Aires
- Coronato A, Meglioli A, Rabassa J (2004) Glaciations in the Magellan Straits and Tierra del Fuego, Southernmost South America. In: Ehlers J, Gibbard P (eds) *Quaternary glaciations—extent and chronology, part III. Developments in quaternary science, vol 2C*. Elsevier, Amsterdam, pp 45–48
- Coronato A, Fanning P, Salemm M, Oría J, Pickard J, Ponce JF (2011) Aeolian sequence and the archaeological record in the Fuegian steppe, Argentina. *Quatern Int* 245:122–135
- Crosta S, Villarreal ML, Coronato A (2014) Formación de cristales de halita en la Laguna Escondida, norte de Tierra del Fuego. III Reunión Argentina de Geoquímica de la Superficie. In: Massone H, Miglioranza K (eds) *Universidad Nacional de Mar del Plata-IIMYC-CONICET. CD-Rom*, pp 57–61

- Dangavs N (1979) Presencia de dunas de arcilla fósiles en la Pampa Deprimida. *Revista Asociación Geológica Argentina* 34(1):35–39. Buenos Aires
- del Valle HF, Rostagno CM, Coronato FR, Bouza PJ, Blanco PD (2008) Sand dune activity in north-eastern Patagonia. *J Arid Environ* 72(4):411–422
- del Valle HF, Blanco PD, Metternicht GI, Zinck JA (2010) Radar remote sensing of wind-driven land degradation processes in Northeastern Patagonia. *J Environ Qual* 39:62–75
- Diraison M, Cobbold P, Gapais D, Rosello E, Le Corre C (2000) Cenozoic crustal thickening, wrenching and rifting in the foothills of the southernmost Andes. *Tectonophysics* 316:91–119
- Gaiero D, Gili S, Koestner E, Farid C (2015) What is the real isotopic signature of dust emitted from Tierra del Fuego? In: VI Congreso Argentino de Cuaternario y Geomorfología, Abstracts, 91. Asociación Argentina de Cuaternario y Geomorfología. Buenos Aires
- Gile LH (1975) Holocene soils and soil-geomorphic relations in an arid region of southern New Mexico. *Quatern Res* 5:321–360
- Gili S, Gaiero D, Goldstein S, Chemale F Jr, Koester E, Jweda J, Vallelonga P, Kaplan M (2016) Provenance of dust to Antarctica: a lead isotopic perspective. *Geophys Res Lett* 43:2291–2298. doi:10.1002/2016GL068244
- Goudie AS, Wells GL (1995) The nature, distribution and formation of pans in arid zones. *Earth-Sci Rev* 38:1–69
- Hutchinson E (1957) A treatise of limnology. Geography, physics and chemistry. New York, 1015 pp
- Mazzoni E (2001) Distribución espacial y caracterización geomorfológica de “bajos sin salida” de la Patagonia Austral Extracordillerana. *Anales Instituto de la Patagonia, Serie Ciencias Naturales* 29:5–24
- Meglioli A (1992) Glacial geology of Southernmost Patagonia, the Strait of Magellan and Northern Tierra del Fuego. Unpublished PhD Dissertation, Lehigh University, Bethlehem, U S A
- Moore D (1983) Flora of Tierra del Fuego. Anthony Nelson, Missouri 396 pp
- Olivero EB, Malumíán N, Martinioni DR (2006) Mapa Geológico a escala 1:500 000 de la Isla Grande de Tierra del Fuego e Isla de los Estados, Provincia de Tierra del Fuego, Antártida e Islas del Atlántico Sur. República Argentina. SEGEMAR, Buenos Aires
- Rabassa J, Coronato A, Ponce JF (2009) La depresión Bahía Inútil – Bahía San Sebastián (Tierra del Fuego, Argentina-Chile): una conexión marina inexistente durante el Pleistoceno tardío-Holoceno. In: Salemm M, Santiago F et al (eds) *Arqueología de la Patagonia: una mirada desde el Último Confín*, vol 1. Editorial Utopías. Ushuaia, pp 101–108
- Raedeker LD (1978) Formas del terreno y depósitos cuaternarios en Tierra del Fuego Central, Chile. *Revista Geológica de Chile* 5:3–31
- Seppälä M (2004) Wind as geomorphic agent in cold climates. *Studies in polar research*. Cambridge University Press, Cambridge, 358 pp
- Thornthwaite CW, Mather JR (1957) Instructions and tables for computing potential evapotranspiration and the water balance. *Publ Climatol* 10(3). Thornthwaite Associates, Elmer
- Tuhkanen S (1992) The climate of Tierra del Fuego from a vegetation geographical point of view and its ecoclimatic counterparts elsewhere. *Acta Botánica Fennica* 145:1–64
- Vilas F, Arche A, Ferrero M, Isla F (2000) Subantarctic macrotidal flats, cheniers and beaches in San Sebastian bay, Tierra del Fuego, Argentina. *Mar Geol* 160(3–4):301–326
- Villarreal ML, Coronato A (2014) Desarrollo de nebkhas asociado a *Festuca gracillima* en un ambiente lagunar semiárido, Tierra del Fuego, Argentina. In: XIX Congreso Geológico Argentino, Córdoba 2014. CD ROM, S13-56. Asociación Geológica Argentina. Buenos Aires
- Villarreal ML, Coronato A, Mazzoni E, López R (2014) Deflación en las lagunas semipermanentes de la estepa fueguina (53°S), Argentina. *Revista de la Sociedad Geológica de España* 27(2):81–96

Epibiosis on Brachiopods from Patagonia, Argentina (40°–55°S): Composition, Spatial Variation, and Preservation

Gisela A. Morán, Sandra Gordillo and M. Sol Bayer

Abstract Epibiosis is the association between two or more living organisms belonging to the same or different species as a result of surface limitation. Besides the ecological significance, epibiosis is of interest in paleoecological studies of both recent and fossil organisms. Brachiopods provide an ideal biogenic substrate for studying paleoecological questions relating to encrusting biotas. The aim of this preliminary study is to describe brachiopods and their epibionts in living/recent/Holocene shelled assemblages located along the Argentine coast between 40° and 55°S, at different depths. Representative brachiopod samples were collected. Living/recent samples were grouped into latitudinal areas to characterize organisms of high latitude (55°S approx.) and mid-latitude (40°S approx.), and benthic and coastal, depending on the bathymetric location where they were sampled. Six epibiont taxa were found on the living/recent valves of *M. venosa* and *T. dorsata*. The most frequent and abundant epibionts on both species were bryozoans and algae. Additional organisms such as polychaeta, barnacles, brachiopods, and molluscs were found. Benthic samples from high latitudes showed a higher overall rate of occurrence of epibionts. This difference is possibly determined by the bryozoans, which have the highest percentage of occurrence in this area and are usually predominant in these environments. The epibiont algae were found in greater amounts in the mid-latitude coastal samples. The absence of encrusting biotas on the Holocene shells of this study is attributed to the fact that many of these individuals are young and small. From this preliminary study, we intend to continue and deepen the analysis to assess potential ecological patterns and contribute to the knowledge of the epibionts and encrusting communities of Patagonian Quaternary brachiopods.

Keywords Epibiosis · Brachiopods · Patagonia · South Atlantic ocean · Argentina

G.A. Morán (✉) · S. Gordillo · M.S. Bayer
Centro de Investigaciones en Ciencias de la Tierra (CICTERRA), Consejo Nacional de Investigaciones Científicas y Técnicas (CONICET)/Universidad Nacional de Córdoba (UNC), Av. Vélez Sarsfield 1611 X5016GCA, Córdoba, Argentina
e-mail: gisela.amoran@gmail.com

1 Introduction

1.1 *Epibiosis in Marine Environments and in the Fossil Record*

In marine environments, the sessile mode of life is dominant in the majority of benthic communities, and finding a hard, stable substrate for colonization is an important event in the life cycle of this kind of organism. In this scenario, epibiosis takes place in spatially close associations between two or more living organisms belonging to the same or different species as a result of surface limitation. In epibiosis, the organism providing a substrate is called *basibiont*, while the organism growing attached to a living surface is called *epibiont* (Wahl 1989; Harder 2008). This association has a profound ecological impact, since the presence of epibionts affects (positively, negatively or both) the fitness of basibionts directly as well as indirectly, by modulating its interactions with the abiotic and biotic environment (Wahl 2008).

The main factors affecting epibiosis are probably latitude and depth (Wahl 1989; Barnes and Clarke 1995; Vasconcelos et al. 2007), although the other biological and physical processes, such as developmental stages, species or physical abrasion by water movement, can also determine the development of the epibiotic communities (Wahl 1989; Barnes and Clarke 1995; Schejter et al. 2007, 2011).

Besides the ecological significance, epibiosis is of interest in paleoecological studies of both recent and fossil organisms (Waugh 2004; Schneider 2013; Rodland 2014) since this association can be preserved in the fossil record and is an ancient phenomenon that can be traced as far back as the Cambrian (Palmer 1982; Taylor and Wilson 2003; Schneider 2013). Through this association, we can understand not only the lifestyles of these organisms, but also their common paleoenvironments and paleocommunities.

1.2 *Brachiopods as Basibionts*

Due to the widespread occurrence of brachiopods and their abundance on the Paleozoic, epibiosis in this group has been well documented for that geological period (e.g., Richards 1972; Alexander and Scharpf 1990; Bordeaux and Brett 1990; Gibson 1992; Lescinsky 1997; Zhan and Vinn 2007; Zatón and Borszcz 2013). However, the brachiopods suffered greatly in the Permo-Triassic extinction event and never regained their former diversity. Nowadays, they are abundant in just a few sites and habitats (Brey 1995), and are, therefore, relatively little understood; the epibiosis of Quaternary brachiopods in particular has received scarce attention (i.e., Rodland et al. 2004, 2014).

Quaternary brachiopod shells, consisting of low-Mg calcite, have been mentioned in Pleistocene and Holocene deposits from different regions (Harper 1995; Craig 1999; Ruggiero and Annunziata 2002; Wood et al. 2006; Zezina 2010;

Simões et al. 2011; Rodland 2014). In Patagonia, Argentina, and Quaternary brachiopods were first mentioned by Feruglio (1950), who described the presence of two species as follows: *Terebratella dorsata* and *Magellania venosa*. Later, Gordillo (1990) described the presence of the same species for mid-Holocene deposits along the Beagle Channel, in the southernmost point of South America. At present, the existence of three living species of brachiopods, *T. dorsata*, *M. venosa*, and *Liothyrella uva*, are recognized in Argentina (Cooper 1973; Roux and Bremec 1996).

Quaternary brachiopods, therefore, provide an ideal biogenic substrate for studying the paleoecological questions of encrusting biotas, relationships between hosts and colonizing epibionts, and taphonomic pathways in the past and present communities (e.g., Alexander and Scharpf 1990; Bordeaux and Brett 1990; Lescinsky 1993). In addition, an increasing understanding of encrustation on brachiopods from the present day can be used to address macroevolutionary questions, for example, whether encrustation varies as a function of productivity (Vermeij 1995). Evaluation of encrustation trends through the Phanerozoic could also be used as a proxy for productivity issues through time. In any case, the evaluation of macroevolutionary patterns in epibiont faunas requires a firm understanding of modern patterns in analogous settings. Additionally, if epibionts are to be used as ecological proxies, taphonomic, and observational effects must be understood so that the information they provide can be discerned from useful paleoecological information.

Given the above, the aim of this preliminary study is to describe brachiopods and their epibionts in living/recent/Holocene shelled assemblages located along the Argentine coast between 40° and 55°S, at different depths. This provides information on latitudinal and bathymetric variations, as well as valuable insights into the what can be preserved and what cannot be preserved elements of the fossil record.

2 Materials and Methods

Representative brachiopod samples were previously collected from different localities along the Argentine coast between Río Negro and Tierra del Fuego provinces (Fig. 1). The samples included living/recent material (benthic samples from 4 localities between 20 and 75 m depth), recent material (coastal samples from 13 localities along the modern beach), and paleontological samples (Holocene marine deposits and paleontological samples from two localities along the Beagle Channel). For the analysis, living/recent samples were grouped into latitudinal areas to characterize organisms of high latitude (55°S approx.) and mid-latitude (40°S approx.), and benthic and coastal, according to the bathymetric location where they were sampled (Table 1). For the dorsal and ventral valves of each specimen, the presence/absence of epibionts was analyzed, and the occurrence percentage of each epibiont group was calculated for each area and valve.



Fig. 1 Sampling sites for brachiopods on the Argentine coast between Río Negro and Tierra del Fuego

Table 1 Sampling localities of brachiopods along the Argentine coast between Río Negro and Tierra del Fuego. Samples were grouped into latitudinal and bathymetric areas for the analysis

Depth	Latitude	
	Mid	High
Coastal	Playas Doradas	Beagle Channel A (Holocene)
	Punta Colorada	Beagle Channel B (Holocene)
	Puerto Lobos	
	Puerto Pirámides	
	El Doradillo	
	Puerto Madryn	
	Playa Unión	
	Playa Elola	
	Bahía Bustamante	
	Rada Tilly	
	Caleta Olivia	
	Cabo Blanco	
	Puerto Deseado	
	Benthic	San Jorge Gulf
Tierra del Fuego B		
Tierra del Fuego C		

3 Results

Two brachiopod species have been found as follows: 110 specimens belonged to *M. venosa* and 32 were *T. dorsata*. Epibionts were found on 51% of the *M. venosa* valves, and on 46.9% of those of *T. dorsata*. For all the living/recent brachiopods, 30% of the samples did not have epibionts, and in the Holocene specimens, epibiosis was not observed at all. In all specimens with epibionts, 64% occurred in the ventral shell and 36% in the dorsal shell.

The main epibionts found in the samples were bryozoans and algae, followed by polychaete (i.e., serpulid tubes, sabellids, *Spirorbis* sp.), barnacles, brachiopods, and molluscs (Fig. 2). Algae represent 26% of the total observations and bryozoans do so for 24%. For both epibiont groups, there were more observations on ventral than on dorsal valves (Fig. 3).

Preliminary results showed a higher overall rate of occurrence of epibionts in benthic samples from higher latitudes, compared with the rest (Fig. 4). The epibiont algae were found in greater amounts in the mid-latitude coastal samples than in other areas (Fig. 5). The sabellid polychaetes were only found in benthic samples and were not observed in the coastal samples (Figs. 6 and 7).

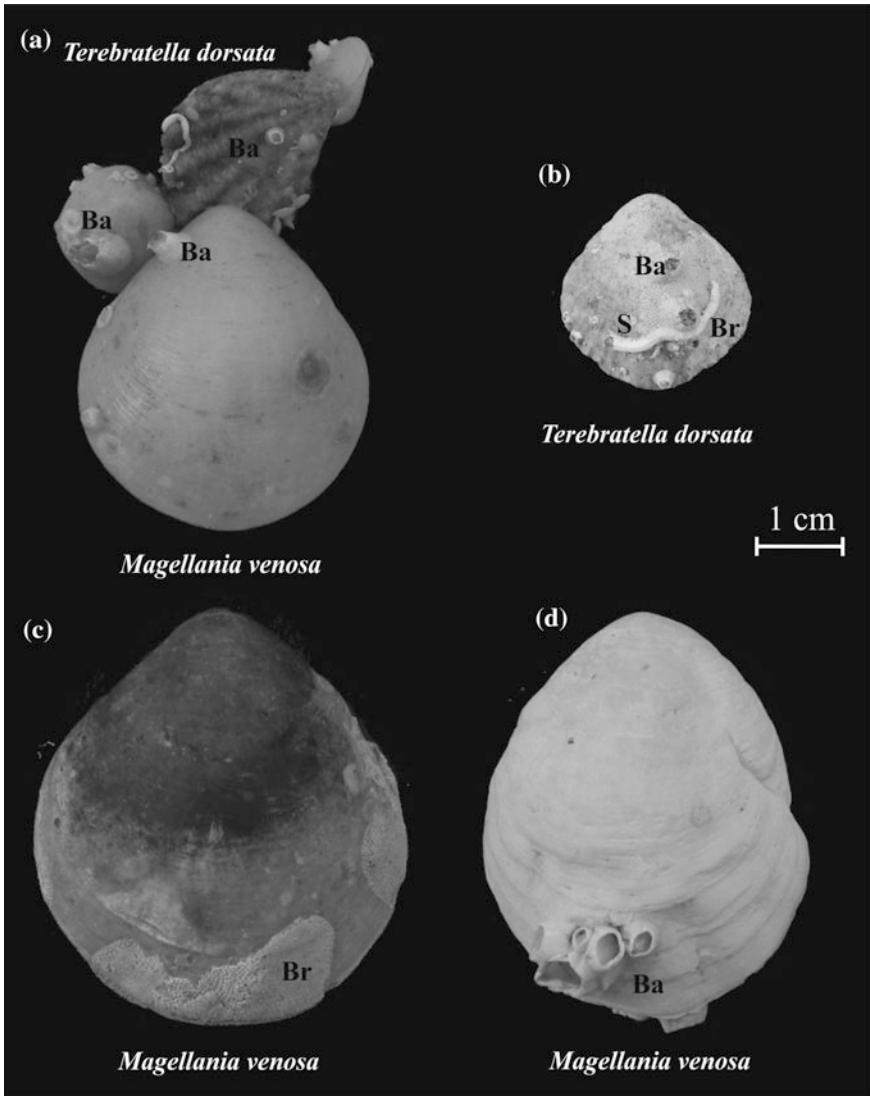


Fig. 2 Epibiont organisms on brachiopods from the Argentine coast. **a** Aggregation of two species of brachiopods, *Magellania venosa*, and *Terebratella dorsata*. Both species have some barnacle epibionts, and the small brachiopods are using the big *Magellania venosa* as a substrate. **b** *Terebratella dorsata* with bryozoans, serpulid tubes, and several barnacles. **c** *Magellania venosa* with bryozoans. **d** *Magellania venosa* with barnacles. Acronyms: *Ba* Barnacles, *Br* Bryozoos, and *S* Serpulid

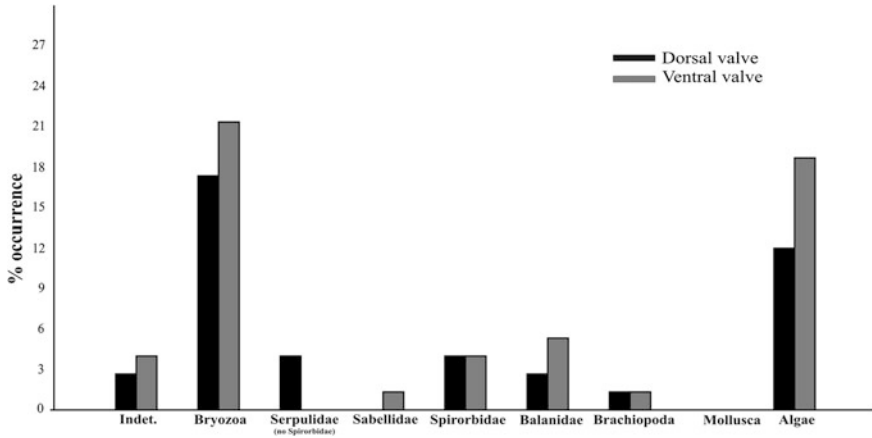


Fig. 3 Frequency of occurrence of epibionts on each valve of brachiopods (based on presence–absence data)

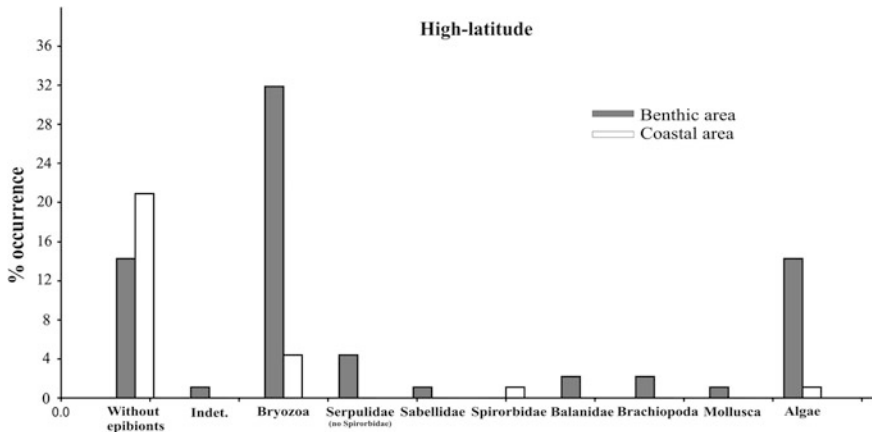


Fig. 4 Frequency of occurrence of epibionts on brachiopods in high latitudes for benthic and coastal areas (based on presence–absence data)

4 Discussion

Six epibiont taxa were found on the living/recent valves of *Magellania venosa* and *Terebratella dorsata* from Patagonia. The most frequent and abundant epibionts on both species were bryozoans and algae. Additional organisms such as polychaeta, barnacles, brachiopods, and molluscs occurred as part of the fauna closely related to the epibiont association. This study represents the first approach to the investigation of this interaction for brachiopods in Patagonia.

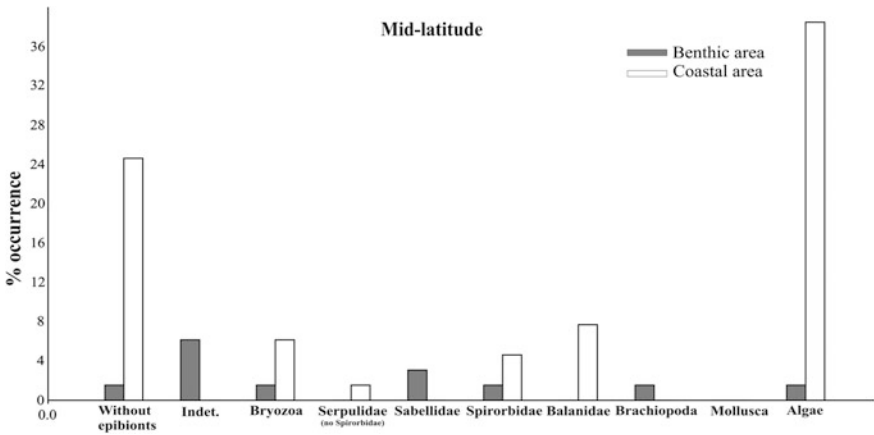


Fig. 5 Frequency of occurrence of epibionts on brachiopods in mid latitudes for benthic and coastal areas (based on presence–absence data)

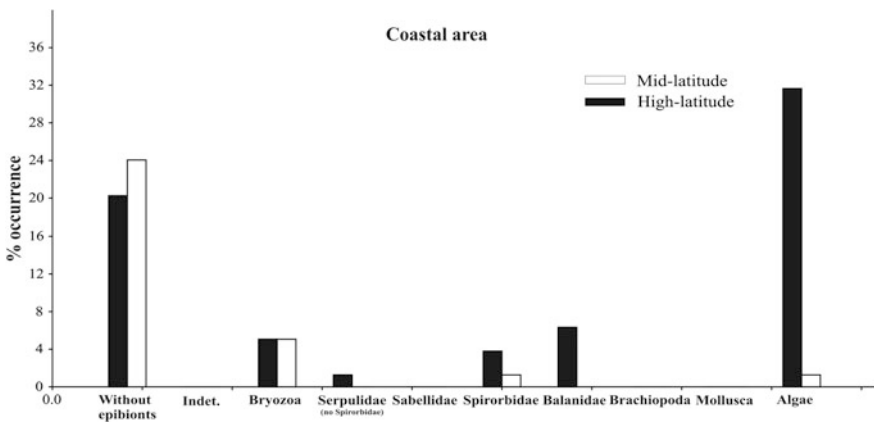


Fig. 6 Frequency of occurrence of epibionts on brachiopods in coastal areas for mid- and high-latitude (based on presence–absence data)

Although both valves were encrusted, the ventral valves had a higher occurrence percentage for the most epibiont groups. *M. venosa* and *T. dorsata* are sedentary species that have a limited swimming capacity (Camacho 1966). Epibionts can settle on both valves, depending on the living position adopted by the brachiopod, which seems to be more frequent with the dorsal valve close to the substrate (Camacho 1966).

Different occurrence percentages were observed in epibionts from different areas. Benthic samples from higher latitudes showed the highest overall rate of occurrence of epibionts. This difference is possibly determined by bryozoans, which have the highest percentage of occurrence in this area and are usually

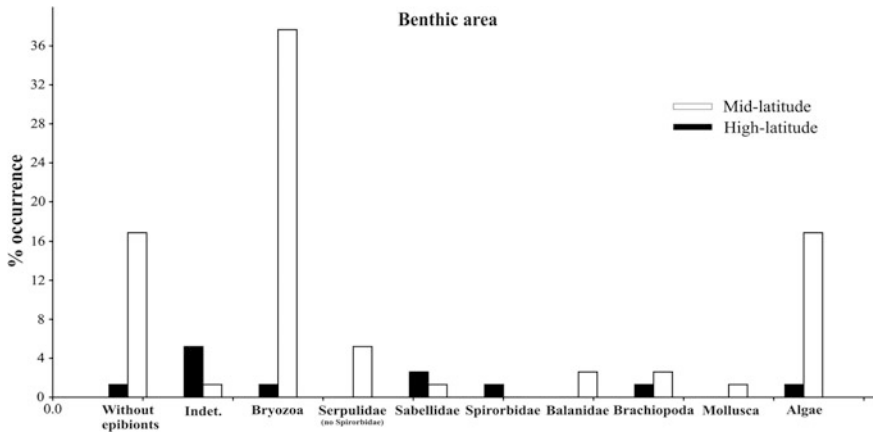


Fig. 7 Frequency of occurrence of epibionts on brachiopods in benthic areas for mid- and high-latitude (based on presence–absence data)

predominant in these environments. Gappa (2000) reported a higher species richness and an abundance of bryozoans for these latitudes in benthic environments in the Atlantic Ocean compared to that of coastal and mid-latitude environments. The epibiont algae were found in greater amounts in the mid-latitude coastal samples, probably because of the greater availability of sunlight in such environments. Sabellid polychaetes were only found in benthic samples and were not observed in coastal samples. This result was attributed to the few chances of preservation due to their non-calcified structure (i.e., mucus agglutination with small sediments) and the highly erosive coastal environments. By contrast, other epibiont groups such as *Spirorbis* sp., or other serpulid polychaete, balanids, and bryozoans, have a greater chance of preservation because of their calcified structures, which would allow us to find them in paleontological samples (Waugh 2004). The absence of encrusting biotas on the Holocene shells of this study is attributed to the fact that many of these individuals were young and small, so there may not have been enough exposure time for colonization. The colonization process of a solid surface, a brachiopod shell in this case, is intimately related to the length of time of exposure to colonizers (Wahl 1989). We expected larger (older) organisms to be more heavily encrusted than the smaller (younger) ones if no mechanisms for deterrence were acting. The interpretation in the absence of epibionts in younger/smaller specimens in Holocene specimens from the Beagle Channel is reinforced because barnacles on scallop shells were also recovered in the same fossil assemblage (Gordillo 1999). From this preliminary study, we intended to continue and deepen the analysis in order to assess potential ecological patterns and to contribute to the knowledge of the epibionts and encrusting communities of Patagonian Quaternary brachiopods.

5 Final Remarks

- (a) Six epibiont taxa were found on the living/recent valves of *M. venosa* and *T. dorsata* from Patagonia.
- (b) The most frequent and abundant epibionts in both species were bryozoans and algae. Additional organisms such as polychaeta, barnacles, brachiopods, and molluscs occurred as part of the fauna closely related to the epibiont association.
- (c) Different occurrence percentages were observed on epibionts from different areas. Benthic samples from higher latitudes showed the highest overall rate of occurrence of epibionts. The epibiont algae were found in greater amounts in the mid-latitude coastal samples than in other areas. Sabellid polychaetes were only found in benthic samples and were not observed in coastal samples.
- (d) The absence of encrusting biotas on the Holocene shells of this study was attributed to the fact that many of these individuals were young and small.

References

- Alexander RR, Scharpf CD (1990) Epizoans on Late Ordovician brachiopods from southeastern Indiana. *Hist Biol* 4(3–4):179–202
- Barnes DK, Clarke A (1995) Epibiotic communities on sublittoral macroinvertebrates at Signy Island, Antarctica. *J Mar Biol Assoc U K* 75(03):689–703
- Bordeaux YL, Brett CE (1990) Substrate specific associations of epibionts on Middle Devonian brachiopods: implications for paleoecology. *Hist Biol* 4(3–4):203–220
- Brey T, Peck LS, Gutt J, Hain S, Arntz WE (1995) Population dynamics of *Magellania fragilis*, a brachiopod dominating a mixed-bottom macrobenthic assemblage on the Antarctic shelf. *J Mar Biol Assoc U K* 75(04):857–869
- Camacho HH (1966) *Invertebrados fósiles*, vol 5. Eudeba, Buenos Aires
- Cooper GA (1973) *Vema's Brachiopoda (recent)*. Smithsonian Institution Press
- Craig RS (1999) The brachiopod fauna of the Plio-Pleistocene Ascot Formation, Perth Basin, Western Australia. *Rec-West Aust Mus* 19(4):451–464
- Feruglio E (1950) Descripción geológica de la Patagonia. YPF, tomo 3, Buenos Aires
- Gibson MA (1992) Some epibiont-host and epibiont-epibiont relationships from the birdsong shale member of the lower Devonian Ross formation (west-central Tennessee, USA). *Hist Biol* 6(2):113–132
- Gordillo S (1990) Braquiópodos del Holoceno Medio del Canal Beagle, Tierra del Fuego, Argentina. XI Congreso Geológico Argentino. 2, pp 215–218
- Gordillo S (1999) Holocene molluscan assemblages in the Magellan region. *Sci Mar* 63(S1):15–22
- Harder T (2008) Marine epibiosis: concepts, ecological consequences and host defense. Springer
- Harper DA, Doyle EN, Donovan SK (1995) Palaeoecology and palaeobathymetry of Pleistocene brachiopods from the Manchioneal Formation of Jamaica. *Proc Geol Assoc* 106(3):219–227
- Lescinsky HL (1993) Taphonomy and Paleoecology of Epibionts on the Scallops *Chlamys hastata* (Sowerby 1843) and *Chlamys rubida* (Hinds 1845). *Palaios*, pp 267–277
- Lescinsky HL (1997) Epibiont communities: recruitment and competition on North American Carboniferous brachiopods. *J Paleontol* 71:34–53
- Gappa JL (2000) Species richness of marine Bryozoa in the continental shelf and slope off Argentina (south-west Atlantic). *Diversity Distrib* 6(1):15–27

- Palmer TJ (1982) Cambrian to Cretaceous changes in hardground communities. *Lethaia* 15:309–323
- Richards RP (1972) Autecology of Richmondian brachiopods (Late Ordovician of Indiana and Ohio). *J Paleontol* 46:386–405
- Rodland DL, Kowalewski M, Simoes MG, Carroll M (2004) Colonization of a “Lost World”: encrustation patterns in modern subtropical brachiopod assemblages. *Palaios* 19:381–395
- Rodland DL, Simoes MG, Krause RA, Kowalewski M (2014) Stowing away on ships that pass in the night: Sclerobiont assemblages on individually dated bivalve and brachiopod shells from a subtropical shelf. *Palaios* 29(4):170–183
- Roux A, Bremec C (1996) Brachiopoda collected in the Western South Atlantic by R/V Shinkai Maru cruises (1978–1979). *Revista de Investigación y Desarrollo Pesquero* 10:109–114
- Ruggiero ET, Annunziata G (2002) Bioerosion on a *Terebratulina scillae* population from the Lower Pleistocene of Lecce area (Southern Italy). *Acta Geológica Hispánica* 37(1):43–51
- Schejter L, Bremec CS (2007) Epibionts on *Flexopecten felipponei* (Dall, 1922), an uncommon scallop from Argentina. *Am Malacol Bull* 22(1):75–82
- Schejter L, Escolar M, Bremec C (2011) Variability in epibiont colonization of shells of *Fusitriton magellanicus* (Gastropoda) on the Argentinean shelf. *J Mar Biol Assoc U K* 91(04):897–906
- Schneider CL (2013) Epibiosis across the Late Devonian biotic crisis: a review. *Proc Geol Assoc* 124:893–909
- Simões MG, Chiesi CM, Kotzian CB, Pätzold J (2011) Late Pleistocene (Ionian-Tarantian) brachiopods from the Rio Grande do Sul shelf, as recorders of cold climate conditions near the Brazil-Malvinas confluence zone. In: *Congresso da Associação Brasileira de Estudos do Quaternário*, vol 13, p 5
- Taylor PD, Wilson MA (2003) Palaeoecology and evolution of marine hard substrate communities. *Earth-Sci Rev* 62(1):1–103
- Vasconcelos P, Curdia J, Castro M, Gaspar MB (2007) The shell of *Hexaplex (Trunculariopsis) trunculus* (Gastropoda: Muricidae) as a mobile hard substratum for epibiotic polychaetes (Annelida: Polychaeta) in the Ria Formosa (Algarve coast-southern Portugal). *Hydrobiologia* 575(1):161–172
- Vermeij GJ (1995) Economics, volcanoes, and Phanerozoic revolutions. *Paleobiology*, 125–152
- Wahl M (1989) Marine epibiosis. I. Fouling and antifouling: some basic aspects. *Mar Ecol Prog Ser* 58:175–189
- Wahl M (2008) Ecological lever and interface ecology: epibiosis modulates the interactions between host and environment. *Biofouling* 24(6):427–438
- Waugh D, Feldmann R, Crawford R, Jakobsen S, Thomas K (2004) Epibiont preservational and observational bias in fossil marine decapods. *J Inf* 78(5)
- Wood SLB, Krause RA, Kowalewski M, Wehmiller J, Simões MG (2006) Aspartic acid racemization dating of Holocene brachiopods and bivalves from the southern Brazilian shelf, South Atlantic. *Quat Res* 66(2):323–331
- Zatón M, Borszcz T (2013) Encrustation patterns on post-extinction early Famennian (Late Devonian) brachiopods from Russia. *Hist Biol* 25(1):1–12
- Zežina ON (2010) Check-list of Holocene brachiopods annotated with geographical ranges of species. *Paleontol J* 44(9):1176–1199
- Zhan R, Vinn O (2007) Cornulitid epibionts on brachiopod shells from the Late Ordovician (middle Ashgill) of East China. *Est J Earth Sci* 56:101–108

The Quaternary of the Laguna de los Pozuelos Basin, Northern Puna, Argentina

María Camacho and Julio J. Kulemeyer

Abstract The Laguna de los Pozuelos basin (LLPB) (22°18′–22°25′S and 65°57′–66°02′W, 3625–4808 m a.s.l.) is located in the northwestern portion of the Province of Jujuy, near the Argentine–Bolivian border. Geomorphologically, the area, which belongs to the Puna, has the distinctive characteristics of a bolson relief, covering an area of ~3650 km². Puna is a large “altiplano,” a high-altitude tableland characteristic of the Central Andes. The depression shapes a morphostructurally low area, limited by generally trending N–S faults. A relatively extensive, shallow salt lake system, which often underwent shrinkage and expansion, became established in this depression in the Late Pleistocene and has survived until present times. Geological and geomorphological aerial photointerpretation, as well as sedimentological, mineralogical, and paleontological studies and physical–geochemical analyses, has been carried out for the sake of this research work (X-ray fluorescence, IC ICP-OES) together with calibrated radiocarbon dating. Four drill holes from McGlue et al. (2013) and four from Camacho et al. (2013) have been considered. The Quaternary record began with alluvial fan deposits of the so-called Level I, which were distributed along the foothill and hillside of the LLPB. These deposits have accumulated during pluvial periods and they form coalescent fans. These are the oldest clastic deposits in this basin, which have been eroded and flattened forming a unique bajada (a natural slope composed of coalescent alluvial fans). They are provisionally ascribed to the Early–Middle Pleistocene, since they have been interpreted to be older than the lacustrine expansion. These sequences are in contact with various Palaeozoic, Mesozoic, and Cenozoic (Paleogene–Neogene) formations and they grade laterally to the deposits of the lacustrine coasts of the Minchin phase and the Late Pleistocene-related deltas (ca. 43 to 23 cal. ka B.P.) (Camacho et al. 2013). During the Last Glaciation period at the regional level (Camacho et al. 2013), vast coastlines were formed at 3695, 3680, and 3665 m a.s.l.

M. Camacho (✉) · J.J. Kulemeyer
School of Engineering, Universidad Nacional de Jujuy,
San Salvador de Jujuy, Argentina
e-mail: mcamacho@fi.unju.edu.ar

J.J. Kulemeyer
e-mail: jjkulemeyer@fi.unju.edu.ar

The last two of them are very well preserved with the growth of bioherms (algal carbonates), ostracods, fine sandy gravels, sands, and calcisiltites. While Gilbert-type deltas developed, with their typical tripartite internal structure: bottomset beds made up of mud, foreset clinofolds with layers of sand showing cross-planar stratigraphy, and fine gravel topset beds, the section is exposed today thanks to ~ 15 -ka-old tectonic faults, at the mouth of the Río Corral Blanco. Deltas also represent coastal littoral environments which occurred together with three lacustrine expansions and shrinkages according to the paleolimnological interpretation by Camacho et al. (2013). Alluvial fan deposits were formed laterally; this is Level II (sandy gravel and sand) with an age of ~ 26 to 19 cal ka B.P., based on geomorphological–stratigraphical positions, and in McGlue et al. (2013) paleogeographic dating diagram. Meanwhile, the lake underwent another lacustrine shrinkage due to more arid and warmer climate at the beginning of the studied period. This caused gypsum precipitation in rosettes of around 5 cm in diameter and also Halite deposition. Afterward, a recovery of an ephemeral lake (Playa Lake) took place since the Last Glacial Maximum (LGM) (~ 23 to 15 cal. ka B.P.). Carbonate–siliciclastic mud, gypsum, and halite with ostracods and gyttja fossil are found in these lacustrine sediments. Climatic and tectonic adjustment at the end of the LGM reduced it to an ephemeral and shallow lake with a surface of only 264 km² and 10 m deep. Early Holocene shores at 3625 m a.s.l. (11.7 ka) signal the beginning of the present interglacial period with a larger lacustrine shrinkage of 112 km² per meter in depth, ranging from 70 km² per 0.50 m, to become dry in some years. Alluvial fan deposits surround the lake; these are known as Level III (sands, gravels, and silts), which were deposited from ~ 3 cal. ka B.P. until present times (McGlue et al. 2013). These deposits are covered by eolian deposits toward the southern side of LLPB. Deltas were formed at the mouths of the Cincel, Colquimayo, and Santa Catalina Rivers. The stratigraphic chart is completed with floodplain and riverbed deposits, made up of sands, silts, and salt precipitation.

Keywords Quaternary · Puna · Central Andes · Argentina · Stratigraphy · Geomorphology · Palynology · Paleoenvironments

1 Introduction

The Laguna de Los Pozuelos Bolson (LLPB) (22°18′–22°25′S and 65°57′–66°02′ W, 3625–4808 m a.s.l.) is located in northwestern Province of Jujuy, near the Argentine–Bolivian border (Fig. 1a, b). From a geomorphological point of view, the area belongs to the Puna morphostructural unit and has the distinctive characteristics of a bolson relief, covering an area of ~ 3650 km² and having internal or endorheic drainage. Puna is a large “altiplano,” a high-altitude tableland characteristic of the Central Andes. It is a biogeographical unit extending from Chile, Bolivia, Peru, and northwestern Argentina, consists of plateaus which they are

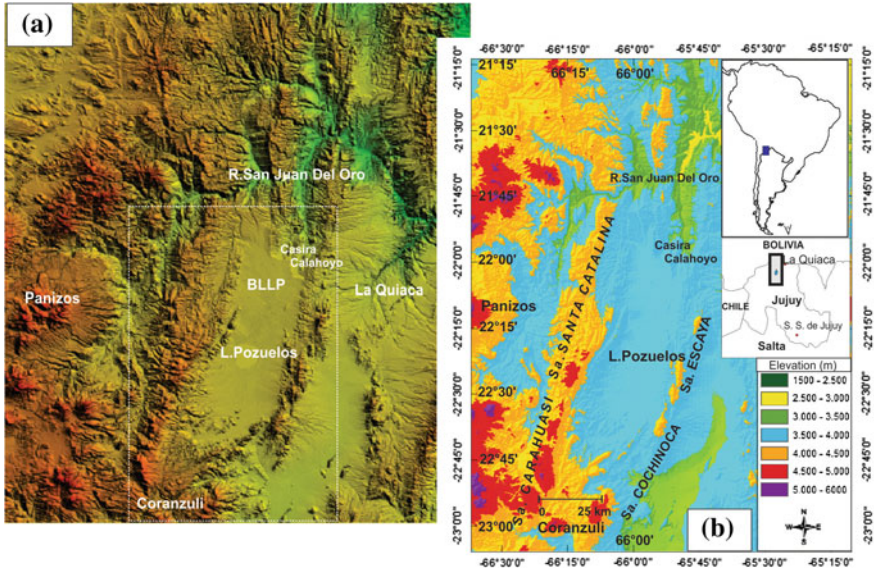


Fig. 1 a Satellite image of the LLPB and b Shuttle Radar Topography Mission (SRTM) digital elevation model of LLPB illustrating the shape of the basin and retrograde erosion in the northern limit by the Calahoyo and Casira basins and excavating the north closure of the Bolson Laguna Los Pozuelos

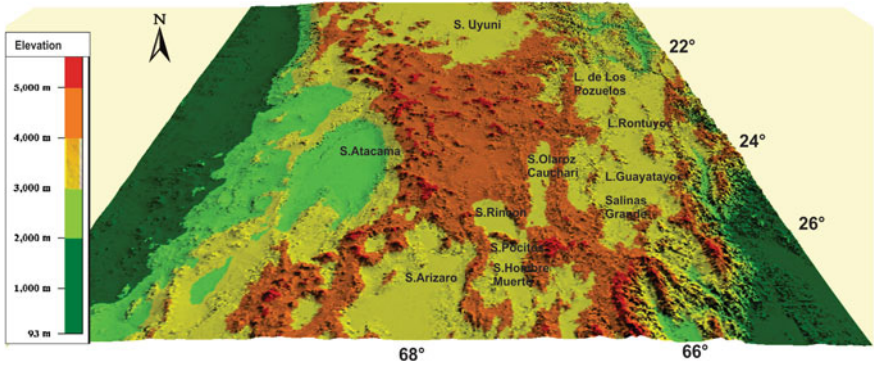


Fig. 2 Digital elevation model of the Puna (SRTM), showing the location of various shallow salt lakes and saline basins, forming endorheic depressions

located between 3400 and 3800 meters above sea level (m a.s.l.). These plains or “bolsones,” which are split by parallel mountain ranges from north to south, lack of drainage into the sea (Fig. 2). As a result, the water in low rainfall or snowfall in the region accumulates in a central depression the bolson, forming large and shallow lagoons. The depression was formed in a morphostructurally low area, limited by generally trending N–S faults. A relatively extensive shallow salt lake system,

which often underwent shrinkage and expansion, developed in this depressed area during the Late Pleistocene and has persisted until Recent times.

At present, the existing record of water and sediment is consistent with the variability of rainfall, produced mainly by anomalies of surface temperature of the Pacific Ocean. This strong seasonal cycle has been described as the South American Summer Monsoon (SASM) by Zhou and Lau (1998), associated with the El Niño/Southern Oscillation (ENSO), as in most of the Puna and the Bolivian “altiplano.”

Laguna Los Pozuelos basin is highly favored by its geographical location, allowing you to receive more precipitation in the range of 300–400 mm annually. It is classified as semiarid area by Bianchi and Yáñez (1992).

The Laguna Los Pozuelos is one of the few lakes in the Puna, which has not evolved to a salt flat, both for its geographical position and climate added to the water quality of its main tributaries (Río Santa Catalina from the north and Río Cincel from the south) with pH = 7.

Camacho et al. (2013) analyzed four incomplete records of rainy period 1972–1990, the stations belonging to the Provincial Direction of Hydraulics of the province of Jujuy (DHJ), Argentina, Cieneguillas, Tafna, Oratorio, Santa Catalina, in the basin of the Laguna de Los Pozuelos, which unfortunately stopped working, and a fifth station of the National Weather Service (NWS), La Quiaca (neighboring basin), with complete records from 1934 to 1987, published by Bianchi and Yáñez (1992). There have been excessively high rainfalls during the year 1984 in the towns of Santa Catalina (1046 mm), Cieneguillas (742 mm), Rinconada (1046 mm), since the region recorded a significant increase in rainfall (Fig. 3).

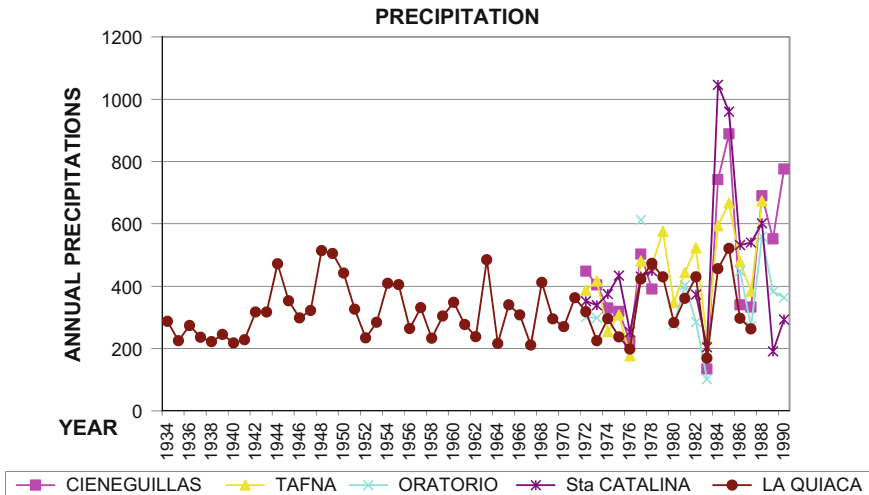


Fig. 3 Comparative study of the 5 meteorological stations reflected in this graph a significant increase in rainfall from about the year AD 1980, with a peak between AD 1984 and AD 1986 stands out

However, sediments of shallow lacustrine deposits of the Late Pleistocene reveal a close relationship between the central Andean climate and surface temperature gradients North Atlantic Ocean, as well as in the lakes of the Bolivian “Altiplano” (McGlue et al. 2013; Placzek et al. 2013).

An isotopic and chemical study of Lake Titicaca (Cross et al. 2001) indicates that the Late Pleistocene climate was 20% more humid and 5 °C cooler than the current climate (Argollo Bautista and Iriondo 2008).

Although the largest Pleistocene moisture increase affects the Argentine Puna in general, one of the basins most benefited was the Laguna de Los Pozuelos, coinciding with the regional glacial maximum expansion affecting the Sierra de Santa Victoria, the northernmost orographic element of the Cordillera Oriental morphostructural region (Igarzábal 1978), located to the east of the study area.

The aim of this work is to present the results of the geological and stratigraphical research done so far in the LLPB. Based on paleolimnological and paleoclimatic research, this paper also intends to explain the Quaternary evolution of the Laguna de los Pozuelos.

2 Methodology

Based upon the interpretation of aerial photographs, preliminary maps were prepared at a 1:50,000 scale, with field survey of stratigraphy and tectonics. Quaternary-type profiles were obtained in the area, with their associated textural analysis and determination of lithofacies, sedimentary structures, and fossil content. Mineralogical studies have been carried out by means of polarization microscopy, X-Ray Diffraction (XRD), Scanning Electron Microscope (SEM), and physical-geochemical analysis (X-ray Fluorescence X, IC ICP-OES; Camacho et al. 2013).

Analyses have been run on sediments acquired from a hole drilled by the National Centre of Competence in Research on Climate–Switzerland (NCCR–Climate), including 6 radiocarbon dates (Camacho and Kunz 2011), and a 100-m drill hole in the foothill area (Camacho 2009). Two ^{14}C Late Pleistocene ($\sim 14\text{--}13$, 7 ka ^{14}C B.P.; thousands of years before present; Camacho et al. 2009), and other Late Holocene (around 2 ka ^{14}C B.P.) paleosols dating were obtained in the Tritium and Radiocarbon Laboratory (LATYR) at the Universidad Nacional de La Plata; Kulemeyer et al. (2009). Besides, the radiocarbon dates obtained in four cores performed in the Laguna de los Pozuelos were taken into consideration. The cores and dating were completed by the Central Energy and Resources Science Center, US Geological Survey, Denver, Colorado, USA, and the University of Arizona, Tucson, Arizona, USA (McGlue et al. 2013).

3 Results and Discussion

The first geological records in the Laguna de Los Pozuelos Bolson began with the deposition of powerful, sandy–muddy, marine sedimentary sequences during the Ordovician. On the western side of the basin, these sedimentary sequences display features related to a talus zone, proximal to an external to middle marine platform. On the eastern side of this depression, a succession of bimodal (dacitic–basaltic alkaline), basically non-explosive, eruptions took place, concomitant with the sedimentation. These were associated with an extensional regime, which could have developed in relation to (or as a consequence of) a 467-Ma-old (millions of years ago) oblique subduction system. Interconnected extensional basins belonging to the “Salta Group Basin” developed during the Cretaceous. They were connected to a syn-rift stage and to an alkaline volcanism, represented by ~114–77 Ma trachy-andesitic lava flows.

During the Late Eocene–Early Oligocene, the Inka Tectonic phase brought about the interruption of the Salta Group deposition, forming vast foreland basins to the east of the deformation front. Inter-hill basins, where the clastic successions were deposited, were formed during the Late Oligocene–Early Miocene as a consequence of the Pehuenche phase compressive stage. Cenozoic volcanism in the region starts between 28 to 20 Ma, with reduced signs of calco-alkaline affinities registered in the Moreta Formation. Ephemeral fluvial lacustrine sedimentary facies come next, bringing the fallout of tephra or pyroclastic flows from the Tiomayo Formation (ca. 14 Ma).

Between 12 and 10 Ma, the San Juan de Oro surface was formed. This is a well-known regional discontinuity in the Northern Puna, the High-Puna plateau, and the Eastern Andes of Bolivia. From this period onwards, the tectonics of the region underwent a transition from a compressive to a distension area due to direction changes. On the other hand, sediments slowly started to accumulate within the basins.

A voluminous siliceous volcanism began between ca. 10–5 Ma. This volcanism, mainly composed of ignimbrites, settled over the San Juan de Oro surface. The most important periods of the crustal shortening and thickening of the Puna (the Quechua Phase) took place during the Middle to Late Miocene. After 5 Ma, following the Quechua Phase, sedimentary basins were formed. These basins were filled up with conglomerates, sandstones, mudstones, tuffs and tuffites from the Tafna Formation, of Pliocene age.

Quaternary tectonic movements, 2 Ma old, studied by Gubbles et al. (1993), caused a general uplift of the area and the active excavation of deep canyons. These processes primarily affected mountain ranges and hills, reactivating previous structures and creating an uneven or broken relief, comprised of ridges and open inter-hill extended valleys, which had endorheic drainage and varied according to the direction of the fracturing E–W and NNW–SSE.

3.1 *Paleozoic–Ordovician*

Acoite Formation (Harrington and Leanza 1957)

This formation is composed of sandstones, siltstones, and marine shales, which outcrop at the western margin of LLPB, at “Los Altos de Yoscaba”, “Sierra de la Rinconada”, “Carahuasi Mountain Range”, and “Alto Médanos” (Fig. 4). It extends over as a belt in a north–south direction and disappears southwards underneath the Neogene volcanic complex. The Sierra de la Rinconada Ordovician sediments include quartz veins which bear Au, As, Fe, Cu, Zn, Sb sulfides, and Ag sulfate salts, all related to the volcanic and volcanoclastic facies of the western side.

Environment: Bahlburg (1990) interpreted the Ordovician sequences as turbidite lobed deposits and turbidite interrelated channels.

Age: Lower–Middle Ordovician (Turner 1964), based on abundant existing fossils in the region and the surrounding area, among which the following should be mentioned: Graptolites: *Didymograptus v-deflexus* Harris, *Didymograptus nitidus* Hall, *Phyllograptus* sp., *Tetragraptus* sp., etc.; Cephalopoda: *Protocycloceras* cf. *Calligramma stefani* Ceccioni and Brachiopoda: *Orthis* cf. *Calligramma Dalman*, etc.

Cochinoca–Escaya magmatic–sedimentary complex (Coira et al. 2004)

This complex outcrops along the Escaya mountain chain, and the Cochinoca and Quichagua ranges, forming the eastern side of LLPB. It is comprised of two separated rock associations, (a) sandstones, siltstones, clays, dacitic, and spilitic lava mantles, and (b) dacitic–rhyolitic domical sub-volcanic bodies, spilitic lavas, autoclastic hyaloclastite breccia, saddles and dykes.

Environment: This intense volcanism, partially simultaneous with the Ordovician sedimentation, is related to the development of a magmatic arch (the Escaya–Cochinoca mountain chain), connected to an ocean crust subduction. Toward the east of the arch, the Pumahuasi–Aguilar platform deposits area is found, and toward the west (i.e., the Rinconada and Carahuasi ranges, among others) the antiarc deposits area appears.

Age: Early–Middle Ordovician, based on the fossil record, with a numerical age of 467 ± 1 Ma, using U–Pb dating on monazites obtained from migmatite rocks from the area of Cochinoca (Middle Ordovician).

3.2 *Mesozoic–Cretaceous (Fig. 4)*

Salta Group (Turner 1959)

Pirgua (sensu lato) Subgroup (Reyes and Salfity 1973)

These sediments are composed of red sandstones, silty–clays, and conglomerates. Toward the south of LLPB, small outcrops occur following tectonic lines on the Pan de Azúcar and Tucsurá Ranges, and between the Quichagua and Queta Hills.

Environment: These deposits settled in rift basins, in a terrigenous–fluvial environment, and they were connected to a basic alkaline volcanism.

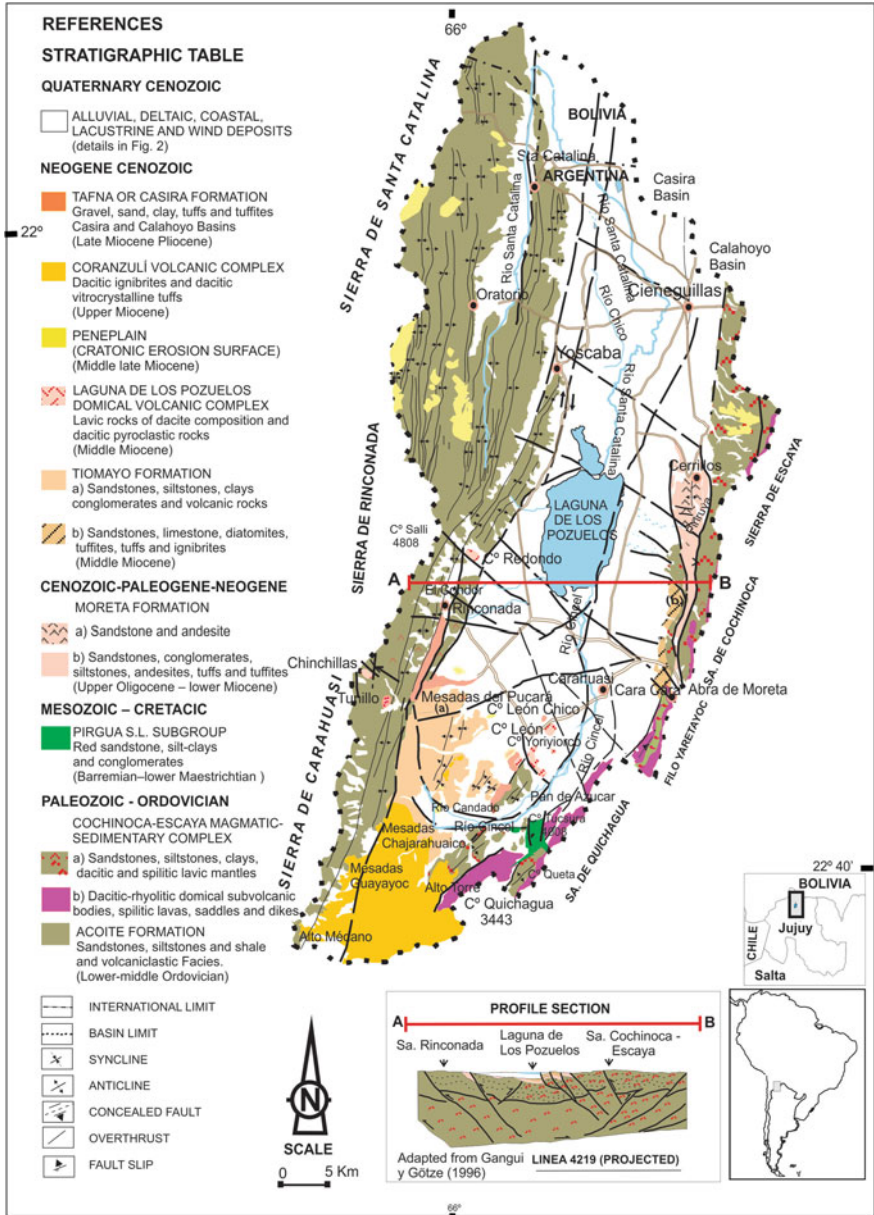


Fig. 4 Pre-Quaternary geological map of the LLPB

Age: The radiometric dating of volcanic rocks shows a K/Ar age of 114–77 Ma. Barremian–Early Maestrichtian.

3.3 *Cenozoic–Paleogene–Neogene (Fig. 4)*

Moreta Formation (Coira 1979)

This formation comprises fluvial and alluvial clastic deposits, among which lava and pyroclastic levels of andesitic–dacitic composition merge showing a central compound magmatism. It is possible to map two big rock associations, (a) sandstones and andesites and (b) sandstones, conglomerates, siltstones, andesites, tuffs, and water-lain tuffs. These rocks appear in Abra de Moreta, Cerrillos, Pan de Azúcar and in the inter-hill sub-basin at the eastern edge of the Rinconada ranges.

Environment: The emerging sediments are typically continental. They belong to a fluvial regime, inter-hill basins, both from channels and alluvial plains; in certain cases, they were possibly formed in shallow water bodies. The sequence composed of primary pyroclastic rocks, followed by re-elaborated volcanoclastic rocks, shows the activity of one or various lava-explosive centers occurring in a subsequent stage within the basin.

Age: Late Oligocene–Early Miocene. K/Ar radiometric dating of andesitic–dacitic rocks from the Pirurayo complex, belonging to the Moreta Formation, yielded an age of 28 ± 3 to 20 ± 2 Ma.

3.4 *Cenozoic–Neogene (Fig. 4)*

Tiomayo Formation (Seggiaro and Aniel 1989)

This formation comprises sandstones, siltstones, conglomerates, limestones, diatomites, water-lain tuffs, tuffs and ignimbrites which show different colors, ranging from grayish, pinkish, reddish, and yellowish to brownish and greenish. The outcrops are located on the eastern shore of LLPB, toward the west of the Escaya mountain chain, and on the LLPB western shore, in Sierra de Rinconada eastern edge, on the Pucará table mountains.

Environment: The sedimentary facies suggest a fluvial environment, with transition to brief lacustrine episodes, toward their end. Tephra and pyroclastic flows, probably coming from a distant volcanic center closer to the Coranzulí Volcano, reached these lakes.

Age: Middle Miocene, supported by isotopic dating on merging tuff levels, in the Cara Cara profile, showed an age of 14.26 ± 0.10 Ma.

Laguna de los Pozuelos dome volcanic complex (Coira et al. 2004)

This complex includes lava rocks of dacite composition and dacitic pyroclastic rocks (block-and-ash flow deposits, ignimbrite flows, wave-like pyroclastic flows,

and associated mudslide deposits. This is portrayed by small sub-volcanic intrusive bodies, related to pyroclastic rocks which outcrop on the area of the Pan de Azúcar mine, Cerro León, Cerro León Chico, Chinchillas and Tunillo mines, Cerro Redondo, and their surroundings. These bodies intrude both the Ordovician basement (the Acoite Formation) and the Moreta Formation rocks.

Environment: During the Middle Miocene, the Pan de Azúcar and Cerro Redondo complex domical systems appeared in the southern and central areas of the Pozuelos depression. In the LLPB western edge, on the eastern side of Cerro Rinconada, another coeval, domical explosive-lava dacitic complex emerged, at Chinchillas and Tunillo. The Pan de Azúcar and Cerro Redondo domical complexes could represent the latest magmatic phases of a Middle Miocene caldera magmatic system, suffocated by the sedimentary cover in-filling the Pozuelos depression.

Age: Isotopic dating has registered ages of 12 ± 2 Ma for Pan de Azúcar, 12.54 ± 1.1 Ma for Cerro Redondo, and 13 ± 1 Ma for Chinchillas, which certainly place these units in the Middle Miocene.

“Peneplain” (Cratonic Erosion Surface) (Gubbels et al. 1993)

During this period, LLPB remained a cratonic high area, lacking clastic sedimentary deposits. A planation surface, whose elevation and distribution can easily be observed on aerial photographs, is exposed surrounding the entire LLPB. This area can be compared to the high area erosion surface named as San Juan del Oro, which emerged along the Central Andes, sometime between 12 and 10 Ma ago. This regional discontinuity is also found in Puna Norte, the Altiplano, and the Bolivian Eastern Mountain Range.

Coranzulí volcanic complex (Coira et al. 2004)

These rocks comprise mainly dacitic ignimbrites and dacitic vitro-crystalline tuffs. These rocks occur in the southeastern end of LLPB, forming the Chajarahuaico and Guayayoc table mountains, and extend discontinuously toward the north, along the Pucará table mountain.

Environment: During the Late Miocene, dacitic ignimbrites, erupting from the Coranzulí volcanic complex, flew into the depression of Pozuelos entering from the south, covering preexisting rocks and causing the southern closure of the LLPB.

Age: These rocks recorded an age of 6.6–6.5 Ma (Late Miocene).

Tafna Formation (Turner 1964), similar to the Casira Formation (Claire 1969)

This formation is represented by gravels, sands, clays, tuffs, and water-lain tuffs emerging on the northern shore of the LLPB from underneath the Quaternary sediments, in the Casira and Calahoyo basins.

Environment: All the materials were deposited on sedimentary basins by alluvial and/or fluvial currents, undergoing transitions of various lacustrine episodes. Volcanic ashes accumulated during these episodes, interbedded with eolian deposits (dunes).

Age: Pliocene, based upon the paleontological finding of a mesotherine, in the Casira Formation, Calahoyo (Anaya et al. 1989), together with the recent findings

of the following Xenarthra (Mammalia): *Eosclerocalyptus lineatus* Ameghino (Cingulata, Glyptodontidae) and *Macrochorobates chapalmalensis* Ameghino (Cingulata, Dasypodidae), in the Tafna Formation, at the site of Calahoyo, by Camacho et al. (2015). This age should be adjusted by future radiometric dating in tuffs.

3.5 Quaternary–Cenozoic (Fig. 5)

Pleistocene (sensu lato) (Igarzábal 1978, Camacho 2009)

Alluvial deposits (bajadas)—Level I (Camacho 2009)

These units are basically composed of fine gravel, a sandy supporting matrix, stratified fine gravel, sand with large clasts, fine to very thick sand, silty–sand, laminated silt–mud and solid mud. The measured thickness may vary from 100 m in the Colqui drill hole (Río Chorrión) to ~6 m in the Casira Basin outcrop. They spread all over the LLPB hillside. These sediments accumulated during pluvial periods, forming coalescent fans. They are the oldest Quaternary clastic deposits, which have been eroded and flattened forming a single slope or bajada. These sequences are clearly different from the aforementioned Paleozoic, Mesozoic, and Cenozoic formations (Paleogene–Neogene) (Fig. 5).

Environment: At the beginning, sediments were carried by alluvial and/or fluvial currents held by different sub-basins. There was no defined development of alluvial fans in a mountain system.

Age: These sediments are momentarily assigned to the Pleistocene, sensu lato, probably Early–Middle Pleistocene, because they are considered to be older than the Late Pleistocene lacustrine expansion. Due to the fact that this area shows a bolson-like relief, sediments previously deposited are drowned by newer ones preventing age estimation.

3.6 Late Pleistocene

Lacustrine coastline deposits (Minchín) (Igarzábal 1991, Camacho et al. 2013)

These deposits are mainly formed by fine sandy gravel, with bioherm development (algal carbonates), calcisiltite, and ostracods (Fig. 6). The lacustrine expansion began with the Last Glaciation (the Minchín Phase). During this glacial event, at the regional level, long coastlines were formed at 3695, 3680, and 3665 m a.s.l. (Fig. 7). These last two coastlines are very well preserved in the landscape.

Environment: These coastlines represent littoral coastal environments which accompany three lacustrine expansions and shrinkages, according to paleolimnological interpretation (Camacho et al. 2013). They were also complemented by the

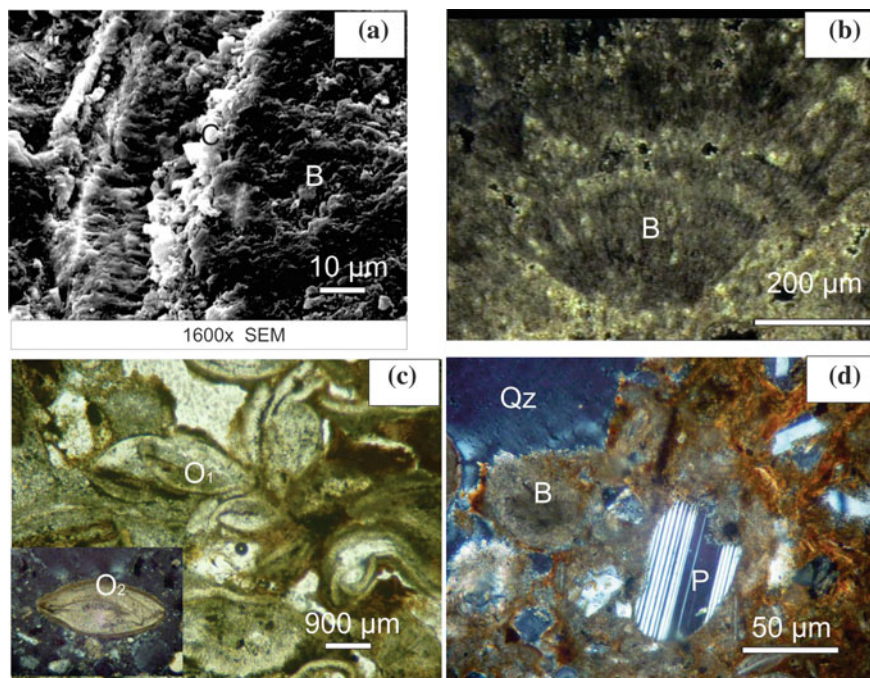


Fig. 6 **a** (SEM) scanning electron microscope image of bioherm development (*B*) and of crystalline calcite (*C*); **b** thins section photomicrograph of de coastal sediments showing their algal filaments and cone cone structure of the bioherms (*B*); **c** thins section photomicrograph of de ostracods in parallel polarizers (*O1*) in crossed polarizers (*O2*); **d** Remains of bioherms (*B*), quartz (*Qz*), plagioclase (*P*) constituting calcisiltites

development of fan-deltas (McGlue et al. 2013) and transverse Gilbertian deltas (Camacho and Bossi 2013).

Age: The first radiocarbon age, 27 ka ^{14}C B.P., was obtained by Igarzábal (1991). Later research (McGlue et al. 2013) on 4 cores extracted from the modern lake (squares 1-2-3-4, Fig. 5) allowed the correlation of these units with a probable age of ca. 43–23 cal. ka B.P.

Gilbert-type delta deposits (Minchín Phase) (Camacho and Bossi 2013)

These deposits outcrop at the mouth of the Río Corral Blanco, presenting the typical deltaic tripartite structure: (1) bottom sedimentary layers made up of mud, “bottomsets”; (2) foreset-type clinofolds, with sand layers showing cross-planar stratigraphy and (3) fine gravel “topset” layers. All these units are exposed due to neotectonic faults which have an age of ~ 15 ka. From the architectural analysis of the outcrop, a three lobe structure is easily observed. These three deltaic lobes are separated by third-order contacts (Fig. 8).

Environment: Coastal littoral, accompanying Minchín lacustrine coastlines.

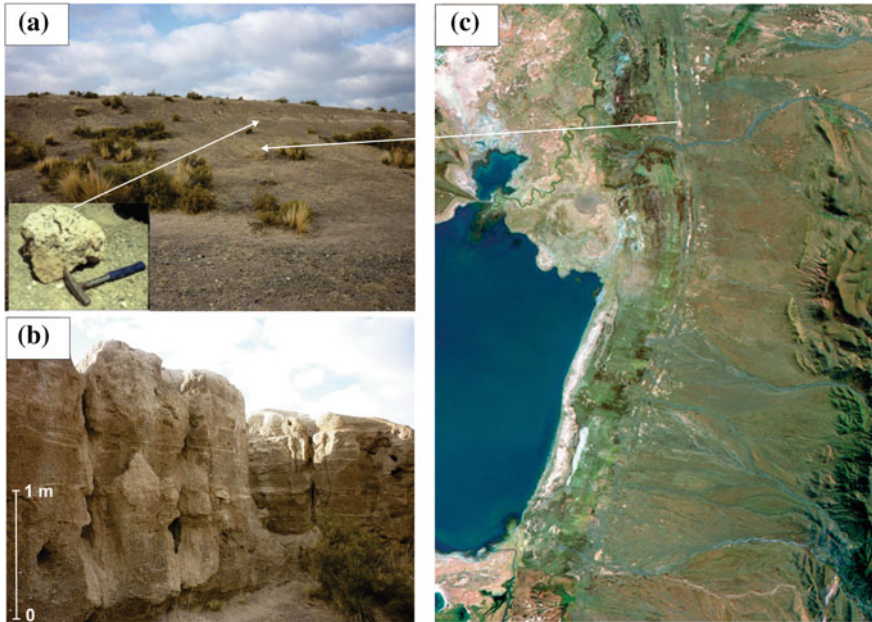


Fig. 7 Lacustrine coastline deposits (Minchín)

Age: Deltaic facies were formed during the Late Pleistocene (ca. 43 a 23 ka), at the mouth of braided rivers, during the well-known Minchín lacustrine floods and shrinkages, in the Bolivian Plateau and the Argentine Puna.

Alluvial fan deposits—Level II (Camacho 2009)

Thick gravels (cobbles and pebbles) with sandy supporting matrix, in which debris flow predominate. These units are located close to the Pleistocene s.l. deposits, the Level I alluvial fans and in erosive unconformity, at the foothill second level. They are bound both by a fault of the slope and to important variations of the general and local gradient due to neotectonic adjustment. They cover the deltaic deposits partially and the Minchín Phase delta fans and spread toward the lowest areas of the landscape. During the catastrophic events that occurred at the end of the LGM (~ 15 ka), these deposits moved forward as muddy currents within the lake, causing the lateral closure or partial obstruction of the Minchín lacustrine deposits in the towns of Pasaje and Abra Moreta (Fig. 9), and forming a peninsula near the site of Guayatayoc.

Environment: The materials of the fans were carried by alluvial and/or fluvial currents outdone by mixed hyper-concentrated flows (Gani 2004).

Age: From ca. 26 to 15 ka, based upon the morphological–stratigraphic positions, which were established based on photogeological mapping and field sections (Camacho 2009), and stimulated by neotectonic catastrophic events at the end of the Last Glaciation Maximum (~ 15 ka). The sediments were dated in the Pozuelos

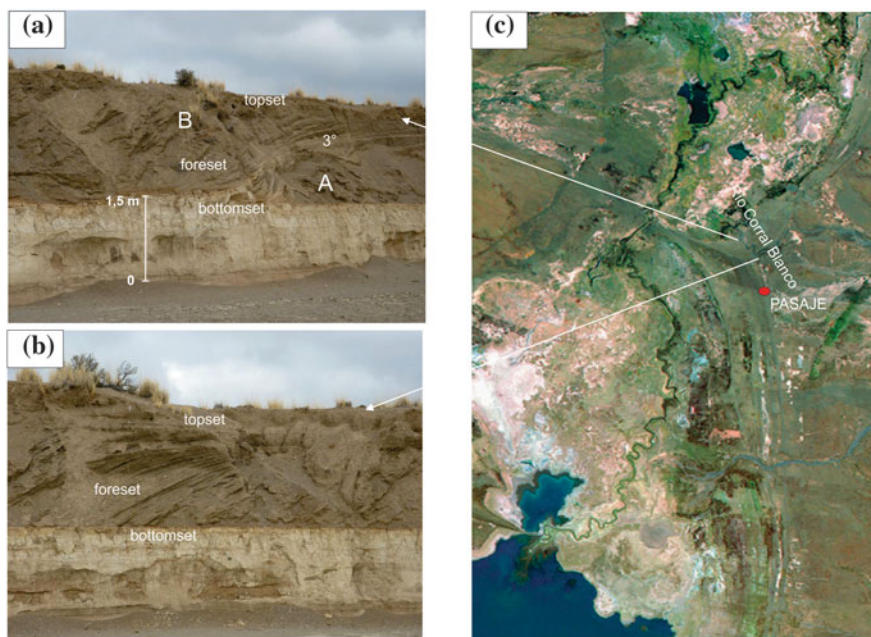


Fig. 8 View of the northeast edge of lake showing Gilbert-type delta deposits (Minchín Phase), **a** Two deltaic lobes (A and B) are separated by third order contacts; **b** Deltaic tripartite structure: bottomsets, foreset and topset layers; **c** LANDSAT satellite image

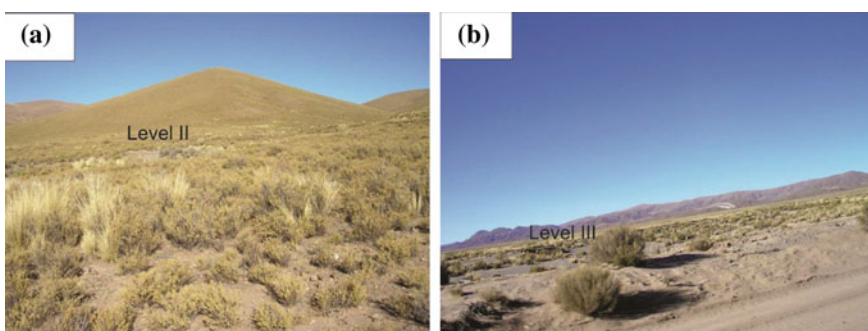


Fig. 9 View of the southeast edge of lake showing alluvial fan deposits **a** Level II and **b** Level III

drilling on the NE side of the Laguna de los Pozuelos (Camacho and Kunz 2011) and they were confirmed by the radiocarbon dating of the paleogeographic diagram suggested by McGlue et al. (2013).

Lacustrine deposits (Playa Lake) (Camacho et al. 2013)

These deposits (Fig. 10) are made up of carbonate–siliciclastic muds, gypsum, halite, together with fossil ostracods and gyttja (Fig. 11a, b). They are located toward the inner part of the Minchín lacustrine coasts.

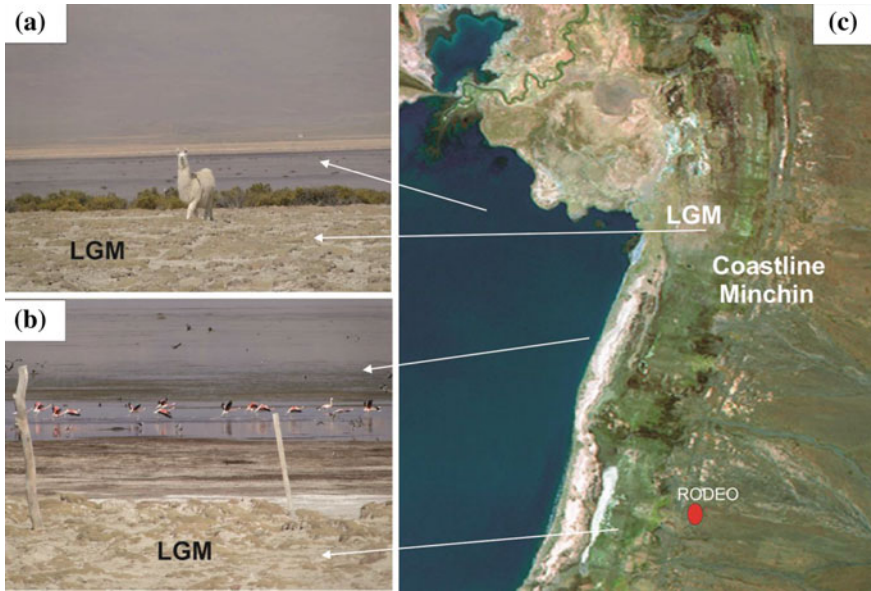


Fig. 10 View of the eastern edge of the lake showing the lacustrine deposits (Playa Lake) of the Last Glacial Maximum (LGM). **a** Lama (South American Camelidae) “llama,” standing on deposits of the LGM; **b** high-altitude water birds (flamingos) in the Laguna de Los Pozuelos, feeding in a shallow lake, of Holocene–Present age; **c** LANDSAT satellite image of the region

Environment: It began with a salt lake which signals the beginning of a more arid and, perhaps, warmer climate. This caused the precipitation of gypsum rosettes of 5 cm in diameter as well as small percentages of halite (Fig. 11c, d). Later on, there was a recovery of a short-lived lake (a Playa Lake). No coastlines were formed, only beach remnants, and the environment underwent neotectonic movements ca. 15 ka ago, reducing the area of sedimentation of the lake.

Age: Last Glacial Maximum (LGM), from ca. 23 to 15 cal. ka B.P. (Camacho and Kunz 2011).

Late Pleistocene Paleosols (Camacho et al. 2009)

These soils are representative of an extended paleopedological phase at the LLPB foothill. They are luvisols, with A-B2t-C-type profiles, presenting ochraceous epipedon and superficial argilic horizon. These paleosols are not included in Fig. 5 map due to the scale used. At depths which range from 10 to 240 cm, within Level I and Level II alluvial fans, these paleosols are covered by modern alluvial–colluvial sediments.

Age: These soils have been assigned to the Late Pleistocene, based upon a ~14–13.7 cal. year radiocarbon dating, carried out at LATYR-Universidad Nacional de La Plata, Argentina (Camacho et al. 2009). It is herein suggested that the paleosols documented conditions of greater moisture than present ones, and reflected a massive intensification of the South American Summer Monsoon (SASM), in response to northern hemisphere cooling during the Heinrich I event

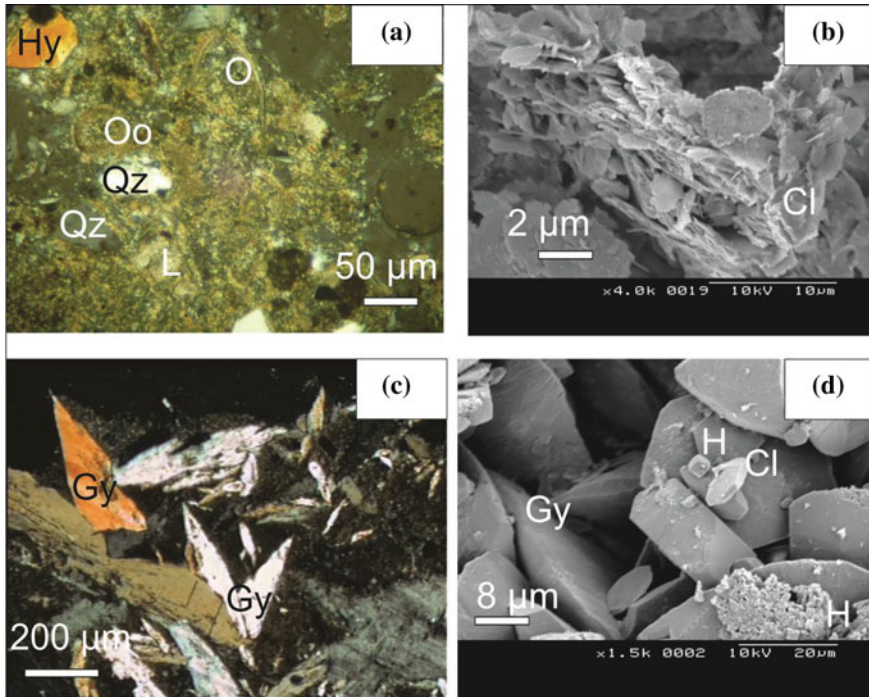


Fig. 11 Thin-section photomicrographs of the LGM sediments: **a** carbonate-siliciclastic muds with fossils of ostracods (*O*), oolites (*Oo*), quartz (*Qz*), hypersthene (*Hy*), limestone (*L*); **b** SEM image of clays (*Cl*); **c** thin-section photomicrograph of the salt lake sediments at the end of the Minchin phase, with gypsum rosettes (*Gy*); **d** SEM image of gypsum (*Gy*), halite (*H*) and clays (*Cl*)

and the resultant southward shift of the intertropical convergence zone (ITCZ) and La Niña-like conditions in the eastern equatorial Pacific Ocean (Zech et al. 2009). These conditions are correlated with the final lake transgression phase on the Altiplano-Coipasa ($\sim 13.8 \pm 1.5$ ka, Zech et al. 2009).

3.7 Holocene

Lacustrine deposits (Playa Lake) (Camacho et al. 2013)

These deposits are mainly composed of clay and silt, with a prevalence of preexisting calcareous (limestone) rocks (calcisilites), and saline precipitation (gypsum and halite). Traces of Cypris ostracods, algae (Bacillariophyceae, Cyanophyta, Chlorophyta), diatoms, and gytija are also found in the area (Fig. 12). This environment forms a natural ecosystem with very little anthropic modification, which serves as nesting area for thousands of migratory birds. These deposits are located in the central and lower part of the LLPB (Figs. 5 and 13a, b) and form the shallow lake known as Laguna de Los Pozuelos, which has been characterized as a

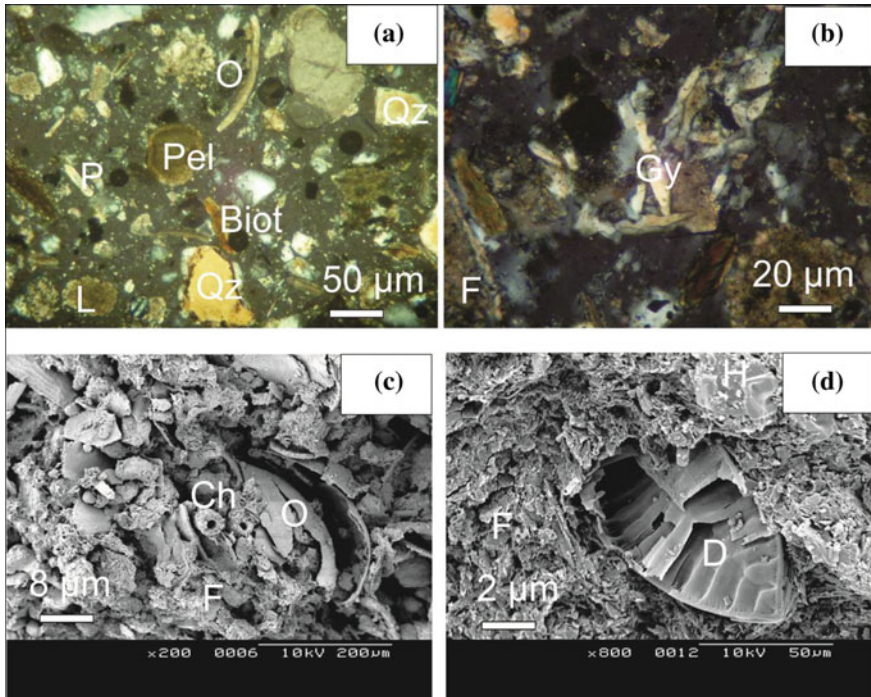


Fig. 12 Thin-section photomicrographs of the Holocene sediments: **a** carbonate-siliciclastic muds with fossils of ostracods (*O*), limestone (*L*), peloid (*Pel*), biotite (*Biot*), quartz (*Qz*), plagioclase (*P*); **b** gypsum rosettes (*Gy*); **c** SEM image of mud (*F*) with fossils of ostracods (*O*), charophytes algae (*Ch*); **d** SEM image of mud (*F*), halite (*H*), with fossils of diatoms (*D*)

biosphere reserve (IUCN category IX) and a national monument (IUCN category II), registered by the International Union for the Conservation of Nature.

Age: From the beginning of the Holocene (~11.7 ka) until present times.

Lacustrine coastline deposits (Camacho et al. 2013)

These deposits range from one to several centimeters in thickness and are composed of calcareous massive mud, with ostracods and algae. They are overlain with organic mud due to the presence of decomposed organic matter, a gyttja. The coastlines (Fig. 13a) rarely show geomorphological expressions, and their geometry is defined by its wetter zone, which appear colored as dark gray in satellite images, which displays the advances and recession of the lake, subject to climate oscillations.

Age: Beginning of the Holocene (~11.7 ka) until present times.

Flooding pools due to which the lake has been named Laguna de Los Pozuelos (Camacho 2009)

These wetlands are very unstable, both in terms of space and time (e.g., lake extension and hydro-chemistry) and display high ecological fragility. These two

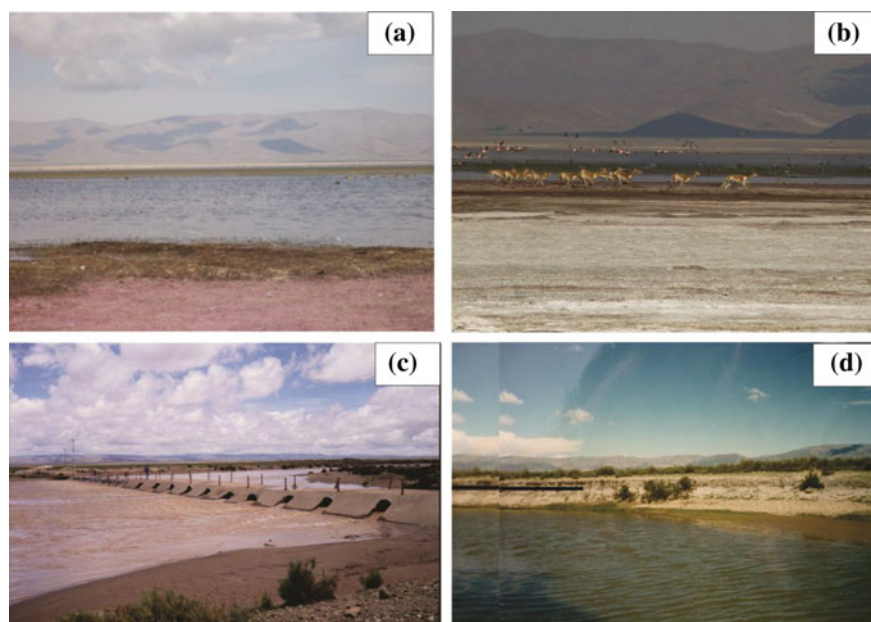


Fig. 13 View of the Laguna de Los Pozuelos in present times: **a** coastal environments marked by the growth of algae; **b** high-altitude water birds (flamingos) in flight and South American Camelidae “vicugna” (“vicuña”) in a stampede; **c** Río Santa Catalina with high discharge during the southern hemisphere Summer; **d** Río Cincel, showing peat deposits of *blackish color*, Holocene age, at the margins of the stream

traits are related to natural causes, such as prolonged droughts, high irradiation, strong winds, extreme temperature amplitudes, and underground water variations. Every pool or wetland provides habitat, resources, and alternative functions for the region and for the wildlife species in the area. The ponds and wetlands are located in low lands which used to be part of the wet Minchín phase lake, during the Late Pleistocene, but today they are empty. Besides, there are plenty of pools and wetlands behind the coastlines, formed at the Minchín phase optimal climatic conditions.

Age: Due to their stratigraphic position, these pools should be considered of Holocene age.

Level III Alluvial fan deposits (Camacho 2009)

These deposits are composed of sands, gravels, and silt with a tendency to decrease grain size. They form the foothill third level, crushed by a third level of erosion. Their distribution is very heterogeneous, located at different levels of the foothill (Fig. 9b).

Environment: After the catastrophic events that occurred ~ 15 ka ago, basement blocks reactivation changed the LLPB landscape. The course of streams acting as collectors also changed. These changes caused alluvial fans to overlay forming isolated patches scattered along the different deposits and on the alluvial fan of the

Levels I and II, expand toward depressed areas and cut not only the Minchín lacustrine coastlines, but also the LGM's lacustrine beaches.

Age: ca. 3 cal. ka B.P., based on radiometric dating of paleosols (Kulemeyer et al. 2009), related to the higher phreatic levels in valleys and probably connected to higher moisture conditions during the Middle Holocene and the older part of the Late Holocene.

Eolian deposits (dunes) (Camacho 2009)

These dunes are predominantly formed by sands and silts. They are more frequent on both banks of the Río Cincel toward the south, near Cerro León Grande and opposite to Cerro Yoritorco and the Pan de Azúcar mine (Fig. 5). Thin eolian deposits of a smaller size climb up the coastal lacustrine lines acting as a barrier preventing them from moving forward. They are eolian deposits associated both with deflation basins and dunes.

Age: Because of their stratigraphic position—they are located over the Level III alluvial fans—their estimated age is <3 ka, indicating a drier period.

Deltaic deposits (McGlue et al. 2012)

These units are composed of sands and silty clays located at the mouth of the Cincel, Colquimayo, and Santa Catalina Rivers (Fig. 5).

Riverbed and floodplain deposits (Camacho 2009)

These deposits are formed by sand, silt, and salt precipitation accumulations. They occupy the LLPB central part, on the flood plains of the meandering Cincel and Santa Catalina Rivers (Fig. 13c, d), and areas of braided transversal tributaries, which drain the sediments located east and west of the LLPB.

These sediments are spread over restricted depressed areas of the LLPB (Fig. 5).

Age: Holocene, due to its stratigraphic position.

4 Conclusions

- (1) The sedimentation in the area of LLPB began during the Oligocene-Miocene typified by deposition in a closed piggyback-type basin. Quaternary tectonic movements (ca. 2 Ma) defined a broken relief, comprised of ridges and wide, elongated intermountain valleys, depending on the dominant direction of the E–W, NNW, and SSE fractures, with endorheic drainage in the area of Laguna de Los Pozuelos.
- (2) The outcropping units in the area of the LLPB are as follows: (a) Acoite Formation, related to the Ordovician–Paleozoic Cochino–Escaya magmatic–sedimentary eruptive rocks; (b) Late Cretaceous Pírgua subgroup; (c) Late Oligocene–Early Miocene Moreta Formation; (d) Tiomayo Formation (Middle Miocene); (e) Domic Volcanic Complex Laguna de Pozuelos (Middle Miocene); (f) Coranzulí Volcanic Complex (Late Miocene), and (g) Tafna Formation, equivalent to the Casira Formation (Pliocene).

The Quaternary is represented by (1) Level I alluvial deposits (“bajadas”) previous to the lacustrine expansion (Pleistocene s.l.); (2) (a) Minchín deposits of lacustrine coastlines, (b) Gilbert-type deltaic deposits, (c) Level II alluvial deposits, (d) lacustrine LGM deposits (Playa Lake) (Late Pleistocene); and (3) (a) Lacustrine deposits (Playa Lake) (b) coastal deposits, (c) eolian deposits (sand dunes and dunes), (d) floodplain and riverbed deposits formed during the Holocene.

- (3) During the Late Pleistocene, a deep to shallow lake appeared in LLPB, in response to the climatic events occurred in the Last Glaciation, at the global level. The lacustrine expansion began with the “Minchín phase” (from ca. 43 to 23 ka B.P.). The lake reached an extension of ~ 900 to 572 km^2 in surface and a depth of ≥ 20 m. Long coastlines were formed around it, at 3695, 3680, and 3665 m a.s.l., with the development of bioherms (algal carbonates), fan-deltas, and Gilbert-type deltas. Climatic and tectonic adjustments at the end of the LGM (from ~ 23 to 15 ka B.P.) and at the Coipasa transgression phase on the Altiplano (ca. ~ 14 – 13.7 ka B.P.) reduced it to an ephemeral lake of 264 km^2 and less than 10 meters in depth. Early Holocene coastlines at 3625 m a.s.l. (11.7 ka B.P.) depict the beginning of the interglacial with a larger lacustrine expansion of 112 km^2 and only 1 m deep, ranging from 70 km^2 and 0.50 m deep, to becoming almost dry as it happened in AD 1958, 1983, and 1992. However, LLPB shows a firm recovery from 3 ka to the present with a tendency to increased rainfall.

References

- Anaya D, Pacheco FJ, Pili LA (1989) Hallazgo de Mesotherinos en la Formación Kasira (Terciario) en el Sud Boliviano (provincia Omiste, departamento Potosí). Servicio Geológico de Bolivia, Boletín, Serie A 4(1):41–46 (La Paz)
- Argollo Bautista J, Iriando MH (2008) El Cuaternario de Bolivia y regiones vecinas. Museo Provincial de Ciencias Naturales “F. Ameghino”, 378 p., Corrientes, Argentina
- Bahlburg H (1990) The “Faja Eruptiva de la Puna Oriental” in the northern Argentinian Puna revisited: granitoid emplacement in a Late-Ocloyic (Silurian?) sinistral strike-slip zone. In: 11° Congreso Geológico Argentino -1° Congreso de Exploración de Hidrocarburos, Actas, vol 2, Buenos Aires, pp 297–300
- Bianchi AR, Yáñez CE (1992) Las precipitaciones en el Noroeste argentino. 2da ed., Instituto Nacional de Tecnología Agropecuaria (INTA), Estación Experimental Agropecuaria, 383 p., Salta, Argentina
- Camacho M (2009) Sedimentología y mineralogía de los depósitos superficiales aluviales y lacustres del Bolsón de La Laguna de Los Pozuelos (BLLP), Puna Jujeña, Argentina. Unpublished doctoral thesis, Facultad de Ciencias Naturales e Instituto Miguel Lillo, Universidad Nacional de Tucumán, 205 p., Argentina
- Camacho M, Alcalde FG, Escalante JR (2009) Paleosuelos del Pleistoceno Superior en el Bolsón de la Laguna de Los Pozuelos y su significado paleoclimático, Puna jujeña, Argentina. In: Investigaciones en Facultades de Ingenierías del NOA. Facultad de Ingeniería Universidad Nacional de Salta (eds), Ciencias de la Tierra vol 1, Salta, Argentina, pp 77–81

- Camacho M, Kunz A (2011) Sedimentos del testigo de la perforación al NE de La Laguna de Los Pozuelos Actual, Puna jujeña, Argentina. In: Investigaciones en Facultades de Ingeniería del NOA. Facultad de Tecnología y Ciencias Aplicadas, Universidad Nacional de Catamarca (eds) Ciencias de la Tierra vol 1, Catamarca, Argentina, pp 375–382
- Camacho M, Zamar MI, Kulemeyer JJ (2013) Sedimentología, Mineralogía y Paleontología de los sedimentos costeros del Pleistoceno tardío-Holoceno, de la Cuenca de la Laguna de Los Pozuelos [CD]. In: Investigaciones en Facultades de Ingeniería del NOA. Facultad de Ingeniería Universidad Nacional de Santiago del Estero (eds) Ciencias de la Tierra, vol 15, Santiago del Estero, Argentina, 8 p
- Camacho M, Bossi GE (2013) Desarrollo de delta “Tipo Gilbert” transversal, durante el Pleistoceno tardío, en una cuenca lacustre de la Puna jujeña. In: Investigaciones en Facultades de Ingeniería del NOA. Facultad de Ingeniería Universidad Nacional de Santiago del Estero (Eds.), Ciencias de la Tierra, (13): 8 p., Santiago del Estero, Argentina
- Camacho M, Zurita A, Miño-Boilini AR, Rodríguez-Bualó SM, Canavidez DH, Scillato-Yane GJ (2015) El Paleambiente de la Comarca de Calahoyo, Puna Norte, Argentina. In: 3° Simposio del Mioceno-Pleistoceno del Centro y Norte de Argentina. Resúmenes, 7–8. Corrientes, Argentina
- Claire H (1969) Estudio geológico de la región de Chagua-Kasira. Unpublished doctoral thesis, Universidad Mayor de San Andrés, 58 p. La Paz, Bolivia
- Coira B (1979) Descripción geológica de la Hoja 3c, Abra Pampa, Provincia de Jujuy: Carta geológico-económica de la República Argentina, escala 1: 200.000. Servicio Geológico Nacional, SEGEMAR, Boletín 170, 90 p. Buenos Aires, Argentina
- Coira B, Caffé P, Ramírez A, Chayle W, Díaz A, Rosas S, Pérez A, Pérez B, Orosco O, Martínez M (2004) Hoja Geológica 2366-I/2166-III Mina Pirquitas. Servicio Geológico Minero Argentino, Boletín 269, 131p
- Cross S, Seltzer G, Fritz S, Dunbar R (2001) Late Quaternary climate and hydrology of tropical South America inferred from an isotopic and chemical model of Lake Titicaca, Bolivia and Peru. *Quatern Res* 56:1–9
- Gani MR (2004) From turbid to lucid: a straightforward approach to sediment gravity flows and their deposits. *Sediment Rec* 2(3):4–8
- Gubbels TL, Isacks BL, Farrar E (1993) High level surfaces, plateau uplift, and foreland development, Central Bolivian Andes. *Geology* 21:695–698
- Harrington HJ (1957) Ordovician formations of Argentina. In: Harrington HJ, Leanza AF (eds) Ordovician trilobites of Argentina. Department of Geology, University Kansas. Special Publication 1:1–59
- Igarzábal AP (1978) La laguna de Pozuelos y su ambiente salino. Departamento de Rinconada Provincia de Jujuy, *Acta Geologica Lilloana* 15(1):79–103 (Tucumán, Argentina)
- Igarzábal AP (1991) Evaporitas cuaternarias de la Puna Argentina. In: Génesis de formaciones evaporíticas: Modelos Andinos e Ibéricos. Pueyo JJ (Coord.), Universitat de Barcelona, Pub 2:333–373 (Barcelona)
- Kulemeyer JJ, Camacho M, Escalante JR (2009) Paleosuelos del Holoceno Superior en el Norte de la Puna Jujeña, Argentina. In: 4° Congreso Argentino de Cuaternario, Actas, vol 301
- McGlue MM, Ellis GS, Cohen AS, Swarzenski PW (2012) Playa-lake sedimentation and organic matter accumulation in an Andean piggyback basin: the recent record from the Cuenca de Pozuelos, north-west Argentina. *Sedimentology* 59:1237–1256
- McGlue MM, Cohen AS, Ellis GS, Kowler AL (2013) Late Quaternary stratigraphy, sedimentology and geochemistry of an underfilled lake basin in the Puna plateau (northwest Argentina). *Basin Res* 25:1–21
- Placzek CJ, Quade J, Patchett PJ (2013) A 130 ka reconstruction of rainfall on the Bolivian Altiplano. *J Earth Planet Sci Lett* 363:97–108
- Reyes FC, Salfity JA (1973) Consideraciones sobre la estratigrafía del Cretácico (Subgrupo Pirgua) del Noroeste Argentino. In: 5° Congreso Geológico Argentino, Actas vol 3, pp 354–385

- Seggiaro RE, Aniel B (1989) Los ciclos piroclásticos del área Tiomayo-Coranzulí, Provincia de Jujuy. *Revista de la Asociación Geológica Argentina* 44(1-4):394-401 (Buenos Aires, Argentina)
- Turner JC (1959) Estratigrafía del cordón de Escaya y de la Sierra de Rinconada (Jujuy). *Revista de la Asociación Geológica Argentina* 13(1-2):15-39 (Buenos Aires)
- Turner JC (1964) Descripción geológica de la hoja 2, La Quiaca, Provincia de Jujuy: Instituto Nacional de Geología y Minería, Boletín 103, 90p (Buenos Aires)
- Zech J, Zech R, Kubik PW, Veit P (2009) Glacier and climate reconstruction at Tres Lagunas, NW Argentina, based on ^{10}Be surface exposure dating and lake sediment analyses. *Palaeogeogr Palaeoclimatol Palaeoecol* 284:180-190
- Zhou J, Lau KM (1998) Does a monsoon climate exist over South America? *J Clim* 11:1020-1040

Calcium Biomineralizations Associated with Bioclastic Deposits in Coastal Pedostratigraphic Sequences of the Southeastern Pampean Plain, Argentina

Margarita Osterrieth, Natalia Borrelli, Celia Frayssinet, Lucrecia Frayssinet and Juan Cresta

Abstract The biomineralization process is genetically controlled, and it is the result of the metabolic activity of different organisms. Microorganisms, plants and animals produce calcium biomineralizations, calcium oxalates and carbonates being the most representative. The Quaternary pedosedimentary sequences of the southeastern coast of Buenos Aires province evolved from bioclastic and loess sediments, reworked by water and/or wind action. Calcium biomineralizations play an important role in the development of soils and contribute to differentiate sedimentary levels affected by pedogenesis. This work aims to characterize calcium biomineralizations in bioclastic, loessic and fluvio-eolian pedosedimentary sequences, typical of coastal environments of the southeastern Buenos Aires province. Modal soil profiles were defined in pedosedimentary sequences of the fluvio-eolian and coastal plains, in which disturbed and undisturbed samples were analyzed. Samples were analyzed at different scales of resolution: mesoscopic, microscopic and submicroscopic, using optical microscopy and scanning electron microscopy/energy-dispersive X-ray spectroscopy (SEM/EDX). Organic matter

M. Osterrieth (✉) · N. Borrelli · C. Frayssinet · L. Frayssinet · J. Cresta
Facultad de Ciencias Exactas y Naturales, Instituto de Geología
de Costas y del Cuaternario, Universidad Nacional de Mar del Plata,
C.C. 722, Correo Central, 7600 Mar del Plata, Argentina
e-mail: mosterri@yahoo.com.ar

M. Osterrieth · N. Borrelli
Instituto de Investigaciones Marinas y Costeras, Universidad Nacional
de Mar del Plata and CONICET, Peña, 4046 Mar del Plata, Argentina

N. Borrelli
CONICET, Buenos Aires, Argentina

M. Osterrieth
CIC, Comisión de Investigaciones Científicas, Buenos Aires Province, Argentina

content, pH, particle size distribution, mineralogy and calcium content were also quantified. Three geopedological units were differentiated in a sequence developed on loess mantle deposits: dunes and interdunes, coastal lagoon/paleo-coastal lagoon and shell ridges. In soils with incipient development, calcium biomineralizations are scarce, mainly associated with isolated bioclasts. In soils with more pedological development, bioclasts are affected by bioerosion through microorganism action (fungi and algae), and subsequently calcium re-precipitated as secondary oxalates and carbonates (biomineralizations). These biomineralizations also weakly add or bind skeletal components, incorporating themselves into the matrix of soils and sediments. The type and diversity of calcium biomineralizations increase directly in relation with time and pedogenetic evolution; so, these biomineralizations have been determinant in the origin, evolution and resistance to natural and anthropic degradation of the late Quaternary pedosedimentary sequences of southeastern Buenos Aires province, Argentina.

Keywords Calcium oxalate · Calcium carbonate · Calcimorphic soils · Microorganisms · Mineral chemistry

1 Introduction

The biomineralization process is genetically controlled; it generates paracrystalline or crystalline biominerals and amorphous compounds, produced by the metabolic activity of different organisms. Biomineralizations have accompanied the evolution of life from the earliest appearance of biota on the planet, thus being present at all levels of the biosphere (Lowenstan 1981; Osterrieth 2004; Coe et al. 2014). Biomineralizations give a selective advantage to organisms that produce them and favor several biological functions; for example, biominerals and amorphous compounds act as a sink of ions that can be reutilized when necessary (Simkiss and Wilbur 1989). Calcium, iron and silicon biomineralizations are the most common in the planet, and among them, calcium carbonate polymorphisms are the most widely found (Mann 2001).

Calcium biomineralizations are produced by microorganisms (bacteria, algae, fungi, actinomycetes), plants and animals (Graustein et al. 1977; Osterrieth and Oyarbide 1998; Osterrieth et al. 1998). Calcite, vaterite and aragonite are the major minerals in animals, whereas in plants, calcium oxalate—both whewellite (dihydrated, $\text{CaC}_2\text{O}_4 \cdot 2\text{H}_2\text{O}$) and weddellite (polyhydrated, $\text{CaC}_2\text{O}_4 \cdot (2+x)\text{H}_2\text{O}$)—is the most representative (Arnott 1982). These biomineralizations originate through processes mediated by an organic matrix, structure or mold: organisms constitute a structure or mold where the ions are introduced and induced to precipitate and crystallize. In fungi, from the first identification by Schmidt in 1847 (Horner et al. 1983), the presence of calcium biomineralization has been widely studied in

vegetative and reproductive structures (Osterrieth et al. 1998). The biomineralization process occurs intra- and/or extracellularly, and it is associated with vegetative growth, degradation of organic resource and the activity of mycorrhizal species. The latter produces calcium oxalate salts on the walls of the hyphae by the reaction of excreted oxalic acid and calcium available in the environment (Verrecchia et al. 1993). Species producing calcium oxalate crystals include mycorrhizal basidiomycetes: *Hysterangium crassum*, *Paxillus involutus* (Lapeyrie et al. 1990); ascomycetes: *Dasyscypha capitata*; and mucorales: *Mucor mucedo*, *M. phimbesis*, *Cunninghamella echinulata* (Horner et al. 1983; Cromack et al. 1979) and *Trichoderma koningii* recently included among the fungi that produce calcium biomineralizations (Osterrieth et al. 1998; Oyarbide et al. 2001).

Calcium biomineralizations generate structures with a variable structural complexity ranging from single crystals to aggregates (Mann 2001). The aggregated units are usually placed in an order, and the crystallographic axes are partially or entirely aligned. These ordered structures are generally differentiated in a number of microarchitectural units, each of which is wrapped by a film, coating or organic membrane called *biofilm* (Lowenstam 1981; Jahren 1996; Addadi et al. 2003).

In the last thirty years, calcium biomineralizations have been widely reported in sedimentary sequences of different environments in the world (James 1972; Klappa 1980; Verrecchia et al. 1993, 1996). Research has also increased on the role in the pedological processes of Calcimorphic and Rendzina soils, among others (Verrecchia et al. 2006; Tuason et al. 2009; Aragno et al. 2010; Dhami et al. 2013) and in the genesis and degradation of calcretes (Verrecchia and Verrecchia 1994; Verrecchia 1990, 1994; Verrecchia et al. 1995). The latter processes are the result of a biochemical sequence that starts as calcium oxalate—whewellite ($\text{CaC}_2\text{O}_4 \cdot \text{H}_2\text{O}$) and/or weddellite ($\text{CaC}_2\text{O}_4 \cdot 2\text{H}_2\text{O}$)—and ends as calcite (CaCO_3) in a stable and definitive form (Verrecchia and Verrecchia 1994; Verrecchia 1990, 1994; Verrecchia et al. 1993; Loysi et al. 1999; Osterrieth 2005).

Bioerosion is another process associated with biomineralization. It occurs due to the dissolution or erosion of the surface of minerals, fissures and the drilling of minerals and/or biominerals. This process has been underestimated by scientists, in spite of its high impact on all environments, especially in calcium biomineralizations developed in aqueous environments (Warme 1975). These processes are of great interest in the research on corrosion of both natural and artificial materials (archaeological and paleontological materials, artwork, monuments, metal alloys, steels, etc.).

The Quaternary pedosedimentary sequences of the southeastern coast of Buenos Aires province evolved from bioclastic and loess sediments, reworked by water and/or wind action. They have been affected by a succession of marine and terrestrial actions, associated with sea level changes, which have generated landforms and microlandforms in a changing water regime. During the last sixty years, they have been studied from geological, sedimentary, paleontological and paleoecological perspectives (Ameghino 1908; Frenguelli 1935, 1950; Fidalgo et al. 1973,

1991; Violante 1992; Violante et al. 2001; Isla 1989; Schnack et al. 1982, 1984; Schnack and Gardenal 1979; Tricart 1973; Osterrieth and Martínez 1993; Osterrieth and Schnack 1984; Osterrieth 2005; Bortolus et al. 2001; Espinosa 1994, etc.).

Closely associated with coastal landforms, different soil types are developed, in which calcium biomineralizations play an important role. Soil is open, complex, pluri-structural and multifunctional, with numerous definitions according to the discipline involved in its analysis. In summary, “soil is a natural resource that varies continuously in space and time,” whose structure and function are little known, and whose properties are transient and change in space and time (Jenny 1941; Simonson 1959; Ibáñez et al. 2000).

The coastal pedosedimentary sequences developed during the late Quaternary have acquired diagnostic features and experienced environmental changes of varying intensity in short time intervals, resulting in a succession of specific soil bodies (Osterrieth and Schnack 1984; Osterrieth and Martínez 1993; Osterrieth 1998). Differentiating sedimentary levels affected by pedogenesis is not always easy: it depends on the intensity with which it disturbed the parent materials, and on whether there were erosional processes, diagenetic calcification or decalcification, saturation conditions, syn- or post-pedogenetic processes, etc. Few studies use tools originated in pedosedimentary studies based on interdisciplinary biomineralogical studies. Our approach is part of the challenge to pursue studies in a field that is still weak in Argentina.

This work aims to characterize calcium biomineralizations in bioclastic, pedosedimentary sequences, typical of coastal environments of southeastern Buenos Aires province.

2 Materials and Methods

The site under study is located in the coastal areas of Mar Chiquita and General Pueyrredón counties, Buenos Aires province (34°–39°S and 57°–63°W) (Fig. 1). After detailed preliminary field studies, modal soil profiles were defined in pedosedimentary sequences of the fluvio-eolian plain and coastal plain (Schnack et al. 1982). Across a toposequence, the horizons of the modal profiles, disturbed and undisturbed samples were described according to Soil Taxonomy (1996) (Figs. 1 and 2).

For each sample, pH in 1:1 paste was measured with a digital Orion Research 501 pH meter, the organic matter content was calculated (Walkley 1965; Black 1965) and the particle size distribution was assessed with sieve and pipette analysis (Ingram 1971; Galehouse 1971). Calcium content was determined according to Dawis and Freitas (1970).

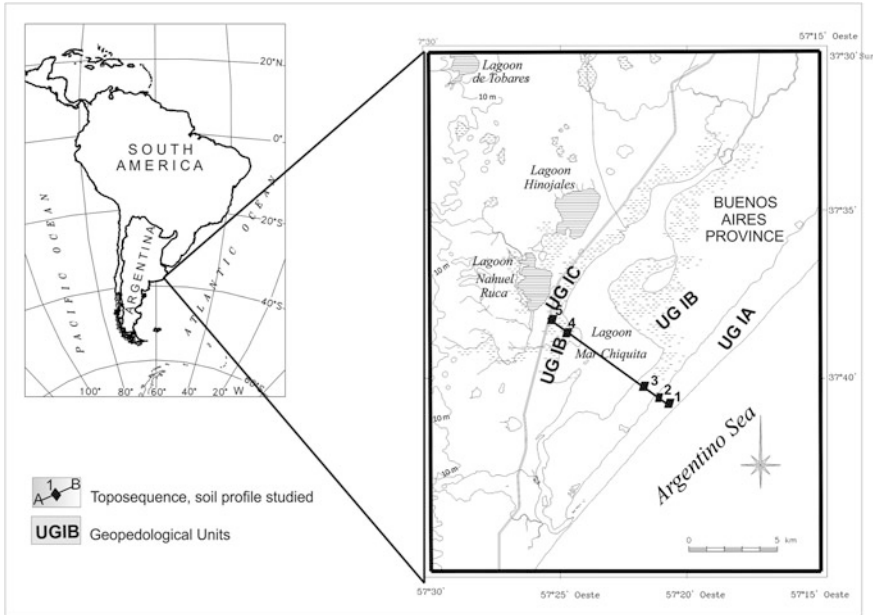


Fig. 1 Map of the study area. Location of toposequence and geopedological units (UGIA, UGIB, UGIC), and profiles studied (1–5)

In all the disturbed samples, loose grains, peds, skeletal fraction and matrix were analyzed at different scales of resolution: mesoscopic (binocular magnifying glass), microscopic (polarization microscope, PM, Olympus BX51P) and submicroscopic (scanning electron microscopy—SEM—JEOL JSM 6460 LV), and semi-quantitative studies of elementary components through microdispersive analysis with X-ray spectrometer (EDXS), operating between 15 and 25 kV. Mineralogical studies were carried out concentrating light and heavy minerals with sodium polytungstate at a density of 2.89 g/cm³.

Undisturbed samples of 30 × 30 mm and 1 × 1 mm were analyzed with polarized and scanning electron microscopy according to Brewer (1964) and Bullock et al. (1985). The identification and description of calcium oxalates and calcium carbonates were carried out according to Verrecchia et al. (1995) and Verrecchia and Verrecchia (1994), respectively. The characterization of calcified filaments was carried out based on the definition of Klappa (1979).

Dating by ¹⁴C was performed at LATYR (Universidad Nacional de La Plata, Argentina) on bioclastic material of *Heleobia* sp., *Tagelus plebeius* and *Mactra isabelliana*.

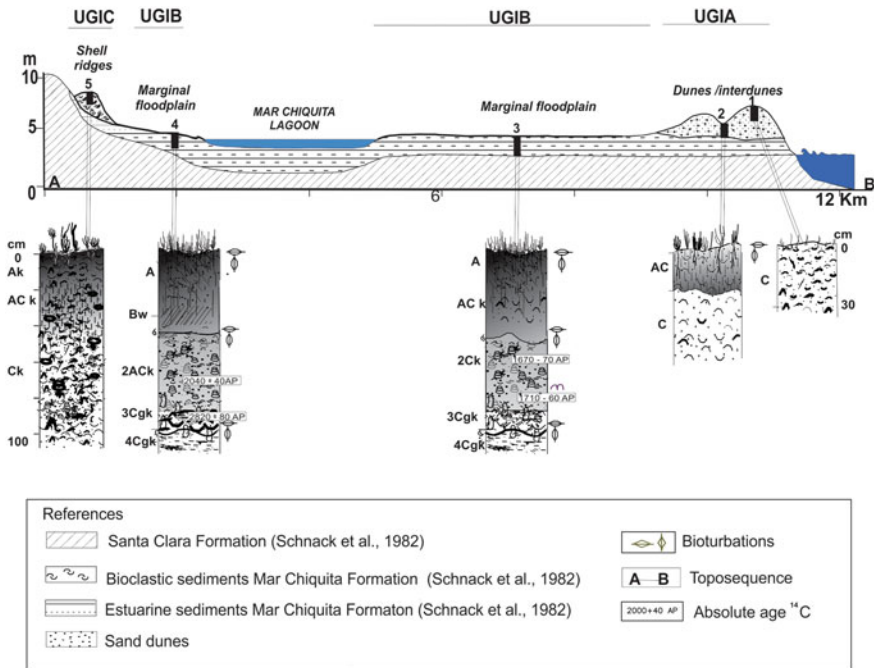


Fig. 2 Toposequence, geopedological units, pedosedimentary and modal profiles studied (modified of Schnack et al. 1982)

3 Results and Discussion

The study area is located in the coastal lagoon of Mar Chiquita and is part of the Pampa, as defined by Frenguelli (1950). The study site includes the following geomorphological zones: coastal dunes, marginal plains, shell ridges and continental deposits (Schnack and Gardenal 1979) (Figs. 1 and 2). The sedimentary characteristics vary in relation to the climate, the water body and the alternation of transgressive–regressive coasts from the Late Pleistocene to the present. The studied sequences evolved from ancient coastal deposits linked to the last transgressive–regressive cycle of the Late Pleistocene and Holocene. Discordant deposits of the Mar Chiquita Formation are located over the Santa Clara Formation (Schnack et al. 1982), composed by Pampean loess and silts (Frenguelli 1950). The Mar Chiquita Formation is composed of both marine beach facies, formed by ridges of an age of approximately 6000 years BP (Schnack et al. 1982) and coastal lagoon facies formed by estuarine deposits with abundant whole and partially fragmented bioclasts. These mollusk shells include *Heleobia* sp., radiocarbon dated at 1670 ± 70 year BP, *T. plebeius*, dated between 1710 ± 60 and 2880 ± 90 year BP, and *M. isabelliana*, at the bottom of the profile, dated at 2820 ± 80 year BP

(Schnack et al. 1982; Osterrieth 1998). This area of study has been closely associated with the evolution of the coastline and/or to the fluctuations of the sea level which took place during the transgressive–regressive cycle of the Holocene (Schnack et al. 1982).

The climate is mesothermic and subhumid, with little or no water deficiency (Burgos and Vidal 1951). The annual precipitation averages 809 mm. The average annual temperature is 13.7 °C; the mean minimum temperature reaches 8.1 °C in June, with an average maximum of 19.8 °C in January (Servicio Meteorológico Nacional of Argentina at the city of Mar del Plata, according to the 1920–1980 records).

The study area is an ecotone with specific biotic characteristics. These environments, broadly characterized as wetlands, are among the richest in the world in terms of their high biological diversity of both vertebrates and invertebrates (Mistch and Gopsselink 1993). Plant communities of coastal lagoons support very complex food chains, the dominant communities being “flechillar,” wet meadows, salty meadows, “Espartillar,” “Duraznillar,” “Hunquillar” and dune vegetation (Vervoorst 1967; Isacch 2001).

The dominant soil assemblages in the study area are composed of Udipsamments on coastal dunes, calcimorphic soils and Rendzinas on shell ridges, saline and calcimorphic soils, Endoaquolls, Calciaquolls and Hapludolls on estuarine sediments of the low and flooded areas surrounding the Mar Chiquita lagoon.

Such geopedological characteristics have conditioned the evolution of this complex coastal system, where pedological processes associated with calcic biomineralizations have furthered the understanding of their genesis. The work was made on five modal profiles across a toposequence (12 km), in the coastal and mixed typical geopedological units (Figs. 1 and 2).

4 Mixed Coastal Environment

Three geopedological units were differentiated in a sequence developed on loess mantle-shaped deposits: dunes and interdunes (UGIA) (Profiles 1 and 2), coastal lagoon/paleo-coastal lagoon in the Mar Chiquita lagoon marginal floodplain (UGIB) (profiles 3 and 4) and shell ridges (UGIC) (Profile 5).

5 Geopedological Unit of Dunes and Interdunes (UGIA)

The studied soils are located in the dune barrier extending from the Mar Chiquita lagoon to Punta Rasa (Fasano et al. 1982) (Figs. 1 and 2).

Soils in dune crests (Profile 1) are subject to strong wind and marine activities (Fig. 3a). They are sandy Mineral soils (typic Udipsamment) with textural unimodal distribution, and the medium and fine sands being the main fractions (Table 1). Soils are light gray (10YR 7/2), exhibiting little evidence of pedogenic

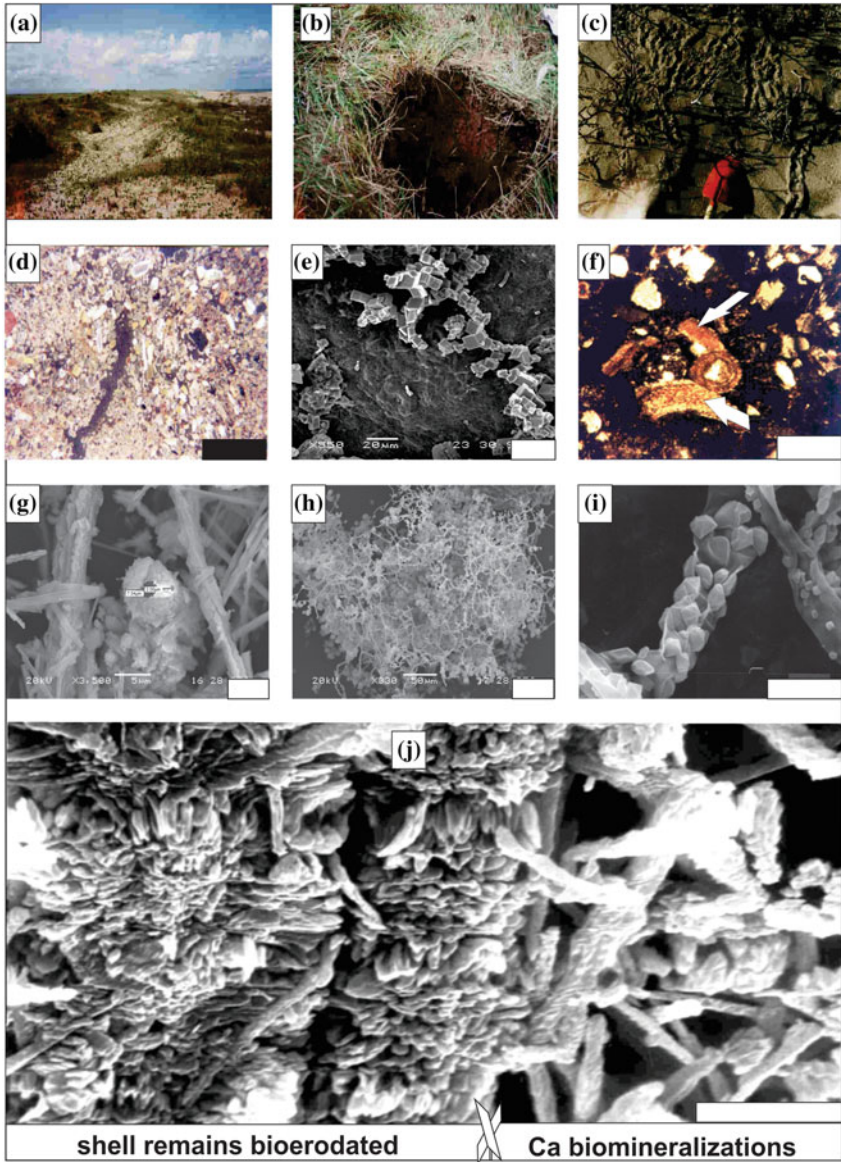


Fig. 3 **a** Panoramic view of UGBI, and plant communities. **b** Detail of oxyaquic Udipsammits (P2). **c** Detail of bioturbations in present soils. **d** Mesoscopic view of apedal microstructure in AC horizon (P2), bar: 100 μ m. **e** SEM image of an oxalate crystal to fungal activity in isolated grain (P1), bar: 20 μ m. **f** Microscopic microstructure (PM) view with bioclasts (*white arrow*) of AC, P2, bar: 100 μ m. **g** SEM image of filaments and tubes calcified (AC, P2), bar: 100 μ m. **h** SEM image of filaments and tubes associated with fungal hyphae, in AC, P2, bar: 50 μ m. **i** SEM image of oxalate crystals in the fungal hyphae filaments, bar: 5 μ m. **j** SEM image interface in shell/Ca biomineralizations, bar: 100 μ m

Table 1 Chemical, grain size and mineralogical characteristics of the pedosedimentary sequences studied

Soil profile	Horizon	Depth (cm)	Organic carbon (%)	Organic matter (%)	pH	CaCO ₃ (%)	Grain size (%)			Light minerals (%)	Heavy minerals (%)
							Sand	Silt	Clay		
P1	C	0-30*	0.08	0.14	8.2	12	99	1	0	82	18
	AC	0-20	0.30	0.62	8.4	18	83	16	1	91	9
	C	20-50*	0.08	0.14	8.8	15	92	8	0	83	17
P3	A	0-22	4.60	8.00	7.0	5	50	28	22	93	7
	ACk	22-45	1.80	3.20	8.1	20	46	34	20	94	6
	2Ck	45-75	0.35	0.65	8.5	38	73	25	2	88	12
	3Cgk	75-90	0.34	0.64	8.6	27	46	44	10	93	7
	4Cgk	90-100*	0.21	0.30	8.2	15	33	53	14	98	2
P4	A	0-25	3.90	6.70	7.8	19	39	41	20	95	5
	Bw	25-40	3.60	6.30	7.7	16	35	39	26	98	2
	2ACk	40-85	1.20	2.07	8.0	23	63	24	13	92	8
	3Cgk	85-100*	0.20	0.30	8.4	17	32	48	20	96	4
	4Cgk	100*	0.11	0.21	8.3	15	17	64	19	92	8
P5	Ak	0-35	4.70	8.22	8.0	23	40	33	27	96	4
	ACk	35-68	0.60	1.03	8.7	40	28	66	6	91	9
	C	68-200*	0.20	0.30	8.9	36	17	80	3	90	10

development, with no organic matter. They are colonized by scarce vegetation (*Spartina ciliata*, *Panicum racemosum*), except in those areas undergoing fixing and afforestation. They are excessively drained and highly permeable soils, and they are impacted by bioturbations of both vertebrates and invertebrates (Fig. 3c). They have a higher content of calcium carbonate associated with the presence of abundant shell remains, which, added to the influence of sea spray, generates a moderately alkaline pH (Table 1).

Light and heavy minerals in the medium and fine sand fractions indicate higher levels of rounded shells, as most of the observed minerals. Due to coastal dynamics (Teruggi 1959), the maximum concentration of heavy minerals was found in the fine sand fraction, where pyroxene, epidote, amphibol, opaque minerals, biotite, garnet and tourmaline prevail. Lighter minerals are characterized by quartz, plagioclase, lithic fragments, volcanic glass and abundant bioclasts (Table 1; Fig. 3f).

The bioclasts or shell fragments are fibrous and rounded, granular and/or partially weathered. At the surface, there are few fibrous calcium biomineralizations, with crystal morphologies (filaments and rods or rollers) of varying sizes, ranging from 0.5 to 10 μm (Fig. 3e, g–j).

Soils in the interdune area (Profile 2) have slight development (oxyaquic Udipsamment) with AC and C horizons; they are of a yellowish brown color (10YR 5/2), and present abundant shell remains and an important density of Bioturbations by both invertebrates (carabids) and vertebrates (*Ctenomys talarum*) (Antenuchi and Busch 1992) (Fig. 3b, c). The physico-chemical characteristics are similar to the dune crest profile, but most vegetation cover (*S. ciliata*, *Androtrichum trygynum*, *Cakile maritima*) generates an increase of 0.6% in organic matter content. The reaction is slightly alkaline and carbonate content is highest in the AC pedogenetic horizon (25%) (Table 1). They are sandy soils with a predominance of very fine, fine and medium sand fractions. The textural distribution is irregular, with poly-modal design in pedological horizons, showing an increase in the fine silts reaching up to 16% (Table 1).

The light minerals are predominant and are composed of quartz, plagioclase, lithic fragments, volcanic glass and abundant bioclasts (Fig. 3f). Heavy minerals do not exceed 17% in the AC/C horizons, including pyroxene, epidote, amphibol, opaque minerals, biotite and abundant minerals covered by iron oxides (Table 1, Fig. 3d).

The microstructure of the AC horizon is apedal (with some instances of very weak pedality); the loose grain is slightly connected by low mineralized organic matter, amorphous iron and/or little biogenic oxalates and calcium carbonate. It has a great number and variety of holes where bioturbation structures filled with materials enriched with MOS and/or iron oxides are common (Fig. 3d, f).

The microdispersive analyses (EDXS) with beryllium window (unable to detect C and O) showed that the matrix is predominantly composed of carbon, calcium, sodium and chlorine. In the coating of mineral grains, calcium, iron and sodium predominate, whereas in the coating of bioclasts there is a predominance of calcium oxalates and carbonates, followed by sodium and magnesium.

6 Calcium Biomineralizations

The shells are always present, with maximum values in the C horizon. They are rounded, with a cloudy appearance, and have abundant calcium biomineralizations associated with remnants of shells, forming an intricate network of very small calcified organic filaments (Fig. 3e, g–j). The term “filament” describes any tubular and/or rod-like organic structure that is not, or is slightly, calcified. The term “calcified filament” describes a structure where biogenic calcium carbonate replaces the filament and has precipitated on the shells (incrustation) or inside the shells (impregnation) (Klappa 1979). International studies on these biomineralizations are numerous (Arnott 1982; Verrecchia et al. 1993, 1995). These calcified filaments, on the bioclastic material of the AC horizon, conform an intricate network of elongated tubes of several tens of microns long and 3–8 μm wide; they are dichotomous, with a central hollow channel of 0.5–4 μm . Solid elongated rods of 20 μm of length and 0.5–1 μm of width are also present (Fig. 3g–j). The shells have a fibrous and porous appearance, and the depressions on their surface are very common, perhaps due to bioerosion processes (Warne 1975; Jahren 1996) (Fig. 3j). There are few variations in the surface elemental composition of the tubes and shells; calcium predominates, whereas iron is abundant in the wall of the shell but almost unnoticeable in the calcified filament. In some calcified filaments, secondary calcite and some stylets typical of calcium oxalate of fungal origin (Verrecchia and Verrecchia 1994) were observed, in oxyaquic Udipsamment soils predominantly (Fig. 3g–j).

In summary, calcium biomineralizations are scarce in typical Udipsamment (crest of the dunes), associated mainly with isolated bioclasts with different sand sizes. In the AC/C pedological horizon of the interdune soils, there is a greater number of bioclasts impacted by bioerosion. These dissolution processes are generated by the action of microorganisms (fungi and algae), which subsequently re-precipitated as secondary oxalates and calcium carbonates (biomineralization), coating the bioclasts and other mineral grains. Moreover, they weakly add or bind skeletal components, incorporating themselves into the matrix of soils and sediments. In general, they are fibrous and have various crystal morphologies such as filaments, rods and tubes (Fig. 3e, g–j).

7 Geopedological Unit of Coastal Lagoon/Paleo-Coastal Lagoon (UGIB)

The pedosedimentary sequences have developed in the marginal plain of the Mar Chiquita lagoon, from estuarine sediments linked to the last transgressive–regressive cycle of the Holocene (Schnack et al. 1982). The relief is flat and irregular, characterized by a microrelief associated with the presence of marshes, old tidal

channels and reworked bioclastic deposits. Whole and partially fragmented individuals of *Heleobia* sp., *T. plebeius*, and *Mactra* sp. are abundant, with ^{14}C ages between 1670 ± 70 and 2820 ± 80 (Schnack et al. 1982; Osterrieth 1998). In the area, grassland “espartillares” predominate, mostly composed by *Spartina densiflora* and *S. alterniflora* (Vervoorst 1967; Isacch 2001). Soils are moderately developed (without the full solum): mainly Endoaquolls, Natraquolls, Calciaquolls and Hapludolls; they are conditioned by hydrological variations related to the dynamics of the coastal lagoon.

Profile 3 developed from reworked bioclastic sediments, located between the Mar Chiquita lagoon and the dune barrier, and it is impacted by hydrological changes and episodic sea entries (Figs. 1 and 2).

The vegetation covers the soils completely, and it consists of *Cortaderia selloana*, *P. racemosum*, *Juncus* sp., etc. (Fig. 4a).

The soils have epipedons of a length of more than 20 cm, composed of surface horizons A-AC. Bioclasts are abundant and increase toward the base of the profile. The colors range from very dark grayish brown (10YR 3/1) to pale gray (10Y 7/2). They are imperfectly drained soils with slow permeability due to the presence of secondary calcium carbonate that hardened bioclastic levels. Concretions and iron coatings evidence hydromorphism conditions, which allow us to classify them as typic Endoaquolls (Fig. 4b).

Soil reaction ranges from moderately alkaline in the surface to alkaline at the base of the sequence. The organic matter content is moderate in the A horizon, descending sharply toward the base of the profile. The calcium carbonate content, associated with bioclastic materials, increases toward the lower horizons (Table 1).

The sequence is texturally homogeneous, the fine and very fine sand fractions being dominant. Distribution is mostly unimodal, except in the pedological horizons: this is due to a slight increase in clays and silts.

The lighter minerals dominate the entire sequence, composed of bioclasts (Fig. 4e), feldspar, lithoclasts, volcanic glass, minerals coated by brown to reddish oxides or amorphous, quartz and muscovite. Heavy minerals are composed of pyroxene, opaque minerals, covered minerals, amphibol, epidote, tourmaline, garnet and zircon, in order of importance. In the silt fraction, other amorphous silica biomineralizations, like silicophytoliths and diatoms, predominate (Table 1).

The microstructure of the pedological horizons (A, ACk) is weak pedality; the grain is connected by mineralized organic matter, amorphous iron, and common biogenic oxalates and calcium carbonate (Fig. 4d). The coarse minerals (or pedological horizon skeleton) consist of fine sand-silty, with a predominance of lighter and heavy minerals abundant shells and remains of shells (Fig. 4d).

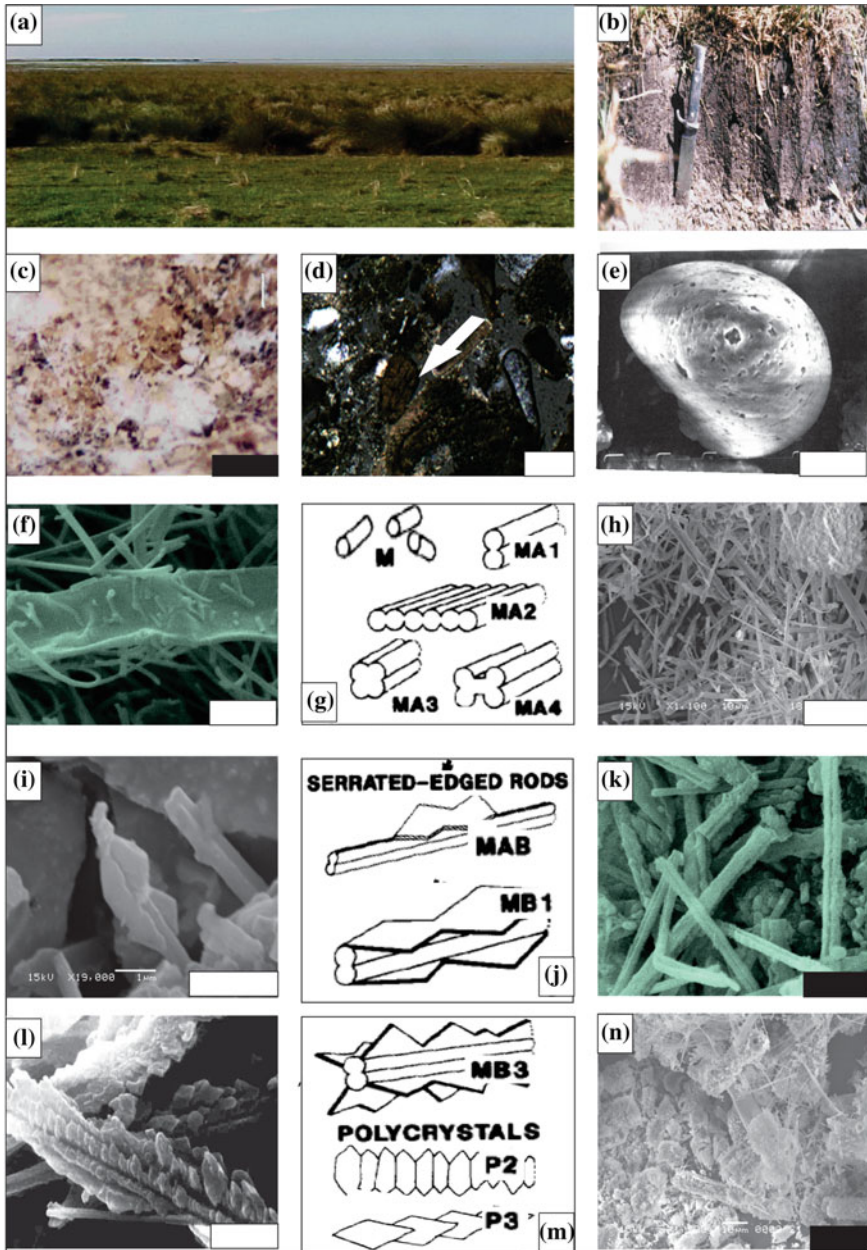


Fig. 4 **a** Panoramic view of UGBI, and plant communities in profile 3. **b** Detail of typical Endoaquoll. **c** Mesoscopic view of “lubinite” in ACK Hz, bar: 1000 μ m. **d** Microstructure (PM) view with bioclasts (white arrow) of ACK, bar: 100 μ m. **e** Eroded bioclast. **f–n** Different habits, according morphologies described by Verrecchia and Verrecchia (1994). **f–g** Monocrystals M, bar: 2 μ m. **g–h** M and MA, paired rods, bar: 20 μ m. **i–j** MA serrated plates, MAB: intermediate forms from the smooth coupled rods, bar: 2 μ m. **j–k** General view of M, MAB, bar: 10 μ m. **l–m** General view of M, MAB MB3 and Polycrystalline chains P2, l: bar 10 μ m. **n** bar 20 μ m

8 Calcium Biomineralizations

Although bioclasts are present in all horizons, they are more relevant in the ACK horizons. The bioclastic material is affected by dissolution and re-precipitation of calcium carbonates and oxalates of biogenic origin. The re-precipitation process is relevant in bioclasts and in the matrix between grains and bioclasts, as noted in Profile 2. The matrix is fibrous and very white and could be defined as “lublinite” (Ivanoff 1906), or as calcite with a particular habit (Stoops 1976) (Fig. 4c). Peds have dense crystalline forms: calcified filaments and tubes, rods, and short and long needles with sharp or straight ends (Fig. 4f–n). All these morphologies have been precisely described in different types of calcretes (Verrecchia and Verrecchia 1994) (Fig. 4f–n).

- (a) Monocrystals **M**: individual microrods of 0.3 μm width and 1 μm length (Fig. 4f–h).
- (b) Large monocrystalline rods **MA**: 0.5–2 μm width and < 100 μm length (Fig. 4f–k).
 - MA 1: paired rods that have a cross section in the shape of an “eight” figure
 - MA 2: three or more pairs of rods that form planes (Fig. 4f–k).
 - MA 3: two pairs of rods that have a cross section in the shape of an X (Fig. 4k).
 - MA 4: two pairs of rods that have a cross section in the shape of a bar bell.
- (c) Complex forms **MB**: paired monocrystalline rods with serrated plates along their length. There are three different habits, according to the number of plates and their orientation relative to the rod (Fig. 4i, h, n).
 - MB 1: two plates are situated at the top and bottom of the “8” formed by the crystal in the cross section (Fig. 4j–l).
 - MB 2: two plates are oriented at 90° to those in MB 1.
 - MB 3: four plates form an X in cross section (Fig. 4k–n).
 - MAB: intermediate forms from the smooth coupled rods to rods with serrated edges (Fig. 4i–n).
- (d) Polycrystalline chains **P**: P1, P2 and P3 morphologies (Fig. 4l–m).

The MA, MB and MAB habits are most often found and are formed by cementation and precipitation of calcium carbonate caused by biogeochemical processes (Fig. 4c–n), (Verrecchia et al. 1993). Some of them have been defined as raphides and styloids of whewellite (monohydrate) or weddellite (polyhydrate) (Osterrieth et al. 1998; Oyarbide and Osterrieth 2000), typical of pedogenic calcium oxalates mediated by fungal biomineralization (Verrecchia et al. 1993). Thus, in general, all morphologies are associated with fungal hyphae, forming an intricate mesh of needles: filaments, rods and tubes that coated peds, pores and the matrix of bioclastic–matrix interface (Fig. 4h, n).

Profile 4 is representative of a polycyclic pedosedimentary sequence, located in the W-NW sector of the marginal floodplain of the Mar Chiquita lagoon, in a flat relief with a 0.5% slope. Soils have evolved from sediments of an ancient coastal lagoon, linked to the last transgressive–ingressive Holocene cycle. Vegetation cover is complete, composed of *S. densiflora*, *Panicum* sp., *Distichlis spicata*, *Sarcocornia* sp. and other grasses. Soil drainage and permeability are moderate (Fig. 5a).

These soils have a moderate development, with a 40-cm-thick solum composed of a mollic epipedon of 25 cm and dark color (10YR 2/1), and a weak endopedion Bw, classified according to the USDA Soil Taxonomy (1996) as acucic Hapludolls. Then, the 2ACk horizon has abundant and well-preserved *Heleobia* sp. that has lived 1670 ± 70 year BP. This soil is based on a 3Cgk sedimentary level, of gray color (5Y 5/1), with sandy loam, where *T. plebeius* and *M. isabelliana* have lived there around 2040 ± 40 year BP and 2820 ± 80 year BP, respectively. The sequence is based on clayey silt sediments of the Santa Clara Formation, with colors ranging from gray to bluish gray and gray light brown (10YR 6/2), partially to fully calcretized in the top and very bioturbated by crabs (Schnack et al. 1982) (Fig. 5b).

The organic matter content is high on the A horizon and moderate on the 2ACgk horizon; the pH is slightly to moderately alkaline. Carbonates are present as whole or fragmented shells, scattered in the soil mass from Bw horizon, with higher values in the bioclastic levels (Table 1).

The distribution of the different particle sizes is variable. In the superficial horizons, muddy sediment values reach 50%, in addition to fine and very fine sands. In the 2ACk horizon, a discordance is evident due to substantial increase in sand and bioclastic fractions. The distribution is bimodal in the pedological horizons and polymodal in the two lower sedimentary levels (Table 1).

The mineralogy is recurrent with 92–98% of light minerals and 8–2% of heavy ones, and is characterized by the same minerals as Profile 3. In addition, silicobioliths reach values exceeding 15% in the pedological horizons, with a common presence of diatoms and their remains in 3 and 4Cgk horizons.

The microstructure is moderately pedal. The solum, in terms of fine mineral components, the factor B (“birefringence”) is composed of silt and clay grains, organic matter, amorphous iron; and calcium oxalates and carbonates with an important presence in sub-superficial horizons (Bw to 4Cgk). Also, present matrix with weak cristic fabric and scarce calcitans. The organic components of the basal mass are formed by decomposed Organic materials, mostly monomorphic, forming a homogeneous mass in color and density. There is a high density of interconnected channels and chambers, with irregular morphologies and varied size and layout, which could be attributed to insect activity (Genise and Poire 1998) (Fig. 5c). Many calcium biomineralization coatings were observed around sand and silt grains, associated with biogenic structures, minerals and/or humified organic matter (Fig. 5c–f).

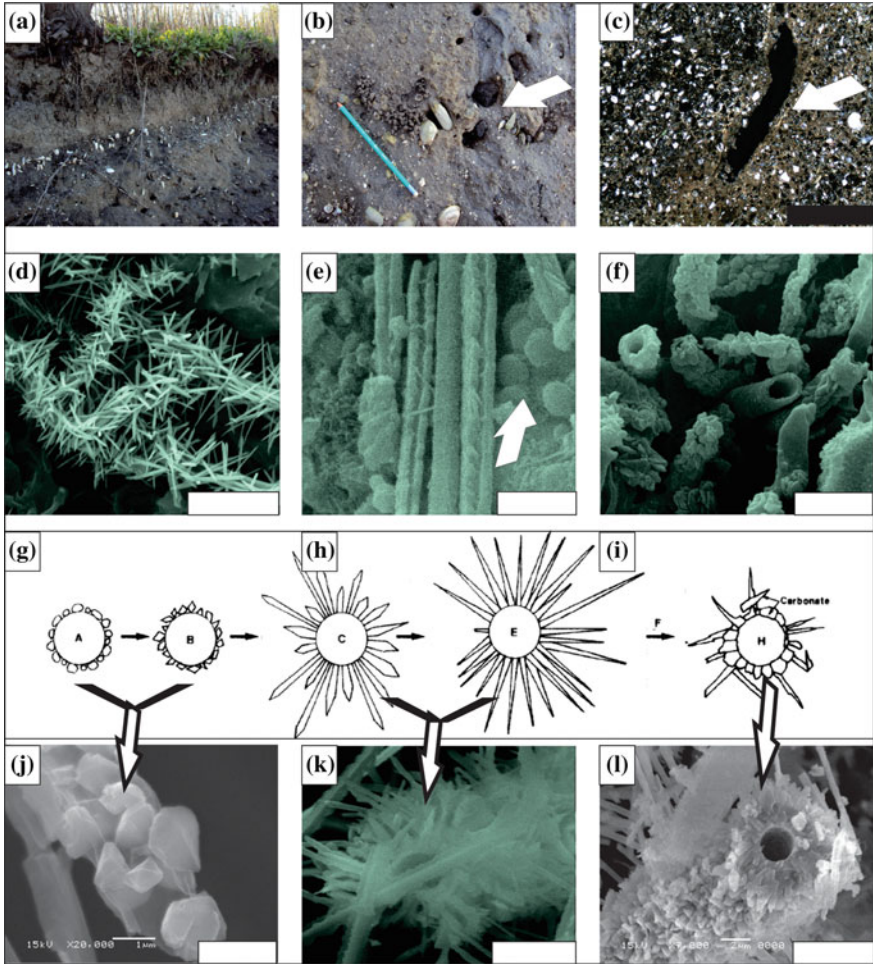


Fig. 5 **a** View of UGBI, profile 4, acuc Hapludoll. **b** Crabs bioturbations. **c** View of pedal microstructure with chambers bioturbation (*white arrow*), in A horizon bar: 100 μ m. **d** SEM image of styloids of weddellite crystal associated with the fungal mycelia, bar: 20 μ m. **e** SEM image filaments and bacteria (*white arrow*), in 2ACK Hz, bar: 2 μ m. **f** SEM image algae and fungus covering on the shells in 3ACgk Hz, bar: 10 μ m. **g–i** Different habits, according morphologies described by Verrecchia and contributors (1993), **g**, **j** SEM image of weddellite pseudo-rombohedral crystals bar: 2 μ m. **h**, **k** SEM image of styloids Ca oxalates surrounding the exterior of the filaments, bar: 5 μ m. **i**, **l** SEM image of calcite surrounding the hollow fungal filaments, bar: 5 μ m

9 Calcium Biomineralizations

In peds, the bioclastic material is affected by dissolution and re-precipitation of calcium oxalates and carbonates through the fungi and algae action (Fig. 5d–l). The re-precipitation processes are more conspicuous than in previously analyzed profiles, because they become part of a granular matrix with white and fibrous irregular areas. These calcium biomineralizations have variable sizes and morphologies: filaments (5 μm width, 60 μm length), rods (0.6–1.2 μm width and 15 μm length, with straight or pointed ends, and very fine needles, with 0.2 μm width and 10 μm length) and some ovoid structures and composed rods that could be calcified bacteria (Fig. 5d–f) (Verrecchia 1990, 1994; Verrecchia and Verrecchia 1994; Verrecchia et al. 1993, 1995, 1996; Wright 1984, 1986). The presence of algae covering the shells of current mollusks has been described (Fig. 5f). This would suggest that, under saturation conditions and adequate biogeochemistry, algae could also generate calcium biomineralizations. In this regard, there are numerous research studies about the influence of mucus or biofilms, rich in algae and Bacteria, involved in the creation of an environment that enables the precipitation of calcite (Coleman 1993; Jones 1995) (Fig. 5e, f, l).

The study of crystals by EDAX confirms the presence of calcium and variable carbon content according to the stage of development of calcium oxalates (primary nuclei in close association with the hyphae and/or more developed crystals: rosettes or druses) (Osterrieth et al. 1998). All the described morphologies coincide with the findings of Verrecchia et al. (1993); they explained the transformation of weddellite into whewellite by dehydration, in addition to the evolution to more stable forms, such as calcite (Fig. 5g–i). The most stable forms of calcium oxalate are the styloids of weddellite (Fig. 5d). These could lead to more stable forms by processes of dehydration: the raphides and styloids of whewellite. These biomineralizations can be transformed, in turn, into needles and other forms of calcium carbonate by the action of soil microfauna (Verrecchia et al. 1993). It is reported that microorganisms may form calcite crystals directly and/or act as catalysts by releasing metabolic products (Fig. 5d, k) (Loisy et al. 1999).

Rods and filaments are very common and are composed of sharpened bundles associated with the mycelia that are generated by chitinolytic and cellulolytic processes during the degradation of the organic substrate (Fig. 5d, j, k). These processes show a considerable time sequence, from the formation of an alveolar substructure to the subsequent random arrangement through diagenesis (Fig. 5d, e).

The structures are associated with very small calcified, crystalline, ellipsoidal, spherical bacteria. They are isolated and they coat mineral grains; they are grouped into chains in the micropores of the matrix, or joined by calcified strands (Fig. 5 e) (Perry 1999).

10 Geopedological Unit of Shell Ridges (UGIC)

The pedosedimentary sequence is represented by Profile 5, a moderately developed soil, well drained and with very rapid permeability, which has evolved over the shell ridges. These ridges form a narrow strip, slightly wavy, parallel to Route 11, which runs along the western margins of the Mar Chiquita lagoon (Figs. 1 and 2). Currently, there are only remnants, as the soil has been used in roadwork. The shell levels are constituted by more than 90% of bioclasts; they have been studied in the east-northeast of the Buenos Aires province by several authors (Cortelezzi 1977; Fidalgo et al. 1973; Violante 1992) (Fig. 6a–c). The morphological, physico-chemical and mineralogical properties of the soil profile show a pedological cycle from bioclastic materials of ancient regressive deposits that form elevations of 1.5 m in the marginal plain. The vegetation cover is dominated by communities of grass affinity and a modern arboreal stratum. These soils evolved from bioclastics, calcium-enriched sediments called typical Calciudolls.

The content of soil organic matter is high in the A horizon and very low in the underlying horizons. There is a high percentage of carbonates, represented by complete shells, remains of shells, and a massive to powdery carbonate with a strong reaction to HCl. The reaction is alkaline at soil surface, increasing progressively toward the base of the profile.

The particle size of these soils is essentially psephitic, bioclastic and sandy. In the mollic epipedon and transitional horizon, the texture (excluding the psephitic fraction), is sandy loam with polymodal distributions. The largest proportion of heavy minerals is found in the very fine sand fraction of the parent material (Ck), decreasing toward the surface.

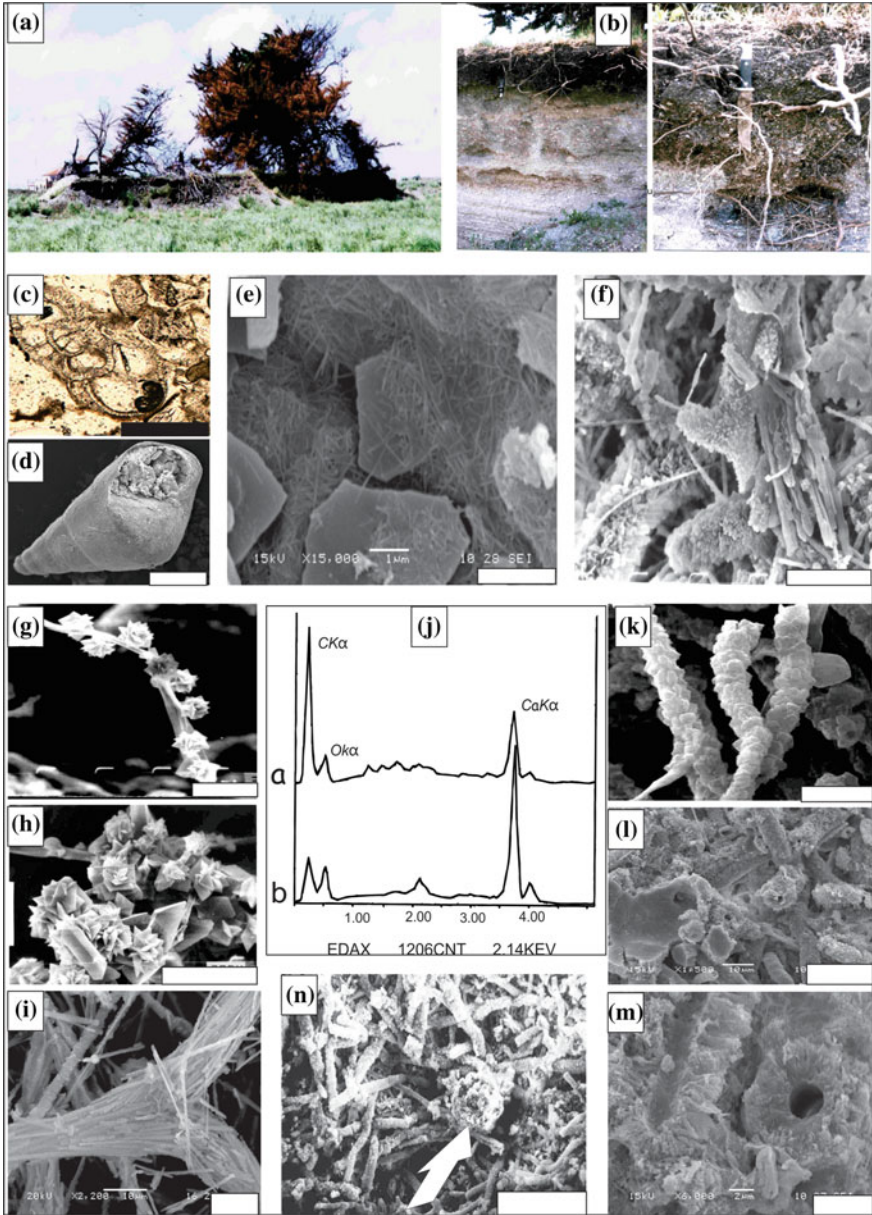
The light and heavy minerals are very similar to those previously described, with slight intra-profile variations. At the base of the profile, quartz, tourmaline and zircon are more abundant.

The microstructure is moderately pedal, in the mollic epipedon (Ak and ACk horizons), with cristic fabrics, calcitans, hipo- and neocalcitans and alveolar micro fabrics (Fig. 6). The matrix is enriched in calcium oxalates and carbonates, organic matter and bioclasts (Fig. 6c, e).

11 Calcium Biomineralizations

Peds have white efflorescences of different morphology. In all horizons, there are shells of *Heleobia* sp., bivalves, and many bioclastic fragments, all under the effect of dissolution and re-precipitation of calcium oxalates and carbonates (Fig. 6c, d).

These biomineralizations conform dense white mats, of varying sizes, which appear from the surface, reaching their maximum expression from 68 cm onwards. They are common in the matrix of aggregates, where they join clasts, minerals, in addition to amorphous materials, bioclasts and aggregates, as well as aggregates



◀**Fig. 6** **a** Panoramic view shell (UGIC). **b** Detail of typical Calciudolls profile 5. **c** Microstructure (PM) view calcic matrix with bioclast, in Ak Hz, bar: 1000 μm . **d** SEM image of *Heleobia* sp. with marks bioerosion of Ak Hz, bar: 500 μm . **e** SEM image of microstructure of calcified filaments, on the bioclastic and clastic material of the Ak horizon, bar: 2 μm . **f** SEM image of filaments and tubes in the ACk matrix bar: 10 μm . **g** SEM image of “rosettes” bar: 10 μm . **h** SEM image of “druses,” bar: 10 μm . **i** SEM image of acicular crystals surrounding the exterior of the fungal miscelia, bar: 10 μm . **j** Spectra of counts registered by the EDXS microprobe of different crystals, filaments, tubes, *a* calcium oxalates, *b* calcium carbonates. **k** SEM image of unbranched calcified tubes in Ak Hz, bar: 10 μm . **l** SEM image of calcified tubes in matrix (ACk), bar: 20 μm . **m** SEM image of calcite tubes in matrix of Ck Hz, bar: 4 μm . **n** SEM image of pelletiform calcified structures (*white arrow*), immersed in calcified mats of filaments and tubes (Ak Hz), bar: 50 μm

with each other (Fig. 6a–e). Others with a tubular and compact appearance form dense networks of calcified filaments distributed superficially, in some cases forming a compact crust. The presence of these white masses filling the pores is common (Fig. 6e, f).

The morphologies found show a series of specific forms and compositions associated with fungal mats that have been defined as:

1. Calcium oxalate biominerals: whewellite ($\text{CaC}_2\text{O}_4 \cdot \text{H}_2\text{O}$) and weddellite ($\text{CaC}_2\text{O}_4 \cdot (2+x)\text{H}_2\text{O}$). They are the product of fungal activity favored by the presence of an organic horizon of several cm (Graustein et al. 1977; Cromack et al. 1979; Osterrieth et al. 1998). Crystals of weddellite occur in all stages of development as pseudo-rhombohedral crystals or pyramids (Horner et al. 1983; Osterrieth et al. 1998): “primary nuclei” (1–4 μm), “rosettes” (2–5 μm) and “druses” (8–12 μm), a stage of greater complexity (Fig. 6g, h). In all cases, the close relationship between the crystals and the fungal cell wall is evident: the “primary nuclei” are located within the hyphae (Figs. 3i, 4f, 5j); the “rosettes” are closely associated with the wall, but in an external position (Fig. 6g), and the “druses” have little visible relationship to the hyphae (Fig. 6h) (Arnott 1982; Horner et al. 1983; Verrecchia et al. 1993; Osterrieth et al. 1998).
2. Calcium carbonate biominerals: acicular calcite and elongated needle-fiber monocrystalline crystals of habit type M, MA and MB, of $0.5 \times 5 \mu\text{m}$ average sizes, linked to the fungal cell wall and oxalates that cover it (Fig. 6i). The coexistence of calcite and calcium oxalate biominerals in different proportions is recurrent, but with a marked increase in calcite at the base of the profile (Fig. 6f, i, m). This coincides with the findings of Verrecchia et al. (1993), who argue that there is a chronological sequence beginning with the precipitation of polyhydrated calcium oxalates (weddellite), then transformed into more stable monohydrated calcium oxalates (whewellite) by dehydration, which subsequently become calcium carbonate by bacterial activity and diagenesis (Franceschi and Horner 1980; Verrecchia et al. 1993; Cromack et al. 1979).

Water availability and high content of organic matter in the upper levels of the soil profile promote microbial activity and the process of biomineralization. The coexistence of both calcium oxalate and calcite, which increases toward the base,

indicates a response to moisture changes that occurred in the environment, favored by the macroporosity of the profile and bioclastic calcareous materials. In addition, we have characterized the genera *Penicillium*, *Trichoderma* and *Absidia* as fungi associated with crystals in the Ak and ACK horizons (Osterrieth et al. 1998, Oyarbide and Osterrieth 2000).

Y-shaped branching and the diameter of the filaments and calcified tubes revealed their fungal nature (Fig. 6f, i, k–n). Unbranched tubes, which could be linked to actinomycetes and algae, were also present, but in a lower proportion (Fig. 6f, j–n).

The crystals are composed almost entirely of calcium, whereas the matrix of the aggregates has a calcium-enriched elemental composition with little to moderate silicon content, and traces of aluminum, sodium chlorine, iron and potassium.

The elemental composition of the crystals in mollic horizons, analyzed without the Be window permitted measurement of light elements (C and O) in addition to Ca, confirms the presence of calcium and varying carbon contents according to their developmental stage: primary nuclei, rosettes or druses of calcium oxalates (Fig. 6j, a, g, h); and acicular and rhombohedral calcite (Fig. 6j, b, i, k–m) (Osterrieth et al. 1998). The detailed characterization of morphologies and their mineralo-chemical study indicate that fungal biomineralization processes, even when they coexist in the same horizons, may have different origins. Filaments and tubes probably associated with species that develop surface crystals, and others that may have formed within ectomycorrhizic pods and then released by decomposition, were differentiated. Some of these needle bundles retain their parallel arrangement to a main longitudinal axis and are alveolar microfactories (Fig. 6e–m). In addition, in these mollic epipedons, the presence of pelletiform calcified structures immersed in calcified mats of filaments and tubes has been recurrent; their shapes and sizes could be associated with the action of fungivore mesofauna (Fig. 6n).

12 Final Considerations and Conclusions

The pedostratigraphic sequences of the current and past coastal plains or marshes have monocyclic and polycyclic soils. These soils are linked to the active coastal morphodynamics, the evolution of the lagoon, and the water changes from the maximum transgressive period, around 7000 year BP to the present. In addition, the calcium biomineralizations associated with bioclastic and silty-sandy deposits have conditioned their pedological evolution.

In these coastal environments, bioclasts and/or their remains, essentially aragonite, are dissolved by the action of microorganisms (fungi, actinomycetes, bacteria and algae) generating bioerosion. Subsequently, the microflora re-precipitates calcium oxalates and carbonates (biomineralizations) are incorporated as coatings of clasts and bioclasts, and to the matrix of soils and sediments.

These calcium biomineralizations, present in all the soils studied, become more conspicuous and abundant as one moves from the east to the west of the

toposequence. The type and diversity of these biomineralizations increase directly in relation with time and pedogenetic evolution.

Morphologically, biomineralizations are barely visible in soils of dunes and interdunes, but they are evident in the pedosedimentary sequences of the Mar Chiquita lagoon's marginal plain and shell ridges, where they reach their maximum expression. They are yellowish-white, pink to white and, in general, they display an earthy and fibrous appearance. Their morphologies are varied: calcified filaments and tubes, rods, short and long needles with sharp or straight ends, among others. Their size also varies from 0.2 to >100 μm .

The microstructure of these sequences ranges from apedal in dune environments to pedal with cristic factories, calcitans, hipo- and neocalcitans and alveolar microfactories. In addition to matrices which are massive or have a filliform appearance, they have the same appearance in faces, pores, chambers and cavities.

The interaction between organic and mineral horizons, rhizosphere fungi-bacteria and present- and paleo-soils, generates gels and biofilms where bacteria which are isolated or joined in chains may calcify and persist in the micro- and mesopores, and in the matrix of the peds. These bacteria, with calcium contents above 85%, are always associated with calcified filaments, rods, etc.

A remarkable variety of dichotomous tubes was found, as clear evidence of fungal origin, in addition to elongated tubes of multiple sizes and diameters, and complex interdigitated crystalline textures of oxalate and calcium carbonates.

The presence of calcified pelletiform structures of various shapes and sizes, present in fibrous and complex matrices, is linked to the activity of fungivore mesofauna, common in mollic epipedons of soils with moderate development.

The chemical composition of calcified structures shows calcium as the main element, in addition to oxygen and Carbon. Mineralo-chemical studies confirm the presence of calcium and varying carbon contents, depending on the stage of development of the crystals: the early stages, in close association with the walls of the hyphae (primary nuclei), or the more developed stages of crystals, which expand to the environment (rosettes and druses). Thus, it was possible to define the genetic sequence of calcite via calcium oxalate (weddellite and whewellite) associated with hyphae, algae, soil bacteria and actinomycetes. Most morphologies match the studies of Verecchia et al. (1995), where the transformation of weddellite into whewellite by dehydration is explained, in addition to the evolution into more stable forms, such as calcite. Based on the elemental composition, a relationship has been established between them, which indicate the loss of carbon and oxygen as calcium oxalate crystals evolve into needles and tubes of calcium carbonates.

Calcium biomineralizations allowed us to characterize and confirm biogenic processes and to define the biological evidence masked by sedimentary and post-pedological processes. Moreover, from the point of view of plant nutrition, they are an important reservoir of calcium in the soil. Given their magnitude, they also play an important role in the calcium biogeochemical cycle, linked to the availability of other fundamental macronutrients for the development of the biota, such as phosphorus (Osterrieth et al. 1998).

While there are still many unanswered questions in this area of multidisciplinary interaction, this research adds important data to the results provided by other evidence and proxies. Calcium biomineralizations are good mineralo-biochemical indicators for a better understanding of both current and past pedological environmental processes.

Acknowledgements This study was financially supported by the Universidad Nacional de Mar del Plata (EXA 741/15), the National Agency for Science and Technology Promotion of Argentina (ANPCyT, BID-PICT N°1583). The authors are especially grateful to Ing. José Vila for their assistance with SEM-EDXS analysis.

References

- Addadi L, Raz S, Weiner S (2003) Taking advantage of disorder: amorphous calcium carbonate and its roles in biomineralization. *Adv Mater* 15(12):959–970
- Ameghino F (1908) Las formaciones sedimentarias de la región litoral de Mar del Plata y Chapadmalal. *Anales Museo Nacional Buenos Aires* 10(3):343–428
- Antinuchi CD, Busch C (1992) Burrow structure in the subterranean rodent *Ctenomys talarum*. *Z. Saugetierkunde* 57:163–168
- Aragno M, Verrecchia E, Job D, Cailleau G, Braissant O, Khammar N, Ferro K, Mota M, Guggiari M, Martin G (2010) Calcium carbonate biomineralization in ferrallitic, tropical soils through the oxalate-carbonate pathway. *Bulletin de la Société Suisse de Pédologie* 30:127–130
- Arnott HJ (1982) Calcium oxalate (weddellite) crystals in forest litter. *Scan Elect Microsc* 3:1141–1149
- Bortolus A (2001) Marismas en el Atlántico sudoccidental. In: Iribarne O (ed) *Reserva de la biosfera Mar Chiquita: características físicas, biológicas y ecológicas*, pp 83–92
- Brewer R (1964) *Fabric and mineral analysis of soils*. Wiley, New York, p 470
- Bullock P, Fedoroff N, Jongerious A, Stoops G, Tursina T, Babel U (1985) *Handbook for soil thin section description*. Wayne Research Publications, Wolverhampton, p 150
- Burgos JJ, Vidal AL (1951) Los climas de la República Argentina, según la nueva clasificación de Tornthwaite. *Meteoros* 1(1):3–32
- Coe HH, Osterrieth M, Fernández Honaine M (2014) Phytoliths and their applications. In: Gomes CH, Osterrieth M (eds) *Synthesis of some phytolith studies in South America*. Nova Publishers, New York, pp 1–26
- Coleman M (1993) Microbial processes: controls on the shape and composition of carbonate concretions. *Marine Geol* 113:127–140
- Cortelezzi CR (1977) Dataciones de las formaciones marinas del Cuaternario en las proximidades de La Plata-Magdalena, Buenos Aires. *LEMIT II* 342:77–93
- Cromack K, Sollins P, Graunstein W, Spiedel K, Todd A, Spycher C, Todd R (1979) Calcium oxalate accumulation and soils weathering in mats of the hypogeous fungus *Hysterangium crassum*. *Soil Biochem* 11:463–468
- Dawis J, Freitas F (1970) Physiological and chemical methods of soil and water analysis. *Soil Bull* 10:39–51
- Dhami NK, Reddy MS, Mukherjee A (2013) Biomineralization of calcium carbonates and their engineered applications: a review. *Front Microbiol* 4:314. doi:10.3389/fmicb.2013.00314
- Espinosa M (1994) Diatom paleoecology of the Mar Chiquita lagoon delta, Argentina. *J Paleolimnol* 10:17–23
- Fasano J, Hernández M, Isla F, Schnack E (1982) Aspectos evolutivos y ambientales de la Laguna Mar Chiquita (provincia de Buenos Aires, Argentina). *Oceanologica Acta*, Nti SP, pp 285–292

- Fidalgo F, Colado U, De Francesco O (1973) Sobre ingresiones marinas cuaternarias en los partidos de Castelli, Chascomús y Magdalena (provincia de Buenos Aires). In: V Congreso Geológico Argentino, Buenos Aires, vol 3, pp 227–240
- Fidalgo F, Riggi J, Gentile R, Correa H, Porro N (1991) Los “sedimentos pampeanos” continentales en el ámbito sur bonaerense. *Revista Asociación Geológica Argentina* 46(3–4):239–256
- Franceschi VR, Horner HT Jr (1980) Calcium oxalate crystals in plants. *Bot Rev* 46:361–427
- Frenguelli J (1935) Diatomeas de la Laguna Mar Chiquita al norte de Mar del Plata (Buenos Aires). *Notas Museo de La Plata* 1:121–140
- Frenguelli J (1950) Rasgos generales de la morfología y la geología de la Provincia de Buenos Aires. *LEMIT* 2(33):72
- Galehouse JS (1971) Sedimentation analysis. In: Carver J (ed) *Procedures in sedimentary petrology*. Wisconsin, Wiley Interscience, USA, pp 69–94
- Genise JF, Poire DG (1998) Icnofósiles: estudio y aplicación. Tercera Reunión Argentina de Icnología and Primera Reunión de Icnología del Mercosur. Cuadernillo de apuntes, 92 p
- Graustein WC, Cromack K, Sollins P (1977) Calcium oxalate: occurrence in soils and effects on nutrient and geochemical cycles. *Science* 198:1252–1254
- Horner H, Tiffani L, Cody A (1983) Formation of oxalate crystal associated with apothecia of the Discomycete *Dasyscypha capitata*. *Mycologia* 75(3):423–435
- Ibáñez J, de Alba S, García Álvarez A (2000) Una disciplina en crisis: bases para un cambio de paradigma en edafología (el suelo, su clasificación e inventario). XVIII Congreso Argentino de la Ciencia del Suelo, Mar del Plata. CD
- Ingram RL (1971) Sieve Analysis. In: Carver J (ed) *Procedures in sedimentary petrology*. Wisconsin, Wiley Interscience, USA, pp 41–68
- Isach JP (2001) Mapa de vegetación de la Reserva Mar Chiquita. In: Iribarne O (eds) *Reserva de la biosfera Mar Chiquita: características físicas, biológicas y ecológicas*, pp 79–80
- Isla F (1989) Holocene sea-level fluctuations in the southern hemisphere. *Quat Sci Rev* 8:359–368
- Iwanoff LL (1906) Ein Wasserhaltiges Calcium Carbonat Aussen Umgebungen von Nowo-Alexandria (gub. Lublin). *Annalen der Geologie und Mineralogte der Russland* 8: 23–25.
- Jahren AH (1996) How and why do phytoliths form? *Biom mineralization*. *Phytolitharien Bull* 9: 2–10
- James NP (1972) Holocene and Pleistocene calcareous crust (caliche) profiles: criteria for subaerial exposure. *J Sed Petrol* 42(4):817–836
- Jenny L (1941) *Factors of soils formation*. McGraw Hill Book Company, New York
- Jones B (1995) Processes associated with microbial biofilms in the Twilight zone of caves: example from the Cayman Islands. *J Sediment Res* 65(3):552–560
- Klappa CF (1979) Calcified filaments in Quaternary calcretes: organo-mineral interactions in the subaerial vadose environment. *J Sediment Petrol* 49(3):955–968
- Klappa C (1980) Rhizoliths in terrestrial carbonates: classification, recognition, genesis and significance. *Sedimentology* 27:613–629
- Lapeyrie F, Picatto C, Gerard J, Dexheimer J (1990) TEM study of intracellular and extracellular calcium oxalate accumulation of ectomycorrhizal fungi in pure culture or in association with *Eucalyptus* seedlings. *Symbiosis* 9:163–166
- Loisy C, Verrecchia E, Dufour P (1999) Microbial origin pedogenic micrite associated with a carbonate paleosol (Champagne, France). *Sediment Geol* 126:193–204
- Lowenstam R (1981) Minerals formed by organisms. *Science* 211:1126–1131
- Mann S (2001) *Biom mineralization: principles and concepts in bioinorganic materials chemistry*. Oxford University Press, New York
- Mitsch S, Gosselink J (1993) *Wetlands*. Van Nostrand Reinhold (eds) New York
- Osterrieth ML (1998) Paleosols and their relation to sea level changes during the Late Quaternary in Mar Chiquita, Buenos Aires, Argentina. *Quat Int* 43–44
- Osterrieth ML (2004) *Biom minerales y Biom mineralizaciones*. *Cristalografía de Suelos*. Sociedad Mejicana de Cristalografía (ed), pp 206–218

- Osterrieth ML (2005) Biomineralizaciones de hierro y calcio, su rol en procesos biogeoquímicos de secuencias sedimentarias del sudeste bonaerense. XVI Congreso Geológico Argentino 3:255–262
- Osterrieth ML, Martínez G (1993) Paleosols on Late Cainozoic Sequences in the Northeastern side of Tandilia Range, Buenos Aires, Argentina. *Quat Int* 17:57–65
- Osterrieth ML, Oyarbide F (1998) Calcium oxalate biominerals generated by fungi in Argiudolls of the Pampean plains, Argentina. A problem? II International Meeting of Phytolith Research 2:43
- Osterrieth M, Schnack E (1984) El perfil de Mar de Cobo (partido de Mar Chiquita, provincia de Buenos Aires). Características de sus paleosuelos y posibles correlaciones. Symposium on Oscilaciones del nivel del mar durante el último hemicycle deglacial en la Argentina, pp 101–117
- Osterrieth M, Oyarbide F, Bordas V (1998) Biominerales de oxalato de calcio en suelos de Laguna de Los Padres, Buenos Aires. *Revista Argentina Ciencias Suelo* 18(1):1–9
- Oyarbide RF, Osterrieth M (2000) Presencia y desarrollo de biominerales de calcio de origen fúngico en suelos del sudeste de la provincia de Buenos Aires (Argentina). Congreso Universitario Internacional de Edafología Nicolás Aguilera 1–2:81–88
- Oyarbide F, Osterrieth M, Cabello M (2001) *Trichoderma koningii* as a biomineralizing fungous agent of calcium oxalate crystals in typical Argiudolls of the Los Padres Lake natural reserve (Buenos Aires, Argentina). *Microbiol Res* 156:113–119
- Perry C (1999) Biofilm-related calcification, sediment trapping and constructive micrite envelopes: a criterion for the recognition of ancient grass-bed environments? *Sedimentology* 46:33–45
- Schmidt C (1847) Ueber das Vorkommen des oxalsauren Kalks in den einfachsten Zellenpflanzen und dem Secret der Schleimhaute. *Ann. Chem. Pharm. (Heidelberg)* 61:288–306
- Schnack EJ, Gardenal M (1979) Holocene transgressive deposits, Mar Chiquita lagoon coast, Buenos Aires province, Argentina. Proc. Int. Symposium on coastal evolution in the quaternary, pp 419–425
- Schnack EJ, Fasano JL, Isla FI (1982) The evolution of Mar Chiquita Lagoon, Province of Buenos Aires, Argentina. In: Colquhoun DJ (ed) Holocene sea-level fluctuations: magnitudes and causes. IGCP 61, University of South Carolina, Columbia, pp 143–155
- Schnack EJ, Alvarez, J, Cionchi J (1984) El carácter erosivo de la línea de costa entre Mar Chiquita y Miramar, provincia de Buenos Aires. Symposium Oscilaciones del Nivel del Mar durante el último Hemicycle Deglacial en la Argentina, pp 118–130
- Simkiss K, Wilbur K (1989) Biomineralization: cells biology and mineral deposition. Acad. Press Inc., New York, p 327
- Simonson RW (1959) Outline of a generalized theory of soil genesis. *Soil Sci Soc Am Proc* 23:152–156
- Soil Survey Staff (1996) Keys to soil taxonomy, 7th edn. Department of Agriculture, USA, p 631
- Stoops GJ (1976) On the nature of “lublinite” from Hollanta (Turkey). *Am Mineralogist* 61:172
- Teruggi ME (1959) Las arenas de la costa de la provincia de Buenos Aires entre Cabo San Antonio y Bahía Blanca. LEMIT II, 77, La Plata
- Tricart JL (1973) Geomorfología de la pampa deprimida. *INTA* 12:202
- Verrecchia E (1990) Lithodiagenetic implications of the calcium oxalate-carbonate biogeochemical cycle in semi-arid calcretes, Nazareth, Israel. *Geomicrobiol J* 8:89–101
- Tuason MMS, Arocena JM (2009) Calcium oxalate biomineralization by *Piloderma fallax* in response to various levels of calcium and phosphorus. *Appl Environ Microbiol* 75(22):7079–7085
- Verrecchia E (1994) L’origine biologique et superficielle des croûtes zonaires. *Bull Soc Geol France* 165(6):583–592
- Verrecchia E, Verrecchia K (1994) Needle-Fiber calcite: review and classification. *J Sediment Res* 64(3):650–664
- Verrecchia E, Yair A, Ribier J, Kidron G, Rolko-Verrecchia KE (1993) Le role des Cyanobactéries dans la fixation des sols sableux désertiques: un exemple pris dans le désert de Néguev (Nizzana area, Israel). *Palynosciences* 2:255–266

- Verrecchia E, Dumont JL, Verrecchia K (1995) Role of calcium oxalate biomineralization by fungi in the formation of calcretes: a case study from Nazareth, Israel. *J Sediment Petrol* 65: 1060–1066
- Verrecchia E, Van Grootel G, Guillemet G (1996) Classification of Chitinozoa (Llandoveryan, Canada) using image analysis. *Microscopy Microanal Microstruct* 5–6:461–466
- Verrecchia EP, Braissant O, Cailleau G (2006) The oxalate-carbonate pathway in soil carbon storage: the role of fungi and oxalotrophic bacteria. In: Gadd GM (eds) *Fungi in biogeochemical cycles*. Cambridge University Press, Cambridge, pp 289–310
- Vervoorst F (1967) La vegetación de la República Argentina. VII. Las comunidades vegetales de la depresión del Río Salado, Provincia de Buenos Aires. INTA. Buenos Aires
- Violante R (1992) Ambientes sedimentarios asociados a un sistema de barrera litoral del Holoceno en la llanura costera al sur de Villa Gesell, Provincia de Buenos Aires. *Revista de la Asociación Geológica Argentina* 47(2):201–214
- Violante RA, Parker G, Cavallotto JL (2001) Evolución de las llanuras costeras del este bonaerense entre la Bahía Samborombón y la Laguna Mar Chiquita durante el Holoceno. *Revista Asociación Geológica Argentina* 56(1):51–66
- Walkley B (1965) In: Black C (ed) *Methods of soil analysis*. American Society of Agronomy, pp 1372–1375
- Warne J (1975) Boring as trace fossils and the process of marine bioerosion. In: Fray RY (ed) Springer, New York, pp 191–229
- Wright VP (1984) The significance of needle-fibre calcite in Lower Carboniferous palaesol. *Geol J* 19:23–32
- Wright VP (1986) Pyrite and the drowning of a paleosol. *Geol J* 21:139–149

Index

A

- Abiotic, 226
- Abiotic components, 54
- Abiotic environment, 52
- Abiotic nature attributes, 53
- Aboriginal occupation, 174
- Abrasion, 6, 8, 9
- Absolute stability, 127
- A-B2t-C-type profiles, 252
- Accommodation, 54
- Accumulation landforms, 204, 221, 222
- Accuracy statistics, 131
- Acicular and rhombohedral calcite, 281
- Acicular calcite, 280
- Acicular crystals, 279
- Acoite Formation, 243, 246, 256
- Aconquija, 124
- Aconquija Range, 122
- Actinomycetes, 262, 281, 282
- Activities, 54
- Acuic Hapludoll, 276, 275
- Aeolian action, 204
- Aeolian deflation, 204
- Aeolian dust mantle, 218
- Aeolian erosion, 3, 220
- Aeolian influx, 78, 82
- Aeolian landforms, 204
- Aeolian mantles, 204, 217, 219–222
- Aeolian models, 204
- Aeolian pans, 80
- Aeolian plumes, 204
- Aeolian processes, 204
- Aerial photograph, 123, 136, 164, 165
- Aesthetic appreciation, 53
- Aesthetic value, 59
- Afforestation, 270
- Africa, 28
- Aggradation, 91
- Aggregated units, 263
- Aggregates, 263, 280
- Agricultural intensive activities, 185
- Ag sulfate salts, 243
- Algae, 225, 229, 231, 253, 254, 262, 271, 276, 277, 281, 282
- Algal carbonates, 247
- Algorithm, 125, 186
- Aligned ridges, 213
- Alkaline, 270, 272, 275, 279
- Alkaline pH, 270
- Alkaline volcanism, 242, 243
- Allochthonous streams, 161
- Alluvial clastic, 245
- Alluvial–colluvial sediments, 252
- Alluvial deposits, 96, 247, 257
- Alluvial fan, 95, 150, 181, 183, 187, 189, 191, 192, 194, 196, 198, 237, 238, 247, 250, 252, 255, 256
- Alluvial fan deposits, 250
- Alluvial fan relict, 93, 95, 77, 81, 82
- Alluvial plains, 31, 77, 81, 96, 163, 168, 198, 245
- Alteration mantles, 37
- Altiplano, 237, 238, 240, 241, 246, 257
- Altiplano–Coipasa, 253
- Altitude, 127
- Altitudinal gradient, 121
- Aluminum, 281
- Alveolar cavities, 18
- Alveolar hollow, 1, 18, 24, 26, 30, 34
- Alveolar hollowsm tafoni, 45
- Alveolar micro fabrics, 279
- Alveolar microfactories, 281, 282
- Alveolar substructure, 277
- Amorphous, 272
- Amorphous compounds, 262
- Amorphous iron, 270, 272, 275
- Amorphous materials, 280
- Amorphous silica, 272

- Amphibol, 270, 272
Ancient regolith mantle, 37
Andean, 120
Andean climate, 241
Andean Cordillera, 38, 40, 41, 43, 141, 142, 164
Andean Cordillera landscape, 169
Andean desert, 56
Andean piedmont, 143
Andean ranges, 4, 143
Andes, 55, 120, 144, 146
Andesites, 28, 90, 245
Andesitic–dacitic, 245
Andesitic–dacitic rocks, 245
Angle of friction, 129, 137
Anglican missionary, 52
Animals, 261, 262
Annual calm days, 207
Annual rainfall, 183
Anortoclase, 38
Antarctica, 56
Anthropic aspects, 187
Anthropic indicators, 186
Anthropogenic activities, 102
Anthropogenic alteration, 108
Anthropogenic factor, 103
Anthropogenic modification, 107
Anthropogenic perturbation, 137
Anthropogenic variables, 181, 183
Apedal, 270, 282
Apedal microstructure, 268
Aqueous environments, 263
Aquic Haplocalcids, 96
Aquic Torrifluvents, 96
Aquifer, 102, 103, 106, 110, 112, 158
Aquifer recharge, 102
Aquitard/Aquiclude, 106
Aragonite, 262, 281
Arboreal stratum, 279
ArcGis, 147
ArcGis v.10, 205
ArcGIS 9x, 186, 187
Archaeological and paleontological materials, 263
Archaeological record, 168
Area, 187
Area slope, 127
Area Under the ROC Curve (AUC), 131
Argentina, 1–4, 28, 49–51, 54, 77, 101, 120, 121, 142, 143, 148, 149, 152, 164, 170, 173, 174, 181–183, 216, 220, 237, 238, 262, 264
Argentina brachiopods, 227
Argentine coast, 225, 227–229
Argentine Congress of Quaternary and Geomorphology, 49
Argentine coast, 227
Argentine National Historical Monument, 52
Argentine Pampas, 204
Argentine Patagonia, 141, 203
Argentine Puna, 241, 250
Argentine sector, 52
Argentine southern Patagonia, 141
Argillic, 82
Argillic horizon, 90, 93, 252
Arid, 124
Arid conditions, 81
Aridic, 80
Aridisols, 82
Artwork, 263
As, 243
Ascomycetes, 263
Ash fall, 11, 28
Ashfall tuffs, 37, 38, 40
Ash mantles, 41
Aspect, 123, 127, 135, 136
Aspect map, 186
Aspect networks, 186
Assessment of model accuracy, 130
Associated mudslide deposits, 246
ASTER-GDEM, 127, 129
Asymmetrical shapes, 217
Atlantic, 42, 103
Atlantic coast, 152
Atlantic Ocean, 40, 55, 152, 155, 164, 206, 216, 233
Atlantic Ocean coast, 57, 141–143, 150, 152, 154, 155, 164
Atlantic Ocean shore, 210
Atmospheric correction, 106
Atmospheric dust, 222
Atriplex lampa, 82, 91, 96
Attractions, 54
Au, 243
Austral Basin, 143, 146
Autoclastic hyaloclastite breccia, 243
Availability of sand, 102
Average consumption, 107
Avulsion, 198
Azonal ecosystems, 159
- B**
Bacillariophyceae, cyanophyta, chlorophyta, 253
Bacteria, 262, 276, 277, 281, 282
Bacterial activity, 280
Badland, 17, 29, 45
Badland landscape, 35

- Badland morphology, 30
 Bahadas, 150
 Bahía Brown, 59
 Bahía Cambaceres, 58, 68
 Bahía Harberton, 59
 Bahía Inútil, 211
 Bahía Laura group, 3, 28, 37
 Bajadas, 91, 96, 237, 247, 257
 Bajo Pobre formation, 28
 Bajos sin salida, 170, 204
 Banded schists, 122
 Bandurria austral (*Theristicus melanopis*), 160
 Barda Colorada, 1, 45
 Barda Colorada formation, 13, 45
 Barda Colorada ignimbrite, 12
 Barda de los Perros, 18
 Barnacles, 225, 229–231, 233
 Barremian–Early Maestrichtian, 245
 Barrier chains, 102
 Barriers, 102
 Barrier sands, 106
 Basalt flow, 156, 160
 Basaltic lava flow, 4
 Basaltic mesetas, 204
 Basaltic outcrops, 158
 Basaltic tablelands, 155, 158, 170
 Basalts, 90
 Basalts rock, 28
 Base level, 186, 210
 Basibiont, 226
 Basin areas, 123
 Basin level, 119
 Basins, 213, 214, 216, 220, 221
 Bathymetric, 227
 Bathymetric areas, 229
 Bathymetric location, 225
 Bays, 213
 Beagle channel, 51, 55, 57, 58, 60, 69, 227, 233
 Bedrock front, 28
 Bedrock landforms, 40
 Bedrock outcrops, 41
 Bee hives, 34
 Belts and fans fluvial plains, 198
 Benthic, 225, 227, 229
 Benthic areas, 233
 Benthic communities, 226
 Benthic samples, 227, 234
 Berberis buxifolia, 144
 Beryllium, 270
 Bike and trekking path, 69
 Binary splits, 106
 Binocular magnifying glass, 265
 Biochemical sequence, 263
 Bioclast, 262, 266, 268, 270–274, 279–281
 Bioclastic, 261, 263, 264, 271, 272, 275, 277, 279–281
 Bioclastic calcareous materials, 280
 Bioclastic deposits, 272
 Bioclastic material, 265, 274
 Bioclastic–matrix, 274
 Bioclastic sediments, 272
 Bioerosion, 262, 263, 271, 279, 281
 Bioerosion processes, 271
 Biofilm, 263, 277, 282
 Biogenic, 282
 Biogenic calcium carbonate, 271
 Biogenic origin, 274
 Biogenic oxalates, 270, 272
 Biogenic structures, 275
 Biogenic substrate, 225, 227
 Biogeochemical processes, 274
 Biogeographical unit, 238
 Bioherm development, 247
 Bioherms (algal carbonates), 238, 257
 Biological diversity, 267
 Biological evidence, 282
 Biological functions, 262
 Biological processes, 226
 Biomes, 56
 Biomineralization, 262, 271, 272, 275, 280–282
 Biomineralization process, 263
 Biomineralogical, 264
 Biominerals, 262, 263
 Biosphere, 262
 Biosphere reserve, 254
 Biota, 52, 147, 262, 282
 Biotic, 226, 267
 Biotic information, 53
 Biotite, 5, 38, 39, 270
 Bioturbated, 275
 Bioturbations, 268, 270
 Bioturbation structures, 270
 Bird, 163, 172, 174
 Bird species, 160
 Bird wildlife, 223
 Birefringence, 275
 Bivalves, 280
 Bivariate.Seemultivariate
 Block-and-ash flow deposits, 245
 Bluffs, 29
 Bogs, 71
 Bolivia, 238, 242
 Bolivian Eastern Mountain Range, 246
 Bolivian Plateau, 250
 Bolson, 237–239, 242, 247
 Bolsones, 239

- Boolean logic, 120
 Bornhardts, 1, 22
 Bottomset beds, 238
 Bottomsets, 249
 Boulder, 22, 25, 188
 Bowl, 8, 14
 Brachiopod, 225–229, 231, 233
 Brachiopoda
 Orthis cf. Calligramma Dalman, 243
 Brackish water, 104
 Braided, 256
 Braided drainage pattern, 43
 Braided pattern, 31, 161
 Braided rivers, 250
 Brazil, 54
 Breccias, 35
 Brochures, 72
 Brownish, 38
 Bryozoans, 225, 229–231
 Bryozoos, 230
 Buenos Aires, 101, 103, 104
 Buenos Aires Province, 261, 264, 279
 Buffer, 136
 Bundles, 277
 Buried palaeohills, 42
- C**
- ¹⁴C, 265
¹⁴C ages, 272
 Ca-HCO₃, 106
 Cabo Nombre, 210
 Caducifoliated species, 144
 Calcareous concretions, 39, 43
 Calcareous (limestone) rocks, 253
 Calcareous massive mud, 254
 Calciacuolls, 267, 272
 Calcic, 82
 Calcic biomineralizations, 267
 Calcic Lithic Petrocalcids, 82
 Calcic matrix, 279
 Calcids soil suborder, 78
 Calcified, 277
 Calcified bacteria, 277
 Calcified filament, 265, 271, 274, 279, 280, 282
 Calcified mats, 279, 281
 Calcified organic filaments, 271
 Calcified pelletiform structures, 282
 Calcified strands, 277
 Calcified structures, 233, 281, 282
 Calcified tubes, 279, 281
 Calcimorphic, 263
 Calcimorphic soils, 267
 Calcsiltite, 238, 247, 253
 Calcitans, 275, 279, 282
 Calcite, 262, 263, 271, 274, 276, 277, 280, 282
 Calcite crystals, 277
 Calcite tubes, 279
 Calcitic concretions, 90
 Calcium (Ca), 262, 263, 270, 271, 275, 277, 279, 281, 282
 Calcium biogeochemical cycle, 282
 Calcium biomineralization, 261–264, 270, 271, 274, 277, 280–283
 Calcium carbonate, 38, 265, 270–272, 274, 277, 279, 280, 282
 Calcium carbonate biominerals, 280
 Calcium carbonate content, 272
 Calcium carbonate polymorphisms, 262
 Calcium content, 262, 264
 Calcium oxalate, 261, 262, 265, 270, 271, 275, 277, 279–281
 Calcium oxalate biominerals, 280
 Calcium oxalate crystals, 263, 282
 Calcium oxalate salts, 263
 Calcium oxalate—whewellite, 263
 Calco-alkaline, 242
 Calcretes, 263, 274
 Calcretization, 78
 Calcretized, 275
 Caldera, 5, 11
 Caldera formation, 5
 Cambrian, 226
 Canadian Arctic zone, 204
 Cañadón de la Buitrera, 17, 19
 Cañadón del Loro, 18
 Canyons, 242
 Ca oxalates, 276
 Carabids, 270
 Carbajal-Tierra Mayor-Lashifasaj, 55
 Carbon (C), 270, 281, 282
 Carbonate, 93, 261, 262, 270, 275, 277, 279–281
 Carbonate content, 270
 Carbonate–siliciclastic, 238
 Carbonate–siliciclastic muds, 251
 Carbon content, 277, 281
 Carex banksii, 96
 Carmen Sylva Creek, 215
 Carmen Sylva formation, 206
 Cartographic analysis, 209
 Cartography, 141, 174
 Caruhué tuff member, 38
 Carving, 159
 Cascos, 146
 Casira Formation, 246, 256
 Castillo Formation, 206
 Castle koppies, 1, 22, 25, 29, 30, 25, 45

- Catalysts, 277
 Catastrophic episodes, 199
 Catastrophic events, 255
 Catchment area, 185
 Cattle, 52, 145, 159, 167
 Cattle raising, 146, 185
 Cattle rising, 168
 Cavern, 1, 14, 18, 19, 30, 45, 156
 Caves, 1, 2, 14, 18, 30, 45
 Cavities, 18, 282
 CBERS 2B, 123
 Cellulolytic, 277
 Cementation, 274
 Cemented, 38
 Cenozoic, 242, 247
 Cenozoic alluvial fans, 183
 Cenozoic–Neogene, 237, 245
 Cenozoic–Paleogene–Neogene, 245
 Central Andes, 237, 238, 246
 Central Energy, 241
 Cephalopoda, 243
 Cerro Barcino formation, 80, 91
 Cerro Cornú, 59
 Cerro Cortado, 27
 Cerro de la Sociedad Científica, 24–26
 Cerros mesa, 158
 Cespitose species, 209, 220
 Chachahuen volcanoes, 4
 Chambers, 282
 Chambers bioturbation, 276
 Changes, 182
 Channel, 6, 188, 206, 211, 215, 245
 Channel flow, 188
 Channel network, 186
 Channel reaches, 187
 Channel route, 102
 Channel slope, 188
 Characterization studies, 103
 Charles Darwin, 69
 Chemical composition, 282
 Chemical quality, 101, 106, 114
 Chemical weathering, 1, 20, 79
 Chenier, 206, 211, 214, 220–222
 Chenier pans, 211, 213
 Chico and Grande rivers, 214–216
 Chile, 50, 55, 143, 152, 155, 164, 166, 170, 216, 238
 Chimney, 33
 Chimney rocks, 33
 Chi-square, 126
 Chitinolytic, 277
 Chlorine, 270
 Chon Aike, 3
 Chon Aike formation, 28, 45
 Chon Aike ignimbrites, 28, 30, 45
 Chon Aike (Province of Santa Cruz), 1
 Chubut, 2
 Chubut group, 80, 90, 91, 93, 96
 Chubut Province, 77, 79
 Chuquiraga avellanadae, 91, 93, 96
 Cieneguillas, 240
 Cinder, 38
 Cinder flow, 4
 Cinder matrix, 38
 Cineritic tuff, 38
 Circular, 222
 Circular dunes, 217
 Circular shape, 206, 213–216
 Cirques, 56, 57
 Ciudad en Nombre de Jesús, 152
 Classification, 174
 Classification of the scenic resources, 142
 Classification of the soils, 80
 Clastic, 279
 Clastic aquifers, 103
 Clastic component, 3
 Clay coatings, 90
 Clay dunes, 204
 Clayey shale, 69
 Clays, 243, 246
 Clays formation, 79
 Cliffs, 29, 30, 44, 45, 150
 Climate, 56, 80, 104, 110, 122–124, 147, 153, 183, 207, 252, 254, 266, 267
 Climate–Switzerland, 241
 Climatic analysis, 206
 Climatic aridness, 166
 Climatic changes, 37, 42, 44, 45, 69, 103
 Climatic conditions, 143, 144, 203
 Climatic cycles, 45
 Climatic events, 257
 Climatological data, 208
 Climbing dunes, 217
 Clinopyroxene, 5
 Closed depressions, 56, 204
 Coal, 173
 Coal deposits, 169
 Coalescent alluvial fans, 77, 237
 Coalescent explosion centers, 156, 160
 Coalescent fans, 237, 247
 Coalescent pyroclastic flow, 13
 Coal mining, 146, 172, 173
 Coal seams, 169
 Coarse stratification, 38
 Coastal, 225, 227
 Coastal aquifer, 102–104
 Coastal areas, 231, 232, 264
 Coastal barrier, 104

- Coastal deposits, 257, 266
- Coastal desertic lands, 204
- Coastal dunes, 102, 103, 266, 267
- Coastal dynamics, 270
- Coastal environments, 220, 233, 261, 281
- Coastal environments of southeastern Buenos Aires province, 264
- Coastal erosion, 103
- Coastal lagoon, 266, 267, 272, 275
- Coastal lagoon/paleo-coastal lagoon, 262, 267, 271
- Coastal lagoon facies, 266
- Coastal landforms, 264
- Coastal landscape, 55, 150
- Coastal littoral, 249
- Coastal littoral environments, 238
- Coastal morphodynamics, 281
- Coastal pedosedimentary sequences, 264
- Coastal plain, 210, 213, 261, 264, 281
- Coastal population, 102
- Coastal region, 104, 174
- Coastal samples, 233, 234
- Coastal sand dunes, 102
- Coastal sedimentation, 150
- Coastal surface environments, 220
- Coastal system, 102, 267
- Coastal zone, 214
- Coastline, 57, 171, 107, 210, 211, 237, 247, 252, 254, 255, 257, 267
- Coasts, 56
- Coating, 270, 275, 281
- Cochinoca–Escaya magmatic–sedimentary, 243
- Coefficients, 124
- Cohesion, 134, 137
- Cohesion errors, 137
- Cohesion values, 135
- Cold/subhumid environments, 204
- Cold/temperate, 207
- Cold temperatures, 222
- Collapsed depressions, 170
- Colliguaja integerrima, 95
- Collision, 55
- Collón Curá ashfall tuffs, 43
- Collón Curá formation, 37, 38, 40, 42, 43
- Collón Curá Formation (Middle to Late Miocene), 37
- Collón Curá Graben, 43
- Collón Curá river, 38
- Colluvial deposit, 38
- Colonization, 226
- Colonizers, 233
- Columnar jointing, 13, 38, 44
- Columnar structure, 14
- Comallo, 4
- Communities of grass affinity, 279
- Compaction, 30
- Competence, 192, 198
- Complex domical systems, 246
- Complex movements, 123
- Complex volcanic relief, 156
- Composed rods, 277
- Concave profile, 27, 33
- Concave slopes, 33
- Concentric buffer, 136
- Concretions, 38, 272
- Conglomerate, 2, 12, 37, 38, 242, 245
- Conglomerates and sandstones with carbonate cement, 122
- Consequent, 42
- Conservation, 54, 69, 72
- Conservation of resources, 54
- Conspicuous moraines, 56
- Constant western winds, 209
- Consumption and management of water reserves, 103
- Continental climate, 144
- Continental Cretaceous sediments, 77
- Continental deposits, 266
- Continental environment, 39
- Continental intraplate region, 79
- Continental landmass, 50
- Continental or marine, 55
- Continental plain, 105, 106
- Continental shelf, 164
- Contour maps, 110
- Converging, 44
- Cooling, 15, 30, 45
- Cooling unit, 12, 14, 21, 23, 39, 44
- Coppice dunes, 217
- Coranzulí volcanic complex, 246, 256
- Cordilleran, 174
- Cordilleran landscape, 172
- Cordillera Oriental morphostructural region, 241
- Corestones, 30
- Corners, 31
- Corridor, 6, 14, 23, 30, 45
- Corrosion, 8, 28, 263
- Corrosion plain, 37
- Coupled rods, 273, 274
- Cover vegetation, 188
- Crabs, 275
- Crabs bioturbations, 276
- Crack, 14
- Craters, 170
- Cratonic areas, 2
- Cratonic massifs, 2

- Creeks, 24
 Crests, 1, 29–31, 43, 45, 156
 Cretaceous, 28, 80, 96, 122, 169, 242
 Cretaceous planation surface, 20
 Cretaceous rocks, 122
 Critical success index, 131
 Cross section, 188
 Crustal shortening and thickening, 242
 Crustal stability, 2
 Cryoclastic processes, 169
 Cryoclastic product, 8
 Cryogenic structures, 143, 174
 Crystalline, 277
 Crystalline basement, 37, 42
 Crystalline biominerals, 262
 Crystalline clasts, 2
 Crystalline rocks, 136
 Crystalline textures, 282
 Crystallization, 28, 45
 Crystallographic axes, 263
 Crystals, 277, 279–282
 Crystals of weddellite, 280
 Crystic fabric, 275, 279
 Crystic factories, 282
 Ctenomys talarum, 270
 Cu, 243
 Cuestas, 26
 Cultural dimension, 146
 Culture, 52
 Cumbres Calchaquies, 124
 Current interglacial time, 69
 Curvature, 55
 Cutoff-independent statistic methods, 121
 Cypris ostracods, 253
- D**
- Dacite, 245
 Dacitic, 243
 Dacitic–basaltic alkaline, 242
 Dacitic ignimbrite, 21, 38, 246
 Dacitic pyroclastic rocks, 245
 Dacitic–rhyolitic, 243
 Dacitic vitro-crystalline tuffs, 246
 Damage degree, 187
 Darwin Range, 55
 Data sheet, 50, 58–60, 62, 64, 66, 68, 70
 Davisian, 40
 Debris, 26
 Debris avalanches, 123
 Debris flow, 123, 124, 127, 136, 250
 Debris-flow susceptibility, 121
 Debris slope, 27
 Decomposed organic matter, 254
 Decomposition, 281
 Deep chemical weathering, 2, 37, 39, 82
 Deep leaching, 79
 Deeply welded, 46
 Deeply welded zone, 44
 Deep weathering processes, 45
 Deficit, 207
 Deflation, 6, 20, 170, 204, 210, 217, 219, 221, 222
 Deflation basins, 220, 256
 Deflation energy, 210
 Deflation hollow, 155, 204, 207, 214, 222
 Deflation particles, 220
 Deflation plume, 210
 Degasification tube, 15, 30
 De Geer moraines, 168
 Deglaciation, 167
 Degraded vegetation, 218
 Degree of welding, 2, 12, 30, 43
 Dehydration, 277, 282
 Deltaic deposits, 250, 256
 Deltaic facies, 250
 Deltaic lobes, 249
 Deltaic tripartite structure, 249
 Deltas, 238
 Demographic increase, 103
 Demoiselle, 17, 33, 45
 DEM resolution, 185
 Dendritic drainage pattern, 163
 Density estimation, 120
 Denudation, 21, 22, 38, 45
 Denudation rate, 156
 Dependent dichotomous variable, 124
 Dependent variables, 126
 Deposition, 54
 Deposits, 238, 241, 243
 Depression bottoms, 210
 Depressions, 211, 213, 216, 217, 220–222
 Depth of failure surface, 129
 Descaling, 27
 Deseado Massif, 3, 28, 29
 Desert pavements, 80, 91
 Desert varnish, 18
 Desiccation, 210, 218, 219, 221, 222
 Desiccation cracks, 218
 Dessicating process, 218
 Destructive phenomenon, 186
 Detaching, 20
 Detailed dataset, 120
 Deterministic methods, 120
 Deterministic model FS, 136
 Deterministic models, 120
 Developmental stages, 226
 Devitrification, 28, 45
 Diagenesis, 277, 280

- Diagenetic calcification or decalcification, 264
 Diatomites, 245
 Diatoms, 253, 272, 275
 Dichotomous tubes, 282
 Didymograptus nitidus Hall, 243
 Didymograptus v-deflexus Harris, 243
 Difference vegetation index (NDVI), 125
 Differential erosion, 25, 30, 33, 35
 Differential resistance, 45
 Differential weathering, 3
 Digital Elevation Model (DEM), 125, 127, 129, 133, 136, 137, 141, 147, 183–186
 Digital Elevation Model-SRTM (Shuttle Radar Topography Mission), 185
 Digitalization, 80
 Digital Orion Research 501 pH meter, 264
 Digital terrain model MDE-Ar, 205
 Digital terrain models, 222
 3-dimension digital models, 141
 Diminished river, 161
 Direct assessment sheet, 58
 Direct insolation, 127
 Direct solar insolation, 136
 Discharge, 161, 185, 187, 191, 194
 Discharge areas, 102
 Discharge glaciers, 164
 Discharge values, 185
 Dismantling, 28, 45
 Dissolution, 263, 274, 277, 280
 Dissolution processes, 271
 Distance to stream channels, 125
 Distension area, 242
 Distributaries systems, 181
 Distribution, 3
 Distribution histogram, 134
 Diversity, 52, 226
 Divides, 40, 41
 DL index, 214, 216
 Dome, 11, 22
 Dome-like landforms, 30
 Domestic water service, 103
 Domestic wells, 104, 114
 Domical complexes, 246
 Domical explosive-lava dacitic complex, 246
 Domic Volcanic Complex, 256
 Dominant communities, 81
 Dorsal shell, 229
 Dorsal valve, 227, 229, 232
 Down-warped blocks, 43
 Drainage, 103, 187, 275
 Drainage basins, 216
 Drainage lines, 206, 211, 213
 Drainage network, 30, 40, 42, 187, 191–193
 Drinking water, 223
 Drinking water supply, 114
 Drinking water supply systems, 116
 Droughts, 255
 Drought season, 210
 Drumlin field, 51, 56, 58, 66, 69, 166, 167
 Drumlinoid forms, 164
 Druses, 277, 279–282
 Dry beds, 204
 Dry bottoms, 210, 220
 Dry climatic periods, 204
 Dry valleys, 163
 Dune, 103, 108, 217–220, 256, 262, 267, 271, 282
 Dune barrier, 267, 272
 Dune crest, 267, 270
 Dune destruction, 103
 Dune environments, 282
 Dune fringe, 103
 Dune migration, 204
 Dune sands, 106
 Duraznillar, 267
 Duricrust, 34
 Dust, 217, 221
 Dust clouds, 221
 Dust supply, 223
 Dynamic equilibrium, 210
 Dynamic modelling, 120
 Dynamics, 272
 Dystichlis sp., 96
- E**
- Earliest Miocene, 40
 Early Cretaceous, 55
 Early Holocene, 238, 257
 Early–Middle Ordovician, 243
 Early–Middle Pleistocene, 206, 237, 247
 Early Miocene, 245
 Early Miocene basalts, 40
 Early Palaeozoic, 20, 37
 Early Pleistocene, 4, 154
 Early Tertiary (Maastrichtian-Danian), 11, 169
 Early to Middle Miocene, 206
 Earth pillars, 33
 Eastern Andes, 242
 Eastern coastal areas, 209
 Eastern coast of the Province of Buenos Aires, 103
 Eastern margin of the pan, 210
 Ecological fragility, 254
 Ecological impact, 226
 Ecological patterns, 225, 233
 Ecological proxies, 227
 Ecological significance, 225, 226
 Economic activities, 72, 103

- Economic damages, 182
 Ecotone, 267
 Ecotourism, 54, 141, 174
 Ecotouristic potential, 53
 Ecotourists, 53
 Ectomycorrhitic pods, 281
 Education, 72
 Educational function, 54, 72
 EDXS microprobe, 279
 Effective cohesion, 129
 Efflorescences, 280
 Electric isoconductivity maps, 106
 Elevation, 127
 Ellipsoidal, 277
 Elliptical, 214
 Elliptical shape, 206, 214, 221, 222
 El Loro, 13
 El Nevado, 4, 5
 El Niño/Southern Oscillation (ENSO), 240
 El Niño southern oscillation phenomena, 123
 Elongated needle-fiber monocrystalline
 crystals, 280
 Elongated rods, 271
 Elongated tubes, 271, 282
 El Portezuelo formation, 5
 Encrustation, 227
 Encrusted, 233
 Encrusting, 225
 Encrusting biotas, 225, 227, 233, 234
 Endoaquolls, 267, 272
 Endopedion, 275
 Endorheic basins, 31, 82, 96, 206, 209, 214
 Endorheic depressions, 204
 Endorheic drainage, 238, 242, 256
 Endorheic drainage systems, 155
 English, 59
 Entisols, 79
 Environmental changes, 171
 Environmental factors, 120
 Environments, 267
 Eocene, 37
 Eocene-Oligocene boundary, 20
 Eolian abrasion, 38
 Eolian action, 20, 155
 Eolian activity, 155
 Eolian deflation, 170
 Eolian deposit, 38, 167, 171, 238, 246, 256,
 257
 Eolian erosion, 1, 6, 11, 45
 Eolian flux, 9
 Eolian processes, 141
 Eosclerocalyptus lineatus, 247
 Epeirogenic cycles, 143
 Ephedra ochreatea, 91, 95
 Ephemeral lake, 238, 257
 Ephemeral regime, 185
 Ephemeral runoff systems, 185
 Ephemeral shallow lakes, 214
 Ephemeral, shallow water lakes, 219
 Ephemeral streams, 163, 172, 209
 Epibiont, 225–227, 229, 231–234
 Epibiont algae, 225, 233
 Epibiont organisms, 230
 Epibionts pathways, 227
 Epibiosis, 225, 226
 Epibiotic, 226
 Epiclastic sequence, 38
 Epidote, 270, 272
 Epipedons, 272
 Episodic sea entries, 272
 Equilibrium analysis, 127
 Erdas, 147
 Erosion, 1, 22, 37, 40, 54, 91, 204, 209, 218,
 219, 222, 263
 Erosion action, 6
 Erosional and depositional landforms, 56
 Erosional geomorphic surface, 95
 Erosional processes, 264
 Erosion and deposition, 187
 Erosion and sedimentation, 186
 Erosion cycle, 80
 Erosion escarpments, 82
 Erosion features, 188, 191
 Erosion landform, 17, 43, 45, 220
 Erosion potential, 222
 Erosion processes, 2, 27, 30
 Erosion rates, 3
 Erosion surface, 22
 Erratic boulder, 56, 164
 Erratic boulder field, 51
 Error propagation map, 134
 Eruption centres, 174
 Eruption products, 38
 Eruptive vent, 5, 38, 170, 172
 Escaping gas, 15, 30
 Espartillar, 267, 272
 Estancia Harberton, 52
 Estancias, 146, 174
 Estuarine deposits, 266
 Estuarine sediments, 271
 Estuary, 150, 162, 172, 174
 Etching plain, 37
 Etching processes, 28
 Etchplain, 22, 39
 Europe, 204
 Evapotranspiration (ETP), 104, 204, 206, 207
 Excreted oxalic acid, 263
 Exfoliation, 9

- Exhumation, 37
 Exhumed planation surface, 77, 81, 82, 91
 Exploitation, 103
 Explosive eruption, 5
 Explosive volcanic eruptions, 2
 Explosivity, 156
 Extensional basins, 242
 Extensional Province, 79
 Extensional regime, 242
 Extra-Andean Patagonia, The, 78, 168, 220
 Extraction volumes, 114
- F**
- Fabric, 2, 37, 44
 Faces, 282
 Factor of Safety (FS), 119, 127, 137
 Fact sheet, 58
 Failure, 127, 137
 False Negative areas (FN), 131
 False negative errors, 137
 False negative/false positive, 137
 False negatives, 137
 False Positive areas (FP),, 131
 False positive errors, 137
 Fan, 191, 196, 198
 Fan-deltas, 249, 257
 Fault, 55
 Faulting, 55, 57
 Fault scarp, 181
 Fe and Mn, 106, 114
 Feldspar, 5, 17, 35, 272
 Fe precipitation, 18
 Ferdinand of Magellan, 152
 Festuca gracillima, 174
 Fiammes, 12
 Field and postgraduate courses, 52
 Field hydrological evidence, 181, 187
 Field observation, 209
 Field trip, 49, 51, 52, 58
 Filament, 268, 270, 271, 274, 276, 277, 279, 281
 Filliform, 282
 Fine gravel, 247
 First Phase of the Andean movements, 42
 Fissure eruptions, 155
 Fissures, 38, 263
 Fissure volcanic eruptions, 28
 Fixation, 107
 Fixation process, 107
 Fixed dune, 108, 110, 115
 Fixed dune and urbanized area, 107
 Flaking, 20
 Flared slope, 33
 Flares slopes, 34
 Flash flood, 181–183, 185–188, 192, 196, 197
 Flash flood hazard, 181, 183, 188, 195, 198
 Flash flood hazard assessment, 181
 Flash flood hazard map, 188
 Flash flood hazard map analysis, 198
 Flash flood risk, 182
 Flash flood susceptibility, 181, 189, 191–193
 Flash flood susceptibility map, 187
 Flechillar, 267
 Flood, 182, 183, 185, 191, 194
 Flood discharge, 194
 Flood duration, 185
 Flooded areas, 267
 Flood events, 182, 192
 Flood flash hazard, 197, 198
 Flood hazard, 182, 185
 Flooding, 182, 199
 Flooding plains, 43
 Flooding pools, 254
 Flooding probability, 186, 187
 Flood marks, 194
 Flood plain, 161, 169, 188, 257
 Floodplain and riverbed deposits, 238
 Flood susceptibility, 186
 Flora and fauna, 53
 Flow, 123, 188, 191
 Flow energy, 187
 Flow meter, 187
 Flow pathways, 192
 Flow unit, 3, 26
 Flow velocity, 188
 Flow volume, 102
 Flutes, 166
 Fluvial and fluvio-glacial channelled landscape, 161
 Fluvial and glaciofluvial valleys, 204
 Fluvial belts, 187
 Fluvial deposits, 222
 Fluvial dissection, 214
 Fluvial-eolian plain, 187, 192
 Fluvial erosion, 40
 Fluvial landscape, 148
 Fluvial modelling, 222
 Fluvial network, 40
 Fluvial process, 81, 141
 Fluvial regime, 245
 Fluvial streams, 173
 Fluvial systems, 181, 187, 199
 Fluvial valleys, 154
 Fluvio-eolian, 261
 Fluvio-eolian plain, 264
 Folding, 55
 Foliation, 55
 Food chains, 267

- Foreland basins, 242
 - Foreset clinoforms, 238
 - Foreset-type clinoforms, 249
 - Forest, 69, 169, 173
 - Forest cover, 137
 - Forested mountains, 56
 - Forest fires, 169
 - Formation of the Andes, 69
 - Forms, 54
 - Forward Stepwise technique, 125
 - Fossil assemblage, 233
 - Fossil littoral environment, 211
 - Fossil mammal bones, 39
 - Fossil mammal teeth, 39
 - Fossil marshes, 211
 - Fossil organisms, 225, 226
 - Fossil record, 226, 227
 - Fossils, 54
 - Fossil tide-channels, 211
 - Fractures, 12, 42
 - Fracture systems, 30, 37
 - Franquenian sp., 93
 - Freshwater, 101
 - Freshwater aquifer, 106
 - Freshwater-brackish water interface, 106
 - Freshwater recharge, 116
 - Freshwater reserves, 103
 - Freshwater reservoirs, 102
 - Freshwater-saltwater interface, 106, 114
 - Freshwater supply, 103
 - Freshwater supply system, 103
 - Friability, 43
 - Friable sedimentary rocks, 45
 - Frozen soils, 156
 - FS model, 131, 134–137
 - Fuegian Andes, 52, 55, 57
 - Fuegian Archipelago, 50, 56
 - Fuegian ecotone, 56
 - Fuegian geotourist itinerary, 71
 - Fuegian landscapes, 69, 71
 - Fuegian steppes, 204, 207
 - Fungal, 271
 - Fungal activity, 268, 280
 - Fungal biomineralization, 274
 - Fungal biomineralization processes, 281
 - Fungal cell wall, 280
 - Fungal filaments, 276
 - Fungal hyphae, 268, 274
 - Fungal hyphae filaments, 268
 - Fungal mats, 280
 - Fungal miscelia, 279
 - Fungal mycelia, 276
 - Fungal nature, 281
 - Fungal origin, 282
 - Fungi, 262, 263, 271, 276, 277, 281
 - Fungivore mesofaunan, 281, 282
 - Furrow, 8
 - Future landslides, 126
 - Fuzzy logic, 120
- G**
- Gable island, 58, 64
 - Galleries, 30, 45
 - Garnet, 270, 272
 - Gastronomy, 146
 - Gaussian distribution, 133
 - Gaussian mixture model, 120
 - Gels, 282
 - General Pueyrredón counties, 264
 - Geo-activities, 54
 - Geoconservation, 54
 - Geo-description, 58
 - Geo-diversity, 54
 - Geo-ecology, 79
 - Geo-environmental, 120
 - Geo-environmental factors, 127
 - Geographical, 72
 - Geographical characteristics, 56
 - Geographical data, 124
 - Geographical environments, 172
 - Geographical features, 150
 - Geographical Information System (GIS), 107, 205, 182
 - Geographical position, 174
 - Geographical Setting, 55
 - Geographical zones, 205, 220
 - Geographic space, 146
 - Geographic tourism, 53
 - Geoheritage, 50, 53
 - Geohistory, 54
 - Geohydrological environment, 114
 - Geo-interpretation, 54, 58, 59, 71
 - Geological, geomorphological and hydrological basic studies, 183
 - Geological, 143, 263
 - Geological and geomorphological features, 49
 - Geological and geomorphological map, 184
 - Geological and geomorphological setting, 49, 53, 72
 - Geological aspects, 186
 - Geological features, 52, 54
 - Geological heritage, 54, 69
 - Geological history, 55
 - Geological interest, 58
 - Geological park, 160
 - Geological period, 226
 - Geological processes, 141, 174
 - Geological resources, 54

- Geological setting, 122
- Geological structure, 2
- Geological topics, 69
- Geological tourist attractions, 52
- Geological units, 141
- Geology, 53, 54, 71
- Geology and geomorphology, 53
- Geomorphic process, 45, 78
- Geomorphic surface, 77, 80–82, 95–97
- Geomorphological, 181, 182
- Geomorphological agent, 78, 203
- Geomorphological analysis, 45, 187, 191
- Geomorphological and anthropic variables, 187
- Geomorphological and hydrological indicators, 195
- Geomorphological aspects, 186
- Geomorphological changes, 101
- Geomorphological characteristics, 106, 110, 194
- Geomorphological emplacement, 204, 212, 220
- Geomorphological environment, 106, 191, 221
- Geomorphological feature, 143, 150, 156, 160, 193, 222
- Geomorphological hazards, 182
- Geomorphological interest, 51
- Geomorphological landscapes, 53
- Geomorphological maps, 120
- Geomorphological methodologies, 199
- Geomorphological processes, 120, 141
- Geomorphological regional map, 187
- Geomorphological response, 222
- Geomorphological scenario, 187
- Geomorphological singularity, 152
- Geomorphological–stratigraphical, 238
- Geomorphological studies, 46
- Geomorphological unit, 77, 80, 93, 96, 97, 204–206, 212, 214–216, 220–222
- Geomorphological variables, 183
- Geomorphological zones, 266
- Geomorphologic emplacements, 220
- Geomorphologic
 - (morphometric-morphodynamic) indicators, 186
- Geomorphologists, 71
- Geomorphology (processes, features)
 - networks, 186
- Geomorphology, 53, 71
- Geomorphology-soil relationship, 97
- Geomorphometric parameters, 127
- Geopedological characteristics, 267
- Geopedological Unit, 262, 265–267, 271, 279
- Geo-processes, 58
- Georesource, 49, 54, 58–60, 62, 64, 66, 68–72
- Geosciences, 72
- Geosite, 52–54
- Geo-systems, 58, 146
- Geotechnical aspects, 186
- Geotechnical parameters, 136
- Geotourism, 49, 50, 52–54, 59, 72, 141
- Geotourist, 71, 72
- Geotourist destination, 72
- Geotourist itinerary, 49, 58, 72
- Geotourist potential, 54
- Geotourist practice, 52
- Geo-trails, 54
- Giant inselberg, 3
- Gilbert's skill score, 131
- Gilbertian deltas, 249
- Gilbert-type delta deposits (Minchín Phase), 249
- Gilbert-type deltaic deposits, 257
- Gilbert-type deltas, 238, 257
- GIS-Based landslide susceptibility models, 119
- GIS environment, 121, 123, 124, 126
- GIS framework, 147
- Glacial action, 174
- Glacial advances, 164
- Glacial alignments, 167
- Glacial and fluvial action, 169
- Glacial and glaciofluvial landscape, 148, 164
- Glacial deposits, 55, 154, 222
- Glacial environment, 168
- Glacial episodes, 143
- Glacial event, 164, 247
- Glacial landforms, 69
- Glacial landscape, 165, 170, 172
- Glacial lobes, 168
- Glacial maximum expansion, 241
- Glacial morphology, 161, 163, 164
- Glacial processes, 141
- Glacial topography, 158
- Glacial troughs, 57
- Glacières National Park, 170
- Glaciations, 55–57, 164, 206, 211
- Glacier, 165, 206
- Glaciofluvial and glaciolacustrine sediments, 167
- Glaciofluvial deposits, 30, 56
- Glaciofluvial fan, 206, 214, 215, 216, 221
- Glaciofluvial fan pans, 215, 220
- Glaciofluvial or paleodrainage fans, 220
- Glaciofluvial plains, 164
- Glaciofluvial processes, 150
- Glaciofluvial sediments, 167, 169
- Glass shard, 21, 38, 43
- Glassy layer flow, 23
- Global cooling, 20

- Global frictional angle, 129
 Global Mapper, 147
 Global sea level, 152, 211
 Global sensitivity analysis, 119, 133
 Global warming, 20
 Globular type, 36
 Gnammas, 26, 27
 Gneisses rock, 2, 37
 Gondwana, 28
 Gondwana paleosurfaces, 82
 Google Earth, 51, 57, 58, 123, 147, 187
 Google Earth®, 205
 Google Earth® image, 219
 Gorges, 17, 22, 30
 Graben, 43
 Grain size, 3
 Grande and Chico rivers, 205
 Granite environments, 28, 45
 Granite landscape, 44, 45
 Granite rock landforms, 44
 Granitic landscape, 2, 22, 25, 27
 Granitic rock, 23, 37
 Granitic rock landscapes, 1
 Granular disintegration, 27
 Graptolites, 243
 Grass cover, 174
 Grassland, 144, 169, 204, 272
 Grasslands and shrublands, 207
 Grassland steppe, 168
 Grasslands vegetation, 124
 Grass steppe, 96
 Grassy vegetation, 217
 Gravel beaches, 57
 Gravel ridges, 211
 Gravels, 246
 Gravel spit Península El Páramo, 210
 Grayish white tuff, 247
 Great Patagonian Glaciation, 164
 Grindelia chilensis, 95
 Groove, 5, 6, 8
 Groovy channel, 6
 Groundwater, 102, 103, 106, 136, 137
 Groundwater levels, 102
 Groundwater recharge areas, 102
 Groundwater regime, 103
 Groundwater reserves, 101, 112
 Groundwater system, 110
 Guided tours, 54
 Guided visits, 49
 Gullies, 13, 105
 Gullies and rills, 17
 Gypsic, 82
 Gypsum, 93, 122, 238, 251
 Gypsum and halite, 253
 Gypsum precipitation, 238
 Gypsum rosettes, 252
 Gytja, 238, 251, 253, 254
- H**
- Habit, 273, 274, 276
 Habitats, 223
 Halite, 218, 238, 251, 252
 Halophilous vegetation, 221
 Halophyte vegetation, 217
 Haplargids, 78
 Haplocalcids, 78, 93
 Hapludolls, 267, 272
 Harberton, 51, 52
 Harberton peatbog, 58, 70, 71
 Hazard, 120, 181, 186, 198, 199
 Hazard assessment, 119
 Hazard flood, 183
 HCl, 279
 Headwater erosion, 172
 Heavy minerals, 270, 272, 279
 Heinrich I event, 252
 Heliophany, 144
 Hemispheric Reserve Network of Beach Birds, 150
 Herb species, 207
 Heuristic approach, 120
 Heuristics methods, 120
 Hexagonal column, 13
 Hierarchical classification, 80
 Hierarchical structures, 146
 High coasts, 57
 High-degree ignimbrites, 2
 Higher atmosphere dust, 204
 Higher mean monthly temperature, 207
 High irradiation, 255
 Highly welded, 30
 High mountain scenery, 57
 Highplains, 43
 High-Puna plateau, 242
 High resolution multitemporal satellite images, 123
 High-resolution satellite imagery, 164
 High tide amplitude, 210
 Hipo- and neocalcians, 279, 282
 Hollow, 14, 18, 35, 205, 213–215, 222
 Hollow density, 215
 Holocene, 4, 155, 204, 225–227, 233, 234, 253–257, 266, 267, 271, 275
 Holocene paleosols, 51
 Homocline structure, 21, 169
 Homocline inclination, 26
 Hoodoo, 1, 31, 33, 37, 45

- Horizon, 264, 268, 270–272, 274–276, 279, 281
 Horizon sequence, 82, 91
 Horizontal jointing, 26
 Hornitos, 156
 Horns, 57
 Horse riding, 146
 Hosmer-Lemeshow test, 126
 Human activity, 174
 Human colonization, 168
 Human consumption, 104
 Human populations, 159
 Human settlement, 163
 Human settlement and infrastructure, 120
 Humid winds, 121
 Humified organic matter, 275
 Hummocks, 158
 Hunquillar, 267
 Hyalite deposition, 238
 Hydraulic radius, 188
 Hydrochemical behaviour, 106
 Hydrochemistry, 110
 Hydrodynamic behaviour, 106
 Hydrodynamic diagram, 105
 Hydro-eolian depressions, 155
 Hydrogeological characteristics, 106
 Hydrogeological data, 103, 104
 Hydrogeology, 103
 Hydro-geomorphological features, 188
 Hydrographical network, 102
 Hydrological, 181
 Hydrological analysis, 182
 Hydrological balance, 207, 208
 Hydrological balance analysis, 206
 Hydrological basin level, 121
 Hydrological basins, 123
 Hydrological behaviour, 103
 Hydrological changes, 272
 Hydrological conditions, 120
 Hydrological cycle, 102
 Hydrological data, 181
 Hydrological deficit, 124, 219
 Hydrological excess, 209
 Hydrological factors, 125
 Hydrological models, 182
 Hydrological point of view, 150, 158
 Hydrological system, 101, 104, 110
 Hydrological variables, 183
 Hydrological variations, 101, 272
 Hydrologic aspects, 186
 Hydrologic basin scale, 137
 Hydrology, 147
 Hydrology features, 184
 Hydromorphic soils, 79
 Hydromorphism conditions, 272
 Hyper-concentrated flows, 250
 Hypertropical climates, 82
 Hyphae, 263, 277, 280, 282
- I**
- Ice block, 171
 Ice disintegration, 166
 Ice disintegration processes, 164
 Ice lobes, 57, 165
 Ice modelling, 57
 Ice sheet, 55
 Identification, 142
 Igneous rock, 2, 11, 28, 45, 57
 Ignimbrite, 1–3, 5, 14, 17, 20, 28, 30, 34, 37, 38, 39, 43, 44, 45, 46, 242
 Ignimbrite flow, 1, 13, 22, 23, 40, 44, 245
 Ignimbrite landscapes, 45
 Ignimbrite mantle, 5, 26, 30
 Ignimbrite modelling, 44
 Ignimbrite plateau, 13, 28, 44
 Ignimbrite rocks, 2
 Ignimbrite sedimentary packages, 29
 Ignimbrite sheets, 6, 31
 Illuvial clay, 90
 Impervious areas, 102
 Impervious surfaces, 101, 108, 114, 115
 Impregnation, 271
 Incrustation, 271
 Independent variables, 126
 Independent variables (control factors), 125
 Independent visits, 54
 Indirect heuristic approach, 120
 Indurated porous surfaces, 34
 Infiltration, 101, 103, 104, 108, 110, 112, 115
 Infiltration capacity, 102, 112
 Infiltration ponds, 103
 Infiltration value, 107, 110
 Infinite slope model, 120, 127–129
 Inflated surfaces, 156
 Inka Tectonic phase, 242
 Inner friction, 43
 Insect activity, 275
 Insect nests, 38
 Inselberg, 1, 20
 Insolation, 135
 Instability factors, 120
 Instrumentation, 185
 Instruments, 58
 Integrative discovery, 53
 Interannual variations, 112
 Inter-drumlin interpretation centre, 69
 Interdune area, 270
 Interdune environments, 220

- Interdunes, 262, 267, 282
 Interdune soils, 271
 Interglacial, 257
 Interglacial period, 238
 Intermediate plagioclase, 38
 Intermontane drainage basins, 38
 Intermountain valleys, 256
 International importance site, 150
 International Union for the Conservation of Nature., 254
 Inter-oceanic pathway, 152
 Interpretation, 54
 Interpretation and learning, 54
 Interpretation centre, 69
 Interpretation materials, 54
 Interpretation services, 53
 Interpretative board, 52
 Interpretative facilities, 53
 Interpretative materials, 49
 Interpretative media, 52
 Interpretative panels, 69
 Intertidal plains, 150, 152
 Intertropical convergence zone (ITCZ), 253
 Intra-formational breccias, 38
 Intrazonal soils, 79
 Inventory, 123, 174
 Inventory map, 120
 Inversion of relief, 156
 Inversion of the regional slope, 40
 Invertebrates, 267, 270
 Ionic solutions, 79
 Ions, 262
 Iron (Fe), 243, 262, 270, 271, 281
 Iron coatings, 272
 Iron oxides, 270
 Irrigation, 102, 103
 Irrigation supply, 223
 Isla Gable, 51
 Isla Grande de Tierra del Fuego, 50, 205, 210, 220
 Isla Grande of Tierra del Fuego, 203
 Iso-electrical conductivity, 113
 Isohyet, 183
 Isophreatic curve, 106
 Isotopic and chemical study, 241
 Isotopic dating, 246
 Italy, 121
- J**
- Jarava speciosa, 93
 Jaya River basin, 121, 122, 123, 124, 127, 129, 136
 Joint, 12, 18, 30, 42
 Jointing, 13, 17
 Jointing set, 25
 Joint plane, 19
 Joint surface, 19
 Joint system, 23, 24
 Jujuy, 237
 Juncos sp., 96
 Junellia tridactylis, 96
 Junielia tridens, 144
 Jurassic, 11, 37, 39, 45
- K**
- K/Ar, 245
 Kettles holes, 167
- L**
- La Buitrera, 13
 Lacustrine beaches, 256
 Lacustrine coastline deposits, 254
 Lacustrine coastline deposits (Minchín), 247
 Lacustrine coastlines, 257
 Lacustrine deposits (Playa Lake), 251, 253
 Lacustrine episodes, 245, 246
 Lacustrine expansion, 238, 247, 257
 Lacustrine shrinkage, 238
 Lacustrine terraces, 219
 Lago Fagnano, 51, 55
 Lagoon, 281
 Laguna Amalia, 218
 Laguna Azul, 160
 Laguna de los Pozuelos, 237, 238, 240–242, 251, 253, 254, 256
 Laguna de los Pozuelos dome volcanic complex, 245
 Laguna de Pozuelos, 256
 Laguna Los Pozuelos, 240
 Lagunas Secas Drift, 211
 La Horqueta canyon, 13
 Lake Arturo, 218
 Lakes, 174
 Lake Titicaca, 241
 La Matilde formation, 3, 28, 30
 Laminar runoff (interfil), 78
 Laminated silt–mud, 247
 Land cover, 124
 Land cover/land use, 106
 Landform, 29, 54, 71, 143, 150, 152, 160, 163–169, 204–206, 209, 211, 213, 214, 217, 218, 220, 221, 223, 263
 Land mammal fossil remains, 38
 Landsat 7 images, 147
 Landsat images, 141
 Landsat TM satellites images, 125

- Landscape, 17, 29, 52–54, 57, 137, 141–143, 145–150, 154–156, 158–161, 163, 164, 166–170, 174, 204, 206, 222
- Landscape cartography, 141
- Landscape classification, 147
- Landscape component, 147
- Landscape depressions, 42
- Landscape diversity, 146
- Landscape evolution, 39
- Landscape formation, 20, 69
- Landscape of Endorheic basins, 170
- Landscape Type Associations (LTA), 147
- Landscape Types (LT), 141, 142, 147, 148
- Landscape units (LU), 56, 141, 142, 146, 147, 154, 170
- Landscape variability, 141
- Landslide, 120, 123, 125, 126, 131, 136, 137, 150
 distribution of, 123
 types of, 123
- Landslide/debris-flow inventory maps, 119
- Landslide density, 127
- Landslide depths, 120
- Landslide events, 123
- Landslide initiation, 124
- Landslide inventory, 123, 124
- Landslide inventory map, 129
- Landslide map, 127
- Landslide model, 121
- Landslide presence, 127
- Landslide processes, 137
- Landslide spatial distribution, 127
- Landslide susceptibility, 120, 121, 123, 124, 137
- Landslide susceptibility maps, 130
- Landslide susceptibility models, 119–121, 124, 130, 131
- Landslide susceptibility zoning, 121
- Landslides zonation, 126
- Landslide types, 120
- Landslide volumes, 120
- Landsliding, 120, 127, 137
- Land use, 101–104, 107–110, 112, 116, 185
- Land-use characteristics, 106
- Land-use planning, 101, 137, 182
- Land use planning and management, 199
- La Niña-like conditions, 253
- La Pampa (central Argentina), 2
- La Quiaca, 240
- Las Bayas tuff member, 38
- Last Glacial Maximum (LGM), 51, 56, 238, 250
- Last Glaciation, 69, 237, 247, 257
- Late Cretaceous, 256
- Late Cretaceous continental sediments, 39
- Late Cretaceous sedimentary rocks, 37
- Late Eocene, 20
- Late Eocene–Early Oligocene, 242
- Late Holocene, 204, 241, 256
- Late Jurassic, 39
- Late Jurassic–Early Cretaceous rocks, 55
- Late Jurassic to Early Cretaceous volcanic pyroclastic rocks, 55
- Late Jurassic weathering, 37
- Late Mesozoic, 37
- Late Miocene, 158, 246, 256
- Late Miocene and Early Pliocene basalts, 37
- Late Oligocene, 20, 245
- Late Oligocene–Early Miocene, 242, 256
- Late Oligocene warming, 20
- Late Palaeocene, 37
- Late Pleistocene, 5, 11, 45, 237, 240, 241, 247, 250, 252, 255, 257, 266
- Late Pleistocene climate, 241
- Late Pleistocene lacustrine, 247
- Late Pleistocene paleosols, 252
- Late Pliocene, 155
- Late proterozoic, 20
- Late quaternary, 264
- Late Quaternary pedosedimentary sequences, 262
- Lateral moraine, 165
- Latest Oligocene, 40
- Late Triassic, 28, 37, 45
- Latin hypercube procedure, 134
- Latitudinal position, 56
- LATYR-Universidad Nacional de La Plata, 252
- Lava-explosive centers, 245
- Lava flow, 4, 11, 28, 156, 160, 163, 170, 174
- Lavas, 155, 156
- Least populated regions, 72
- Leeward coast, 221
- Leeward depressions, 220
- Leeward direction, 210
- Leeward margin, 217, 221
- Leisure, 50, 53, 59, 72
- Lenga (*Nothofagus pumilio*), 169
- Lesser welded ignimbrites, 30
- Lichen colonization, 27
- Light and heavy minerals, 265, 270, 272, 279
- Light elements, 281
- Lighter minerals, 270, 272, 275
- Lihuel Calel, 21
- Lihuel Calel ignimbrite, 21, 45
- Lihuel Calel (province of La Pampa), 1
- Limestone, 122, 245
- Liothyrella uva, 227

- Lithic fragments, 5, 270
 - Lithic instruments, 174
 - Lithic Torriothents, 82
 - Lithic tuffs, 38, 42
 - Lithoclast, 2, 6, 12, 19, 30, 35, 272
 - Lithological, 2, 143
 - Lithological aspects, 186
 - Lithological map, 127
 - Lithologic types, 38
 - Lithology, 2, 3, 58, 123, 127, 134
 - Lithostratigraphic units, 42
 - Littoral coastal environments, 247
 - Littoral erosion, 152
 - Littoral landscape, 172
 - Littoral morphology, 211
 - Littoral processes, 141
 - Littoral ranges, 214
 - Littoral ridge, 152, 206, 220, 221
 - Littoral ridges pans, 211, 214
 - Living organisms, 225
 - Llambías, 5
 - Lobes, 158
 - Lobe structure, 249
 - Local heritage, 71
 - Local relief, 156, 170, 209
 - Lodgement, 146
 - Loess, 261, 263
 - Loessic, 261
 - Loess mantle, 262, 267
 - Logistic regression (LR), 119, 120, 125, 126, 131, 132, 136
 - Logistic regression (LR) analysis, 124
 - Logistic regression (LR) model, 119, 124, 127, 131, 135–137
 - Lonco Trapial Formation, 79, 82
 - Los Adobes formation, 80
 - Loss of human lives, 182
 - Low area, 239
 - Low cliffs, 1
 - Lower member, 12
 - Lower–middle ordovician, 243
 - Lower tuffaceous member, 40
 - Low-grade ignimbrites, 2
 - Low-hill topography, 56
 - Lowland plain, 183
 - Low-Mg calcite, 226
 - Low mountain chains, 204
 - Low permeability rocks, 181
 - Lublinite, 273, 274
 - Lunette, 204, 217, 222
 - Luvic calsisols, 252
 - Lycium ameghinoi, 82, 93, 96
- M**
- Maar, 155, 156, 160, 170, 174
 - Macro- and micro-landforms, 1
 - Macrochorobates chapalmalensis, 247
 - Macroevolutionary patterns, 227
 - Macroevolutionary questions, 227
 - Macronutrients, 282
 - Macroporosity, 280
 - Macrotidal, 150
 - Mactra isabelliana, 266, 275
 - Mactra sp., 272
 - Magellan-Fagnano Fault, 51, 55
 - Magellania venosa, 225, 227, 229–232, 234
 - Magellan penguin rockery, 52
 - Magellan penguins, 152
 - Magellan strait, 142, 150, 152, 164, 165, 174, 211
 - Magmatic activity, 11
 - Magmatic arch, 243
 - Magmatic episode, 28
 - Magnesium, 270
 - Magnitude landslides, 120
 - Maihuenia patagonica, 95
 - Mallines, 96, 144, 159
 - Mallines (Aquentes), 79
 - Mammals, 154
 - Management, 54, 103, 174
 - Man-made action, 204
 - Manning, 181, 188, 194
 - Mantle shaped runoff, 191
 - Mar Chiquita, 264, 266
 - Mar Chiquita formation, 266
 - Mar Chiquita lagoon, 267, 271, 272, 275, 279, 282
 - Marginal floodplain, 267, 275
 - Marginal plain, 266, 271, 279, 282
 - Marine, 263
 - Marine and deltaic environments, 206
 - Marine and glaciofluvial origin, 222
 - Marine beach facies, 266
 - Marine deposits, 28
 - Marine environments, 226
 - Marine platform, 242
 - Marine salt water, 104
 - Marine sedimentary sequences, 242
 - Marine shales, 243
 - Marine transgression, 206, 211, 222
 - Marsh, 150, 152, 174, 220, 221, 222
 - Marsh areas, 206
 - Marsh basins, 214
 - Marsh morphology, 217
 - Marsh pans, 211, 213
 - Marsh plains, 221
 - Marshy, 222

- Marshy protected area, 172
 Mass-movement processes, 150, 152, 155, 158, 169, 170
 Materials, 58
 Mat-forming grasses, 144
 Matrix, 6, 262, 265, 274, 277, 279–282
 Matrix of glassy shards, 2
 Maturity, 42
 Maturity stage, 40
 Maximum amplitude (Am), 205
 Maximum length (Lm), 205
 MC analysis, 134
 MC method, 133
 Meadows, 144
 Mean annual precipitation, 104, 110, 207
 Mean annual temperature, 143, 207
 Meandering pattern, 161, 168
 Meanders, 168, 187
 Mean deviation, 134, 135
 Mean perimeter (L), 216
 Mean temperature of the coldest month, 207
 Medium and fine sands, 267
 Megaflutes, 166
 Mega-inselberg, 21, 22
 Megaripples, 217
 Melton ruggedness number (MRN), 125
 Meltwater, 162
 Meltwater activity, 174
 Mesas, 26
 Meseta Latorre, 155
 Mesetas, 43
 Mesh denoising algorithm, 125
 Mesic, 80
 Mesophile forest, 144
 Mesoscopic, 261
 Mesotherine, 246
 Mesothermal, 183
 Mesothermic, 267
 Mesozoic, 2, 143, 237, 247
 Mesozoic–Cretaceous, 243
 Metabolic products, 277
 Metadata file, 106
 Metal alloys, 263
 Metamorphic and granitic rocks, 183
 Metamorphic rock, 11, 57
 Micro- and mesopores, 282
 Microarchitectural units, 263
 Microbial activity, 280
 Microdispersive analysis, 265, 270
 Microfauna, 277
 Microflora, 281
 Micro-grained groundmass, 21
 Micro-landforms, 46, 263
 Micro-landscape, 220
 Micro-modelling, 1
 Micro-modelling landform, 2, 18
 Microorganism, 261, 262, 271, 277, 281
 Micropores, 277
 Micro-relief, 34, 271
 Micro-relief landforms, 43
 Microrods, 274
 Microscopic, 261
 Microscopic microstructure, 268
 Microstructure, 273, 279, 282
 Micro-yardang, 6
 Middle Cretaceous, 39
 Middle Eocene, 11, 20, 45
 Middle Holocene, 152, 206, 211, 256
 Middle Jurassic, 28
 Middle Jurassic age, 77, 79
 Middle Miocene, 40, 206, 245, 246, 256
 Middle Miocene caldera magmatic system, 246
 Middle Miocene climatic optimum, 20
 Middle Ordovician, 243
 Middle Pleistocene, 152, 206, 211, 222
 Middle Tertiary, 141
 Middle Tertiary age, 154
 Middle to Late Jurassic, 28
 Middle to Late Miocene, 2, 37–39
 Middle to Late Palaeozoic, 37
 Migmatites and igneous intrusive rocks, 122
 Migmatites rock, 37, 243
 Migratory birds, 253
 Mildly metamorphosed, 55
 Minchín, 250, 257
 Minchín lacustrine coastlines, 249, 256
 Minchín lacustrine coasts, 251
 Minchín lacustrine deposits, 250
 Minchín phase, 237, 247, 250, 255, 257
 Minchín phase lake, 255
 Mineral grains, 270, 277
 Mineralo-biochemical indicators, 283
 Mineralo-chemical studies, 282
 Mineralogical composition, 37
 Mineralogical properties, 279
 Mineralogical studies, 241, 265
 Mineralogy, 262, 275
 Minerals, 263, 272
 Mineral soils, 267
 Minerlogical transformation, 37
 Mining, 173
 Mining structures, 169
 Miocene, 28, 55, 154, 242
 Miocene tuffs, 42
 Mixed Coastal Environment, 267
 Mixed hills and valleys, 56
 Mn precipitation, 18
 Mobile dune, 107, 108, 110, 112, 115

- Mobile slice, 128
 Modelling of sandstones, 44
 Model prediction capacity, 137
 Modern alluvial fans, 77, 81, 82, 96
 Moisture, 210
 Moisture changes, 280
 Moisture regime, 80
 Mollic, 281
 Mollic epipedon, 275, 279, 281, 282
 Molluscs, 225, 229, 231
 Mollusk shells, 266
 Monazites, 243
 Monitoring network, 104
 Monocrystalline rods, 274
 Monocrystals, 273, 274
 Monocyclic and polycyclic soils, 281
 Monogenetic, 44
 Monogenetic landscape, 11, 45
 Monohydrated calcium oxalates, 280
 Monomorphic, 275
 Monsoon, 123
 Monsoon storm regime, 122
 Monte Carlo (MC) approach method, 133
 Monte Olivia, 59
 Monuments, 263
 Moraine, 164, 168, 170, 210
 Moraine systems, 164
 Morainic belts, 211
 Moreta formation, 242, 245, 246, 256
 Morphoclimatic, 11, 20, 44–46
 Morphodynamic analysis, 191
 Morphogenesis periods, 78, 91
 Morphogenetic agent, 20, 44, 45
 Morphogenetic system, 11, 20, 45, 46
 Morphogenetic units, 147, 204
 Morphological, 279
 Morphological changes, 102
 Morphological types, 2
 Morphometric analysis, 205
 Morphometric and morphological characteristics, 221
 Morphometric causal factors, 124
 Morphometric changes, 221
 Morphometric characteristics, 188, 204, 209, 213, 216, 221
 Morphometric factors, 125
 Morphometric indicators, 188
 Morphometric parameters, 222
 Morphometric values, 215
 Morphostratigraphic position, 82
 Morphostructurally, 239
 Morphostructural unit, 3, 143, 237, 238
 Mountain and piedmont areas, 182
 Mountain and piedmont basins, 181
 Mountain basin, 185, 192
 Mountainous, 55
 Mountainous and coastal environments, 52
 Mountainous terrain, 56
 Mountainous topography, 57
 Mountain systems, 57
 Mountain uplift, 55
 MRN, 135
 Mucorales, 263
 Mucus, 277
 Mucus agglutination, 233
 Mud, 238
 Muddy currents, 250
 Mudstone, 90, 96, 242
Mulguraea ligustrina, 82, 91, 93
Mullinum spinosum, 82
 Multiclass overlay, 120
 Multi-date classification, 106
 Multiple eruption vents, 39
 Multi-spectral, 141
 Multi-temporal analysis, 101, 106
 Multivariate, 120
 Multivariate logistic regression, 120
 Muscovite, 272
 Mushroom, 1, 33, 37
 Mushroom rocks, 31, 33, 45
 Mushroom shape, 6
 Mycelia, 277
 Mycorrhizal, 263
 Mycorrhizal basidiomycetes, 263
- N**
- Na-Cl, 106
Nadrophillum obtusipolium, 93
Nardophyllum obtusifolium, 82, 91, 93
Nassauvia axilaris Colliguaja integerrima, 93
Nassauvia glomerulosa, 82, 91, 93
Nassauvia sp., 93
Nassauvia ulicina, 91, 96
 National Centre of Competence in Research, 241
 National road 3, 52
 National road number 3, 52
 National route 40, 141, 142, 174
 Natracoulls, 272
 Natrargids, 78
 Natric, 82
 Natric horizon, 91
 Natural and anthropic degradation, 262
 Natural and cultural resources, 53
 Natural attractions, 59
 Natural bridge, 3
 Natural fauna, 145
 Natural fragility, 181, 186

- Natural hillslopes, 127
 Natural infiltration, 102
 Natural landscape, 54, 142
 Natural logarithm, 127
 Natural resources, 71, 147
 Natural scenery, 71, 72
 Nature tourism, 54
 Nebkas, 80
 Nebkhas, 217, 218, 221, 222
 Needle bundles, 281
 Needles, 29, 30, 44, 45, 274, 277, 282
 Neogene, 28, 122, 211, 256
 Neogene volcanic, 243
 Neoproterozoic, 28
 Neotectonic activity, 183
 Neotectonic adjustment, 250
 Neotectonic catastrophic events, 250
 Neotectonic faults, 249
 Neotectonic movements, 252
 Ñire (*Nothofagus antarctica*), 169
 Ñirihuau marine basin, 43
 North Atlantic Ocean, 241
 Northeastern Santa Cruz province, 3
 Northeast Uruguay, 103
 Northern Patagonia, 37, 38, 42, 54, 155
 Northern Patagonian Massif, 4, 37, 42, 43
 Northern Puna, 242
 Northern Tierra del Fuego, 51, 205, 221, 222
 Northwestern Argentina, 119
 Nothofagus, 169
 Nothofagus Antarctica, 144
 Nothofagus forest, 169
 Nothofagus pumilio, 144
 Nothofagus sp. forest, 57
 Nubbins, 1, 22, 25, 29, 30, 45
- O**
- Oblique subduction system, 242
 Observational effect, 227
 Observation networks, 103
 Occupation of space, 147
 Ocean crust subduction, 243
 Ochraceous epipedon, 252
 Off shore, 146
 Oligocene, 40
 Olivine, 5
 Ollier, 2, 22
 Opaque minerals, 270, 272
 Optic microscopy, 261
 Ordovician, 242, 243, 246
 Ordovician–Paleozoic, 256
 Organic and mineral horizons, 282
 Organic horizon, 280
 Organic materials, 275
 Organic matrix, 262
 Organic matter, 264, 270, 272, 275, 280
 Organic matter content, 262
 Organic membrane, 263
 Organic mud, 254
 Organic resource, 263
 Organic substrate, 277
 Organisms, 225–227, 233, 261, 262
 Orogenic movements, 40, 42
 Orographic barrier, 121
 Orographic storms, 144
 Orthogonal jointing, 45
 Ostracods, 238, 247, 251, 254
 Outcrops, 43
 Outdoors adventure, 174
 Outwash plain, 162
 Outwash plains with kettles, 56
 Overflow, 191, 192, 194, 198
 Overgrazing, 204, 209
 Ovoid structures, 277
 Oxalate and calcium carbonates, 282
 Oxalate crystal, 268
 Oxalates, 271, 274, 280
 Ox-bow lakes, 168
 Oxidation, 30
 Oxides, 272
 Oxyaquic Udipsamment, 270, 271
 Oxygen (O), 281, 282
- P**
- Pacific, 40, 42
 Pacific and Atlantic oceans, 152
 Pacific Ocean, 55, 240, 253
 Paired rods, 273
 Palaeocene, 11, 20, 28
 Palaeoclimate, 2
 Palaeoclimatic, 38
 Palaeoenvironmental, 38
 Palaeogene volcanic rocks, 42
 Palaeolandforms, 42
 Palaeosols, 40, 42
 Palaeosurface, 37
 Palaeovalleys, 42
 Palaeoweathering, 37
 Palaeozoic, 11, 28, 237
 Palaeozoic and Mesozoic age, 57
 Paleo-bay, 206, 220–222
 Paleobay basins, 216
 Paleo-bay geomorphological units, 221
 Paleobay pans, 216
 Paleoclimate history, 71
 Paleoclimatic research, 241
 Paleo-coastline, 152
 Paleocommunities, 226

- Paleo-drainage, 219
 Paleo-drainage environments, 220
 Paleo-drainage hollows, 222
 Paleodrainage pans, 216
 Paleodrainage system, 206, 216
 Paleo-drainage unit, 216, 221
 Paleoecological information, 227
 Paleoecological perspectives, 263
 Paleoecological questions, 227
 Paleoecological studies, 225, 226
 Paleoenvironmental history, 143
 Paleoenvironments, 226
 Paleo-floods, 182
 Paleogene, 122
 Paleogene–Neogene, 247
 Paleogene rocks, 122
 Paleo-hydraulic, 188, 194
 Paleo-hydraulic method, 181, 188
 Paleo-lacustrine environments, 220
 Paleolimnological, 238
 Paleolimnological interpretation, 247
 Paleolimnological research, 241
 Paleo-littoral environment, 216
 Paleontological, 263
 Paleontological samples, 227, 233
 Paleopedological phase, 252
 Paleo-soils, 282
 Paleosols, 79, 91, 241, 247, 252, 256
 Paleozoic, 226, 247
 Paleozoic–Ordovician, 243
 Pali-Aike volcanic field, 155, 174
 Pampa, 266
 Pampean loess, 266
 Pan, 204–206, 209–223
 Pan density, 206, 215, 221
 Panels, 69, 72
 Pan perimeter, 215
 Paracrystalline, 262
 Parameters model, 135
 Parametric assessment sheet, 58
 Parametric values, 120
 Parent material, 264, 279
 Particle releasing, 9
 Particle remotion, 221
 Particle size distribution, 262
 Particle sizes, 188
 Partido de La Costa, 101, 104, 107
 Paso del Sapo, 3
 Past landslide events, 120
 Past pedological, 283
 Patagonia, 2, 39, 49, 52, 54, 55, 72, 143, 152, 154, 158, 161, 174, 204, 231, 234
 Patagonia brachiopods, 227
 Patagonian, 152, 204
 Patagonian and Fuegian Andes, 204
 Patagonian Cordilleran range, 164
 Patagonian destinations, 55
 Patagonian enchantments, 72
 Patagonian glaciations, 164
 Patagonian Gravels tablelands, 204
 Patagonian landscapes, 174
 Patagonian mountain ice-sheets, 164
 Patagonian plains, 154
 Patagonian Quaternary brachiopod, 225, 233
 Patagonian region, 147
 Patagonian Shingle formation, 154
 Patterned ground features, 143
 Payún Liso, 4
 Payún Liso volcano, 5, 6
 Payún Matrú, 4–6
 Payún Matrú caldera, 5
 Payún Matrú eruptions, 11
 Payún Matrú volcanic complex, 4
 Payún Matrú volcano, 5
 Payunia volcanic district, 3, 4
 Peak discharge, 185, 187, 196
 Peatbog, 57, 71
 Peaty plains, 56
 Pedal, 275, 279, 282
 Pedality, 270, 272
 Pedal microstructure, 276
 Pedestal, 26, 33
 Pedestal rocks, 33, 37
 Pediment, 22, 27, 77, 78, 82, 91
 Pediment associations, 81, 91
 Pedimentation, 82
 Pediment level, 91, 93
 Pedisediment, 77, 82
 Pedisediment level, 81, 82, 90, 91
 Pedogenesis, 261, 264
 Pedogenetic evolution, 262, 281
 Pedogenetic horizon, 270
 Pedogenic calcium oxalates, 274
 Pedogenic carbonate, 95
 Pedogenic development, 270
 Pedogenic gypsum nodules, 91
 Pedogenic periods, 78, 91
 Pedogenized cretaceous sedimentites, 93
 Pedological contents, 97
 Pedological cycle, 279
 Pedological development, 262
 Pedological evolution, 281
 Pedological horizon, 271, 272, 275
 Pedological processes, 263, 267
 Pedologic components, 77
 Pedologic evolution, 96
 Pedosedimentary, 266

- Pedosedimentary sequence, 261, 264, 271, 275, 279, 282
 Pedosedimentary studies, 264
 Pedostratigraphic sequences, 281
 Peds, 265, 274, 277, 280, 282
 Pehuenche phase compressive stage, 242
 Pellet formation, 217
 Pelletiform, 281
 Pelletiform calcified structures, 279
 Peneplain (Cratonic Erosion Surface), 246
 Penguin rockery, 152
 Peninsula Valdés, 204
 Peperite, 35, 36
 Perched dune, 217–219, 221, 222
 Periglacial environment, 156
 Perimeter (L), 205
 Perimeter development (DL), 205, 206, 213–216, 222
 Peripheral dip, 42
 Permafrost, 143, 156
 Permanent hydrological regime, 185
 Permeability, 163, 198, 272, 275, 279
 Permeable soils, 270
 Permian, 28, 37
 Permian–Early Triassic, 20
 Permian period, 21
 Permo-Triassic extinction, 226
 Peru, 238
 Petrocalcic, 82
 Petrocalcic crust, 82, 95
 Petrocalcic horizons, 95
 Petrographic studies, 3
 Petrologic point of view, 2
 Petrology, 2
 PH, 262, 264, 275
 Phanerozoic, 227
 Phillip II, 152
 Phosphorus, 282
 Photogeological mapping, 250
 Phreatic aquifer, 104
 Phreatic level, 210, 256
 Phreatic morphology, 110
 Phreato-magmatic explosions, 170
 Phyllograptud sp., 243
 Physical abrasion, 226
 Physical and chemical weathering, 170
 Physical dimension, 146
 Physical environment characteristics, 147
 Physical–geochemical, 241
 Physical landscape, 71
 Physical natural processes, 71
 Physical processes, 226
 Physical weathering, 1, 7, 13
 Physico-chemical, 279
 Physiographic features, 58
 Physionomy, 147
 Phytogenetic dunes, 217, 221
 Piedmont, 181–183, 185, 186, 188, 191–194, 198
 Piedmont alluvial fans, 187
 Piedmont area, 181–183
 Piedmont fluvial basin, 183
 Piedmont glaciations, 174
 Piedmont glaciers, 164
 Piedmont lobes, 164
 Piedmont plains, 183, 192
 Piedmont slope, 93
 Piedra Parada, 3
 Piedra Parada Caldera, 11
 Pierce's skill score, 131
 Piggyback-type basin, 256
 Pilcaniyeu (province of Río Negro), 1
 Pilcaniyeu-Comallo region, 37
 Pilcaniyeu ignimbrite, 2, 4, 37, 38, 43, 46
 Pilcaniyeu ignimbrite member, 38
 Pillow-lava flows, 36
 Pillow lavas, 35
 Pillows, 35
 Pinnacles, 1, 29
 Piping, 3, 14, 17, 30, 45
 Pirgua (sensu lato) Subgroup, 243
 Pirgua subgroup, 256
 Pits, 27
 Pixel, 106
 Plagioclase, 270
 Plains, 204
 Planation surface, 2, 3, 20, 22, 39, 246
 Planning, 54, 103
 Planning management, 182
 Plant communities, 267, 268, 273
 Plant cover, 144, 155, 169, 172
 Plant nutrition, 282
 Plant remains, 39
 Plants, 261, 262
 Plants and animals, 262
 Plateau, 13, 28, 29, 56, 238
 Playa Lake, 252, 257
 Pleistocene, 4, 51, 80, 143, 164, 226, 241, 247, 250, 257
 Pleistocene alluvial terrace, 77
 Pleistocene glaciations, 161
 Pleistocene glaciers, 210
 Pleistocene–Holocene boundary, 4
 Pleistocene ice advance, 164
 Pliocene, 154, 242, 256
 Pliocene piedmont deposits, 37
 Pliocene–Pleistocene, 55
 Plumes, 172

- Pluvial period, 237, 247
 Pluviometers, 185
 Poisson model, 120
 Polar Front, 223
 Polarization microscope, 241, 265
 Polish, 59
 Polished surface, 9
 Polychaeta, 225, 229, 231
 Polycrystalline, 273
 Polycrystalline chains, 274
 Polycyclic, 275
 Polygenesis, 44, 46, 78, 91
 Polygenetic landscape, 20
 Polygonal, 143
 Polyhydrated calcium oxalates, 280
 Polymodal, 275
 Polymodal design, 270
 Polymodal distributions, 279
 Ponds, 167, 168, 174
 Poorly welded, 30, 46
 Poorly welded zone, 43
 Population, 114, 172, 174
 Population growth, 104, 107
 Pores, 274, 280, 282
 Porphyritic rock, 2
 Porphyritic texture, 21, 38
 Portezuelo (province of Mendoza), 1
 Portezuelo de los Payunes, 5, 6, 8, 45
 Portezuelo ignimbrite, 3, 5–44
 Posters, 54
 Post-pedological processes, 282
 Potash feldspar, 38
 Potassium, 281
 Potential evapotranspiration, 110, 208
 Pre- and post-caldera lavas, 5
 Precambrian-Paleozoic, 183
 Precipitation(P), 102, 110, 121–124, 158, 172, 181, 183, 185, 187, 206–208, 267, 274, 277, 280, 281
 Precipitation data, 107
 Precipitation gradient, 144, 168, 183
 Pre-Collón Curá, 42
 Pre-Collón Curá formation landscape, 42
 Prediction accuracy, 119
 Prediction models, 133
 Predictive capacity, 136
 Predictive mapping, 199
 Pre-existing landscape, 43
 Pre-Jurassic highly deformed metamorphic rocks, 55
 Pre-Miocene, 41
 Preservation, 233
 Primary nuclei, 280–282
 Primary pyroclastic rocks, 245
 Prismatic columns, 29
 Probabilistic methods, 120
 Probabilistic model, 120
 Probability of landslide occurrence, 124
 Probability of occurrence, 186
 Processes, 54
 Productivity, 227
 Productivity indexes, 97
 Prosopis denudans, 82, 93, 96
 Protected birds, 152
 Proterozoic, 11
 Protocycloceras cf. Calligramma stefani Ceccioni, 243
 Province of Buenos Aires, 101, 104
 Province of Córdoba, 181–183
 Province of Chubut, 3, 11
 Province of Jujuy, 238, 240
 Province of Mendoza, 4
 Province of Santa Cruz, 28, 142, 143, 204
 Province of Tierra del Fuego, 51
 Province of Tucumán, 119, 121, 123
 Provinces of Mendoza (western Argentina), 2
 Provinces of Río Negro, Neuquén, 2
 Provincial road “j”, 52
 “Pseudo-pillow” landforms, 35
 Pseudo-rhombohedral crystals, 276, 280
 Pseudo-rhombohedral crystals, 276
 Pseudo-stratification, 18, 22, 25, 45
 Pseudo-stratification layer, 18
 Pseudo-stratification planar surface, 13
 Pucará table mountain, 245, 246
 Puerto Almanza, 52
 Pumice, 5, 6, 12, 19, 30, 35
 Pumice rock, 4
 Pumping field, 114, 115
 Puna, 237, 238, 240
 Puna Norte, 246
 Punta Sinái, 51
 Pyramids, 45, 280
 Pyroclastic deposit, 5, 13
 Pyroclastic flow, 2, 5, 6, 11, 19, 28, 30, 36, 44, 242
 Pyroclastic flow deposit, 4
 Pyroclastic levels, 245
 Pyroclastic matrix, 30
 Pyroclastic rock, 11, 28, 37, 246
 Pyroclastic sediments, 42
 Pyroclastic–volcanic complex, 3
 Pyroxene, 270, 272
- Q**
 Qualitative maps, 120
 Quartz, 34, 38, 270, 272, 279

- Quaternary, 20, 55, 166, 237, 241, 242, 246, 247, 256, 257
 Quaternary alluvial deposit, 38
 Quaternary brachiopod, 226, 227
 Quaternary–Cenozoic, 247
 Quaternary glacial sediments, 38
 Quaternary glaciations, 57
 Quaternary pedosedimentary sequences, 261, 263
 Quechua Phase, 242
 Quickbird satellite images, 205
- R**
- Radar diagram, 131
 Radiance spectra, 107
 Radiocarbon, 249, 266
 Radiocarbon age, 152
 Radiocarbon dating, 237, 241, 251, 252
 Radiometric ages, 156
 Radiometric dating, 5, 245, 256
 Raindrop-splash, 78
 Rainfall, 80, 181, 182, 183, 194, 198, 257
 Rain forest, 122, 124
 Rain gauge, 107
 RAL index, 221
 Ranches, 159
 Random field map, 133
 Random fields, 135
 Ranney wells, 114
 Raphides, 274
 Raster format, 187
 Rb–Sr isochrone, 21
 Real evapotranspiration, 110
 Recent, 240
 Recharge, 101–104, 107, 109, 110, 115, 207
 Recharge area, 103, 106
 Recharge of the aquifer, 108
 Recharge reduction, 112
 Recurrence, 186
 Redox depletions, 96
 Reference evapotranspiration, 107
 Regional faults, 183
 Regional landscapes, 147
 Regional palaeosols, 38
 Regional touristic development, 146
 Regolith, 22, 28, 30, 37, 45
 Regolith denudation, 37
 Regolith pediment, 22
 Regression equation, 125
 Regressive deposits, 279
 Relationship of Axes Length (RAL), 205
 Relationship of Axes Longitude (RAL), 206, 213–217, 222
 Relative frequency model, 120
 Relict geomorphic surfaces, 80
 Relict landforms, 31, 80
 Relict pedisediment, 90
 Relief, 193
 Relief modelling, 12
 Remote sensing, 137
 Remote sensing analysis, 222
 Remote sensing techniques, 204
 Rendzinas, 267
 Rendzina soils, 263
 Renguenao Formation, 90
 Reservoir, 101, 116
 Residential purposes, 137
 Resources Science Center, 241
 Retro-arc position, 4
 Rhizosphere fungi–bacteria, 282
 Rhyodacitic ignimbrite, 38
 Rhyolites, 90
 Rhyolitic flow, 23
 Rhyolitic ignimbrites, 12, 20
 Rhyolitic plateau, 20
 Ribbed moraines, 168
 Ridges, 279
 Rift basins, 243
 Rill, 6
 Rinconada, 240
 Río Avilés, 215
 Río Chico, 207, 214–216
 Río Chico Conglomerate member, 38
 Río Chico–Río Grande, 206, 214
 Río Chico valley, 163
 Río Chubut, 11
 Río Chubut valley, 3
 Río Cincel, 240
 Río Corral Blanco, 238
 Río Coyle watershed, 155
 Río Gallegos, 142, 155, 162, 166, 172, 173
 Río Gallegos basin, 155
 Río Gallegos estuary, 154, 155
 Río Gallegos valley, 154, 161, 163–165
 Río Gallegos watershed, 142, 143, 146, 147, 161
 Río Grande, 51, 207
 Río Grande–Río Chico, 210
 Río Lasifashaj, 59
 Río Negro, 228, 229
 Río Negro province, 4, 227
 Río Pichileufu, 4
 Río Santa Catalina, 240
 Río Turbio, 142, 146, 155, 169, 172
 Riparian vegetation, 160
 Risk, 137, 199
 Riverbed and floodplain deposits, 256
 Riverbed deposits, 257

- Road network, 186, 187
- Road network analysis, 187, 192
- ROC-curve, 131, 132, 136
- Rock arches, 45
- Rock-art, 24, 174
- Rock bridges, 45
- Rock cliff, 14
- Rock falls, 123, 158
- Rock monuments, 44
- Rock painting, 159
- Rocks, 54
- Rock-shelter, 1, 6, 18, 24, 45
- Rock towers, 43
- Rock walls, 44, 45
- Rock weathering, 123
- Rocky arcs, 3
- Rodados Patagónicos, 154
- Rods, 271, 274, 277, 282
- Root Mean Square Error (RMSE), 133
- Rosettes, 277, 279–282
- Roughness coefficient, 183, 188
- Rounded hills, 42
- Rowars, 45
- Runoff, 187
- Runoff direction, 186
- Runoff paths, 198
- Runoff spatial distribution, 187
- Rural and urban settlements, 182
- Rural tourism, 174

- S
- Sabellid polychaetes, 229, 233, 234
- Sabellids, 229
- Saddles and dykes, 243
- Safety factor, 128
- SAGA GIS, 127, 129
- SAGA GIS software, 186
- Saline and Calcimorphic soils, 267
- Saline content, 209
- Saline precipitation, 253
- Salinity, 106, 223
- Salt, 220
- Salta Group, 242, 243
- Salta Group Basin, 242
- Saltation, 8, 11
- Salt flat, 240
- Salt lake, 252
- Salt lake system, 237, 239
- Salt precipitation, 238, 256
- Saltwater intrusion, 101, 103, 110, 116
- Saltwater wedge, 114
- Salt weathering, 204
- Salty meadows, 267
- Samborombón Bay, 105
- San Clemente del Tuyú, 101
- Sand compaction, 107
- Sand-covered crests, 6
- Sand dune, 106, 107, 108, 204
- Sand dune barrier, 101, 104, 106, 108, 115
- Sand-dune environment, 101, 112
- Sand fractions, 270, 272
- Sands, 246
- Sandstone, 2, 37, 38, 44, 96, 122, 242, 243, 245
- Sandstones and andesites, 245
- Sand wedges, 143
- Sand with large clasts, 247
- Sandy coast, 102, 103
- Sandy supporting matrix, 247
- Sandy tuffs, 38
- Sanidine, 38
- San Juan de Oro surface, 242
- San Miguel de Tucumán, 121
- San Sebastián Bay (SSB), 204–206, 210–213, 217, 222
- San Sebastián Drift, 210
- Santa Catalina, 240
- Santa Clara formation, 266, 275
- “Santacrucense-Friasense” stage, 39
- Santa Cruz, 2
- Santa Cruz Formation, 154, 172
- Santa Cruz Province, 141, 147, 172
- Santa Teresita, 101
- Sarcocornia sp., 150
- SA studies, 121
- Satellite image Landsat, 205
- Satellite imagery, 136, 166, 169, 220
- Satellite images, 137, 147, 156
- Saturation conditions, 264
- Sb sulfides, 243
- Scallop shells, 233
- Scanning Electron Microscope (SEM), 241, 265
- Scanning electron
 - microscopy/energy-dispersive X-ray spectroscopy (SEM/EDX), 261
- Scarce vegetation, 204
- Scenery, 50, 53, 71
- Scenic attractions, 145
- Scenic landscape resources, 170
- Scenic value, 163
- Schists rock, 37
- Science, 50, 53, 59, 72
- Scientific disciplines, 72
- Scientific intermediation, 71
- Scientific talents, 71
- Scientific tourism, 166, 174
- Scoria and cinder cones, 155

- Scotia plate, 51, 55
 Scraping, 27
 Sea, 222
 Sea level, 103, 267
 Sea level changes, 263
 Seaside resorts, 103
 Seasonal variation, 106
 Sea spray, 270
 Seawater intrusion, 101–103, 114
 Secondary calcium carbonate, 272
 Secondary oxalates, 262
 Secondary permeability, 103, 158
 Sedentary species, 232
 Sedimentary, 263
 Sedimentary rock, 2, 11, 28, 37, 39, 45, 122
 Sedimentary rock landscapes, 1
 Sedimentary rocks of marine origin, 55
 Sedimentary sequences, 263
 Sediment distribution, 188
 Sedimentological, 181
 Sedimentological analysis, 191
 Sedimentological indicators, 186
 Sedimentological variables, 183
 Sediment retention, 187
 Sediments, 54, 262, 271
 Seismic, 57
 Semi-arid, 124
 Semi-arid climate, 124, 220
 Semi-arid conditions, 207
 Semi-arid zones, 222
 Semi-fixed dune, 107, 108, 110, 112, 114, 115
 Senecio filaginoides, 82
 Sensitive, 137
 Sensitivity, 133
 Sensitivity analysis (SA), 121, 133, 136
 Sensitivity and uncertainty analysis, 121
 Sensitivity indices, 135
 Serpulid, 230
 Serpulid tubes, 229
 Sessile mode of life, 226
 Sewage system, 103, 104
 Shallow and temporary water body, 209
 Shallow depressions, 211
 Shallow lacustrine, 241
 Shallow lake, 204, 207, 209, 210, 218, 220, 223
 Shallow landslides, 123, 124
 Shallow translational landslides, 128
 Shallow water, 211
 Shallow water body, 209
 Shape, 213
 Sharp edges, 57
 Shearing, 146
 Shear plane, 129
 Sheep, 52, 145, 159
 Sheep breeding, 146, 159
 Sheep farming, 168
 Sheep rising, 172
 Sheet of water surrounded by mountains, 69
 Shell, 270–272, 275–277, 279
 Shell/Ca biomineralizations, 268
 Shell ridges, 262, 266, 267, 279, 282
 Shelter, 26
 Shelters form, 34
 Shield volcano, 5
 Shrinkages, 247
 Shrubby steppe, 96, 209
 Shrubby vegetation, 217
 Shrublands, 204
 Shrubs, 144, 155
 Shrub species, 207
 Shrub-steppe, 91, 93
 Shuttle Radar Topography Mission (SRTM), 147, 184
 Sierra de la Rinconada Ordovician, 243
 Sierra de Lihuel Calel, 3, 20–23, 27
 Sierra de Pichiñán, 78, 93
 Sierra de Rinconada, 245
 Sierra de Santa Victoria, 241
 Sierras Grandes de Córdoba, 181, 183, 198
 Sierras Pampeanas, 181, 182
 Sierras Pampeanas geological setting, 183
 Sieve and pipette analysis, 264
 Siliceous volcanism, 242
 Silicobioliths, 275
 Silicon, 281
 Silicon biomineralizations, 262
 Silicophytoliths, 272
 Silt fraction, 272
 Silts, 266
 Siltstones, 122, 243, 245
 Silty-sand, 247
 Single crystals, 263
 Singularity, 51, 58
 Sites of interest, 59
 Sixth Argentine Congress of Quaternary and Geomorphology, 51
 Skeletal components, 262, 271
 Skeletal fraction, 265
 Slide plane, 129
 Slides, 123
 Slope, 123, 127, 128, 135–137, 186
 Slope angle, 123, 129
 Slope class, 127
 Slope map, 186
 Slope networks, 186
 Slope stability module, 129
 Slope steepness, 57

- Slumping, 13, 14, 43, 158
- Slumps, 150
- Small-scale structure, 3
- Snow fall, 222
- Snow melting, 207
- Snow precipitation, 207
- Snow storms, 207
- Social housing program, 172
- Sodic Haplocalcids, 96
- Sodium, 270
- Sodium chloride, 281
- Sodium polytungstate, 265
- Software Simlab, 134
- Soil, 78, 96, 103, 106, 129, 147, 163, 169, 204, 207, 220, 221, 252, 261, 262, 264, 267, 268, 270–272, 275, 277, 279, 281, 282
- Soil bacteria, 282
- Soil chronosequences, 79
- Soil cohesive strength, 120
- Soil control profiles, 80
- Soil degradation, 79
- Soil development, 79, 160, 169
- Soil freezing, 222
- Soil-geomorphic, 79
- Soil-geomorphic relationship, 81
- Soil-geomorphology, 79
- Soil matrix, 155
- Soil mining, 185
- Soil organic matter, 279
- Soil parent materials, 77, 81, 82
- Soil-plant relationships, 79
- Soil profile, 80, 93, 261, 279, 280
- Soil profile development, 82
- Soil properties, 79
- Soil-quality index, 97
- Soil taxonomy, 264
- Soil thickness, 120
- Soil use, 147, 163
- Solar direct insolation map, 127
- Solar insolation, 136
- Solar radiation maps, 137
- Solid mud, 247
- Soluble salts, 93
- Solum, 272, 275
- South America, 28, 103, 152, 154, 203, 227
- South American continent, 164
- South American plate, 51, 55
- South American Summer Monsoon (SASM), 240, 252
- South Atlantic Ocean, 28
- Southeast Brazil, 103
- South-easterly winds (“sudestadas”), 103
- Southeastern coast, 261
- Southeastern coast of Buenos Aires province, 261, 262, 263
- Southern Andes, 55
- Southern Argentina, 3
- Southern Austral Basin, 141, 143
- Southern end of South America, 50
- Southern hemisphere, 204
- Southern hemisphere oceans and atmosphere, 223
- Southernmost end of South America, 204
- Southernmost territories with temperate continental ecosystems, 72
- Southern Pacific Ocean, 144, 223
- Southern Pacific Ocean Anticyclone, 143
- Southern Patagonia, 148, 149
- Southern Patagonian Andes, 141, 143, 169
- Southern South America, 223
- Southern Tierra del Fuego, 49, 53, 72
- Southern Winter months, 204
- South Pacific Anticyclone, 203, 207
- Spatial, 226
- Spatial landslide risk assessment, 120
- Spatial multicriteria evaluation, 120
- Spatial prediction validation, 121
- Specimen, 227, 229
- Spectral features, 106
- Spheniscus magallanicus, 152
- Spherical bacteria, 277
- Spherulitic crystallization, 21
- Spilitic lava mantles, 243
- Spilitic lavas, 243
- Spillway channel, 27
- Spiral form, 34
- Spirorbis sp., 229
- Sporting fishery, 163
- Springs, 159
- SPSS statistical package, 124
- SRTM DEM, 133
- SRTM 30 m, 133
- SRTM 30-m digital elevation model., 125
- Stability of a slope, 127
- Stable tectonic environments, 82
- Stable terrains, 131
- Stagnant water, 187
- Stakeholders, 69
- Standard deviation, 133–135
- Static model, 120
- Statistical analysis, 107, 125
- Statistical and heuristics models, 120
- Statistical index (Wi), 120
- Statistical indicators, 119, 137
- Statistical methods, 120, 124, 125
- Statistical performance, 137
- Statistical techniques, 119

- Steels, 263
 Steep cliffs, 44
 Steppe, 56, 144, 163, 207
 Stepped plains, 206
 Steppe landscape, 223
 Steppe plains, 56
 Stopovers, 69
 Storm event, 185
 Storm waves, 103
 Straits of Magellan, 152
 Stratified fine gravel, 247
 Stratigraphic units, 154
 Stratovolcanoes, 11
 Stream channels, 187
 Stream networks, 42
 Stream Power Index (SPI), 125
 Structure, 58, 147
 Styloids, 274, 276, 277
 Sub-Andean grasslands, 146
 Sub-Antarctic landscape, 223
 Sub-Antarctic mixed forest, 56
 Sub-Antarctic species, 52
 Sub-circular cavities, 18
 Subglacial landform, 166, 171
 Subhumid, 207, 267
 Submarine volcanic activity, 55
 Submicroscopic, 261
 Subsequent, 42
 Sub-shrubby steppe, 93, 95
 Sub-superficial etching, 3, 37
 Subsurface flow, 120
 Subtropical, 122
 Subtropical climate, 123
 Subtropical regions, 122
 Subtropical river basin, 119
 Sub-volcanic bodies, 243
 Sub-volcanic intrusive bodies, 11, 246
 Summits, 41
 Super-eruption, 5
 Superficial runoff system, 209, 213
 Superimposed subglacial processes, 168
 Supra- and inter-tidal environments, 211
 Supratidal deposits, 204
 Surface (A), 205
 Surface runoff, 102, 110
 Surface temperature, 240, 241
 Surficial runoff, 166
 Surficial runoff conditions, 216
 Surficial sediments, 204
 Surroundings, 205
 Susceptibility, 120, 131, 136, 181, 186–188, 190, 192, 193, 197–199
 Susceptibility analysis, 188
 Susceptibility classification, 130
 Susceptibility map, 119, 127, 136
 Susceptibility models, 131
 Susceptibility value, 187
 Sustainability paradigm, 54
 Sustainable development, 72
 Sustainable economic activities, 72
 Sustainable engineering work, 199
 Swamps, 167
 Swimming capacity, 232
 Syn- or post-pedogenetic, 264
 Syn-rift stage, 242
- T**
 Tableland, 55, 143, 148, 150, 154–156, 158, 163, 168, 172, 220, 237, 238
 Tableland landscape, 143, 154, 163, 170, 174
 Taffoni, 2
 Tafna formation, 242, 246, 247, 256
 Tafoni, 1, 6, 18, 24, 26, 33, 34, 38, 44
 Tafoni hollows, 30
 Tagelus plebeius, 266, 272, 275
 Taphonomic effect, 227
 Taphonomic pathways, 227
 Tectonic activity, 54
 Tectonically active area, 57
 Tectonic basins, 43
 Tectonic block, 183
 Tectonic depression, 211
 Tectonic movements, 256
 Tectonic origin, 206, 210
 Tectonic plates, 51, 55, 56
 Tectonic stability, 2
 Temperate/cold climate, 204
 Temperature, 267
 Temperature amplitudes, 255
 Temporal dimension, 146
 Tephra and pyroclastic flows, 245
 Tephra flow, 242
 Terebratella dorsata, 225, 227, 229–232, 234
 Terminal and basal moraines, 164
 Terminal and ground moraines, 220
 Terminal moraines, 164, 167
 Terrace level, 161
 Terraced areas, 57
 Terrain, 137, 148
 Terrain classes, 132
 Terrain slopes, 120
 Terrain unit, 137
 Terrestrial, 263
 Territorial planning, 174
 Territory, 204, 205
 Tertiary, 30
 Tertiary rocks, 55
 Tertiary sedimentary rocks, 143

- Tetraraptus sp., 243
- Textural analysis, 241
- Texture, 2
- Thematic itineraries, 54
- Thematic panels, 59, 71
- Thematic trails, 49
- Thermal contraction joints, 158
- Thomas Bridges, 52
- Thomas Goodall, 52
- Threat, 186–188, 194, 196–199
- Threat analysis, 194
- Threat score. critical success index, 131
- Tidal channels, 272
- Tidal influence, 209
- Tidal paleochannels, 220
- Tidal plains, 206, 211
- Tierra del Fuego, 49, 51, 52, 55–57, 72, 204, 220, 221, 228, 229
- Tierra del Fuego archipelago, 55
- Tierra del Fuego National Park, 71
- Tierra del Fuego Provinces, 227
- Timbering, 169
- Tiomayo Formation, 242, 245, 256
- Tobas del Portezuelo, 2, 5
- Tolhuin, 51
- Topographical contrasts, 198
- Topographical factors, 133, 134
- Topographical parameters, 134, 136
- Topographic lowlands, 204
- Topographic maps, 185
- Topographic Wetness Index (TWI), 125
- Topography, 56, 167, 169
- Toposequence, 264–267, 281
- Topset, 249
- Topset beds, 238
- Torrential hydrologic regimen, 185
- Torrential regime, 181, 198
- Torres del Paine National Park, 170
- Torrifluvents, 78
- Torriorthens, 78
- Torriorthens, 91
- Tors, 1, 22, 25, 26
- Tourism, 54, 104
- Tourism industry, 59
- Tourist awareness, 54
- Tourist destinations, 53
- Touristic development, 182
- Touristic planning, 142
- Touristic point of view, 142, 147
- Touristic potential, 141
- Touristic purposes, 159
- Touristic resources, 141, 174
- Tourist infrastructure, 52
- Tourist products, 52
- Tourists, 103, 142
- Tourist supply, 54
- Tourmaline, 270, 272, 279
- Tours, 54
- Trachy-andesitic lava flows, 242
- Trachyte layer, 4
- Trachytic face, 5
- Trachytic-trachyandesitic type, 5
- Traditional architecture, 172
- Training basins, 124
- Trans-American, 150
- Transect, 52, 58, 71, 72
- Transect singularities, 49
- Transect Ushuaia-Estancia Harberton, 56, 59, 72
- Transform type, 55
- Transgressive–ingressive, 275
- Transgressive period, 281
- Transgressive–regressive, 266, 271
- Transgressive–regressive coasts, 266
- Transgressive–regressive cycle, 267
- Transitional intermediate zone, 56
- Transitory or ephemeral stream channels, 206
- Transitory water bodies, 221, 222
- Translocation of particles, 79
- Transport capacity, 192, 198
- Transport dynamics, 107
- Transported sediment, 186
- Tree classification algorithm, 106
- Tree roots, 187
- Trekking, 174
- Treks, 52
- Triassic period, 21, 39
- Triassic sedimentary rocks, 28
- Tributary glaciers, 56
- Tributary streams, 189
- Tritium and Radiocarbon Laboratory (LATYR), 241
- Tropical climate, 21
- Troughs, 56
- Trout fishing, 146
- True Negative, 136
- True Negative areas (TN), 131
- True Positive, 136
- True Positive areas (TP), 131
- Truncated spurs, 57
- Tubes, 156, 268, 271, 274, 279, 281, 282
- Tubes and chambers, 30
- Tucson, 241
- Tuff, 12, 28, 30, 245, 246
- Tuffs and ignimbrites, 245
- Tuffs and tuffites, 242
- Tumulus, 156
- Tunnel, 14, 30, 45, 156

- Tunnelling, 3, 17, 30, 45
 Turbidite interrelated channel, 243
 Turbidite lobed, 243
 Turbidity, 223
 Turbulence, 9
 Twisters, 217
 Type of use, 58
 Typic Calciudolls, 279
 Typic Endoacuoll, 272, 273
 Typic Haplargids, 93, 96
 Typic Haplocalcids, 90, 91, 93
 Typic Natrargids, 93, 96
 Typic Torrifluvents, 96
 Typic Torriorthents, 91, 93, 96
 Typic Udipsamments, 271
- U**
 Udipsamment, 267
 Unbranched calcified tubes, 279
 Unbranched tubes, 281
 Uncertainty Analysis (UA), 121, 133, 135
 Uncertainty and sensitivity analysis, 133
 Unconventional tourism, 141
 Underground water, 156, 255
 Undulated relief, 183
 Undulating relief, 192
 Ungauged catchments, 182
 Ungauged piedmont basin, 181
 Unique geographical position, 50
 Uniqueness, 49, 51
 Universidad Nacional de La Plata, 241
 University of Arizona, 241
 Unstable terrain, 131
 U–Pb dating, 243
 Uplift, 38, 40
 Uplifting, 20
 Upper member, 12
 Uranium ore deposit, 77, 79
 Urban areas, 102
 Urban centers, 146
 Urban design, 172
 Urban development, 114
 Urban expansion, 182
 Urban growth, 103
 Urbanization, 101–103, 107, 112, 116, 182
 Urbanization process, 101, 115
 Urbanized area, 108, 110, 112, 114, 185, 198
 Urbanized surfaces, 108
 Urban landscape, 172
 Urban pattern, 172
 Urban structure, 172
 USDA Soil Taxonomy, 275
 US Geological Survey, 241
 Ushuaia, 51, 52
 Ushuaia and Estancia Harberton, 72
 Ushuaia-Estancia Harberton transect, 49, 50, 53, 58
 Utah (USA.), 33
- V**
 Validation, 131, 133
 Valle Carbajal, 52, 58, 62
 Valle de las Pinturas, 24
 Valle de las Pinturas (Arroyo de las Sierras), 25
 Valley depth, 186
 Valley depth networks, 186
 Vapour-phase, 28, 45
 Vaterite, 262
 Vector format, 187
 Vegas, 144
 Vegetal cover, 168
 Vegetation, 81, 102, 107, 108, 122, 125, 143, 144, 155, 169, 188, 192, 196, 198, 207, 209, 217, 270, 275
 Vegetation cover, 143, 163, 204, 220, 270, 279
 Vegetation cover factor (NDVI index), 125
 Vegetation influence, 187
 Vegetative and reproductive structures, 263
 Vegetative growth, 263
 Velocity, 9, 187, 188, 194, 196–198
 Velocity, competence and transport capacity, 181
 Velocity values, 181
 Ventana formation, 37
 Ventifacts, 155
 Ventral shell, 229
 Ventral valves, 227, 229, 232
 Vents, 174
 Vertebrate fossils, 154
 Vertebrates, 267, 270
 Vertical joint, 6
 Vertical jointing, 29, 31
 Vesicular horizons, 91
 Viewpoints, 49, 54
 Visitor centres, 54
 Vitroclasts, 2, 38
 Vitrophyric, 12, 21
 Volcanic, 143
 Volcanic activity, 155, 156
 Volcanic and plutonic, 57
 Volcanic ashes, 246
 Volcanic bomb field, 4
 Volcanic breccias, 21
 Volcanic center, 158, 245
 Volcanic chimneys, 158
 Volcanic complex, 20
 Volcanic cones, 4, 156, 160, 163
 Volcanic ejecta, 39

- Volcanic episode, 28
- Volcanic event, 28
- Volcanic field, 155, 160, 172
- Volcanic glass, 270, 272
- Volcanic glass shard, 18
- Volcanic islands, 55
- Volcanic landforms, 4
- Volcanic landscape, 46, 155, 170, 172
- Volcanic lithoclast, 5
- Volcanic mesetas, 220
- Volcanic necks, 158
- Volcanic processes, 54, 141
- Volcanic–pyroclastic complex, 3, 11
- Volcanic relief, 160
- Volcanic rock, 11, 28, 37, 39, 154
- Volcanic tablelands, 170
- Volcanic vents, 155
- Volcanism, 21, 155
- Volcanoclastic rock, 14, 28, 245
- Volcanoes, 172
- Volcano-karst, 43
- Vulnerability, 120, 136, 199

- W**
- Wadis, 163, 172
- Wadi systems, 155
- Wandering channels, 168
- Warmest month, 207
- Washboard moraines, 168
- Water, 145, 261
- Water availability, 280
- Water balance, 101, 107, 110, 114
- Water body, 160, 219, 221
- Water consumption, 114
- Water currents, 216, 219
- Water deficiency, 267
- Water demand, 107
- Water discharge, 185, 187
- Water excess infiltration, 103
- Water flow, 186, 187, 193, 198
- Water flow direction, 187
- Water flowing, 186
- Waterfront, 172
- Water height, 196, 197
- Water height values, 194
- Water input, 110, 206
- Water-lain tuffs, 30, 38, 245–247
- Water level, 112, 185, 187, 188, 196
- Water level and velocity, 187
- Water-level change, 110
- Water management, 104
- Water output, 206
- Water purification, 114
- Water regime, 263
- Water removal velocity, 186
- Water reservoirs, 103
- Water resource, 104, 114, 159, 185
- Water service, 104
- Water supply, 101, 104, 114, 159
- Water supply network, 104, 114
- Water supply service, 104
- Water surface, 194
- Water surplus, 110
- Water system, 101, 104, 115
- Water table, 96, 103, 104, 110, 111, 129, 134
- Water transfer, 198
- Water treatment, 104
- Water values, 194
- Water velocity, 187, 188
- Wave action, 209, 221
- Wave erosion, 210, 217
- Wave-like pyroclastic flows, 245
- Weathered crystalline rocks, 123
- Weathered particles, 217
- Weathered product, 22
- Weathering, 14, 17, 26, 34, 37, 54
- Weathering front, 2, 20, 22, 25, 28, 37, 45
- Weathering mantles, 2, 20, 30
- Weathering processes, 23, 28
- Weathering profile, 21
- Weddellite, 262, 263, 276, 277, 280, 282
- Weddellite (polyhydrate), 274
- Wedge, 8
- Weight of evidence (WE) model, 119, 126, 131, 132, 134–136
- Welded, 12, 21
- Welded ignimbrite, 14, 27, 30, 39, 45
- Welding, 17, 19, 30, 38, 45, 46
- Welding degree, 1, 3, 5, 38
- Welding facies, 3, 46
- Welding types, 46
- Wellpoint systems, 114
- Well stratified, 38
- Westerlies, 221, 222
- Westerly winds, 172, 210
- Western Argentina, 3
- Western coasts, 209
- Western Río Negro province, 37
- Wet grasslands, 159
- Wetland, 96, 145, 163, 167, 168, 174, 254, 255, 267
- Wetlands (mallines), 77, 81, 96
- Wet meadows, 267
- Wet perimeter, 188
- Whaleback, 1, 25
- Whewellite, 262, 277, 280, 282
- Whewellite (monohydrate), 274
- Wildlife, 159, 163, 167, 174, 255

Wind, 78, 203, 204, 207, 210, 217, 221–223, 255

Wind abrasion, 6

Wind action, 6, 8, 261, 263

Wind direction, 208

Wind energy, 221

Wind erosion, 6, 8, 210

Wind intensity, 204

Wind-transported particles, 217

Wind velocity, 9

Windward margin, 210

Winter sport centres, 52

X

Xenarthra, 247

Xerophyte vegetation, 122, 124

X-Ray Diffraction (XRD), 241

X-ray fluorescence, 237, 241

X-ray spectrometer (EDXS), 265

Y

Yardang landscape, 3

Yardangs, 1–3, 5, 6, 33, 45

Younger Dryas episode, 257

Yungas, 122

Z

Zircon, 272, 279

Zn, 243

Zonal biomes, 144